FACULTY OF MEDICINE, MASARYK UNIVERSITY

# Analysis of cardiomyocyte contraction for drug testing, hereditary cardiomyopathies, and quantification of arrhythmias in vitro

---

**MUDr. Martin Pešl, Ph.D.**

HABILITATION THESIS

B R N O 2 0 2 6

Acknowledgements

I would like to express my sincere gratitude to my mentors:

Professor Jaroslav Meluzín, M.D., Ph.D., Associate Professors Tomáš Kara MD. Ph. D. and Zdeněk Stárek, M.D., Ph.D., for introducing me to cardiology, arrhythmology, and cardiac electrophysiology, and for their invaluable guidance, insightful discussions, expert advice, and patience throughout our consultations.

Mgr. Vladimír Rotrekl, Ph.D., Professor Petr Dvořák, Ph.D., and Professor Dan Kaufman, M.D., Ph.D., for introducing me to molecular biology, particularly the differentiation of cardiomyocytes, for their inspiring scientific insights, valuable advice, and for their patience with my clinically oriented way of thinking.

I am also deeply grateful to the heads of the First Department of Internal Cardioangiology and the Institute of Biology for fostering an inspiring environment for scientific research, namely Professor Petr Dvořák, Professor Jiří Vítovec, Professor Lenka Špinarová, Professor Ondřej Slabý, and Professor Jan Krejčí.

My sincere thanks also go to my colleagues and collaborators: Mgr. Jan Přibyl, Ph.D., Associate Professor Kristian Brat, M.D., Ph.D., MSc, Ivana Acimovic, Ph.D., Mgr. Šárka Jelínková, Ph.D., Guido Caluori, Ph.D., Mgr. Šimon Vrána Klimovič, Ph.D., Mgr. Deborah Beckerova, Martin Ščurek, M.D., Ph.D., Lucie Masarová, M.D., Ph.D., and Katarína Melajová, M.D. I would also like to thank the entire electrophysiology team at St. Anne's University Hospital and the Institute of Biology for their invaluable assistance with sample collection, cell culture experiments, and data analysis.

Finally, my deepest gratitude belongs to Lucie, Lucinka, and Martínek for their endless patience, unwavering support, and understanding throughout this journey.

# OBSAH

**1 COMMENTARY ..... 8**

*1.1 Introduction: Cardiomyocyte contraction and relaxation for inherited cardiomyopathies ..... 8*

*1.2 Aims ..... 9*

1.2.1 Describe the force and frequency of contractions of a cluster of cardiomyocytes differentiated from stem cells ..... 9

1.2.2 To measure absolute contractile force values along with contraction frequency in cellular models. 9

1.2.3 To extend analysis beyond mechanics and include other related modalities ..... 9

1.2.4 To apply technology in genetic models ..... 9

1.2.5 To apply technology in pharmacological analysis ..... 9

1.2.6 To apply technology in specific area of arrhythmology – conductive arrhythmias ..... 9

*1.3 Key words ..... 9*

*1.4 Methods ..... 9*

1.4.1 Atomic force microscopy ..... 10

1.4.2 Microelectrode array ..... 10

1.4.3 Calcium Imaging ..... 11

*1.5 Obtained Results ..... 11*

**2 Biosensing of cardiomyocyte contraction and relaxation (p1) ..... 13**

*2.1 Introduction ..... 15*

*2.2 Materials and methods ..... 17*

2.2.1 Preparation of hiPSC and hESC cardiomyocyte clusters ..... 17

2.2.2 Clusters seeding and measurement set-up ..... 18

*2.3 Recording of mechanocardiograms ..... 19*

*2.4 Results and discussion ..... 21*

*2.5 Conclusions ..... 29*

*2.6 Acknowledgments ..... 30*

*2.7 Appendix A. Supporting information ..... 30*

**4 Improvements in biosensing by addition of electrophysiological recordings (p2a) ..... 31**

*4.1 Commentary ..... 31*

*4.2 Introduction ..... 34*

*4.3 Materials and methods* ..... *36*

4.3.1 hPSC culture and cardiac differentiation ..... 36

4.3.2 Microelectrode arrays cleaning and coating ..... 37

4.3.3 BCCs plating on MEA chips ..... 37

4.3.4 Setup preparation and experimental protocols ..... 38

4.3.5 Data recording and evaluation ..... 40

*4.4 Results and discussion* ..... *41*

4.4.1 Simultaneous electromechanical recording ..... 41

4.4.2 Differential drug response and correlation analysis is indispensable to distinguish cell-type dependency of cardiac parameters ..... 43

4.4.3 Calcium trials ..... 43

4.4.4 Isoproterenol trials ..... 46

4.4.5 Verapamil trials ..... 46

*4.5 Conclusions* ..... *47*

*4.6 Acknowledgments* ..... *48*

*4.7 Appendix A. Supporting information* ..... *48*

**5 Improvements in biosensing by addition calcium imaging (p2b) ..... 49**

*5.1 Commentary* ..... *49*

*5.2 INTRODUCTION* ..... *52*

*5.3 METHODS* ..... *56*

5.3.1 Preparation of hESC-derived CM clusters ..... 56

5.3.2 Clusters seeding and measurement setup ..... 57

5.3.3 Data recording ..... 58

5.3.4 Data extraction and filtration ..... 59

*5.4 RESULTS* ..... *61*

5.4.1 Evaluation of different filtration methods ..... 62

5.4.2 Evaluation of caffeine effect on calcium and contraction signals ..... 64

*5.5 DISCUSSION* ..... *64*

*5.6 CONCLUSIONS* ..... *67*

*5.7 FUNDING INFORMATION* ..... *67*

**6 Disease phenotype description by AFM (p3) ..... 69**

*6.1 Commentary* ..... *69*

*6.2 INTRODUCTION* ..... *72*

*6.3 MATERIALS AND METHODS* ..... *73*

6.3.1 Cell Lines, Cultivation, Reprogramming, and hPSC Differentiation Into Cardiomyocytes via Embryoid Bodies ..... 73

6.3.2 Immunodetection ..... 75

6.3.3 Quantitative Real-Time PCR ..... 77

6.3.4 Measurements of Intracellular Cytosolic $Ca^{2+}$ Variations by Fluorescent Confocal Microscopy ..... 77

6.3.5 Electrophysiological Recordings Through Patch-Clamp ..... 78

6.3.6 Atomic Force Microscopy Measurements ..... 78

6.3.7 Free Troponin Analysis ..... 79

6.3.8 Statistical Analysis ..... 79

*6.4 RESULTS* ..... *79*

6.4.1 DMD-CCs Do Not Express Full-Length Dystrophin Protein ..... 79

6.4.2 Dystrophin Deficiency Leads to Cardiac Differentiation With Lower Yield of Spontaneously Beating EBs 82

6.4.3 DMD-CCs Display Altered Electrophysiological Properties ..... 84

6.4.4 DMD-CCs Exhibit Abnormal Intracellular $Ca^{2+}$ Handling ..... 87

6.4.5 Aberrant L-Type Voltage-Dependent $Ca^{2+}$ Channel Expression in DMD-CCs ..... 88

6.4.6 DMD-EBs Display Hypocontractility, Bradycardia, and Higher Heart Rate Variability ..... 91

6.4.7 Loss of Dystrophin Leads to β-Adrenergic Remodeling and Cardiomyocyte Wasting ..... 93

*6.5 DISCUSSION* ..... *96*

*6.6 LIMITATIONS OF THE STUDY* ..... *101*

*6.7 CONCLUSIONS* ..... *101*

*6.8 SUPPLEMENTARY MATERIAL* ..... *102*

**7 Pharmacological (p4) ..... 104**

*7.1 Commentary* ..... *104*

*7.2 INTRODUCTION* ..... *106*

*7.3 MATERIALS AND METHODS Cell Cultivation* ..... *108*

7.3.1 Atomic Force Microscopy Measurements ..... 110

7.3.2 Multielectrode Array Measurements ..... 110

7.3.3 Measurement of HL-1 Viability ..... 111

7.3.4 Statistical Analyses ..... 111

*7.4 RESULTS* ... *112*
7.4.1 Positive Chronotropic and Inotropic Effects of Aminophylline on hPSC-CMs ... 112
7.4.2 Positive Chronotropic Effect of Aminophylline on HL-1 ... 114
7.4.3 Exposure to Aminophylline Causes Spontaneous $Ca^{2+}$ Releases Leading to Arrhythmia ... 115
*7.5 DISCUSSION* ... *116*

**CONCLUSION/SUMMARY ... 121**

*7.6 STUDY LIMITATIONS* ... *121*
*7.7 FUNDING* ... *122*
*7.8 ACKNOWLEDGMENTS* ... *122*
*7.9 SUPPLEMENTARY MATERIAL* ... *122*

**8 Pharmacological (p5) ... 123**

*8.1 Commentary: Synergic effect of salbutamol and aminophylline on hPSC-CMs* ... *123*
*8.2 Introduction* ... *125*
*8.3 Materials and Methods* ... *126*
8.3.1 Cell Cultivation ... 126
8.3.2 Atomic Force Microscopy measurements ... 126
8.3.3 Beat rate variability (BRV) analysis ... 127
8.3.4 Statistical analysis ... 128
*8.4 Results* ... *129*
8.4.1 Inotropic and anti-arrhythmic effect of salbutamol on hPSC-CMs ... 129
8.4.2 Synergic effect of salbutamol and aminophylline on hPSC-CMs ... 131
8.4.3 Activation of nitric oxide synthase (NOS) reduces aminophylline induced arrhythmia. ... 134
*8.5 Discussion* ... *136*
*8.6 Funding* ... *139*
*8.7 Acknowledgments* ... *140*

**9 Arrhythmology application (p6) ... 141**

*9.1 Commentary: hESC derived cardiomyocyte biosensor to detect the different types of arrhythmogenic properties of drugs* ... *141*
*9.2 Introduction* ... *144*
*9.3 Materials and methods* ... *146*
9.3.1 Cell lines, cultivation, and differentiation into embryoid bodies ... 146

9.3.2 Cultivation dish preparation and EBs seeding ..... 146
9.3.3 Processing of video sequences mechanocardiograms (MCG). ..... 147
9.3.4 Atomic force microscopy ..... 148
9.3.5 $Ca^{2+}$ imaging ..... 149
9.3.6 Immunocytochemistry ..... 150
*9.4 Results and discussion ..... 150*
9.4.1 Formation and characterization of functional syncytium ..... 151
9.4.2 Detection of caffeine-induced arrhythmia by AFM based biosensor and Fluo-4 ..... 152
*9.5 Conclusion ..... 159*
*9.6 Acknowledgments ..... 159*
*9.7 Appendix A. Supplementary data ..... 159*
**10 Final Conclusion and Future Perspectives ..... 160**
*10.1 Disease modeling ..... 160*
*10.2 Pharmacological Analysis and Arrhythmia Detection ..... 161*
*10.3 Clinical Relevance and Precision Medicine ..... 161*
**11 References ..... 162**

# 1 COMMENTARY

## 1.1 Introduction: Cardiomyocyte contraction and relaxation for inherited cardiomyopathies

Cardiomyocyte (CM) contraction and relaxation are functional parameters that are fundamentally altered in most cardiac pathologies. The phenotypic characteristics of these myocardial diseases range from entirely asymptomatic forms to symptomatic heart failure and death resulting from malignant tachycardias (Martinez et al. 2021), with the underlying cause often residing at the cellular and genetic levels (Aistrup et al. 2009; Stienen 2015). Understanding the genetic-phenotypic associations of hereditary cardiac diseases enables more effective risk stratification (Stroeks et al. 2025), which improves clinical surveillance and risk management for both the patient and family members at risk of preventable cardiovascular morbidity and mortality (Carrick et al. 2024). Particularly in the era of precision medicine, this understanding provides the first opportunities for targeted therapy—for example, regarding a patient's ability to metabolize propafenone (Smíšek et al. 2025) or using Recursive Piecewise Data Assimilation (RPDA) to quantify alterations in ion channels, demonstrating the potential of this method as a drug toxicity counter-screen (Wells et al. 2025).

Since 1998, human cellular models became widespread, initially derived from human embryonic stem cells (hESC) (Thomson et al. 1998) and in the next decade in patient-specific induced pluripotent stem cells (hiPSC) (Takahashi and Yamanaka 2006), collectively called human pluripotent stem cells (hPSC). The cardiomyocytes differentiation methods quickly developed in co-culture, monolayers or clusters (three dimensional embryoid bodies, EBs) (reviewed in (Acimovic et al. 2014)). Resulting progenitor and maturing cells are important in drug screening and disease modeling(reviewed in (Svobodova et al. 2021)). The analysis of cardiomyocytes contractility phenotype represents an initial phase for further mechanical studies relevant for drug development and disease modeling (Martin Pesl et al. 2023; Caluori et al. 2019). Beating force and contraction frequency of the CMs contractions can be recorded by micromechanical transducers, a platform for cell-based biosensors (CBB). Strategies involving CBBs represent a powerful tool to understand and specifically treat human heart diseases.

We have constructed a sensitive setup that involves human pluripotent stem cell-derived cardiomyocytes (hPSC-CMs), combined with an atomic force microscopy (AFM) force sensing platform, to measure biomechanical properties (absolute values of contractile forces together with the beat rate) in complex conditions and cellular models (Pesl et al. 2013) and continuously develop this setup for clinically relevant purposes.

## 1.2 Aims

The habilitation thesis is a commentary on a set of publications containing analysis of cardiomyocytes by atomic force microscopy, where the applicant is the first author, corresponding author or co-author. The works are organized into 6 chapters according to aims.

- **1.2.1** Describe the force and frequency of contractions of a cluster of cardiomyocytes differentiated from stem cells.
- **1.2.2 To measure absolute contractile force values along with contraction frequency in cellular models.**
- **1.2.3 To extend analysis beyond mechanics and include other related modalities**
- **1.2.4 To apply technology in genetic models**
- **1.2.5 To apply technology in pharmacological analysis**
- **1.2.6 To apply technology in specific area of arrhythmology – conductive arrhythmias**

## 1.3 Key words

Human pluripotent stem cells; cardiomyocytes; excitation-contraction coupling; atomic force microscopy; drug testing; three-dimensional heart models; inherited heart diseases.

## 1.4 Methods

The three basic methods utilized across the research works are briefly summarized in Table 1. This methodological framework consists of Atomic Force Microscopy (AFM) for recording mechanocardiograms, Microelectrode Arrays (MEA) for electrophysiological recordings, and Calcium Imaging for the direct monitoring of intracellular calcium transients.

| METHOD | WHAT IT MEASURES | KEY ADVANTAGES |
|---|---|---|
| **AFM (MECHANOCARDIOGRAMS)** | Contractile force, beat rate, relaxation time | High sensitivity (200 pN), real-time mechanical readout |
| **MEA (ELECTROPHYSIOLOGY)** | Field potentials, beat frequency, arrhythmia risk | Correlates electrical excitation with mechanical output |
| **CALCIUM IMAGING** | Intracellular $Ca^{2+}$ transients (timing & amplitude) | Direct insight into excitation–contraction coupling |

*Tab.: 1. Overview of utilized methods*

### 1.4.1 Atomic force microscopy

AFM-based biosensor noninvasively characterizes the contractile mechanics of clusters of human pluripotent stem cell–derived cardiomyocytes. Uncoated silicon-nitride cantilevers were mounted in a fluidic chamber at physiological conditions (~37 °C, buffered culture medium). Setup record continuous real-time mechanical force-time curves—termed mechanocardiograms (MCGs). These capture beat-to-beat contraction force, beat rate, and relaxation dynamics. This setup has excellent sensitivity, with a detection limit down to ~200 pN and ~20 nm vertical displacement, providing robust, low-computational readouts

To optimize signal accuracy across the entire syncytium, cantilever parameters such as feedback gain and spring constant (optimized around 6 nN) were fine-tuned (Pribyl, Pesl et al. 2019), and it was demonstrated that uncoated (non-coated) cantilevers provide enhanced thermal stability for prolonged measurements lasting hours to days

. This method also enables pharmacological testing—for instance, measuring inotropic responses to isoproterenol, aminophylline, salbutamol, or β-blockers—thereby translating mechanical changes into quantifiable indicators of drug effect (Kabanov et al. 2024, Klimovic et al. 2022).

### 1.4.2 Microelectrode array

To complement the mechanical insight, the AFM platform was integrated with microelectrode arrays (MEAs)—exactly aligning beating clusters of cardiomyocytes cultured atop MEA chips

with simultaneous cantilever probing. In this dual-modal electromechanical system, extracellular field potentials (FPs)—including beat frequency, waveform morphology, and arrhythmic events—were captured via MEA electrodes, while the AFM cantilever recorded mechanical outputs from the same biological structure.

This configuration enabled precise correlation between electrical excitation (FP signals) and mechanical contraction, offering a richer, multidimensional phenotype readout. Optical–mechanical synchronization involved inverted optical microscopy enabling simultaneous visualization and data alignment for the two modalities.

### 1.4.3 Calcium Imaging

The third methodological pillar is the combination of AFM with optical calcium imaging, enabling direct monitoring of intracellular calcium dynamics alongside mechanical contraction. In their conference abstract, Pešl et al. reported the first simultaneous recordings of mechanocardiograms (via AFM) and local calcium wave dynamics (likely using fluorescent $Ca^{2+}$-sensitive dyes) in cardiomyocyte clusters—delivering rich data on excitation-contraction coupling within embryoid bodies (EBs) (Odstrcilik et al. 2015)

Signal processing employed ensemble empirical mode decomposition (EEMD), which they found optimally balanced signal-to-noise ratio and minimized distortion. They validated the system by applying caffeine—a known modulator of calcium handling—and observed the expected physiological effects: ~5.5 % increase in calcium transient duration and ~14.5 % increase in contraction amplitude. This AFM-$Ca^{2+}$ integration thus empowers real-time correlation between $Ca^{2+}$ spike timing, amplitude, and mechanical force generation. (Cmiel 2017).

## 1.5 Obtained Results

Atomic Force Microscopy (AFM) is novel high-fidelity nanomechanical transducer with a sensitivity down to ~200 pN, using non-coated silicon nitride cantilevers with a 5–6 nN setpoint provides the thermal stability necessary for continuous, non-invasive recordings of cardiac activity lasting up to 8 hours

The platform achieved the first-ever synchronous recording of extracellular field potentials (via MEA) and mechanical force (via AFM) in 3D cardiac models. This integration allowed for the quantification of the electro-mechanical delay (EMD), providing a novel and critical parameter for assessing excitation-contraction coupling in vitro.

By utilizing patient-specific hiPSCs and CRISPR/Cas9-edited lines, the human Duchenne Muscular Dystrophy (DMD) phenotype was described. Key findings included a distinctive signature of hypocontractility, bradycardia, increased heart rate variability, and impaired calcium handling marked by diastolic calcium leaks

Research on aminophylline identified two parallel arrhythmogenic actions: a "deterministic" concentration-dependent chronotropic effect (sinus tachycardia) and a "stochastic" concentration-independent occurrence of rhythm irregularities (resembling atrial fibrillation). The study of the salbutamol-aminophylline combination revealed that salbutamol acts as an anti-arrhythmic agent by mitigating aminophylline-induced irregularities. This effect was mechanistically linked to the activation of nitric oxide synthase (NOS) via β2-adrenergic receptors.

The development of a dual 3D cardiac syncytium connected by a functional cellular bridge allowed for the detailed study of conduction disturbances. By utilizing lateral AFM deflection measurements, the biosensor detected the loss of synchrony and signal spreading defects characteristic of fibrillation-like behaviour.

**Following will be shortened description of each of 7 papers (p1, p2a, p2b, p3, p4, p5, p6),** citations and literature is compiled in the end of work as single citation body. Figures and tables shall be numbered by appropriate chapter as Fig.: 1.1.

## 2 Biosensing of cardiomyocyte contraction and relaxation (p1)

Cell-based biosensor (CBB) stands for device combining cell of interest, in this case CMs with measurement equipment comprehending and managing various phenotypes of human diseases, notably heart diseases, which stand as a primary cause of mortality in developed nations (Pilkerton et al., 2015). Many of these diseases harbor underlying causes at cellular and genetic levels (Aistrup et al., 2009; Stienen, 2015), not readily accessible for diagnostics due to the invasiveness and risk associated with heart biopsy (Holzmann et al., 2008; Imamura et al., 2015). Since the emergence of pluripotent stem cells (PSCs), particularly human embryonic stem cells (hESC) (Thomson et al., 1998), and disease-specific induced pluripotent stem cells (hiPSC) (Takahashi et al., 2007), along with their differentiation into cardiomyocytes (Mummery et al., 2002), these cell types have become crucial models for drug and disease screening (reviewed in Acimovic et al., 2014, Svobodova et al. 2021).

The electrophysiological phenotype of individual cardiac cells is extensively studied, offering insights into pacemaker or messenger functions. However, the syncytium of cardiac myocytes (CMs) emerges as a critical parameter in biosensor assembly, with unstable signals observed in individual or small clusters of cells (Kaneko et al., 2007, 2014). Various methods, predominantly focusing on action potential, cell-to-cell conductivity, or electrical cell-substrate impedance, have been employed (Giaever and Keese, 1984). Recently, xCELLigence RTCA Cardio multiwell sensor combined with primary neonatal rat cells has shown promise in monitoring the effects of antiarrhythmic drugs (Guo et al., 2011). Nonetheless, the interplay between electrophysiological data and mechanical triggers remains challenging, particularly for diseases affecting electro-mechanical coupling. Therefore, biosensing of CM contraction and relaxation emerges as a crucial step in in vitro disease modeling.

Indirect methods of contraction measurement, such as optical ones based on optical fiber deformation and image analysis, have limitations, especially with in vitro differentiated CMs. Furthermore, the combination of optical analysis with direct methods measuring contraction force on artificially assembled structures is significantly influenced by substrate stiffness. The most promising structure for studying the contraction properties of human cardiac syncytium appears to be uniformly sized clusters of differentiated CMs in the form of PSCs-derived embryoid bodies. Consequently, a direct approach using atomic force microscopy (AFM) to assess the EBs' cardiac syncytium mechanical properties in real-time under alternating

biophysical and biochemical conditions is opted for. AFM, a three-dimensional high-resolution topographic technique, offers suitability for biological applications in native conditions with the ability to measure cantilever probe bending with extremely high precision. It serves as a mechanical nanosensor or micromechanical transducer for biosensor construction. Modified AFM tip biosensors have found applications in various studies, including Alzheimer's disease analysis, cell penetration studies, drug effect sensing, and growth factor studies.

In this study, uniformly sized EBs containing hiPSC-derived cardiomyocytes are integrated into an AFM force sensing platform to establish a high-fidelity contraction pattern as a unique CBB for measuring absolute values of contractile forces along with beat rate in complex conditions and cellular models. The development and optimization of the entire measurement setup are described, with proposed applications for characterizing cardiac cell clusters and testing the effects of model drugs. Key results of the work include:

**a) Long-term stability** (up to 8 hours) was achieved using non-coated silicon nitride cantilevers and a preferred 6 nN set point, which allowed for the measurement of 95% of maximum contraction force while minimizing mechanical stimulation of the cells.

b) **Homogeneity**: Biomechanical properties, including contraction force and beat rate, were found to be homogeneous across the surface of the EB, which offers a significant advantage in robustness over single-cell based sensors

c) **Calcium Sensitivity:** The biosensor demonstrated that contraction force increased proportionally with extracellular calcium concentrations (0.2–5.4 mM), while the beat rate simultaneously decreased.

d) **Pharmacological Validation**: The system accurately quantified the effects of cardiac drugs: the beta-blocker metoprolol decreased both force and rate, while the beta-agonist isoproterenol induced an increase in both parameters.

e) **Arrhythmia Detection:** The platform successfully visualized and quantified fast arrhythmic processes, such as the "stop-and-go" effect triggered by caffeine.

Biosensors and Bioelectronics 85 (2016) 751–757

Contents lists available at ScienceDirect

Biosensors and Bioelectronics

journal homepage: www.elsevier.com/locate/bios

# Atomic force microscopy combined with human pluripotent stem cell derived cardiomyocytes for biomechanical sensing

Martin Pesl [a,b,1], Jan Pribyl [c,1], Ivana Acimovic [a], Aleksandra Vilotic [a], Sarka Jelinkova [a], Anton Salykin [a,b], Alain Lacampagne [d], Petr Dvorak [a,b], Albano C. Meli [a,d], Petr Skladal [c,*], Vladimir Rotrekl [a,b]

[a] Department of Biology, Faculty of Medicine, Masaryk University, Brno, Czech Republic
[b] ICRC, St. Anne's University Hospital, Brno, Czech Republic
[c] CEITEC, Masaryk University, Brno, Czech Republic
[d] PhyMedExp, INSERM U1046, University of Montpellier, Montpellier, France

ARTICLE INFO

*Article history:*
Received 15 March 2016
Received in revised form
11 May 2016
Accepted 23 May 2016
Available online 28 May 2016

*Keywords:*
Micromechanical biosensor
Human stem cell
Cardiomyocyte contraction
Drug testing

ABSTRACT

Cardiomyocyte contraction and relaxation are important parameters of cardiac function altered in many heart pathologies. Biosensing of these parameters represents an important tool in drug development and disease modeling. Human embryonic stem cells and especially patient specific induced pluripotent stem cell-derived cardiomyocytes are well established as cardiac disease model.. Here, a live stem cell derived embryoid body (EB) based cardiac cell syncytium served as a biorecognition element coupled to the microcantilever probe from atomic force microscope thus providing reliable micromechanical cellular biosensor suitable for whole-day testing.

The biosensor was optimized regarding the type of cantilever, temperature and exchange of media; in combination with standardized protocol, it allowed testing of compounds and conditions affecting the biomechanical properties of EB. The studied effectors included calcium , drugs modulating the catecholaminergic fight-or-flight stress response such as the beta-adrenergic blocker metoprolol and the beta-adrenergic agonist isoproterenol. Arrhythmogenic effects were studied using caffeine. Furthermore, with EBs originating from patient's stem cells, this biosensor can help to characterize heart diseases such as dystrophies.

© 2016 Elsevier B.V. All rights reserved.

## 2.1 Introduction

Cell based biosensor (CBB) devices represent a novel tool to understand and treat various human diseases including heart diseases which are leading cause of death in developed countries (Pilkerton et al., 2015). Most of them have hidden cause at the cellular and genetic levels (Aistrup et al., 2009; Stienen, 2015) not easily accessible for diagnostics, as heart biopsy is invasive procedure with significant risk (Holzmann et al., 2008; Imamura et al., 2015). Since the discovery of pluripotent stem cells (PSCs), such as human embryonic stem cells (hESC) (Thomson et al., 1998) and especially disease specific induced pluripotent stem cells (hiPSC) (Takahashi et al., 2007) and their differentiation into cardiomyocytes (Mummery et al., 2002), these cell types represent an important cellular model in drug and disease screening (reviewed in Acimovic et al., 2014).

The electrophysiological phenotype of individual cardiac cells is often studied providing information representing pacemaker or messenger function. Despite most of studies use single cells, the CMs syncytium seems to be a critical parameter in biosensor assembly as unstable signals are obtained in case of individual or small cluster of cells (Kaneko et al., 2007, 2014). These methods follow mostly action potential, cell to cell conductivity or electrical cell-substrate impedance (Giaever and Keese, 1984). Recently, xCELLigence RTCA Cardio multiwell sensor combined with primary neonatal rat cells was used to monitor the effect of antiarrhythmic drugs on cell growth and contractions (Guo et al., 2011). However, the electrophysiological data cannot be fully separated from the mechanical triggers and consequences (Kelly et al., 2006) rendering the method not suitable for large group of diseases affecting electro-mechanical coupling. Thus CM contraction and relaxation biosensing represents an indispensable step for the in vitro disease modeling. Indirect methods of contraction measurement, such as optical ones based on optical fiber deformation (Fearn et al., 1993) and image analysis (Neagoe et al., 2003) have limited potential especially in case of in vitro differentiated CMs, which do not fully match the shape of the isolated CMs and often require dissociation of the syncytium and analyzing the individual cells in microposts (Rodriguez et al., 2014). Furthermore, the combination of optical analysis and the direct methods measuring contraction force on artificially assembled structures are significantly impacted by stiffness of the substrate, such as the twitch power in the case of dissociated cells plated on substrate with varying stiffness (Rodriguez et al., 2011). Further the increasing cell number negatively impacted the force-length relationship measured directly on neonatal cardiac cells self-assembled on fibrin fibers (Sondergaard et al., 2012), again rendering the syncytium analysis at least difficult. Thus it seems that the most promising structure for studying the contraction properties of human cardiac syncytium might be uniformly sized clusters of differentiated CMs in the form of PSCs-derived embryoid bodies (Pesl et al., 2014). Therefore we opted for a direct approach to assess the EBs' cardiac syncytium mechanical properties in real time and under the alternating biophysical and biochemical conditions using atomic force microscopy (AFM).

AFM is a three-dimensional high resolution topographic technique. It is suitable for biological applications in native conditions (Vahabi et al., 2013) with the ability to measure bending of

the cantilever probe with extremely high precision (Sundararajan and Bhushan, 2002). It allows AFM to be used as a mechanical nanosensor (Wang et al., 2015), or as a micromechanical transducer for the construction of biosensors (Lavrik et al., 2004). Furthermore, modified AFM tip biosensor has been used in numerous studies, including the analysis of Alzheimer's disease process (Hane et al., 2014), as mechanical sensor in the study of cell penetration by nanoneedles (Obataya et al., 2005), in cell-based biosensing of drug effects (Wang et al., 2009) and in study of growth factor effects on epidermal cells (Zhang et al., 2014).

In this study, our previously developed uniformly sized EBs containing human induced pluripotent stem cell-derived cardiomyocytes (hiPSC-CMs) (Pesl et al., 2014) are integrated into the AFM force sensing platform to perform a high fidelity contraction pattern as a unique CBB for the measurement of absolute values of contractile forces together with frequency of the beat rate in complex conditions and cellular models. Development and optimization of the whole measurement setup is described with proposed application for characterization of cell clusters of cardiac cells and testing effects of model drugs.

## 2.2 Materials and methods

### 2.2.1 Preparation of hiPSC and hESC cardiomyocyte clusters

Measurements were performed using the hESC lines CCTL14 and CCTL12, characterized previously (Dvorak et al., 2005; International Stem Cell Initiative et al., 2007; Krutá et al., 2013). The hiPSC line cl1 was obtained from Dr. Majlinda Lako, Institute of Genetic Medicine, Newcastle University and the iPSC lines MDMD2Se were derived in our laboratory from human skin biopsies (Krutá et al. 2014). The hESCs and iPSC lines were propagated on mitotically inactivated mouse embryonic fibroblasts (Dvorak et al., 2005). Regular round shape of embryoid bodies was achieved by forced aggregation in silicone mold preformed microwells (1.5% agarose, VWR) (Dahlmann et al., 2013), their differentiation and maturation was achieved using our previously described method (Pesl et al., 2014). For statin samples, PSC were cultivated with pravastatin (20 mM, Sigma) for 4 days prior to EB formation.

### 2.2.2 Clusters seeding and measurement set-up

Beating EBs cultured for 28 days after initiation of differentiation were selected for round shape and adequate size and seeded onto adherent 30 mm Petri dishes (TPP Technoplastic Products, Trasadingen, Switzerland). The cultivation media was replaced by Tyrode solution (135 mM NaCl, 10 mM HEPES, 5.4 mM KCl, 0.9 mM $MgCl_2$, pH 7.4) and suplemented with 10 mM glucose and $CaCl_2$ (in desired concentration) and the EBs were maintained at 37 °C in a standard $CO_2$ incubator. Before experiment, a dish equipped with media exchange tubes was placed on the motorized stage of an inverted microscope (Olympus IX-81S1F-3, Tokyo, Japan) and the AFM recording head (BioAFM NanoWizard 3, JPK, Berlin, Germany) was finally placed on top of the sample. The AFM set-up was modified in order to provide real-time biomechanical characterization of CMs cell clusters (Fig. 3.1).

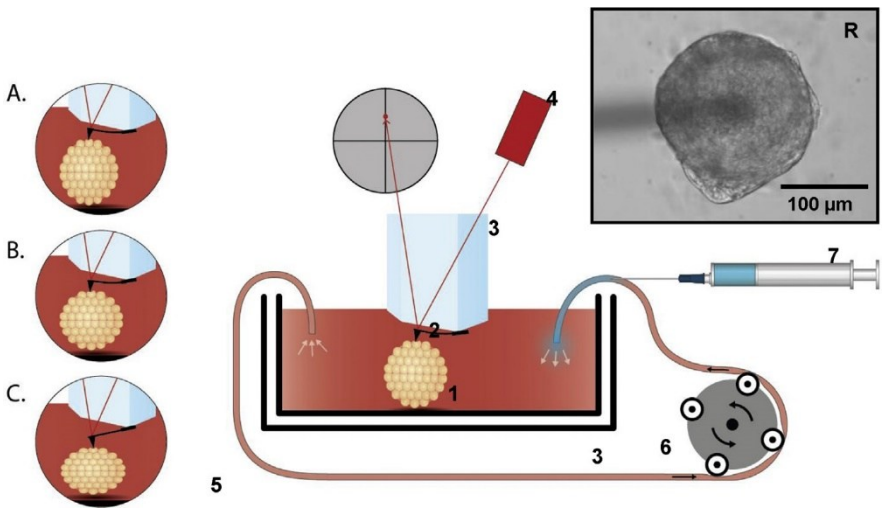



*Fig. 3.1. Scheme of the biosensor setup used for biomechanical characterization of cardiomyocyte clusters. Most important parts are schematically shown and are labeled as follows: 1 – Embryonic body (EB, cluster of living cells) in plastic Petri dish, (3 cm in diameter), 2 – AFM cantilever, equipped with a sharp tip, 3 – glass cantilever holder block, 4 – AFM laser source (a) (left) and photodetector of laser (b), position, 5 – plastic (PP) tubing, i.d. 0.2 mm (an arrow shows the flow direction), 6 – peristaltic pump, driving the flow direction and rate (rotation direction is shown by an arrow), 7 – medical syringe (total*

*volume of 1.0 ml) for drug injection, 8 – Petri dish heater (to keep constant temperature of 37 °C). The little insets on the left (A, B and C) show the subsequent stages of the EB contractile movement as this is measured by the AFM cantilever. Image (R) in the top-right corner shows real image of EB cluster with cantilever on its surface (captured by optical microscope). The size of the EB cluster is 175 µm.*

### 2.3 Recording of mechanocardiograms

The mechanocardiogram (MCG) curve shows the interaction force between the AFM tip and the surface of the beating cells cluster recorded in a real time. The force between the AFM probe and the studied surface was kept constant as defined by the set point (SP) value, carried out by the feedback loop. Intensity of feedback is given by integral and proportional gain parameters (IGain/PGain). The various AFM cantilever probes used are described in the supplementary material (SM) part 2.3.
https://www.sciencedirect.com/science/article/pii/S0956566316305036#s0095

In order to determine the effect of the set point value on the measured force (MCG curves), the cantilever (Hydra-6R, AppNano, Mountain View, CA, USA) was left to land onto the beating CM cell cluster stabilized for 15 min at 37 °C. The MCGs were recorded in 10 min intervals using SP set to 0, 1, 3, 6, 9, 12, 15 and 18 nN (whole measuring range of the biosensor setup given by stiffness and sensitivity), where the SP=0 value means operation in the so-called passive mode, i.e. it does not follow the cell movement (zero interaction force) and only the living beating cell cluster is leveling the cantilever, similar as in the literature (Liu et al., 2012).

The effect of temperature stability on MCG recording and behavior of CM clusters at different temperatures are provided in SM parts 2.4 and 2.5, respectively. The protocol for studying effect of different concentration of calcium is given in the SM as linked above.

**Surface homogeneity of the biomechanical properties**

EB is a spherical cluster (300µm in diameter) consisting of approximately 2000 cells; fluorescent images of EB are provided in Fig. S1. In order to map the homogeneity of the beating force on the surface of the CMs cluster, nine points of the surface of the cell cluster were screened (scheme included in Fig. 3). The uncoated silicon nitride cantilever Hydra-6R-200N (AppNano), characterized by spring constant of 0.025 N/m and sensitivity 10.1 nm/V was used. Motorized stage of the AFM microscope was used to move the AFM probe between the positions, when the Z-driving piezo was in the retracted state and the probe was 50 mm above the cell surface. When in place, AFM cantilever was landed onto the beating cell cluster of cardiomyocytes (EB), preheated and stabilized. The MCG curve was recorded for 10 min in each position with constant set point value of 6 nN. 5 min recordings of MCG curves were evaluated for the force and beat rate comparison.

**Evaluation of signal traces**

Time-series data saved from the Nanowizard AFM were preprocessed and analyzed by in-house developed algorithm using MATLAB 2015a (ver. 8.5, The MathWorks Inc., Natick, USA). After resampling (noise and dataset size reduction), the local maximum and its corresponding local minimum for each contraction were identified and processed to obtain the force of each individual contraction (R-S amplitude) and beat rate of EB. The MannWhitney's U-test was used to evaluate two group comparisons.

**Statistical evaluation of data**

Quantitative data are presented as the mean, the standard error of the mean from 3 to 6 experiments (indicated as N in the appropriate graph). The normality of data distribution was evaluated by the Shapiro-Wilk method thus proving the data normality at the 0.05 level. One way Student's t-test was used to test statistical difference of the measured data sets at the level 0.05 (maps of force on the cell cluster) when they were compared to the mean value. One way ANOVA method implementing the Bonferroni test was employed to compare statistical significance of measured signals (force/beat rate) at different concentrations of calcium, significance was compared either at different levels (po0.05, po0.01, po0.005) or was

calculated as value. Microcal Origin 7.0 software (Microcal, Northampton, MA, USA was used for statistical processing of the data.

## 2.4 Results and discussion

CMs cluster biosensor construction

The multicellular biosensor device was constructed by implementing the embryoid body inside the AFM measurement chamber as shown in Fig. 3.1. The major difference compared to previously reported approach (Liu et al., 2012) was the use of the embryoid body as multicellular syncytium rather than individual cardiomyocytes. EBs were characterized by immunofluorescence using anti α-actinin antibody and DAPI staining (Fig. 3.1SA), providing distribution of cardiomyocytes within the syncytium. After dissociating the beating EB into individual cells, the obtained DAPI/α-actinin and DAPI/cardiac troponin T fluorescence patterns (Fig. 3.1SB) were as expected for mature cardiomyocytes.

The use of the cluster of CMs seems to be a significant advantage regarding robustness of the resulting system. Typically, the CMs-based biosensing experiments were running successfully for up to 8 h. A fresh sterile medium was exchanged when needed, however, the experiments were otherwise carried out in nonsterile conditions inside the acoustic isolation chamber containing the microscopes. The AFM cantilever contacting surface of the cell cluster was kept fixed in the horizontal plane and the contraction force was monitored in real time by the vertical bending of the cantilever. Other parameters such as beating frequency and kinetics of the responses were precisely determined by the data post-processing.

The effect of various set point values on the AFM biosensor with the CMs-based EB was tested. The force and "heart" beat rate (BR) of the EB were recorded (Fig. 3.2A) while the set point value was gradually increased from 1 nN up to 18 nN (Fig. 3.2B). The BR values did not differ significantly within the tested range demonstrating robustness of the biosensor set-up and also suggesting that the force application does not lead to BR changes due to the activation of mechano-sensitive ion channels normally present in cardiomyocytes. Interestingly, the initial significant and steep increase in contraction force between the set point 0 and 5 nN was

observed. The explanation for the initial ramp below 5 nN is demonstrated by the curves of force measured with 3 different values of set point (0, 6 and 10 nN) shown in Fig. 3.2A.

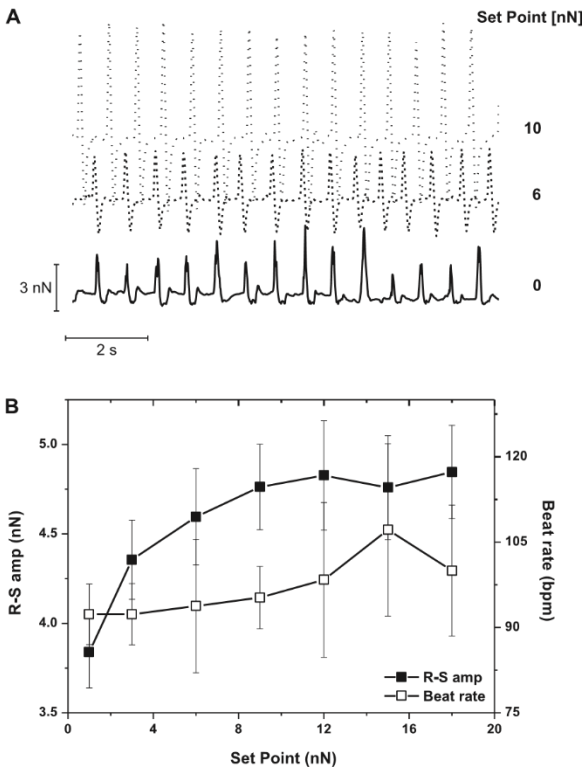



*Fig. 3.2. A Comparison of real time curves recorded during the passive (set point value 0 nN) and active mode, with two different values of set point. B Effect of set point value on force (r-S amp) and beat rate of EB. Average of median values is shown in the graph, error bars are equal to standard deviation of values, N=2.*

The curve measured with SP=0 nN (passive mode) is missing the feedback loop resulting from the EB relaxation rendering the data incomplete. Application of 6 nN of SP force to the cantilever resulted in recording complete dataset of force needed to compensate the EB cluster movement. Thus, the active mode was preferred to the passive one (Liu et al., 2012), possibly due to the limited mechanical integrity of dissociated CMs on the non elastic surface. Further increase in SP force to 10 nN led to subsequent insignificant increase in contraction force; however, based on the curve shape (Fig. 3.2(A), can be explained by mechanical stimulation of the cells in the cluster and activation of mechanosensitive ion channels (e.g. Lin et al., 2007)

rather than by inability to record full contraction with SP=6 nN as in case of the passive mode (0 nN).

Therefore, the optimal value of set point for experiments was set at 6 nN, this is also close to the average values of EBs contraction forces. Such set point force allows for the measurement of 95% of maximum contraction force (4.6 nN vs. 4.85 nN, when SP was 6 and 18 nN, respectively), with no effect on BR therefore minimizing the effect of the mechanical stimulation. On the other hand, further increase in SP force, stimulating the mechano-sensitive ion channels and/or adherent junctions present in the syncytium, enables the EB containing biosensor to be useful for modeling and/or drug screening in case of hypertension and stretch related hypertrophy (Yamazaki et al., 1998) or cardiac injury related tension changes between myocyte and fibroblast (Thompson et al., 2011).

**Biomechanical properties are homogenous on the EB surface**

The effect of localization of the AFM probe on the surface of the cell cluster was tested; the measuring position ideally should not significantly influence the resulting biomechanical parameters. Nine points homogenously located on the EB surface were chosen (Fig. 3) and the contraction force and BR were determined. Furthermore, to evaluate potential influence of the EB phenotype, these experiments were repeated for three different types of EBs including normal control EBs generated under hypoxic conditions (Hypoxia), disease model EBs with pathologically affected excitation-contraction coupling (CPVT) (Meli et al., 2011 and unpublished data), and EBs derived from the cells treated with statins (Jelinkova et al., unpublished). Consistent values of the contraction force and beating frequency were found by screening of a single EB across the nine detection points and even the EB-to-EB values covered quite *narrow interval (Fig. 3; the detailed statistical values are included as Table S1 in SM).* However, the contraction force variability on peripheral detection points implicates some positional effect and possibly the effect of biomagnetic fields produced by the EB's electric activity and stresses the importance to choose the detection point with highest response for further analysis. The highest reproducibility was observed for the normal (Hypoxia) EBs. The minor effect of the exact positioning of the microcantilever probe at biosurface seems to be the most important advantage of the cluster of (several hundredths) cells compared to experiments

carried out on individual cardiomyocytes. Single cells either separately adhering to the surface or as part of the two-dimensional layer are typically much more affected by the contacting cantilever, and if present, the sharp tip might damage the cell membrane. In the case of cell cluster, damage of few surface-located cells contacting the probe is not very significant. From the practical point of view, this is quite significant advantage of the cluster of cells serving as the biorecognition element.

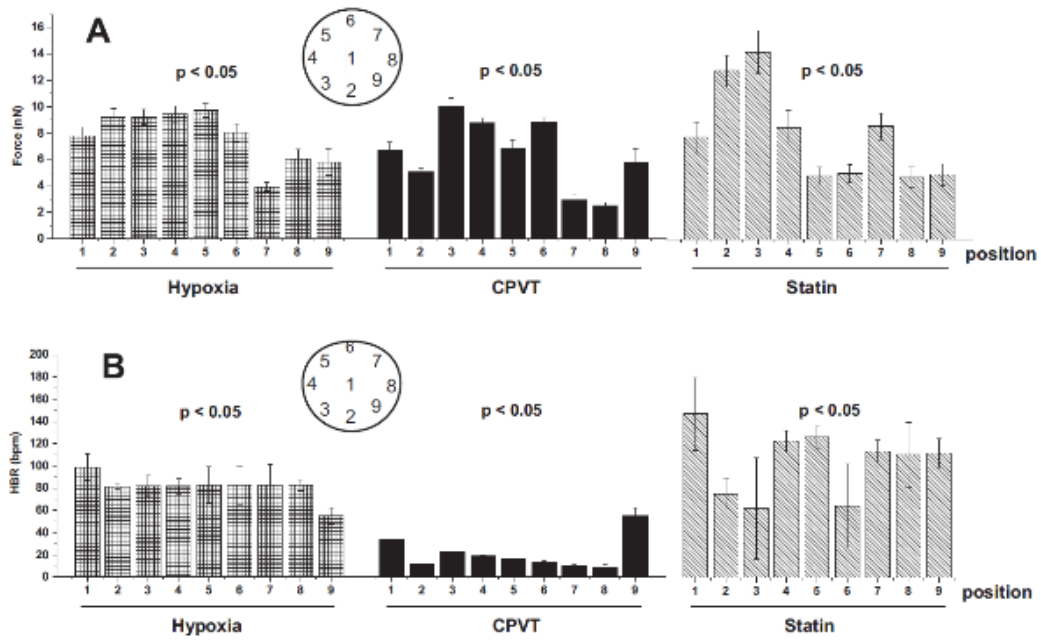



*Fig. 3.3. Mapping of the force on the surface of the EB cluster. Average of median values of beating force (A) and beat rate (B) recorded in different positions on cell cluster surface are presented in the graphs as data sets (groups) of values measured for every cell cluster. Map of positions on EB surface is shown in the upper part of both graphs., error bars are equal to standard deviation of values, The data normality was confirmed by Shapiro Wilk test at 0.05 level. All the data sets were found not to be significantly different from the mean value at the same level (0.05), as indicated in the graph.*

**Effect of temperature on the cardiomyocytes-based biosensor**

Temperature affects the beat rate as well as arrhythmogenic cardiomyocyte potential (Chen et al., 2003). Furthermore, temperature affects also stability of the cantilever and its coupling with EB in the biosensor set-up. Contrary to the desired effect of temperature on the cardiomyocyte function (biorecognition process), its effect on the stability of the transducer system should be

eliminated by choosing suitable components and optimal conditions. To characterize the effect of cantilever type and its temperature instability independent of the EB activity, live but non beating EB coupled with variety of AFM probes were evaluated between 30 and 37 °C; details are discussed in SM and shown in Fig. S2. The instability usually results from the bimetallic effect combined with adsorption events on the hydrophobic surface of the coating metal layer (Samori, 2009). Thus, the uncoated silicon nitride cantilever (HYDRA-6R, pyramidal tip) provided most stable force reading and higher reflection of laser beam comparing to the tip-less version (HYDRA TL). Gold-coated SNL-10 probe exhibited the highest variability in the force signal, suggesting limited usefulness of metal coated probes. The cantilever equipped with colloid nanosphere (bio650) provided reasonable temperature stability but high signal noise, probably due to hydration of the colloidal probe, again limiting its use for mechanical transduction. Generally, the work in liquids of elevated temperatures (e.g. physiological) causes instability of the AFM laser signal reflected to the detector (Amano and Takahashi, 2013). Here, the use of non-coated probes eliminated most complications and allowed stable measurements over long time periods. At the cellular level, temperature modulates contraction force and BR of CMs clusters; this effect can serve as an example of physiological conditions affecting heart function, conveniently studied using the developed EB-based biosensor. Data were collected for the contraction force (median of the r-S amplitude) and BR in the range from 26 to 37 °C (Fig. S3).

The temperature dependence showed slightly increasing values of the relative force with rising temperature, with plateau at 34 and 35 °C (88% of maximal force) and absolute maxima (quite fluctuating beating force) at the maximal temperature point. This indicates that the beating EBs are highly sensitive to temperature variation, suggesting that the constant temperature is a major factor for reliable use of the biosensor as well as it provides a great tool for arrhythmogenic drug effect detection under non standard temperature, resembling hypothermia or fever, in agreement with previously described temperature dependency in murine neonatal ventricle slices and hESC co-culture models (Pillekamp et al., 2007).

**Effect of extracellular calcium level on contraction force and beat rate**

Calcium is a principal mediator of the cardiac excitation-contraction coupling initiating the contraction. We then explored the effect of increased extracellular calcium concentration on EB using this biosensor set-up. The cardiac physiological concentration of $Ca^{2}$þ range from 0.1 to 5 mM (Meli et al., 2011) while 1.8 mM is common for patch clamp and other cardiomyocyte in vitro studies (Bébarová, 2012). Real time force traces (Fig. 3.4A) recorded with 0.2, 1.0, 1.8, 3.6 and 5.4 mM extracellular $Ca^{2}$þ present not only ability of the biosensor to determine the absolute contraction force (Fig. 3B) and BR (Fig. 3.3C) data, but also to detect and quantify irregular contractions and arrhythmias evident from traces in Fig. 3.4A. Such application of the biosensor enables both to detect and characterize the arrhythmias on the cellular level as well as to determine the arrhythmogenic effect of tested drugs or conditions.

Data obtained by evaluation of these curves were relativized as the absolute value for every EB sample is slightly different and therefore difficult for absolute comparison. The contraction force increased with the $Ca^{2}$þ concentration (Fig. 4B), in agreement with well-known fact that the force of contraction is proportional to the calcium uptake in atrial and ventricular cardiomyocytes (Winegrad, 1961, Hellam and Podolsky, 1969; Katz and Lorell, 2000).

Simultaneously, BR decreased with increasing concentration of extracellular calcium (Fig. 4C). This also corresponds to the previously published non reciprocal relationship between force and BR (Burridge et al., 2014; Liu et al., 2012). Interestingly, the BR data presented higher variability for low (0.2 mM) as well as high (3.6 mM) levels of calcium, confirming dependence of coupling of excitation and contraction on calcium (Winegrad, 1961). Winegrad presented periodical drops in BR at 2.5 and 3.75 mM $Ca^{2}$þ, almost perfectly matching our data showing uncoupling at 3.6 mM calcium (Fig. 3.4C). This demonstrates that the EB based biosensor can be used to study both the excitation-contraction coupling as well as to screen drugs targeted for such effects. Moreover, arrhythmogenic effect of higher calcium concentrations (3.6 and 5.4 mM) can be observed in CMG curves (Fig. 3.4A).

**Beta-adrenergic receptors' stimulation/inhibition followed by the biosensor**

The cardiomyocytes-based biosensor is not presented as purely analytical tool for measuring concentrations; its principal task is quantification of biochemical activity of the tested drugs affecting biomechanics of the cardiac syncytium. To demonstrate such application, baseline signal for different EBs was initially standardized in Tyrode buffer; afterwards, the tested compound was injected to the working chamber; the experiments included the beta-adrenergic receptor antagonist metoprolol (Beta, final concentration 70 mM), the beta-adrenergic agonist isoproterenol (1 mM) and the calcium discharger caffeine (1 mM) triggering arrhythmia (Fig. 5).

The basal physiological values of the contractile movement were characterized by R-S amplitude corresponding to force of 22.0 nN and beat rate of 67.4 per minute (bpm). In agreement with published data on beta adrenergic antagonizing activity of metoprolol (Blinova et al., 2014), its addition decreased the average force down to 18.8 nN accompanied by reduction of beat rate to 53.7 bpm. On the other hand, isoproterenol (Pillekamp et al., 2012), in agreement with published data on its adrenergic stimulatory activity, induced an increase of the beat force value to 23.4 nN and beat rate to 78.8 bpm (Fig. 3.5).

Finally, the addition of caffeine well illustrates the ability of the biosensor to visualize very fast processes like arrhythmias. From the mathematical point of view, it is difficult to describe the arrhythmic, so called stop-and-go effect. The beating force was rather constant during the active intervals. However, the average frequency provides rather low value (58.9 bpm), it is very high (85.0 bpm) during the active period. The high deviation value stems from the irregular biological movement and not from low measurement reproducibility.

The presented data on beta adrenergic stimulation and inhibition demonstrated that the β-adrenergic signaling was mature in both hESC- and hiPSC-CMs syncytium, rendering the biosensor useful for both studying the mechanism of beta adrenergic stimulation and beta adrenergic modulatory drug screening as well as dissecting the mechanism of induced arrhythmias.

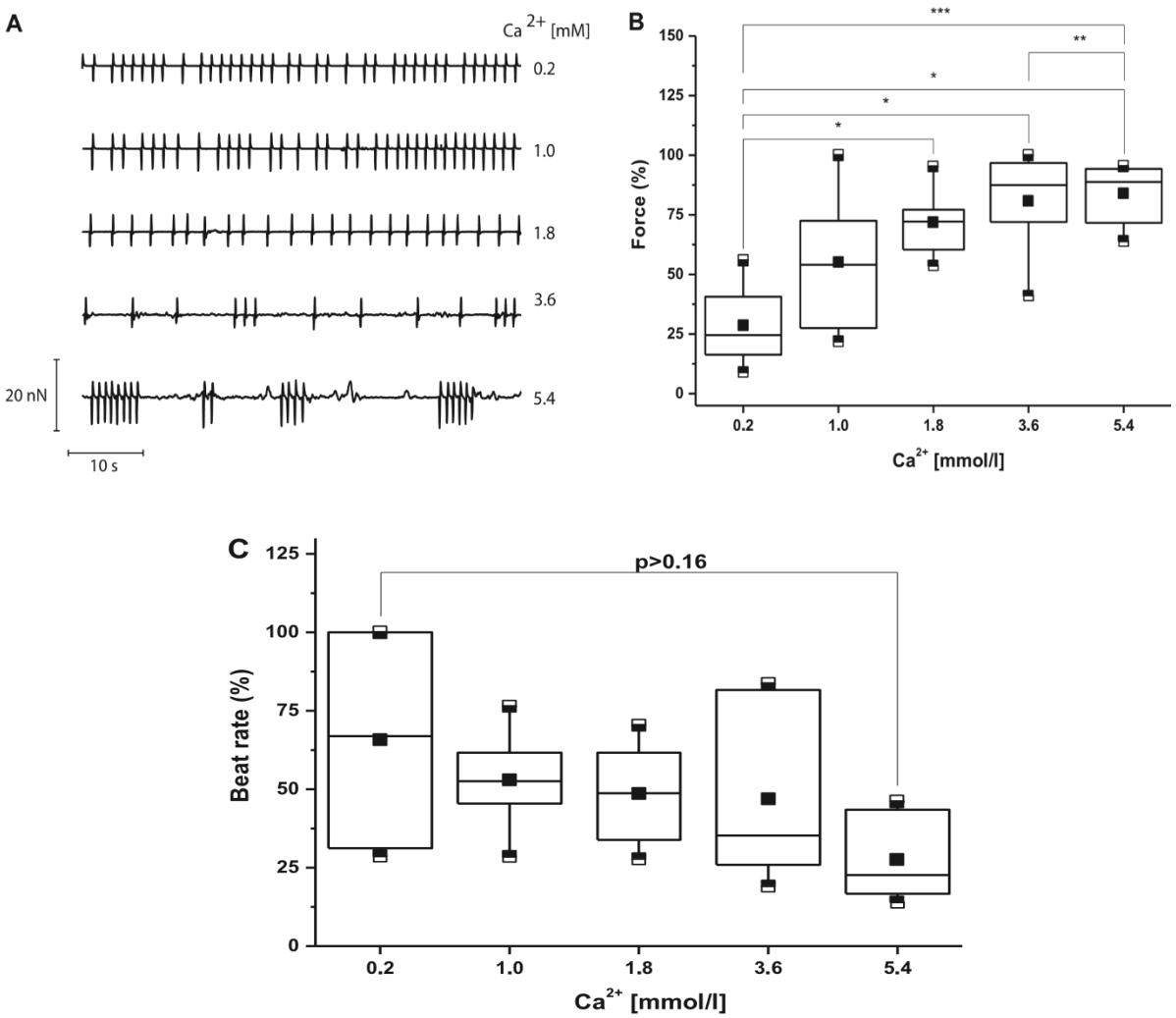



*Fig. 3.4. Effect of calcium concentration on the beating force (r-S amp) and beating rate (BR) characterized by AFM microscope. Real time curves recorded in the presence of calcium concentrations indicated in the graph A. Corresponding dependencies of force (B) and beat rate (C) on the concentration of calcium. The main bars of data show middle quartile of measured data with line as median and quartiles represented by whiskers (graphs B and C). The main bars show middle quartile of the measured data which were compared using the Bonferroni test for their signal as median and quartiles represented by whiskers (graphs B and*

*C), N at different levels. Statistical significance * p < 0.05, tested by the ANOVA one way method, when the means<.01,and * p <0.005, the level of significance is indicated numerically in the graph C*

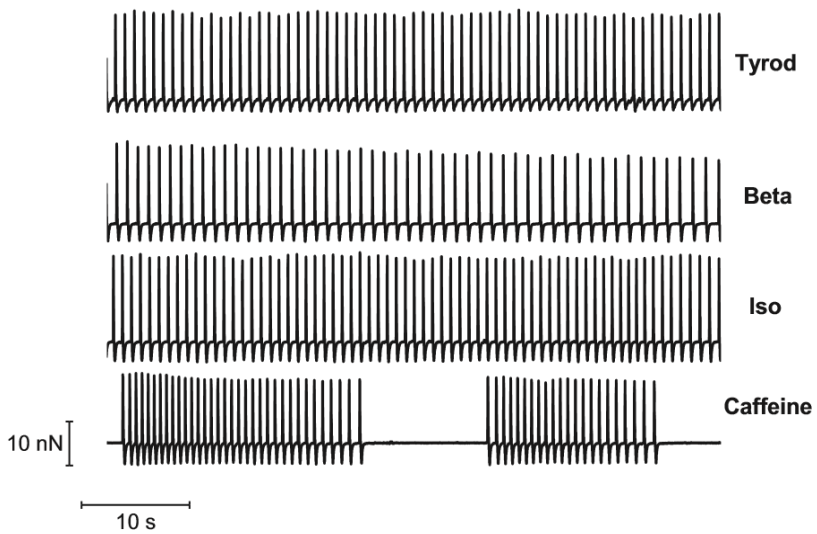



*Fig. 3.5. Real traces of force of the beating EB measured by the AFM microscope as a response to the presence of various drugs in the measuring chamber, as indicated close to the curves.*

## 2.5 Conclusions

The cardiomyocytes-based embryoid body as a biorecognition element was coupled to the microcantilever probe from atomic force microscope providing micromechanical cellular biosensor. Beating force and rate of the EB contractions was transduced by AFM cantilever thus providing a robust biosensor platform suitable for whole-day testing. The cellular biosensor was optimized regarding the type of cantilever, thermostatic parameters, exchange of media and addition of tested compounds. The resulting reliable biosystem in combination with standardized protocol allowed for complex testing of compounds and conditions affecting the biomechanical properties of the embryoid body. The studied effector molecules included calcium ions, drugs as beta-blocker metoprolol and stimulant isoproterenol, arrhythmic effects were initiated by caffeine. Furthermore, when embryoid bodies containing cardiomyocytes derived from patient's own cells via reprogrammed pluripotent stem cells are employed, the resulting biosensor can be conveniently used as the in vitro model for detailed

biomechanical characterization of heart diseases such as dystrophies, including screening of novel drugs in near physiological conditions.

## 2.6 Acknowledgments

We wish to thank Martina Vodinská and Miroslava Nehybová for their technical support, Guido Caluori from University of Genoa for reading the manuscript. We also thank Majlinda Lako from NewcastleUniversity for the cl1iPSCs line, The work has been supported by CEITEC - Central European Institute of Technology

(CZ.1.05/1.1.00/02.0068 and LQ1601), FNUSA-ICRC (CZ.1.05/1.1.00/ 02.0123 and LQ1605) from the European Regional Development Fund and the National Program of Sustainability II., Grant Agency of the Czech Republic (P302/12/G157 and GA13-19910S). This work has also been supported by SoMoPro – Marie Curie Actions – South Moravian Region and by the European Society of Cardiology (ESC) (R12042FF).

## 2.7 Appendix A. Supporting information

Supplementary data associated with this article can be found in the online version at http://dx.doi.org/10.1016/j.bios.2016.05.073.

# 4 Improvements in biosensing by addition of electrophysiological recordings (p2a)

## 4.1 Commentary

While observing the beating of CMs is relatively straightforward (e.g., via video microscopy, (Laurila et al., 2015), understanding the associated beating force is often crucial in pathologies like dystrophinopathies and cardiomyopathies (Vatta et al., 2005). Alterations in beating force are linked to pathophysiological electro-mechanical coupling, often leading to mechanical heart failure (Pesl et al., 2016a). Prior studies on dilated cardiomyopathy employed biomechanical measurements using the stretcher device (Knoll et al., 2002), while more detailed investigations utilized cantilevers and AFM for real-time evaluation with individual CMs (Liu et al., 2012a, 2012b). Hence, combining AFM for biomechanical changes with MEA sensing electric signals holds promise for elucidating complex events in CMs derived from patient-specific stem cells, demonstrating the capabilities of the organ-on-a-chip system in disease-related CMs. hPSC-derived CMs recapitulate the morphological, genetic, and functional characteristics of the heart muscle, including cardiac excitation-contraction coupling (cECC), responsible for the heart's pumping function (Bers, 2002). While hPSC-CMs can be derived as 2D or 3D cultures, the latter appear more physiologically relevant (Regmi and Jeong, 2016). Various differentiation protocols exist, involving modulation of signaling pathways like the Wnt/β-catenin pathway for monolayer cultures and spontaneous differentiation for 3D cultures (Pesl et al., 2014). Physical methods such as electro-mechanical stimulation can enhance differentiation and maturation efficiency (Bauwens et al., 2016). Purified hPSC-CMs offer potential in drug development, cardiotoxicity assays, disease modeling, and regenerative therapies (Doppler et al., 2013), although achieving cardiac maturation remains a focus of ongoing research.

Characterization of hPSC-derived cardiac models involves functional assays, among which atomic force microscopy (AFM) has played a significant role in evaluating sample mechanics and topography in native culture environments (Alonso and Goldmann, 2003; Kilpatrick et al., 2015). Integration of AFM with 3D cardiac models has been proposed as a cell-based biosensor (CBB) in previous studies (Pesl et al., 2016a). Most AFM systems now integrate with optical and confocal microscopy, enabling combined measures of AFM and calcium

imaging (Liu et al., 2012b; Caluori et al., 2018), described later, nevertheless microelectrode arrays (MEA) offer a complementary approach, allowing multiprobe extracellular field potential (EFP) measurements of electroactive cells (Spira and Hai, 2013). Here, we present an electromechanical in vitro system for the combined study of cECC on 3D cardiac models, employing both AFM and MEA platforms.

The study utilized 3D BCCs differentiated from hESC and patient-derived hiPSC carrying a DMD mutation. These cardiac models were plated onto 60-channel MEA chips coated with a laminin and fibronectin mixture to promote stable cell adhesion. Once stabilized, the clusters were simultaneously probed using a soft silicon nitride cantilever from an AFM, which was calibrated using the thermal noise method and maintained at a constant contact force of 5 nN. The system enabled the synchronous recording of extracellular field potentials (EFP) and mechanocardiograms (MCG) at a 5 kHz sampling frequency through a custom LabVIEW interface. The resulting data were post-processed using MATLAB algorithms to quantify specific functional parameters, including the beating rate, contractile force, and the electro-mechanical delay (EMD).

The implemented electromechanical system demonstrated high stability and resilience, supporting continuous recordings of cardiac activity for 4 to 5 hours without inducing adverse effects or contaminating the biological samples. While basal functional parameters—such as beating frequency and contractile force—were not significantly different across the healthy and diseased cell lines, differential drug trials revealed distinct phenotypic signatures. Notably, this paper provided the first distinctive measurement of the beating-force relationship in a 3D DMD cardiac model, identifying a significant, dose-dependent increase in the EMD (up to 257% of basal delay) when exposed to increasing calcium concentrations. Pharmacological trials with isoproterenol and verapamil further validated the biosensor's sensitivity, as the DMD-derived cells showed unique ionotropic and chronotropic responses that served as critical discriminants between the healthy and pathological models. Ultimately, the system proved effective for high-resolution disease modeling and drug testing in an "organ-on-a-chip" format.

Biosensors and Bioelectronics 124–125 (2019) 129–135

Contents lists available at ScienceDirect

Biosensors and Bioelectronics

journal homepage: www.elsevier.com/locate/bios

# Non-invasive electromechanical cell-based biosensors for improved investigation of 3D cardiac models

Guido Caluori[a,b,c], Jan Pribyl[a], Martin Pesl[b,d,e], Sarka Jelinkova[d], Vladimir Rotrekl[d], Petr Skladal[a,*], Roberto Raiteri[c,*]

[a] Central European Institute of Technology, Masaryk University, Kamenice 5, 62500 Brno, Czech Republic
[b] International Clinical Research Centre of Saint Anne Hospital Brno, Pekarska 53, 60200 Brno, Czech Republic
[c] Department of Informatics, Bioengineering Robotics and Systems Engineering, University of Genova, Via All'Opera Pia, 13, 16145 Genova, Italy
[d] Department of Biology, Faculty of Medicine, Masaryk University, Kamenice 5, 62500 Brno, Czech Republic
[e] 1st Department of Cardiovascular Diseases, St. Anne's University Hospital and Masaryk University, Pekarska 53, Brno, Czech Republic

ARTICLE INFO

*Keywords:*
Excitation-contraction coupling
Human pluripotent stem cells
Cardiomyocytes
Atomic force microscopy
Microelectrode array
Drug testing

ABSTRACT

Cardiomyocytes (CM) placed on microelectrode array (MEA) were simultaneously probed with cantilever from atomic force microscope (AFM) system. This electric / nanomechanical combination in real time recorded beating force of the CMs cluster and the triggering electric events. Such "organ-on-a-chip" represents a tool for drug development and disease modeling. The human pluripotent stem cells included the WT embryonic line CCTL14 and the induced dystrophin deficient line reprogrammed from fibroblasts of a patient affected by Duchenne Muscular Dystrophy (DMD, complete loss of dystrophin expression). Both were differentiated to CMs and employed with the AFM/MEA platform for diseased CMs' drug response testing and DMD characterization. The dependence of cardiac parameters on extracellular $Ca^{2+}$ was studied. The differential evaluation explained the observed effects despite variability of biological samples. The β-adrenergic stimulation (isoproterenol) and antagonist trials (verapamil) addressed ionotropic and chronotropic cell line-dependent features. For the first time, a distinctive beating-force relation for DMD CMs was measured on the 3D cardiac in vitro model.

Supplementary material related to this article can be found online at doi:10.1016/j.bios.2018.10.021.

## 4.2 Introduction

In the field of cell-based biosensors, CMs are often used as models to study heart related diseases. The monitoring of electric activities of CMs is typically chosen; (multi)electrode transducers seem well established and widely available as MEA (Rothermel et al., 2005). The beating of CMs can be followed relatively easily (e.g. by video microscopy, Laurila et al., 2015), though in many situations the missing information on the associated beating force is of paramount importance in heart remodeling pathologies, such as dystrophinopathies and cardiomyopathies (Vatta et al., 2005). Beating force is associated with pathophysiological electro-mechanical coupling, and its alterations result often in mechanical heart failure (Pesl et al., 2016a). Such biomechanical measurements investigating the dilated cardiomyopathy were previously done on CMs using the stretcher device (Knoll et al., 2002). More detailed investigations were later done using cantilevers as nanomechanical transducers and atomic force microscope (AFM) as the evaluation system in real time with individual cardiomyocyte cells (Liu et al., 2012a,2012b) or cell clusters (Pesl et al., 2016a). Thus, combination of AFM for biomechanical changes with MEA sensing electric signals described here seems naturally promising for elucidating complex events in cardiomyocytes obtained from patient derived stem cells. This approach provides a robust and convenient example of the organ-on-a chip system demonstrating its capabilities on disease related CMs.

The introduction of human pluripotent stem cells (hPSC, either embryonic, hESC, or induced pluripotent, hiPSC) and cardiac differentiation protocols allowed almost two decades of study on the cardiac organogenesis and functionality. In particular, patient-specific hiPSC representing a direct supply of healthy and mutation-carrying samples (Sinnecker et al., 2014) allow for description of the disease progression involved in heart failure (Moretti et al., 2013). To improve the comparison between in vitro models, CRISPR-Cas9 technology has recently gained an outstanding popularity for its efficiency and flexibility in inducing precise mutations in cell lines, providing researchers with isogenic controls (Motta et al., 2017). hPSC-derived cardiomyocytes and models recapitulate the morphological, genetic and functional characteristics of the heart muscle, specifically the subcellular cascade known as cardiac excitation-contraction coupling (cECC), responsible for heart pumping function (Bers, 2002). Cardiomyocytes from hPSC can be derived as 2D or 3D stem cell cultures. However, the 3D

models seem to be superior and more physiologically relevant compared to the 2D ones (Regmi and Jeong, 2016). For monolayer culture, the multiple existing protocols with high differentiation efficiency involve modulation of the canonical Wnt/β-catenin pathway (Lian et al., 2012; Burridge et al., 2014), with high differentiation efficiency. For 3D cultures, the protocols exploit the spontaneous differentiation triggered from the aggregation of hPSC into embryoid bodies, which is driven to cardiac phenotypes using hypoxia and small molecules cocktails (Pesl et al., 2014). The efficiency of differentiation and grade of maturation can vary according to protocol and cell lines, and can be improved by physical methods, as in electro-mechanical stimulation (Bauwens et al., 2016). Purified hPSC-CMs can be further reassembled in precise geometries, such as in the engineered heart tissue (Tzatzalos et al., 2016). From gene expression to functionality, hPSC-CMs present an embryonic-like cardiac phenotype, with immature sarcomeres, sarcoplasmic reticulum and calcium cycling (Mummery et al., 2012; Acimovic et al., 2014). An immature phenotype has also been proven for hESC embryoid body-derived cardiac models (Doevendans et al., 2000). Nevertheless, hPSC-CMs play a key role in future drug development with reduced attrition rate (Liang et al., 2013; Zheng et al., 2013), in cardiotoxicity assays (Takeda et al., 2018), disease modeling (Dell'Era et al., 2015) and in cell-based regenerative therapies (Doppler et al., 2013), and further studies to achieve cardiac maturation are ongoing. This aspect is also investigated by our proposed approach, to assess its robustness.

The hPSC-derived cardiac models can be characterized by functional (or phenotypic) properties though multiple in vitro assays, reviewed in another work from our group (Pesl et al., 2016b). Among these, atomic force microscopy has in the past three decades achieved remarkable role in the evaluation of biological samples mechanics and topography (Alonso and Goldmann, 2003; Kilpatrick et al., 2015) in native culture environment. In particular, it has been employed in important studies on single CMs (Liu et al., 2012a). A combination of AFM and 3D cardiac models has already been proposed as cell-based biosensor (CBB) in our previous work (Pesl et al., 2016a). Most AFM systems are now currently integrated with optical and confocal microscopy, which allows the implementation of combined measures of AFM and calcium imaging (Liu et al., 2012b; Caluori et al., 2018), but further systems can be included if properly miniaturized. Small biosensors, such as microelectrode arrays (MEA), can be engineered to comply with AFM and optical microscopy systems for cardiac investigation

(Cogollo et al., 2011). The attractiveness of MEA-based electrophysiology resides in its ability to multiprobe extracellular field potentials (EFP) of electroactive cells in a non-destructive fashion, which allows for prolonged and complex measurements of cells and tissues (Spira and Hai, 2013).

In this work, we present an electromechanical in vitro system for the combined study of cECC on 3D cardiac models, employing both AFM and MEA platforms together. The aim of this work is to provide an improved method for cardiac model characterization and drug testing in the format of an organ (heart)-on-a-chip. For this reason, we have confronted a model of cardiac maturation with respect to its control, and employed a disease model of Duchenne muscular dystrophy (DMD), a progressively invalidating pathology of the striated muscle, including the myocardium (Finsterer and Stöllberger, 2003).

## 4.3 Materials and methods

### 4.3.1 hPSC culture and cardiac differentiation

The cardiac cells clusters were obtained using the hESC line CCTL14 (Adewumi et al., 2007) and one hiPSC line reprogrammed from fibroblasts of a patient affected by Duchenne Muscular Dystrophy (DMD). The patient carries a deletion of exons 45–50 of the DMD gene causing a complete loss of dystrophin expression. The line has been fully characterized for pluripotency markers (https://hpscreg.eu/cellline/MUNIi001-A) and the differentiated CMs were tested for presence of striated pattern of sarcomeres labeled with cardiac troponin T (sc8121, Santa Cruz), and cytoplasmic presence of dystrophin (NCL-DYSB, Leica) (see Supplementary material, SFig. 1). Pluripotent cells were firstly thawed and seeded on mitotically-inactivated mouse embryonic fibroblasts (feeder cells). The hPSC colonies were cultivated in DMEMF12 (Thermofisher, Waltham, MA, USA) supplemented with 15% KnockOut fetal bovine serum Serum Replacement (FBS, Life Technologies, Carlsbad, CA, USA), 1% L-glutamine (Thermofisher), 0.5% penicillin/streptomycin (Thermofisher), 1% 2-mercaptoethanol (Thermofisher), 1% non-essential amino acids (Life Technologies), and 4 ng $ml^{-1}$ and 10 ng $ml^{-1}$ human fibroblast growth factor 2 (hFGF2, Peptrotech, London, UK) for hESC and hiPSC, respectively. Medium was changed daily and colonies were propagated for at least 5 passages, by manual fractioning. hESC cells were divided in a control group (CTRL) and another group

(DORSO) undergoing an exposure to 500 nM of dorsomorphin (Sigma Aldrich, St. Louis, MO, USA) 4 days to the differentiation protocol, to improve cardiac commitment (Hao et al., 2008).

Cardiac differentiation was started by embryoid body formation, as described elsewhere (Pesl et al., 2014). Briefly, compact, round colonies were manually cut and scratched from the culture surface. For DMD iPSC, the colonies were kept intact, carefully detached from the culturing surface as a whole. The cell leaflets were transferred in hypoxic incubation atmosphere (5% $O_2$) and underwent a sequential cytokine modulation in KnockOut DMEM (Life Technologies), supplemented with 10% FBS, 1% L-glutamine, 1% PS, 1% 2-mercapthoethanol, 1% non-essential amino acids (further referred simply as culture medium). Beating cardiac clusters (BCC, Supplementary Fig. 1) were visible from day 14 and were transferred into normoxic atmosphere. After day 22, they were kept in the culture medium with 10 µg $ml^{-1}$ ascorbic acid (Sigma Aldrich).

### 4.3.2 Microelectrode arrays cleaning and coating

Before beating CMs cluster plating, 60 channel MEAs (60MEA200/ 30iR-Ti/ITO, Multichannel Systems, Reutlingen, Germany) were cleaned using a 0.1% w/v solution of Tergazyme detergent (Alconox, White Plains, NY, US) in MilliQ water for at least 8 h. The culture well (i.e. the area inside the plastic ring) was then thoroughly washed with MilliQ water to remove the excess detergent. The preparation of the device was moved to a UV-sterilized clean box (Biosan, Riga, Latvia). Each MEA was placed in 100 mm sterile Petri dish (TPP, Trasadingen, Switzerland), and the MEA culture well was sterilized by filling it with 70% ethanol solution. After 30 min, the sterilizing solution was removed, the culture well on MEA was rinsed twice with 0.2 µm-filtered MilliQ water and let dry. The sensing area (i.e. the electrode array area) was then coated with 20–50 µl of 0.1 mg $ml^{-1}$ laminin (Sigma Aldrich) and fibronectin (Sigma Aldrich) mixture, 1:1 ratio, to promote cell adhesion. The MEAs were put in a cell incubator at 37 °C, 5% $CO_2$, overnight. The next day, MEAs were rinsed twice with filtered MilliQ water to remove excess of adhesion factor from the surface.

### 4.3.3 BCCs plating on MEA chips

Suspended BCCs were collected and plated on MEA sensing area with 30 µl droplet of the culture medium. This amount of medium was a safe tradeoff between sample wobbling

limitation and the need of hydrated environment. Samples were manually placed on top of electrode array, then put in standard cell incubator and kept in this overnight (with loosely fitted lid and additional droplets were placed separately around the well to prevent evaporation). The following day, medium was gently added atop up to 1 ml. The BCCs were allowed to stabilize up to 3 days in vitro to ensure appropriate adhesion, spreading and formation of cell-electrode contacts. Fig. 4.1A and Supplementary Fig. 3 show typical BCCs properly placed on MEA, before beginning the experiments. Supplementary video recording presents movements of the adhered BCC clearly demonstrating the regular beating events.

.

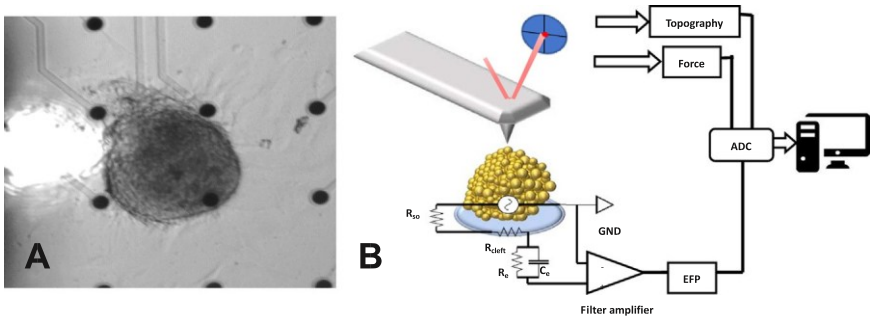



*Fig. 4.1. Real case and schematic of the proposed electromechanical cell-based system. A) A beating cardiac cluster (BCC) placed on a microelectrode array (MEA) sensing area. The bright spot on the left side represents the AFM laser reflecting from the cantilever. Scale bar is 200 µm. B) Schematic representation of the implemented setup. The BCC acts as a periodic micro-voltage generator sensed by the planar electrode, while the AFM measures the topographical displacement and the exerted force. The synchronous acquisition is guaranteed by the common acquisition board and computer*

### 4.3.4 Setup preparation and experimental protocols

The MEA chip containing the samples was housed in a customized holder made of an aluminum plate with adhesive heating pads and Pt100 temperature probe (RS Components, Corby, UK), and an electronic board with contacts to interface with the MEA electrodes. The electronic board was equipped with 60-channels unity-gain amplifiers to provide low impedance tracks and noise shielding. A second filtering-amplifying stage provides a pass-band of 10–3000 Hz and a total gain of 60 dB. The described holder was then fixed on the motorized stage of an inverted microscope (Olympus IX-81S1F-3, Tokyo, Japan). An AFM

scanner head with 15 µm vertical range (BioAFM NanoWizard 3, JPK, Berlin, Germany) was placed above the sample. A soft silicon nitride cantilever SNL-10-D (Bruker, Billerica, MA, USA; nominal spring constant 30 pN $m^{-1}$) was used as nanomechanical probe to ensure stable contact without applying disruptive forces on the sample. The cantilever spring constant was calibrated before each experiment using the thermal noise method (Butt and Jaschke, 1995). A contact force of 5 nN was found optimal compromise between baseline stability and absence of visible adverse effects on the sample, as previously showed (Pesl et al., 2016a). Each experiment was performed in Tyrode solution (135 mM NaCl, 10 mM HEPES, 5.4 mM KCl, 0.9 mM $MgCl_2$, pH 7.4) supplemented with 10 mM glucose and 1.8 mM $CaCl_2$. After solution exchange, the calibrated cantilever was immersed in liquid and put in contact with the sample several times to identify the superficial center of contraction (i.e. the point with highest vertical positive displacement). Once the center of contraction was found, the drug trials started at an interval of 5 min of recording and 10 min settling time after drug administration or washout (a schematic is provided in Supplementary Fig. 4).

Calcium chloride solution was obtained in Tyrode buffer to give a stepwise increment of 1.1 mM after each addition. Isoproterenol stock solution (30 µM) was made in sterilized MilliQ water to prevent it from quenching: the selected step increment was 300 nM. Finally, Verapamil hydrochloride (Lekoptin, Lek Pharmaceuticals, Ljubljana, Slovenia) stock solutions (127.5 µM) were made in Tyrode, for a step increment of 255 nM. The added volume of drug solution never exceeded 5% of the basal volume in the MEA chip (2 ml).

| Parameter name | Description |
|---|---|
| Beating rate | Reciprocal of time distance between two adjacent events |
| Electro mechanical delay | Time between the electrical event and 10% of the next contraction maximum amplitude |
| Contraction time | Time between 10% of the peak amplitude and the peak, on the rising side |
| Relaxation time | Time between the event peak and the point corresponding to 10% of the peak amplitude on the falling side |
| Duration time | The sum of contraction and relaxation times |
| Average speed of contraction | Mean of the first derivative of the rising part of contraction |
| Time constant | Time parameter obtained by fitting the relaxation time interval with a decreasing exponential function |
| Force | The uncompensated force peak-to-peak during the contraction |
| Z height | The peak excursus of the AFM Z-piezo following the contraction |

*Table 4.1 Description of extracted parameters.*

### 4.3.5 Data recording and evaluation

All the presented protocols were repeated on 3 biological replicates of each cell line. Electromechanical recordings were acquired at 5 kHz sampling frequency through a LabVIEW virtual instrument and a proprietary data acquisition board PCI6071E (National Instruments, Austin, TX, USA). Fig. 4.1B shows a schematic of the acquisition system. Cell mechanocardiogram (MCG) comprehends the time-dependent topographical changes (i.e. the vertical displacement of the AFM piezo actuator, in µm) and the uncompensated force (in nN). The cell-cantilever contact was never lost during drug injections or medium washout. The obtained data were post-processed and analyzed using a Matlab R2016b (Natwick, MA, USA)

GUI, using state of the art algorithms. From each recording, the parameters listed in Table 4.1 and defined in Supplementary Fig. 5 were determined. Statistical analysis was performed in Prism 5.0 (GraphPad Software, La Jolla, CA, USA) and numerical results are presented as mean ± SEM, after passing normality test. Datasets were compared for statistical significance using 1-way analysis of variance (ANOVA) with Bonferroni post-test, or repeated measures 2-way ANOVA with matching on drug concentration levels. Statistical significance was accepted with p-values below 0.05.

## 4.4 Results and discussion

### 4.4.1 Simultaneous electromechanical recording

The implemented setup allowed the simultaneous visualization, synchronous recording and coupled analysis of the electromechanical features of the cECC (Fig. 4.2A).

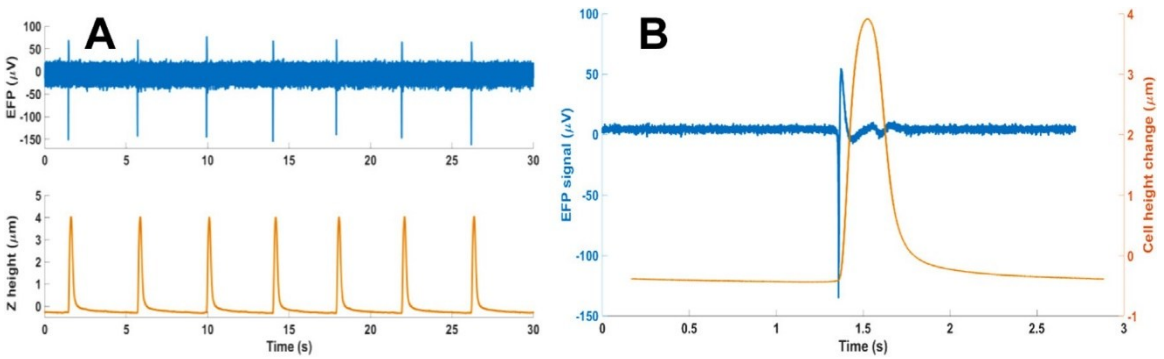



*Fig. 4.2. Representative recording obtained with the implemented electromechanical system, and its post-processed part. A) Simultaneously and synchronously acquired extracellular field potential (top) and mechanical contraction (bottom). B) Averaged curves from the same recording; it is possible to appreciate the noise reduction due to filtering. The two traces are separated by the mean calculated delay.*

The lowest observable noise level in the MEA-EP traces was 33.3 µVpp, whereas the average noise in the force and in the Z height traces were 18.3 pN and 24.5 nm respectively. Online and post-processing digital filtration allowed the analysis of EFPs with signal-to-noise ratio even close to 0 dB. Nevertheless, approximately half of the plated samples were able to produce a visible EFP trace, while mechanically beating. This issue is most probably due to scarcely-conductive coupling between the MEA planar electrodes and the BCC. Extracellular biopotentials morphology is fundamentally dependent on the conductive sample/electrode proximity and high resistance cleft (Spira and Hai, 2013). As BCC present a mixed cell population of cardiomyocytes and fibroblast-like cells (Supplementary Fig. 1A), as also previously reported (Ma et al., 2011); it is plausible that a non-conductive patch might adhere to the electrode area. In fact, fibroblast-like cells are found to be dedicated into BCC adhesion and spreading (Supplementary Fig. 2). This drawback is easily amendable, since it is possible to remove gently and re-plate BCCs in sterile conditions.

Each measurement lasted between 4h and 5h, without any remarkable alteration of cardiac activity, if not due to drug stimulation. This can be also seen in the absence of morphological alteration between beginning and end of protocol (Supplementary Fig. 3). Although probed in not completely sterile conditions, it was found that if refilled with antibiotics-containing medium, at the end of the experiments, the samples can keep on without visible contamination up to 4 days. This is particularly useful when testing overnight or realizing several-day treatments. Such evidence shows, like previously reported, how the adopted BCC model presents an outstanding resilience. Since an applied force of 5 nN did not elicit any spontaneous change in the measured parameters, in time, one can infer that the implemented CBBs are really following alteration of cECC and not mechano-electric feedback from stretch-induced depolarization (Zhang et al., 2008).

An accurate peak detection and averaging period selection allowed the reconstruction of important physiological parameters described in Table 4.1, namely beating rate, contraction speed, cardiac cycle duration and, most importantly, a coupled parameter such as the electro-mechanical delay (EMD). To our best knowledge, this is the first time that such parameter is measured on 3D cardiac in vitro model. Fig. 2B shows the obtainable averaged electromechanical events, corrected by the calculated EMD.

### 4.4.2 Differential drug response and correlation analysis is indispensable to distinguish cell-type dependency of cardiac parameters

Once the feasibility and features of the implemented electromechanical CBBs were assessed, we firstly asked whether basal conditions would be sufficient to distinguish diseased and healthy hPSC derived BCC. The baseline beating frequency for all the cell lines tested was not significantly different (0.327 ± 0.023 Hz for CTRL, 0.325 ± 0.062 Hz for DORSO and 0.468 ± 0.103 Hz for DMD). The same evidence was found for other important functional parameters, such as the basal force (2.1 ± 1.9 nN for CTRL, 12.0 ± 4.7 nN for DORSO and 0.89 ± 0.46 nN for DMD) and EMD (23.0 ± 1.3 ms for CTRL, 22.0 ± 3.0 ms for DORSO and 25.6 ± 5.3 ms for DMD).

Therefore, different stimulation / inhibition drug protocols were tested to validate the adopted models versus the expected cardiac response and assess the presence of cell type-dependent differences.

### 4.4.3 Calcium trials

Initially, the dependence of cardiac parameters on extracellular $Ca^{2+}$ concentration was tested. This ion and its extracellular availability are in fact of primary importance for cECC, particularly for the hPSC-derived CMs, which possess an immature calcium handling toolkit (Keung et al., 2014) and rely mostly on membrane transport (Youm, 2016). Cell type-dependency was found by 2-way ANOVA for beating rate ($p = 0.007$), contraction duration ($p = 0.0003$), time decay ($p < 0.0001$) and EMD ($p = 0.026$). A difference close to significance was reached for the average speed of contraction ($p = 0.069$). The effect of the $Ca^{2+}$ concentration was found significant only in relationship to the beating rate ($p < 0.0001$). All cell lines experienced a decrease in beating rate proportional to $Ca^{2+}$ concentration. The CTRL and DORSO groups plateaued around ¾ of the basal rate (67 ± 10% and 68.6 ± 5.1%, respectively), while the DMD group decreased to 89.5 ± 3.2% of its basal rate. The beating rate phenotype of mutation carrying cell line correlates with previously described pre-existing calcium stress impairing inward ion flux (Fanchaouy et al., 2009). This frequency decrease was paralleled by an increase of exerted force in all the cell lines (120.3 ± 9.4% for the CTRL group, 110 ± 14% for DORSO and 112 ± 19% for DMD). This phenomenon is due to the immature

contractile phenotype of hPSC-derived CMs, which possess negative frequency-force relationship (Pesl et al., 2016b). The observed change of contractile events was found as an increase of the relaxation period, expressed by the decay time constant for the CTRL and DORSO groups (108.1 ± 3.5% and 110.5 ± 4.2%, respectively) and a decrease for DMD (84.3 ± 5.2%). The $Ca^{2+}$ dependent decay time decrease in dystrophin mutation-carrying line is in correlation with previously described pre-existing calcium overload (Fanchaouy et al., 2009), which may limit the contraction dilation due to saturated sarcomere, probably resulting in limited ability of the DMD CBB to employ force-imposed reaction during cluster stretch as imposed in healthy tissue by Frank Starling mechanisms. The EMD, a parameter directly connected to electromechanical coupling, did prove statistically significant for cell-type. CTRL did not show a dose-dependent relation with the $Ca^{2+}$ concentration (109–99% variation range); DORSO showed a similar trend with only non-significant increase with respect to CTRL (142–131%), validating the CBB's robustness toward line specific variability in differentiation efficiency. Conversely, the DMD group showed a dose- dependent trend (up to 257 ± 71% of the basal delay); it is possible that increasing calcium levels are gradually impairing the already elevated activity of an altered ryanodine receptor to coordinate the calcium-induced calcium release (Fauconier et al., 2010). The previous results are summarized in Fig. 4.3A-C.

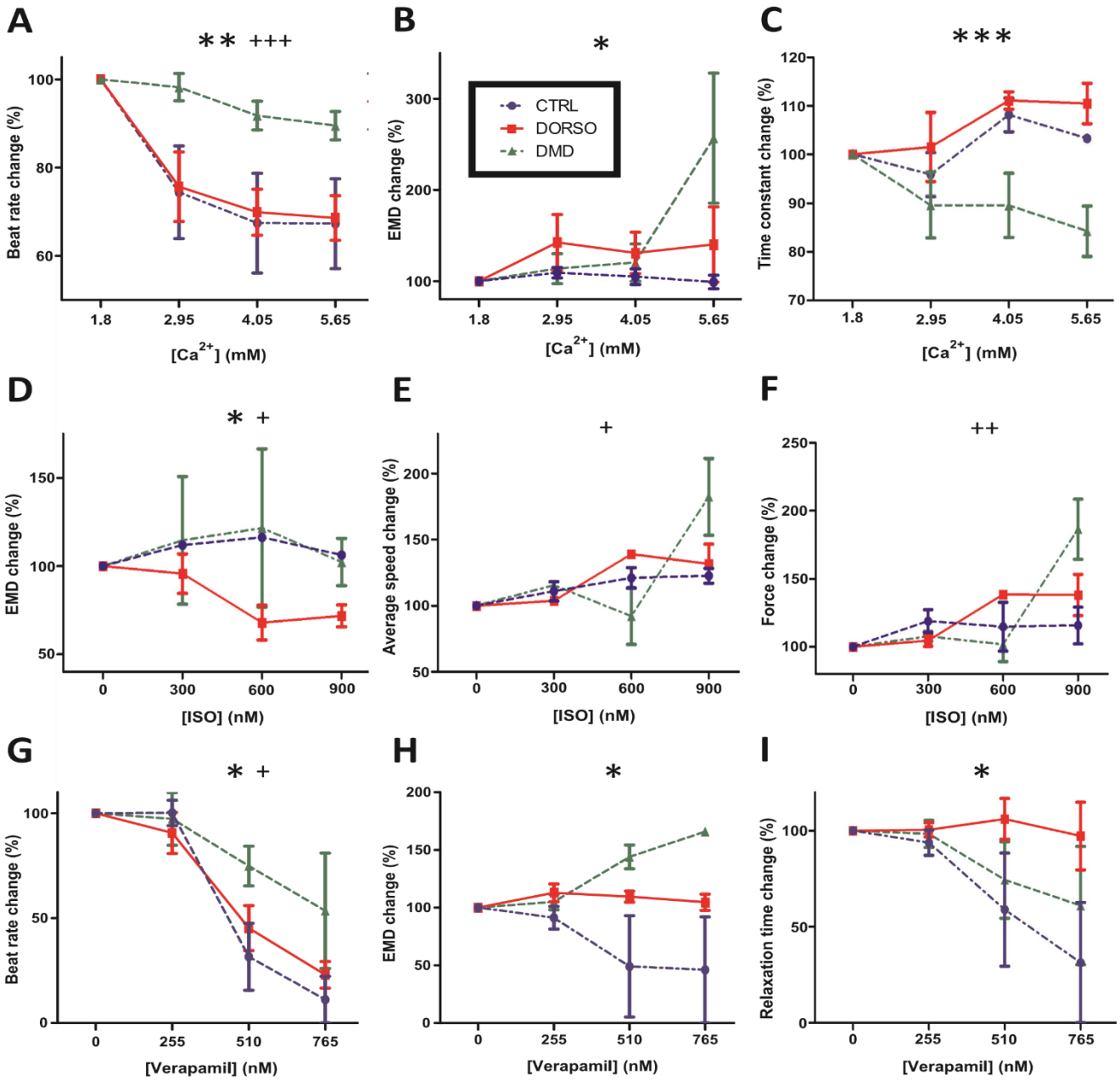



*Fig. 4.3. Selected results of drug trials performed with the presented electrochemical cell-based biosensor. The top row (A-B-C) represents extracellular calcium concentration trials. The middle row (D-E-F) β-adrenergic stimulation trials (Isoproterenol). The bottom row (G-H-I) represent class IV antiarrhythmic / calcium channel blocker trial (Verapamil). The * symbol indicates statistically significant difference according to the beating cardiac cluster type. The + symbol indicates statistically significant difference due to the chemical concentration. One symbol indicates a p-value < 0.05, two*

*symbols < 0.01, three symbols < 0.001. All the comparisons are carried on with repeated measurements 2-way ANOVA with row matching (drug concentration).*

### 4.4.4 Isoproterenol trials

The β-adrenergic stimulation was performed via increasing isoproterenol concentration to assess the ionotropic and chronotropic cell line-dependent features. Surprisingly, no extracted parameter showed significant dependency over the cell type, except for the EMD ($p = 0.0130$), which was also significantly concentration dependent ($p = 0.012$). Other concentration-dependent parameters were the average speed of contraction ($p = 0.031$) and the exerted force ($p = 0.006$), with DMD group showing marked increase at end concentration (182 ± 29% and 186 ± 22% respectively). In contrast, DORSO experienced roughly 1/3 increase of these parameters (132 ± 15% for average speed and 138 ± 15% for force) and CTRL only 1/5 increase (122.7 ± 5.5% and 116 ± 14% respectively). Isoproterenol effect appears to have a threshold concentration between 300 and 600 nM. After this threshold, the CTRL and DMD groups slightly altered EMD (101.0 ± 6.0% and 96.6 ± 2.7%, respectively), whereas the DORSO group decreased its measured EMD to 73.0 ± 7.6% of the baseline value. This difference might be explained with better differentiation grade of dorsomorphin-treated groups, since dorsomorphin is an inhibitor of BMP signaling and promotes cardiac differentiation (Kattman et al., 2011). It is therefore plausible that an improved differentiation guarantees a better BCC syncytium, able to improve cECC timing in response to adrenergic stimulation. The notable results are shown in Fig. 4.3D-F. The same negative beating rate/ force relationship was also noticed for all the cell lines, except when an arrhythmic behavior (e.g., multiple beating modes) was induced.

### 4.4.5 Verapamil trials

The antagonist trials were carried on L-type calcium channels to observe the reaction of different BCCs to class IV antiarrhythmics. Verapamil, as an example of this class, was shown to improve skeletal muscle force in DMD patients but led also to adverse cardiac side effect. However, no data on mechanism of such adverse effect exists (Nascimento Osorio et al., 2018). Previously, the growing CMs were coupled to RTCA impedance system, which allowed to quantify only beat rate effects of Verapamil (Wang et al., 2013). Here, the beat rate influence of drug showed to be cell type-dependent ($p = 0.019$) and dose dependent ($p = 0.001$). The

EMD parameter was found to be only cell-type dependent ($p = 0.0316$), together with the relaxation time ($p = 0.030$). The measured exerted force and Z height change were found solely dose-dependent ($p = 0.015$ and $p = 0.019$ respectively). The DMD cells showed decrease in beating rate down to 53 ± 27% of baseline, compared to 11 ± 11% of CTRL and 23.0 ± 6.3% of DORSO groups. The EMD shows different trends for each cell line: for the CTRL groups, the delay drops to 46 ± 46% of the baseline; DORSO group upped to 112% of the baseline and ended the trial at 104.0 ± 7.1%; the DMD group showed an increase of 143% to finish the trial at 111 ± 55%. These distinct trends can be due to the different biological backgrounds of the BCC models: CTRL group may respond to L-type channel inhibition by referring to the inositol-3-phosphate complex, which spontaneously produces calcium influx in embryonic cardiac phenotype (Youm, 2016); dorsomorphin-treated BCC might express higher number of functional L-type calcium channels, therefore being more resilient to the same drug concentration and present delayed coupling, with stable force level. DMD samples can present calcium leaking at the membrane level (Burr and Molkentin, 2015), although cECC delay is linearly increasing, which together with the decreasing force suggests impairment of the contractile machinery (Li et al., 2014). The mentioned notable results are shown in Fig. 4.3G-I.

## 4.5 Conclusions

We have successfully implemented and tested the electro-mechanical cell-based biosensor for the simultaneous and synchronous probing of cardiac excitation-contraction coupling. The system allows the characterization of cardiac models through differential drug trials and sample-type discrimination. For the first time, to our knowledge, a distinctive beating-force relation was shown for Duchenne muscular dystrophy cardiac models. The bioelectromechanical parameters derived from the cardiomyocyte cluster-based models provide important insights into heart pathologies and sometimes (such as in β-adrenergic stimulation assays) serve as the only discriminant between different models. Current limitations of the systems regard the non-sterility of the measurement environment, and the localized probing of a 3D model with a single MEA electrode and AFM cantilever. The system also suffers from a substantial biological sample variability, which requires more experimental repetitions to achieve better accuracy of results; this can be overcome by suitable choice of

drug treatment regimens to focus the data collection toward the desired disease phenotype. Future improvement with higher-density electrode arrays and tip-less cantilevers providing a wider surface contact should provide a higher information content and improve stability of models, respectively.

## 4.6 Acknowledgments

This research has been financially supported by the Ministry of Education, Youth and Sports of the Czech Republic under the project CEITEC 2020 (LQ1601) and ICRC (LQ1605), the CIISB research infrastructure project LM2015043 supported the AFM measurements at the Core Facility Nanobiotechnology, and the Grant Agency of the Czech Republic (GACR) provided support through grant no. P302/12/G157.

## 4.7 Appendix A. Supporting information

Supplementary data associated with this article can be found in the online version at doi:10.1016/j.bios.2018.10.021.

# 5 Improvements in biosensing by addition calcium imaging (p2b)

## 5.1 Commentary

Excitation-contraction coupling is a complex and adaptive process, governed by the rhythmic contraction of cardiomyocytes triggered by cellular depolarization. This depolarization leads to the generation of action potentials, which are subsequently converted into mechanical contractions through the mediation of intracellular calcium ions (Ca2+). Central to cardiac functionality is the intricate handling of calcium ions, which play a crucial role in initiating and regulating muscle contractions. Systolic calcium cycling involves two primary sources: inward ionic currents flowing through voltage-dependent transmembrane calcium channels and the release of calcium from specialized intracellular compartments known as the sarcoplasmic reticulum (SR). The release of calcium from the SR predominantly occurs through ryanodine receptors (RyR), particularly the RyR2 isoform in cardiac muscle. Following an action potential, a massive release of calcium ions from the SR triggers mechanical contraction, while mechanisms such as the Na+/Ca2+ exchanger and sarco-endoplasmic reticulum calcium ATPase work to maintain intracellular calcium homeostasis.

In vitro models of cultured cardiac myocytes offer unique advantages for studying cardiac tissue development, pathophysiology, and pharmacology. These models, including monolayer cultures of primary neonatal rat ventricular cardiomyocytes and adult rodent cardiomyocytes, allow for direct manipulation and control of environmental parameters without the confounding effects of in vivo feedback mechanisms. Additionally, novel models utilizing cellular multilayers or human stem cell-derived cardiomyocytes hold promise for recapitulating physiopathological conditions and studying patient-specific disease states.

hESC combined with AFM, may provide additional information using fluorescence microscopy. This integrated approach enables simultaneous mechanical and chemical measurements, offering real-time visualization of calcium dynamics and contractility in 3D cardiac models. The study utilized 3D BCCs generated through the forced aggregation of hESC from the CCTL14 line within agarose microwells. To enable simultaneous recording, these clusters were loaded with the calcium-specific fluorescent dye Fluo-4 AM and placed in a specialized setup consisting of an AFM scanner positioned above an inverted microscope

equipped with a scientific complementary metal-oxide-semiconductor (sCMOS) camera. Mechanical contractility was recorded as MCG using a soft silicon cantilever maintained at a constant 5 nN contact force, while calcium waves were captured via epifluorescence video at approximately 50 frames per second. The asynchronous signals were subsequently processed using MATLAB algorithms, where multiple filtration methods—including finite impulse response (FIR), median, and ensemble empirical mode decomposition (EEMD) filters—were evaluated for their ability to increase the signal-to-noise ratio (SNR) without distorting biological parameters. The robustness of this integrated biosensor was validated through caffeine stimulation (10 mM) to trigger and characterize a known pharmacological cardiac response.

We achieved the first simultaneous recording of cardiac contractility and calcium waves on 3D in vitro cardiac models. The optimized biosensor demonstrated excellent stability, with the clusters withstanding the measurement environment for over one hour while maintaining native average beating rates between 0.74 and 2.35 Hz. In terms of data processing, the EEMD filter was identified as the superior method because it significantly improved the SNR of calcium signals (e.g., from 7.35 dB to 14.61 dB during caffeine trials) while preserving the original character and morphology of the signals better than FIR or median filtering. Validation with caffeine produced the expected physiological responses, including an increase in beating frequency (approx. 8.4%), a 3.9-fold rise in basal fluorescence, and a reduction in contraction peak amplitude (-24.7%). Technical challenges, such as interference from the AFM infrared laser on the optical path, were effectively mitigated by interposing a near-infrared filter before the camera detector. These results confirm that the combined AFM-fluorescence platform provides a high-information and reliable system for the real-time evaluation of cardiac phenotypic traits and drug responses.

# Simultaneous study of mechanobiology and calcium dynamics on hESC-derived cardiomyocytes clusters

Guido Caluori[1,2] | Jan Pribyl[2] | Vratislav Cmiel[3] | Martin Pesl[1,4] | Tomas Potocnak[3] | Ivo Provaznik[3] | Petr Skladal[2] | Vladimir Rotrekl[4]

[1] International Clinical Research Centre of Saint Anne Hospital of Brno (FNUSA-ICRC), Interventional Cardiac Electrophysiology Group, Brno, Czech Republic

[2] Nanobiotechnology Group, Central European Institute of Technology of Masaryk University (CEITEC-MU), Brno, Czech Republic

[3] Department of Biomedical Engineering, Brno University of Technology, Faculty of Electrical Engineering and Communication, Brno, Czech Republic

[4] Department of Biology, Masaryk University, Faculty of Medicine, Brno, Czech Republic

**Correspondence**
Jan Pribyl, Central European Institute of Technology of Masaryk University (CEITEC-MU), Nanobiotechnology Group, Kamenice 5, 62500 Brno, Czech Republic.
Email: jan.pribyl@ceitec.muni.cz

**Funding information**
CIISB research infrastructure, Grant/Award Number: LM2015043; Ministry of Education, Youth and Sports of the Czech Republic, Grant/Award Number: CEITEC 2020 (LQ1601); Czech Science Foundation, Grant/Award Number: GA18-24089S

## Abstract

Calcium ions act like ubiquitous second messengers in a wide amount of cellular processes. In cardiac myocytes, $Ca^{2+}$ handling regulates the mechanical contraction necessary to the heart pump function. The field of intracellular and intercellular $Ca^{2+}$ handling, employing in vitro models of cardiomyocytes, has become a cornerstone to understand the role and adaptation of calcium signalling in healthy and diseased hearts. Comprehensive in vitro systems and cell-based biosensors are powerful tools to enrich and speed up cardiac phenotypic and drug response evaluation.

We have implemented a combined setup to measure contractility and calcium waves in human embryonic stem cells-derived cardiomyocyte 3D clusters, obtained from embryoid body differentiation. A combination of atomic force microscopy to monitor cardiac contractility, and sensitive fast scientific complementary metal-oxide-semiconductor camera for epifluorescence video recording, provided correlated signals in real time. To speed up the integrated data processing, we tested several post-processing algorithms, to improve the automatic detection of relevant functional parameters. The validation of our proposed method was assessed by caffeine stimulation (10mM) and detection/characterization of the induced cardiac response.

We successfully report the first simultaneous recording of cardiac contractility and calcium waves on the described cardiac 3D models. The drug stimulation confirmed the automatic detection capabilities of the used algorithms, measuring expected physiological response, such as elongation of contraction time and $Ca^{2+}$ cytosolic persistence, increased calcium basal fluorescence, and transient peaks. These results contribute to the implementation of novel, integrated, high-information, and reliable experimental systems for cardiac models and drug evaluation.

**KEYWORDS**

atomic force microscopy, biosignals filtering, caffeine, calcium imaging, cardiac differentiation, embryoid bodies, fluorescence microscopy, human stem cell-derived cardiomyocytes

**List of Abbreviations:** AFM, atomic force microscopy; AM, acethoxymethylester; BCC, beating cardiac clusters; CM, cardiomyocytes; EB, embryoid body; ECC, excitation-contraction coupling; EEMD, ensemble empirical mode decomposition; FIR, finite impulse response; hESC, human embryonic stem cells; MCG, mechanocardiogram; PW, peak width; ROI, region of interest; RT/FT, rising time/falling time; RyR, ryanodine receptor; sCMOS, scientific complementary metal-oxide-semiconductor; SNR, signal-to-noise ratio; SR, sarcoplasmic reticulum

Guido Caluori, Jan Pribyl, and Vratislav Cmiel contributed equally to this work.

This article is published in Journal of Molecular Recognition as part of the virtual Special Issue 'AFM BioMed Krakow 2017, edited by Malgorzata Lekka, IFJ PAN, and Pierre Parot, CEA, France, and Jean-Luc Pellequer, IBS, France'.

 © 2018 John Wiley & Sons, Ltd. 

## 5.2 INTRODUCTION

The heart muscle provides the necessary pressure to the blood stream to circulate the necessary nutrients, oxygen, and metabolites around the organism. This function is achieved by rhythmic contraction of the cardiac muscle cells, of cardiomyocytes (CMs) (Nickerson DP: 2005) through a phenomenon typical of the muscular phenotype called excitation-contraction coupling (ECC) (Bers 2002). The ECC is a complex and adaptive set of subcellular processes, retained in in vitro cultures of dissociated CMs, both at the single cell level and at the tissue level(Rapila et al. 2008). The process is triggered by induced/spontaneous cellular depolarization up to the threshold to elicit an action potential, which are subsequently converted into mechanical contraction by the mediation of intracellular $Ca^{2+}$ ions. An appropriate $Ca^{2+}$ handling is of paramount importance for cardiac functionality. Systolic $Ca^{2+}$ cycling has mainly two sources: inward ionic currents flowing through voltage-dependent transmembrane calcium channels (mostly L-type)(Satin et al. 2008) and a specialized subcellular compartment known as the sarcoplasmic reticulum (SR)(Dibb et al. 2010).

$Ca^{2+}$ release from the SR occurs mostly through a specialized channel known as the ryanodine receptor (RyR), specifically, in cardiac muscle, the RyR2 isoform(N. Liu 2006). Following an action potential, $Ca^{2+}$ ions stored in the SR are massively released, initially triggered by $Ca^{2+}$ inward current, which stimulates the collective opening of grouped RyRs in a process known as calcium-induced calcium release (Fabiato et al. 1985). While contraction occurs, at the membrane level, $Ca^{2+}$ is promptly pumped out by the $Na^{+}/Ca^{2+}$ exchanger or segregated into subsarcolemmal mitochondria by the same mechanism. The high $Ca^{2+}$ concentration inside the SR is re-established by the sarco-endoplasmic reticulum calcium ATPase, which transports calcium ions from the cytosol inside the lumen of the SR. The extremely sophisticated organelles and receptors and buffers for the uptake and release of $Ca^{2+}$ goes generally under the name of calcium-signalling toolkit (Berridge, Bootman, and Roderick 2003).

In vitro models of cultured cardiac myocytes offer many advantages for developmental, pathophysiological, and pharmacological studies of cardiac tissue through cell-based biosensors, as they allow direct cell manipulation and control of environmental parameters, without interference from the compensatory feedback mechanisms that exist in vivo (Bursac et al. 1999. Monolayer cultures of primary neonatal rat ventricular CMs represent a frequently employed model to study cardiac processes, (Martherus, Zeijlemaker, and Ayoubi 2010) as the isolated CMs retain contractility and reassociate in functional syncytium in vitro. (Eschenhagen and Zimmermann 2005) Adult rodent CMs are preferred for single cell study as they present mature morphology (eg, Z-disk structures or ion channels expression) and functional features. (Yang, Pabon, and Murry 2014) Nevertheless, new realistic models are being researched with the use of cellular multilayers(Sperelakis 1989) or human stem cells-derived CMs. (Gepstein 2013) These are able to generate functional cardiac muscle cells that recapitulate existing physiopathological conditions and can be derived in a 2D monolayer form or in a 3D structure from the formation of embryoid bodies (EBs). (Pesl et al. 2016; Davis et al. 2012; Acimovic et al. 2014). The 3D models derived from EBs have proven to produce beating foetal-like CMs, (Jung et al. 2017). which control the differentiated cluster contractility and electrophysiology. (Mummery et al. 2012) Recently, these models have also been proved to recapitulated patient-specific disease conditions. (Spitalieri et al. 2018) For more details on otherwise obtained 3D cardiac constructs, the reader is referred to the dedicated literature (Mathur et al 2016).

Overall, in vitro cardiac models have allowed to obtain precise physiological insights, such as the difference between atrial and ventricular populations in calcium handling. (Bootman et al. 2011) Furthermore, they have revealed key aspects and consequences of calcium signaling remodeling when cardiac pathologies occur. For example, usually minor calcium toolkits, such as inositol triphosphate (InsP3)/$Ca^{2+}$ signaling can be hyperstimulated by the presence of cardiac hormones due to atrial arrhythmias. (Berridge 2012) Dystrophic mutations (such as Duchenne's muscular dystrophy) severely hamper the $Ca^{2+}$ current inactivation and the SR uptake, leading to $Ca^{2+}$ overload. (Koenig et al. 2013) Genetic mutations can involve specific intracellular receptors, such as in RyR2-specific catecholaminergic polymorphic ventricular tachycardia, which causes leaky SR inducing sudden cardiac death during exercise. (Marks 2013) It has been demonstrated that induced persistent $Ca^{2+}$ overload, due to prolongation of action potentials, directly induces CMs death through a mitochondria-mediated necrotic

pathway. (Nakayama et al. 2007) Eventually, reduced $Ca^{2+}$ transients, prolonged duration and impaired uptake lead to abnormal cardiac output, muscular remodeling, and heart failure.[2](Gorski, Ceholski, and Hajjar 2015) Dynamics of $Ca^{2+}$ are becoming an elective drug target to avoid tissue remodeling followed by development of congestive heart failure, ischemia or arrhythmias. (Nattel et al. 2007; Driessen, Bourgonje, and Vos 2014)

$Ca^{2+}$ dynamics are visualized by imaging techniques that require calcium-specific fluorescent probes or fluorophores. These are a class of natural or artificial light-excitables/emitting (bio)molecules able to detect specific chemical species. (Molecular Probes 2010; Bootman et al. 2013) Fluo-4 acethoxymethylester (AM), used in this study, is a high yield non-ratiometric (i.e., not able to determine concentration) fluoresceine-based dye conjugated with the 1,2-bis (o-aminophenoxy)ethane-N,N,N′,N′-tetraacetic acid, a calcium-specific chelating agent, linked to AM groups. It is briefly recalled that AM-neutralizing group allows cytosolic irreversible internalization via lipophilic affinity and de-esterification within the cell membrane. (Tsien 1981) The use of high-performance dyes goes in parallel with the design of high-speed sensitive cameras. Microscopy embedded video imaging (Swandulla et al. 1991) and the use of electron multiplying charge coupled device and scientific complementary metal-oxide-semiconductor (sCMOS) cameras (Lasser-Ross et al. 1991; Bigas et al. 2006) have been key innovative steps for calcium imaging. The high signal strength of the fluorescent probes in combination with these emerging technologies allowed for real-time fluorescence observations of biological processes at the single-cell level.

As previously mentioned, $Ca^{2+}$ dynamics is directly responsible for the proper function of the contractile machinery and therefore the exerted force by CMs. Cardiac contractility and mechanics in vitro can be assessed by several methodologies (eg, force-transducing elements, optical tweezers, video analysis of particle tracking, and impedance spectroscopy), (Pesl et al. 2016) among which the most sensitive is atomic force microscopy (AFM). Atomic force microscopy-based nanoindentation has been applied for almost 30 years to the investigation of cellular mechanics. (Radmacher 2007) Atomic force microscopy can also serve as nano sensitive tool to measure time-resolved cell height change, contractility rate, and transverse exterted force or single CM(Domke et al. 1999; Sun et al. 2012) and 3D organoids through mechanocardiograms (MCGs). (Pesl et al. 2016) An important technological integration among

experimental systems is the one between optical microscopy (or later confocal microscopy) and AFM. The integration of optical microscopy and confocal microscopy within life sciences has proved particularly beneficial, because it unlocked the ability to simultaneously apply and measure local mechanical forces, while tracking biological responses/pathways with fluorescent dyes, antibodies, or genetic incorporation of fluorescent fusion proteins such as green fluorescent protein. Common optical microscopy techniques like bright-field illumination, phase contrast, and especially differential interference contrast, reveal high-contrast topography information, as well as location and/or distribution of internal structural features (e.g., cell organelles). (Bank 2005; Madl et al. 2006; Pelling et al. 2007) Fluorescence microscopy has proven to be a powerful tool for selective and specific visualization of labelled molecules down to the single-molecule level, rendering it possible to follow cellular processes and to monitor the dynamics of living cell components. (Hinterdorfer et al. 2001) The advantages and benefits of AFM and fluorescence microscopy complement each other, allowing a more detailed characterization of cellular structures and processes. (Hards et al. 2005; Raiteri et al. 2015) A prime example of this is the visualization of calcium dynamics during cardiomyocyte contractions; AFM is used as an ultrasensitive force detector or is measuring the mechanical pulsations of living cells, with cantilever probe touching at a constant force the cell. (Haupt et al. 2006). Employing simultaneous fluorescence-AFM, these local mechanical pulsations can be linked directly to intracellular calcium oscillations. (Pelling et al. 2007) Simultaneous calcium imaging and AFM contractility recording has been successfully tested for drug response on single CM, (Haupt et al. 2006) but to our best knowledge, no such method has been implemented for 3D cardiac models.

Therefore, we defined an integrated experimental setup that would allow to harness the detecting capabilities of the two techniques simultaneously. In this work, we employed size-controlled EBs, differentiated in beating cardiac clusters (BCCs) from human embryonic stem cells (hESC), (Pesl et al. 2013) as our cell-based biosensors model for detection of cardioactive chemicals. We have expanded our previously established mechanical methods (Pesl et al. 2016) with calcium imaging, to provide combined information of two biophysical aspects of cardiac function. As integrated measures lead to a proportional increase of information, an automatic functional parameter extraction is desirable. The choice of the best automatic analysis

algorithm was bound to its versatility in processing different signals and most importantly to performance. Specifically, we looked for increase of the signal-to-noise ratio (SNR) absence of morphological alterations on the baseline and reduction of imposed signal delay for future synchronization. Therefore, we explored different data handling algorithms to put the base of a robust method for automatic analysis.

## 5.3 METHODS

### 5.3.1 Preparation of hESC-derived CM clusters

In this work, the cardiac models were obtained using the hESC line CCTL14 as previously described (Dvorak et al. 2005, Pesl et al. 2013). Cells were thawed and seeded on mitotically inactivated mouse embryonic fibroblasts.(Dahlman et al. 2013) hESC colonies were cultivated in DMEM-F12 (Thermofisher, Waltham, MA-USA), supplemented with 15% knockout serum replacement (fetal bovine serum (FBS), Life Technologies, Carlsbad, CA-USA), 1% L-glutamine (Thermofisher), 0.5% penicillin/streptomycin (Thermofisher), 1% 2mercaptoethanol (Thermofisher), 1% nonessential amino acids (Life Technologies), and 4 ng/mL human fibroblast growth factor 2 (hFGF2, Peptrotech, London, UK). Colonies were propagated for at least five passages, by scratching and fractioning using 1-mL pipette tip. To prepare monolayer cultures, colonies were passaged and transferred to 1:100 Matrigel (Corning, Tewksbury, MA-USA) coated dishes. Monolayer cultures were carried on in Modified Eagle's Medium (MEF)-conditioned medium supplemented with 10 ng/mL hFGF2. Upon reaching 80% confluence, hESC were passaged using TrypLE Express dissociating agent (Thermofisher). Cells underwent at least two feeder-free passages. Regular and size-controlled EBs were obtained by forced aggregation of $2 \times 10^6$ cells/ milliliters. Aggregation wells were prepared in 1.5% w/v agarose gel (VWR, Radnor, PA-USA), and each EB contained approximately 1000 cells. Cardiac differentiation was achieved using our previously described method, (Krutá et al 2014) by sequential cytokine modulation in KnockOut DMEM (Life Technologies), supplemented with 10% FBS, 1% L-Glutamine, 1% penicillin/streptomycin, 1% β-mercapthoethanol, 1% nonessential amino acids, and 10 $\mu g/mL^{-1}$ ascorbic acid. Beating cardiac clusters were visible from day 11, and after day 20, they were counted and divided from non-beating clusters. Typical dimensions of the measured BCCs ranged between 300 and

400 μm in diameter. By visual observation, BCCs contain both contracting cells and fibroblast-like ones, the latter involved in adhesion to the substrate.

### 5.3.2 Clusters seeding and measurement setup

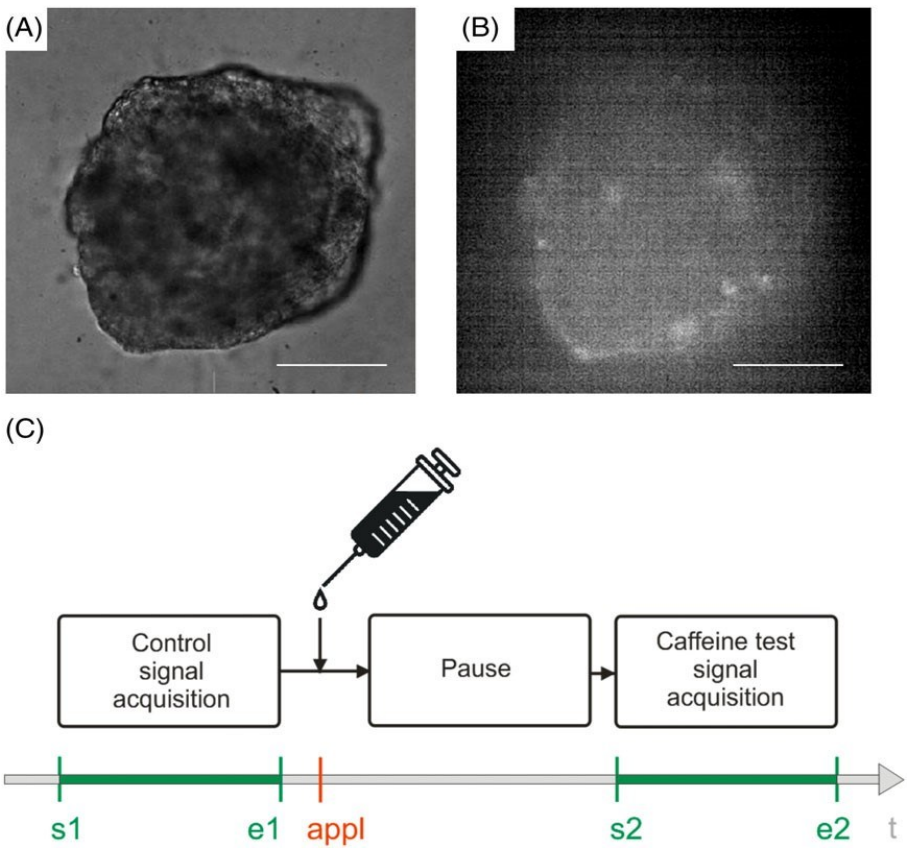
Differentiated BCCs were selected according to spheroidal regular shape and seeded onto 0.1% gelatin-coated (Sigma Aldrich, St. Louis, MO-USA) 34-mm Petri dishes (TPP Technoplastic Products, Trasadingen, Switzerland) and let adhere for 24 hours. Beating cardiac clusters were maintained at 37°C in a standard 5% $CO_2$ incubator. Prior to experiments, the samples were exposed for 60 minutes to a 3μM concentration of Fluo-4 AM (Life Technologies) in culture medium and incubating atmosphere. After loading, the sample were gently rinsed twice with KnockOut DMEM to remove excess of calcium dye, replenished with culture medium, and let in incubator for further 30 minutes to allow fluorophore de-esterification. Ultimately, the medium was removed and replaced by Tyrode solution (135mM NaCl, 10mM HEPES, 5.4mM KCl, 0.9mM $MgCl_2$, 10mM glucose, and 1.8mM $CaCl_2$, pH 7.4). For drug testing, a caffeine (Sigma) solution of 10mM concentration in complete Tyrode was used. All other chemicals when not specified were purchased from Sigma.

The prepared sample dish was equipped with media exchange tubes and placed on the motorized stage of an inverted microscope (Olympus IX-81S1F-3, Tokyo, Japan). An AFM scanner of 15 μm vertical range (BioAFM NanoWizard 3, JPK, Berlin, Germany) was then placed above the sample. A soft semicoated silicon cantilever Hydra2R (AppNano) was used as mechanical probe to ensure a stable contact without applying disruptive forces on the sample. A Petri dish heater (JPK) was used to keep the temperature constant at 37°C. The upper optical path of the optical microscope was used to record fluorescence image sequences with an sCMOS camera Andor Zyla 5.5 (Andor Technology, Belfast, Northern Ireland). A Thorlabs MD498 dichroic mirror was used for light wavelength selection. A Thorlabs FES650 shortpass type optical filter (650 nm) was inserted to the optical path before the camera detector to cut off the interference of the AFM laser light.

### 5.3.3 Data recording

BCC contraction and calcium transient signals were obtained simultaneously but in an asynchronous way. Scanning probe microscope Control Software v.5 (JPK) was used for AFM control and data acquisition at 1 kHz rate. The cantilever was placed in contact with the sample using a set point of 5 nN, with feedback loop parameter I = 50 and P = 0.05. This level of force was previously found to be the smallest force necessary to ensure stable contact and showed no visible functional alteration of clusters' contractility rate of exerted force. (Pesl et al 2016) The location was selected by consecutive trials to find the region with best vertical displacement. The observable MCG showed the temporal displacement on the AFM vertical piezoelectric crystal following the beating of the BCC, to maintain constant force with the sample. Calcium imaging video sequences were recorded at 200× using Andor Solis 64-bit control and acquisition software. The camera was connected via USB 3.0 to the computer station, while a high throughput solid-state drive disc was included to enable fast and long enough video acquisition by increasing the acquisition capacity. Camera resolution was set to 1700 × 1700 px and framerate to 49.67 frames per second. Data were obtained using spooling mode in form of data fractions and converted to AVI files. The time points of data acquisition protocol are shown in Figure 1 C. Mechanocardiogram signals were acquired for 10-minute intervals while only 60 seconds of image sequence was recorded from the start point of MCG, due to the memory-consuming data size.

*Fig.: 5.1 Microscopy images of the cardiac EB loaded with Flou-4 under the combined setup (magnification 20× and scale bar 100 µm). A, Brightfield image of the adhered EB. B, Epifluorescence view, with visible AFM laser artefact on bottom left corner. Biological fluorescence is still visible on the edges. C, Experimental method for caffeine stimulation, all time point distances indicate 10 minutes. E1-S2 resting time of 10 minutes was necessary for appropriate chemical diffusion in the sample*




### 5.3.4 Data extraction and filtration

Atomic force microscopy data and fluorescence image sequences were processed using Matlab 2015b and its image processing toolbox. Figure 5.2 shows a schematization of the mixed signal acquisition and post-processing. Contraction signals were extracted as text files while $Ca^{2+}$ traces were obtained from images stacks by selection of appropriate region of interest (ROI). Absolute fluorescence was retrieved as sum of the ROI pixel values ($F_{ROI}$) and corrected using a background fluorescence ROI ($F_{back}$) from each image in the sequence. Raw signals were then filtered and analyzed. Linear min-max normalization was performed to allow comparison between filtration and drug stimulation trials. However, to distinguish the change in amplitude

of the control and test signal, the relative ratio was recorded prior to normalization. Both MCG were corrected for baseline drift, filtered through different digital algorithms to provide the best noise reduction and parameter detection. The applied filters were

1 finite impulse response low-pass filter, with 5 Hz cut-off frequency;

2 median filter of fixed-length moving window (11 samples for MCG, 5 for Ca2+ transients);

3 ensemble empirical mode decomposition (EEMD) filter. This method works by analyzing the signal to find its main components

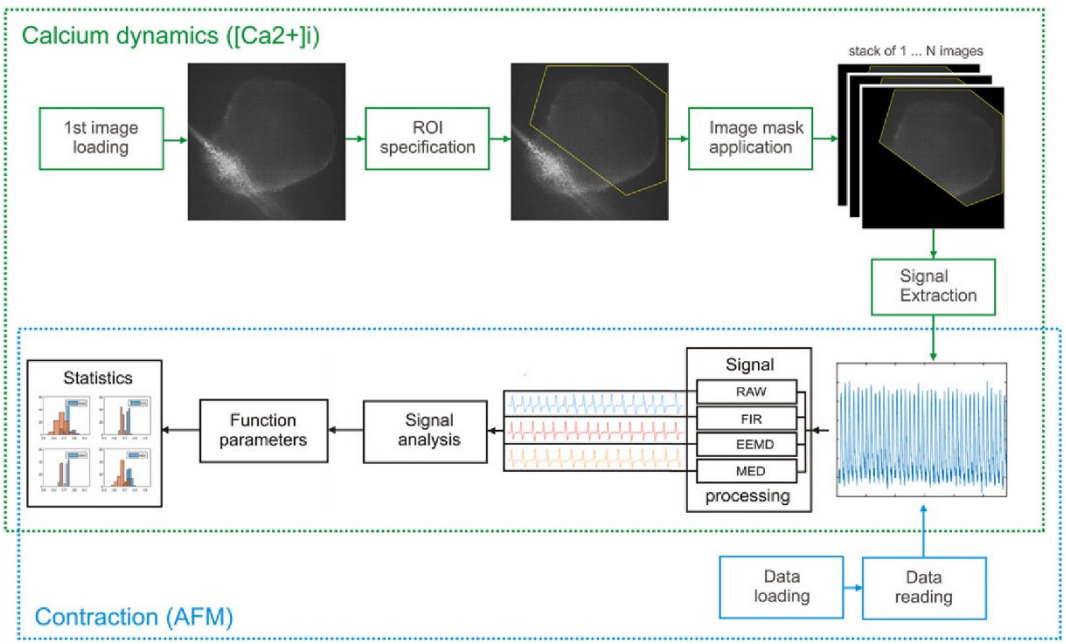



*Fig 5.2.: Schematic representation of data manipulation, from extraction to integration, conditioning and parameter extraction (intrinsic mode functions [IMF]) and remove them selectively in a process called sifting. (Huang eta al. 1998) Two and three IMFs were excluded for Ca2+ traces and MCG, respectively, after which the signals were recomposed. The EEMD algorithm was set up to maximum 10 sifting process per IMF with 200 ensembles cycles.*

After filtration, signal peaks were detected and parameters of interest (Figure 4, bottom row) were extracted and compared in at least 30 events per sample. For the raw and filtered data sets, the noise reduction was quantified calculating the SNR with the formula

$$SNR=20\ \log_{10}{}^{App}/_{4}\sigma 1$$

where $A_{pp}$ is the maximum amplitude of the single contraction or transient event, and σ is the standard deviation of the random noise detected on the baseline. Increase of noise standard deviation was considered a sign of undesired morphological artefacts.

## 5.4 RESULTS

Repeated recordings were performed after setup optimization over three different clusters. Figure 5.1 A, B show a representative BCC after calcium dye loading. The samples were able to withstand measurement environment for more than 1 hour. The native average beating rate calculated from MCG spanned between 0.74 and 2.35 Hz. The interference coming from the AFM laser module was attenuated on the common path for video acquisition but could not be eliminated. Nevertheless, simultaneous recording was achieved, when AFM backscattering was kept at the edge of the BCC. Figure 5.3 shows MCG and $Ca^{2+}$ traces recorded from the same sample, before normalization.

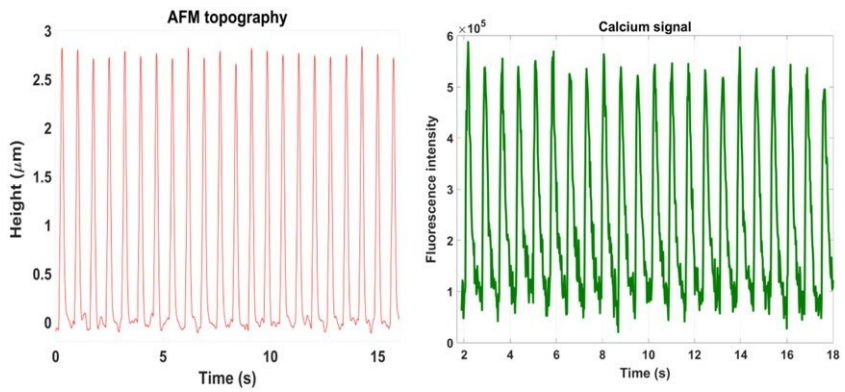



*Fig.: 5.3.: Typical traces of mechanocardiogram (MCG, left) and calcium transients (right) coming from the same recording*

### 5.4.1 Evaluation of different filtration methods

A correction of MCG drift is achieved by the direct linear interpolation method between two adjacent peaks. $Ca^{2+}$ signal is not affected by baseline drift when corrected appropriately for background intensity. Due to low number of samples, a 1:3 oversampling was performed to increase filtration working points. Original SNRs of the two signals were 19.73 and 14.11 dB for MCG and calcium transients, respectively.

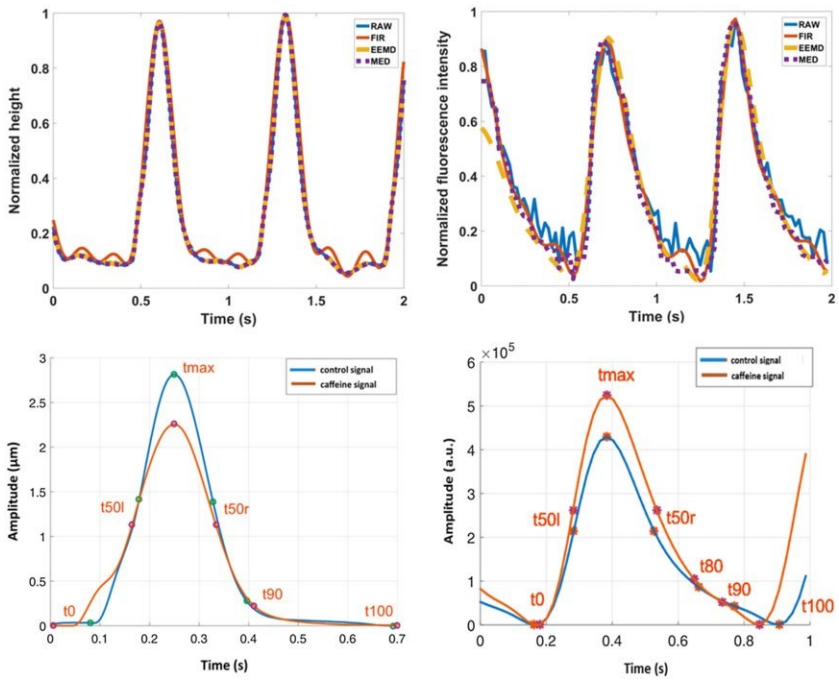



*Fig.: 5.4.: Filtration results and drug effect on the signals traces. MCG traces before and after filtration, where corrugation of the FIR filter is visible (top left). Calcium transients before and after oversampling (1:3) and filtering, where the best effect for EEMD method can be observed (top right). Averaged (n = 39) contraction events detected in MCG before and after caffeine stimulation, where one can see the mean event elongation and the lowering of the peak probably due to contraction pattern changes (bottom left). Averaged (n = 32) calcium cycling events before and after caffeine stimulation, where one can observe the elongating peak width (t50l-t50r), due to persistence of calcium in cytosol, and the increase of peak amplitude most probably due to increased calcium storage depletion (bottom right)*

Finite impulse response filtering increased the SNR to 20.49 dB and 20.97 dB for MCG and calcium transients, respectively. Over filtering of MCG produced corrugation artefacts that impaired proper extraction of time-related parameters. For instance, the mean contractile event duration increased up to 15.67% due to filtration-induced error in the automatic detection algorithm. Calcium traces on the contrary were partially smoothed, inducing a mean event time contraction of 4.59%.

Ensemble empirical mode decomposition filtering respected the signal shape with stochastic shifts of peaks on calcium traces, with respect to the raw signals. Signal-to-noise ratio did not improve for MCG (19.71 dB), but it increased for $Ca^{2+}$ transients (21.80 dB). No corrugation of morphological artefact was found using this filtering method. Mean event duration remained stable for MCG (0.08%) and saw a 6.82% elongation of the $Ca^{2+}$ ones.

Median filtering window width was empirically optimized for each separate signal. Signal-to-noise ratio again did not raise for MCG traces (19.73 dB) but saw mild improvement for calcium transients (16.81 dB). Mean duration of the events was slightly elongated in both cases, at 1.98% for calcium transients and 0.56% for contractility. Representative performance of the different filtering methods is summarized in Figure 4, top row. Because of the general best performance of EEMD filtering method, we will show only the results following this filtration method (Table 1). The results of signal filtration efficiency are included in Table 5.1.

| Parameter | Meaning |
|---|---|
| $t_X$ | Time with x indication percentage of the event total time |
| tmax | Time to maximum |
| T50I/T50R | Time to half of maximum in rising/falling |
| PW | Peak width (T50R-T50I) |
| RT/FT | Rising/falling time |

*Table 5.1 Parameter identification and description*

| | Contraction Signal (AFM) | | | | Calcium Transients (Optical Measurement) | | | |
|---|---|---|---|---|---|---|---|---|
| SNR, dB | Raw | FIR | EEMD | Median | Raw | FIR | EEMD | Median |
| Control signal | 19.73 | 20.49 | 19.71 | 19.73 | 14.10 | 20.97 | 21.80 | 16.81 |
| Caffeine signal | 20.73 | 21.82 | 20.70 | 20.73 | 7.35 | 14.22 | 14.61 | 11.62 |

*Table 5.2. Representative effect of different filtration methods on SNR (N of events > 30) Abbreviations: AFM, atomic force microscopy; EEMD, ensemble empirical mode decomposition; FIR, finite impulse response; SNR: signal-to-noise ratio.*

### 5.4.2 Evaluation of caffeine effect on calcium and contraction signals

To validate the robustness of our recording system automatic detection approach, we conducted caffeine stimulation on BCCs. The expected cardiac response was seen in contraction signal, as reduction of peak amplitude (24.7%) and increasing peak width (14.5%), as combination of elongation in rising time (25.2%) and falling time (5.1%). Event frequency increased 8.3%. Similar trend was observed in $Ca^{2+}$ signals in frequency increase (8.43%), with corresponding faster rising time (−3.7%) and longer falling time (13.4%). Basal fluorescence increased 3.9 times and peak width rose up of 5.5%. While the MCG traces did not benefit largely from the filtration in terms of SNR (from 20.73 to 20.70 dB), EEMD filtration doubled $Ca^{2+}$ signals SNR (7.35 dB to 14.61 dB), aiding significantly the reliability of the detection. These results are summarized in Tables 5.2 and 5.3.

## 5.5 DISCUSSION

A trustworthy and rapid investigation of in vitro cardiac cellular models is of fundamental importance to validate new drugs and investigate cardiac pathologies at the level of basic science. So far, in vitro models of CMs are examined through multiple alternative techniques (increasing sample variability) or powerful techniques affected by low throughput (e.g., patch clamp electrophysiology). $Ca^{2+}$ imaging is a powerful technique that brings precious insights in the adaptation of ECC at the single cell and tissue level. (Herron et al. 2012) Atomic force microscopy can, due to its versatility, integrate the information of chemical signaling with information on the cell/tissue mechanics, leading to better inference when an abnormal effect is observed.(Franz and Puech 2008) For this reason, we have implemented a combined optical and scanning probe microscopic setup, tested it on a defined 3D cardiac model, and validated

it with a known cardiac drug response. To increase the throughput of the experimental method, we have also tested different data conditioning methods to improve the accuracy of automatic detection of important parameters.

| Parameter | Contraction Signal (MCG, % Change) | Calcium Transients (% Change) |
|---|---|---|
| Beating rate | 8.83 | 8.42 |
| Peak amplitude | −24.70 | 20.85 |
| Rising time | 25.20 | −3.70 |
| Falling time | 5.20 | −13.40 |
| Peak width | 14.50 | 5.50 |

*Table 5.3 Representative effect of caffeine stimulation over observed parameters ($N_{events}$ > 30) Abbreviations: MCG, mechanocardiogram.*

We successfully recorded for the first time, to the best knowledge of the authors, simultaneous $Ca^{2+}$ cycling and contractility of intact BCC. We experienced how hardware technological integration of the two techniques is not a trivial point. Because the sCMOS camera shares the optical path with the AFM infrared laser, the non-reflected portion of the laser beam was often sufficient to disturb epifluorescence emission detection. The interposition of a near infrared filter on the camera optical path greatly attenuated the unwanted artefact, but it could not eliminate it completely. This problem was related to the high sensitivity of the employed camera and the nature of the technique. Similar artefacts were not visible with CCD cameras or confocal microscopy, albeit these two alternatives present different disadvantages: the former one comports the loss of the sensitivity necessary to detect events at high resolution, while the latter is technologically expensive and less flexible. Therefore, great attention on light filtration must be taken into consideration for different AFM producers.

After data extraction, we explored different filtration methods and quantified them in terms of SNR increase and undesired signal alteration. Due to the asynchronous recording, filtration-

induced delays were not quantified. The aim behind filtering is to improve the automatic detection of points of interest in noisy signal, when diverse sources of electronic noise are present from distinctive systems. The noise affecting the $Ca^{2+}$ transients come primarily from the processes associated with image acquisition by sensor array and camera electronics. This electronic and thermal detector noise is typically of high frequency nature with respect to the biological signals of interest. Nevertheless, due to the relatively low acquisition rate, oversampling is recommendable to ensure reliable performance of subsequent filtration. In the contraction signals obtained by AFM, a source of the signal noise comes from uncompensated environmental vibrations, but baseline drift, due to the soft sample creeping or temperature-induced bimetallic effect on the probe, are preeminent disturbances and need to be compensated. Due to the low frequency of drifts, a simple peak-between-peak linear interpolating algorithm is enough correct for this noise source.

In general, all three filtering methods led to beneficial increase of the SNR for the $Ca^{2+}$ signals, in basal condition and in caffeine-stimulated ones. The MCGs present higher SNR due to the AFM detecting method (optical lever amplification) and low noise electronics, which allows force sensing at the nanoscale. In this case, FIR filtering can lead to over-filtration artefacts. Median filtering was the worst performing option in terms of improvement of SNR, although signal parameter alterations were in the order of units of percent. Ensemble empirical mode decomposition filtering met the SNR improvement performance with the low signal alteration; therefore, it became the filtering elective choice for both signals. This algorithm is very adaptive, low-demand, and effective for high-frequency white noise elimination, while at the same time preserving the original signal character. Our selection does not exclude the possibility to employ other harmonic-based methods, like Fourier transform, although EEMD works without the assumption of stationary signals. Averaging filters could also provide an alternative method for functional parameters calculation, provided that the events alignment jitter induced by the noise is neglectable.

To test the detection of biological drug response, we employed caffeine stimulation. Caffeine is a well-known agonist of the RyR2 receptor of cardiac SR, as it induces calcium release in the cytoplasm.(Kong et al. 2008) This effect can be appreciated by the augmented basal

fluorescence, reflecting the presence of more unbound $Ca^{2+}$ in the cytosol.(O'Neill and Eisner 1990) The increase peak amplitude and elongated width of $Ca^{2+}$ transients can also be explained with the stimulated and prolonged depletion of the SR storage. The observed reduction of SNR in caffeine-stimulated conditions can be due to chaotic activation of local calcium sparks.(Izu et al. 2013) Rise in beating rate can be explained with the depolarized state induced by cytosolic unbound calcium,(Youm 2016) a condition initiated by caffeine and probably maintained by neighboring coupled fibroblasts.(Vasquez et al. 2011) Consequently to the beating rate increase, $Ca^{2+}$ transients rising time decreased, probably due to the augmented activation of L-type voltage-gated channels.(Leroy et al. 2002) Falling time decreased as well, most probably from enhanced activity of the $Na^{+}/Ca^{2+}$ exchange mechanism,(J. S. Rodriguez et al. 2014) deputed to restore low calcium cytosolic levels.(Ottolia et al. 2013) The change of peak amplitude at the MCG level can be attributed to the immature contractile machinery of hESC-derived CMs,(Martin Pesl, Pribyl, Caluori, et al. 2016) and to different activation pattern of the 3D cardiac cluster. Local monitoring of the BCC contraction using a pyramidal tip cantilever, like the one employed in this study, faced the influence of changing contractile patterns in heterogeneous sample. For future study, a colloidal probe with appropriate diameter (over 20 μm), or a tipless cantilever, might suffer less from this phenomenon.

## 5.6 CONCLUSIONS

In the presented work, we have proven the feasibility of the combination of AFM mechanical probing and epifluorescence recording of chemical events in 3D cardiac in vitro models. We have also proposed a best data handling and filtration method to speed up reliable and robust automatic analysis of data. This will hopefully contribute to the implementation of new and reliable integrated experimental systems, with high-information content, for cardiac in vitro models and cardiac drugs evaluation.

## 5.7 FUNDING INFORMATION

CIISB research infrastructure project LM2015043 funded by MEYS CR is gratefully acknowledged for the financial support of the measurements at the CF Nanobiotechnology. Work was supported by the projects no. LQ1601 (CEITEC 2020) and LQ1605 from the National Program of Sustainability II (MEYS CR) and by the project FNUSA-ICRC no.

CZ.1.05/1.1.00/02.0123 (OP VaVpI). Czech Science Foundation GACR supported this work with grant number GA18-24089S.

## 6 Disease phenotype description by AFM (p3)

### 6.1 Commentary

Duchenne Muscular Dystrophy (DMD is an X-linked genetic disorder leading to progressive muscle degeneration and heart failure, particularly due to dilated cardiomyopathy (DCM), which is the most common cause of death in DMD patients. While the mechanisms of muscle wasting and cardiac dysfunction in DMD are recognized, the dynamics of heart failure development remain poorly understood. Since 2014 group of Roman Panovsky pioneered cardiac Magnetic resonance in DMD patients (Panovský et al. 2019) and female carriers (Kincl et al. 2020). The DMD mouse model exhibits mild cardiac symptoms, which contrasts with the severe manifestations in humans. The present study, using patient-specific induced pluripotent stem cell-derived cardiac cells (DMD-hiPSCs) and CRISPR/Cas9-engineered dystrophin-deficient human embryonic stem cells (DMD-hESCs), investigates the molecular and functional abnormalities that contribute to cardiac dysfunction in DMD, providing new insights into the altered excitation-contraction coupling (ECC) observed in these cells.

Several independent dystrophin-deficient hPSC lines were employed, including patient-specific hiPSC and an isogenic hESC line generated via CRISPR/Cas9 gene editing. These lines were differentiated into 3D beating cardiac clusters (BCC, embryoid bodies, EBs) using a differentiation described above in section 3. AFM was used to record MCG, confocal fluorescent microscopy with Fluo4-AM was employed to monitor intracellular calcium transients; and whole-cell patch-clamp was used to measure electrophysiological action potentials. Additionally, we quantified free cardiac troponin T (cTnT) levels in the culture medium using a high-sensitivity immunochemical system to track progressive cardiomyocyte death over time. We demonstrated that DMD-derived cardiac cells lacked the full-length 427 kDa dystrophin protein and exhibited a significantly lower yield of spontaneously beating EBs compared to wild-type controls. We also showed that DMD-CMs exhibited lower differentiation efficiency, as evidenced by a reduced yield of beating embryoid bodies (EBs) compared to wild-type (WT) cells. Despite similar relative expression of known cardiac markers, DMD-CMs showed a tendency toward increased Connexin 43 expression, suggesting remodeling mechanisms in the absence of functional dystrophin, as seen in previous models of DMD. This diminished differentiation may be linked to DNA damage and errors in cell fate

determination, potentially caused by deregulated nitric oxide synthase (NOS) activity, which interferes with stem cell renewal and multipotency.

Functional analysis revealed a distinctive pathological phenotype characterized by hypocontractility (reduced contraction force), bradycardia, and increased heart rate variability. The inter-beat interval (IBI) in DMD-EBs was more variable, with increased heart rate variability, which is characteristic of early-stage cardiac dysfunction. These mechanical impairments were linked to altered calcium dynamics and voltage-gated ion channel activity, which may predispose DMD patients to arrhythmias and reduced cardiac output. Calcium transient dynamics, including prolonged rising and decay times, were observed, correlating with calcium overload due to sarcoplasmic reticulum (SR) dysfunction. There were elongated time-to-peak and a significantly higher frequency of diastolic calcium events (leaks), which contribute to arrhythmic risk.

Furthermore, while patient-specific DMD models overexpressed β-adrenergic receptors, they paradoxically exhibited a blunted response to pharmacological modulation with isoproterenol and metoprolol. Electrophysiological measurements showed that DMD-CMs and WT-CMs exhibited similar action potential (AP) properties, such as resting membrane potential, amplitude, and AP duration. Both cell types displayed various AP shapes, including atrial- and nodal-like APs. However, DMD-CMs showed an increased expression of the inward rectifier potassium channel Kir2.1, which may indicate altered AP duration and a reduced effective refractory period, potentially contributing to arrhythmias. . Interestingly, CRISPR/Cas9-modified cDMD-EBs displayed a β-adrenergic response similar to WT-EBs, suggesting a compensatory mechanism in the engineered line. This highlights a dysregulated β-adrenergic signaling pathway in DMD, which may contribute to heart failure progression. Additionally, DMD-CMs exhibited higher expression of the L-type calcium channel (LTCC) α2 subunit, suggesting a gain-of-function mechanism that could further contribute to arrhythmic risk. Finally, the detection of significantly elevated free cTnT in the medium starting from day 35 confirmed that the model effectively recapitulates the progressive cardiomyocyte wasting and death observed clinically in DMD patients.

frontiers in Bioengineering and Biotechnology

ORIGINAL RESEARCH
published: 19 June 2020
doi: 10.3389/fbioe.2020.00535

# DMD Pluripotent Stem Cell Derived Cardiac Cells Recapitulate *in vitro* Human Cardiac Pathophysiology

*Sarka Jelinkova[1,2], Aleksandra Vilotic[1], Jan Pribyl[3], Franck Aimond[4], Anton Salykin[1], Ivana Acimovic[1], Martin Pesl[1,2,5], Guido Caluori[2,5], Simon Klimovic[6], Tomas Urban[1], Hana Dobrovolna[7], Vladimir Soska[7,8], Petr Skladal[5,6], Alain Lacampagne[4], Petr Dvorak[1,2], Albano C. Meli[1,4*†] and Vladimir Rotrekl[1,2*†]*

[1] Department of Biology, Faculty of Medicine, Masaryk University, Brno, Czechia, [2] International Clinical Research Center ICRC, St. Anne's University Hospital Brno, Brno, Czechia, [3] CEITEC, Masaryk University, Brno, Czechia, [4] PhyMedExp, University of Montpellier, INSERM, CNRS, Montpellier, France, [5] First Department of Internal Medicine—Cardioangiology, Faculty of Medicine, Masaryk University, Brno, Czechia, [6] Department of Biochemistry, Faculty of Science, Masaryk University, Brno, Czechia, [7] Department of Clinical Biochemistry, St. Anne's University Hospital of Brno, Brno, Czechia, [8] Second Clinic of Internal Medicine, Masaryk University of Brno, Brno, Czechia

OPEN ACCESS

**Edited by:**
*Monica Boffito,*
*Politecnico di Torino, Italy*

**Reviewed by:**
*Monica Mattioli-Belmonte,*
*Marche Polytechnic University, Italy*
*Hannes Todt,*
*Medical University of Vienna, Austria*

***Correspondence:**
*Albano C. Meli*
*albano.meli@inserm.fr*
*Vladimir Rotrekl*
*vrotrekl@med.muni.cz*

*†These authors have contributed equally to this work*

**Specialty section:**
*This article was submitted to Biomaterials, a section of the journal Frontiers in Bioengineering and Biotechnology*

**Received:** *15 December 2019*
**Accepted:** *04 May 2020*
**Published:** *19 June 2020*

**Citation:**
*Jelinkova S, Vilotic A, Pribyl J, Aimond F, Salykin A, Acimovic I, Pesl M, Caluori G, Klimovic S, Urban T, Dobrovolna H, Soska V, Skladal P, Lacampagne A, Dvorak P, Meli AC and Rotrekl V (2020) DMD Pluripotent Stem Cell Derived Cardiac Cells Recapitulate in vitro Human Cardiac Pathophysiology. Front. Bioeng. Biotechnol. 8:535. doi: 10.3389/fbioe.2020.00535*

Duchenne muscular dystrophy (DMD) is a severe genetic disorder characterized by the lack of functional dystrophin. DMD is associated with progressive dilated cardiomyopathy, eventually leading to heart failure as the main cause of death in DMD patients. Although several molecular mechanisms leading to the DMD cardiomyocyte (DMD-CM) death were described, mostly in mouse model, no suitable human CM model was until recently available together with proper clarification of the DMD-CM phenotype and delay in cardiac symptoms manifestation. We obtained several independent dystrophin-deficient human pluripotent stem cell (hPSC) lines from DMD patients and CRISPR/Cas9-generated DMD gene mutation. We differentiated DMD-hPSC into cardiac cells (CC) creating a human DMD-CC disease model. We observed that mutation-carrying cells were less prone to differentiate into CCs. DMD-CCs demonstrated an enhanced cell death rate in time. Furthermore, ion channel expression was altered in terms of potassium (Kir2.1 overexpression) and calcium handling (dihydropyridine receptor overexpression). DMD-CCs exhibited increased time of calcium transient rising compared to aged-matched control, suggesting mishandling of calcium release. We observed mechanical impairment (hypocontractility), bradycardia, increased heart rate variability, and blunted β-adrenergic response connected with remodeling of β-adrenergic receptors expression in DMD-CCs. Overall, these results indicated that our DMD-CC models are functionally affected by dystrophin-deficiency associated and recapitulate functional defects and cardiac wasting observed in the disease. It offers an accurate tool to study human cardiomyopathy progression and test therapies *in vitro*.

**Keywords: duchenne muscular dystrophy, DMD, human pluripotent stem cells, cardiomyocytes, intracellular calcium, excitation-contraction coupling, adrenergic response, cardiomyocyte death**

## 6.2 INTRODUCTION

Duchenne muscular dystrophy (DMD, prevalence 1/3,500–6,000 boys) is an X-linked genetic disorder which impairs striated muscles and results in severe disability and premature death in young men(Mah et al. 2014) (Mah et al., 2014; Vry et al., 2016; Stehlíková et al., 2017). DMD is often associated with dilated cardiomyopathy (Manzur et al., 2008), which develops in affected patients during their teenage years. It is represented by a slowly progressing decline in diastolic function, systolic ejection fraction, and fractional shortening (Markham et al., 2006). Mechanical degeneration is associated with progressive cardiomyocyte (CM) wasting and spreading of fibrosis throughout the ventricular wall (Finsterer and Stöllberger, 2003; Panovský et al., 2019), which leads to intracardiac conduction disturbances, inducing atrial and life-threatening ventricular arrhythmias (Chenard et al., 1993; Himmrich et al., 2000). Gradual dilatation of the ventricle, thinning of the wall (Wagner et al., 2007), and consequent loss of contractility lead to repeated episodes of heart failure, which recently became the most frequent mortality cause in DMD patients worldwide (Finsterer and Stöllberger, 2003; Fayssoil et al., 2010).

DMD is caused by mutations in the dystrophin gene (*DMD*), which can result in a total lack of functional dystrophin or presence of a truncated inactive form of the protein (Blake et al., 2002). Dystrophin plays a major role in the organization of dystrophin glycoprotein complex (Clarac et al., 2009) responsible for sarcolemmal adhesion to the basal lamina and intracellular pathway regulations. Whereas, skeletal muscle degeneration is extensively studied, the cellular mechanisms of the cardiac pathophysiology are still unclear. Available studies point out the role of oxidative stress and DMD-induced $Ca^{2+}$ mismanagement (Williams and Allen, 2007; Jung et al., 2008; Caluori et al., 2019), with subsequent cytosolic imbalance and cell damage (Gerke et al., 2005).

In DMD (muscular dystrophy on X chromosome, *mdx)* mice, we have shown that dystrophin deficiency caused posttranslational remodeling of the cardiac ryanodine receptor (RyR2) macromolecular complex, due to S-nitrosylation and Calstabin2 (FKBP12.6) depletion, which leads to intracellular diastolic $Ca^{2+}$ leak and ventricular arrhythmias (Fauconnier et al., 2010).

Intracellular $Ca^{2+}$ leak from the sarcoplasmic reticulum (SR) was also associated with deregulation of stretch-activated channels (SAC) though reactive oxygen species (ROS)-mediated hyperactivity (Jung et al., 2008).

Further studies in animal models showed misregulation of other ion channels such as voltage-gated Nav1.5 and L-type calcium channel (LTCC) hyperactivation (Koenig et al., 2011), as well as upregulation of inflammation-related induced nitric oxide synthase (iNOS) (Fauconnier et al., 2010; Peterson et al., 2018). Such observations remain to be validated in human DMD. Furthermore, to this day, there are only limited studies of human DMD cardiac cell (CC) models, describing some of the discrepancies eventually leading to DMD-CM damage (Eisen et al., 2019; Pioner et al., 2020). In the present study, we thus focused, for the first time, on evaluating the impact of dystrophindeficiency on some molecular properties of the excitationcontraction coupling (ECC) and flight-or-fight response in some patient-specific DMD human pluripotent stem cell-derived cardiac cells (DMD-hPSC-CCs) as well as in CRISPR/Cas9 engineered hPSC-CCs (summarized in **Graphical abstract chapter 6.8**).

## 6.3 MATERIALS AND METHODS

A wide selection of methods was used for analysis of the model starting from generation of the hPSC lines to analysis of 3D contracting clusters and dissociated CCs; thus, the methodological approach has been summarized in **Figure 6.1**.

### 6.3.1 Cell Lines, Cultivation, Reprogramming, and hPSC Differentiation Into Cardiomyocytes via Embryoid Bodies

Patient-specific DMD human induced pluripotent stem cell (hiPSC) lines (DMD02 and DMD03) and CRISPR/Cas9 dystrophin-deficient human embryonic stem cell (hESC) line (cDMD) were used (described in Jelinkova et al., 2019a,b). The fibroblasts of two DMD patients were derived from skin/muscle (for DMD02/DMD03, respectively) biopsies. Informed consents approved by Ethics Committee (Faculty of Medicine, Masaryk University) were signed by parents of the patients beforehand and the investigation conformed to the principles outlined in the Declaration of Helsinki.

Control human embryonic stem cell (hESC) line CCTL14 (serving as isogenic control for cDMD) as well as CCTL12 hESC line (further referred to as WT hESC) derived in Masaryk University, Brno, and previously characterized (International Stem Cell Initiative et al., 2007), were used. hiPSC control line UEFhfiPS1.4 (Qu et al., 2013) and cl.4 obtained from Majlinda Lako (NewCastle, UK) (further called WT-hiPSC) were used for comparison with DMD-hiPSC to reduce the effect of reprogramming on the CC phenotype.

All human pluripotent stem cell (hPSC) lines were routinely maintained on feeder layer of mitotically inactivated mouse embryonic fibroblasts (mEF) as previously described (Dvorak et al., 2005; Krutá et al., 2014; Jelinkova et al., 2019a).

Cardiac differentiation and eventual subsequent dissociation of hPSC-CCs were performed for confocal fluorescent intracellular $Ca^{2+}$ measurements, patch-clamp, atomic force microscopy (AFM), and immunocytochemistry as previously described (Pesl et al., 2014) with minor modifications. Briefly, grown colonies were cut into pieces with a pipette tip and clumps were transferred into differentiating embryonic body (EB) medium (86% KnockOut Dulbecco modified eagle medium, 10% fetal bovine serum, 1% L-glutamine, 1% penicillin/streptomycin, 1% nonessential amino acids, 0,1mM 2-mercaptoethanol) with

10 ng/ml bone morphogenic protein 4 (BMP4, R&D) and 10 µg/ml ascorbic acid (Sigma Aldrich) where they formed EBs. After 2 days, the medium was changed into EB medium with 5 ng/ml basic fibroblast growth factor (FGF2, Peprotech), 10 ng/ml BMP4, 6 ng/ml Activin A (R&D) and 10 µg/ml ascorbic acid (Sigma Aldrich) and incubated for 4 days. The next 3 days consisted of EB medium supplemented with 10 ng/ml vascular endothelial growth factor (VEGF, R&D), 10 µM IWR1 (Sigma Aldrich), and 10 µg/ml ascorbic acid. The EBs were further cultivated in EB medium with 10 µg/ml ascorbic acid, 10 ng/ml VEGF, and 5 ng/ml FGF2 for 12 days with medium changed every 4 days, and then with EB medium with 10 µg/ml ascorbic acid until further analysis. The differentiation procedure was performed for 13 days in hypoxic conditions (5% oxygen). Then, the EBs were moved into normoxic conditions (20% oxygen) for further cultivation.

### 6.3.2 Immunodetection

Immunocytological analyses utilized [antibody specific against N-terminal (1:50 ICC/1:50-1:300 WB, Cat# NCL-DYSB, Leica Biosystems), and antibody specific against C-terminal (1:100 ICC/1:1000 WB, Abcam, Cat# ab15277)], for cardiac markers cardiac troponin T (cTnT; SantaCruz, Cat# sc-8121, 1:200) α-actinin (SigmaAldrich, Cat# A7180, 1:500) L-type channel (LTCC, dihydropyridine receptor DHPR alpha 2 subunit/CACNA2D1 antibody abcam, Cat# ab2864, 1:200), assays were performed as described previously (Krutá et al., 2013). For cTnT and α-actinin, cells were fixed using 4% paraformaldehyde at room temperature for 10-15 min. Cells for dystrophin labeling were fixed with 2% paraformaldehyde for 10 min at room temperature, then with ice cold methanol for 5 min, and incubated with pre-extraction buffer (25 mM HEPES, 50 mM NaCl, 1 mM EDTA, 3 mM MgCl2, 200 mM sucrose, 0.5% Triton X-100) before continuing to blocking steps.

The cells were permeabilized and blocked with blocking solution 1 (1% bovine serum albumin, BSA, 0.2% Triton X100 in phosphate buffer saline, PBS, 15 min on ice) and blocking solution 2 (1% BSA, 1% NaN3, 0.05% Tween 20 in PBS, 60 min on ice). Primary antibodies were diluted in PBS/Tween (0.05%) and incubated overnight at 4˚C. Samples were extensively washed with PBS/Tween (0.05%) and incubated with appropriate fluorescent secondary antibody for 1 h at room temperature. For nuclear counterstain, 4′,6-Diamidine-2′phenylindole dihydrochloride (DAPI) was used. All fluorescent and confocal microscopy experiments were performed using Confocal LSM700 microscope and processed using Zen software (both Carl Zeiss, Oberkochen, Germany). For dystrophin immunoblots, protein samples from cell lysates were run in 4–12% gradient polyacrylamide gel for 70 min/170V/400mA, blotted at 100 V/300 mA for 2 h, and labeled with antibody against dystrophin protein. After dystrophin detection, the membrane was incubated with antibody against lamin B as loading control (1:1000, Santa Cruz, sc6217). Adrenergic receptors (AR) were analyzed using β1 specific (Thermo Fisher, PA5-28808, 1:500) and β2 specific (abcam, ab137494, 1:500) antibody. Human heart atrial tissue was obtained as procedural surplus material, available during bicaval orthotopic heart transplantation from donor organs and was used as positive control as previously described (Pesl et al., 2020).

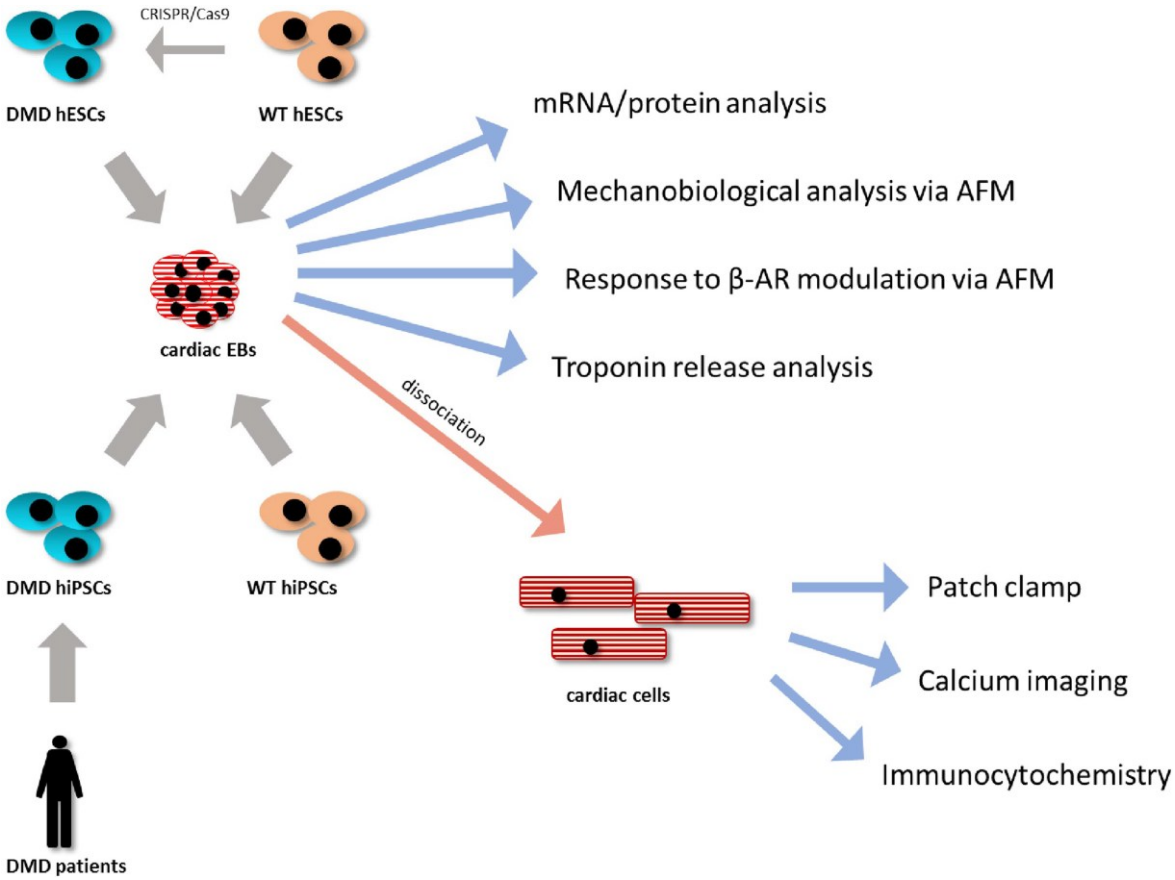



*FIGURE 6.1 Methodological approach. DMD-hiPSC lines from two Duchenne muscular dystrophy (DMD) patients were generated and analyzed compared to*

*WT-hiPSC lines. DMD-hESC line was generated using CRISPR/Cas9 technology by targetted deletion of the DMD gene from a healthy WT hESC line serving as*

*isogenic control. All hPSC lines were differentiated using 3D cell aggregates (embryonic bodies, EBs). These EBs were then used for molecular and mechanobiological analysis methods or were enzymatically dissociated into isolated cardiac cells, which were further analyzed using single cell specific analysis as protein localization and ion fluxes analyses.*

### 6.3.3 Quantitative Real-Time PCR

CardiacEBs30–50days old and human heartsamples (obtained as surplus material from donor hearts during cardiac transplantations) were lysed using RNA Blue reagent (TopBio, Prague, Czech Republic) according to the manufacturer's instructions, and the total mRNA was isolated using the RNeasy Micro Kit (Qiagen, Hilden, Germany). RNA concentration and purity were determined using NanoDrop (NanoDrop technologies, Wilmington, DE, USA). cDNA was synthesized by Moloney Mouse Leukemia Virus (M-MLV) reverse transcriptase (Invitrogen, Carlsbad, CA, USA) at 37˚C for 1 h followed by 5 min at 85˚C. For quantitative real-time PCR (qRTPCR), LightCycler® 480 SYBR Green Master kit (Roche, Basel, Switzerland) was used according to manufacturer's instructions, and PCR was performed, with annealing temperature 60˚C and 55 cycles on LightCycler LC480 Instrument (Roche). The PCR primers (Generi-Biotech, Hradec Kralove, Czech Republic) are shown in **Supplementary Table 1**.

### 6.3.4 Measurements of Intracellular Cytosolic $Ca^{2+}$ Variations by Fluorescent Confocal Microscopy

The contracting EBs were dissociated to single CCs by incubation in $Ca^{2+}$-free solution [120 mM NaCl, 5.4 mM KCl, 5 mM $MgSO_4$, 5 mM sodium pyruvate, 20 mM glucose, 20 mM taurine, 10 mM HEPES (all Sigma Aldrich), pH6.9] at room temperature and enzymatically treated with 0.8 mg/ml type II collagenase (Gibco) and 0.037 mg/ml type XIV proteinase (Sigma Aldrich) in the same solution for 3 min at 37˚C. The clusters were then incubated in dissociating solution (85 mM KCl, 30 mM $K_2HPO_4$, 5 mM $MgSO_4$, 1 mM EGTA, 5 mM sodium pyruvate, 5 mM creatine, 20 mM taurine, 20 mM glucose, 2 mM disodium pyruvate, pH = 7.4) for 20 min at 37˚C and plated on gelatin coated 35 mm glass bottom culture dishes (MatTek) in EB medium until the next day. On the day of measurements, cells were incubated in a Tyrode's solution (140 mM NaCl, 5 mM HEPES, 4 mM KCl, 1 mM $MgCl_2$, 1.8 mM $CaCl_2$, 10 mM glucose, pH 7.4) with 3 μM Fluo4-AM (Invitrogen, Carlsbad, CA, USA) for 20 min at room temperature. After the incubation with Fluo4-AM, the solution was replaced with the fresh Tyrode's solution and the cells were placed on the stage of an inverted microscope. $Ca^{2+}$ images in line-scan mode were recorded with a laser scanning confocal microscope Zeiss LSM Exciter (Carl Zeiss), with 40x water immersion objective, in x–y mode, 1 image/0.495 s. Electrical pacing was set up with frequency 0.5, 1 Hz (20 V, 0.5 ms duration and 1 ms delay).

The kinetic properties of intracellular $Ca^{2+}$ variations including $Ca^{2+}$ transients and diastolic events were analyzed by inhouse developed PeakInspector software (https://asalykin.github.io/PeakInspector/) as previously described (Acimovic et al., 2018).

### 6.3.5 Electrophysiological Recordings Through Patch-Clamp

Electrophysiological recordings were obtained using whole-cell patch-clamp technique on an Axopatch 200B (Axon Instruments, Foster City, CA) at room temperature (22–24˚C). The recording pipettes contained: 120 mM KCl, 8 mM EGTA, 10 mM HEPES, 6.8 mM $MgCl_2$, 3 mM $CaCl_2$, 4 mM $ATPNa_2$, 0.4 mM $GTPNa_2$ (pH 7.2). The bath solution contained: 130 mmol/L NaCl, 4 mM/L KCl, 1.8 mM/L $MgCl_2$, 1.8 mM/L $CaCl_2$, 10 mM/L HEPES, 11 mM/L glucose (pH 7.4). Action potentials (APs) were measured in the current-clamp configuration in response to brief (1–2 ms) depolarizing current injections at 1 Hz. The resting membrane potential, the amplitude and duration (APDs) at 20, 50, and 90% repolarization of the APs were measured

(respectively indicated as $APD_{20}$, $APD_{50}$, and $APD_{90}$). 7 DMDhPSC-derived CCs (DMD-CCs) and 18 WT-hPSC-derived CCs (WT-CCs) were analyzed. Cells arrhythmogenicity was tested using application of successive 10 s runs in the current clamp configuration defined by 5 brief (1 ms) depolarizing current injections at 2 Hz followed by a resting period. Data were analyzed using the Clampfit 10.0 (Axon Instruments) software.

### 6.3.6 Atomic Force Microscopy Measurements

Atomic force microscope (JPK NanoWizard 3, JPK, Berlin, Germany), combined with an inverted light microscope (IX-81S1F-3, Olympus, Tokyo, Japan), was used to obtain mechanocardiograms of beating EBs as previously described (Pesl et al., 2014; Caluori et al., 2019; Pribyl et al., 2019). Drug response tests were performed after initial equilibration in Tyrode's solution, followed by addition of 70 µM metoprolol, 10 min of stabilization time, and then 10 min of measurement. Isoproterenol (1 µM) was subsequently added into the solution, and mechanocardiograms were measured after 20 min of stabilization. The mechanical properties of beating EBs were expressed as force of contraction in nN as previously described (Pesl et al., 2014); however, the values were relativized for final comparison.

### 6.3.7 Free Troponin Analysis

The EBs were formed and cardiac induction was initiated as described above. On day 18, individual EBs homogenous in size and shape were separated onto 12 well plate coated with gelatin and 1ml of proper induction medium was added. From day 21 to 51 with frequency of 4 days, medium sample was collected, spun, and the supernatant frozen in −20˚C until all samples were harvested. The samples were then analyzed for free troponin T concentration using two epitopes based immunochemical system Cobas e602 (Basel, Switzerland) specifically high sensitive short turnaround time (STAT) kit Elecsys Tropo T hs STAT 100 (Roche diagnostics, Basel, Switzerland; Hess et al., 2008) according to the manufacturer's instructions.

### 6.3.8 Statistical Analysis

Statistical evaluation was carried out in GraphPad Prism 8.3 software (GraphPad Software, Inc., La Jolla, CA, USA). Available normality tests were performed for the obtained data, and Student's two-tailed *t*-test or ANOVA was used to assess statistically significant differences on normally distributed group pairs. Where normality tests failed, non-parametric tests were used. Individual statistical test used was specified in individual figure legends.

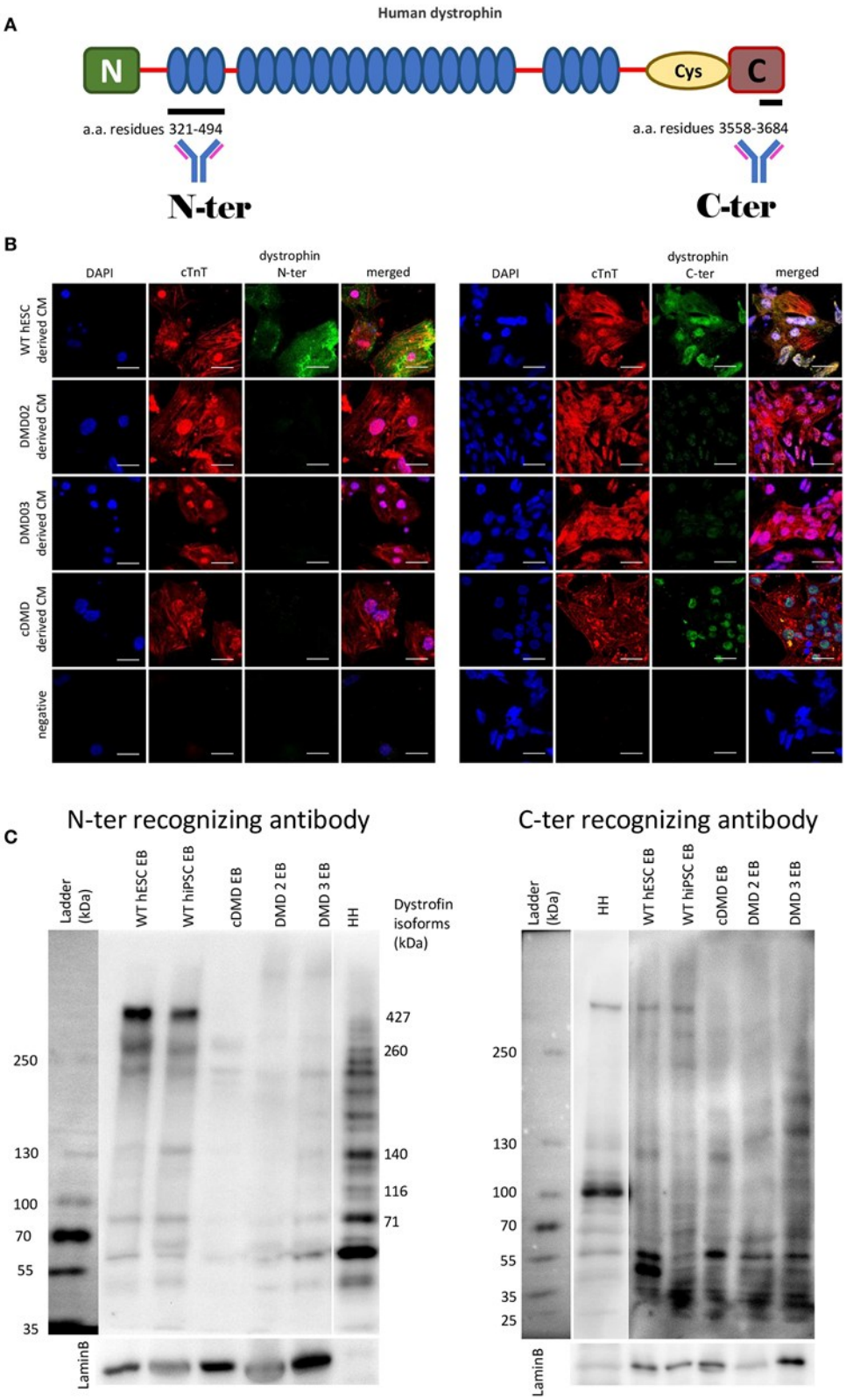
## 6.4 RESULTS

### 6.4.1 DMD-CCs Do Not Express Full-Length Dystrophin Protein

Three previously described patient-specific DMD-hiPSC and one CRISPR/Cas9-mediated DMD-hESC lines (Jelinkova et al., 2019a,b) were differentiated into CMs (Pesl et al., 2014). WT hESC [hESC CCTL12 (hPSCreg name MUNIe005-A, passages 15–61) and CCTL14 (hPSCreg name MUNIe007-A, passages 15–63) derived in Masaryk University, Brno, and characterized previously (International Stem Cell Initiative et al., 2007)] and WT-hiPSC [cl.4 (passages 43–84) obtained from Dr. Majlinda Lako (Newcastle University, UK) (Armstrong et al., 2010) and hfiPSC (passages 20–52) (Qu et al., 2013)] were used as controls. The obtained DMD-CCs were evaluated for dystrophin presence. The strategy for antibody detection is illustrated in **Figure 6.2A**. Dystrophin expression was evaluated using immunocytology with specific antibodies against high molecular weight isoform of dystrophin (antibody specific to Nterminus detecting the full-length 427 kDa isoform, **Figure 6.2B**, left panel), as well as

shorter isoforms (antibody specific to C-terminus, which is present in various lower molecular weight dystrophin isoforms, **Figure 6.2B**, right panel). Dystrophin expression was observed with both antibodies in WT-CCs as membranous signal of the antibody (**Supplementary Figure 2**). No membranous/cytoplasmic protein signal was detected in any DMD-CCs (**Figure 6.2B**). Nuclear signal of dystrophin was detected by C-ter antibody (which can detect shorter dystrophin isoforms, most likely the Dp71 isoform), and no cytoplasmic/membranous signal was observed in CCs derived from either DMD-hPSC lines. Furthermore, western blot analysis with N-ter and C-ter antibodies showed expression of some shorter dystrophin isoforms (Dp140, Dp116, and Dp71) in the DMD cell lines, but none in the full high molecular band (Dp427) (**Figure 6.2C**, full membranes in **Supplementary Figure 2**).

*FIGURE 6.2 DMD-hPSC differentiate into cardiac cells (CCs), which do not express dystrophin. (A) Antibodies against dystrophin N-terminal (N) aminoacid (a.a.) residues 321–494 and C-terminal aminoacid residues 3558–3684 were used. (B) hPSC derived CCs were analyzed for presence of dystrophin (in green). WT hESCderived CCs dissociated from spontaneously beating EBs presenting with positive signal for cardiac troponin T (red) showed positive signal for dystrophin labeled by N-terminus specific antibody as well as by C-terminus specific antibody. None of the DMD-hPSC lines (DMD02, DMD03, and cDMD) derived CCs showed any signal for dystrophin. DAPI was used for nuclear counterstain. Ruler represents 50 μm. (C) The differentiated EBs were lyzed and western blot analysis was performed to identify the individual isoforms expressed. Both used WT-hPSC derived EBs show expression of various dystrophin isoforms including Dp427, Dp260, Dp140, and Dp71. The CRISPR/Cas9 generated cDMD-EBs show no expression of either isoform, while only shorter isoforms were identified in patient DMD-hiPSC-EBs with promoters downstream of the patient's mutations. Human heart tissue (HH) was used as positive control. LaminB was used as loading control*


A
Human dystrophin
N
Cys
C
a.a. residues 321-494
a.a. residues 3558-3684
N-ter
C-ter
B
DAPI
cTnT
dystrophin N-ter
merged
DAPI
cTnT
dystrophin C-ter
merged
WT hESC derived CM
DMD02 derived CM
DMD03 derived CM
cDMD derived CM
negative
C
N-ter recognizing antibody
C-ter recognizing antibody
Ladder (kDa)
WT hESC EB
WT hiPSC EB
cDMD EB
DMD 2 EB
DMD 3 EB
HH
Dystrofin isoforms (kDa)
427
260
140
116
71
250
130
100
70
55
35
25
LaminB

### 6.4.2 Dystrophin Deficiency Leads to Cardiac Differentiation With Lower Yield of Spontaneously Beating EBs

Next, we aimed at characterizing the impact of dystrophin deficiency on the cardiac differentiation of hPSCs through the EB-based method as previously published (Pesl et al., 2014). We compared the yield of beating EBs upon differentiation of all DMD and WT-hPSC lines. First of all, we used the spontaneous beat in 3D EB clusters as a criterion to evaluate the cardiac differentiation success. The differentiation efficacy represented by the fraction of spontaneously beating EBs (detected at day 29 after cardiac differentiation start) was decreased in DMDEBs compared to WT-EBs (**Figure 6.3A**, statistical evaluation in **Supplementary Table 6.2**). At the cellular level, the beating EBs from all tested cell lines contained CCs (**Figure 6.3B**) with striated pattern of cardiac troponin T (cTnT) and α-actinin. The differentiation efficacy was also measured in age-matched groups of DMD- and WT-EBs aged 25–29 days by qRT-PCR of well-known cardiac markers [*NKX2.5 (p* = 0.42*)*, myosin heavy chain α (*MYH6*, *p* = 0.71), myosin heavy chain β (*MYH7, p* = 0.82), myosin light chain 2 (*MYL2, p* = 0.17), myosin light chain 7 (*MYL7, p* = 0.42), ryanodine receptor 2 (*RYR2*, *p* = 0.61), cardiac muscle alpha actin (*ACTC1, p* = 0.78), connexin43 (*GJA1, p* = 0.36)], showing no significant difference in relative mRNA expression. However, a tendency for lower yield of most of the markers in the obtained DMD clusters was observed, with the exception for *MYH7* and *GJA1* (**Figure 3C**). Inward rectifier potassium channels Kir2.1, Kir2.2, and Kir2.3 were also tested (*KCNJ2*, *KCNJ4*, and *KCNJ12*, respectively) with significant increase in Kir2.1 expression (*p* = 0.004); SERCA (*ATP2A*) shows no difference in mRNA expression.

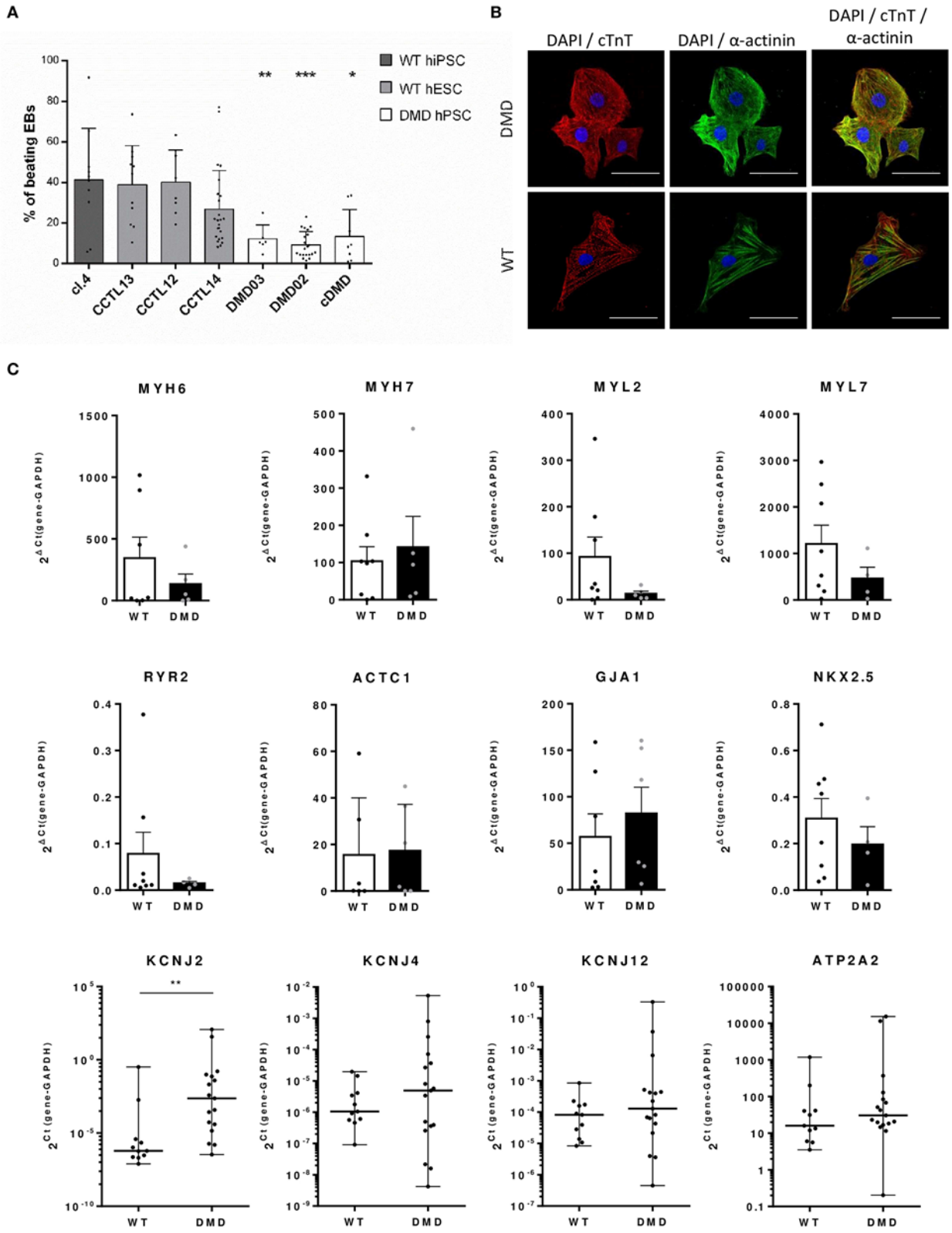



*FIGURE 6.3 Differentiation efficacy is lower in DMD-hPSC lines. (A) All DMD-hPSC and WT-hPSC lines were differentiated into spontaneously contracting EBs containing*

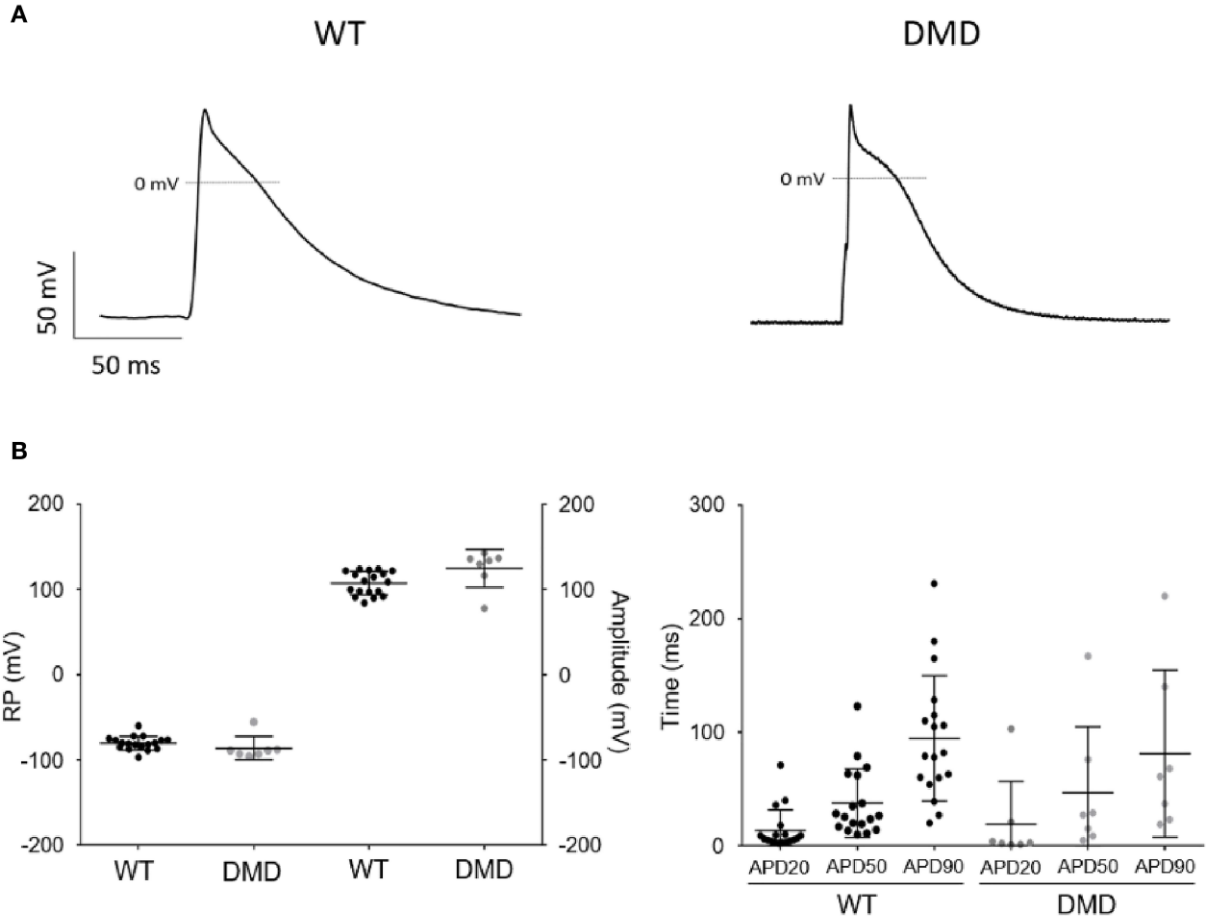
*cardiomyocytes and cardiac cells. The ratio of these spontaneously contracting clusters was evaluated and compared to wild-type (WT) controls (n = 36 for CCTL14 EBs, n = 8 for CCTL12 EBs, n = 13 for CCTL13, n = 12 for cl.4 EBs, n = 25 for DMD02 EBs, n = 6 for DMD03 EBs, n = 19 for cDMD-EBs). Lesser yields of beating EBs were identified in all DMD-hPSC lines. Statistical difference was calculated by one-way ANOVA and multiple comparison with Dunn's test. Significance (*p < 0.05, p < 0.01, *p < 0.01) is visualized as asterisks for the lowest values; for individual p-values, see Supplementary Table 1. (B) EBs were dissociated and cells labeled for cardiac markers α-actinin (in green) and cardiac troponin T (cTnT, in red) (DAPI is labeling the nuclei). WT and DMD-CCs presented similar level of typical striated pattern of sarcomeres. Line represents 50 µm. (C) Differentiation efficacy was evaluated by rt qPCR on mRNA levels of cardiac markers showing only non-significant differences in expression of various markers (MYH6, n = 7 for WT and n = 5 for DMD; MYL2, n = 8 for WT and n = 4 for DMD; MYL7, n = 8 for WT and n = 4 for DMD; RYR2, n = 8 for WT and n = 4 for DMD; ACTC1 n = 6 for WT and n = 5 for DMD; NKX2.5, n = 8 for WT and n = 4 for DMD, ATP2A2, n = 11 for WT and n = 17 for DMD) and non-significant increase in MYH7 (n = 8 for WT and n = 5 for DMD) and GJA1 (n = 7 for WT and n = 6 for DMD). Potassium channels were analyzed using Kir2.x isoforms mRNA expression (KCNJ2 – Kir2.1, KCNJ4 – Kir2.2 and KCNJ12 – Kir2.3, for all n = 11 for WT and n = 17 for DMD). Statistical significance on pooled DMD and pooled WT data sets was calculated using Mann–Whitney test; exact value for each is represented by • in each graph.*

### 6.4.3 DMD-CCs Display Altered Electrophysiological Properties

Next, we tested whether dystrophin deficiency alters the cardiac electrophysiological properties and arrhythmogenicity of single hPSC-derived CCs. Action potential (AP) properties (resting membrane potential (RP), amplitude, and duration (APD) in DMD- (26–46 days old) and WT-CCs (36–41 days old) were recorded using the patch clamp technique. Age matching of the CCss was not possible in this instance due to technical reasons as only a limited number of CCs were analyzed. Both DMD- and WT-CCs mostly exhibited triangular-shaped APs with various APD90 durations ranging from 20 to 380 ms (**Figures 6.4A,B**) similarly to WT with measured APD90 ranging from 20 to 520 ms. More occasionally, plateau-shaped APs with longer (>300 ms) APD90 durations were observed (**Figures 6.4 A, B**, **Supplementary Figure 7**). No significant difference was observed in RP, amplitude, and durations between DMD- ($n$ = 7)

and WT-CCs ($n$ = 18) APs (**Figure 6.4B**). Occurrence of fast pacing induced delayed afterdepolarization (DAD) events was observed and quantified. No difference ($p$ = 0.25) between DMD-CCs (50%; 1.2 ± 0.3 events/10 s, $n$ = 7) and WT-CCs (35%; 1.9 ± 0.4 events/10 s, $n$ = 18) in the occurrence of DAD was observed (**Figure 6.4C**).

*FIGURE 6.4 AP recordings showed no difference in WT and DMD-CCs. (A) Representative AP recordings obtained from WT and DMD-hiPSC derived CCs, under current clamp configuration. (B) Scatter plot of RP (mV) and amplitude (mV) (left) and APD 20, 50, and 90 durations (right) of WT (n = 18) and DMD (n = 7) hPSC-CCs are represented. No significant difference was observed among these parameters between WT and DMD-hPSC-CCs. Exact n value for each is represented by • in each graph. Mean ± SEM are represented. (C) Representative arrhythmic events recorded in WT-CCs (left) and DMD-CCs (right). Upper panels show representative recordings of non-arrhythmogenic cells from WT-CCs and DMD-CCs and bottom panels show representative recordings of arrhythmogenic cells showing extra events, such as DAD (Asterisks).*


A
WT
DMD
0 mV
0 mV
50 mV
50 ms
B
200
100
0
-100
-200
RP (mV)
Amplitude (mV)
WT
DMD
WT
DMD
300
200
100
0
Time (ms)
APD20
APD50
APD90
APD20
APD50
APD90
WT
DMD
C
WT
DMD
20 mV
1 sec

### 6.4.4 DMD-CCs Exhibit Abnormal Intracellular $Ca^{2+}$ Handling

Intracellular SR $Ca^{2+}$ handling has been shown to be affected in several DMD models, in particular through RyR2 mediated $Ca^{2+}$ leak (Andersson and Marks, 2010; Fauconnier et al., 2010; Andersson et al., 2012). Using confocal fluorescent microscopy as we previously showed in hPSC-CCs (Pesl et al., 2014; Acimovic et al., 2018), we investigated the enzymatically dissociated single cell $Ca^{2+}$ handling in DMD and WT-CCs matched between 40 and 50 days after differentiation. We chose this age as a safe timepoint to interpret the eventual differences as prevalently caused by the DMD mutation: it is in fact reported that calcium machinery in hPSC-CCs reaches a "stationary state" between 21 and 30 days after induction (Hwang et al., 2015). We acquired intracellular $Ca^{2+}$ transients in resting state and under physiological pacing conditions (0.5 and 1 Hz). We analyzed spontaneous frequency of calcium transients, together with their time parameters, and occurrence of secondary small diastolic calcium events possibly triggering increased automaticity.

A lower frequency was observed in the major $Ca^{2+}$ transients in DMD- compared to WT-CCs in resting conditions (1.262 ± 1.608 Hz vs. 2.416 ± 3.441 Hz respectively, $p < 0.0001$). $Ca^{2+}$ transient dynamics resulted altered in DMD single CCs: either in resting or in paced conditions, the time to peak, dependent on the SR $Ca^{2+}$ release properties, was significantly elongated in dystrophin deficient cells ($p < 0.0001$, **Figure 5A**). $Ca^{2+}$ transient

decay time, expression of the features of calcium reuptake, was increased in DMD in resting state (+59.24 ms average increase, $p = 0.013$, **Figure 5B**); this prolongation was non-significant in pacing conditions. Transient duration, which determines the contraction cycle and possible $Ca^{2+}$-induced arrhythmogenicity, was also elongated in DMD-CCs (**Figure 5C**; 63.53 ms in resting state, $p = 0.002$, and 71.51 ms under 0.5 Hz pacing, $p = 0.025$). These data suggest that the lack of dystrophin affects DMDCCs during spontaneous and triggeed SR $Ca^{2+}$ release, affecting overall calcium dynamic.

We then observed and quantified the occurrence of secondary small-amplitude $Ca^{2+}$ release events occurring after a main transient during diastole (relaxation and baseline, **Figure 5D**) and found significantly increased frequency of these events in DMD-CCs ($p = 0.0172$, **Figure 5E**).

### 6.4.5 Aberrant L-Type Voltage-Dependent $Ca^{2+}$ Channel Expression in DMD-CCs

To further understand how dystrophin deficiency affects $Ca^{2+}$ homeostasis and ECC in DMD-CCs, we verified the expression pattern of LTCCs using dihydropyridine receptor (DHPR) α2 subunit/CACNA2D1 antibody. At the protein level, DHPR α2 subunit expression was increased in patient-specific DMDCCs (DMD02 and 03, **Figure 5F**). No difference was observed on the mRNA level of the CACNA1C (encoding Cav1.2) or CACNA1D (encoding Cav1.3) between the WT and DMD groups (**Figure 5G**). We then tested the cellular localization of the L-type channels using DHPR immunostaining. In line with previous protein analysis, DMD-CCs (detected by cTnT labeling) showed stronger signal of the LTCC, and no other difference was detected (**Figure 5H**).

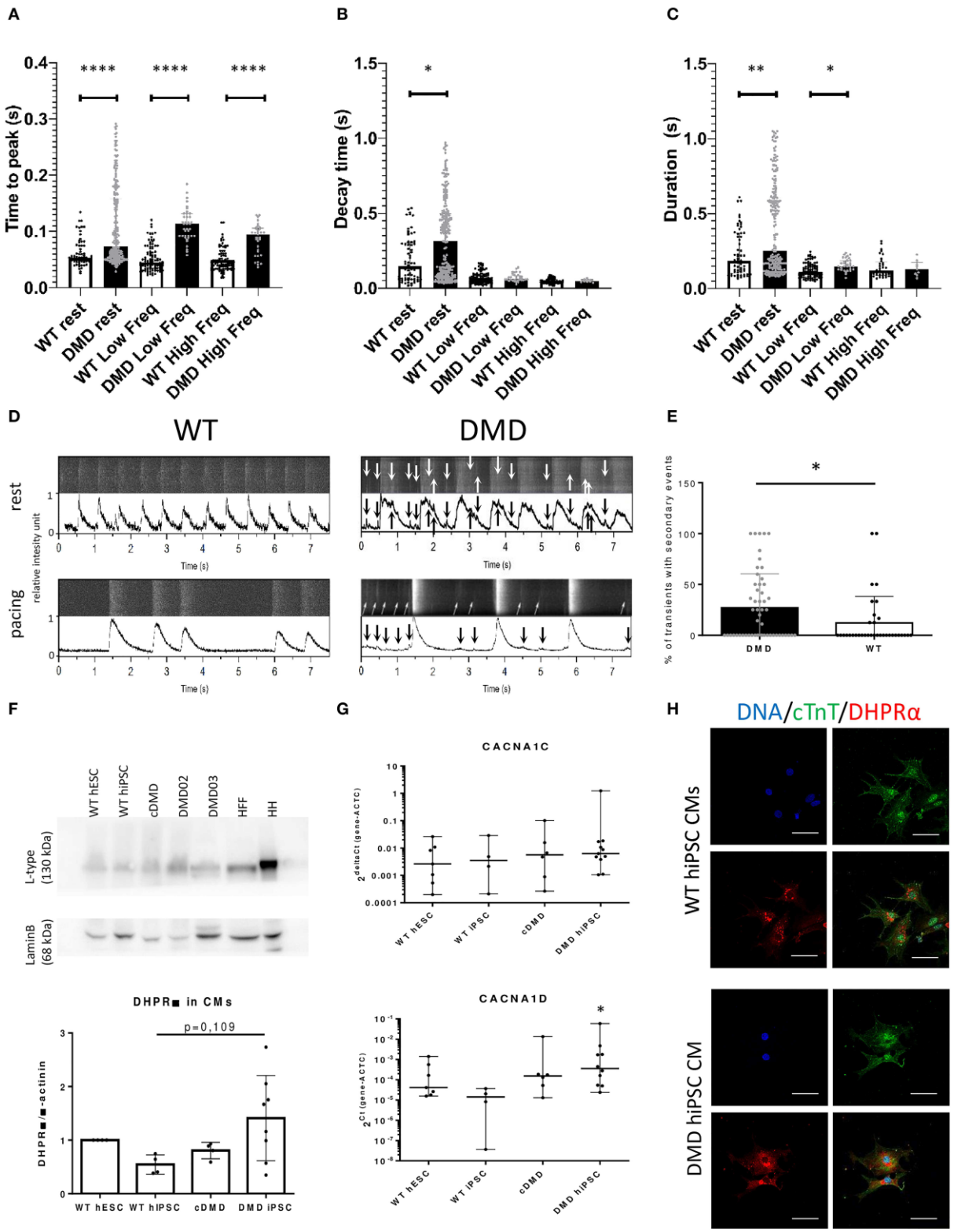

A
Time to peak (s)
0.4
0.3
0.2
0.1
0.0
****
****
****
WT rest
DMD rest
WT Low Freq
DMD Low Freq
WT High Freq
DMD High Freq
B
Decay time (s)
1.5
1.0
0.5
0.0
*
C
Duration (s)
1.5
1.0
0.5
0.0
**
*
D
WT
DMD
rest
pacing
relative intesity unit
Time (s)
E
% of transients with secondary events
150
100
50
0
*
DMD
WT
F
WT hESC
WT hiPSC
cDMD
DMD02
DMD03
HFF
HH
L-type (130 kDa)
LaminB (68 kDa)
DHPR■ in CMs
p=0,109
DHPR■/■-actinin
WT hESC
WT hIPSC
cDMD
DMD iPSC
G
CACNA1C
2^-delta Ct (gene-ACTC)
WT hESC
WT iPSC
cDMD
DMD hiPSC
CACNA1D
2^-Ct (gene-ACTC)
*
H
DNA/cTnT/DHPRα
WT hiPSC CMs
DMD hiPSC CM

*FIGURE 6.5 The dynamics of Ca2+ release and re-pumping is affected by dystrophin deficiency. Release of Ca2+ transients was measured using Fluo4 dyes in enzymatically dissociated DMD (91 cells and n = 278 transients were analyzed for resting conditions; 20 cells and n = 83 transients were analyzed for low frequency paced at 0.5Hz) and WT-CCs (30 cells and n = 262 transients were analyzed for resting conditions; 15 cells and n = 128 transients were analyzed for low frequency paced at 0.5Hz) in the age 40–50 days of differentiation. (A) Time to peak, (B) decay time, and (C) contraction duration time were analyzed for the main Ca2+ transients. The DMD-CMs showed significantly higher Ca2+ amplitude and longer time to release and repump/extrude the Ca2+ back into the SR/out of the cell in comparison to WT. The exact values are plotted in the graphs; red line represents the median. Significance (*p < 0.05) is visualized as asterisks as calculated by Mann–Whitney one-sided test (*p < 0.05, p < 0.01, p < 0.0001). The Ca2+ leakage is demonstrated by Ca2+ events of low-amplitude (arrows) among the main Ca2+ transients [D—the obtained data from microscope with line scanning (upper bar) and transferred into peak graph by PeakInspector (lower bar) with and without electrical pacing of 0.5Hz]. The occurrence of these small events is increased in DMD-CCs transients (E) as analyzed by Mann–Whitney test (n = 54 and n = 35 analyzed cells, for DMD and WT, respectively). (F) L-type channel (DHPR subunit) expression was characterized, showing non-significant increase in protein expression in DMD-hiPSC compared to WT-EBs as calculated by one-way ANOVA (n = 4, n = 4, n = 4 and n = 8 for WT hESC, WT-hiPSC, cDMD, and DMD-hiPSC-EBs). HH was used as positive control, HFF (human foreskin fibroblasts) as non-CM cell sample. (G) CaV isoform's (CACNA1C and CACNA1D) mRNA expression of LTCC subunits were analyzed using rt qPCR showing no difference between the groups. The values were calculated for CMs using ACTC for normalization. At least three biological repetitions were used for the analysis with exact value for each represented by • in the graph. Statistical difference was calculated using one-way ANOVA. (H) ICC analysis showed stronger signal for LTCC (in red) in DMD-hiPSC CCs recognized by cTnT labeling (in green). Line represents 50μm.*

### 6.4.6 DMD-EBs Display Hypocontractility, Bradycardia, and Higher Heart Rate Variability

DMD-associated dilated cardiomyopathies is characterized by thinner left ventricle, reduced cardiac output, and hypocontractility of the heart (Hajjar et al., 1993; Bondue et al., 2018; Amedro et al., 2019). We thus tested whether DMDCCs contained in 3D cardiac clusters (EBs) exhibit weaker contractile properties by measuring the contraction force and beat rate by AFM as we previously published (Pesl et al., 2014, 2016; Acimovic et al., 2018). We observed weaker spontaneous contraction force in DMD-EBs (**Figure 6.6 A**, $p < 0.0001$) while they exhibited similar overall beat rate compared to WT-EBs (**Figure 6.6 B**, $p = 0.139$; for separate data of each line, see Supplementary **Figure 6.6**). We noticed a peculiar variability in the inter-beat interval (IBI, **Figure 6.6 C**, $p = 0.0039$) (examples of AFM curves are shown in **Supplementary Figure 6.6 A**) across the different samples. While WT-EBs showed consistent IBI with few exceptions, DMD-EBs showed high heterogeneity (**Figure 6.6 C**, **Supplementary Figures 6.5 B–D**). We observed not only different variability in recorded IBI but also prevalence in shorter IBI in WT-EBs compared to DMD-EBs (1 ± 1.0 s, and 0.96 ± 0.35 s for WT-hESC- and hiPSC-EBs respectively, 2.4 ± 1,6 s for DMD02EBs, 2.1 ± 1.2 s for DMD03-EBs and 1.9 ± 1.2 s for cDMD-EBs, *p*-values in **Supplementary Table 3**) (**Figures 6.6 D–G**).

Moreover, DMD-EBs displayed more dispersed IBI scatter plot and histogram than WT-EBs (**Figures 6.6 H,I**). Using representative Poincaré plots, a quantitative measure of the evolvement in time of the IBI, we found more scattered inter-contraction pattern in DMD-EBs compared to WT-EBs (**Figures 6.6 J,K**) showing a higher beat rate variability.

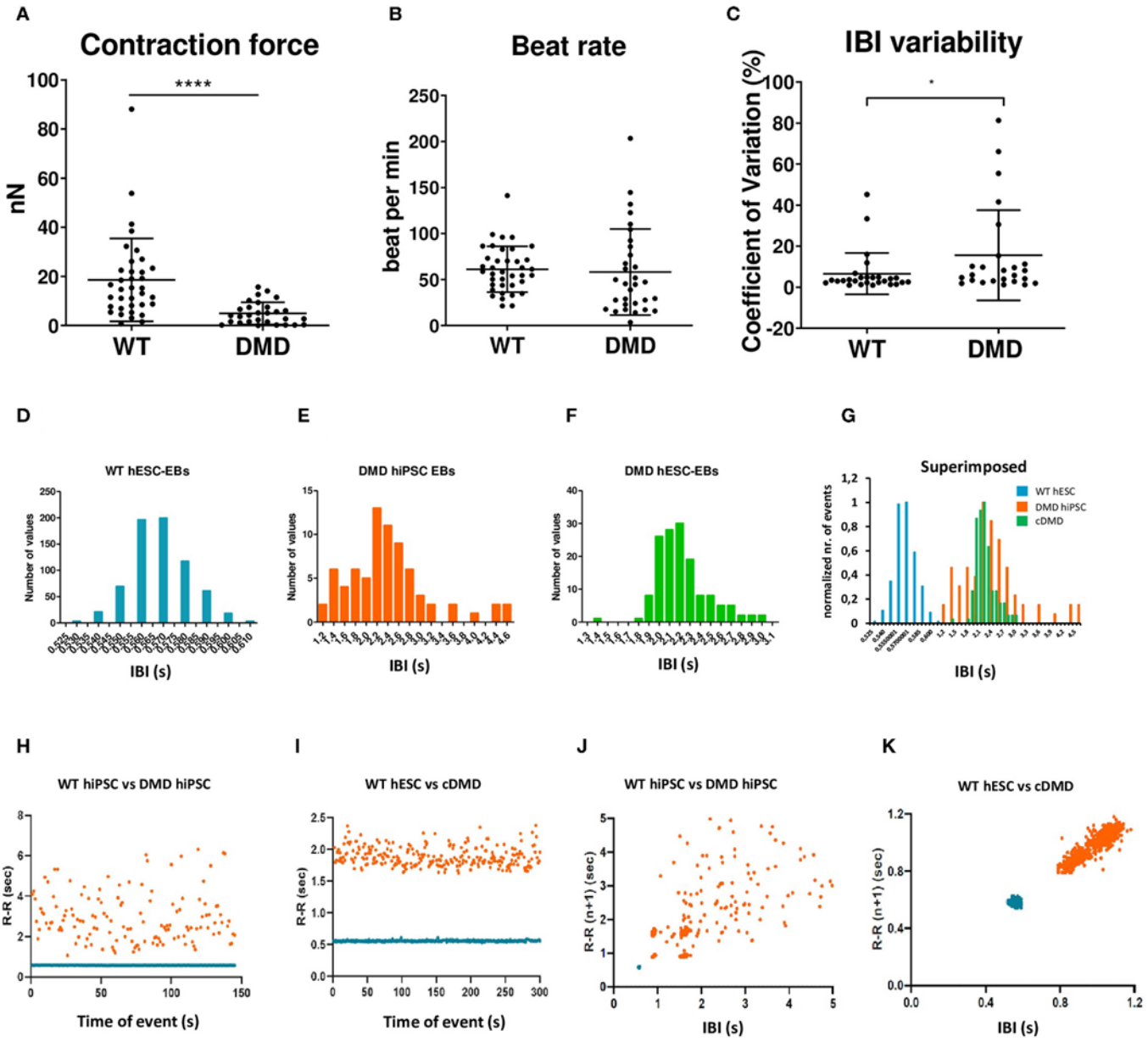



*FIGURE 6.6 The spontaneously contracting EBs lacking dystrophin showed weaker contraction force and signs of arrhythmias. The EBs were analyzed by AFM-based methods. (A,B) Contraction force is decreased in DMD-hPSC derived EBs (n = 36 for WT, n = 29 for DMD-EBs), beat rate is not affected by DMD mutation (n = 38 for WT, n = 31 for DMD-EBs). The statistical difference was calculated by Mann-Whitney test (*p < 0.05, p < 0.0001). At least five biological repetitions were used in each differentiated line; exact value for each is represented by • in each graph. Beat rate variability was identified in DMD-EBs. Graph shows coefficient of variation analysis (C) of pooled control and DMD groups. The data were cleaned of outliers by ROUT test (q = 1%), and normality was tested by available*

*tests showing non-normal distribution. Statistical difference was calculated using Mann–Whitney test. Representative IBI histograms of control (D, n = 712 peaks of the representative EB analyzed), DMD-hiPSC (E, n = 76 peaks of the representative EB analyzed), and DMD-hESC (F, n = 165 peaks of the representative EB analyzed) EBs and superimposed example of all three groups with normalized values (G). Superimposed representative inter-beat-interval (IBI) scatter plots of control hiPSC with DMD-hiPSC-EBs (n = 145 time points for each EB) (H) and control hESC with DMD-hESC-EBs (n = 334 time points for each EB) (I). Superimposed Poincaré plots of control hiPSC with DMD-hiPSC-EBs (J, same representative EBs as in H) and control hESC with DMD-hESC-EBs (K, same representative EBs as in I).*

### 6.4.7 Loss of Dystrophin Leads to β-Adrenergic Remodeling and Cardiomyocyte Wasting

Dystrophin-deficient mouse CMs have been shown to display aberrant response to β-AR stimulation (Li et al., 2014). Thus, we evaluated the β-adrenergic response in DMD-EBs to investigate the effect of stress. We monitored the mechanobiological properties of the contracting clusters upon a selective β1-AR inhibitor (metoprolol, METO) followed by a non-selective β-AR activator (isoproterenol, ISO). In presence of METO, the WThPSC-EBs exhibited a significant decrease in contraction force ($p = 0.0042$ for WT hESC, $p = 0.0156$ for WT-hiPSC) and beat rate ($p = 0.0051$ for WT hESC, **Figures 6.7A,B**). DMD-hiPSCEBs showed no response in beat rate nor contraction force to modulation by ISO nor METO. cDMD-EBs showed a response in contraction force to METO application similarly to its isogenic control ($p = 0.0003$ for contraction force and $p = 0.103$ for beat rate). WT-EBs responded to subsequent β-adrenergic stimulation by ISO application (partially competing with METO) through marginally significant increase in relative contraction force ($p = 0.0596$ for WT hESC, $p = 0.03$ for WT hiPSC, **Figure 6.7A**),

DMD-EBs did not show statistically significant responses to ISO nor METO. cDMD-hESC line, however, responded similarly to its isogenic WT control in contraction force increase (with significant change in response to modulation, $p = 0.0039$). The pharmacokinetic answer to ISO has been additionally tested by exclusion of METO response using division of Tyrode and ISO value still showing response in WT-EBs ($p = 0.0021$) with no significant change in DMD-EBs ($p = 0.1309$) (as shown in **Supplementary Figure 4C**).

These mechanobiological data suggest that the DMD-EBs exhibit much weaker response to stress conditions in presence of β-AR modulation. Thus, we compared the expression of the β1, β2, and β3 AR at the protein level between DMD- and

WT-EBs. While DMD-EBs derived from patient hiPSC showed increased β1 ($p = 0.0103$) and β2 AR expression ($p = 0.0162$) compared to isogenic WT-EBs, cDMD-EBs show similar or lower expression of both (**Figures 6.7C–E**). β3 expression was analyzed by quantitative rt qPCR showing no significant differences in between WT- and DMD-EBs (**Supplementary Figure 4D**).

A pathological overexpression of β-AR together with the blunted drug response and hypocontractility above described lead us to ask whether our derived CCs are already undergoing complex changes leading to their death, with consequential depletion and mechanical function deterioration in our 3D model. Thus, CC death was quantified, over time after differentiation, via cTnT concentration in the culture medium, originating from the dying CCs in the EBs. DMD lines showed from day 35 a significantly increased free cTnT level in their medium, compared to WT samples (**Figure 6.7F**, statistical evaluation in **Supplementary Table 4**). Interestingly, the DMDEB kept beating even late after cardiac induction, even over the observed increased CM death (**Supplementary Video 1**).

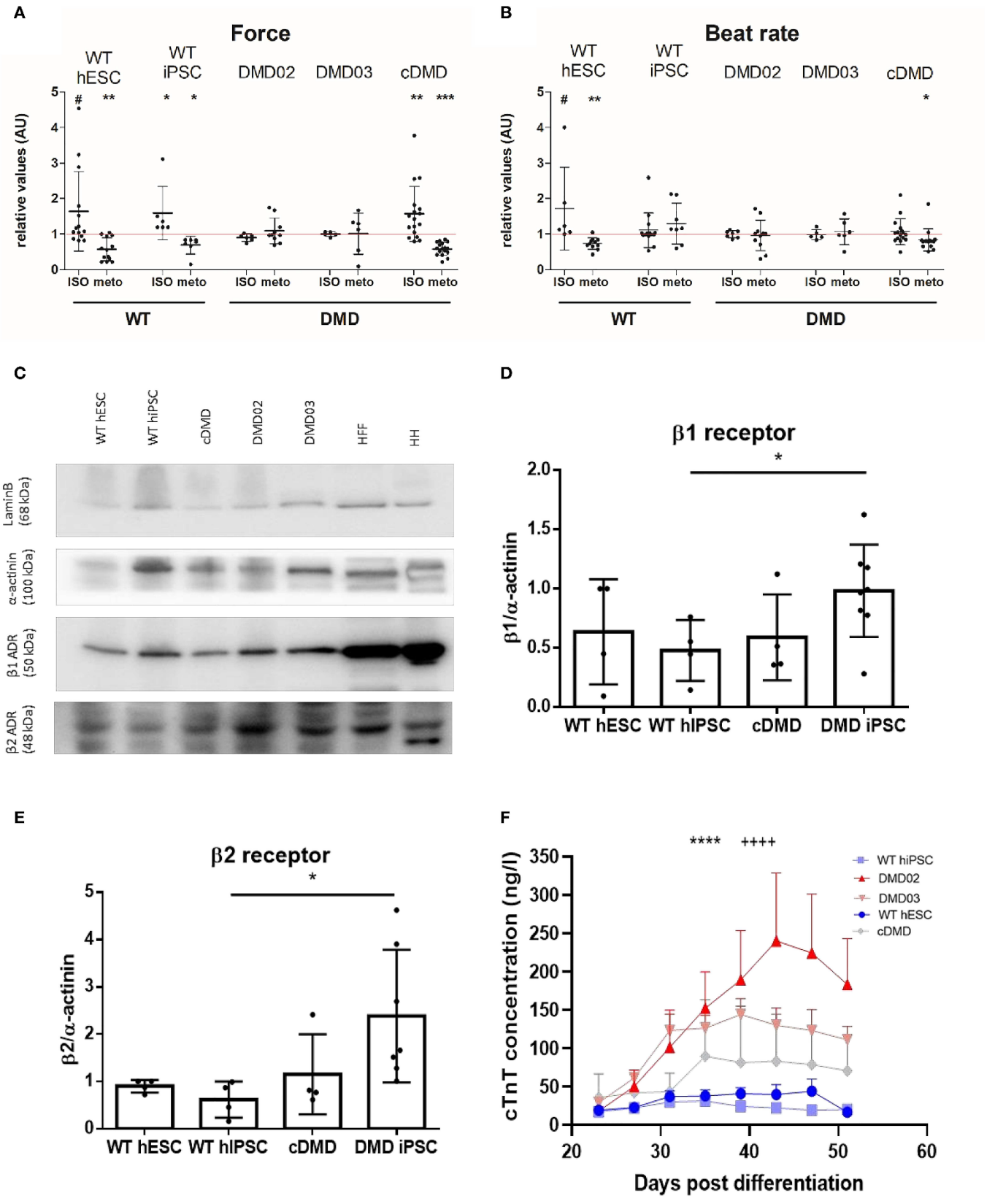



*FIGURE 6.7 DMD-CCs show remodeled b-adrenergic response and increased death. The contraction force and beat rate were measured using an AFM-based method and tested for b adrenergic response with isoproterenol (ISO, activator) and metoprolol (METO, inhibitor)*

*(A). WT-CMs show increase in contraction force (n = ISO/METO: n = 14/13 for WT hESC, n = 6/7 for WT-hiPSC-EBs, n = 6/10 for DMD02 EBs, n = 5/6 for DMD03 EBs, n = 17/17 for cDMD-EBs, exact value for each is represented by • in each graph) and (B) beat rate (n = ISO/METO: n = 6/11 for WT hESC, n = 14/8 for WT-hiPSC-EBs, n = 7/11 for DMD02 EBs, n = 5/6 for DMD03 EBs, n = 15/15 for cDMD-EBs, exact value for each is represented by • in each graph) after ISO treatment and decrease in both parameters under METO treatment. The DMD-hiPSC-EBs remained unresponsive to any of these stimulations. cDMD derived EBs show similar response in contraction force to its isogenic WT control. The red line represents the ratio of 1 for better orientation in change. Significance calculated by Wilcoxon test (*p < 0.05, p < 0.01, *p < 0.01, #p < 0.1) is visualized as asterisks. (C–E) Western blot analysis of b receptors shows higher expression of b1 in DMD-hiPSC derived EBs compared to WT-EBs; cDMD line shows similar expression to its isogenic WT control (calculates as b1 signal/actinin signal). b2 receptor showed increased levels in DMD-hiPSC-EBs. Human heart (HH) sample was used as positive control, human foreskin fibroblasts (HFF) as CM negative sample. Lamin B was used as loading control. Exact value for each is represented by • in each graph. Statistical difference was calculated by Mann-Whitney test for both b1 and b2 receptor expression. (F) CM death in the EBs was evaluated using free troponin level analysis in the medium. All DMD-EBs show significantly increased free cTnT levels compared to WT-EBs. Statistical difference was calculated using two-way ANOVA with uncorrected Fisher's post hoc test. p < 0.0001 according to cell line factor (WT vs. DMD) and + + ++p < 0.0001 according to day of differentiation factor.*

## 6.5 DISCUSSION

Dilated cardiomyopathy, ultimately leading to heart failure, is the most common outcome in patients with dystrophin mutations (Kamdar and Garry, 2016; Papa et al., 2017), and it develops in DMD patients due to muscle wasting, but remains mostly unexplained in its dynamics. The DMD (*mdx)* mouse model has critical limitations since it develops only mild symptoms of heart failure with slow progression and unaffected lifespan compared to control mice (Carnwath and Shotton, 1987; Coulton et al., 1988; Shirokova and Niggli, 2013). In the present study, we provided a detailed description of patient-specific hiPSCCCs and CRISPR/Cas9 engineered hESC-CCs. DMD-CC exhibited several molecular and functional abnormalities including an altered $Ca^{2+}$ handling, irregular bradycardic beating, hypocontractility, and remodeling processes such as βAR alteration and CMs wasting. Our

evidences on the alteration of ECC are in agreement with symptoms described in DMD patients.

Our results showed that dystrophin deficiency leads to lower efficacy in differentiating hPSCs into CCs. Interestingly, DMD-CCs exhibited a similar relative expression of known cardiac markers, and with trending increased Connexin 43 expression, similarly observed in *mdx* and *mdx:utr* CMs as a remodeling mechanism following functional dystrophin absence, with potential fatal arrhythmias in presence of β adrenergic stimulation (Patrick Gonzalez et al., 2015). Lower differentiation efficacy can point to cell fate errors: these can result from increased DNA damage caused by deregulated NOS activity (Jelinkova et al., 2019a). This process can lead to loss of stemness both at the commitment and self-renewal level (Rossi et al., 2007; Inomata et al., 2009). DNA damage can also affect multipotent stem cells division, rendering muscular differentiation ineffective (Dumont et al., 2015). Dystrophin loss was recently associated, in advanced CM *in vitro* models, with delayed contractile machinery formation, suggesting a mutationderived impairment even at the latest stage of CM development (Pioner et al., 2020).

Then, we inquired whether and to what extent the mutation affected the single cell and EB ECC. We measured the electrophysiological properties and found similar AP features between DMD- and WT-CCs. While most of the recorded AP displayed atrial-like AP properties, our results suggested that dystrophin deficiency does not alter the electrophysiological properties of the derived hPSC-CCs. The AP durations we obtained indicate mixed population of various type of excitable cells from ventricular-like CMs (APD90 $\geq$ 300 ms), through atrial- and nodal-like CMs (APD90 $\geq$ 160 ms) and undefined/immature cardiomyocyte-like cells (APD90 < 100 ms) similarly to what others previously found (He et al., 2003; Zhu et al., 2016). Nevertheless, a significant increase of Kir2.1 mRNA expression level point to a possible alteration of APD, which results in reduced effective refractory period during diastole *in vivo*. Furthermore, regarding the voltage-gated ion channels expression, DMD-CCs exhibited increased expression of DHPRα subunit of L-type $Ca^{2+}$ channels but no difference in Cav1.2 and Cav1.3 isoform expression. L-type $Ca^{2+}$ channels presenting gain-of-function mechanism was reported in dystrophic hearts (Koenig et al., 2014). In a recently published work (Eisen et al., 2019), it was shown that prolongation of APD in DMD-CMs was caused by increased $I_{Ca,L}$ density, which can be matched to prolonged diastole in DMD patients (Panovský et al., 2019). APD alterations, both at the potassium and calcium current levels, can lead to ventricular tachycardia (Choi

et al., 2002; McNally et al., 2015), or premature ventricular beats, possibly degenerating into Torsades-de-Pointes ventricular fibrillations (Weiss et al., 2010).

Correlated with the mentioned calcium channels alterations, we measured the intracellular $Ca^{2+}$ transients on dissociated CCs and observed a reduced spontaneous firing in DMD-CCs, with a significantly higher occurrence of small $Ca^{2+}$ events in diastolic phase. For $Ca^{2+}$ dynamics, DMD-CCs presented

prolonged rising time under resting and paced conditions with high variability. The $Ca^{2+}$ transient decay time mean was significantly longer in resting conditions for DMD-CCs, even if this difference was abolished during pacing. This led to a measured prolonged duration of the transients, except under the 1 Hz physiological pacing.

Altered $Ca^{2+}$ transients dynamics correlate with cellular alteration of ECC, as previously shown in our work and others (Sato et al., 2007; Caluori et al., 2019; Pioner et al., 2020). In particular, longer rising time might be correlated to a state of calcium overload, derived from sarcolemmal tears (Danialou et al., 2001) and SR leakage by remodeling of RyR2 by Snitrosylation (Fauconnier et al., 2010; Oda et al., 2015) or loss of the closed-state stabilizer calstabin2 (Fauconnier et al., 2010). RyR2 misregulation can explain also that the presence of small $Ca^{2+}$ amplitude events by random firing is a state of overload. Prolonged cytosolic $Ca^{2+}$, as expressed by increased duration of the transients, can contribute to arrhythmic events via inverse $Na^{+}$-$Ca^{2+}$-exchange activation (Voigt et al., 2012) and electromechanical dissociation. However, it should be noted that young DMD boys rarely exhibit arrhythmias (Villa Chet et al., 2015). We performed patch-clamp experiments and observed no difference in the number of arrhythmic events in WT- and DMD-CCs. In our previous work, we have shown how DMD-EBs are insensitive to positive chronotropic effect of high extracellular $Ca^{2+}$ concentration, most likely due to low diffusion gradients in case of constant cytosolic overload (Caluori et al., 2019). Nevertheless, WT-EBs tolerated high levels of extracellular $Ca^{2+}$ by modulating their contractile activity, while DMD-EBs presented an increased and erratic electromechanical coupling delay, together with an increased calcium reuptake time. In accordance with the presented evidences, we have previously shown how DMD-EBs are less sensitive to Verapamil L-type channels inhibition.

From the single cell electrochemical experiments, and previous results in the DMD-EB electromechanical alterations, we focused on the study of 3D mechanical behavior and its

modulation. EBs showed that the overall spontaneous beat rate of WT and DMD groups did not differ at rest.

However, we identified an increased heart rate variability though IBI analysis and its time-dependent correlation, similarly to Eisen et al.'s observations (Eisen et al., 2019), which also showed high heterogeneity in beat rate variability in dissociated DMD-hiPSC-CCs. Heart rate variability via L-type inactivation can be increased and even become pro-arrhythmogenic in case of spontaneous SR leakage (Johnson et al., 2013), a condition proven in the case of DMD models. The measured contraction force in DMD-EBs was significantly lowered compared to WT-EBs, as previously shown in single cell models (Pioner et al., 2020) and correlated to the ejection fraction decrease in reported patient's hearts (Corrado et al., 2002; Villa Chet et al., 2015; Panovský et al., 2019). Both lower contraction force and arrhythmic events occur in DMD patient's heart from a very young age and before dilated cardiomyopathy onset. In fact, 25% of pediatric DMD patients under 10 years old already showed decreased ejection fraction and have developed sinus tachycardia (Sadek et al., 2017). Overall, our model presents functional alterations of an early-stage cardiac manifestation of DMD.

For the first time, we further evaluated the ECC modulation abilities by pharmacological response in DMD-CCs through the β-AR response. We found an impaired response in DMD-EBs through lack of contraction force and beat rate modulation similarly to *mdx* hearts (Meyers et al., 2019). Our data showed visible changes in contraction force and beat rate in WT-EBs in the presence of isoproterenol (nonselective β adrenergic agonist) or metoprolol (β1 receptor inhibitor) but no change of both parameters in DMD-EBs. Surprisingly, the CRISPR/Cas9-induced cDMD-EBs reacted to β adrenergic modulation similarly to WT-EBs. The response might involve an unknown compensatory mechanism proper of the engineered line. As further confirmation, cDMD-CCs presented similar levels of β-AR with respect to its isogenic hESC-derived WT-CCs. In contrast, patient-specific DMDEBs showed an increased expression in β1 and β2 receptors compared to WT-EBs. It has been previously shown that *mdx* CMs present lowered density of β1-AR (Li et al., 2014) with blunted β-adrenergic signaling pathway (Lu and Hoey, 2000; Li et al., 2014). Here, patient-specific DMD-CCs showed increased protein expression level of both, still with blunted response to adrenergic modulation.

That is also similar to non-DMD heart failure, where β1 overexpression is quite common (Engelhardt et al., 1999); trying to compensate for the weak contractility of the organ and the overactivation of the receptors then leads to receptor dysfunction in signaling, thus their insensitivity (Bristow et al., 1982; Rengo et al., 2009; de Lucia et al., 2018). The impaired contraction force observed in DMD-EBs can also be caused by β3 inhibitory function (Skeberdis, 2004). β3 normally acts as β-adrenergic break, but has been also shown to temper with mechanical properties of skeletal muscle together with nNOS expression increase leading to elevated ROS production (Puzzo et al., 2016). However, our results indicated that β3 expression was unchanged in DMD-CCs although we cannot exclude difference in β3 cellular distribution. The use of β-AR modulators has been shown to be challenging in management of cardiomyopathy in DMD patients due to severe hypotension events (McNally et al., 2015). Investigations using β blockers in DMD cardiomyopathy have turned up mixed results, with some studies demonstrating a clear benefit while others showed little effect of β-AR blockade on outcomes signaling lack of response to the modulation (Kajimoto et al., 2006; Matsumura et al., 2010; Viollet et al., 2012). The β-AR responsiveness might as well be linked to the type of mutation of the *DMD* gene, which might explain why one of our models lacked dystrophin expression yet was responsive to adrenergic modulation. Nevertheless, the beat rate and contraction force response to adrenergic modulation in patient-specific DMD-EBs suggested that the human DMD phenotype is accompanied by altered density of the β-AR on the sarcolemma and less sensitive β-AR pathway. The latter can involve a hampered lusitropic effect, resulting in a hypocontractile $Ca^{2+}$-saturated sarcomere (Culligan et al., 2002; Asp et al., 2013).

As a further original contribution, we finally investigated whether ECC alterations and regulatory pathways remodeling were associated in the dish with CCs wasting. Serum concentration of cTnT is a routinely used marker of CMs death, especially for acute myocardial infarction, although with high sensitivity assays it is also a prognostic marker of non-ischemic cardiac diseases (Park et al., 2017). We have indeed observed how even *in vitro* early stage models of DMD undergo progressive CMs injury, with detected levels of free cTnT up to 10 times the one of age-matched control lines. Dystrophin mutations, with severe symptomatology like in Duchenne's or milder like in Becker's, are all characterized with progressive cardiac symptoms stemming from loss of CMs, remodeling of the cardiac tissue with substitutive fibrosis, and ventricular dilation leading to heart failure accompanied by non-CM cell population depletion (Pesl et al., 2020). CM death can be indirectly caused by high levels of cytosolic $Ca^{2+}$, reportedly present in DMD through several mechanisms,

which increases proteolysis and triggers mitochondrial dysfunctions with consequent ATP exhaustion (Meyers and Townsend, 2019; Tsurumi et al., 2019). Despite the fact that troponin levels measured by immunoassay methods in the media cannot define the mechanisms of cardiomyocyte injury, nor prove if the cell remains viable after such injury or became apoptotic, our findings confirmed that clinical assays can be used together with our model to follow subclinical stages of DMD cardiac involvement. Remarkably, this progressive CCs death is not correlated with loss of contractility. Pioner at al. demonstrated how up to 100 days of cultivation DMD models preserved their contractile function assuming a hypertrophic phenotype (Pioner et al., 2020). A similar mechanism could explain the similar evidence we observed in our 3D model, where CM depletion might be compensated by surviving CM hypertrophy. This evidence opens further uses of our presented model to study progressive cellular adaptation at different stages of the diseases.

## 6.6 LIMITATIONS OF THE STUDY

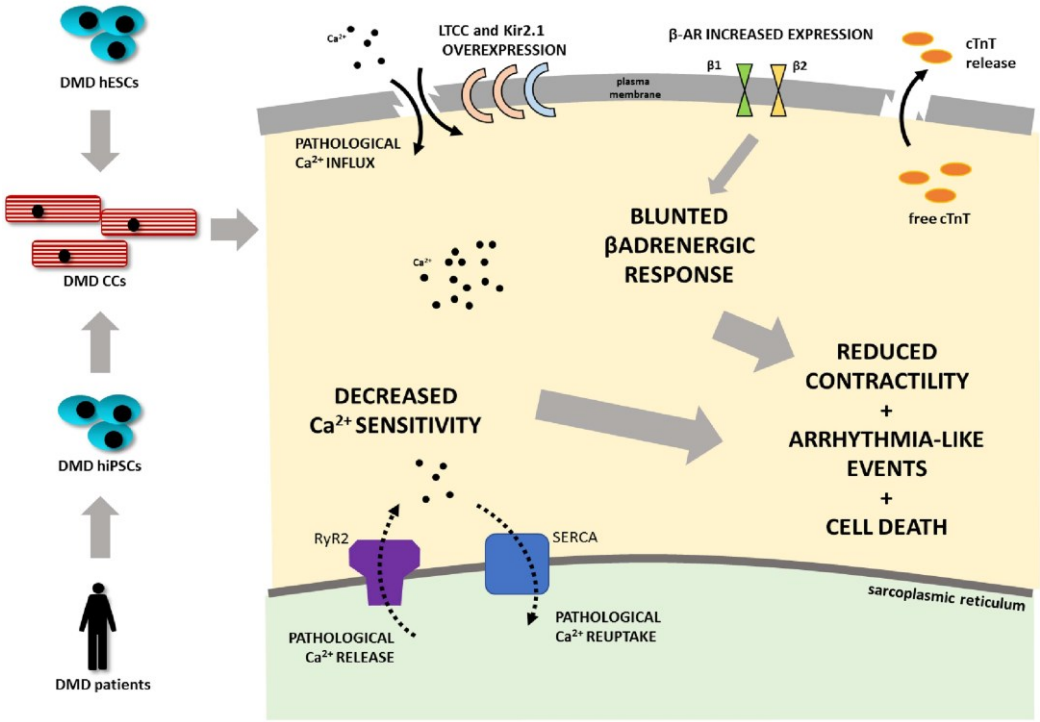
The reported study presents several limitations. The electrophysiological analysis via patch clamp lacks a proper age matching; therefore, the highly variable parameters might have masked mutation-related changes. Furthermore, no channel-specific study was performed to make a causative link between the presented channels overexpression to the calcium handling and contractile alterations observed. We did not directly characterize the age effect on calcium handling and contractility on hPSC-CC. However, we have relied on existent information on the topic to exclude a significant contribution of incomplete maturation to the reported differences.

## 6.7 CONCLUSIONS

The purpose of this work was to model some key cardiac molecular properties in DMD cardiomyopathy using DMD patient-specific and engineered CRISPR/Cas9 isogenic hPSC derived cardiac cells. Our results indicated that our DMD models in the dish are functionally affected by dystrophin deficiency and recapitulate functional defects and cardiac wasting observed in the disease. This work contributes to determine cardiac defects in DMD patients. It offers an accurate tool to study human cardiomyopathy progression and test therapies in the dish.

## 6.8 SUPPLEMENTARY MATERIAL

The Supplementary Material for this article can be found online at: https://www.frontiersin.org/articles/10.3389/fbioe. 2020.00535/full#supplementary-material




*GRAPHICAL ABSTRACT Duchenne muscular dystrophy (DMD) is associated with progressive dilated cardiomyopathy eventually leading to heart failure as the main cause of death in DMD patients. A human cardiomyocyte (CM) model was developed from several independent dystrophin-deficient human pluripotent stem cell (hPSC) lines from DMD patients and hESC line with deletion of DMD gene generated by CRISPR/Cas9 technology. DMD hPSC were differentiated into CMs. DMD mutation-carrying cells are less prone to differentiate into CMs. DMD CMs further demonstrate an enhanced cell death rate. Ion channel expression was altered in terms of potassium (Kir2.1 overexpression) and calcium handling (DHPR overexpression). DMD-CMs exhibited mishandling of calcium demonstrated by increased time of calcium release. Further mechanical impairment (hypocontractility), bradycardia, increased beat rate variability, and blunted b-adrenergic response connected with remodeling of b-adrenergic receptors' expression was found in DMD-CMs (LTCC L-type calcium channel, cTnT - cardiac troponin T, Kir2.1 - potassium channel).*

***Abbreviations:*** *ACTC1, cardiac muscle alpha actin; AFM, atomic force microscopy; AP, action potential; APD, action potential duration; AR, adrenergic receptor; BMP4, bone morphogenic factor 4; CC, cardiac cell; cDMD, CRISPR/Cas9 generated DMD-hESC line; cl4, control hiPSC line; CM, cardiomyocyte; cTNT, cardiac troponin T; DAD, delayed after depolarization; DAPI, 4',6-Diamidine-2'-phenylindole dihydrochloride; DCM, dilated cardiomyopathy; DHPR, dihydropyridine receptor; DMD, Duchenne muscular dystrophy; EB, embryonic body; ECC, excitation-contraction coupling; FGF2, fibroblast growth factor (basic, or 2); FKBP12. 6, calstabin 2; GJA1, connexin43; hESC, human embryonic stem cells; hiPSC, human induced pluripotent stem cells; hPSC, human pluripotent stem cells; IBI, inter-beat variability; ISO, isoproterenol; Kir2.1, Kir2.2, Kir2.3, potassium channels encoded by KCNJ2, KCNJ4, and KCNJ12 genes respectively; LTCC, L-type calcium channel; mdx; mdx:utr, muscular dystrophy on X chromosome, mouse model lacking dystrophin; utrophin and dystrophin lacking mouse model; mEF, mouse embryonic fibroblasts; METO, metoprolol; MYH6, myosin heavy chain α; MYH7, myosin heavy chain β; MYL2, myosin light chain 2; MYL7, myosin light chain 7; NKX2.5, NK homeobox 5; NOS, nitric oxide synthase, inducible (iNOS), neuronal (nNOS); qRT-PCR, quantitative real-time PCR; ROS, reactive oxygen species; RyR2, ryanodine receptor 2; SAC, stretch activated channels; SERCA (ATP2A), Sarcoplasmic/endoplasmic reticulum calcium ATPase 1; SR, sarcoplasmic reticulum; VEGF, vascular endothelial growth factor; WT, wild type control.*

## 7 Pharmacological (p4)

### 7.1 Commentary

Aminophylline, is a commonly used bronchodilator for chronic obstructive pulmonary disease COPD and asthma, having anecdotical linked to a variety of adverse effects, including arrhythmias (Zafar Gondal and Zulfiqar 2026). These effects, which are often observed in patients taking therapeutic or overdose doses of the drug, include an increased risk of cardiovascular mortality and arrhythmias, particularly atrial fibrillation (AF). Despite this, the mechanisms behind aminophylline-induced arrhythmias remain unclear, with previous studies focusing largely on animal models and providing limited insights into how aminophylline affects human cardiomyocytes (CMs).

The research utilized 3D BCC differentiated from hPSC and validated the findings using the HL-1 murine cardiac muscle cell line. The experimental protocol involved exposing these models to increasing concentrations of aminophylline, a methylxanthine bronchodilator, with doses ranging from 10 µM to 10 mM for hPSC-CMs and 8 µM to 512 µM for HL-1 cells. Biomechanical and electrophysiological parameters were captured using AFM recorded MCG from the 3D clusters and MEA, which captured field potentials from HL-1 monolayers; and confocal calcium imaging with Fluo-8 AM monitored intracellular calcium transients. Automated analysis of these signals was performed using custom scripts to quantify beat-to-beat variability and identify arrhythmic events, which were defined by extreme R-R intervals exceeding specific cut-off thresholds (3 seconds for hPSC-CMs and 1 second for HL-1). The study identified two parallel arrhythmogenic mechanisms of action: a concentration-dependent ("deterministic") positive chronotropic effect and a concentration-independent ("stochastic") occurrence of rhythm irregularities. A significant increase in beat rate was observed at severe overdose levels (10 mM) in hPSC-CMs, whereas a positive inotropic effect—manifested as increased contraction force—was evident at lower therapeutic concentrations (10 µM). All tested concentrations of aminophylline significantly increased the frequency of arrhythmic events, characterized by repeated tachycardia-like periods followed by long pauses. Calcium imaging further revealed that high-dose treatment induced a significantly higher number of calcium sparks and a decreased calcium wave decay time, suggesting that the arrhythmogenicity is driven by microdomain-related diastolic calcium leakage from the sarcoplasmic reticulum. Washout experiments demonstrated that these functional changes were reversible, confirming the drug's pharmacological action rather than irreversible cellular damage.

frontiers in Pharmacology

ORIGINAL RESEARCH
published: 17 January 2022
doi: 10.3389/fphar.2021.789730

# Aminophylline Induces Two Types of Arrhythmic Events in Human Pluripotent Stem Cell–Derived Cardiomyocytes

*Simon Klimovic*[1,2,3†], *Martin Scurek*[4,5†], *Martin Pesl*[2,6,7†], *Deborah Beckerova*[2,6], *Sarka Jelinkova*[2], *Tomas Urban*[2,7], *Daniil Kabanov*[1,2,3], *Zdenek Starek*[6,7], *Marketa Bebarova*[8], *Jan Pribyl*[1], *Vladimir Rotrekl*[2,6] and *Kristian Brat*[4,5,6*†]

[1]CEITEC, Masaryk University, Brno, Czechia, [2]Department of Biology, Faculty of Medicine, Masaryk University, Brno, Czechia, [3]Department of Biochemistry, Faculty of Science, Masaryk University, Brno, Czechia, [4]Department of Respiratory Diseases, University Hospital Brno, Brno, Czechia, [5]Faculty of Medicine, Masaryk University, Brno, Czechia, [6]International Clinical Research Center, St. Anne's University Hospital, Brno, Czechia, [7]First Department of Internal Medicine—Cardioangiology, Faculty of Medicine, St. Anne's University Hospital, Masaryk University, Brno, Czechia, [8]Department of Physiology, Faculty of Medicine, Masaryk University, Brno, Czechia

OPEN ACCESS

**Edited by:**
*Paulo Correia-de-Sá, University of Porto, Portugal*

**Reviewed by:**
*Bruno Bragança, Centro Hospitalar do Tâmega e Sousa, Portugal, Portugal*
*Jean-Sebastien Rougier, University of Bern, Switzerland*

***Correspondence:**
*Kristian Brat*
*Brat.Kristian@fnbrno.cz*

[†]*These authors have contributed equally to this work*

**Specialty section:**
*This article was submitted to Cardiovascular and Smooth Muscle Pharmacology, a section of the journal Frontiers in Pharmacology*

**Received:** *05 October 2021*
**Accepted:** *17 November 2021*
**Published:** *17 January 2022*

**Citation:**
*Klimovic S, Scurek M, Pesl M, Beckerova D, Jelinkova S, Urban T, Kabanov D, Starek Z, Bebarova M, Pribyl J, Rotrekl V and Brat K (2022) Aminophylline Induces Two Types of Arrhythmic Events in Human Pluripotent Stem Cell–Derived Cardiomyocytes. Front. Pharmacol. 12:789730. doi: 10.3389/fphar.2021.789730*

Cardiac side effects of some pulmonary drugs are observed in clinical practice. Aminophylline, a methylxanthine bronchodilator with documented proarrhythmic action, may serve as an example. Data on the action of aminophylline on cardiac cell electrophysiology and contractility are not available. Hence, this study was focused on the analysis of changes in the beat rate and contraction force of human pluripotent stem cell–derived cardiomyocytes (hPSC-CMs) and HL-1 cardiomyocytes in the presence of increasing concentrations of aminophylline (10 µM–10 mM in hPSC-CM and 8–512 µM in HL-1 cardiomyocytes). Basic biomedical parameters, namely, the beat rate (BR) and contraction force, were assessed in hPSC-CMs using an atomic force microscope (AFM). The beat rate changes under aminophylline were also examined on the HL-1 cardiac muscle cell line via a multielectrode array (MEA). Additionally, calcium imaging was used to evaluate the effect of aminophylline on intracellular $Ca^{2+}$ dynamics in HL-1 cardiomyocytes. The BR was significantly increased after the application of aminophylline both in hPSC-CMs (with 10 mM aminophylline) and in HL-1 cardiomyocytes (with 256 and 512 µM aminophylline) in comparison with controls. A significant increase in the contraction force was also observed in hPSC-CMs with 10 µM aminophylline (a similar trend was visible at higher concentrations as well). We demonstrated that all aminophylline concentrations significantly increased the frequency of rhythm irregularities (extreme interbeat intervals) both in hPSC-CMs and HL-1 cells. The occurrence of the calcium sparks in HL-1 cardiomyocytes was significantly increased with the presence of 512 µM aminophylline. We conclude that the observed aberrant cardiomyocyte response to aminophylline suggests an arrhythmogenic potential

**Abbreviations:** sAFM, atomic force microscope; bpm, beats per minute; CBBs, cell-based biosensors; CCTL, center for cell therapy line; CM, cardiomyocyte; EB, embryoid body; ECC, excitation–contraction coupling; hESC, human embryonic stem cell; hiPSC, human-induced pluripotent stem cell; hPSC, human pluripotent stem cell (hESC and hiPSC); hPSC-CMs, pluripotent stem cell–derived cardiomyocytes.

## 7.2 INTRODUCTION

Theophylline (1,3-dimethylxanthine) and its more soluble form aminophylline (a complex of two theophylline molecules and ethylenediamine) are well-known bronchodilators used mostly for therapy of COPD and asthma. These drugs are also recommended for the treatment of emphysema (Zatloukal et al., 2020). Other indications have been suggested, for example, treatment of apnea in premature neonates (Ye et al., 2019). Unfortunately, a narrow therapeutic range and frequent adverse effects make their use controversial (Singh et al., 2019). An increased mortality rate in theophylline users has been reported by multiple research teams (Lee et al., 2009; Horita et al., 2016). A higher percentage of cardiovascular deaths was observed in asthma patients who received aminophylline (Suissa et al., 1996), as well as in patients with COPD (Lee et al., 2009), and also in a general patient population overdosed with theophylline (Shannon, 1999).

The adverse effects of theophylline/aminophylline include arrhythmias, even at their therapeutic plasma concentrations (Bittar and Friedman, 1991). In a meta-analysis of several randomized clinical trials, 13% incidence of arrhythmias or palpitations after intravenous aminophylline infusion has been observed (Nair et al., 2012). More than 20% of patients experience cardiac arrhythmias during an aminophylline overdose episode (Shannon, 1999). Supraventricular arrhythmias have been observed most frequently, usually represented by atrial fibrillation (AF) (Varriale and Ramaprasad, 1993; Huerta et al., 2005). Concurrently, COPD is an independent risk factor of AF (Goudis, 2017). The risk of arrhythmias is further enhanced by hypokalemia (Hoppe et al., 2018), which may develop as a side effect of aminophylline treatment, particularly occurring in cases of intentional overdose (Ellis, 1985; Charytan and Jansen, 2003).

Mechanisms of theophylline-/aminophylline-induced arrhythmias are not clear. It is well known that methylxanthines non-specifically inhibit phosphodiesterases (hence increasing the cAMP level) and adenosine receptors (Ukena et al., 1993). These effects may explain the sinus tachycardia often observed in clinical practice. In contrast, this does not explain the origin of AF associated with aminophylline treatment. Effects of theophylline/aminophylline on cardiac electrophysiology were studied mostly in animal models (Komadina et al., 1992; Onodera et al., 2001; Shamsuzzaman et al., 2016). However, a conclusive explanation of their proarrhythmic action has not been provided, and data from human cardiomyocytes (CMs) embedded in cardiac syncytia have been missing completely.

This study was aimed to reveal changes of basic functional characteristics (contraction force and beat rate) of human cardiac tissues induced by aminophylline at a wide range of concentrations. A clinically relevant model was employed, for example, 3D structures called embryoid bodies (EBs) derived from human pluripotent stem cells subsequently differentiated into cardiomyocytes (hPSC-CMs). The model was originally described in previous studies (Burridge et al., 2012; Pesl et al., 2014). Its functional properties were further validated using atomic force microscopy (Liu et al., 2012; Dinarelli et al., 2018; Pribyl et al., 2019), a method enabling real-time monitoring of contractions and thus also beating properties of single cardiomyocytes or cardiac cell clusters, alone or in combination with other methods such as microelectrode array (Caluori et al., 2019b) or calcium imaging (Odstrcilik et al., 2015; Caluori et al., 2019a). This model was recently used for disease modeling in studies by Acimovic et al., 2018; Jelinkova et al., 2019. The effects of aminophylline were further validated on an independent model of HL-1 cardiomyocyte cells. The overall scheme of all experiments within this study is presented in Figure 1. This approach has provided the first experimental data well-corresponding with the aminophylline-induced arrhythmias observed in clinical medicine.

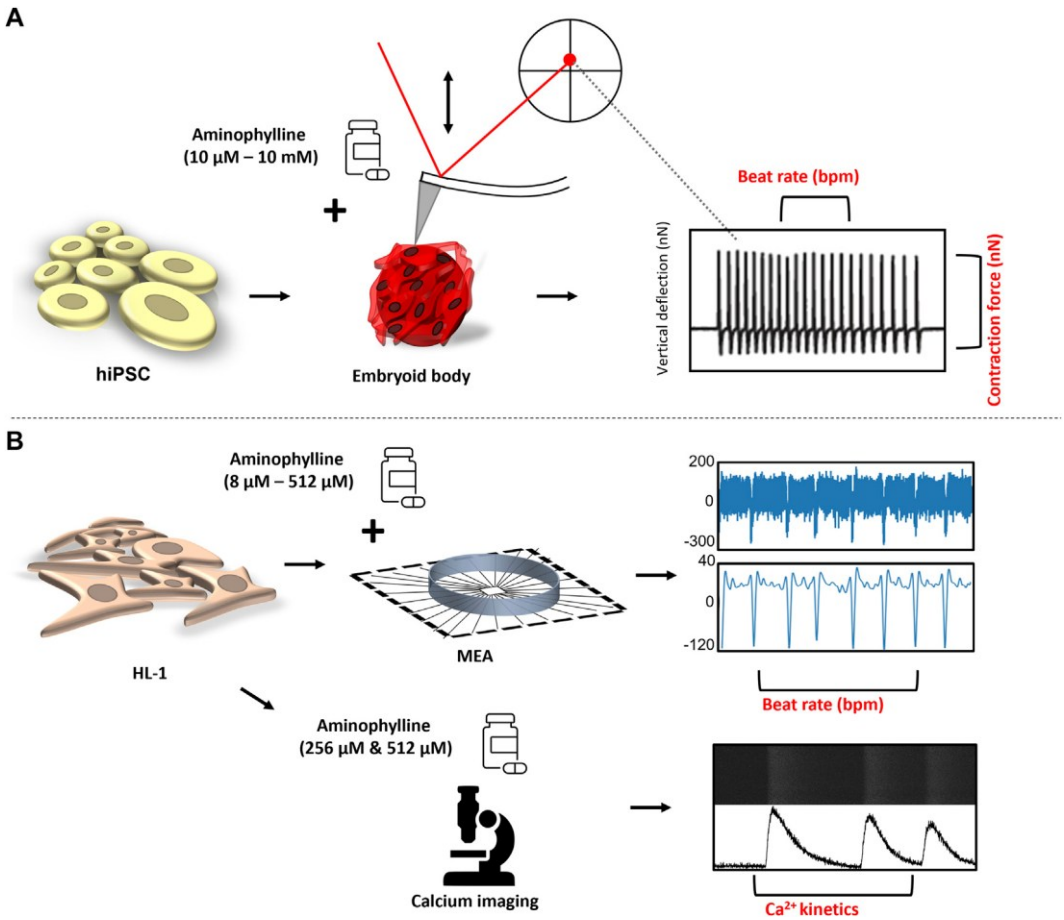


*FIGURE 7.1 Experimental design: (A) hPSCs were differentiated in the form of EBs into contracting 3D clusters of cardiomyocytes, and under the influence of increasing concentrations of aminophylline, the mechanocardiogram (MCG) was recorded was recorded by an atomic force microscope. The BR and contraction force values of each contractive event were further analyzed and compared. (B) Field potential by the multielectrode array (MEA) system, together with intrinsic Ca2+ kinetics via Fluo-8 AM, a calcium-binding dye, was assessed on HL-1 cells to further confirm the arrhythmogenic effect of aminophylline.*

## 7.3 MATERIALS AND METHODS Cell Cultivation

The hESC line CCTL14 (46 XX) derived at Masaryk University, Brno, and previously characterized (International Stem Cell Initiative et al., 2007) was routinely maintained on a feeder layer of mitotically inactivated mouse embryonic fibroblasts as previously described (Dvorak et al., 2005; Krutá et al., 2014; Jelinkova et al., 2020). Differentiation into CMs via embryoid bodies (EBs) and measurements by an AFM were performed as previously described (Pesl et al., 2014), with minor modifications. Briefly, hESC colonies were collected 4 days after seeding and subsequently broken down into smaller clumps which were seeded into the EB medium (86% KO DMEM, 10% FBS, 1% L-glutamine, 1% penicillin/streptomycin, 1% non-essential amino acids, 0.1 mM 2-mercaptoethanol, and 10 µg/ml ascorbic acid) with 10 ng/ml BMP4 (R&D) and placed in hypoxic conditions (5% $O_2$, 5% $CO_2$,) where they spontaneously formed EBs. After 3 days, the medium was removed and replaced with fresh EB medium supplemented with 5 ng/ml FGF2 (Peprotech), 10 ng/ml BMP4, and 6 ng/ml activin A (R&D) for a 4-day incubation. A 3-day incubation in EB medium supplemented with 10 ng/ml VEGF (R&D) and 10 µM IWR1 (R&D). The next induction medium was the EB medium supplemented with 10 ng/ml VEGF and 5 ng/ml FGF2, with a medium exchange every 4 days. After four days in this medium (day 14 of differentiation), the EBs were transferred into a normoxic incubator (21% $O_2$, 5% $CO_2$) for the remaining 8 days of this induction period. From then onward, EBs remained in normoxia and were fed with the EB medium every 4 days until analysis. Beating EBs were selected and transferred on a gelatin-coated PM3 dish to adhere to for measurement. These cellular constructs of the cardiac syncytium were coupled to an AFM force sensor to perform a high-fidelity contraction pattern as an hPSC-CM–based biosensor (Pesl et al., 2014). The constant size of clusters of hPSC-CMs allows comparable and stable beating pattern evaluation allowing for force- and rhythm-related drug effect tracking.

For the immunocytochemistry experiment, either whole or dissociated EBs attached on coverslips were fixed with 4% PFA, blocked and permeabilized by 1% BSA (Sigma) in 0,1% Triton-X (Sigma) or 0,05% TWEEN (Sigma) in PBS, and incubated with anti–troponin T antibody (1:5,000, Cell Signaling, 5,593, Rb) overnight in 4 C. Anti-rabbit Alexa 594 (1:500, Invitrogen) was left to incubate for an hour at room temperature, and the slips were mounted on slides with Mowiol containing DAPI (Sigma). The images were obtained using a Zeiss LSM 700 confocal microscope. The contracting clusters were previously checked for expression and checked by immunostaining for cardiac troponin T (cTnT) and ryanodine receptor RyR2 as described elsewhere (Pesl et al., 2014; Souidi et al., 2021). The expression of myosin heavy chain MYH6/7 and MYH7, RyR2, and the striated pattern of cTnT in dissociated cardiomyocytes was used to assess the progress in CM maturation. The clusters consisted of all three CM subtypes as described elsewhere; in brief, nodal-like CMs had an AP duration at 90% of repolarization shorter than 100 ms (about 16%), slightly more frequent were atrial-like cells, and recorded AP mainly demonstrated a typical ventricular-like shape (Acimovic et al., 2018). EB responses to basic heart modulators, such as β adrenoceptor agonist and blocker, isoproterenol, and metoprolol, were previously measured (Supplementary Figure S1). EBs from the same cultivation batch were checked for the presence of cTnT in the clusters as well as in the dissociated EBs by immunostaining to demonstrate the batch-to-batch differentiation consistency (Figure 2).

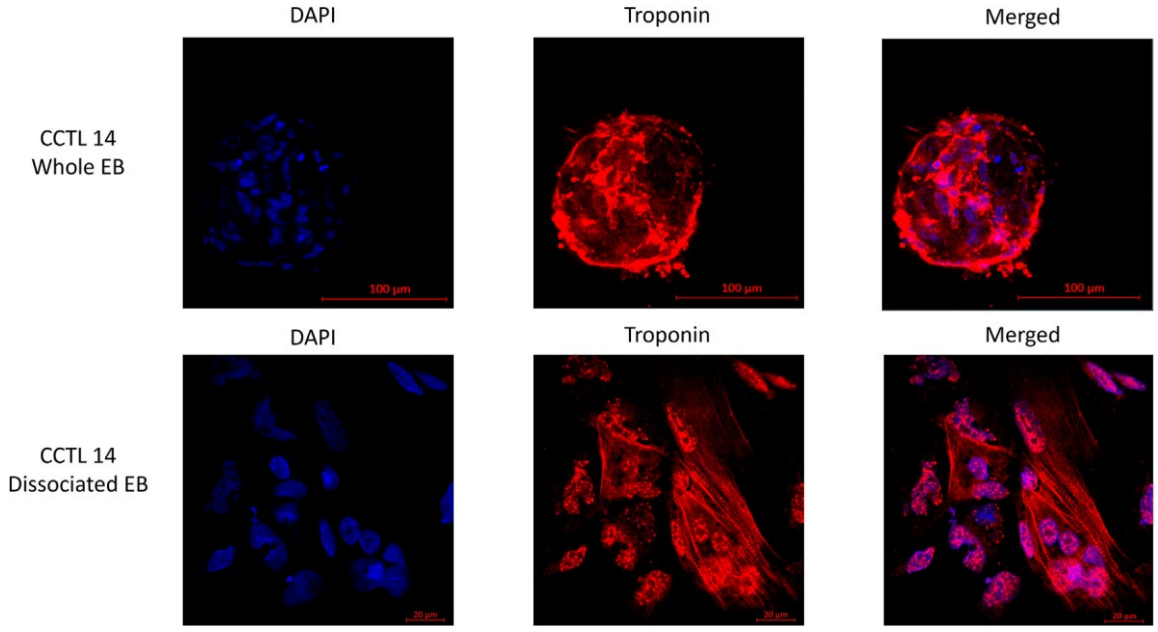



*FIGURE 7.2 Fluorescence staining of whole and dissociated CCTL14 EBs (cell cluster) illustrates the presence of matured cardiomyocytes identified by the presence of troponin T (red color); cells are localized with DAPI staining of the nucleus (blue color).*

The HL-1 Cardiac Muscle Cell Line (Sigma) was routinely maintained on fibronectin-coated dishes in Claycomb medium (Sigma) supplemented with 10% FBS, 100 U/ml:100 µg/ml penicillin-streptomycin, 0.1 mM norepinephrine, and 2 mM L-glutamine. The cells were passaged with trypsin after reaching full confluency, usually every 3–4 days, in a ratio of 1:3. For experiments with MEA, the HL-1 cells were cultivated on MEA chips coated with fibronectin in 0.02% gelatin (5 mg/ml; Sigma). The HL-1 response to β-adrenoceptor agonist isoproterenol was measured (Supplementary Figure S1).

### 7.3.1 Atomic Force Microscopy Measurements

NanoWizard 3 AFM (Bruker-JPK) combined with inverted light microscope IX-81 (Olympus) was used to obtain mechanocardiograms (MCGs) of beating EBs as previously described (Pesl et al., 2014; Caluori et al., 2019b; Pribyl et al., 2019). Drug response tests were performed after initial equilibration of EBs in Tyrode's solution (composition in mM: NaCl 135, KCl 5.4, $MgCl_2$ 0.9, $CaCl_2$ 1.8, HEPES 10, $NaH_2PO_4$ 0.33, and glucose 5.5; pH 7.4 adjusted with 3M NaOH) (Bébarová et al., 2017). The addition of increasing concentrations of aminophylline (10 µM, 100 µM, 1 mM, and 10 mM; Fagron) followed. Each concentration was prepared in Tyrode's solution from 1 mM stock solution of aminophylline. The MCG was recorded for further analysis; each measurement point consisted of 10 min of stabilization time, followed by 10 min of measurement. Control experiments were conducted in the same setting without aminophylline in the treatments. The contraction of beating EBs was recorded as a force value in time (MCG). In-house built MATLAB-based script located R and S peaks for each contractive event and their respective vertical deflection and time values. From these values, R-R (sec), R-S (contraction force; nN), and BR (beat rate; beats per minute) were calculated, averaged, and normalized to the respective baseline values recorded in Tyrode's solution.

### 7.3.2 Multielectrode Array Measurements

The field potential of the HL-1 cells was measured using MEA2100-mini-60 (Multi Channel Systems). Drug responses were measured after initial equilibration in Claycomb medium, followed by the increasing concentrations of aminophylline in Claycomb medium (8, 16, 32, 64, 128, 256, and 512 µM). Measurement points consisted of 3 min of stabilization time, followed by 5 min of measurement. As a monolayer, HL-1 cells are more sensitive to a treatment than hPSC-CM clusters. Therefore, treatment measurement times and concentration ranges were modified. MEA recordings were analyzed using Multi-Channel

Analyzer software and in-house Python script, which processed the data in a similar way; however, the resulting parameters were only R-R (sec) and BR (beat rate; beats per minute). R-S (amplitude; μV) values in case of MEA recordings do not correlate with R-S values measured via AFM; therefore, they were not used in this study. Noisy and non-representative MEA channels were eliminated, and at least 3 channels were then used for calculations. Measurements of Intracellular Cytosolic $Ca^{2+}$

HL-1 cells were passaged and seeded onto an imaging dish with a polymer coverslip bottom (Ibidi) and allowed to adhere. Fluo-8 (490/525; AAT Bioquest) was added into the medium (final concentration 2 μM; stock solution in DMSO 2 mM), and the cells were incubated for 20 min at 37°C. After the incubation, the solution was replaced with fresh medium, and the cells were placed on the heated stage (37°C) of an inverted microscope. $Ca^{2+}$ images in the line-scan (line size 3.37 μm, 100 Hz) mode were recorded using a laser scanning confocal microscope Olympus FL1200 (Olympus) with a ×40 water immersion objective, in the x–y mode. Kinetic properties of intracellular $Ca^{2+}$ were analyzed via the in-house Python-based script (Kabanov, 2021).

### 7.3.3 Measurement of HL-1 Viability

The HL-1 cells were passaged and mixed with PBS containing aminophylline (final concentration 512 μM) or only PBS for control. The cells were incubated for 8 min after which their viability was analyzed via the trypan blue dye exclusion method (Vicell-XR, Beckman Coulter).

### 7.3.4 Statistical Analyses

Statistical evaluation was carried out with the use of GraphPad Prism 8.5 software (GraphPad Software). All data were tested for outliers by the ROUT (Q 1%) method, and available normality tests were performed for the obtained data. In case of hPSC-CM measurements, Brown–Forsythe ANOVA with Games–Howell multiple comparisons test was used to assess the statistical significance of the differences on normally distributed group pairs. In the case of arrhythmia analysis, R-R for each contractive event was extracted via processing scripts as mentioned before. R-R values over 1 or 3 s (cut-off) in HL-1 and hPSC-CMs, respectively, were quantified in all treatment groups and compared to controls. Choice of the cut-off value for hPSC-CMs was based on clinical experience with arrhythmia in human patients. The cut-off value for HL-1 was reduced with respect to the fact that HL-1 is a murine cell line with a higher overall beat rate. The resulting contingency tables were

statistically evaluated by using the chi-square test with Yates's correction. The use of the individual statistical test is specified in appropriate figure legends and in Supplementary Data. Additionally, datasets containing complete raw data from all measurements are available at the online open-access repository (Klimovic et al., 2021).

## 7.4 RESULTS

### 7.4.1 Positive Chronotropic and Inotropic Effects of Aminophylline on hPSC-CMs

In the case of hPSC-CMs, two groups of treatment concentrations were determined according to the literature (Aslaksen et al., 1981; Goldberg et al., 1986; Rowe et al., 1988; Higgins et al., 1995; Shannon, 1999). The "therapeutic concentration/overdose" group consisted of 10 μM, 100 μM, and 1 mM of aminophylline treatments, while the 10-mM aminophylline treatment was considered "severe overdose" concentration. Consistent presence of troponin-positive cardiomyocytes in whole and dissociated embryoid bodies (EBs) was confirmed by immunostaining (representative example shown in Figure 7.2).

The positive chronotropic effect of aminophylline on hPSC CMs was seen only in the 10 mM concentration of aminophylline (Figures 3A,B; $p < 0.05$; the remaining p-values are given in Supplementary Table S1 and Supplementary Table S2). The positive inotropic effect was evident by a significantly increased contraction force of EBs in lower concentrations of aminophylline that was in contrast to its chronotropic effect (Figure 3D; $p < 0.0001$; the remaining p-values are given in Supplementary Table S3). Statistical analysis showed that this effect was significant in 10 μM concentration, with a similar trend in the concentrations of 100 μM and 1 mM (Figure 3C; $p < 0.01$; the remaining p-values are given in Supplementary Table S4). Linear regression analysis showed that the beat rate increase correlates with the concentration of aminophylline (Supplementary Figure S2A,B, $p < 0.0001$). On the contrary, this relationship was not proven in case of contraction force (Supplementary Figure S2A,B). To further strengthen the presented results, the washout experiment was performed on hPSC-CMs. The results showed that the BR of EBs increases significantly after administration of aminophylline; however, it decreased again during the washout period, suggesting that the chronotropic and inotropic effects is likely due to the effect of aminophylline and not due to irreversible cellular damage (Supplementary Figure S3).

In order to further explain molecular mechanisms, hPSC-CM cells were treated with 1 μM adenosine, followed by a combination of 1 μM adenosine and 1 mM aminophylline, a well-known non-selective adenosine receptor antagonist. The results showed an insignificant trend toward the adenosineantagonizing aminophylline effect (Supplementary Figure S3B).

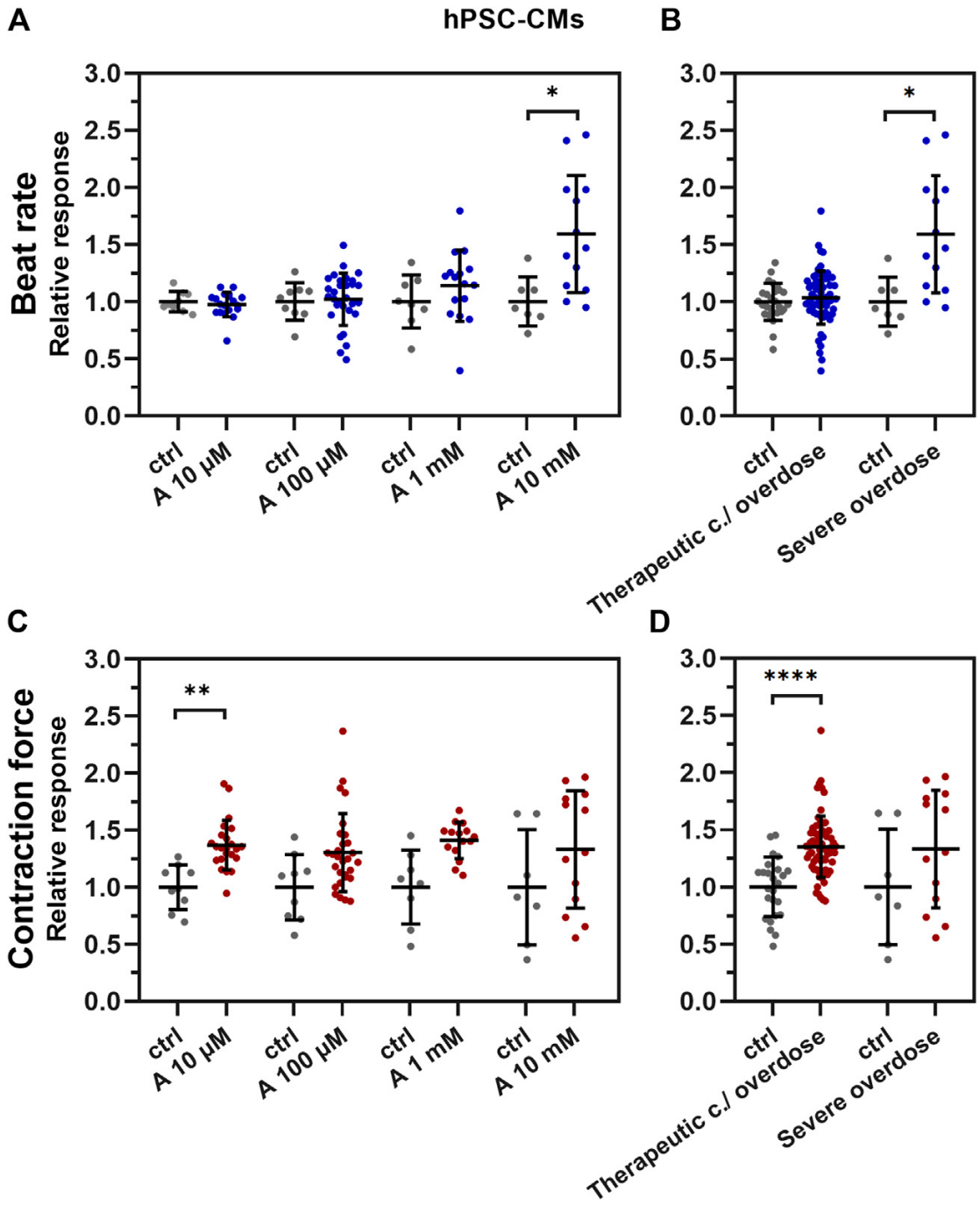



*FIGURE 7.3 Effect of aminophylline (A) on contractile properties of 3D cardiac clusters. Scatterplots (mean ± standard deviation) of the BR (blue) and contraction force (red) overall*

*changes, normalized to a baseline measurement (relative response) and to control measurement means (n = 19 for A 10 μM, n=30 for A 100 μM, n=16 for A 1 mM, n=13 for A 10 mM, n= 9 for BR ctrl and n=7 for contraction force ctrl). At least four biological repetitions were used in each column. (A) BR of the measured EBs with 10 mM aminophylline (A 10 mM) was significantly increased compared to that of the control ($p < 0.05$). (B) Similarly, the BR of EBs treated with 10 mM concentration of aminophylline was significantly increased over that of the controls ($p < 0.05$). (C) Contraction force of EBs with 10 μM aminophylline treatment was significantly increased over that of the control ($p < 0.05$), with a similar trend in higher concentrations. (D) Group analyses then showed a strong statistically significant effect of therapeutic concentration / overdose (10 μMand 100 μMand 1 mM) aminophylline over the controls. (Brown–Forsythe and Welch ANOVA tests were used in all analyses).*

### 7.4.2 Positive Chronotropic Effect of Aminophylline on HL-1

To test whether chronotropic effects of aminophylline are modelindependent, field potential measurements of the HL-1 cardiac cell line treated with aminophylline were conducted. The concentrations of aminophylline in a range of 8 up to 512 μM were used. Higher concentrations turned out to be toxic for the cells, which can be explained by higher treatment efficacy on the cellular monolayer of HL-1, as opposed to the cellular cluster of hPSC-CMs. Non-toxicity of selected concentrations was experimentally tested by trypan blue staining (Supplementary Figure S3C).

The results of these experiments showed a similar positive chronotropic effect with increasing concentration of aminophylline. Compared to controls, the BR was significantly increased only in the cells treated with 256 μM aminophylline; however, we observed a similar non-significant trend also in the case of the 512-μM treatment (Figure 4; 256 μM aminophylline vs. the control $p < 0.05$; 512 μM aminophylline vs. the control $p < 0.06$; the remaining p-values are given in Supplementary Table S5).

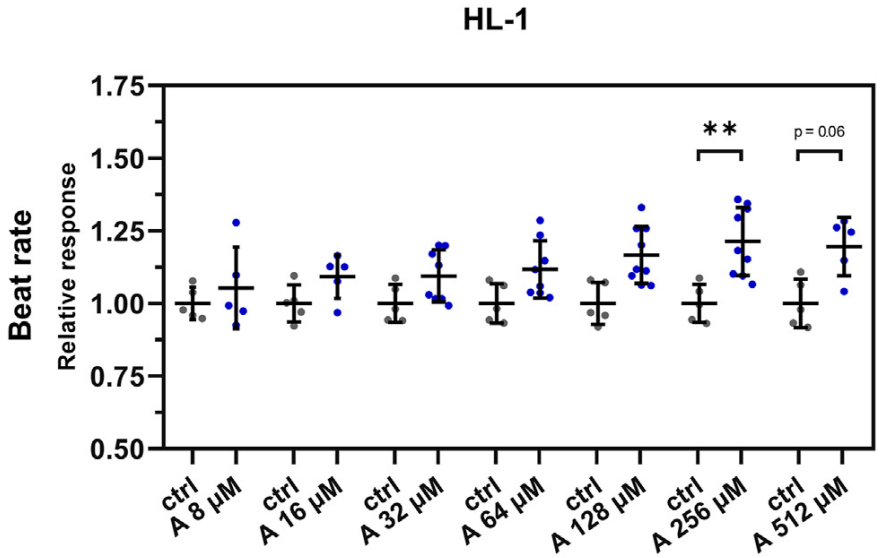



*FIGURE 7.4 Effect of aminophylline (A) on the BR of HL-1 cells. Scatterplots (mean ± standard deviation) of the BR (blue) normalized to a baseline measurement (relative response) and to controlmeasurement means (n = 5 for A 8 and 16 µM, n = 8 for 32 and 64 µM, n = 9 for 128 and 256 µM, n = 5 for 512 µM and n = 5 for ctrl). At least three biological repetitions were used in each column. Results showed linear increase of BR correlating with a higher concentration of aminophylline, with statistically significant and partially significant changes of BR 256 and 512 µM measurements compared that of the control (A 256 vs. ctlr p < 0.01, A 526 vs. ctlr p 0.06, ordinary oneway ANOVA).*

### 7.4.3 Exposure to Aminophylline Causes Spontaneous $Ca^{2+}$ Releases Leading to Arrhythmia

Among the adverse effects of aminophylline apparent in clinical practice, arrhythmias are most frequent. To test whether this effect is also present in our in vitro hPSC-CM model and HL-1 cardiomyocytes, we assessed the number of R-R intervals (interbeat interval length) over 3 s or 1 s, respectively. Our results showed that the frequency of cutoff R-R values in measurements with aminophylline was significantly higher than that in controls in both models (Figure 5; p-values in Supplementary Table S6 and Supplementary Table S7).

To further investigate this effect, intracellular cytosolic $Ca^{2+}$ events were measured on HL-1 cells in the presence of 256 and 512 µM aminophylline. A significantly higher number of $Ca^{2+}$ sparks was detected in the presence of 512 µM aminophylline than the control (Figure 6, 512 µM aminophylline vs. the control $p < 0.0001$). A similar effect was not detected in the presence of 256 µM aminophylline. Higher concentrations of aminophylline cause arrhythmic events presented by calcium leakage events (sparks). This is in good agreement with the measurement of electrical activity of cells (Figure 5B), where the concentration of

256 μM did not cause a significantly higher occurrence of arrhythmia; however, the concentration of 512 μM leads to rhythm irregularities. Last, the time to peak and decay time of main calcium waves were analyzed. While aminophylline caused no change in time to peak, the decay time significantly decreased, corresponding to an increased BR (Figures 6B,C).

## 7.5 DISCUSSION

This is the first study demonstrating the proarrhythmic action of aminophylline on human cardiomyocytes in vitro. To monitor aminophylline's effect at a wide range of concentrations, AFM was used on cell clusters [embryoid bodies (EBs)] formed by aggregation of human pluripotent stem cell–derived cardiomyocytes. Furthermore, the effect of aminophylline was investigated via a multielectrode array and by means of intracellular cytosolic $Ca^{2+}$ measurement on HL-1 cells. Despite the differences between the models such as monolayer growth, cellular populations, or the fact that it is a murine cell type, HL-1 cells are considered a standard drug screening platform; therefore, we chose them to confirm our findings. A missing link between the previous experimental data and aminophylline-induced arrhythmias observed in clinical practice was identified. Our most important finding was that aminophylline had two principal actions of arrhythmogenicity, the first being concentration-dependent ("deterministic") and the second one concentration-independent ("stochastic"). First, we observed a linear concentration-dependent positive chronotropic effect with increasing aminophylline concentrations in hPSCCMs (Figures 3A,B and Supplementary Figure S2A,B). Moreover, this effect was also confirmed to an extent on the HL-1 cellular line (Figure 4). This may be related to previous clinical findings that demonstrated that theophylline's higher plasmatic levels were associated with an increased heart rate (sinus tachycardia); the relationship was linear and concentration-dependent (Vestal et al., 1983; Nadkarni et al., 1988). This effect is sometimes used to treat severe, atropine resistant bradycardia (Pasnoori and Leesar, 2004) or other indications (Conte et al., 2017). The inotropic effect was nonlinear in our study. An increased inotropic effect was present only in lower aminophylline concentrations. This response may be attributed to reaching peak-shortening amplitude, as a physical parameter of cells and cluster, respectively, and partial immaturity may be responsible for lower number of present sarcomeres and, thus, lower shortening capability of the cells (Fraticelli et al., 1989).

In parallel to the "deterministic" effect, we observed a second arrhythmogenic action of aminophylline expressed as a concentration-independent occurrence of RR interval abnormities. This action was stochastic, independent of the applied aminophylline concentration. It consisted of repeated tachycardia-like periods followed by bradycardia-like periods (not illustrated), which is reflected by the extreme R-R intervals in Figure 5 that occurred significantly more often in the cells exposed to aminophylline. Even though certain beat rate variability was present in spontaneously beating hPSC-derived CMs in previous studies (Mandel et al., 2012; Binah et al., 2013; Niehoff et al., 2019), similar events have never been previously described to our best knowledge. We speculate that this effect may be an experimental equivalent to the sick sinus syndrome (Tse et al., 2017) or to tachy–brady alternating episodes in patients with AF, an arrhythmia that was previously observed both in aminophylline overdose cases and at therapeutic levels of the drug (Laaban et al., 1988; Bittar and Friedman, 1991; Varriale and Ramaprasad, 1993).

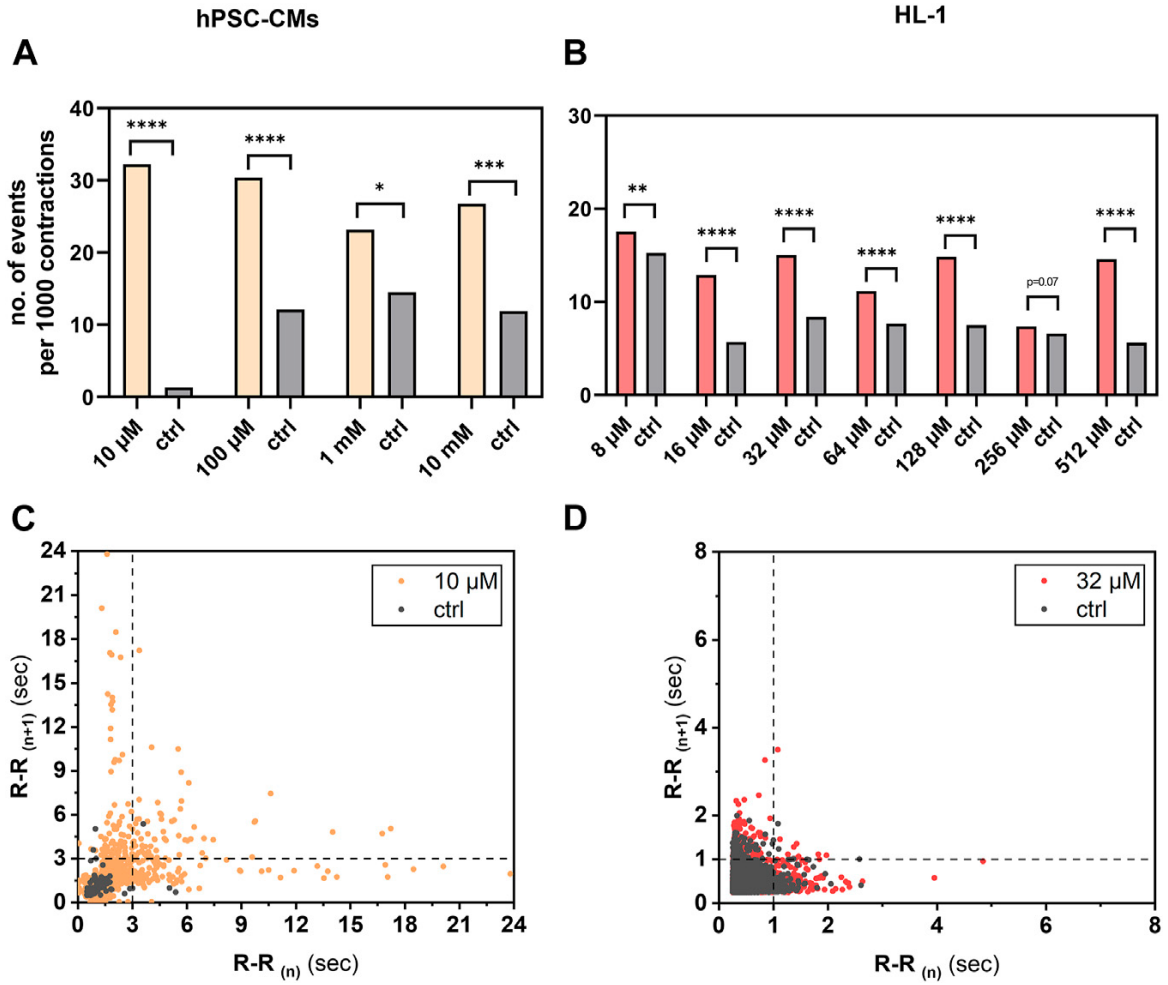



*FIGURE 7.5 Analysis of arrhythmogenic effect of aminophylline on hPSC-CMs and HL-1 cells. R-R values over 3 s in case of hPSC-CM measurements or 1 s in case of HL-1 of*

*aminophylline and control measurements were subtracted, and the resulting contingency tables were statistically analyzed. Column graphs show sums of cutoff R-R values (arrhythmic events) per 1,000 contractions in each treatment group and controls of (A) hPSC-CMs and (B) HL-1 experiments (chi-square test with Yates' correction). Results show significant or partially significant higher frequency of aminophylline group cutoff values compared to that of the control. Poincaré plots of R-R values of representative concentration for (C) hPSC-CMs and (D) HL-1 experiments with visible cutoff lines.*

Attempts to reveal mechanisms of the arrhythmogenic action of aminophylline/theophylline have been performed previously, using various animal models. In rats, aminophylline induced tachycardia and elevated blood pressure and potential cardiac ischemia (Shamsuzzaman et al., 2016), which may be related to theophylline-induced myocardial fibrosis found as a long-term concentration-/dose-dependent side effect in a notable portion of rats (Onodera et al., 2001). In a canine model, aminophylline significantly enhanced AV nodal and His–Purkinje conduction; this effect was potentiated in combined therapy with metaproterenol (Komadina et al., 1992).

Studies published so far have not provided a clear clue to the genesis of proarrhythmic effects of aminophylline/theophylline, namely, AF. Aminophylline effects (likely an equivalent of the sinus tachycardia in patients) may be explained by the effect of elevated cAMP and the absence of the inhibitory effect of adenosine (Belardinelli et al., 1995) on cardiac ionic currents (see insignificant trend in Supplementary Figure S3B).

As studied in detail by Kong et al. (2008), caffeine (another type of methylxanthine), aminophylline, and theophylline preferentially potentiated luminal $Ca^{2+}$ activation of the ryanodine type 2 (RyR2) receptor, reduced the threshold for spontaneous $Ca^{2+}$ release, and increased the basal activity, inducing repeated quantal $Ca^{2+}$ releases. As is well-known, the accumulation of $Ca^{2+}$ in the cytoplasm may result in delayed afterdepolarizations, which can trigger arrhythmia. Considering the increased occurrence of $Ca^{2+}$ sparks in HL-1 cardiomyocytes treated with 512 µM aminophylline (Figure 6), the concentration-independent "stochastic" effect of aminophylline observed in our study may be a consequence of microdomain cAMP level–related diastolic release of $Ca^{2+}$ via independent clusters of RyR2 receptors (Berisha et al., 2021). Such transient $Ca^{2+}$ accumulation may induce an increased BR and, following $Ca^{2+}$ depletion, results in a pause in the investigated cardiac cell's beating clusters. Such chain of events might also be amplified by the local

cAMP level–induced alteration of the current amplitude via modulation of hERG potassium channel phosphorylation (Cui et al., 2000). Detailed subcellular mechanisms of this effect should be studied in the future. To our best knowledge, this is the first study reporting results of experiments with aminophylline conducted on human cardiomyocytes derived from hPSCs. As such, this set of experiments showed that our comprehensive monitoring system is a unique and valuable tool for cardiotoxicity vs. safety testing of various molecules or drugs. Our results may present the missing link between the described subcellular mechanisms of methylxanthine arrhythmogenesis and the clinical variability of arrhythmic events related to the theophylline treatment in clinical practice.

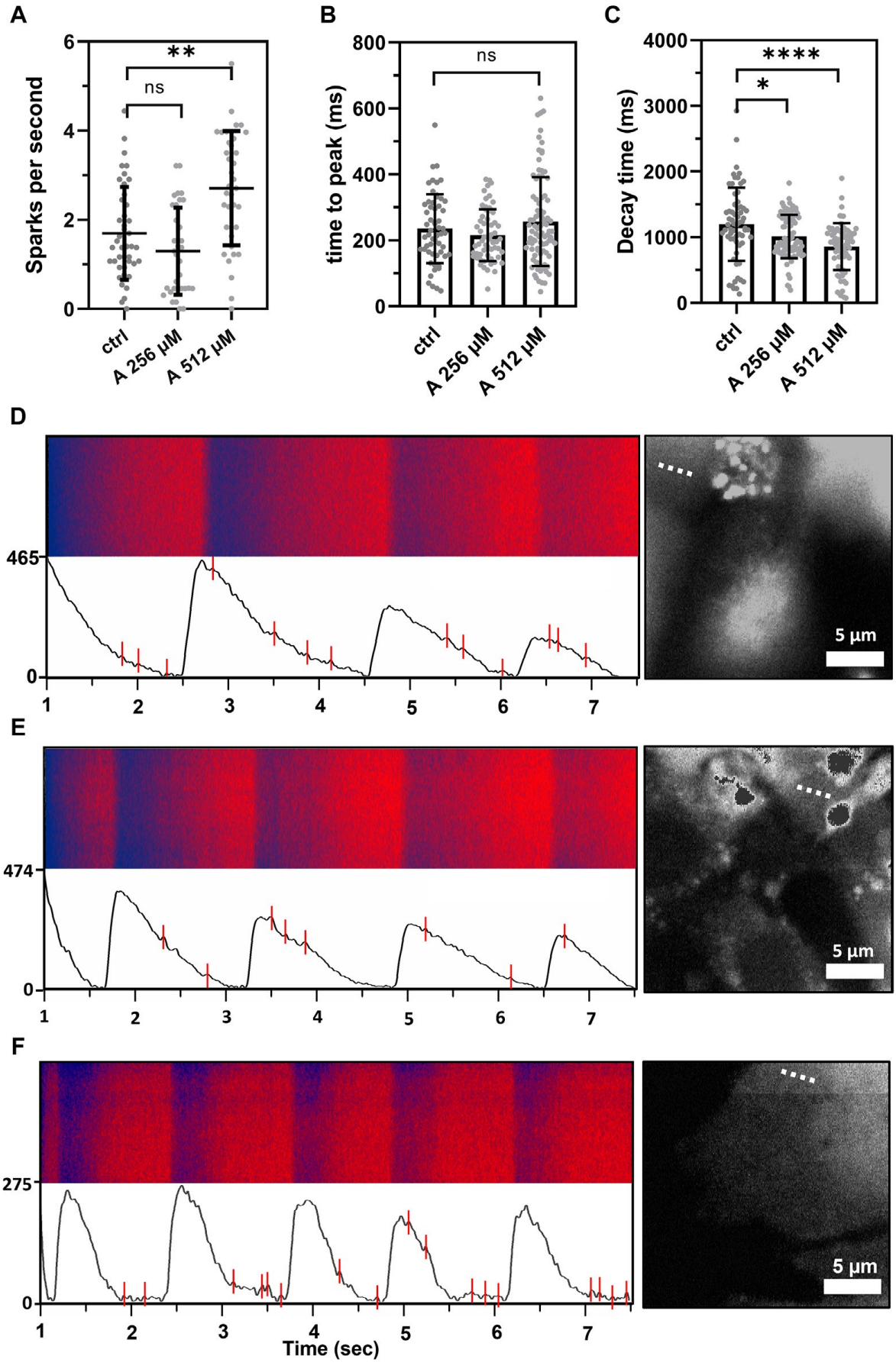

A
Sparks per second
6
4
2
0
**
ns
ctrl
A 256 µM
A 512 µM
B
time to peak (ms)
800
600
400
200
0
ns
ctrl
A 256 µM
A 512 µM
C
Decay time (ms)
4000
3000
2000
1000
0
****
*
ctrl
A 256 µM
A 512 µM
D
465
0
1
2
3
4
5
6
7
5 µm
E
474
0
1
2
3
4
5
6
7
5 µm
F
275
0
1
2
3
4
5
6
7
Time (sec)
5 µm

*FIGURE 7.6 Calcium sparks measured as extra events in the fluorescence in-time signal, showing leakage of calcium from the sarcoplasmic reticulum. (A) Scatterplot (mean ± standard deviation) showing calcium leakage events in a one-second period in control cells compared to the treatment by 256 and 512 μM aminophylline (A; n _ 43 for ctlr, n _ 33 for 256 μM and n _ 37 for 512 μM). The frequency of calcium leakage events of cells treated with 512 μM aminophylline was significantly higher than that of the control (A 512 vs. ctlr $p < 0.01$, ordinary one-way ANOVA). (B,C) Scatterplots (mean ± standard deviation) showing times to peak and decay times of the control compared to the treatments. Aminophylline caused no significant change to time to peak compared to the control; however, decay time significantly decreased in a linear trend (n _ 65 for ctrl, n _ 89 for A 256 μM, n _ 77 for A 512 μM; ctlr vs. A 256 μM $p < 0.05$, ctlr vs. A 512 μM $p < 00.001$; Kruskal–Wallis test). (D–F) Fluorescence line profiles were measured in time, typical recordings together with fluorescence–time curves were filtered for the presence of noise, and calcium sparks were found—labeled as red lines (B _ control, C _ 256 μM, D _ 512 μM). Each recording is accompanied with a fluorescence image showing the exact location of line scan on the cell (dashed line).*

**CONCLUSION/SUMMARY**

We conclude that aminophylline had two parallel arrhythmogenic mechanisms of action on EBs: a concentration-dependent ("deterministic") effect, presenting with an increased beat rate (potential clinical correlate: sinus tachycardia), and a concentration-independent ("stochastic") effect, which was characterized by tachycardia-like episodes alternating with long pauses (potential clinical correlate: atrial fibrillation). Our comprehensive monitoring system is a unique and valuable tool for cardiotoxicity vs. safety testing of various molecules or drugs.

## 7.6 STUDY LIMITATIONS

The study presents the effect of aminophylline on contractile properties of human hPSC-CMs along with results of field potential measurements on the HL-1 cardiac cell line that further confirmed the effects. First, it has to be considered that hPSC-derived CMs represented immature/neonatal phenotype possibly affecting drug effect kinetics [e.g., altered IK1 levels which may affect resting potential, repolarization, and depolarization dynamics (Sartiani et al., 2007)]. Second, if different hPSC lines are used to generate embryoid bodies, it is likely that there will be different degrees of maturity and the effect of

aminophylline might also differ. The last limitation is that field potential measurements can generate information about the BR but not about contraction force; therefore, the results with HL-1 cells confirmed only the chronotropic effect of aminophylline.

## 7.7 FUNDING

This study was funded by the Ministry of Health of the Czech Republic (Research Grant No. NU20-06-00156).

## 7.8 ACKNOWLEDGMENTS

We acknowledge further support by the European Regional Development Fund-Project ENOCH (No. CZ.02.1.01/0.0/0.0/ 16_019/0000868) and the Specific University Research Grants of the Masaryk University MUNI/A/1246/2020, MUNI/A/1700/ 2020, and MUNI/A/1133/2021 provided by the Ministry of Education, Youth and Sports of the Czech Republic. We also acknowledge the support by the Internal grant agency of Masaryk University - Project MUNI/IGA/1428/2020. CIISB, Instruct-CZ Centre of the Instruct-ERIC EU consortium, funded by the MEYS CR infrastructure project LM2018127, is gratefully acknowledged for the financial support of the measurements at the CF

Nanobiotechnology.

## 7.9 SUPPLEMENTARY MATERIAL

The Supplementary Material for this article can be found online at: https://www.frontiersin.org/articles/10.3389/fphar.2021.789730/ full#supplementary-material.

# 8 Pharmacological (p5)

## 8.1 Commentary: Synergic effect of salbutamol and aminophylline on hPSC-CMs

This study investigates the combined effects of the methylxanthine aminophylline and the short-acting β-agonist salbutamol—a combination frequently used in clinical practice of COPD or Asthma —on human cardiac tissue to determine their joint impact on force, rhythm, and arrhythmogenesis. We estimated that both compounds will have some degree of arrhythmogenicity stemming from their chemical structure. Thus, we utilized proven model of 3D BCC (cardiac organoids, aka embryoid bodies) differentiated from two human embryonic stem cell lines (CCTL14 and CCTL12) vie protocol described in previous chapters (e.g 3$^{rd}$ and 5$^{th}$ chapter). These clusters were integrated into the AFM as describedand MCGs were recorderd at a stable physiological temperature of 37 °C. The experimental protocol involved measuring the effects of salbutamol alone (10 nM to 10 µM) and in combination with aminophylline (10 µM to 1 mM). Advanced signal processing was conducted using a Python-based script to identify contraction peaks and calculate force and beat rate. Additionally, heart rate/beat rate variability (HRV/BRV) was quantified using the standard deviation of successive differences (SDSD) of R-R intervals to assess the pro- or anti-arrhythmic potential of the treatments.

We revealed that salbutamol alone produced a significant positive inotropic effect (a 40% increase in contraction force at 100 nM) but only a minimal chronotropic response. When salbutamol was combined with aminophylline, the drugs exhibited a synergistic effect, significantly amplifying both the beat rate and contraction force compared to monotherapy. Most importantly, the study identified a significant anti-arrhythmic effect of salbutamol, which successfully reduced the occurrence of rhythm irregularities previously induced by aminophylline. Mechanistic validation showed that this anti-arrhythmic property was completely blocked by butoxamine (a β2 -selective blocker) and L-NAME (a non-specific NOS inhibitor), significantly diminished the anti-arrhythmic effect of salbutamol indicating that salbutamol mitigates aminophylline-induced arrhythmias through the activation of nitric oxide synthase (NOS) via β 2-adrenergic receptors. These findings suggest that salbutamol as an add-on therapy may increase the cardiovascular safety of aminophylline treatments. Future clinical trials are needed to further assess the safety, effectiveness, and potential arrhythmogenic risks of using salbutamol and aminophylline together in patients.

www.nature.com/scientificreports

scientific reports

Check for updates

OPEN

# Salbutamol attenuates arrhythmogenic effect of aminophylline in a hPSC-derived cardiac model

Daniil Kabanov[1,3], Simon Vrana Klimovic[1,3], Deborah Beckerová[2,5], Martin Molcan[5], Martin Scurek[4], Kristian Brat[4], Marketa Bebarova[7], Vladimir Rotrekl[2,5], Jan Pribyl[1,2] & Martin Pesl[2,5,6]

The combination of aminophylline and salbutamol is frequently used in clinical practice in the treatment of obstructive lung diseases. While the side effects (including arrhythmias) of the individual bronchodilator drugs were well described previously, the side effects of combined treatment are almost unknown. We aimed to study the arrhythmogenic potential of combined aminophylline and salbutamol treatment in vitro. For this purpose, we used the established atomic force microscopy (AFM) model coupled with cardiac organoids derived from human pluripotent stem cells (hPSC-CMs). We focused on the chronotropic, inotropic, and arrhythmogenic effects of salbutamol alone and aminophylline and salbutamol combined treatment. We used a method based on heart rate/beat rate variability (HRV/BRV) analysis to detect arrhythmic events in the hPSC-CM based AFM recordings. Salbutamol and aminophylline had a synergistic chronotropic and inotropic effect compared to the effects of monotherapy. Our main finding was that salbutamol reduced the arrhythmogenic effect of aminophylline, most likely mediated by endothelial nitric oxide synthase activated by beta-2 adrenergic receptors. These findings were replicated and confirmed using hPSC-CM derived from two cell lines (CCTL4 and CCTL12). Data suggest that salbutamol as an add-on therapy may not only deliver a bronchodilator effect but also increase the cardiovascular safety of aminophylline, as salbutamol reduces its arrhythmogenic potential.

**Keywords** Salbutamol, Aminophylline, Atomic force microscopy, iPSC, HESC, Cardiomyocytes, Pulmonary drug screening, Drug cardiotoxicity, Biomechanical properties, Arrhythmogenic effects

**Abbreviations**

| | |
|---|---|
| AFM | Atomic force microscopy |
| BPM | Beats per minute |
| BRV | Beat rate variability |
| CBBs | Cell-based biosensors |
| CCTL | Center for cell therapy line |
| CM | Cardiomyocyte |
| EB | Embryoid body |
| ECC | Excitation-contraction coupling |
| hESC | Human embryonic stem cell |
| hiPSC | Human induced pluripotent stem cell |
| hPSC | Human pluripotent stem cell (hESC and hiPSC) |
| hPSC-CMs | Pluripotent stem cell-derived cardiomyocytes |

[1]CEITEC MU, Masaryk University, Brno, Czech Republic. [2]Department of Biology, Faculty of Medicine, Masaryk University, Brno, Czech Republic. [3]Department of Biochemistry, Faculty of Science, Masaryk University, Brno, Czech Republic. [4]Department of Respiratory Diseases, University Hospital Brno and Faculty of Medicine, Masaryk University, Brno, Czech Republic. [5]International Clinical Research Center, St. Anne's University Hospital, Brno, Czech Republic. [6]First Department of Internal Medicine – Cardioangiology, Faculty of Medicine, Masaryk University, St. Anne's University Hospital, Brno, Czech Republic. [7]Department of Physiology, Faculty of Medicine, Masaryk University, Brno, Czech Republic. ✉email: jan.pribyl@ceitec.muni.cz; pesl@fnusa.cz

## 8.2 Introduction

Bronchodilator drugs were designed to relieve symptoms of obstructive respiratory diseases (e.g., asthma and chronic obstructive pulmonary disease, COPD) by relaxing the smooth muscle apparatus of the lower airways. To date, three main classes of bronchodilators have been introduced in clinical practice, namely beta-2 agonists, anticholinergics, and methylxanthines (Zatloukal et al. 2020). These drugs are often used in combination, either in the stable phase of the disease or during asthma or COPD exacerbation (Zatloukal et al. 2020; Levy et al. 2023; Glob. Initiat. Chronic Obstr. Lung Dis. - GOLD, n.d.).

Cardiac adverse events are among the most frequent side effects of beta-2 agonists and methylxanthines. While the pro-arrhythmic activity of aminophylline is well described in the clinical setting (Bittar and Friedman 1991; Shannon 1999) and has recently been examined in our experimental study (Klimovic et al. 2022), there is limited evidence on the effect and adverse events of these two bronchodilator classes used in combination (Rodrigo and Rodrigo 1994; White et al. 2004; Nair et al. 2012).

Salbutamol (also known as albuterol) is the most frequently used short-acting beta-2 agonist (SABA). A wide variety of side effects have been described with salbutamol treatment, especially when the drug is injected into the bloodstream (Price and Clissold 1989). Considering its effects on the heart, positive bathmotropic, chronotropic, and inotropic effects were described (Engel et al. 1985; Overgaard et al. 1999). Salbutamol-induced hypokalemia may also affect cardiac function[19] Serious arrhythmias (even ventricular fibrillation) in patients with preexisting heart diseases were reported (Mettauer et al. 1985; UYSAL et al. 2016)

Using our established and previously described *in vitro* three-dimensional model of cardiac tissue formed by clusters of human pluripotent stem cells-derived cardiomyocytes (hPSC), we aimed to evaluate the effect of salbutamol alone and in combination with aminophylline on cardiac excitability and inotropy with a focus on their impact on arrhythmogenesis (Ramalho et al. 2022; Caluori et al. 2019; Klimovic et al. 2022; Martin Pesl et al. 2017a; Pribyl et al. 2019; Bébarová et al. 2017).

## 8.3 Materials and Methods

### 8.3.1 Cell Cultivation

hESC line "center for cell therapy line" CCTL14 (46 XX) and CCTL12 (46 XX) derived at Masaryk University, Brno, and previously characterized (International Stem Cell Initiative et al. 2007a) was routinely maintained on a feeder layer of mitotically inactivated mouse embryonic fibroblasts. For formation of embryonic bodies (EB), hESC colonies were collected 4 days after seeding and subsequently broken down into smaller clumps which were seeded into EB medium (86% KO DMEM, 10% FBS, 1% L-glutamine, 1% penicillin/streptomycin, 1% nonessential amino acids, 0,1mM 2-mercaptoethanol and 10 µg/ml ascorbic acid) with 10 ng/ml BMP4 (R&D) and placed in hypoxic conditions (5% $O_2$, 5% $CO_2$) where they spontaneously formed EBs. After three days, the medium was removed and replaced with fresh EB medium supplemented with 5 ng/ml FGF2 (Peprotech), 10 ng/ml BMP4, and 6 ng/ml Activin A (R&D) for a four-day incubation. A three-day incubation followed this in EB media supplemented with 10 ng/ml VEGF (R&D) and 10 µM IWR1 (R&D). The following induction media was EB medium supplemented with 10 ng/ml VEGF and 5 ng/ml FGF2 with a media exchange every four days. After four days in this media (day 14 of differentiation), the EBs were transferred into a normoxic incubator (21% $O_2$, 5% $CO_2$) for the remaining 8 days of this induction period. From then onward, EBs remained in normoxia and were fed with EB medium every four days. 1 month old EBs with spontaneous contraction activity were used for analysis. Beating EBs were selected and transferred on a gelatin-coated PM3 dish to adhere to for measurement. These cellular constructs of cardiac syncytium were coupled to an AFM force sensor to perform a high-fidelity contraction pattern as an hPSC-CM-based biosensor (Martin Pesl, Pribyl, Acimovic, et al. 2016).

### 8.3.2 Atomic Force Microscopy measurements

Contraction of beating EBs was assessed by Nanowizard 3 (Bruker-JPK) AFM combined with inverted light microscope IX-81 (Olympus) as previously described (Caluori et al. 2019; Klimovic et al. 2022; Martin Pesl et al. 2017a; Pribyl et al. 2019). Liquid media was preheated to 37 Celsius degree and let to stabilize for at least 10 minutes before each measurement. Temperature was maintained unchanged during all following measurements(Martin Pesl, Pribyl, Acimovic, et al. 2016; Martin Pesl et al. 2017a). A soft silicon nitride cantilever (Nitra-tall B, AppNano) was landed on EB attached to the petri dish (TPP). Real-time changes of force in time applied by contracting EB were recorded while administrating salbutamol (Fagron), its mixes with aminophylline (Fagron) in different concentrations, or butoxamine (Sigma Aldrich). Each measurement was preceded by initial

equilibrium in Tyrode solution (composition in mM: NaCl 135, KCl 5.4, $MgCl_2$ 0.9, $CaCl_2$ 1.8, HEPES 10, $NaH_2PO_4$ 0.33, and glucose 5.5; pH 7.4 adjusted with 3M NaOH), after which increasing concentrations of salbutamol (10 nM, 100 nM, 1 µM, 10 µM), mixes of salbutamol (S) and aminophylline (A) (10 – 1000 nM salbutamol, 10 – 100 µM aminophylline) or butoxamine (3 µM) was added (Bébarová et al. 2017). All stock solutions of substances and treatments were prepared using Tyrode buffer, as both compounds show excellent water solubility (approx. 0.2 M for both), and no stock solutions in organic solvents were needed. Mixes were defined based on previous results of individual measurements of salbutamol in this article and aminophylline in our group's previous article (Klimovic et al. 2022). Each measurement point consisted of 10 min of stabilization time, followed by 10 min of measurement. Control experiments were conducted in the same setting with the Tyrode solution alone and tied to individual experiment groups based on the time the treatment was given to the cells. Therefore, some control groups can repeat thought-out results. Control EBs were taken from each batch to account for variances among batches. During all experiments, the temperature was maintained at 37°C.

The resulting data were processed by a python-based script, which located R and S peaks for all contractive events (Kabanov D. 2021, Repeev N., 2021). Contraction forces (nN), beat rates (bpm), and interbeat intervals (sec) were calculated and statistically evaluated. Representative AFM records of vertical deflection of cells treated with salbutamol, aminophylline, and a mix of both are shown in Figure S5.

### 8.3.3 Beat rate variability (BRV) analysis

. To ensure reliable and valid data, samples invalid for BRV analysis because of multiple sudden irregular pauses in beat rate were excluded using SignalPlant software (ver. 1.2.8.2)(Plesinger et al. 2016). Resulting interbeat RR-intervals were analyzed by domain BRV analysis methods, which compute variability. For analysis of short-term variability, the standard deviation of successive differences (SDSD) was used (Shaffer and Ginsberg 2017). SDSD serves as an index of beat-to-beat variability, primarily determined by external influences on the heart. It measures the variability in the time intervals between successive heartbeats. It is unaffected by linear trends in the heart rate, acting as a statistical filter in which the low-frequency components are removed (Malpas and Maling 1990). In our approximation, R-R intervals that deviated from the median by more than two times were excluded from the analysis to reduce the influence of noise. The PyHRV (“Highlights — pyHRV - OpenSource Python Toolbox for Heart Rate Variability 0.4 Documentation,” n.d.) library for Python was used for SDSD calculations. Internal variability was constant during

the measurement and may be related to the mixed population of all three CM subtypes as described elsewhere; in brief, nodal-like CMs had an AP duration at 90% of repolarization shorter than 100 ms (about 16%), slightly more frequent were atrial-like cells, and recorded AP mainly demonstrated a typical ventricular-like shape(Acimovic et al. 2018).

### 8.3.4 Statistical analysis

Data was processed via the in-house Python-based scripts or Signal plant software as described above. Statistical evaluation was calculated with GraphPad Prism 8.5 software (GraphPad Software). All data were tested for outliers by the ROUT (Q = 1%) method, and their normal distribution was tested via available normality tests. Ordinary one-way ANOVA with the Holm Sidak multiple comparisons test was used to test the statistical significance of the differences in normally distributed group pairs. In cases where equal standard deviations could not be assumed, Brown–Forsythe ANOVA with Games–Howell multiple comparisons test was used. Where normality tests failed, non-parametric tests were used. Cut-off arrhythmia analysis (Figure S2 and S3, Supplementary data) was previously described (Klimovic et al. 2022). Briefly, in that work, inter-beat RR intervals over 3 seconds were subtracted, and the statistical significance of the differences between treatments and controls were tested by the Chi-square test with Yate's correction. An individual statistical test is specified in appropriate figure legends and in Supplementary Data.

## 8.4 Results

### 8.4.1 Inotropic and anti-arrhythmic effect of salbutamol on hPSC-CMs

The AFM-based setup was used to obtain and calculate the contraction force and beat rate of hPSC-CMs in EBs. The contraction force was significantly increased by 40% in the presence of 100 nM salbutamol compared to the normalized control (Figure 1A) and increased non-significantly in higher concentrations. Salbutamol didn't significantly increase the beat rate in the concentration range between 10 nM and 10 µM (Figure 8.1 B). Still, linear regression of beat rate relative responses and measured concentrations showed a significant increase towards 1 µM (Figure 8.1 CD).

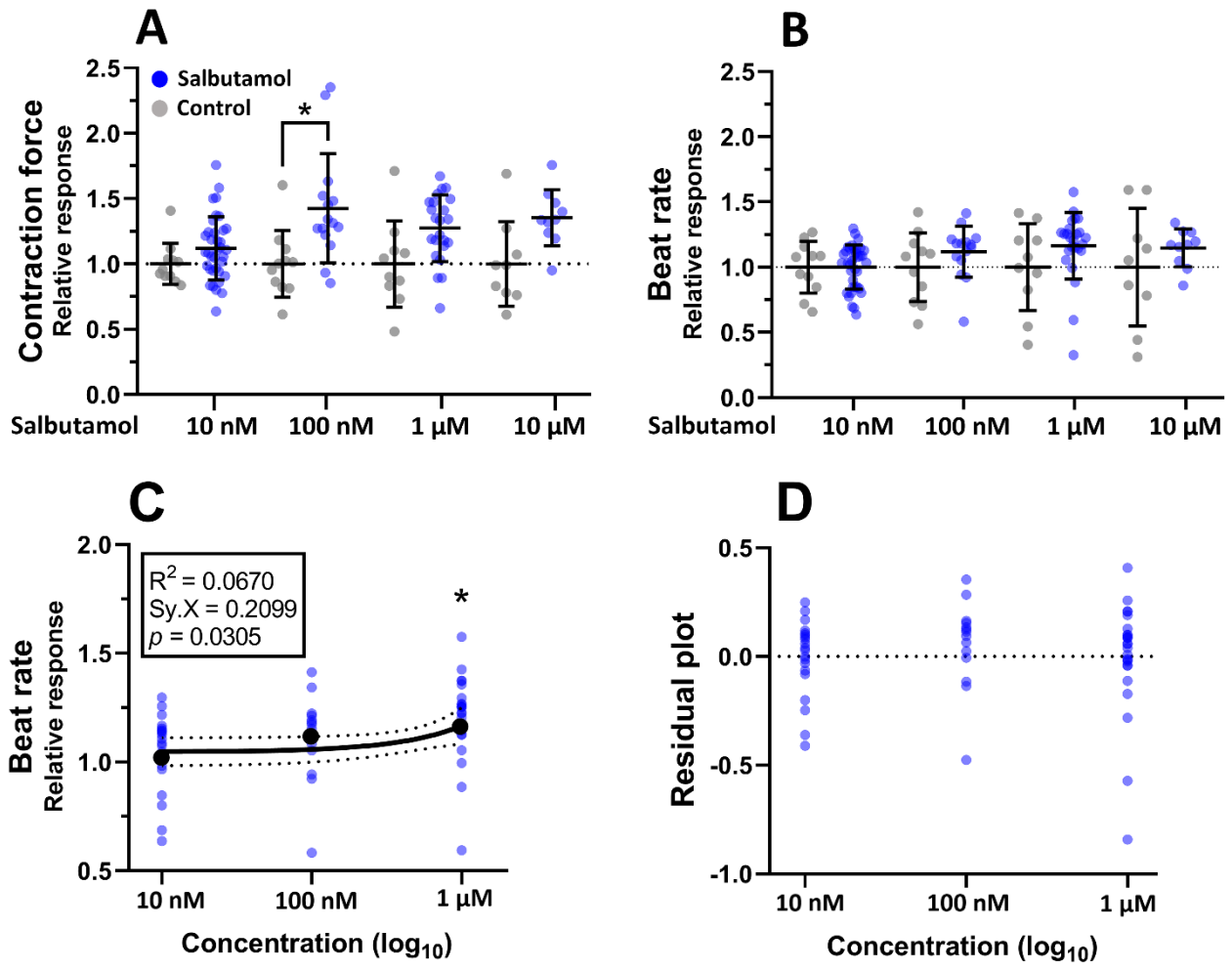



**Figure 8.1** Effect of salbutamol on contraction properties of hPSC-CMs. *Scatter plots with indicated means and standard deviation (SD) of the contraction force and beat rate relative responses normalized to the respective baseline control measurement in the case of salbutamol and to mean values of the control measurement in the case of control (n = 11 for controls, n = 15, 15, 23, and 10 for 10 nM, 100 nM, 1 µM, and 10 µM salbutamol, respectively). At least four biological repetitions were used in each column.* ***(A)*** *The*

*contraction force was significantly increased after administration of salbutamol at the concentration of 100 nM (Kruskal-Wallis test with Dunn's multiple comparisons test, P < 0.05).* ***(B)*** *The beat rate wasn't significantly elevated after administration of salbutamol (P > 0.05).* ***(C, D)*** *Linear regression of beat rate relative responses and measured concentrations coupled with residual plot. Results show a statistically significant non-zero slope (Wald test, P = 0.0305), proving a positive relationship between concentration and relative response.*

The SDSD of short-term beat rate variability was used for the analysis of arrhythmic effects after salbutamol administration. A higher value corresponds to an elevated beat rate variability, *i.e.,* to an increased pro-arrhythmic activity. Interestingly, salbutamol showed a dose-independent trend to reduce the variability of RR intervals compared to controls (Figure 2A). This effect is further illustrated in the Poincaré plot, where measurements with salbutamol are clustered in the left bottom corner of the plot (i.e., showing a low variability), compared to the scattered control values (Figure 2B).

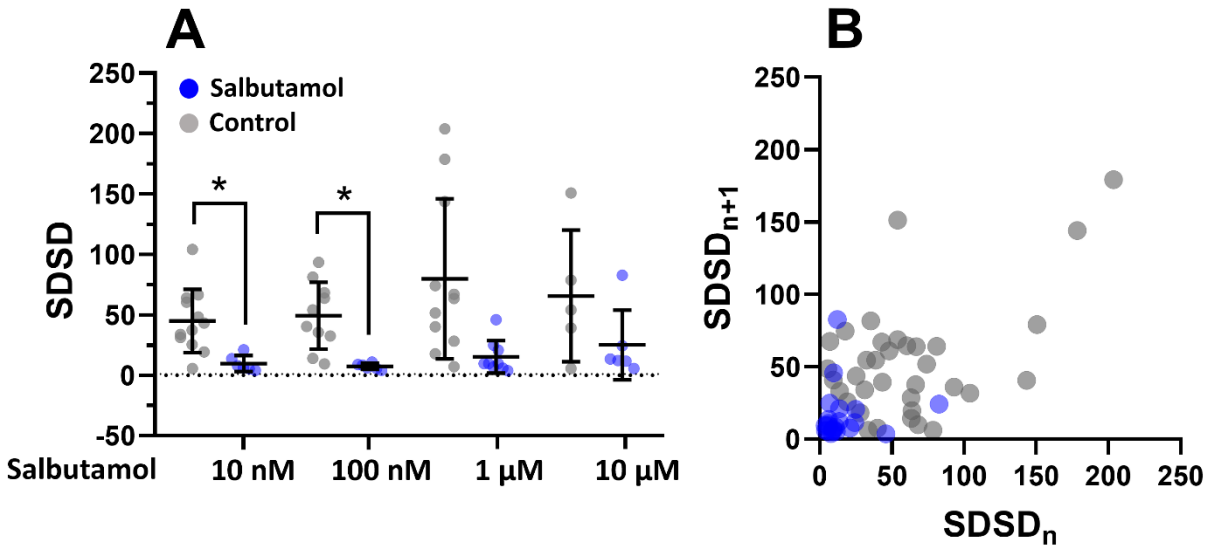



**Figure 8.2** Beat rate variability analysis of hPSC-CMs with salbutamol. **(A)** *Scatters plots with indicated means and SD of the standard deviation of successive differences (SDSD) of EBs measured in salbutamol and control (n = 8, 9, 9, and 6 for 10 nM, 100 nM, 1 µM, and 10 µM salbutamol, respectively, and n = 14, 11, 11, and 5 for the respective controls). SDSD with 10 nM and 100 nM salbutamol were significantly lower compared to controls (Brown-Forsythe and Welch ANOVA test with Holm-Sidak multiple comparisons test, control vs. 10 nM salbutamol, P = 0.0115, control vs. 100 nM salbutamol, P = 0.0139).* **(B)** *Poincaré plots with SDSD intervals.*

We observed a limited effect of salbutamol on the beat rate and contraction force, with the latter significantly increased at 100 nM salbutamol. While a significant anti-arrhythmic effect was present within all tested concentrations (i.e. 10 nM and 100 nM) of salbutamol.

### 8.4.2 Synergic effect of salbutamol and aminophylline on hPSC-CMs

Effects of aminophylline and salbutamol alone were compared with their combined action in various concentrations on EBs prepared from hPSC-CMs derived from the CCTL14 cell line. Significant increases in the beat rate and contraction force were observed when the combinations of 10 nM, 100 nM, and 1 μM salbutamol with 1 mM aminophylline were administered (Figure 3). Strikingly, a comparison with individual effects of salbutamol and aminophylline in the respective concentrations revealed an amplified effect of the combined drugs. The observed effects on the beat rate and contraction force were also validated using a different cell line (CCTL12 hPSC-CMs; Figure S1 in Supplementary data).

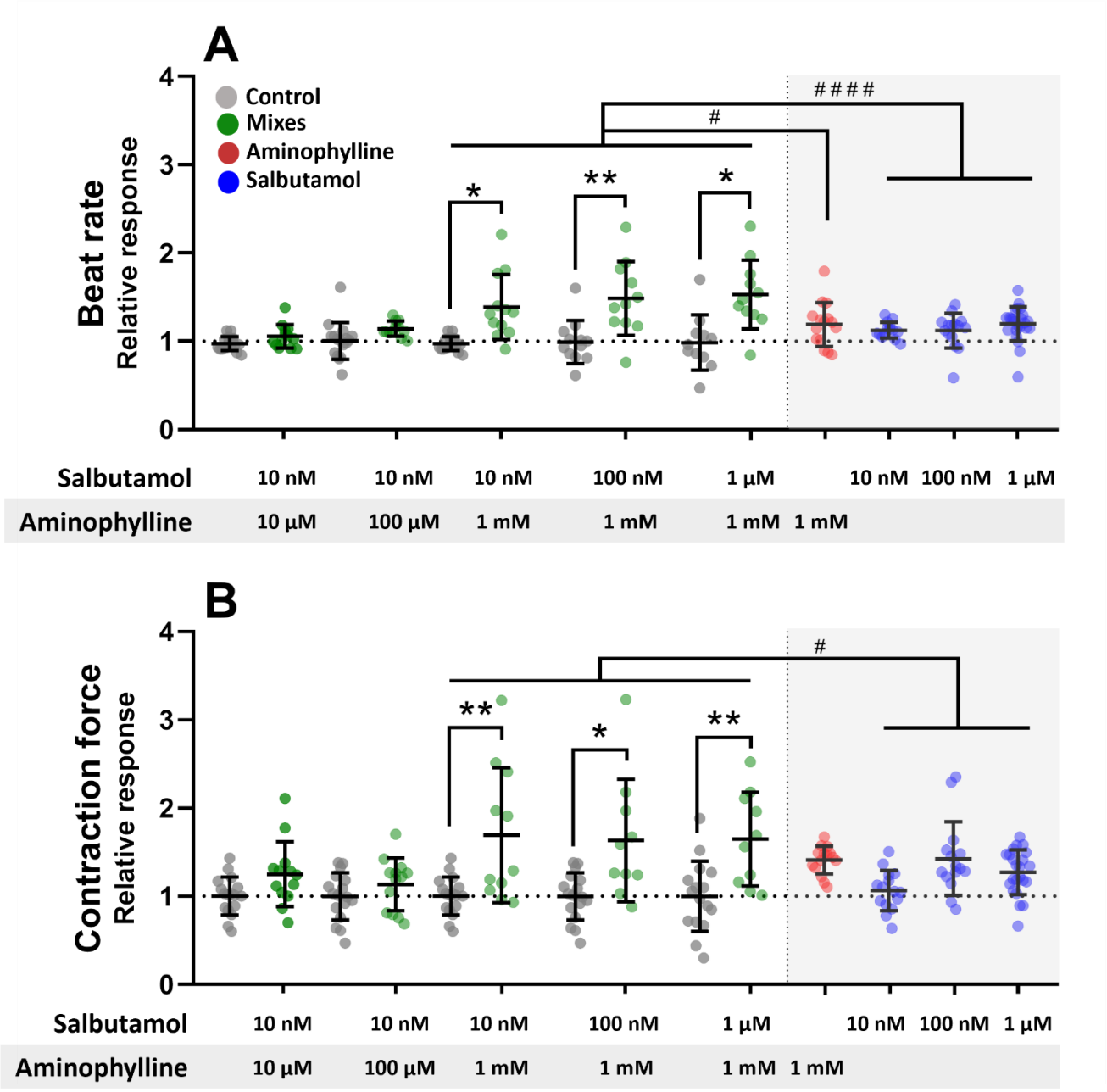



**Figure 8.3** *Synergic effect of salbutamol and aminophylline on contractile properties of hPSC-CMs. * stands for P ≤ 0.05, P ≤ 0.01, compared to control, # stands for P ≤ 0.05 and #### stands for P ≤ 0.0001. Scatter plots with indicated means and standard deviation (SD) of the beat rate (A) and contraction force (B) relative responses normalized to the respective baseline control measurement in the case of salbutamol and aminophylline and to mean values of the control measurement in the case of control (n = 17 for controls, n = 13, 13, 11, 10, 10, 15, 15, 23, and 15 for treatments, P values in Table S1 in Supplementary data, Brown-Forsythe and Welch ANOVA test was used for contraction force results, ordinary one-way ANOVA for the beat rate results and Kruskal-Wallis test was applied to compare contraction force and beat rate results of mixes with individual treatment). The legend in A applies to*

*the whole graph. The results of the mixes consist of two separate experiments, same control dataset used based on time of measurement (the first two controls are the same as the third and fourth, relating to 20 min and 40 min of treatment). The results of separate aminophylline administration originate from our previous paper* (Klimovic et al. 2022). (**A, B)** *The beat rate and contraction force significantly differed from controls in mixed treatments with 1 mM aminophylline and 10 nM, 100 nM, or 1 µM salbutamol. Still, no significant effect was observed in individual treatments. The effect of mixed treatments was amplified when compared to individual treatments.*

Analysis of the short-term beat rate variability with combined salbutamol and aminophylline treatment showed a decreasing arrhythmia tendency across the concentrations, with a significant decrease if 1 µM salbutamol and 1 mM aminophylline were applied (Figure 8.4 AB). In our previous study, we demonstrated the arrhythmogenic potential of aminophylline using the cut-off method of arrhythmia analysis (Klimovic et al. 2022). An analogical cut-off arrhythmia analysis of the current data revealed an anti-arrhythmic effect of salbutamol, alone or administered with aminophylline (Figure S2 and S3).

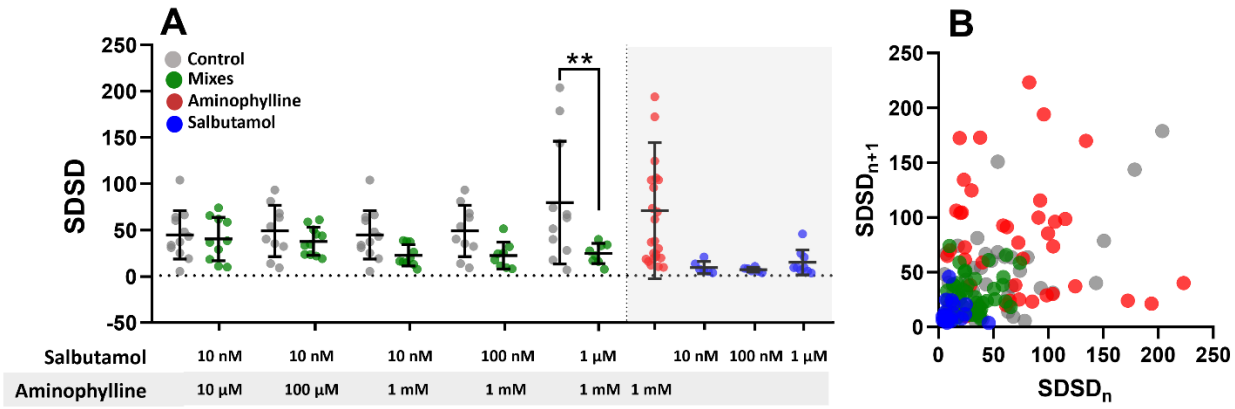



**Figure 8.4** Beat rate variability analysis with combined salbutamol and aminophylline treatments. *Scatter plots indicate means and SDs of SDSDs measured with mixed treatments and control (n = 10 for controls, n = 10, 11, 10, 8, 8, 24, 6, 6, and 9 for treatments, p values in Table S1 in Supplementary data, Ordinary one way ANOVA test was used).* **(A)** *SDSD results of EBs with indicated concentrations of salbutamol and aminophylline supplemented with separate measurements of both treatments for comparison. The results of the mixes consist of two separate experiments, so the same control dataset was used based on time of measurement (the first two controls are the same as the third and fourth, relating to 20 min*

*and 40 min of treatment). The results of separate aminophylline administration originate from our previous paper* (Klimovic et al. 2022). **(B)** *Poincaré plots with SDSD intervals.*

Overall, we observed a synergic effect of salbutamol and aminophylline as both bronchodilators potentiate their individual effects on the contraction force and beat rate; this effect was most apparent with 1 mM concentration of aminophylline. Finally, anti-arrhythmic effect of salbutamol prevailed even aminophylline was co-administered.

### 8.4.3 Activation of nitric oxide synthase (NOS) reduces aminophylline induced arrhythmia.

To exclude a contribution of possible non-specific mechanisms of the salbutamol action, we investigated the role of beta-2 adrenergic receptors ($\beta_2$-AR) in the observed effect. We co-administered butoxamine, a β2-selective blocker, with the mixture of salbutamol and aminophylline, and we observed that butoxamine effectively blocked the anti-arrhythmic effects of salbutamol and synergic effects of the salbutamol-aminophylline combination (Figure 5). Interestingly, when treatment containing salbutamol was administered before any treatment containing butoxamine, the anti-arrhythmic effect was apparent even after the addition of pro-arrhythmic aminophylline alone. (Figure S8.5 in Supplementary data). These results showed that the anti-arrhythmic effect in hPSC-CM is mediated solely through $\beta_2$-AR and could last tens of minutes after salbutamol exposure.

To test whether $\beta_2$-AR activated NOS has a role in antiarrhythmic effect of salbutamol, a well-known non-specific inhibitor of NOS Nω-Nitro-L-arginine methyl (L-NAME) was co-administered with mixture of salbutamol and aminophylline. Figure 8.6 shows that inhibition of NOS led to significant increase of SDSD value compared to mix without the inhibitor. This increase was comparable to results where sole aminophylline was administered (Figure 8.6, $P > 0.01$). These results indicate that mechanism of salbutamol anti-arrhythmic effect depends on activation NOS through $\beta_2$-AR.

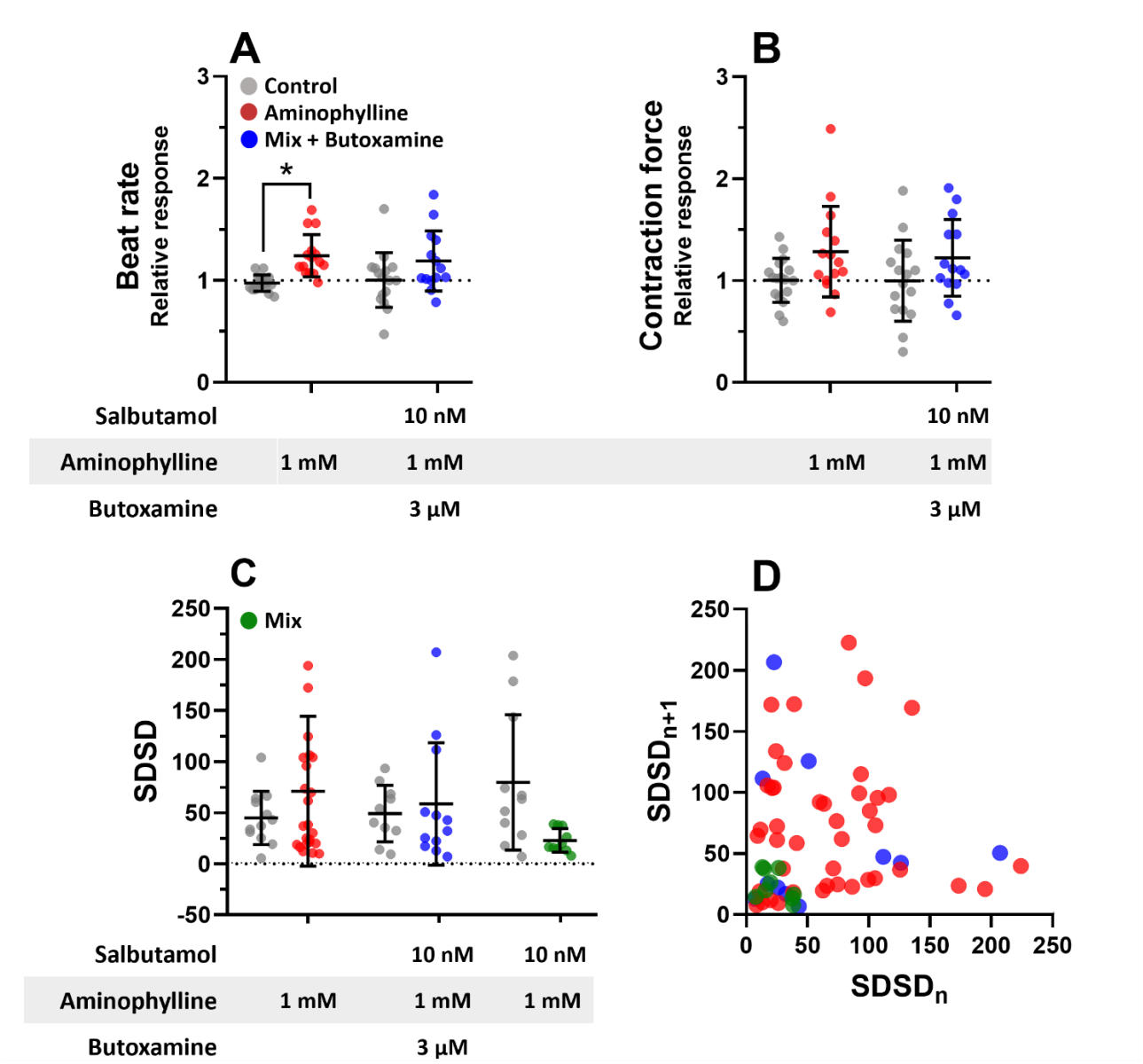



**Figure 8.5** Contractile properties and beat rate variability analysis of hPSC-CMs with salbutamol, aminophylline, and selective $\beta_2$-AR blocker butoxamine. *Scatter plots indicate means and standard deviations (SD) of the beat rate and contraction force relative responses normalized to the respective baseline control measurement in the case of salbutamol and mixed treatments and to mean values of the control measurement.* *Scatter plots with means and SDs of SDSDs measured with mixed treatments and control means (n and P values) are presented in Table S1 in Supplementary data, ordinary one-way ANOVA test was used.* **(A, B)** *The contraction force and beat rate of EBs treated with the mixes of salbutamol, aminophylline, and butoxamine are indicated at the bottom.* **(C)** *Analysis of short-term variability SDSD. Control groups were always paired with treatment groups based on the*

*time they were given, so they were repeated from previous figures.* **(D)** *Poincaré plots with SDSD. If butoxamine was added to the mix, contractile properties were not significantly different from the effect of aminophylline alone. The anti-arrhythmic potential of salbutamol completely diminished when butoxamine was co-administered.*

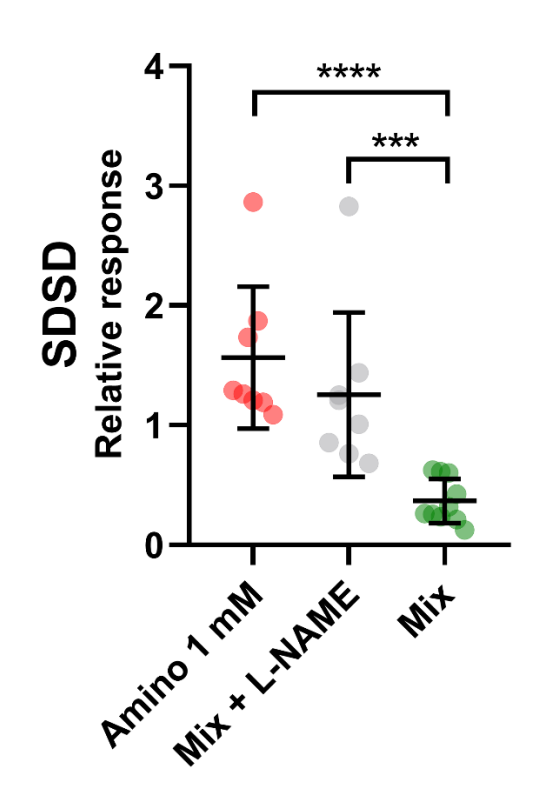



**Figure 8.6:** Beat rate variability analysis of hPSC-CMs with salbutamol, aminophylline, and L-NAME, non-selective inhibitor of NOS. *Figure shows relative responses to the respective baseline control. Results shows that L-NAME is co-administrated with mix of salbutamol (10 nM) and aminophylline (1 mM), SDSD values are comparable to results with aminophylline (1mM) and significantly increased to salbutamol and aminophylline mix without the inhibitor (Amino 1 mM vs. Mix, p = 0.0001, Mix + L-NAME vs. Mix, p= 0.0065, Kruskal-Wallis with Dunn's multiple comparisons test, n = 8 for Amino 1 mM and Mix + L-NAME, n = 10 for Mix).*

## 8.5 Discussion

In the present study, we observed that salbutamol at clinically relevant concentrations up to 1 µM, which should selectively affect $\beta_2$-AR, caused a significant inotropic effect and a non-significant trend toward a chronotropic effect on hPSC-CM clusters. When salbutamol was applied with aminophylline, inotropic and chronotropic effects were more prominent.

Importantly, this is the first report on a significant anti-arrhythmic effect of salbutamol, which reduced the arrhythmia occurrence previously introduced with aminophylline in our hPSC-CMs model. This anti-arrhythmic effect was blocked by a selective $\beta_2$-AR blocker butoxamine and by a non-selective NOS inhibitor L-NAME.

The positive inotropic effect and the concentration-dependent trend to a positive chronotropic effect of salbutamol are consistent with its known stimulatory effect on $\beta_2$-AR (Cullum et al. 1969; Corea et al. 1984; Libretto 1994; Baker 2005). This receptor is primarily expressed in cells of the lower respiratory tract, such as in smooth muscle cells, where its activation leads to relaxation and, thus, to bronchodilation (Johnson et al. 2022). In cardiac cells, there is approximately a 4:1 ratio of $\beta_1$-AR to $\beta_2$-AR; activation of both predominantly leads to chronotropy, inotropy, and lusitropy (Moniotte et al. 2001; Bristow et al. 1986). Similarly, we found lower expression of $\beta_2$ receptors compared to $\beta_1$ in our model (described in our previous work (Jelinkova et al. 2020c)). These effects are mediated by the activation of protein kinase A, which phosphorylates several effector molecules such as phospholamban (PLB), L-type calcium channels (LTCC), or troponin complex (Post et al. 1999; Lucia et al. 2018) which plays a key role in the regulation of inotropy (Keefe et al. 2023). Phosphorylation of troponin during activation of β-adrenergic receptors causes a more intense response even at lower $Ca^{2+}$ concentrations (Lorenz et al. 2017; Keefe et al. 2023). Stimulation of $\beta_1$-AR, but not that of $\beta_2$-AR, may show proarrhythmic effects(Pérez-Schindler et al. 2013), and as suggested, $\beta_2$-AR receptors may even counteract $\beta_1$-AR mediated arrhythmogenic effect(Cerbai et al. 1999). The minimal but significant chronotropic effect of salbutamol is not surprising considering its $\beta_2$ selectivity and preferential activity in the bronchial smooth muscle(Cullum et al. 1969; Baker 2005) as well as much lower expression of $\beta_2$ receptors in healthy myocardium compared with $\beta_1$ receptors(Bristow et al. 1986). The chronotropic effect of isoproterenol, a non-selective β-AR agonist, is much higher. It was shown that salbutamol at concentrations below 1 μM (which primarily stimulate $\beta_2$ receptors and were used in our study) did not cause a chronotropic effect, and its chronotropic effect at higher concentrations was mediated exclusively through $\beta_1$ receptor stimulation(Gonzalez-Muñoz et al. 2011).

As confirmed in this study (with the use of butoxamine), the observed anti-arrhythmic effect of salbutamol was primarily mediated *via* the $\beta_2$-AR. The chronotropic effect was smaller than that of isoproterenol, which corresponds to clinical experience(Akhtar et al. 2023;

Rabbany et al. 2023). Nevertheless intrinsic beat rate variability of the model may contribute to the observed trend.

In patients with obstructive lung diseases, various combinations of bronchodilator drugs are used to relieve symptoms (Zatloukal et al. 2020; Levy et al. 2023; Glob. Initiat. Chronic Obstr. Lung Dis. - GOLD, n.d.). While the side effects of individual bronchodilator drugs on cardiac physiology were studied, the side effects of combinations of these substances have not been clarified sufficiently (Cazzola et al. 2019; M. G. Matera et al. 2020; Maria Gabriella Matera et al. 2016). Hence, we decided to analyze the combined effect of different concentrations of salbutamol and aminophylline. We discovered that the combination of salbutamol and aminophylline in concentrations of at least 10 nM and 1 mM had synergic chronotropic and inotropic effects. These effects were significantly stronger compared to controls but also to individual measurements with aminophylline or salbutamol. Aminophylline, similar to other methylxanthines such as caffeine, nonspecifically inhibits phosphodiesterase (PDE) and antagonizes adenosine receptors (Ukena et al. 1993). Taken together, salbutamol (by activation of $\beta_2$-AR) and aminophylline (by inhibition of PDE and adenosine receptors) co-medication may result in an increased intracellular concentration of cAMP and synergic chronotropic and inotropic effects.

Surprisingly, the pro-arrhythmic effect of aminophylline described in our previous study (Klimovic et al. 2022) was reduced in the presence of salbutamol. The previously proposed mechanism of the aminophylline arrhythmic effect was connected to a microdomain cAMP level-related diastolic $Ca^{2+}$ releases *via* independent clusters of ryanodine receptor 2 (RyR2) channels, reducing the threshold for spontaneous $Ca^{2+}$ release (Domeier et al. 2012b). Since the antiarrhythmic action of salbutamol, both alone and in the presence of aminophylline, cannot be logically mediated by the cAMP-PKA pathway, which is generally known to show an opposite effect(Colombe and Pidoux 2021; Sucharov et al. 2011; Crespo et al. 1995; Molenaar et al. 2006). We were looking for alternative possibilities. Considering the role of the cGMP-eNOS pathway, which may be activated by β2-AR (Balligand 1999; Ghasemi and Jeddi 2022; Domeier et al. 2012a; Tamargo et al. 2010; Bhushan et al. 2012; E. Burger and Feng 2011) and is known to cause a systemic decrease of cytosolic $Ca^{2+}$ concentration and increase in SR load (Domeier et al. 2012a; Tamargo et al. 2010; E. Burger and Feng 2011), thus likely inhibiting spontaneous Ca2+ release from SR, we aimed to prove if the non-specific NOS inhibitor L-NAME could mitigate or even prevent the antiarrhythmic effect of salbutamol. The cGMP pathway also depends on cAMP level (García-Morales et al. 2017;

Balligand 1999). As apparent from Fig. 6, SDSD was not different if both salbutamol and aminophylline were applied in the presence of L-NAME from SDSD in the presence of aminophylline alone and, *vice versa*, it was significantly higher to SDSD in the presence of salbutamol and aminophylline mixture, thus, proving the central role of cGMP-eNOS pathway in the antiarrhythmic action of salbutamol.

Our main finding showing that salbutamol reduces the arrhythmogenic effect of aminophylline may be highly clinically relevant. The arrhythmogenic effect of aminophylline is widely known, occurring in about 13% of patients after intravenous administration of the drug or even in 20% of overdosed patients (Shannon 1999; Nair et al. 2012). Aminophylline-induced arrhythmia presents most frequently as atrial fibrillation, but more severe arrhythmias may also occur (Huerta et al. 2005). The dual treatment with salbutamol and aminophylline is a frequently used treatment combination in clinical practice, mainly in the hospital setting during acute exacerbations of asthma or COPD (Zatloukal et al. 2020; Levy et al. 2023; Glob. Initiat. Chronic Obstr. Lung Dis. - GOLD, n.d.). No randomized trials have been reported on the combined effect of aminophylline and salbutamol in patients with COPD or asthma. Only sparse data on the potential toxicity of this combination have been reported previously (White et al. 2004). Our data show two types of results, i.e., that salbutamol added to aminophylline may cease some arrhythmia mechanisms while enhancing the chronotropic and inotropic effects can lead to increased tachycardia, similar to literature (Insulander et al. 2004; Futyma 2019).

This study first showed that salbutamol at clinically relevant concentrations may reduce the pro-arrhythmic potential of aminophylline if both these drugs are combined. This effect was mediated *via* $\beta_2$-AR activated NOS. The clinical relevance of this finding may be high, representing a potential way to reduce pharmacotoxicity during aminophylline treatment. The combined effect of the two molecules, their safety profile, and potential arrhythmogenicity need further investigation in prospective randomized clinical trials.

### 8.6 Funding

This work was supported by the Ministry of Health of the Czech Republic, research grant no. NU20-06-00156.

### 8.7 Acknowledgments

A4L_ACTIONS, supported by European Union's Horizon 2020 under grant agreement No. 964997 and CIISB, Instruct-CZ Centre of Instruct-ERIC EU consortium, funded by MEYS CR infrastructure project LM2023042 and European Regional Development Fund-Project "UP CIISB" (No. CZ.02.1.01/0.0/0.0/18_046/0015974), is gratefully acknowledged for the financial support of the measurements at the CF Nanobiotechnology. The work was furthermore supported by project National Institute for Research of Metabolic and Cardiovascular Diseases (Program EXCELES, No. LX22NPO5104) - Funded by the European Union – Next Generation), by the European Commission's Horizon Europe Framework Program under the Research and Innovation Action MUQUABIS GA no. 101070546, and by the Specific University Research Grants of the Masaryk University , MUNI/A/1410/2022, and MUNI/A/1547/2023 provided by the Ministry of Education, Youth and Sports of the Czech Republic.

# 9 Arrhythmology application (p6)

## 9.1 Commentary: hESC derived cardiomyocyte biosensor to detect the different types of arrhythmogenic properties of drugs

The phenomenon of cardiac arrhythmia, characterized by irregular electrical activation leading to abnormal heart contractions, represents a significant clinical challenge. Atrial fibrillation (AF), the most common form of arrhythmia, significantly increases the risk of stroke, heart failure, and mortality(Al-Khatib et al. 2018; Hindricks et al. 2021; Van Gelder et al. 2024). Understanding the mechanisms underlying arrhythmias is paramount for developing effective treatments. Various substances, including thein and caffeine, have been implicated in the onset of arrhythmias(Voskoboinik et al. 2018), but on the population level his effect was found either inconclusive or even AF burden lowering(Casiglia et al. 2018). Methylxanthine's proarrhythmic effects stem from its inhibition of adenosine receptors, leading to increased intracellular calcium concentrations and neuroendocrine effects(Kong et al. 2008). Given the prevalence of arrhythmias and the challenges associated with their treatment, there is a pressing need to explore these abnormalities at the cellular level. Traditional cell models, based on single cells or monolayers, often exhibit unstable signals and fail to accurately mimic physiological tissues. In contrast, three-dimensional (3D) models, such as EBs, differentiated into CBBs offer a more physiologically relevant platform for studying cardiac function. By leveraging hPSCs, we could generate CBBs that closely resemble the developing embryo, providing insights into cardiac physiology and pathology. To create a dual-cluster model, differentiation was performed in hESC lines CCTL14 and CCTL12, into 3D BCCs, standard cultivation dishes were modified with an agarose-based mask to facilitate the precise seeding of two differentiated EBs in close proximity. These clusters were allowed to adhere for at least 24 hours, during which they spontaneously formed a functional conduction-like syncytium through cellular outgrowth. The cellular composition of this connecting bridge was characterized via immunocytochemistry for vimentin (fibroblasts), DDR2 (cardiac fibroblasts), and cardiac troponin T (cardiomyocytes), revealing a phenotype that mimics the neonatal human heart. The spontaneous synchronization of two BCCs after four days was monitored by AFM, coupled with fluorescence calcium imaging.

The primary sensing platform involved a unique application of AFM . A soft silicon nitride cantilever (MLCT-C) was positioned to land on both clusters simultaneously, enabling the recording of standard vertical deflection (beating rate of the whole syncytium) and for the first time also lateral deflection (complex movement and excitation waves spreading across the two clusters). The MCG were collected at 100 Hz. To validate the mechanical data, fluorescence calcium imaging using Fluo-4 AM was employed as a reference method, with line scans (1000 Hz) placed across the full length of the syncytium to monitor intracellular calcium release and synchronization in real-time.

We demonstrated that two independent cardiac clusters could form an electrically and mechanically connected syncytium with fully synchronized beating by $4^{th}$ day of co-culture. The biosensor's sensitivity was validated through the application of 1 mM caffeine, which acted as a model pro-arrhythmic drug. Caffeine induced an immediate shortening of the R-R interval (tachycardia) and a significant increase in the standard deviation of R-R intervals, indicating the onset of rhythm irregularities. A critical finding was the detection of conductive defects through the loss of synchrony between lateral and vertical deflection patterns. Before caffeine addition, vertical and lateral peaks followed each other closely; however, caffeine triggered a series of independent small peaks and ultimately resulted in complete dyssynchrony of lateral and vertical movements. This mechanical dyssynchrony was directly correlated with calcium handling discrepancies observed in the line scans, which revealed different pacing parts in one cluster compared to the other. Unlike single EB models, this dual-cluster setup was able to visualize the loss of complementarity and sequentially in contraction waves, providing a precise in vitro picture of atrial fibrillation-like behavior and conductive anomalies.

This system not only detects tachycardia and bradycardia but also isolates signal spreading defects through the bridge of connecting cells. Although currently limited by factors like biological sample variability and the need for stable cell adhesion, the dual-cluster AFM biosensor provides a high-information and repeatable platform for studying the initiation, progression, and termination of cardiac arrhythmias in a near-physiological environment.

Analytica Chimica Acta 1216 (2022) 339959

Contents lists available at ScienceDirect

Analytica Chimica Acta

journal homepage: www.elsevier.com/locate/aca

# hESC derived cardiomyocyte biosensor to detect the different types of arrhythmogenic properties of drugs

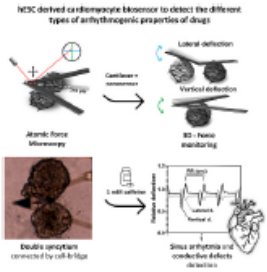
Roberto Pivato [a,b], Simon Klimovic [b,c,d], Daniil Kabanov [c,d], Filip Sverák [a,b], Martin Pesl [a,b,e], Jan Pribyl [d,**], Vladimir Rotrekl [a,b,*]

[a] Department of Biology, Faculty of Medicine, Masaryk University, Kamenice 5, 625 00, Brno, Czech Republic
[b] International Clinical Research Center at St. Anne's University Hospital, Pekarská 53, 65691, Brno, Czech Republic
[c] Department of Biochemistry, Faculty of Science, Masaryk University, Kamenice 753/5, 625 00, Brno, Czech Republic
[d] Central European Institute for Technology, Masaryk University, Kamenice 753/5, 625 00, Brno, Czech Republic
[e] First Department of Internal Medicine - Cardioangiology, Faculty of Medicine, Masaryk University and St. Anne's University Hospital, Pekarská 53, 65691, Brno, Czech Republic

## HIGHLIGHTS

- CBB consists of dual human stem cell-derived CMs cluster forming conductive syncytium.
- AFM based CBB presents relevant arrhythmic response suitable for arrhythmia detection.
- Dual cluster syncytium is able to spontaneously mimic phenotypes present in the neonatal heart.
- CBB derived from patients' specific hiPSCs possesses high potential for precision medicine.

## GRAPHICAL ABSTRACT




## ARTICLE INFO

*Keywords:*
Cell-based biosensor
Atomic force microscopy
Human embryonic stem cells
Cardiac arrhythmia
Cardiomyocytes
Caffeine

## ABSTRACT

In the present work, we introduce a new cell-based biosensor for detecting arrhythmias based on a novel utilization of the combination of the Atomic Force Microscope (AFM) lateral force measurement as a nanosensor with a dual 3D cardiomyocyte syncytium. Two spontaneously coupled clusters of cardiomyocytes form this.

The syncytium's functional contraction behavior was assessed using video sequences analyzed with Musclemotion ImageJ/Fiji software, and immunocytochemistry evaluated phenotype composition.

The application of caffeine solution induced arrhythmia as a model drug, and its spontaneous resolution was monitored by AFM lateral force recording and interpretation and calcium fluorescence imaging as a reference method describing non-synchronized contractions of cardiomyocytes.

The phenotypic analysis revealed the syncytium as a functional contractile and conduction cardiac behavior model. Calcium fluorescence imaging was used to validate that AFM fully enabled to discriminate cardiac arrhythmias in this *in vitro* cellular model. The described novel 3D hESCs-based cellular biosensor is suitable to detect arrhythmic events on the level of cardiac contractile and conduction tissue cellular model. The resulting

* Corresponding author. Department of Biology, Faculty of Medicine, Masaryk University, Kamenice 5, 625 00, Brno, Czech Republic.
** Corresponding author.
*E-mail addresses:* jan.pribyl@ceitec.muni.cz (J. Pribyl), vrotrekl@med.muni.cz (V. Rotrekl).

https://doi.org/10.1016/j.aca.2022.339959
Received 23 February 2022; Received in revised form 16 May 2022; Accepted 17 May 2022
Available online 20 May 2022

## 9.2 Introduction

Introduction of induced pluripotent stem cells (iPSCs)-derived cardiomyocytes (CM) allowed the wide development of cell-based biosensors (CBBs). This leap allowed quantification of CMs biomechanical and biochemical properties to study response to various treatments or cardiomyopathies(Gupta et al. 2019). Sensors are usually based on the multi-electrode array (MEA) (Izumi-Nakaseko et al. 2018; Jans et al. 2017; L. Wang et al. 2013), impedance-based assays (ECIS, xCELLigence®)(Q. Wang et al. 2015; Fleischer et al. 2019), piezoresistive sensor(Kim et al. 2017) or atomic force microscopy (AFM)(Martin Pesl, Pribyl, Acimovic, et al. 2016).

AFM, belonging to the scanning probe microscopy, was at the beginning used predominantly in material research and engineering. Overcoming difficulties related to biological samples allowed it to become a frequently used tool in life sciences. AFM was used to characterize the cell properties, such as phenotype(Warrier et al. 2005; Martin Pesl et al. 2017b) , cell growth(T. Wang et al. 2013)] and stiffness of living cells(Alunda and Lee 2020). Moreover, AFM was successfully used as a sensitive cell-based biosensor (CBB), capable of detecting contractile movements of the cardiac cells (H. Liu et al. 2012) and their clusters (embryonic bodies EBs) (Martin Pesl, Pribyl, Caluori, et al. 2016), or combined with MEA(Caluori et al. 2019). Additionally, arrhythmic (i.e., non-periodical) events in the natural beating pattern, often connected with cardiac non-functionality and heart failure, can be identified in the recorded data by adding drugs or other bioactive molecules(Gupta et al. 2019). AFM microscopy can also be easily combined with other methods such as optical or fluorescence microscopy, as they often create a single unit with AFM(Geisse 2009). AFM can be further combined with Raman spectroscopy, and others to bring a multiparametric description of cardiac cell functions. The main limitation is the need for proper cell adhesion on the surface and maintaining conditions such as a liquid medium and physiological temperature (Miletić et al. 2020).

Cardiac cells within the sinus node generate action potentials spontaneously (cardiac automaticity). This spontaneous activity is retrieved by diastolic depolarization, which brings the membrane potential to the threshold and triggers an impulse propagating through the cardiac conduction system. Cardiac arrhythmia is defined as a deviation from the regular electrical activation of heart contraction, originating in the sinus node(Domke et al. 1999). Human heart rate above 100 BPM is tachycardia, and around 50–60 and lower is bradycardia, arrhythmia often presents irregularly(Al-Khatib et al. 2018). The most

prevalent type of arrhythmia is atrial fibrillation (AF), affecting more than 33 million people worldwide, with an estimated increase of 2–3 times by 2050(Chugh et al. 2014). AF aggravates the risk of stroke, heart failure, and all-cause mortality(January et al. 2014). Recent studies say atrial fibrillation is independently associated with an increased risk of sudden cardiac death(Chen et al. 2013). The mechanisms of cardiac arrhythmias are divided into two categories - abnormal or enhanced formation of ectopic impulses and conduction disturbances. In a structurally normal heart, the ectopic beats seldom progress to sustained arrhythmia. Thus, conduction disturbances in the myocardial tissue are crucial.

A large body of commonly utilized substances and even drugs causing arrhythmias – i.e., antianginals, antibiotics, narcotics, or bronchodilators(Barnes and Hollands 2010). A widely available chemical compound with proarrhythmic effects is caffeine(Voskoboinik et al. 2018) Caffeine acts as a nonselective inhibitor of A1 and A2A adenosine receptors at the cellular level. Cardiovascular effects of caffeine include an increase in blood pressure, changes in heart rate, and neuroendocrine effects. These effects find reason in the blockade of adenosine receptors, causing an increase in intracellular calcium concentrations, the release of norepinephrine, and the sensitization of dopamine receptors(Daly et al. 1999). In clinical practice, caffeine finds application alone, e.g., in selected cases of hypotension(Sawynok 1995) or in combination with analgesics due to its vasoconstricting and anti-inflammatory effects(Daly et al. 1994; Temple et al. 2017). Due to the high prevalence of arrhythmias in the population, their difficult therapy, it is appropriate to address this abnormality burdening the normal functioning of the heart also at the cellular level. This approach is well served by the presented CBB, which can help describe the arrhythmia, its formation, the treatment, and possibly the effect of therapeutical drugs, as even the treatment medication may cause adverse side effects.

Most of the available cell models are based on single cells or smaller clusters of cells, both of which produce unstable signals(Wu et al. 2021). Other models are based on cell monolayers, such as the model proposed by Lian et al.(Lian et al. 2012). The major limitation of these monolayer models is that the environment in which cells are grown does not allow to form 3D syncytia with sufficient similarity to physiological tissues(Zuppinger 2016). Monolayers present a significantly reduced extracellular matrix, connections between cells only at the periphery of the cells, and the answer to drugs is uniform in all cells. Therefore, 3D models such as embryoid bodies (EBs) are more indicated. EBs are 3D aggregates of cells that imitate structures of the developing embryo and can be differentiated from different

lineages such as human embryonic stem cells (hESCs) or patient-specific human induced pluripotent stem cells (hiPSCs), enabling their use in precision medicine(Pettinato et al. 2014). In the present work, hESCs were used. The rationale for using hESCs is that they represent a standard in the field and they do not carry the burden of somatic mutations or reprogramming-induced epigenetic effects(Kobold et al. 2015).

In the present work, we introduce a new biosensor setup based on a combination of atomic force microscope with the hESC derived CMs, where the microcantilever of the microscope creates a sensitive transducer to study cardiac arrhythmias. Computational analysis of image sequences served as a reference method to monitor synchronization of the arrhythmic beating of two cell clusters connected by cardiac conduction-like syncytium. Moreover, the fluorescence calcium imaging supports data obtained by the biosensor setup. The arrhythmic events were induced by caffeine solution. The use of the biosensor setup for a detailed description of the arrhythmia initiation, progression, and termination is presented and discussed.

## 9.3 Materials and methods

### 9.3.1 Cell lines, cultivation, and differentiation into embryoid bodies

Human embryonic stem cell (hESCs) CCTL14 and CCTL 12 were used in the present work. These cell lines have been derived in Masaryk University, Brno, approved by Ministry of Education of the Czech Republic (MSMT approval no.14648/2016-5) and were previously characterized and described(International Stem Cell Initiative et al. 2007b). Cell lines have been maintained on the feeder layer of mouse embryonic fibroblasts (mEF), that have been inactivated mitotically by irradiation as previously described(Jelinkova et al. 2019). Cardiac differentiation was performed as described in Ref. (Jelinkova et al. 2020a).

### 9.3.2 Cultivation dish preparation and EBs seeding

Standard 30 mm cultivation dishes (TPP, cat no. 93040) and low 35 mm ibidi µ-Dishes (ibidi, cat. no. 80136) had to be modified with an agarose-based mask to increase the probability of seeding two differentiated embryoid bodies next to each other. Consequently, we delimited the area to let the EBs adhere when the following protocol was employed. A 0.5 ml Eppendorf tube was cut to obtain 4 mm external diameter sections. The prepared sections were fixed to the bottom of the cultivation dish with a double-sided scotch. The remaining space in the dish was filled with a 1 mm thick layer of 1% agarose dissolved in PBS. Agarose

solution created gel after 20 min of incubation at RT. The addition of 1 ml of PBS stabilized the gel layer after another 10 min. The plastic mask was then removed, the dishes were closed and sealed with a parafilm. The whole process was finished with sterilization by gamma- force spectroscopy mode (1 nN setpoint) using MLCT-C cantilever irradiation at 100 Gy. Dishes were stored for a maximum of one week (Bruker). The cantilever was chosen based on its dimensions, allowing it to land on both EBs simultaneously (see Fig. 9.1). The dish was washed twice with PBS prior to seeding the EBs. The levers from silicon nitride were used due to their properties when bottom of the holes created by the masking process was coated with measuring in liquid. 30 mm cultivation Petri dishes containing either 0,1% gelatin for at least 30 min at 37 ˚C and 5% $CO_2$ to promote the cell distilled water for calibration or double EB were placed to the motorized adhesion. Then, the excess gelatin was removed, 1 ml of cultivation stage with a pre-heated Petri dish heater to 37 ˚C. The laser reflection medium was added, and two differentiated EBs were seeded. Thus, sum was maximized before each experiment, and the laser detector was prepared samples were left for at least 24 h in a standard $CO_2$ incubator centered. After that, cantilever sensitivity and stiffness via the to produce adhered double-EB structure. contact-free method in Bruker-JPK software were determined. Vertical and lateral deflection data was collected in 100 Hz frequency as sampling frequency was chosen three times higher than the frequency required to sample the fastest event in previous recordings.

### 9.3.3 Processing of video sequences mechanocardiograms (MCG).

After seeding of EBs, the development of beating synchronization the QRS complex. Vertical deflection provided information about the was monitored in real-time by analyzing sequences of optical images. R-R interval and its immediate response to caffeine. Beating frequency Monitoring was performed by the everyday acquisition of 20-s videos on was calculated as 60s divided by average R-R interval in seconds during the Zeiss LSM 700 microscope in the bright field and processing them post processing. The lateral (horizontal) deflection representing the using ImageJ/Fiji macro Musclemotion (see supplementary material[37].) complex movement of the syncytium was used to report on the different defects of EB synchronization. Each sample was measured for 1 min in a standard cultivation medium (MEF), followed by 1-min measurements

### 9.3.4 Atomic force microscopy

Cells were treated with 1 mM caffeine in MEF in 0, 5, and 10 after the addition of treatment. Experiments to assess the effect of caffeine (Sigma Aldrich, cat. No. C-0750) on our syncytium has been performed 24 h (AFM) method (JPK Nanowizard 3, JPK-Bruker) was used as described after synchronization of the syncytium. before(Martin Pesl, Pribyl, Acimovic, et al. 2016). In a liquid environment, measurements were conducted in Data analysis obtained from AFM was based on the combination of average RR length, the distance between two R peaks, and standard deviation of the average RR length in vertical and lateral deflection data (Fig. 9.1B, D). These values, recorded for each time point, have been normalized concerning the values registered in standard cultivation medium, i.e., without caffeine. Variation of RR length indicates the onset of tachycardia or bradycardia. The onset of arrhythmic events was assessed by comparing the standard deviation value computed after caffeine treatment concerning the value registered in the standard cultivation medium. Data extraction was performed employing our python script(DaniilKabanov [2021] 2021). Analysis of typical MCG curve recorded by AFM is shown in Fig. 9.1.

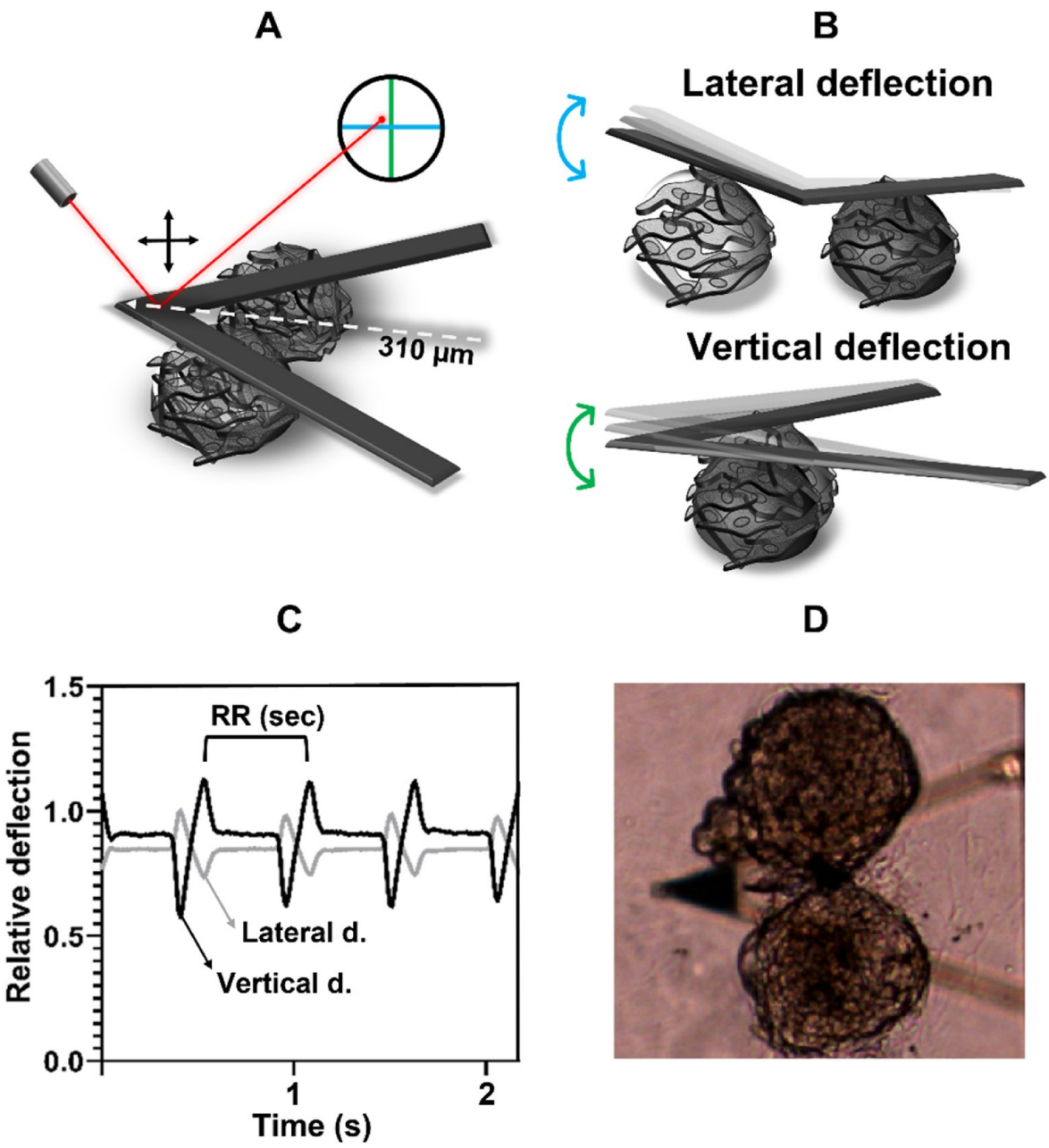



*Fig. 9.1. (A) - Schematic description of the AFM methodological approach. The soft silicon-nitride lever measures the contraction movement of the double-EB in both planes, (B) as lateral and vertical force change deflection of the cantilever. (C) –Representative mechanocardiogram with indicated vertical, lateral synchronized deflection and RR length in seconds (D) - Real image from the top optical microscope captures the cantilever in contact with both EBs, magnification 10×.*

### 9.3.5 $Ca^{2+}$ imaging

The fluorescence staining of cytoplasmic calcium with Fluo-4-AM (Invitrogen, cat. no. F14201) dye was used as a supportive analysis of the contraction movements. This allowed

for monitoring of the contraction by measuring the $Ca^{2+}$ release from sarcoplasmic reticulum. The samples of double EBs were prepared with the same protocol as for AFM measurements; the $Ca^{2+}$imaging experiments were performed 24 h after syncytium synchronization. The staining protocol was adopted from the literature(Klimovic et al. 2021) Briefly, 1.5 µM Fluo-4-AM solution in DMSO was added to the cultivation medium. EBs were then incubated for at least 30 min at 37 ˚C and 5% $CO_2$ in the dark. No washing of the fluorescence dye was necessary. The measurement of $Ca^{2+}$ fluorescence was performed on Zeiss LSM 700 confocal microscope using software Zen Black. Here, line scan analysis was performed (1000 Hz) by placing the line across our syncytium to cover its full length. Line scans were then processed on ImageJ/Fiji(Schindelin et al. 2012). Two regions of interest (ROIs) were applied, one over each EB, and evaluated was each ROI average intensity of the fluorescence signal for every timepoint. Data extracted were then plotted in GraphPad software (GraphPad Software) to analyze the evolution of the mutual interaction between the two EBs in real-time.

### 9.3.6 Immunocytochemistry

To unravel the cellular phenotypes composing our syncytium, immunocytochemistry analysis for three markers was performed. Vimentin (Santa Cruz Biotechnologies, cat. no. sc-7557, dilution 1:250) as a marker of fibroblasts(Tarbit et al. 2019); Discoidin Domain Receptor 2 (DDR2- Santa Cruz Biotechnologies, cat. no. sc-81707, dilution 1:100) marker of cardiac fibroblasts(Camelliti et al. 2005); Cardiac Troponin T (cTnT- R&D Systems, cat. no. MAB1874, dilution 1:100) marker of CMs(Jelinkova et al. 2020b). Briefly, the samples were fixed in ice-cold paraformaldehyde, after permeabilization with 0.2% Triton X, blocking with 2.5% BSA solution in PBS buffer containing 0.1% Tween detergent followed. The incubation of samples with primary antibodies was performed overnight at 4 ˚C. The following day, the secondary antibodies were applied, and cover glasses were mounted on the Mowiol® 4–88 (Sigma, cat. no. 9002- 89-5) layer with DAPI (Thermo Fisher Scientific, cat. no. 62248). Secondary antibodies labeled with the Alexa Fluor 488 (Invitrogen, cat. no. A-21202) and Alexa Fluor 594 (Invitrogen, cat. no. A-21203) dyes were both applied in dilution 1:500.

## 9.4 Results and discussion

In this study, we presented a new stem cell-based model for the study of cardiac arrhythmias coupled with AFM forming together a biosensor capable of detecting arrhythmogenic

properties of drugs. Starting from hESCs, we have been able to form a suspension of hESC's clusters which were differentiated into CMs syncytium. Two such clusters seeded on adherent plate in vicinity spontaneously formed electrically connected syncytium presenting fundamental phenotypes of the human myocardium and its conductive system. Formation of the syncytium, beating synchronization, and study of arrhythmia monitored by the AFM and calcium release are presented and discussed in the following chapter.

### 9.4.1 Formation and characterization of functional syncytium

In this work, two beating clusters were seeded in the vicinity on an adhesive surface allowing cell outgrowth from the EBs. The adhesive surface was previously shown to inhibit cardiogenesis via SRC-family kinases(Zhang et al. 2014), promote cell migration(J. Liu et al. 1999), and fibroblast proliferation(Kilkenny et al. 2003). To investigate the cellular composition of the conductive cell layer connecting the two synchronized EBs, staining of vimentin and discoidin domain receptor 2 (DDR2) was visualized by confocal microscopy (Fig. 9.2). A positive signal for vimentin evenly spread across the cell layer suggested the presence of fibroblast cells. Most cells between the two EBs ('a bridge') proved to be positive for DDR 2, a specific marker of cardiac fibroblasts. The presence of cardiac fibroblasts has been previously shown to be a key factor in the onset of cardiac syncytia synchronization(Jang et al. 2020). Cardiac fibroblasts are also crucial in forming tissue-like architecture(Eder et al. 2016). Finally, the syncytium and the bridge were positively stained for cTnT, structural CMse protein, and synchronization of the contractions of the two EBs was observed on day 4. Considering the hESC-derived CMs have a similar phenotype as fetal/neonatal CMs(Sala et al. 2017) the composition of the connecting cell layer may resemble the composition of the human fetal heart(Dewing et al. 2022). Two EBs were seeded in proximity, thus creating a functional syncytium "bridge" during the following days. Sets of EBs with the suboptimal distance between each other were excluded. The beat rate and synchronicity of the EB pairs were observed in time for 4 days from seeding. Syncytia formed by the two EBs connected by conductive cell layer (Fig. 9.1) with fully synchronized beating were observed at day four for all analyzed samples (Fig. 9.3; 10 EB sets were analyzed).

The unification of the beating frequency of the two EBs and the synchronization of their beats was associated with cell outgrowth on adhesive tissue culture dishes, stemming from both EBs. Correlation between the amount of the cellular outgrowth and synchronization of the beating was observed, suggesting the formation of a conductive cell layer between the

EBs. The cell outgrowth was fundamental for the synchronization of the syncytium. Synchronization may come from the excitable cardiac fibroblast population(Jang et al. 2020) or gap junctions formed between adjacent CMs(Aratyn-Schaus et al. 2016).

### 9.4.2 Detection of caffeine-induced arrhythmia by AFM based biosensor and Fluo-4

An extremely sensitive setup based on the microcantilever of AFM acting as a nanosensor was used to analyze the contractile properties of both EBs (Fig. 9.1). Recorded data were analyzed for both vertical (beating frequency) and horizontal (synchronization) deflections (Fig. 9.4). Caffeine was used to induce arrhythmic events.

Caffeine addition induced shortening of the RR interval and thus the increase in the beat rate of the syncytium (Fig. 9.4). This was reflected by both the change in vertical and lateral deflection (Fig. 9.4a, c). Calculated standard deviation reports on the irregularity/arrhythmic events. A significant increase in standard deviation was observed immediately after caffeine injection (Fig. 9.4b and d, time 0 min) in comparison to other time points, suggesting an arrhythmic event induced by the caffeine. The caffeine-induced increase in standard deviation was observed for both the lateral and the vertical deflection.

The decrease in average RR length is comparable for vertical and lateral deflection after the addition of caffeine (Table S9.1), witnessing that the chronotropic effect of caffeine increases with time. The standard deviation of the RR interval, on the other side, increases only immediately after the addition of caffeine in both the vertical and lateral deflection, while it is lower than the control value in all other time intervals (Table S9.1). The increase in RR standard deviation at time 0 suggests that RR standard deviation reports the caffeine-induced beat rate irregularity (vertical movement) and EBs' synchronization irregularity (lateral movement).

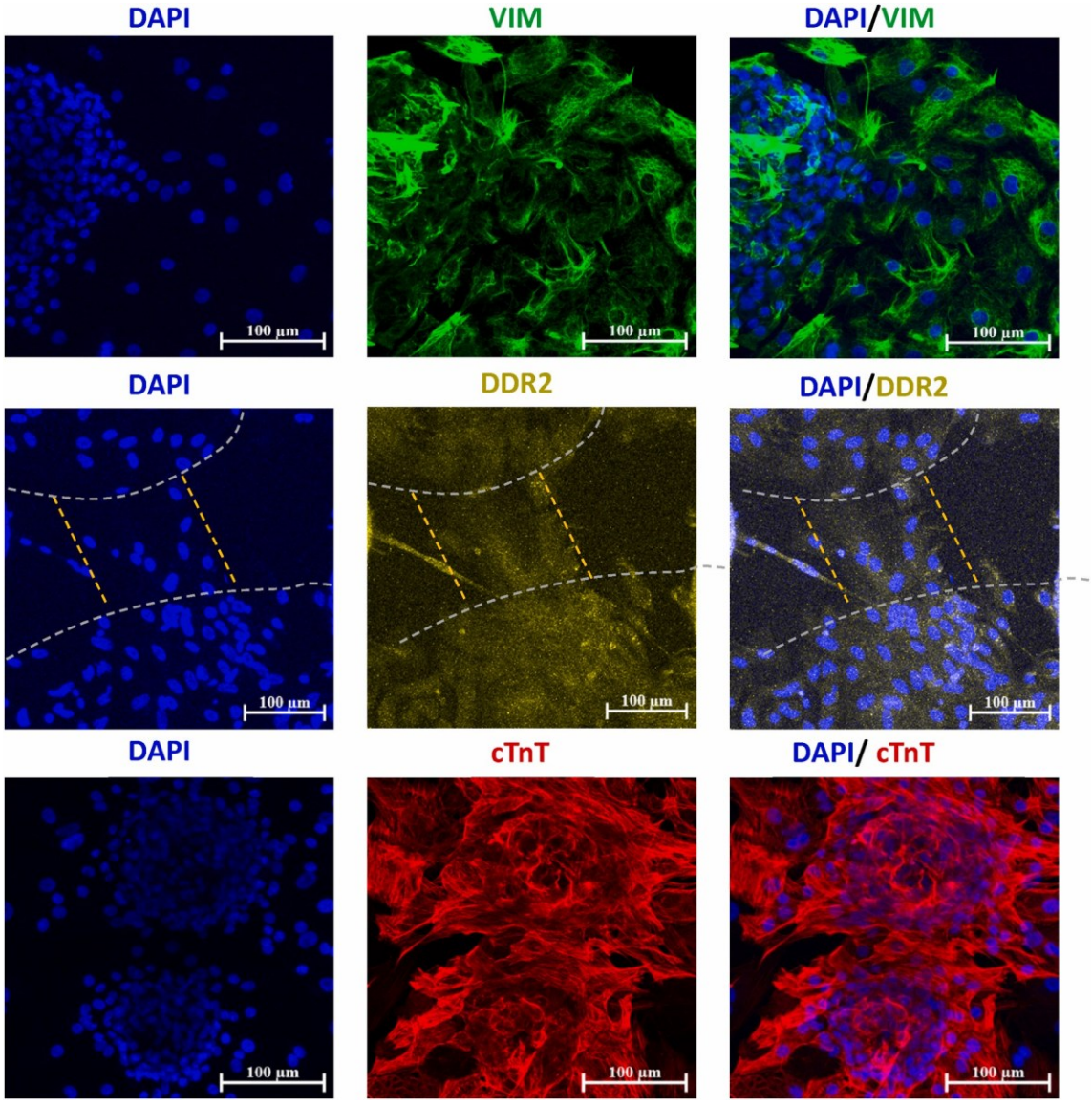



***Fig. 9.2.*** *Cell composition of the connective cell layer between the two adjacent EBs 'a bridge'. The cell layer formed by cell outgrowth from the two EBs on the adhesive surface was stained for the presence of the fibroblast marker vimentin (green), cardiac fibroblast marker DDR2 (yellow), and cardiomyocyte marker cTnT (red). The yellow color was obtained in postprocessing. Orange dashed line helps to recognize connecting 'bridge'; the grey dashed line visualizes partial contours of both EBs. (For interpretation of the references to color in this figure legend, the reader is referred to the Web version of this article.)*

Further, caffeine affected the synchronization of vertical and lateral displacement of the AFM cantilever (Fig. 9.5). The lateral and vertical deflection peaks followed each other closely before adding caffeine, suggesting the spread of contraction waves through the syncytium (Fig. 9.5A). Adding caffeine caused a series of small peaks (independent lateral

and vertical deflections) and ultimately resulted in complete dyssynchrony of the lateral and vertical movement (Fig. 9.5B). That suggests arrhythmic-like events caused by defects in signal spreading through the bridge of cells between the two EBs, resulting in the irregular beat of the two EBs (Fig. 9.5B).

The addition of caffeine induced the loss of synchrony between lateral and vertical deflection resulting in the displacement of the cantilever in both directions (for detail see Fig. 9.5C).

The novel double EB biosensor benefits from atomic force microscopy's real-time measuring mechanical response. Measuring the displacement of a soft cantilever in time gave us information about both cellular clusters' lateral and vertical movements. We hypothesized that vertical movement reports on the beat rate of the whole syncytium while lateral movement can record excitation waves spreading across the double EB set up and report on asynchronous events due to irregular beat of the adjacent EBs.

To validate our hypothesis, our model consisting of two EBs connected in syncytium was subjected to measurement of intracellular cytosolic $Ca^{2+}$ employing fluorescent calcium-sensitive detector Fluo-4. The line scan across the two EBs and their connective layer allowed for the observation of synchronization of the two EBs (Fig. 9.6 C, D, F). Caffeine induced a progressive increase of beat rate, consistent with the observation by AFM. The whole syncytium presents a higher beat rate in caffeine's presence than the MEF media without the caffeine. Caffeine further induced beat rate irregularities and beating discrepancies between the two EBs suggesting the presence of synchronization defects of the two EBs in the double EB biosensor (Fig. 9.6 C and D). Fig. 9.6 also shows a different pacing part of one of the clusters compared to the contraction rate of the syncytium (Fig. 9.6 E and F). To validate our hypothesis, our model consisting of two EBs connected in syncytium was subjected to measurement of intracellular cytosolic $Ca^{2+}$ employing fluorescent calcium-sensitive detector Fluo-4. The line scan across the two EBs and their connective layer allowed for the observation of synchronization of the two EBs (Fig. 9.6 B, D, F). Caffeine induced a progressive increase of beat rate sound with the observation by AFM. The syncytium presents a higher beat rate in caffeine's presence than the MEF media without the caffeine. Caffeine further induced beat rate irregularities and beating discrepancies between the two EBs suggesting the presence of synchronization defects of the two EBs in the double EB biosensor (Fig. 9.6 C and D).

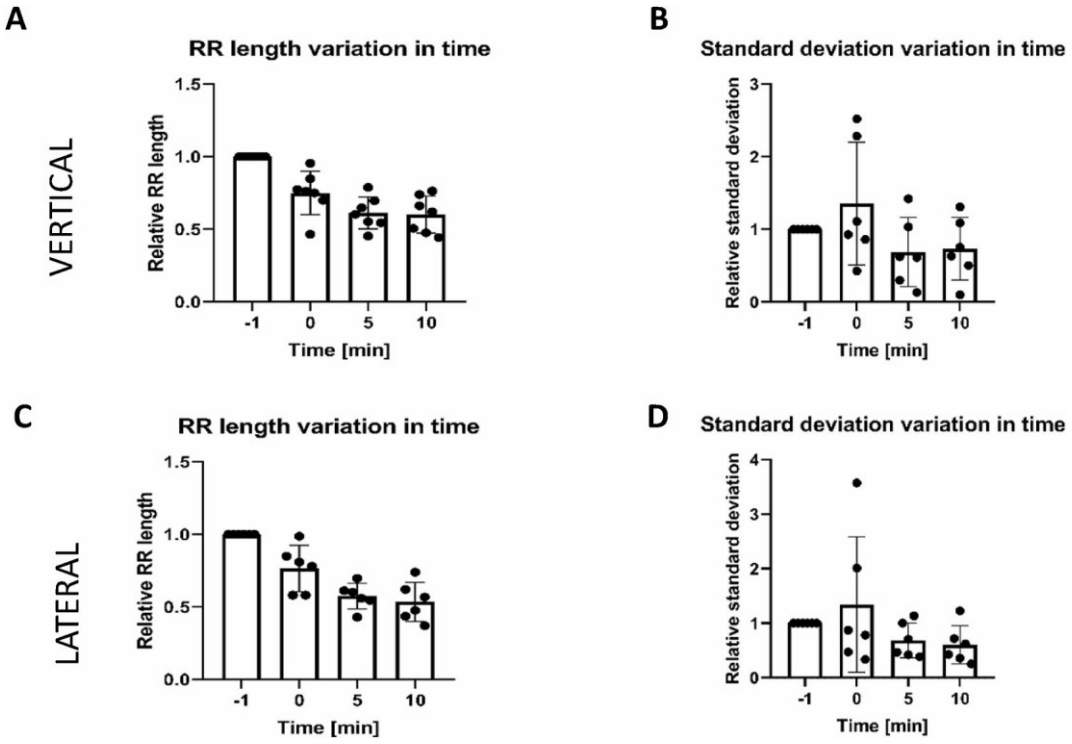



*Fig. 9.4. AFM analysis of the caffeine induced changes in vertical and lateral displacement. Time -1 min indicates measurements conducted in MEF media without caffeine. Caffeine was added at 0 min with subsequent measurements at 5 and 10 min. The vertical displacement (VERTICAL) and lateral displacement (LATERAL) were analyzed. The frequencies of the vertical and lateral movement reporting on the chronotropic effect of caffeine are shown on panels A and C, while the variation of the movement in time is plotted as standard deviation values on panels A and B. Both average RR length and standard deviation have been normalized to the average RR length and standard deviation value before caffeine addition. In both cases, the RR length decreases in time, and the standard deviation increases right after adding caffeine medium.*

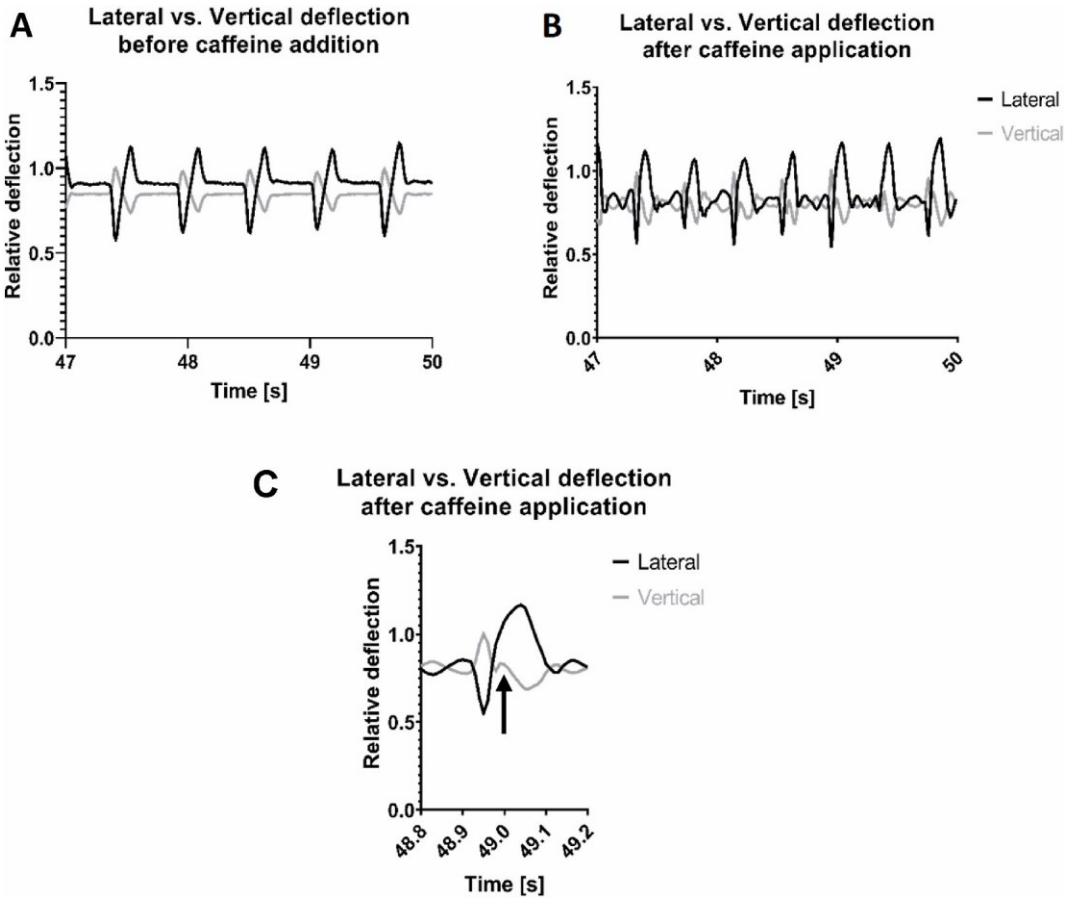



***Fig. 9.5.*** *Caffeine-induced dyssynchrony of the lateral and vertical deflections. Comparison of lateral and vertical deflection before caffeine addition (panel a) and after caffeine addition (panel b). In standard culture medium, vertical and lateral deflection appears to be synchronized with slight time shifts. Caffeine induced irregular small deflections and dyssynchrony of lateral and vertical displacements. (c) Detail of the comparison between vertical and lateral deflection after the application of caffeine. The arrow indicates the instant where dyssynchrony is detected.*

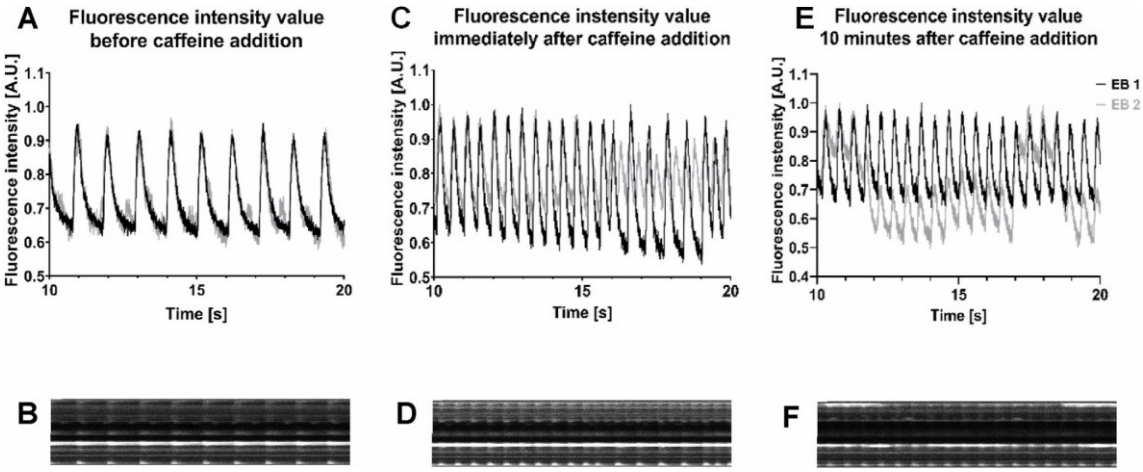



***Fig. 9.6.*** *Calcium imaging analysis of caffeine-induced synchronization defects of the double EB biosensor. Evaluation of the time evolution of the synchronicity of the two EBs (EB1 in black and EB2 in grey) of the double EB biosensor by line scan in high sampling frequency. Panels a and b show representative data of the double EB biosensor in MEF media (control). Panels c to f show three types of beat rate and synchronization defects after caffeine addition. Each curve and image represent 10 s recording before (panels A and B) and after caffeine addition (panels C to F).*

As already mentioned, in the present work, we used a 3D model derived from the model used by Ref.(Pesl et al. 2013). Our model and the single EB model agree on the arrhythmic response caused by caffeine except for the stop-and-go effect not observed in the double EB setup. Moreover, the single EB presents a lower degree of complexity as it does not allow to characterize the effects of chemical compounds on the conductive system employing AFM. Indeed, differentiated EBs present a combination of atrial, ventricular, and nodal CMs (Naumova and Iop 2021) Our model can detect rhythm abnormalities on vertical deflection and conductive disorders on a horizontal deflection by comparing vertical and lateral deflection. In the present study, a conductive defect caused by caffeine equals either ventricular or atrial fibrillation-like behavior and a decrease of contractile function. This is a precise picture of proarrhythmogenic loss of complementarity and sequentiality between vertical and horizontal deflection patterns. This proves that our detection method based on AFM is suitably sensitive for detecting arrhythmic events.

The introduction of the effects caused by the conductive cardiac system and the complex behavior of caffeine represents an advantage of our model compared to 2D models. However, the arrhythmic response of our syncytium is coherent with planar models present

in the literature, whether analyzing tachycardia-like(Balasubramaniam et al. 2005; Korohoda et al. 1995), fibrillation-like(Shafaattalab et al. 2019) or conductive anomalies(Satoh 1993) response. On the other hand, the multicellular system may constitute an eventual limitation as a dual model cannot discreet single-cell phenotype as other 3D(Kawatou et al. 2017) or 2D (Gharanei et al. 2022) models, thus increasing the difficulty of studying the contribution of single cellular phenotypes on the arrhythmic response. The phenotype is a known hurdle in the process of drug screening(Sala et al. 2017). Further, we must acknowledge that our system is unlikely to contain Purkinje bundles, the anatomical structure of the cardiac conduction system, responsible for certain kinds of arrhythmias and it' development(Tusscher and Panfilov 2008). Thus, the involvement of direct Purkinje cells generation from hESCs by cAMP signaling activation(Tsai et al. 2015) might be the next step in developing a complex cardiac conduction system model.

Nevertheless, using this model has a crucial advantage. As a matter of fact, for the differentiation of EBs, it is possible to use both hESCs and hiPSCs (Jelinkova et al. 2020). The use of hiPSCs could be used in the future to introduce patient-specific models that would allow ad hoc drug screening(Kussauer et al. 2019) to select the most appropriate anti-arrhythmic drug for a given patient/pathology.

AFM also comes with limitations as the samples need to adhere, and the question of sterility comes to mind when measuring for a longer time. Some alternatives can be used for mechanical responses measurements, such as traction force microscopy or optical tweezers(Arbore et al. 2019; Lekka et al. 2021; Schaefer and Tranquillo 2016). Those two, however, lack a straightforward sample preparation in the case of the former or are experimentally complex in the case of the latter. Methods based on image processing software such as Musclemotion(Sala et al. 2018), Myocyter(Grune et al. 2019) and others, offer a non-invasive way to measure mechanical response; however, they lack the sensitivity of AFM and information about contraction force. Moreover, optical methods lack exact recognition of CMs cultivated *in vitro* due to their immature morphology compared to isolated CMs and often require dissociation of the syncytium (M. L. Rodriguez et al. 2014). Compared to AFM, calcium imaging required sophisticated image/video postprocessing and analysis. Finally, impedance assay methods were also used for mechanical contraction measurements(Jahnke et al. 2013), but it's unclear whether this method would be feasible with two EBs. Some methods are probing contractile properties in the context of cellular electrophysiology rather than mechanobiology. Those methods include fluorescence

voltage-sensitive or calcium-sensitive dyes, arguably suitable for this model, though, become toxic for the cells after a given time(Ahola et al. 2018; Guatimosim et al. 2011; Herron Todd J. et al. 2012). Compared to AFM, fluorescent calcium indicators require an incubation period and the intracellular presence of the indicator may interfere with cell physiology. Nevertheless, the fluorescent methods can serve as complementary methods.

On the other hand, a multi-electrode array (MEA) is suitable for this model as each EB can sit on a different electrode, allowing simultaneous field potential monitoring of both EBs. Still, such measurement would be complicated by adhering EBs exactly on the electrode. Optimization in this regard, for example, by different types of coating, is very desirable, as this method can be easily combined with AFM. This MEA-AFM setup would give us complex information about electro-mechanical coupling(Caluori et al. 2019), together with the detection of arrhythmic events demonstrated in this paper.

## 9.5 Conclusion

Dual cluster CBB using human stem cell-derived CMs based model presents relevant arrhythmic response and confirms AFM as a suitable device for arrhythmia detection.

Dual cluster syncytium can spontaneously mimic phenotypes present in the neonatal heart, yet its heterogeneity might constitute a limitation. On the other hand, this model already possesses high potential for patient-specific drug screening as future application as patients' hiPSCs derived beating EBs have already been successfully differentiated.

## 9.6 Acknowledgments

The European Regional Development Fund supports this project – Project ENOCH (No. CZ.02.1.01/0.0/0.0/16_019/0000868) and by Brno Ph.D. Talent Scholarship, funded by the Brno City Municipality. CIISB, Instruct-CZ Centre of Instruct-ERIC EU consortium, funded by MEYS CR infrastructure project LM2018127, is gratefully acknowledged for the financial support of the measurements at the CF Nanobiotechnology.

Ministry of Health of the Czech Republic, grant NU20-06-00156 has financially supported this work.

## 9.7 Appendix A. Supplementary data

Supplementary data to this article can be found online at https://doi.org/10.1016/j.aca.2022.339959.

## 10 Final Conclusion and Future Perspectives

The research presented in this habilitation thesis demonstrates the successful development and application of a multi-modal cell-based biosensor (CBB) platform centered on human pluripotent stem cell-derived cardiomyocytes (hPSC-CMs) and Atomic Force Microscopy (AFM). By transitioning from traditional two-dimensional (2D) cultures to three-dimensional (3D) embryoid bodies (EBs) and differentiated BCCs, this work has established a physiologically relevant framework for studying cardiac mechanics, electrophysiology, and pharmacology in vitro.

The core achievement of this research was the optimization of AFM as a high-fidelity nanomechanical transducer capable of recording MCG with a sensitivity down to 200 pN. Initial studies proved that using non-coated silicon nitride cantilevers with a 5-6 nN setpoint provided long-term thermal stability for measurements lasting up to 8 hours. The platform's robustness was further enhanced through the integration of MEA, allowing for the synchronous recording of extracellular field potentials and mechanical force. This integration facilitated the first-ever measurement of the electro-mechanical delay (EMD) in a 3D in vitro model, providing a critical new parameter for assessing cardiac function.

Furthermore, the addition of calcium imaging allowed for the simultaneous monitoring of intracellular calcium transients and mechanical contractions. By employing advanced signal processing methods such as ensemble empirical mode decomposition (EEMD), the biosensor effectively correlated calcium wave dynamics with contractile output, identifying expected physiological responses to caffeine stimulation, such as an 8.4% increase in beating frequency and a significant rise in basal fluorescence.These methods allow for the analysis of key features, such as cell phenotype, stiffness, contraction properties, and the natural beating pattern of cardiac cells, which is critical for understanding heart function and failure. Importantly, the ability to observe arrhythmic events, which indicate non-functional or dysfunctional heart tissue, makes these systems particularly valuable for the study of cardiac health and disease.

### 10.1 Disease modeling

A major pillar of this thesis was the application of these technologies to Duchenne Muscular Dystrophy (DMD). By utilizing patient-specific induced pluripotent stem cells (hiPSCs) and CRISPR/Cas9-edited embryonic lines, the research successfully recapitulated the human DMD phenotype in vitro. The findings revealed a pathological signature characterized by hypocontractility, bradycardia, and significantly increased heart rate variability. Intracellular analysis showed that DMD-CMs exhibit impaired calcium handling, marked by elongated time-to-peak transients and a higher frequency of diastolic calcium leaks. Pharmacological trials uncovered a blunted beta-adrenergic response despite the overexpression of relevant beta-receptors, suggesting a signaling pathway dysfunction similar to that seen in clinical heart failure. Crucially, the detection of elevated free cardiac troponin T (cTnT) in the culture medium from day 35 of differentiation provided a biochemical marker for progressive cardiomyocyte wasting, aligning the in vitro model with clinical diagnostic standards. . This model has been particularly useful also in studying

conditions like Catecholaminergic Polymorphic Ventricular Tachycardia (CPVT), and Diabetic Cardiomyopathy, beyond scope of this thesis.

### 10.2 Pharmacological Analysis and Arrhythmia Detection

The biosensor platform proved to be a highly sensitive tool for drug cardiotoxicity screening. Research on the bronchodilator aminophylline identified two parallel arrhythmogenic mechanisms: a concentration-dependent ("deterministic") chronotropic effect and a concentration-independent ("stochastic") occurrence of rhythm irregularities. Subsequent studies on the combination of aminophylline and salbutamol—a common clinical pairing—revealed a synergistic effect on force and rhythm. Most importantly, salbutamol was found to possess an anti-arrhythmic property that mitigated aminophylline-induced irregularities through the activation of nitric oxide synthase (NOS) via beta2-adrenergic receptors. In the specific area of arrhythmology, the development of a dual 3D cardiac syncytium connected by a functional cellular bridge allowed for the detailed study of conduction disturbances. By utilizing lateral AFM deflection measurements for the first time, the biosensor detected the loss of synchrony and signal spreading defects triggered by pro-arrhythmic drugs. This mechanical dyssynchrony mirrored the non-synchronized contraction patterns characteristic of atrial or ventricular fibrillation.

### 10.3 Clinical Relevance and Precision Medicine

The cumulative findings of this thesis underscore the potential of hPSC-CM biosensors in precision medicine. The ability to create patient-specific dual-cluster syncytia enables ad hoc drug screening tailored to an individual's genetic background and specific conductive pathology. For the first time we initiated systemic study of conduction-related cardiac arrhythmias. The use of dual-cluster PSC-derived CMs has allowed us to explore the complex mechanisms underlying these arrhythmias and better discern the specific conduction and focal arrhythmias. AFM-based biosensors have been particularly effective in detecting subtle arrhythmic events, providing an incredibly sensitive and repeatable platform for cardiac research. The high sensitivity of these sensors makes them ideal for both basic research and clinical applications, where detecting even the smallest disruptions in cardiac function can be critical.

In conclusion, the combination of iPSC-derived cardiomyocytes and advanced biosensor technologies has revolutionized our ability to study and understand cardiac function. The ability to measure both the mechanical and electrical properties of heart cells in real-time, particularly when combined with patient-specific models, holds great promise for the future of precision medicine and personalized drug development. The ongoing development of these technologies, along with their application in disease modeling and drug testing, promises to enhance our understanding of cardiovascular diseases, improve patient outcomes, and reduce the risks associated with drug development. As these systems continue to evolve, they will undoubtedly play a critical role in advancing both basic cardiac research and clinical applications.

## 11 References


Acimovic, Ivana, Marwan M. Refaat, Adrien Moreau, et al. 2018. “Post-Translational Modifications and Diastolic Calcium Leak Associated to the Novel RyR2-D3638A Mutation Lead to CPVT in Patient-Specific hiPSC-Derived Cardiomyocytes.” Journal of Clinical Medicine 7 (11): 423. https://doi.org/10.3390/jcm7110423.

Acimovic, Ivana, Aleksandra Vilotic, Martin Pesl, et al. 2014. “Human Pluripotent Stem Cell-Derived Cardiomyocytes as Research and Therapeutic Tools.” Review Article. BioMed Research International, Hindawi, April 2. https://doi.org/10.1155/2014/512831.

Ahola, A., R. P. Pölönen, K. Aalto-Setälä, and J. Hyttinen. 2018. “Simultaneous Measurement of Contraction and Calcium Transients in Stem Cell Derived Cardiomyocytes.” Annals of Biomedical Engineering 46 (1): 148–58. https://doi.org/10.1007/s10439-017-1933-2.

Aistrup, G. L., Y. Shiferaw, S. Kapur, A. H. Kadish, and J. A. Wasserstrom. 2009. “Mechanisms Underlying the Formation and Dynamics of Subcellular Calcium Alternans in the Intact Rat Heart.” Circulation Research 104 (5): 639–49. https://doi.org/10.1161/CIRCRESAHA.108.181909.

Akhtar, Ayesha, Syed Ali Abbas, Syed Haris M. Zaidi, Adeel Sohail, Muhammad I. Alam, and Liaquat Raza. 2023. “The Acute Effects of the Use of Salbutamol and Ipratropium on the Heart Rates of Patients With Obstructive Airway Disease.” Cureus 15 (10): e46409. https://doi.org/10.7759/cureus.46409.

Al-Khatib, Sana M., William G. Stevenson, Michael J. Ackerman, et al. 2018. “2017 AHA/ACC/HRS Guideline for Management of Patients with Ventricular Arrhythmias and the Prevention of Sudden Cardiac Death: Executive Summary: A Report of the American College of Cardiology/American Heart Association Task Force on Clinical Practice Guidelines and the Heart Rhythm Society.” Heart Rhythm 15 (10): e190–252. https://doi.org/10.1016/j.hrthm.2017.10.035.

Amedro, P., Vincenti, M., De La Villeon, G., Lavastre, K., Barrea, C., Guillaumont, S., et al. (2019). Speckle-tracking echocardiography in children with duchenne muscular dystrophy: a prospective multicenter controlled cross-sectional study. J. Am. Soc. Echocardiogr. 32, 412–422. doi: 10.1016/j.echo.2018.10.017

Andersson, D. C., and Marks, A. R. (2010). Fixing ryanodine receptor Ca leak - a novel therapeutic strategy for contractile failure in heart and skeletal muscle. Drug Discov. Today Dis. Mech. 7, e151–e157. doi: 10.1016/j.ddmec.2010.09.009

Andersson, D. C., Meli, A. C., Reiken, S., Betzenhauser, M. J., Umanskaya, A., Shiomi, T., et al. (2012). Leaky ryanodine receptors in β-sarcoglycan deficient mice: a potential common defect in muscular dystrophy. Skelet. Muscle 2:9. doi: 10.1186/2044-5040-2-9

Alunda, Bernard Ouma, and Yong Joong Lee. 2020. "Review: Cantilever-Based Sensors for High Speed Atomic Force Microscopy." Sensors 20 (17): 4784. https://doi.org/10.3390/s20174784.

Amedro, P., Vincenti, M., De La Villeon, G., Lavastre, K., Barrea, C., Guillaumont, S., et al. (2019). Speckle-tracking echocardiography in children with duchenne muscular dystrophy: a prospective multicenter controlled cross-sectional study.J. Am. Soc. Echocardiogr. 32, 412–422. doi: 10.1016/j.echo.2018.10.017

Andersson, D. C., and Marks, A. R. (2010). Fixing ryanodine receptor Ca leak - a novel therapeutic strategy for contractile failure in heart and skeletal muscle.Drug Discov. Today Dis. Mech. 7, e151–e157. doi: 10.1016/j.ddmec.2010.09.009

Andersson, D. C., Meli, A. C., Reiken, S., Betzenhauser, M. J., Umanskaya, A., Shiomi, T., et al. (2012). Leaky ryanodine receptors in β-sarcoglycan deficient mice: a potential common defect in muscular dystrophy. Skelet. Muscle 2:9. doi: 10.1186/2044-5040-2-9

Armstrong, L., Tilgner, K., Saretzki, G., Atkinson, S. P., Stojkovic, M., Moreno, R., et al. (2010). Human induced pluripotent stem cell lines show stress defense mechanisms and mitochondrial regulation similar to those of human embryonic stem cells. Stem Cells 28, 661–673. doi: 10.1002/stem.307

Asp, M. L., Martindale, J. J., Heinis, F. I., Wang, W., and Metzger, J. M. (2013). Calcium mishandling in diastolic dysfunction: mechanisms and potential therapies. Biochim. Biophys. Acta 1833, 895–900.doi: 10.1016/j.bbamcr.2012.09.007

Aratyn-Schaus, Yvonne, Francesco S. Pasqualini, Hongyan Yuan, et al. 2016. "Coupling Primary and Stem Cell–Derived Cardiomyocytes in an in Vitro Model of Cardiac Cell Therapy." Journal of Cell Biology 212 (4): 389–97. https://doi.org/10.1083/jcb.201508026.

Arbore, Claudia, Laura Perego, Marios Sergides, and Marco Capitanio. 2019. "Probing Force in Living Cells with Optical Tweezers: From Single-Molecule Mechanics to Cell

Mechanotransduction." Biophysical Reviews 11 (5): 765–82. https://doi.org/10.1007/s12551-019-00599-y.

Aslaksen, A., Bakke, O. M., and Vigander, T. (1981). Comparative Pharmacokinetics of Theophylline and Aminophylline in Man. Br. J. Clin. Pharmacol. 11, 269–273. doi:10.1111/j.1365-2125.1981.tb00533.x Bébarová, M., Matejovič, P., Švecová, O., Kula, R., Šimurdová, M., and Šimurda, J. (2017). Nicotine at Clinically Relevant Concentrations Affects Atrial Inward Rectifier Potassium Current Sensitive to Acetylcholine. Naunyn-schmiedeberg's Arch. Pharmacol. 390, 471–481. doi:10.1007/s00210-017-1341-z

Balasubramaniam, Richard, Sangeeta Chawla, Andrew A. Grace, and Christopher L. H. Huang. 2005. "Caffeine-Induced Arrhythmias in Murine Hearts Parallel Changes in Cellular Ca2+ Homeostasis." American Journal of Physiology-Heart and Circulatory Physiology 289 (4): H1584–93. https://doi.org/10.1152/ajpheart.01250.2004.

Balligand, Jean-Luc. 1999. "Regulation of Cardiac β-Adrenergic Response by Nitric Oxide." Cardiovascular Research 43 (3): 607–20. https://doi.org/10.1016/S0008-6363(99)00163-7.

Bank, W. 2005. "Combined AFM and confocal fluorescence microscope for applications in bio-nanotechnology." Confocal and Multiphoton Microscopy 217: 109–116.

Barnes, Brian J., and James M. Hollands. 2010. "Drug-Induced Arrhythmias." Critical Care Medicine 38 (June): S188. https://doi.org/10.1097/CCM.0b013e3181de112a.

Bébarová, Markéta, Peter Matejovič, Olga Švecová, Roman Kula, Milena Šimurdová, and Jiří Šimurda. 2017. "Nicotine at Clinically Relevant Concentrations Affects Atrial Inward Rectifier Potassium Current Sensitive to Acetylcholine." Naunyn-Schmiedeberg's Archives of Pharmacology 390 (5): 471–81. https://doi.org/10.1007/s00210-017-1341-z.

Belardinelli, L., Shryock, J. C., Song, Y., Wang, D., and Srinivas, M. (1995). Ionic Basis of the Electrophysiological Actions of Adenosine on Cardiomyocytes. FASEB J. 9, 359–365. doi:10.1096/fasebj.9.5.7896004Baker, Jillian G. 2005. "The Selectivity of β-Adrenoceptor Antagonists at the Human B1, B2 and B3 Adrenoceptors." British Journal of Pharmacology 144 (3): 317–22. https://doi.org/10.1038/sj.bjp.0706048.

Berisha, F., Götz, K. R., Wegener, J. W., Brandenburg, S., Subramanian, H., Molina, C. E., et al. (2021). cAMP Imaging at Ryanodine Receptors Reveals β2-Adrenoceptor Driven Arrhythmias. Circ. Res. 129, 81–94. doi:10.1161/ CIRCRESAHA.120.318234

Berridge, M. J., M. D. Bootman, and H. L. Roderick. 2003. "Calcium signalling: dynamics, homeostasis and remodelling." Nat Rev Mol Cell Biol 4 (7): 517–529.

Bers, Donald M. 2002. “Cardiac Excitation-Contraction Coupling.” Nature 415 (6868): 198–205. https://doi.org/10.1038/415198a.

Bhushan, Shashi, Kazuhisa Kondo, Benjamin L. Predmore, et al. 2012. “Selective B2-Adrenoreceptor Stimulation Attenuates Myocardial Cell Death and Preserves Cardiac Function After Ischemia–Reperfusion Injury.” Arteriosclerosis, Thrombosis, and Vascular Biology 32 (8): 1865–74. https://doi.org/10.1161/ATVBAHA.112.251769.

Binah, O., Weissman, A., Itskovitz-Eldor, J., and Rosen, M. R. (2013). Integrating Beat Rate Variability: from Single Cells to Hearts. Heart Rhythm 10, 928–932. doi:10.1016/j.hrthm.2013.02.013Berridge, M. J. 2012. "Calcium signalling remodelling and disease." Biochem Soc Trans 40 (2): 297–309.

Bittar, G., and H. S. Friedman. 1991. “The Arrhythmogenicity of Theophylline. A Multivariate Analysis of Clinical Determinants.” Chest 99 (6): 1415–20. https://doi.org/10.1378/chest.99.6.1415.

Bigas, M., E. Cabruja, J. Forest, and J. Salvi. 2006. "Review of CMOS image sensors." Microelectron J 37 (5): 433–451

Blake, D. J., Weir, A., Newey, S. E., and Davies, K. E. (2002). Function and genetics of dystrophin and dystrophin-related proteins in muscle. Physiol. Rev. 82, 291–329. doi: 10.1152/physrev.00028.2001

Bondue, A., Arbustini, E., Bianco, A., Ciccarelli, M., Dawson, D., De Rosa, M., et al. (2018). Complex roads from genotype to phenotype in dilated cardiomyopathy: scientific update from the working group of myocardial function of the european society of cardiology. Cardiovasc. Res. 114, 1287–1303. doi: 10.1093/cvr/cvy122

Bootman, M. D., K. Rietdorf, T. Collins, S. Walker, and M. Sanderson. 2013. "Ca 2+ -sensitive fluorescent dyes and intracellular Ca 2+ imaging." Cold Spring Harb Protoc 2013 (2): 83–99.

Bootman, M. D., I. Smyrnias, R. Thul, S. Coombes, and H. L. Roderick. 2011. "Atrial cardiomyocyte calcium signalling." Biochim Biophys Acta - Mol Cell Res 1813 (5): 922–934.

Bristow, M. R., Ginsburg, R., Minobe, W., Cubicciotti, R. S., Sageman,W. S., Lurie, K., et al. (1982). Decreased catecholamine sensitivity and beta-adrenergic-receptor density in failing human hearts. N. Engl. J. Med. 307, 205–211. doi: 10.1056/NEJM198207223070401

Bristow, M. R., R. Ginsburg, V. Umans, et al. 1986. “Beta 1- and Beta 2-Adrenergic-Receptor Subpopulations in Nonfailing and Failing Human Ventricular Myocardium: Coupling of Both Receptor Subtypes to Muscle Contraction and Selective Beta 1-Receptor down-Regulation in Heart Failure.” Circulation Research 59 (3): 297–309. https://doi.org/10.1161/01.RES.59.3.297.

Burger, DE, Qingping Feng. 2011. “Protective Role of Nitric Oxide Against Cardiac Arrhythmia - An Update.” The Open Nitric Oxide Journal 3 (1). https://benthamopen.com/ABSTRACT/TONOJ-3-38. 10.2174/1875042701103010038

Bursac, N., M. Papadaki, R. J. Cohen, et al. 1999. "Cardiac muscle tissue engineering: toward an in vitro model for electrophysiological studies." Am J Physiol 277 (2 Pt 2): H433–H444.

Burridge, P. W., Keller, G., Gold, J. D., and Wu, J. C. (2012). Production of De Novo Cardiomyocytes: Human Pluripotent Stem Cell Differentiation and Direct Reprogramming. Cell Stem Cell 10, 16–28. doi:10.1016/j.stem.2011.12.013

Caluori, G, Pribyl J, Pesl M, et al. 2019. “Non-Invasive Electromechanical Cell-Based Biosensors for Improved Investigation of 3D Cardiac Models.” Biosensors and Bioelectronics 124–125 (January): 129–35. https://doi.org/10.1016/j.bios.2018.10.021.

Caluori, G., Pribyl, J., Pesl, M., Jelinkova, S., Rotrekl, V., Skladal, P., et al. (2019). Non-invasive electromechanical cell-based biosensors for improved investigation of 3D cardiac models. Biosens. Bioelectron. 124–125, 129–135. doi: 10.1016/j.bios.2018.10.021

Caluori, G., Pribyl, J., Cmiel, V., Pesl, M., Potocnak, T., Provaznik, I., et al. (2019a). Simultaneous Study of Mechanobiology and Calcium Dynamics on hESCDerived Cardiomyocytes Clusters. J. Mol. Recognit. 32, e2760. doi:10.1002/ jmr.2760

Camelliti, P, Borg KT, and Kohl P. 2005. “Structural and Functional Characterisation of Cardiac Fibroblasts.” Cardiovascular Research 65 (1): 40–51. https://doi.org/10.1016/j.cardiores.2004.08.020.

Carnwath, J. W., and Shotton, D. M. (1987). Muscular dystrophy in the mdx mouse: histopathology of the soleus and extensor digitorum longus muscles. J. Neurol. Sci. 80, 39–54. doi: 10.1016/0022-510X(87)90219-X

Carrick, Richard T., Alessio Gasperetti, Alexandros Protonotarios, et al. 2024. "A Novel Tool for Arrhythmic Risk Stratification in Desmoplakin Gene Variant Carriers." European Heart Journal 45 (32): 2968–79. https://doi.org/10.1093/eurheartj/ehae409.

Casiglia, Edoardo, Valérie Tikhonoff, Federica Albertini, et al. 2018. "Caffeine Intake Reduces Incident Atrial Fibrillation at a Population Level." European Journal of Preventive Cardiology 25 (10): 1055–62. https://doi.org/10.1177/2047487318772945.

Cazzola, Mario, Paola Rogliani, and Maria Gabriella Matera. 2019. "Ultra-LABAs for the Treatment of Asthma." Respiratory Medicine 156 (September): 47–52. https://doi.org/10.1016/j.rmed.2019.08.005.

Cerbai, E., R. Pino, M. L. Rodriguez, and A. Mugelli. 1999. "Modulation of the Pacemaker Current If by Beta-Adrenoceptor Subtypes in Ventricular Myocytes Isolated from Hypertensive and Normotensive Rats." Cardiovascular Research 42 (1): 121–29. https://doi.org/10.1016/s0008-6363(98)00291-0.

Charytan, D., and Jansen, K. (2003). Severe Metabolic Complications from Theophylline Intoxication. Nephrology (Carlton) 8, 239–242. doi:10.1046/ j.1440-1797.2003.00181.x

Chen, Lin Y., Nona Sotoodehnia, Petra Bůžková, et al. 2013. "Atrial Fibrillation and the Risk of Sudden Cardiac Death: The Atherosclerosis Risk in Communities Study and Cardiovascular Health Study." JAMA Internal Medicine 173 (1): 29–35. https://doi.org/10.1001/2013.jamainternmed.744.

Chenard, A. A., Becane, H. M., Tertrain, F., de Kermadec, J. M., and Weiss, Y. A. (1993). Ventricular arrhythmia in duchenne muscular dystrophy: prevalence, significance and prognosis. Neuromuscul. Disord. 3, 201–206. doi: 10.1016/0960-8966(93)90060-W

Choi, B.-R., Burton, F., and Salama, G. (2002). Cytosolic Ca2+ triggers early afterdepolarizations and torsade de pointes in rabbit hearts with type 2 long QT syndrome. J. Physiol. 543, 615–631. doi: 10.1113/jphysiol.2002.024570

Chugh, Sumeet S., Rasmus Havmoeller, Kumar Narayanan, et al. 2014. "Worldwide Epidemiology of Atrial Fibrillation: A Global Burden of Disease 2010 Study." Circulation 129 (8): 837–47. https://doi.org/10.1161/CIRCULATIONAHA.113.005119.

Clarac, F., Massion, J., and Smith, A. M. (2009). Duchenne, charcot and babinski, three neurologists of la salpetrière hospital, and their contribution to concepts of the central organization of motor synergy. J. Physiol. Paris 103, 361–376. doi: 10.1016/j.jphysparis.2009.09.001

Conte, L., Pugliese, N. R., and Giannoni, A. (2017). Reversal of Ticagrelor-Induced Arrhythmias and Cheyne-Stokes Respiration with Aminophylline Infusion. J. Cardiovasc. Pharmacol. 70, 290–292. doi:10.1097/FJC.0000000000000518

Corea, L., M. Bentivoglio, P. Verdecchia, et al. 1984. "Noninvasive Assessment of Chronotropic and Inotropic Response to Preferential Beta-1 and Beta-2 Adrenoceptor Stimulation." Clinical Pharmacology and Therapeutics 35 (6): 776–81. https://doi.org/10.1038/clpt.1984.111.

Corrado, G., Lissoni, A., Beretta, S., Terenghi, L., Tadeo, G., Foglia-Manzillo, G., et al. (2002). Prognostic value of electrocardiograms, ventricular late potentials, ventricular arrhythmias, and left ventricular systolic dysfunction in patients with Duchenne muscular dystrophy. Am. J. Cardiol. 89, 838–841.

doi: 10.1016/S0002-9149(02)02195-1

Coulton, G. R., Morgan, J. E., Partridge, T. A., and Sloper, J. C. (1988). The mdx mouse skeletal muscle myopathy: I. A histological, morphometric and biochemical investigation. Neuropathol. Appl. Neurobiol. 14, 53–70. doi: 10.1111/j.1365-2990.1988.tb00866.x

Colombe, A, Pidoux G. 2021. "Cardiac cAMP-PKA Signaling Compartmentalization in Myocardial Infarction." Cells 10 (4): 922. https://doi.org/10.3390/cells10040922.

Crespo, Piero, Teresa G. Cachero, Ningzhi Xu, and J. Silvio Gutkind. 1995. "Dual Effect of β-Adrenergic Receptors on Mitogen-Activated Protein Kinase: EVIDENCE FOR A Bγ-DEPENDENT ACTIVATION AND A Gαs-cAMP-MEDIATED INHIBITION (∗)." Journal of Biological Chemistry 270 (42): 25259–65. https://doi.org/10.1074/jbc.270.42.25259.

Cui, J., Melman, Y., Palma, E., Fishman, G. I., and McDonald, T. V. (2000). Cyclic AMP Regulates the HERG K(+) Channel by Dual Pathways. Curr. Biol. 10, 671–674. doi:10.1016/s0960-9822(00)00516-9

Culligan, K., Banville, N., Dowling, P., and Ohlendieck, K. (2002). Drastic reduction of calsequestrin-like proteins and impaired calcium binding in dystrophic mdx muscle. J. Appl. Physiol. 92, 435–445. doi: 10.1152/japplphysiol.00903.2001Cullum, Valerie A., J.

B. Farmer, D. Jack, and G. P. Levy. 1969. “Salbutamol: A New, Selective β-Adrenoceptive Receptor Stimulant.” British Journal of Pharmacology 35 (1): 141–51. https://doi.org/10.1111/j.1476-5381.1969.tb07975.x.

Daly, John W., Dan Shi, Olga Nikodijevic, and Kenneth A. Jacobson. 1994. “The Role of Adenosine Receptors in the Central Action of Caffeine.” Pharmacopsychoecologia 7 (2): 201–13.

Daly, John W., Dan Shi, Olga Nikodijević, and Kenneth A. Jacobson. 1999. “The Role of Adenosine Receptors in the Central Action of Caffeine.” In Caffeine and Behavior: Current Views & Research Trends. CRC Press.

Danialou, G., Comtois, A. S., Dudley, R., Karpati, G., Vincent, G., Des Rosiers, C., et al. (2001). Dystrophin-deficient cardiomyocytes are abnormally vulnerableto mechanical stress-induced contractile failure and injury. FASEB J. 15,1655–1657. doi: 10.1096/fj.01-0030fje

DaniilKabanov. (2021) 2021. DaniilKabanov/CardioScripts. Jupyter Notebook. September 9, released September 9. https://github.com/DaniilKabanov/CardioScripts.

Davis, R. P., S. Casini, C. W. van den Berg, et al. 2012. "Cardiomyocytes derived from pluripotent stem cells recapitulate electrophysiological characteristics of an overlap syndrome of cardiac sodium channel disease." Circulation 125 (25): 3079–3091.

Deacon, S. P. 1977. “Metabolic Effects of Salbutamol.” British Medical Journal 1 (6061): 639.

de Lucia, C., Eguchi, A., and Koch, W. J. (2018). New insights in cardiac β-adrenergic signaling during heart failure and aging. Front. Pharmacol. 9:904. doi: 10.3389/fphar.2018.00904

Dewing, Jennifer M., Vinay Saunders, Ita O’Kelly, and David I. Wilson. 2022. “Defining Cardiac Cell Populations and Relative Cellular Composition of the Early Fetal Human Heart.” PloS One 17 (11): e0259477. https://doi.org/10.1371/journal.pone.0259477.

Dibb, K. M., A. W. Trafford, and D. A. Eisner. 2010. “Calcium Signaling in Cardiac Muscle.” In Handbook of Cell Signaling. Elsevier BV. https://doi.org/10.1016/B978-0-12-374145-5.00128-5.

Dinarelli, S., Girasole, M., Spitalieri, P., Talarico, R. V., Murdocca, M., Botta, A., et al. (2018). AFM Nano-Mechanical Study of the Beating Profile of hiPSCDerived

Cardiomyocytes Beating Bodies WT and DM1. J. Mol. Recognit 31, e2725. doi:10.1002/jmr.2725

Domeier, Timothy L., Joshua T. Maxwell, and Lothar A. Blatter. 2012a. “β-Adrenergic Stimulation Increases the Intra-Sarcoplasmic Reticulum Ca2+ Threshold for Ca2+ Wave Generation.” The Journal of Physiology 590 (23): 6093–108. https://doi.org/10.1113/jphysiol.2012.236117.

Domeier, Timothy L., Joshua T. Maxwell, and Lothar A. Blatter. 2012b. “β-Adrenergic Stimulation Increases the Intra-Sarcoplasmic Reticulum Ca2+ Threshold for Ca2+ Wave Generation.” The Journal of Physiology 590 (Pt 23): 6093–108. https://doi.org/10.1113/jphysiol.2012.236117.

Domke, J., W. J. Parak, M. George, H. E. Gaub, and M. Radmacher. 1999. “Mapping the Mechanical Pulse of Single Cardiomyocytes with the Atomic Force Microscope.” European Biophysics Journal: EBJ 28 (3): 179–86.

Driessen, H. E., V. J. A. Bourgonje, T. A. B. van Veen, and M. A. Vos. 2014. "New antiarrhythmic targets to control intracellular calcium handling." Neth Heart J 22 (5): 198–213.

Dumont, N. A., Wang, Y. X., von Maltzahn, J., Pasut, A., Bentzinger, C. F., Brun, C. E., et al. (2015). Dystrophin expression in muscle stem cells regulates their polarity and asymmetric division. Nat. Med. 21, 1455–1463. doi: 10.1038/nm.3990

Dvorak, P., Dvorakova, D., Koskova, S., Vodinska, M., Najvirtova, M., Krekac, D., et al. (2005). Expression and potential role of fibroblast growth factor 2 and its receptors in human embryonic stem cells. Stem Cells 23, 1200–1211. doi: 10.1634/stemcells.2004-0303

Eder, A, Vollert I, Hansen A, and Eschenhagen T. 2016. “Human Engineered Heart Tissue as a Model System for Drug Testing.” Advanced Drug Delivery Reviews, Tissue engineering of the heart: from in vitro models to regenerative solutions, vol. 96 (January): 214–24. https://doi.org/10.1016/j.addr.2015.05.010.

Eisen, B., Ben Jehuda, R., Cuttitta, A. J., Mekies, L. N., Shemer, Y., Baskin, P., et al. (2019). Electrophysiological abnormalities in induced pluripotent stem cell-derived cardiomyocytes generated from duchenne muscular dystrophy patients. J. Cell. Mol. Med. 23, 2125–2135. doi: 10.1111/jcmm.14124

Ellis, E. F. (1985). Theophylline Toxicity. J. Allergy Clin. Immunol. 76, 297–301. doi:10.1016/0091-6749(85)90645-1

Engel, Bronia, Rosemarie Einstein, and A. H. Goodman. 1985. “Inotropic Selectivity of Salbutamol and Terbutaline in Anaesthetised, Areflexic Dogs.” European Journal of Pharmacology 116 (1): 97–104. https://doi.org/10.1016/0014-2999(85)90189-X.

Engelhardt, S., Hein, L., Wiesmann, F., and Lohse, M. J. (1999). Progressive hypertrophy and heart failure in beta1-adrenergic receptor transgenic mice.Proc. Natl. Acad. Sci. U.S.A. 96, 7059–7064. doi: 10.1073/pnas.96.12.7059

Eschenhagen, T., and W. H. Zimmermann. 2005. "Engineering myocardial tissue." Circ Res 97 (12): 1220–1231.

Fabiato, A. 1985. "Time and calcium dependence of activation and inactivation of calcium-induced release of calcium from the sarcoplasmic reticulum of a skinned canine cardiac Purkinje cell." J Gen Physiol 85 (2): 247–289.

Fauconnier, J., Thireau, J., Reiken, S., Cassan, C., Richard, S., Matecki, S., et al. (2010). Leaky RyR2 trigger ventricular arrhythmias in duchenne muscular dystrophy. Proc. Natl. Acad. Sci. U.S.A. 107, 1559–1564. doi: 10.1073/pnas.0908540107

Fayssoil, A., Nardi, O., Orlikowski, D., and Annane, D. (2010). Cardiomyopathy in duchenne muscular dystrophy: pathogenesis and therapeutics. Heart Fail Rev. 15, 103–107. doi: 10.1007/s10741-009-9156-8

Finsterer, J., and Stöllberger, C. (2003). The heart in human dystrophinopathies.Cardiology 99, 1–19. doi: 10.1159/000068446

Fleischer, Stephan, Heinz-Georg Jahnke, Enrico Fritsche, Mathilde Girard, and Andrea A. Robitzki. 2019. “Comprehensive Human Stem Cell Differentiation in a 2D and 3D Mode to Cardiomyocytes for Long-Term Cultivation and Multiparametric Monitoring on a Multimodal Microelectrode Array Setup.” Biosensors and Bioelectronics 126 (February): 624–31. https://doi.org/10.1016/j.bios.2018.10.061.

Franz, C. M., and P. H. Puech. 2008. “Atomic Force Microscopy: A Versatile Tool for Studying Cell Morphology, Adhesion and Mechanics.” Cellular and Molecular Bioengineering 1 (4): 289–300. https://doi.org/10.1007/s12195-008-0037-3.

Fraticelli, A., Josephson, R., Danziger, R., Lakatta, E., and Spurgeon, H. (1989). Morphological and Contractile Characteristics of Rat Cardiac Myocytes from Maturation to Senescence. Am. J. Physiol. 257, H259–H265. doi:10.1152/ajpheart.1989.257.1.H259

Futyma, Piotr. 2019. “How to Induce Arrhythmias with Salbutamol.” In Arrhythmia Induction in the EP Lab, edited by Gabriel Cismaru. Springer International Publishing. https://doi.org/10.1007/978-3-319-92729-9_12.

García-Morales, Verónica, María Luaces-Regueira, and Manuel Campos-Toimil. 2017. “The cAMP Effectors PKA and Epac Activate Endothelial NO Synthase through PI3K/Akt Pathway in Human Endothelial Cells.” Biochemical Pharmacology 145 (December): 94–101. https://doi.org/10.1016/j.bcp.2017.09.004.

Geisse, Nicholas A. 2009. “AFM and Combined Optical Techniques.” Materials Today 12 (7): 40–45. https://doi.org/10.1016/S1369-7021(09)70201-9.

Gepstein, L. 2013. "Derivation and potential applications of human embryonic stem cells." Circ Res 91: 866–876.

Gerke, V., Creutz, C. E., and Moss, S. E. (2005). Annexins: linking Ca2+ signalling to membrane dynamics. Nat. Rev. Mol. Cell Biol. 6, 449–461. doi: 10.1038/nrm1661

Gharanei, Mayel, Sanam Shafaattalab, Sarabjit Sangha, et al. 2022. “Atrial-Specific hiPSC-Derived Cardiomyocytes in Drug Discovery and Disease Modeling.” Methods 203 (July): 364–77. https://doi.org/10.1016/j.ymeth.2021.06.009.

Ghasemi, Asghar, and Sajad Jeddi. 2022. “Quantitative Aspects of Nitric Oxide Production in the Heart.” Molecular Biology Reports 49 (11): 11113–22. https://doi.org/10.1007/s11033-022-07889-x.

Global Initiative for Chronic Obstructive Lung Disease - GOLD. n.d. “2023 GOLD Report.” Accessed October 30, 2023. https://goldcopd.org/2023-gold-report-2/.

Goldberg, M. J., Park, G. D., and Berlinger, W. G. (1986). Treatment of Theophylline Intoxication. J. Allergy Clin. Immunol. 78, 811–817. doi:10.1016/0091-6749(86)90066-7

Gonzalez-Muñoz, Carmen, Teodomiro Fuente, Santiago Medin-Aguerre, and Jesús Hernández-Cascales. 2011. “The Increase in Rat Ventricular Automaticity Induced by Salbutamol Is Mediated through B1- but Not B2-Adrenoceptors: Role of Phosphodiesterases.” Life Sciences 88 (25): 1095–101. https://doi.org/10.1016/j.lfs.2011.04.015.

Gorski, P. A., D. K. Ceholski, and R. J. Hajjar. 2015. "Altered myocardial calcium cycling and energetics in heart failure—a rational approach for disease treatment." Cell Metab 21 (2): 183–194.

Goudis, C. A. (2017). Chronic Obstructive Pulmonary Disease and Atrial Fibrillation: An Unknown Relationship. J. Cardiol. 69, 699–705. doi:10.1016/ j.jjcc.2016.12.013

Grune, Tilman, Christiane Ott, Steffen Häseli, Annika Höhn, and Tobias Jung. 2019. "The 'MYOCYTER' – Convert Cellular and Cardiac Contractions into Numbers with ImageJ." Scientific Reports 9 (1): 1. https://doi.org/10.1038/s41598-019-51676-x.

Guatimosim, Silvia, Cristina Guatimosim, and Long-Sheng Song. 2011. "Imaging Calcium Sparks in Cardiac Myocytes." Methods in Molecular Biology (Clifton, N.J.) 689: 205–14. https://doi.org/10.1007/978-1-60761-950-5_12.

Gupta, Niharika, Venkatesan Renugopalakrishnan, Dorian Liepmann, Ramasamy Paulmurugan, and Bansi D. Malhotra. 2019. "Cell-Based Biosensors: Recent Trends, Challenges and Future Perspectives." Biosensors and Bioelectronics 141 (September): 111435. https://doi.org/10.1016/j.bios.2019.111435.

Hajjar, R. J., Liao, R., Young, J. B., Fuleihan, F., Glass, M. G., and Gwathmey, J. K. (1993). Pathophysiological and biochemical characterisation of an avian model of dilated cardiomyopathy: comparison to findings in human dilated cardiomyopathy. Cardiovasc. Res. 27, 2212–2221. doi: 10.1093/cvr/27.12.2212

Hards, A., C. Zhou, M. Seitz, C. Bräuchle, and A. Zumbusch. 2005. "Simultaneous AFM manipulation and fluorescence imaging of single DNA strands." Chemphyschem Eur J Chem Phys Phys Chem 6 (3): 534–540.

Haupt, B. J., A. E. Pelling, and M. a Horton. 2006. "Integrated confocal and scanning probe microscopy for biomedical research." Sci World J 6: 1609–1618.

He, J.-Q., Ma, Y., Lee, Y., Thomson, J. A., and Kamp, T. J. (2003). Human embryonic stem cells develop into multiple types of cardiac myocytes: action potential characterization. Circ. Res. 93, 32–39. doi: 10.1161/01.RES.0000080317.92718.99

Herron Todd J., Lee Peter, and Jalife José. 2012. "Optical Imaging of Voltage and Calcium in Cardiac Cells & Tissues." Circulation Research 110 (4): 609–23. https://doi.org/10.1161/CIRCRESAHA.111.247494.

Hess, G. P. D., Horsch, A. D., and Zdunek, D. D. (2008). Means and Methods for Optimization of Diagnostic and Therapeutic Approaches in Chronic Artery Disease Based on the Detection of Troponin T and NT-proBNP. Available online at: https://patents.google.com/patent/EP1925943A1/en/en22 (accessed December 14, 2019).

Higgins, R. M., Hearing, S., Goldsmith, D. J., Keevil, B., Venning, M. C., and Ackrill, P. (1995). Severe Theophylline Poisoning: Charcoal Haemoperfusion or Haemodialysis. Postgrad. Med. J. 71, 224–226. doi:10.1136/pgmj.71.834.224

"Highlights — pyHRV - OpenSource Python Toolbox for Heart Rate Variability 0.4 Documentation." n.d. Accessed November 23, 2023. https://pyhrv.readthedocs.io/en/latest/index.html.

Himmrich, E., Popov, S., Liebrich, A., Rosocha, S., Zellerhoff, C., Nowak, B., et al. (2000). [Hidden intracardiac conduction disturbances and their spontaneous course in patients with progressive muscular dystrophy]. Z Kardiol. 89, 592–598. doi: 10.1007/s003920070208

Hindricks, Gerhard, Tatjana Potpara, Nikolaos Dagres, et al. 2021. "2020 ESC Guidelines for the Diagnosis and Management of Atrial Fibrillation Developed in Collaboration with the European Association for Cardio-Thoracic Surgery (EACTS): The Task Force for the Diagnosis and Management of Atrial Fibrillation of the European Society of Cardiology (ESC) Developed with the Special Contribution of the European Heart Rhythm Association (EHRA) of the ESC." European Heart Journal 42 (5): 373–498. https://doi.org/10.1093/eurheartj/ehaa612.

Hinterdorfer, P., G. Schütz, F. Kienberger, and H. Schindler. 2001. "Detection and characterization of single biomolecules at surfaces." Rev Mol Biotechnol 82 (1): 25–35.

Hoppe, L. K., Muhlack, D. C., Koenig, W., Carr, P. R., Brenner, H., and Schöttker, B. (2018). Association of Abnormal Serum Potassium Levels with Arrhythmias and Cardiovascular Mortality: a Systematic Review and Meta-Analysis of Observational Studies. Cardiovasc. Drugs Ther. 32, 197–212. doi:10.1007/s10557-018-6783-0

Horita, N., Miyazawa, N., Kojima, R., Inoue, M., Ishigatsubo, Y., and Kaneko, T. (2016). Chronic Use of Theophylline and Mortality in Chronic Obstructive Pulmonary Disease: A Meta-Analysis. Arch. Bronconeumol 52, 233–238. doi:10.1016/j.arbres.2015.02.021

Huerta, C., Lanes, S. F., and García Rodríguez, L. A. (2005). Respiratory Medications and the Risk of Cardiac Arrhythmias. Epidemiology 16, 360–366. doi:10.1097/01.ede.0000158743.90664.a7

Hwang, H. S., Kryshtal, D. O., Feaster, T. K., Sánchez-Freire, V., Zhang, J., Kamp, T. J., et al. (2015). Comparable calcium handling of human iPSC-derived cardiomyocytes generated by multiple laboratories. J. Mol. Cell. Cardiol. 85, 79–88. doi: 10.1016/j.yjmcc.2015.05.003

Inomata, K., Aoto, T., Binh, N. T., Okamoto, N., Tanimura, S., Wakayama, T., et al. (2009). Genotoxic stress abrogates renewal of melanocyte stem cells by triggering their differentiation. Cell 137, 1088–1099.doi: 10.1016/j.cell.2009.03.037

Insulander, Per, Anders Juhlin-Dannfelt, Ulla Freyschuss, and Hans Vallin. 2004. "Electrophysiologic Effects of Salbutamol, a Beta2-Selective Agonist." Journal of Cardiovascular Electrophysiology 15 (3): 316–22. https://doi.org/10.1046/j.1540-8167.2004.03105.x.

International Stem Cell Initiative, Oluseun Adewumi, Behrouz Aflatoonian, et al. 2007a. "Characterization of Human Embryonic Stem Cell Lines by the International Stem Cell Initiative." Nature Biotechnology 25 (7): 7. https://doi.org/10.1038/nbt1318.

International Stem Cell Initiative, Adewumi, O., Aflatoonian, B., Ahrlund-Richter, L., Amit, M., Andrews, P. W., et al. (2007). Characterization of human embryonic stem cell lines by the international stem cell initiative. Nat. Biotechnol. 25, 803–816. doi: 10.1038/nbt1318m Cell Initiative." Nature Biotechnology 25 (7): 803–16. https://doi.org/10.1038/nbt1318.

Izu, Leighton T., Yuanfang Xie, Daisuke Sato, Tamás Bányász, and Ye Chen-Izu. 2013. "Ca2+ Waves in the Heart." Journal of Molecular and Cellular Cardiology 58 (May): 118–24. https://doi.org/10.1016/j.yjmcc.2012.11.014.

Izumi-Nakaseko, Hiroko, Mihoko Hagiwara-Nagasawa, Atsuhiko T. Naito, et al. 2018. "Application of Human Induced Pluripotent Stem Cell-Derived Cardiomyocytes Sheets with Microelectrode Array System to Estimate Antiarrhythmic Properties of Multi-Ion Channel Blockers." Journal of Pharmacological Sciences 137 (4): 372–78. https://doi.org/10.1016/j.jphs.2018.07.011.

Jahnke, Heinz-Georg, Daniella Steel, Stephan Fleischer, et al. 2013. "A Novel 3D Label-Free Monitoring System of hES-Derived Cardiomyocyte Clusters: A Step Forward to In

Vitro Cardiotoxicity Testing." PLOS ONE 8 (7): e68971. https://doi.org/10.1371/journal.pone.0068971.

Jang, Yongjun, Seung-Cheol Choi, Do-Sun Lim, Jong-Hoon Kim, Jongseong Kim, and Yongdoo Park. 2020. "Modulating Cardiomyocyte and Fibroblast Interaction Using Layer-by-Layer Deposition Facilitates Synchronisation of Cardiac Macro Tissues." Soft Matter 16 (2): 428–34. https://doi.org/10.1039/C9SM01531K.

Jans, Danny, Geert Callewaert, Olga Krylychkina, et al. 2017. "Action Potential-Based MEA Platform for in Vitro Screening of Drug-Induced Cardiotoxicity Using Human iPSCs and Rat Neonatal Myocytes." Journal of Pharmacological and Toxicological Methods, Focused Issue on Safety Pharmacology, vol. 87 (September): 48–52. https://doi.org/10.1016/j.vascn.2017.05.003.

January, Craig T., L. Samuel Wann, Joseph S. Alpert, et al. 2014. "2014 AHA/ACC/HRS Guideline for the Management of Patients With Atrial Fibrillation: Executive Summary." Circulation, December. Hagerstown, MD. https://www.ahajournals.org/doi/abs/10.1161/CIR.0000000000000040?url_ver=Z39.88-2003&rfr_id=ori%3Arid%3Acrossref.org&rfr_dat=cr_pub%3Dpubmed#.

Jelinkova, S., Fojtik, P., Kohutova, A., Vilotic, A., Marková, L., Pesl, M., et al. (2019a). Dystrophin deficiency leads to genomic instability in human pluripotent stem cells via NO synthase-induced oxidative stress. Cells 8:53. doi: 10.3390/cells8010053

Jelinkova, S., Markova, L., Pesl, M., Valáškova, I., Makaturová, E., Jurikova, L., et al. (2019b). Generation of two duchenne muscular dystrophy patient-specific induced pluripotent stem cell lines DMD02 and DMD03 (MUNIi001-A and MUNIi003-A). Stem Cell Res. 40:101562. doi: 10.1016/j.scr.2019.101562

Jelinkova, Sarka, Petr Fojtik, Aneta Kohutova, et al. 2019. "Dystrophin Deficiency Leads to Genomic Instability in Human Pluripotent Stem Cells via NO Synthase-Induced Oxidative Stress." Cells 8 (1): 53. https://doi.org/10.3390/cells8010053.

Jelinkova, Sarka, Aleksandra Vilotic, Jan Pribyl, et al. 2020b. "DMD Pluripotent Stem Cell Derived Cardiac Cells Recapitulate in Vitro Human Cardiac Pathophysiology." Frontiers in Bioengineering and Biotechnology 8 (June). https://doi.org/10.3389/fbioe.2020.00535.

Jelinkova, Sarka, Aleksandra Vilotic, Jan Pribyl, et al. 2020c. "DMD Pluripotent Stem Cell Derived Cardiac Cells Recapitulate in Vitro Human Cardiac Pathophysiology." Frontiers

in Bioengineering and Biotechnology 8 (June): 535. https://doi.org/10.3389/fbioe.2020.00535.

Johnson, Donavon B., Brigham J. Merrell, and Connor G. Bounds. 2022. “Albuterol.” In StatPearls. StatPearls Publishing. http://www.ncbi.nlm.nih.gov/books/NBK482272/.

Johnson, D. M., Heijman, J., Bode, E. F., Greensmith, D. J., van der Linde, H., Abi-Gerges, N., et al. (2013). Diastolic spontaneous calcium release from the sarcoplasmic reticulum increases beat-to-beat variability of repolarization in canine ventricular myocytes after β-adrenergic stimulation. Circ. Res. 112, 246–256. doi: 10.1161/CIRCRESAHA.112.275735

Jung, C., Martins, A. S., Niggli, E., and Shirokova, N. (2008). Dystrophic cardiomyopathy: amplification of cellular damage by Ca2+ signalling and reactive oxygen species-generating pathways. Cardiovasc. Res. 77, 766–773. doi: 10.1093/cvr/cvm089

Jung, K. B., Y. S. Son, H. Lee, C. R. Jung, J. Kim, and M. Y. Son. 2017. "Transcriptome dynamics of human pluripotent stem cell-derived contracting cardiomyocytes using an embryoid body model with fetal bovine serum." Mol Biosyst 13 (8): 1565–1574.

Kabanov D, Vrana Klimovic S, Beckerová D, Molcan M, Scurek M, Brat K, Bebarova M, Rotrekl V, Pribyl J, Pesl M. Salbutamol attenuates arrhythmogenic effect of aminophylline in a hPSC-derived cardiac model. Sci Rep. 2024 Nov 9;14(1):27399. doi: 10.1038/s41598-024-76846-4

Kajimoto, H., Ishigaki, K., Okumura, K., Tomimatsu, H., Nakazawa, M., Saito, K., et al. (2006). Beta-blocker therapy for cardiac dysfunction in patients with muscular dystrophy. Circ. J. 70, 991–994. doi: 10.1253/circj.70.991

Kamdar, F., and Garry, D. J. (2016). Dystrophin-deficient cardiomyopathy. J. Am. Coll. Cardiol. 67, 2533–2546. doi: 10.1016/j.jacc.2016.02.081Kawatou, Masahide, Hidetoshi Masumoto, Hiroyuki Fukushima, et al. 2017. “Modelling Torsade de Pointes Arrhythmias in Vitro in 3D Human iPS Cell-Engineered Heart Tissue.” Nature Communications 8 (1): 1078. https://doi.org/10.1038/s41467-017-01125-y.

Keefe, Joshua A., Oliver M. Moore, Kevin S. Ho, and Xander H. T. Wehrens. 2023. “Role of Ca2+ in Healthy and Pathologic Cardiac Function: From Normal Excitation–Contraction Coupling to Mutations That Cause Inherited Arrhythmia.” Archives of Toxicology 97 (1): 73–92. https://doi.org/10.1007/s00204-022-03385-0.

Kilkenny, D.M., Rocheleau J.V., Price J., Reich MB, and Miller G.G,. 2003. “C-Src Regulation of Fibroblast Growth Factor-Induced Proliferation in Murine Embryonic Fibroblasts.” The Journal of Biological Chemistry 278 (19): 17448–54. https://doi.org/10.1074/jbc.M209698200.

Kim, Dong-Su, Yun-Jin Jeong, Bong-Kee Lee, Arunkumar Shanmugasundaram, and Dong-Weon Lee. 2017. “Piezoresistive Sensor-Integrated PDMS Cantilever: A New Class of Device for Measuring the Drug-Induced Changes in the Mechanical Activity of Cardiomyocytes.” Sensors and Actuators B: Chemical 240 (March): 566–72. https://doi.org/10.1016/j.snb.2016.08.167.

Kincl, V, Panovský R, Pešl M, et al. 2020. “Echocardiographic Signs of Subclinical Cardiac Function Impairment in Duchenne Dystrophy Gene Carriers.” Scientific Reports 10 (1): 20794. https://doi.org/10.1038/s41598-020-77882-6.

Klimovic, S, Scurek M, Pesl M, et al. 2022. “Aminophylline Induces Two Types of Arrhythmic Events in Human Pluripotent Stem Cell-Derived Cardiomyocytes.” Frontiers in Pharmacology 12: 789730. https://doi.org/10.3389/fphar.2021.789730.

Klimovic, S., Scurek, M., Pesl, M., Beckerova, D., Jelinkova, S., Urban, T., et al. (2022). Aminophylline Induces Two Types of Arrhythmic Events in Human Pluripotent Stem Cell-Derived Cardiomyocytes - Dataset. doi:10.5281/zenodo.4552607

Kobold, S, Guhr A, Kurtz A, and Löser P. 2015. “Human Embryonic and Induced Pluripotent Stem Cell Research Trends: Complementation and Diversification of the Field.” Stem Cell Reports 4 (5): 914–25. https://doi.org/10.1016/j.stemcr.2015.03.002.

Koenig, X., Dysek, S., Kimbacher, S., Mike, A. K., Cervenka, R., Lukacs, P., et al. (2011). Voltage-gated ion channel dysfunction precedes cardiomyopathy development in the dystrophic heart. PLoS ONE 6:e20300. doi: 10.1371/journal.pone.0020300

Koenig, X., L. Rubi, G. J. Obermair, et al. 2013. "Enhanced currents through L-type calcium channels in cardiomyocytes disturb the electrophysiology of the dystrophic heart." Am J Physiol Heart Circ Physiol 306: H564–H573

Komadina, K. H., Carlson, T. A., Strollo, P. J., and Navratil, D. L. (1992). Electrophysiologic Study of the Effects of Aminophylline and Metaproterenol on Canine Myocardium. Chest 101, 232–238. doi:10.1378/ chest.101.1.232

Kong, H, Jones PP, Koop A, Zhang L, Duff HJ, and Chen S. R.W. 2008. “Caffeine Induces Ca2+ Release by Reducing the Threshold for Luminal Ca2+ Activation of the Ryanodine

Receptor." The Biochemical Journal 414 (3): 441–52. https://doi.org/10.1042/BJ20080489.

Korohoda, W, Jurkiewicz A, Figiel I, and Czyż J. 1995. "A New Model for the Research into Rhythmic Contraction Activity of Cardiomyocytes in Vitro." Biochemistry and Cell Biology 73 (7–8): 431–39. https://doi.org/10.1139/o95-050.

Krutá, M., Bálek, L., Hejnová, R., Dobšáková, Z., Eiselleová, L., Matulka, K., et al. (2013). Decrease in abundance of apurinic/apyrimidinic endonuclease causes failure of base excision repair in culture-adapted human embryonic stem cells. Stem Cells 31, 693–702. doi: 10.1002/stem.1312

Krutá, M., Šeneklová, M., Raška, J., Salykin, A., Zerzánková, L., Pešl, M., et al. (2014). Mutation frequency dynamics in HPRT locus in cultureadapted human embryonic stem cells and induced pluripotent stem cells correspond to their differentiated counterparts. Stem Cells Dev. 23, 2443–2454.doi: 10.1089/scd.2013.0611

Kussauer, S, David R, and Lemcke H. 2019. "hiPSCs Derived Cardiac Cells for Drug and Toxicity Screening and Disease Modeling: What Micro- Electrode-Array Analyses Can Tell Us." Cells 8 (11): 1331. https://doi.org/10.3390/cells8111331.

Laaban, J. P., Iung, B., Chauvet, J. P., Psychoyos, I., Proteau, J., and Rochemaure, J. (1988). Cardiac Arrhythmias during the Combined Use of Intravenous Aminophylline and Terbutaline in Status Asthmaticus. Chest 94, 496–502. doi:10.1378/chest.94.3.496

Lasser-Ross, N., H. Miyakawa, V. Lev-Ram, S. R. Young, and W. N. Ross. 1991. "High time resolution fluorescence imaging with a CCD camera." J Neurosci Methods 36 (2-3): 253–261.

Lee, T. A., Schumock, G. T., Bartle, B., and Pickard, A. S. (2009). Mortality Risk in Patients Receiving Drug Regimens with Theophylline for Chronic Obstructive Pulmonary Disease. Pharmacotherapy 29, 1039–1053. doi:10.1592/phco.29.9.1039

Lekka, M, Gnanachandran K, Kubiak A, Zieliński T, and Zemła J. 2021. "Traction Force Microscopy - Measuring the Forces Exerted by Cells." Micron (Oxford, England: 1993) 150 (November): 103138. https://doi.org/10.1016/j.micron.2021.103138.

Leroy, J, Lignon JM, Gannier F, Argibay JA, and Malécot CO. 2002. "Caffeine-Induced Immobilization of Gating Charges in Isolated Guinea-Pig Ventricular Heart Cells." British Journal of Pharmacology 135 (3): 721–34. https://doi.org/10.1038/sj.bjp.0704520.

Levy, ML., Bacharier LB, Bateman E, et al. 2023. “Key Recommendations for Primary Care from the 2022 Global Initiative for Asthma (GINA) Update.” NPJ Primary Care Respiratory Medicine 33 (1): 7. https://doi.org/10.1038/s41533-023-00330-1.

Li, Y., Zhang, S., Zhang, X., Li, J., Ai, X., Zhang, L., et al. (2014). Blunted cardiac beta-adrenergic response as an early indication of cardiac dysfunction in duchenne muscular dystrophy. Cardiovasc. Res. 103, 60–71. doi: 10.1093/cvr/cvu119

Lian, X, Hsiao CH, Wilson G, et al. 2012. “Robust Cardiomyocyte Differentiation from Human Pluripotent Stem Cells via Temporal Modulation of Canonical Wnt Signaling.” Proceedings of the National Academy of Sciences 109 (27): E1848–57. https://doi.org/10.1073/pnas.1200250109.

Libretto, S. E. 1994. “A Review of the Toxicology of Salbutamol (Albuterol).” Archives of Toxicology 68 (4): 213–16. https://doi.org/10.1007/s002040050059.

Liu, J., C. Huang, and X. Zhan. 1999. “Src Is Required for Cell Migration and Shape Changes Induced by Fibroblast Growth Factor 1.” Oncogene 18 (48): 6700–6706. https://doi.org/10.1038/sj.onc.1203050.

Liu, J., Sun, N., Bruce, M. A., Wu, J. C., and Butte, M. J. (2012). Atomic Force Mechanobiology of Pluripotent Stem Cell-Derived Cardiomyocytes. PLoS ONE 7, e37559. doi:10.1371/journal.pone.0037559

Liu, N. 2006. “Arrhythmogenesis in Catecholaminergic Polymorphic Ventricular Tachycardia: Insights From a RyR2 R4496C Knock-In Mouse Model.” Circulation Research 99 (3): 292–98. https://doi.org/10.1161/01.RES.0000235869.50747.e1.

Liu, Y. 2008. Ryanodine Receptor Function in Intracellular Calcium Signaling. ProQuest.

Liu, Y., J. Feng, L. Shi, et al. 2012. "In situ mechanical analysis of cardiomyocytes at nano scales." Nanoscale 4 (1): 99–102.

Lorenz, K, Rosner MR, Brand T, and Schmitt JP. 2017. “Raf Kinase Inhibitor Protein: Lessons of a Better Way for B-adrenergic Receptor Activation in the Heart.” The Journal of Physiology 595 (12): 4073–87. https://doi.org/10.1113/JP274064.

Lu, S., and Hoey, A. (2000). Changes in function of cardiac receptors mediating the effects of the autonomic nervous system in the muscular dystrophy (MDX) mouse. J. Mol. Cell. Cardiol. 32, 143–152. doi: 10.1006/jmcc.1999.1063

Lucia, C, Eguchi A, and Koch WJ. 2018. “New Insights in Cardiac β-Adrenergic Signaling During Heart Failure and Aging.” Frontiers in Pharmacology 9. https://www.frontiersin.org/articles/10.3389/fphar.2018.00904.

Mah, JK., Korngut L, Dykeman J, Day L, Pringsheim T, and Jette N. 2014. “A Systematic Review and Meta-Analysis on the Epidemiology of Duchenne and Becker Muscular Dystrophy.” Neuromuscular Disorders: NMD 24 (6): 482–91. https://doi.org/10.1016/j.nmd.2014.03.008.

Malpas, SC., Maling JTB. 1990. “Heart-Rate Variability and Cardiac Autonomic Function in Diabetes.” Diabetes 39 (10): 1177–81. https://doi.org/10.2337/diab.39.10.1177.

Madl, J., S. Rhode, H. Stangl, et al. 2006. "A combined optical and atomic force microscope for live cell investigations." Ultramicroscopy 106 (8-9): 645–651.

Mah, J. K., Korngut, L., Dykeman, J., Day, L., Pringsheim, T., and Jette, N. (2014). A systematic review and meta-analysis on the epidemiology of duchenne and becker muscular dystrophy. Neuromuscul. Disord. 24, 482–491. doi: 10.1016/j.nmd.2014.03.008

Mandel, Y., Weissman, A., Schick, R., Barad, L., Novak, A., Meiry, G., et al. (2012). Human Embryonic and Induced Pluripotent Stem Cell-Derived Cardiomyocytes Exhibit Beat Rate Variability and Power-Law Behavior. Circulation 125, 883–893. doi:10.1161/CIRCULATIONAHA.111.045146

Manzur, A. Y., Kinali, M., and Muntoni, F. (2008). Update on the management of duchenne muscular dystrophy. Arch. Dis. Child. 93, 986–990.doi: 10.1136/adc.2007.118141

Markham, L. W., Michelfelder, E. C., Border, W. L., Khoury, P. R., Spicer, R. L., Wong, B. L., et al. (2006). Abnormalities of diastolic function precede dilated cardiomyopathy associated with Duchenne muscular dystrophy. J. Am. Soc. Echocardiogr. 19, 865–871. doi: 10.1016/j.echo.2006.02.003

Marks, A. R. 2013. "Calcium cycling proteins and heart failure: mechanisms and therapeutics." J Clin Invest 123 (1): 46–52.

Martinez, HR., Beasley GS, Miller N, Goldberg JF, and Jefferies JL. 2021. “Clinical Insights Into Heritable Cardiomyopathies.” Frontiers in Genetics 12: 663450. https://doi.org/10.3389/fgene.2021.663450.

Martherus, R. S., V. A. Zeijlemaker, and T. A. Y. Ayoubi. 2010. "Electrical stimulation of primary neonatal rat ventricular cardiomyocytes using pacemakers." Benchmarks 48: 65–67.

Matera, M.G. Page C.P., Calzetta L, P. Rogliani, and M. Cazzola. 2020. “Pharmacology and Therapeutics of Bronchodilators Revisited.” Review Article. Pharmacological Reviews 72 (1): 218–52. https://doi.org/10.1124/pr.119.018150.

Matera, MG, Rogliani P, Calzetta L, and Cazzola M. 2016. “Safety Considerations with Dual Bronchodilator Therapy in COPD: An Update.” Drug Safety 39 (6): 501–8. https://doi.org/10.1007/s40264-016-0402-4.

Mathur, A., Z. Ma, P. Loskill, S. Jeeawoody, and K. E. Healy. 2016. "In vitro cardiac tissue models: current status and future prospects." Adv Drug Deliv Rev 96: 203–213.

Matsumura, T., Tamura, T., Kuru, S., Kikuchi, Y., and Kawai, M. (2010). Carvedilol can prevent cardiac events in duchenne muscular dystrophy. Intern. Med. 49, 1357–1363. doi: 10.2169/internalmedicine.49.3259

McNally, E. M., Kaltman, J. R., Benson, D. W., Canter, C. E., Cripe, L. H., Duan, D., et al. (2015). Contemporary cardiac issues in duchenne muscular dystrophy. Circulation 131, 1590–1598. doi: 10.1161/CIRCULATIONAHA.114.015151

Mettauer, B., J. L. Rouleau, and J. H. Burgess. 1985. “Detrimental Arrhythmogenic and Sustained Beneficial Hemodynamic Effects of Oral Salbutamol in Patients with Chronic Congestive Heart Failure.” American Heart Journal 109 (4): 840–47. https://doi.org/10.1016/0002-8703(85)90648-9.

Meyers, T. A., Heitzman, J. A., Krebsbach, A. M., Aufdembrink, L. M., Hughes, R., Bartolomucci, A., et al. (2019). Acute AT1R blockade prevents isoproterenol-induced injury in mdx hearts. J. Mol. Cell. Cardiol. 128, 51–61. doi: 10.1016/j.yjmcc.2019.01.013

Meyers, T. A., and Townsend, D. (2019). Cardiac pathophysiology and the future of cardiac therapies in duchenne muscular dystrophy. Int. J. Mol. Sci. 20:4098. doi: 10.3390/ijms20174098

Miletić, M, Aškrabić S, Rüger J, et al. 2020. “Combined Raman and AFM Detection of Changes in HeLa Cervical Cancer Cells Induced by CeO2 Nanoparticles – Molecular and Morphological Perspectives.” Analyst 145 (11): 3983–95. https://doi.org/10.1039/C9AN02518A.

Molecular Probes. 2010. The Molecular Probes ® Handbook—Introduction to fluorescence techniques.

Molenaar, P, Chen L, and Parsonage WA. 2006. “Cardiac Implications for the Use of B2-Adrenoceptor Agonists for the Management of Muscle Wasting.” British Journal of Pharmacology 147 (6): 583–86. https://doi.org/10.1038/sj.bjp.0706670.

Moniotte, S., L. Kobzik, O. Feron, J. N. Trochu, C. Gauthier, and J. L. Balligand. 2001. “Upregulation of Beta(3)-Adrenoceptors and Altered Contractile Response to Inotropic Amines in Human Failing Myocardium.” Circulation 103 (12): 1649–55. https://doi.org/10.1161/01.cir.103.12.1649.

Mummery, C. L., J. Zhang, E. S. Ng, D. A. Elliott, A. G. Elefanty, and T. J. Kamp. 2012. "Differentiation of human embryonic stem cells and induced pluripotent stem cells to cardiomyocytes: a methods overview." Circ Res 111 (3): 344–358.

Nadkarni, S., Hay, A. W., Faye, S., and Congdon, P. J. (1988). The Relationship between Theophylline, Caffeine and Heart Rate in Neonates. Ann. Clin. Biochem. 25 ( Pt 4) (Pt 4), 408–410. doi:10.1177/ 000456328802500415

Nair, P., Milan, S. J., and Rowe, B. H. (2012). Addition of Intravenous Aminophylline to Inhaled Beta(2)-Agonists in Adults with Acute Asthma. Cochrane Database Syst. Rev. 12, CD002742. doi:10.1002/14651858.CD002742.pub2

Nakayama, H., X. Chen, C. P. Baines, et al. 2007. "Ca 2+ − and mitochondrial-dependent cardiomyocyte necrosis as a primary mediator of heart failure." J Clin Invest 117 (9): 2431–2444.

Nattel, S., A. Maguy, S. Le Bouter, and Y.-H. Yeh. 2007. "Arrhythmogenic ion-channel remodeling in the heart: heart failure, myocardial infarction, and atrial fibrillation." Physiol Rev 87 (2): 425–456.

Naumova, N, and Iop L. 2021. “Bioengineering the Cardiac Conduction System: Advances in Cellular, Gene, and Tissue Engineering for Heart Rhythm Regeneration.” Frontiers in Bioengineering and Biotechnology 9 (August). https://doi.org/10.3389/fbioe.2021.673477.

Nickerson, D. P. 1994. "Cardiac electro-mechanics: from to the whole heart."

Niehoff, J., Matzkies, M., Nguemo, F., Hescheler, J., and Reppel, M. (2019). The Effect of Antiarrhythmic Drugs on the Beat Rate Variability of Human Embryonic and Human

Induced Pluripotent Stem Cell Derived Cardiomyocytes. Sci. Rep. 9, 14106. doi:10.1038/s41598-019-50557-7

O'Neill, S. C., and D. A. Eisner. 1990. "A Mechanism for the Effects of Caffeine on Ca2+ Release during Diastole and Systole in Isolated Rat Ventricular Myocytes." The Journal of Physiology 430 (November): 519–36. https://doi.org/10.1113/jphysiol.1990.sp018305.

Oda, T., Yang, Y., Uchinoumi, H., Thomas, D. D., Chen-Izu, Y., Kato, T., et al. (2015). Oxidation of ryanodine receptor (RyR) and calmodulin enhance Ca release and pathologically alter, RyR structure and calmodulin affinity. J. Mol. Cell. Cardiol. 85, 240–248. doi: 10.1016/j.yjmcc.2015.06.009

Odstrcilik, J., Cmiel, V., Kolar, R., Ronzhina, M., Baiazitova, L., Pesl, M., et al. (2015). "Computer Analysis of Isolated Cardiomyocyte Contraction Process via Advanced Image Processing Techniques," in 2015 Computing in Cardiology Conference (CinC) (Nice, France: IEEE), 453–456. doi:10.1109/ CIC.2015.7408684

Onodera, K., Shibata, M., Kojima, J., Wachi, M., Sogawa, N., Furuta, H., et al. (2001). Toxicity of Theophylline Depends on Plasma Concentration by Single and Also Repeated Dosing in Rats. Pharmacol. Res. 44, 81–87. doi:10.1006/ phrs.2001.0831

Ottolia, M, Torres N, Bridge J. H. B.,Philipson K.D., and Goldhaber J.I.. 2013. "Na/Ca Exchange and Contraction of the Heart." Journal of Molecular and Cellular Cardiology 61 (August): 28–33. https://doi.org/10.1016/j.yjmcc.2013.06.001.

Overgaard, K, Nielsen O.B., Flatman J.A. and Clausen T. 1999. "Relations between Excitability and Contractility in Rat Soleus Muscle: Role of the Na+-K+ Pump and Na+/K+ Gradients." The Journal of Physiology 518 (Pt 1): 215–25. https://doi.org/10.1111/j.1469-7793.1999.0215r.x.

Panovský, R, Pešl M, Holeček T, et al. 2019. "Cardiac Profile of the Czech Population of Duchenne Muscular Dystrophy Patients: A Cardiovascular Magnetic Resonance Study with T1 Mapping." Orphanet Journal of Rare Diseases 14 (1): 10. https://doi.org/10.1186/s13023-018-0986-0.

Papa, A. A., D'Ambrosio, P., Petillo, R., Palladino, A., and Politano, L. (2017). Heart transplantation in patients with dystrophinopathic cardiomyopathy: review of the literature and personal series. Intractable Rare Dis Res. 6, 95–101. doi: 10.5582/irdr.2017.01024

Park, K. C., Gaze, D. C., Collinson, P. O., and Marber, M. S. (2017). Cardiac troponins: from myocardial infarction to chronic disease. Cardiovasc. Res. 113, 1708–1718. doi: 10.1093/cvr/cvx183

Pasnoori, V. R., and Leesar, M. A. (2004). Use of Aminophylline in the Treatment of Severe Symptomatic Bradycardia Resistant to Atropine. Cardiol. Rev. 12, 65–68. doi:10.1097/01.crd.0000096418.72821.fa

Patrick Gonzalez, J., Ramachandran, J., Xie, L.-H., Contreras, J. E., and Fraidenraich, D. (2015). Selective connexin43 inhibition prevents isoproterenol-induced arrhythmias and lethality in muscular dystrophy mice. Sci. Rep. 5:13490. doi: 10.1038/srep13490

Pelling, A. E., B. M. Nicholls, Y. R. Silberberg, and M. A. Horton. 2007. Approaches for investigating mechanobiological dynamics in living cells with fluorescence and atomic force microscopies

Pérez-Schindler, J, Philp A, and Hernandez-Cascales J. 2013. "Pathophysiological Relevance of the Cardiac B2-Adrenergic Receptor and Its Potential as a Therapeutic Target to Improve Cardiac Function." European Journal of Pharmacology 698 (1–3): 39–47. https://doi.org/10.1016/j.ejphar.2012.11.001.

Pesl, M, Acimovic I, Pribyl J, et al. 2014. "Forced Aggregation and Defined Factors Allow Highly Uniform-Sized Embryoid Bodies and Functional Cardiomyocytes from Human Embryonic and Induced Pluripotent Stem Cells." Heart and Vessels 29 (6): 834–46. https://doi.org/10.1007/s00380-013-0436-9.

Pesl, M, Pribyl J, Acimovic I, et al. 2016a. "Atomic Force Microscopy Combined with Human Pluripotent Stem Cell Derived Cardiomyocytes for Biomechanical Sensing." Biosensors and Bioelectronics 85 (November): 751–57. https://doi.org/10.1016/j.bios.2016.05.073.

Pesl, M, Pribyl J, Caluori G, et al. 2016b. "Phenotypic Assays for Analyses of Pluripotent Stem Cell-Derived Cardiomyocytes." Journal of Molecular Recognition, e2602. https://doi.org/10.1002/jmr.2602.

Pesl M, Pribyl J, Caluori G, et al. 2017a. "Phenotypic Assays for Analyses of Pluripotent Stem Cell–Derived Cardiomyocytes." Journal of Molecular Recognition 30 (6): e2602. https://doi.org/10.1002/jmr.2602.

Pesl M, Pribyl J, Caluori G, et al. 2017b. "Phenotypic Assays for Analyses of Pluripotent Stem Cell–Derived Cardiomyocytes." Journal of Molecular Recognition 30 (6): e2602.

Pesl, M., Jelinkova, S., Caluori, G., Holicka, M., Krejci, J., Nemec, P., et al. (2020). Cardiovascular progenitor cells and tissue plasticity are reduced in a myocardium affected by Becker muscular dystrophy. Orphanet J. Rare Dis. 15:65. doi: 10.1186/s13023-019-1257-4

Pesl, M, Pribyl J, Dvorak P, et al. 2023. "6.1 Cardiovascular Diseases." In 6.1 Cardiovascular Diseases. De Gruyter. https://doi.org/10.1515/9783110989380-011.

Peterson, J. M., Wang, D. J., Shettigar, V., Roof, S. R., Canan, B. D., Bakkar, N., et al. (2018). NF-κB inhibition rescues cardiac function by remodeling calcium genes in a duchenne muscular dystrophy model. Nat. Commun. 9:3431. doi: 10.1038/s41467-018-05910-1

Pettinato, Giuseppe, Xuejun Wen, and Ning Zhang. 2014. "Formation of Well-Defined Embryoid Bodies from Dissociated Human Induced Pluripotent Stem Cells Using Microfabricated Cell-Repellent Microwell Arrays." Scientific Reports 4 (1): 7402. https://doi.org/10.1038/srep07402.

Pioner, J. M., Guan, X., Klaiman, J. M., Racca, A. W., Pabon, L., Muskheli, V., et al. (2020). Absence of full-length dystrophin impairs normal maturation and contraction of cardiomyocytes derived from human-induced pluripotent stem cells. Cardiovasc. Res. 116, 368–382.

Plesinger, F., J. Jurco, J. Halamek, and P. Jurak. 2016. "SignalPlant: An Open Signal Processing Software Platform." Physiological Measurement 37 (7): N38–48. https://doi.org/10.1088/0967-3334/37/7/N38.

Post, Steven R., H. Kirk Hammond, and Paul A. Insel. 1999. "β-ADRENERGIC RECEPTORS AND RECEPTOR SIGNALING IN HEART FAILURE." Annual Review of Pharmacology and Toxicology 39 (1): 343–60. https://doi.org/10.1146/annurev.pharmtox.39.1.343.

Pribyl, Jan, Martin Pešl, Guido Caluori, et al. 2019. "Biomechanical Characterization of Human Pluripotent Stem Cell-Derived Cardiomyocytes by Use of Atomic Force Microscopy." Methods in Molecular Biology (Clifton, N.J.) 1886: 343–53. https://doi.org/10.1007/978-1-4939-8894-5_20.

Pribyl, J., Pešl, M., Caluori, G., Acimovic, I., Jelinkova, S., Dvorak, P., et al. (2019). Biomechanical characterization of human pluripotent stem cell-derived cardiomyocytes

by use of atomic force microscopy. Methods Mol. Biol. 1886, 343–353. doi: 10.1007/978-1-4939-8894-5_20

Puzzo, D., Raiteri, R., Castaldo, C., Capasso, R., Pagano, E., Tedesco, M., et al. (2016). CL316,243, a β3-adrenergic receptor agonist, induces muscle hypertrophy and increased strength. Sci. Rep. 5:37504. doi: 10.1038/srep37504

Qu, C., Puttonen, K. A., Lindeberg, H., Ruponen, M., Hovatta, O., Koistinaho, J., et al. (2013). Chondrogenic differentiation of human pluripotent stem cells in chondrocyte co-culture. Int. J. Biochem. Cell Biol. 45, 1802–1812. doi: 10.1016/j.biocel.2013.05.029

Price, A. H., and S. P. Clissold. 1989. “Salbutamol in the 1980s. A Reappraisal of Its Clinical Efficacy.” Drugs 38 (1): 77–122. https://doi.org/10.2165/00003495-198938010-00004.

Radmacher, M. 2007. "Studying the mechanics of cellular processes by atomic force microscopy." Methods Cell Biol 83: 347–372.

Rabbany, M. A., B. K. Saha, N. Subha, et al. 2023. “Comparative Efficacy of Levosalbutamol and Racemic Salbutamol in the Treatment of Acute Exacerbation of Asthma.” Mymensingh Medical Journal: MMJ 32 (1): 10–17.

Raiteri, R., G. Caluori, M. Tedesco, H. H. Andrade Caicedo, and C. W. Ward. 2015. "A novel AFM-based technique for measuring coupled phenomena in cardiac myocytes." Biophys J 108: 168a.

Ramalho, Nuno Jorge Dourado, Olga Švecová, Roman Kula, Milena Šimurdová, Jiří Šimurda, and Markéta Bébarová. 2022. “Aminophylline at Clinically Relevant Concentrations Affects Inward Rectifier Potassium Current in a Dual Way.” Pflugers Archiv: European Journal of Physiology 474 (3): 303–13. https://doi.org/10.1007/s00424-021-02646-8.

Rapila, Risto, Topi Korhonen, and Pasi Tavi. 2008. “Excitation-Contraction Coupling of the Mouse Embryonic Cardiomyocyte.” The Journal of General Physiology 132 (4): 397–405. https://doi.org/10.1085/jgp.200809960.

Rengo, G., Lymperopoulos, A., and Koch, W. J. (2009). Future g protein-coupled receptor targets for treatment of heart failure. Curr. Treat. Options Cardiovasc. Med. 11, 328–338. doi: 10.1007/s11936-009-0033-5

Rodrigo, C., and G. Rodrigo. 1994. “Treatment of Acute Asthma. Lack of Therapeutic Benefit and Increase of the Toxicity from Aminophylline given in Addition to High Doses

of Salbutamol Delivered by Metered-Dose Inhaler with a Spacer." Chest 106 (4): 1071–76. https://doi.org/10.1378/chest.106.4.1071.

Rodriguez, Jesica S., J. Omar Velez Rueda, Margarita Salas, et al. 2014. "Increased Na+/Ca2+ Exchanger Expression/Activity Constitutes a Point of Inflection in the Progression to Heart Failure of Hypertensive Rats." PLOS ONE 9 (4): e96400. https://doi.org/10.1371/journal.pone.0096400.

Rodriguez, Marita L., Brandon T. Graham, Lil M. Pabon, Sangyoon J. Han, Charles E. Murry, and Nathan J. Sniadecki. 2014. "Measuring the Contractile Forces of Human Induced Pluripotent Stem Cell-Derived Cardiomyocytes with Arrays of Microposts." Journal of Biomechanical Engineering 136 (5): 051005. https://doi.org/10.1115/1.4027145.

Rossi, D. J., Bryder, D., Seita, J., Nussenzweig, A., Hoeijmakers, J., and Weissman, I. L. (2007). Deficiencies in DNA damage repair limit the function of haematopoietic stem cells with age. Nature 447, 725–729. doi: 10.1038/nature05862

Rowe, D. J., Watson, I. D., Williams, J., and Berry, D. J. (1988). The Clinical Use and Measurement of Theophylline. Ann. Clin. Biochem. 25 ( Pt 1), 4–26. doi:10.1177/000456328802500102

Sadek, A. A., Mahmoud, S. M., El-Aal, M. A., Allam, A. A., and El-Halim, W. I. A. (2017). Evaluation of cardiac functions in children with duchenne muscular dystrophy: a prospective case-control study. Electron. Physician. 9, 5732–5739. doi: 10.19082/5732

Sala, Luca, Milena Bellin, and Christine L. Mummery. 2017. "Integrating Cardiomyocytes from Human Pluripotent Stem Cells in Safety Pharmacology: Has the Time Come?" British Journal of Pharmacology 174 (21): 3749–65. https://doi.org/10.1111/bph.13577.

Sala, Luca, Berend J. van Meer, Leon G. J. Tertoolen, et al. 2018. "Musclemotion." Circulation Research 122 (3): 3. https://doi.org/10.1161/CIRCRESAHA.117.312067.

Sartiani, L., Bettiol, E., Stillitano, F., Mugelli, A., Cerbai, E., and Jaconi, M. E. (2007). Developmental Changes in Cardiomyocytes Differentiated from Human Embryonic Stem Cells: a Molecular and Electrophysiological Approach. Stem Cells 25, 1136–1144. doi:10.1634/stemcells.2006-0466

Satin, Jonathan, Ilanit Itzhaki, Sophia Rapoport, et al. 2008. "Calcium Handling in Human Embryonic Stem Cell-Derived Cardiomyocytes." Stem Cells (Dayton, Ohio) 26 (8): 1961–72. https://doi.org/10.1634/stemcells.2007-0591.

Sato, H., Shiraishi, I., Takamatsu, T., and Hamaoka, K. (2007). Detection of TUNEL-positive cardiomyocytes and c-kit-positive progenitor cells in children with congenital heart disease. J. Mol. Cell. Cardiol. 43, 254–261. doi: 10.1016/j.yjmcc.2007.05.011

Satoh, Hiroyasu. 1993. "Positive and Negative Chronotropic Effects of Caffeine in Spontaneously Beating Rabbit Sino-Atrial Node Cells." General Pharmacology: The Vascular System 24 (5): 1223–30. https://doi.org/10.1016/0306-3623(93)90372-5.

Sawynok, Jana. 1995. "Pharmacological Rationale for the Clinical Use of Caffeine." Drugs 49 (1): 37–50. https://doi.org/10.2165/00003495-199549010-00004.

Schaefer, Jeremy A., and Robert T. Tranquillo. 2016. "Tissue Contraction Force Microscopy for Optimization of Engineered Cardiac Tissue." Tissue Engineering Part C: Methods 22 (1): 76–83. https://doi.org/10.1089/ten.tec.2015.0220.

Schindelin, Johannes, Ignacio Arganda-Carreras, Erwin Frise, et al. 2012. "Fiji: An Open-Source Platform for Biological-Image Analysis." Nature Methods 9 (7): 676–82. https://doi.org/10.1038/nmeth.2019.

Shafaattalab, Sanam, Eric Lin, Effimia Christidi, et al. 2019. "Ibrutinib Displays Atrial-Specific Toxicity in Human Stem Cell-Derived Cardiomyocytes." Stem Cell Reports 12 (5): 996–1006. https://doi.org/10.1016/j.stemcr.2019.03.011.

Shaffer, Fred, and J. P. Ginsberg. 2017. "An Overview of Heart Rate Variability Metrics and Norms." Frontiers in Public Health 5 (September): 258. https://doi.org/10.3389/fpubh.2017.00258.

Shamsuzzaman, M., Kavita, G., and Arunabha, R. (2016). Methylxanthine Induced Cardiotoxicity and its Mechanisms: An Experimental Study. MJMS 1, 10.

Shannon, M. 1999. "Life-Threatening Events after Theophylline Overdose: A 10-Year Prospective Analysis." Archives of Internal Medicine 159 (9): 989–94. https://doi.org/10.1001/archinte.159.9.989.

Shirokova, N., and Niggli, E. (2013). Cardiac phenotype of duchenne muscular dystrophy: insights from cellular studies. J. Mol. Cell. Cardiol. 58, 217–224. doi: 10.1016/j.yjmcc.2012.12.009

Singh, D., Agusti, A., Anzueto, A., Barnes, P. J., Bourbeau, J., Celli, B. R., et al. (2019). Global Strategy for the Diagnosis, Management, and Prevention of Chronic Obstructive

Lung Disease: the GOLD Science Committee Report 2019. Eur. Respir. J. 53. doi:10.1183/13993003.00164-2019

Skeberdis, V. A. (2004). Structure and function of beta3-adrenergic receptors. Medicina (Kaunas). 40, 407–413.

Smisek, R., Leinveber, P., Halamek, J., Matejkova, M., Pesl, M., Viscor, I., Jurak, P., Plesinger, F., & Starek, Z. (2025). Reduction of Ultra-High-Frequency ECG Components Following Sodium Channel Blockade by Propafenone: Evidence for Their Electrophysiological Origin. 2025 Computing in Cardiology Conference (CinC). doi:10.22489/CinC.2025.277

Souidi, M., Sleiman, Y., Acimovic, I., Pribyl, J., Charrabi, A., Baecker, V., et al. (2021). Oxygen Is an Ambivalent Factor for the Differentiation of Human Pluripotent Stem Cells in Cardiac 2D Monolayer and 3D Cardiac Spheroids. Ijms 22, 662. doi:10.3390/ijms22020662Sperelakis, N. 1989. "Developmental Changes in Membrane Electrical Properties of the Heart." In Physiology and Pathophysiology of the Heart, 595–623. Springer, Boston, MA.

Spitalieri, P., R. V. Talarico, S. Caioli, et al. 2018. "Modelling the pathogenesis of myotonic dystrophy type 1 cardiac phenotype through human iPSCderived cardiomyocytes." J Mol Cell Cardiol 118: 95–109.

Stehlíková, K., Skálová, D., Zídková, J., Haberlová, J., Vohánka, S., Mazanec, R., et al. (2017). Muscular dystrophies and myopathies: the spectrum of mutated genes in the czech republic. Clin. Genet. 91, 463–469. doi: 10.1111/cge.12839Stienen, G. J. M. 2015. “Pathomechanisms in Heart Failure: The Contractile Connection.” Journal of Muscle Research and Cell Motility 36 (1): 47–60. https://doi.org/10.1007/s10974-014-9395-8.

Stroeks, Sophie L. V. M., Ping Wang, Marco Merlo, et al. 2025. “Impact of Genotype-Phenotype Associations on Prognosis in Dilated Cardiomyopathy.” European Journal of Heart Failure, ahead of print, September 12. https://doi.org/10.1002/ejhf.70040.

Sucharov, Carmen C., Karen Dockstader, Karin Nunley, Timothy A. McKinsey, and Michael Bristow. 2011. “β-Adrenergic Receptor Stimulation and Activation of PKA Protect against A1-Adrenergic Mediated Phosphorylation of PKD and HDAC5.” Journal of Cardiac Failure 17 (7): 592–600. https://doi.org/10.1016/j.cardfail.2011.03.006.

Suissa, S., Hemmelgarn, B., Blais, L., and Ernst, P. (1996). Bronchodilators and Acute Cardiac Death. Am. J. Respir. Crit. Care Med. 154, 1598–1602. doi:10.1164/ajrccm.154.6.8970341

Sun, N., M. Yazawa, J. Liu, et al. 2012. "Patient-specific induced pluripotent stem cells as a model for familial dilated cardiomyopathy." Sci Transl Med 4: 130ra47–130ra47.

Svobodova, Barbora, Sarka Jelinkova, Martin Pesl, et al. 2021. “Cellular Pathology of the Human Heart in Duchenne Muscular Dystrophy (DMD): Lessons Learned from in Vitro Modeling.” Pflugers Archiv: European Journal of Physiology 473 (7): 1099–115. https://doi.org/10.1007/s00424-021-02589-0.

Swandulla, D., M. Hans, K. Zipser, and G. J. Augustine. 1991. "Role of residual calcium in synaptic depression and posttetanic potentiation: fast and slow calcium signaling in nerve terminals." Neuron 7 (6): 915–926.

Takahashi, Kazutoshi, and Shinya Yamanaka. 2006. “Induction of Pluripotent Stem Cells from Mouse Embryonic and Adult Fibroblast Cultures by Defined Factors.” Cell 126 (4): 663–76. https://doi.org/10.1016/j.cell.2006.07.024.

Tamargo, Juan, Ricardo Caballero, Ricardo Gómez, and Eva Delpón. 2010. “Cardiac Electrophysiological Effects of Nitric Oxide.” Cardiovascular Research 87 (4): 593–600. https://doi.org/10.1093/cvr/cvq214.

Tarbit, Emiri, Indu Singh, Jason N. Peart, and Roselyn B. Rose’Meyer. 2019. “Biomarkers for the Identification of Cardiac Fibroblast and Myofibroblast Cells.” Heart Failure Reviews 24 (1): 1–15. https://doi.org/10.1007/s10741-018-9720-1.

Temple, Jennifer L., Christophe Bernard, Steven E. Lipshultz, Jason D. Czachor, Joslyn A. Westphal, and Miriam A. Mestre. 2017. “The Safety of Ingested Caffeine: A Comprehensive Review.” Frontiers in Psychiatry 8 (May). https://doi.org/10.3389/fpsyt.2017.00080.

Thomson, James A., Joseph Itskovitz-Eldor, Sander S. Shapiro, et al. 1998. “Embryonic Stem Cell Lines Derived from Human Blastocysts.” Science 282 (5391): 1145–47.

Tsai, Su-Yi, Karen Maass, Jia Lu, Glenn I. Fishman, Shuibing Chen, and Todd Evans. 2015. “Efficient Generation of Cardiac Purkinje Cells from ESCs by Activating cAMP Signaling.” Stem Cell Reports 4 (6): 1089–102. https://doi.org/10.1016/j.stemcr.2015.04.015.

Tse, G., Liu, T., Li, K. H., Laxton, V., Wong, A. O., Chan, Y. W., et al. (2017). Tachycardia-bradycardia Syndrome: Electrophysiological Mechanisms and Future Therapeutic Approaches (Review). Int. J. Mol. Med. 39, 519–526. doi:10.3892/ijmm.2017.2877Tsien, R. Y. 1981. "A non-disruptive technique for loading calcium buffers and indicators into cells." Nature 290 (5806): 527–528.

Tsurumi, F., Baba, S., Yoshinaga, D., Umeda, K., Hirata, T., Takita, J., et al. (2019). The intracellular Ca2+ concentration is elevated in cardiomyocytes differentiated from hiPSCs derived from a duchenne muscular dystrophy patient. PLoS ONE 14:e0213768. doi: 10.1371/journal.pone.0213768

Tusscher, K. H. W. J. Ten, and A. V. Panfilov. 2008. “Modelling of the Ventricular Conduction System.” Progress in Biophysics and Molecular Biology, Cardiovascular Physiome, vol. 96 (1): 152–70. https://doi.org/10.1016/j.pbiomolbio.2007.07.026.

Ukena, D., C. Schudt, and G. W. Sybrecht. 1993. “Adenosine Receptor-Blocking Xanthines as Inhibitors of Phosphodiesterase Isozymes.” Biochemical Pharmacology 45 (4): 847–51. https://doi.org/10.1016/0006-2952(93)90168-v.

UYSAL, Emin, Suleyman SOLAK, Murat CARUS, Nedim UZUN, and Erdem CEVIK. 2016. “Salbutamol Abuse Is Associated with Ventricular Fibrillation.” Turkish Journal of Emergency Medicine 15 (2): 87–89. https://doi.org/10.5505/1304.7361.2015.33230.

Van Gelder, IC., Rienstra M, Bunting K.V., et al. 2024. “2024 ESC Guidelines for the Management of Atrial Fibrillation Developed in Collaboration with the European Association for Cardio-Thoracic Surgery (EACTS).” European Heart Journal 45 (36): 3314–414. https://doi.org/10.1093/eurheartj/ehae176.

Varriale, P., and Ramaprasad, S. (1993). Aminophylline Induced Atrial Fibrillation. Pacing Clin. Electrophysiol. 16, 1953–1955. doi:10.1111/j.1540-8159.1993.tb00987.x

Vasquez, C, Benamer N, and Morley GE. 2011. “The Cardiac Fibroblast: Functional and Electrophysiological Considerations in Healthy and Diseased Hearts.” Journal of Cardiovascular Pharmacology 57 (4): 380–88. https://doi.org/10.1097/FJC.0b013e31820cda19.

Vestal, R. E., Eiriksson, C. E., Musser, B., Ozaki, L. K., and Halter, J. B. (1983). Effect of Intravenous Aminophylline on Plasma Levels of Catecholamines and Related Cardiovascular and Metabolic Responses in Man. Circulation 67, 162–171. doi:10.1161/01.cir.67.1.162

Villa Chet, R., Czosek Richard, J., Ahmed, H., Khoury Philip, R., Anderson Jeffrey, B., Knilans Timothy, K., et al. (2015). Ambulatory monitoring and arrhythmic outcomes in pediatric and adolescent patients with duchenne muscular dystrophy. J. Am. Heart Assoc. 5:e002620. doi: 10.1161/JAHA.115.002620

Viollet, L., Thrush, P. T., Flanigan, K. M., Mendell, J. R., and Allen, H. D. (2012). Effects of angiotensin-converting enzyme inhibitors and/or beta blockers on the cardiomyopathy in duchenne muscular dystrophy. Am. J. Cardiol. 110, 98–102. doi: 10.1016/j.amjcard.2012.02.064

Voigt, N., Li, N., Wang, Q., Wang, W., Trafford, A. W., Abu-Taha, I., et al. (2012). Enhanced sarcoplasmic reticulum Ca2+-leak and increased Na+-Ca2+-exchanger function underlie delayed afterdepolarizations in patients with chronic atrial fibrillation. Circulation 125, 2059–2070. doi: 10.1161/CIRCULATIONAHA.111.067306

Voskoboinik, Aleksandr, Jonathan M. Kalman, and Peter M. Kistler. 2018. “Caffeine and Arrhythmias.” JACC: Clinical Electrophysiology 4 (4): 425–32. https://doi.org/10.1016/j.jacep.2018.01.012.

Vry, J., Gramsch, K., Rodger, S., Thompson, R., Steffensen, B. F., Rahbek, J., et al. (2016). European cross-sectional survey of current care practices for duchenne muscular dystrophy reveals regional and age-dependent differences.J. Neuromuscul. Dis. 3, 517–527. doi: 10.3233/JND-160185

Wagner, K. R., Lechtzin, N., and Judge, D. P. (2007). Current treatment of adult duchenne muscular dystrophy. Biochim. Biophys. Acta 1772, 229–237. doi: 10.1016/j.bbadis.2006.06.009Wang, L., L. Liu, X. Li, N. Magome, K. Agladze, and Y. Chen. 2013. “Multi-Electrode Monitoring of Guided Excitation in Patterned Cardiomyocytes.” Microelectronic Engineering 111 (November): 267–71. https://doi.org/10.1016/j.mee.2012.11.018.

Wang, Qin, Kaiqi Su, Liang Hu, et al. 2015. “A Novel and Functional Assay for Pharmacological Effects of Marine Toxins, Saxitoxin and Tetrodotoxin by Cardiomyocyte-Based Impedance Biosensor.” Sensors and Actuators B: Chemical 209 (March): 828–37. https://doi.org/10.1016/j.snb.2014.11.150.

Wang, Tianxing, Ning Hu, Jiayue Cao, Jieying Wu, Kaiqi Su, and Ping Wang. 2013. “A Cardiomyocyte-Based Biosensor for Antiarrhythmic Drug Evaluation by Simultaneously

Monitoring Cell Growth and Beating." Biosensors and Bioelectronics 49 (November): 9–13. https://doi.org/10.1016/j.bios.2013.04.039.

Warrier, Sunita, Andriy E. Belevych, Monica Ruse, et al. 2005. "β-Adrenergic- and Muscarinic Receptor-Induced Changes in cAMP Activity in Adult Cardiac Myocytes Detected with FRET-Based Biosensor." American Journal of Physiology-Cell Physiology 289 (2): C455–61. https://doi.org/10.1152/ajpcell.00058.2005.

Weiss, J. N., Garfinkel, A., Karagueuzian, H. S., Chen, P.-S., and Qu, Z.(2010). Early afterdepolarizations and cardiac arrhythmias. Heart Rhythm. 7, 1891–1899. doi: 10.1016/j.hrthm.2010.09.017

Wells SA, Morris PG, Taylor JD, Nogaret A. Estimation of ionic currents and compensation mechanisms from recursive piecewise assimilation of electrophysiological data. Front Comput Neurosci. 2025 Mar 4;19:1458878. doi: 10.3389/fncom.2025.1458878

White, Steven M., Phillip E. Constantin, and William C. Claycomb. 2004. "Cardiac Physiology at the Cellular Level: Use of Cultured HL-1 Cardiomyocytes for Studies of Cardiac Muscle Cell Structure and Function." American Journal of Physiology-Heart and Circulatory Physiology 286 (3): H823–29. https://doi.org/10.1152/ajpheart.00986.2003.

Williams, I. A., and Allen, D. G. (2007). Intracellular calcium handling in ventricular myocytes from mdx mice. Am. J. Physiol. Heart Circ. Physiol. 292, H846–H855. doi: 10.1152/ajpheart.00688.2006Wu, Peng, Gang Deng, Xiyalatu Sai, Huiming Guo, Huanlei Huang, and Ping Zhu. 2021. "Maturation Strategies and Limitations of Induced Pluripotent Stem Cell-Derived Cardiomyocytes." Bioscience Reports 41 (6): BSR20200833. https://doi.org/10.1042/BSR20200833.

Yang, X., L. Pabon, and C. E. Murry. 2014. "Engineering adolescence: maturation of human pluripotent stem cell-derived cardiomyocytes." Circ Res 114 (3): 511–523.

Ye, C., Miao, C., Yu, L., Dong, Z., Zhang, J., Mao, Y., et al. (2019). Factors Affecting the Efficacy and Safety of Aminophylline in Treatment of Apnea of Prematurity in Neonatal Intensive Care Unit. Pediatr. Neonatol 60, 43–49. doi:10.1016/ j.pedneo.2018.03.008

Youm, Jae Boum. 2016. "Electrophysiological Properties and Calcium Handling of Embryonic Stem Cell-Derived Cardiomyocytes." Integrative Medicine Research 5 (1): 3–10. https://doi.org/10.1016/j.imr.2015.12.007.

Zafar Gondal, Anoosh, and Hassam Zulfiqar. 2026. “Aminophylline.” In StatPearls. StatPearls Publishing. http://www.ncbi.nlm.nih.gov/books/NBK545175/.

Zatloukal, Jaromir, Kristian Brat, Katerina Neumannova, et al. 2020. “Chronic Obstructive Pulmonary Disease - Diagnosis and Management of Stable Disease; a Personalized Approach to Care, Using the Treatable Traits Concept Based on Clinical Phenotypes. Position Paper of the Czech Pneumological and Phthisiological Society.” Biomedical Papers of the Medical Faculty of the University Palacky, Olomouc, Czechoslovakia 164 (4): 325–56. https://doi.org/10.5507/bp.2020.056.

Zhang, Xiong, Calvin Simerly, Carrie Hartnett, Gerald Schatten, and Thomas E. Smithgall. 2014. “Src-Family Tyrosine Kinase Activities Are Essential for Differentiation of Human Embryonic Stem Cells.” Stem Cell Research 13 (3, Part A): 379–89. https://doi.org/10.1016/j.scr.2014.09.007.

Zhu, R., Millrod, M. A., Zambidis, E. T., and Tung, L. (2016). Variability of action potentials within and among cardiac cell clusters derived from human embryonic stem cells. Sci. Rep. 6:18544. doi: 10.1038/srep18544

Zuppinger, Christian. 2016. “3D Culture for Cardiac Cells.” Biochimica et Biophysica Acta (BBA) - Molecular Cell Research, Cardiomyocyte Biology: Integration of Developmental and Environmental Cues in the Heart, vol. 1863 (7, Part B): 1873–81. https://doi.org/10.1016/j.bbamcr.2015.11.036.

Biosensors and Bioelectronics 85 (2016) 751–757

Contents lists available at ScienceDirect

Biosensors and Bioelectronics

journal homepage: www.elsevier.com/locate/bios

# Atomic force microscopy combined with human pluripotent stem cell derived cardiomyocytes for biomechanical sensing

Martin Pesl [a,b,1], Jan Pribyl [c,1], Ivana Acimovic [a], Aleksandra Vilotic [a], Sarka Jelinkova [a], Anton Salykin [a,b], Alain Lacampagne [d], Petr Dvorak [a,b], Albano C. Meli [a,d], Petr Skladal [c,*], Vladimir Rotrekl [a,b]

[a] Department of Biology, Faculty of Medicine, Masaryk University, Brno, Czech Republic
[b] ICRC, St. Anne's University Hospital, Brno, Czech Republic
[c] CEITEC, Masaryk University, Brno, Czech Republic
[d] PhyMedExp, INSERM U1046, University of Montpellier, Montpellier, France

ARTICLE INFO

*Article history:*
Received 15 March 2016
Received in revised form
11 May 2016
Accepted 23 May 2016
Available online 28 May 2016

*Keywords:*
Micromechanical biosensor
Human stem cell
Cardiomyocyte contraction
Drug testing

ABSTRACT

Cardiomyocyte contraction and relaxation are important parameters of cardiac function altered in many heart pathologies. Biosensing of these parameters represents an important tool in drug development and disease modeling. Human embryonic stem cells and especially patient specific induced pluripotent stem cell-derived cardiomyocytes are well established as cardiac disease model.. Here, a live stem cell derived embryoid body (EB) based cardiac cell syncytium served as a biorecognition element coupled to the microcantilever probe from atomic force microscope thus providing reliable micromechanical cellular biosensor suitable for whole-day testing.

The biosensor was optimized regarding the type of cantilever, temperature and exchange of media; in combination with standardized protocol, it allowed testing of compounds and conditions affecting the biomechanical properties of EB. The studied effectors included calcium , drugs modulating the catecholaminergic fight-or-flight stress response such as the beta-adrenergic blocker metoprolol and the beta-adrenergic agonist isoproterenol. Arrhythmogenic effects were studied using caffeine. Furthermore, with EBs originating from patient's stem cells, this biosensor can help to characterize heart diseases such as dystrophies.

© 2016 Elsevier B.V. All rights reserved.

## 1. Introduction

Cell based biosensor (CBB) devices represent a novel tool to understand and treat various human diseases including heart diseases which are leading cause of death in developed countries (Pilkerton et al., 2015). Most of them have hidden cause at the cellular and genetic levels (Aistrup et al., 2009; Stienen, 2015) not easily accessible for diagnostics, as heart biopsy is invasive procedure with significant risk (Holzmann et al., 2008; Imamura et al., 2015). Since the discovery of pluripotent stem cells (PSCs), such as human embryonic stem cells (hESC) (Thomson et al., 1998) and especially disease specific induced pluripotent stem cells (hiPSC) (Takahashi et al., 2007) and their differentiation into cardiomyocytes (Mummery et al., 2002), these cell types represent an important cellular model in drug and disease screening (reviewed in Acimovic et al., 2014).

The electrophysiological phenotype of individual cardiac cells is often studied providing information representing pacemaker or messenger function. Despite most of studies use single cells, the CMs syncytium seems to be a critical parameter in biosensor assembly as unstable signals are obtained in case of individual or small cluster of cells (Kaneko et al., 2007, 2014). These methods follow mostly action potential, cell to cell conductivity or electrical cell-substrate impedance (Giaever and Keese, 1984). Recently, xCELLigence RTCA Cardio multiwell sensor combined with primary neonatal rat cells was used to monitor the effect of antiarrhythmic drugs on cell growth and contractions (Guo et al., 2011). However, the electrophysiological data cannot be fully separated from the mechanical triggers and consequences (Kelly et al., 2006) rendering the method not suitable for large group of diseases affecting electro-mechanical coupling. Thus CM contraction and relaxation biosensing represents an indispensable step for the in vitro disease modeling. Indirect methods of contraction measurement, such as optical ones based on optical fiber deformation (Fearn et al., 1993) and image analysis (Neagoe et al., 2003) have limited potential especially in case of in vitro differentiated CMs,

* Correspondence to: Department of Biochemistry, Masaryk University, Kamenice 5, CZ-62500 Brno, Czech Republic.
*E-mail address:* skladal@chemi.muni.cz (P. Skladal).
[1] These authors contributed equally to this work.

http://dx.doi.org/10.1016/j.bios.2016.05.073
0956-5663/© 2016 Elsevier B.V. All rights reserved.

which do not fully match the shape of the isolated CMs and often require dissociation of the syncytium and analyzing the individual cells in microposts (Rodriguez et al., 2014). Furthermore, the combination of optical analysis and the direct methods measuring contraction force on artificially assembled structures are significantly impacted by stiffness of the substrate, such as the twitch power in the case of dissociated cells plated on substrate with varying stiffness (Rodriguez et al., 2011). Further the increasing cell number negatively impacted the force-length relationship measured directly on neonatal cardiac cells self-assembled on fibrin fibers (Sondergaard et al., 2012), again rendering the syncytium analysis at least difficult. Thus it seems that the most promising structure for studying the contraction properties of human cardiac syncytium might be uniformly sized clusters of differentiated CMs in the form of PSCs-derived embryoid bodies (Pesl et al., 2014). Therefore we opted for a direct approach to assess the EBs' cardiac syncytium mechanical properties in real time and under the alternating biophysical and biochemical conditions using atomic force microscopy (AFM).

AFM is a three-dimensional high resolution topographic technique. It is suitable for biological applications in native conditions (Vahabi et al., 2013) with the ability to measure bending of the cantilever probe with extremely high precision (Sundararajan and Bhushan, 2002). It allows AFM to be used as a mechanical nanosensor (Wang et al., 2015), or as a micromechanical transducer for the construction of biosensors (Lavrik et al., 2004). Furthermore, modified AFM tip biosensor has been used in numerous studies, including the analysis of Alzheimer's disease process (Hane et al., 2014), as mechanical sensor in the study of cell penetration by nanoneedles (Obataya et al., 2005), in cell-based biosensing of drug effects (Wang et al., 2009) and in study of growth factor effects on epidermal cells (Zhang et al., 2014).

In this study, our previously developed uniformly sized EBs containing human induced pluripotent stem cell-derived cardiomyocytes (hiPSC-CMs) (Pesl et al., 2014) are integrated into the AFM force sensing platform to perform a high fidelity contraction pattern as a unique CBB for the measurement of absolute values of contractile forces together with frequency of the beat rate in complex conditions and cellular models. Development and optimization of the whole measurement setup is described with proposed application for characterization of cell clusters of cardiac cells and testing effects of model drugs.

## 2. Materials and methods

### 2.1. Preparation of hiPSC and hESC cardiomyocyte clusters

Measurements were performed using the hESC lines CCTL14 and CCTL12, characterized previously (Dvorak et al., 2005; International Stem Cell Initiative et al., 2007; Krutá et al., 2013). The hiPSC line cl1 was obtained from Dr. Majlinda Lako, Institute of Genetic Medicine, Newcastle University and the iPSC lines MDMD2Se were derived in our laboratory from human skin biopsies (Krutá et al. 2014). The hESCs and iPSC lines were propagated on mitotically inactivated mouse embryonic fibroblasts (Dvorak et al., 2005). Regular round shape of embryoid bodies was achieved by forced aggregation in silicone mold preformed microwells (1.5% agarose, VWR) (Dahlmann et al., 2013), their differentiation and maturation was achieved using our previously described method (Pesl et al., 2014). For statin samples, PSC were cultivated with pravastatin (20 μM, Sigma) for 4 days prior to EB formation.

### 2.2. Clusters seeding and measurement set-up

Beating EBs cultured for 28 days after initiation of differentiation were selected for round shape and adequate size and seeded onto adherent 30 mm Petri dishes (TPP Technoplastic Products, Trasadingen, Switzerland). The cultivation media was replaced by Tyrod solution (135 mM NaCl, 10 mM HEPES, 5.4 mM KCl, 0.9 mM $MgCl_2$, pH 7.4) and suplemented with 10 mM glucose and $CaCl_2$ (in desired concentration) and the EBs were maintained at 37 °C in a standard $CO_2$ incubator. Before experiment, a dish equipped with media exchange tubes was placed on the motorized stage of an inverted microscope (Olympus IX-81S1F-3, Tokyo, Japan) and the AFM recording head (BioAFM NanoWizard 3, JPK, Berlin, Germany) was finally placed on top of the sample. The AFM set-up was modified in order to provide real-time biomechanical characterization of CMs cell clusters (Fig. 1).

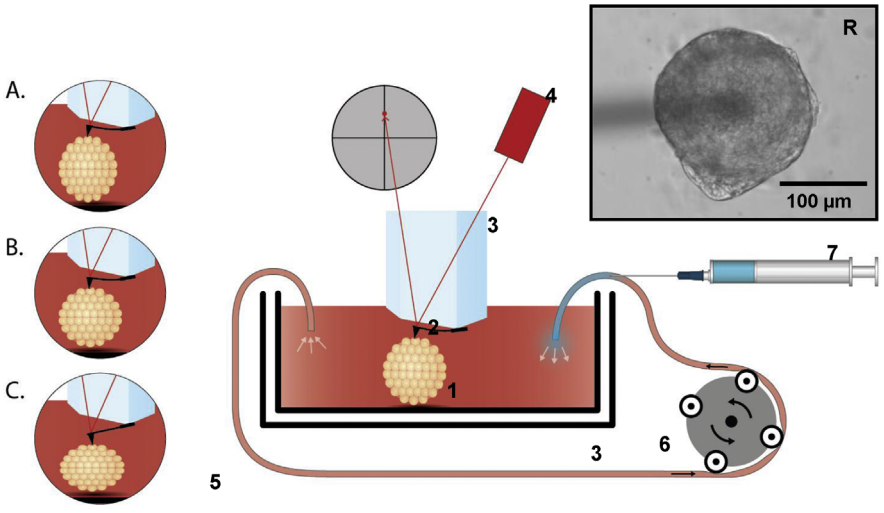



**Fig. 1.** Scheme of the biosensor setup used for biomechanical characterization of cardiomyocyte clusters. Most important parts are schematically shown and are labeled as follows: 1 – Embryonic body (EB, cluster of living cells) in plastic Petri dish, (3 cm in diameter), 2 – AFM cantilever, equipped with a sharp tip, 3 – glass cantilever holder block, 4 – AFM laser source (a) (left) and photodetector of laser (b), position, 5 – plastic (PP) tubing, i.d. 0.2 mm (an arrow shows the flow direction), 6 – peristaltic pump, driving the flow direction and rate (rotation direction is shown by an arrow), 7 – medical syringe (total volume of 1.0 ml) for drug injection, 8 – Petri dish heater (to keep constant temperature of 37.0 ± 0.1 °C). The little insets on the left (A, B and C) show the subsequent stages of the EB contractile movement as this is measured by the AFM cantilever. Image (R) in the top-right corner shows real image of EB cluster with cantilever on its surface (captured by optical microscope). The size of the EB cluster is 175 μm.

The cantilever glass holder placed on the AFM head (scanning by probe, range in X-Y-Z was 100–100–15 μm) was equipped with soft cantilever and the contact part of the head was submersed in the 30 mm Petri dish containing one or more EBs at the bottom of non-treated plastic. The Petri dish heater (JPK, Berlin, Germany) was used to either keep the temperature constant at 37 °C or at 29–37 °C for temperature dependency studies. Scanning probe microscope (SPM) Control Software v.4 (JPK) was used for instrument control and data acquisition at 1 kHz rate. For further details, see part 1.1 of Supplementary Material (SM).

### 2.3. Recording of mechanocardiograms

The mechanocardiogram (MCG) curve shows the interaction force between the AFM tip and the surface of the beating cells cluster recorded in a real time. The force between the AFM probe and the studied surface was kept constant as defined by the set point (SP) value, carried out by the feedback loop. Intensity of feedback is given by integral and proportional gain parameters (IGain/PGain). The various AFM cantilever probes used are described in the supplementary materia (SM) part 2.3.

In order to determine the effect of the set point value on the measured force (MCG curves), the cantilever (Hydra-6R, AppNano, Mountain View, CA, USA) was left to land onto the beating CM cell cluster stabilized for 15 min at 37 °C. The MCGs were recorded in 10 min intervals using SP set to 0, 1, 3, 6, 9, 12, 15 and 18 nN (whole measuring range of the biosensor setup given by stiffness and sensitivity), where the SP=0 value means operation in the so called passive mode, i.e. it does not follow the cell movement (zero interaction force) and only the living beating cell cluster is leveling the cantilever, similar as in the literature (Liu et al., 2012).

The effect of temperature stability on MCG recording and behavior of CM clusters at different temperatures are provided in SM parts 2.4 and 2.5, respectively. The protocol for studying effect of different concentration of calcium is given in the SM part 2.6.

### 2.4. Surface homogeneity of the biomechanical properties

EB is a spherical cluster (300 μm in diameter) consisting of approximately 2000 cells; fluorescent images of EB are provided in Fig. S1. In order to map the homogeneity of the beating force on the surface of the CMs cluster, nine points of the surface of the cell cluster were screened (scheme included in Fig. 3). The uncoated silicon nitride cantilever Hydra-6R-200N (AppNano), characterized by spring constant of 0.025 N/m and sensitivity 10.1 nm/V was used. Motorized stage of the AFM microscope was used to move the AFM probe between the positions, when the Z-driving piezo was in the retracted state and the probe was 50 μm above the cell surface. When in place, AFM cantilever was landed onto the beating cell cluster of cardiomyocytes (EB), preheated and stabilized. The MCG curve was recorded for 10 min in each position with constant set point value of 6 nN. 5 min recordings of MCG curves were evaluated for the force and beat rate comparison.

### 2.5. Evaluation of signal traces

Time-series data saved from the Nanowizard AFM were preprocessed and analyzed by in-house developed algorithm using MATLAB 2015a (ver. 8.5, The MathWorks Inc., Natick, USA). After resampling (noise and dataset size reduction), the local maximum and its corresponding local minimum for each contraction were identified and processed to obtain the force of each individual contraction (R-S amplitude) and beat rate of EB. The Mann-Whitney's *U*-test was used to evaluate two group comparisons.

### 2.6. Statistical evaluation of data

Quantitative data are presented as the mean ± the standard error of the mean from 3 to 6 experiments (indicated as *N* in the appropriate graph). The normality of data distribution was evaluated by the Shapiro-Wilk method thus proving the data normality at the 0.05 level. One way Student's *t*-test was used to test statistical difference of the measured data sets at the level 0.05 (maps of force on the cell cluster) when they were compared to the mean value. One way ANOVA method implementing the Bonferroni test was employed to compare statistical significance of measured signals (force/beat rate) at different concentrations of calcium, significance was compared either at different levels ($p < 0.05$, $p < 0.01$, $p < 0.005$) or was calculated as value. Microcal Origin 7.0 software (Microcal, Northampton, MA, USA was used for statistical processing of the data.

## 3. Results and discussion

### 3.1. Cardiomyocyte cluster biosensor construction

The multicellular biosensor device was constructed by implementing the embryoid body inside the AFM measurement chamber as shown in Fig. 1. The major difference compared to previously reported approach (Liu et al., 2012) was the use of the embryoid body as multicellular syncytium rather than individual cardiomyocytes. EBs were characterized by immunofluorescence using anti α-actinin antibody and DAPI staining (Fig. S1A), providing distribution of cardiomyocytes within the syncytium. After dissociating the beating EB into individual cells, the obtained DAPI/α-actinin and DAPI/cardiac troponin T fluorescence patterns (Fig. 1SB) were as expected for mature cardiomyocytes.

The use of the cluster of CMs seems to be a significant advantage regarding robustness of the resulting system. Typically, the CMs-based biosensing experiments were running successfully for up to 8 h. A fresh sterile medium was exchanged when needed, however, the experiments were otherwise carried out in non-sterile conditions inside the acoustic isolation chamber containing the microscopes. The AFM cantilever contacting surface of the cell cluster was kept fixed in the horizontal plane and the contraction force was monitored in real time by the vertical bending of the cantilever. Other parameters such as beating frequency and kinetics of the responses were precisely determined by the data post-processing.

The effect of various set point values on the AFM biosensor with the CMs-based EB was tested. The force and "heart" beat rate (BR) of the EB were recorded (Fig. 2A) while the set point value was gradually increased from 1 nN up to 18 nN (Fig. 2B). The BR values did not differ significantly within the tested range demonstrating robustness of the biosensor set-up and also suggesting that the force application does not lead to BR changes due to the activation of mechano-sensitive ion channels normally present in cardiomyocytes. Interestingly, the initial significant and steep increase in contraction force between the set point 0 and 5 nN was observed. The explanation for the initial ramp below 5 nN is demonstrated by the curves of force measured with 3 different values of set point (0, 6 and 10 nN) shown in Fig. 2A.

The curve measured with SP=0 nN (passive mode) is missing the feedback loop resulting from the EB relaxation rendering the data incomplete. Application of 6 nN of SP force to the cantilever resulted in recording complete dataset of force needed to compensate the EB cluster movement. Thus, the active mode was preferred to the passive one (Liu et al., 2012), possibly due to the limited mechanical integrity of dissociated CMs on the non elastic surface. Further increase in SP force to 10 nN led to subsequent

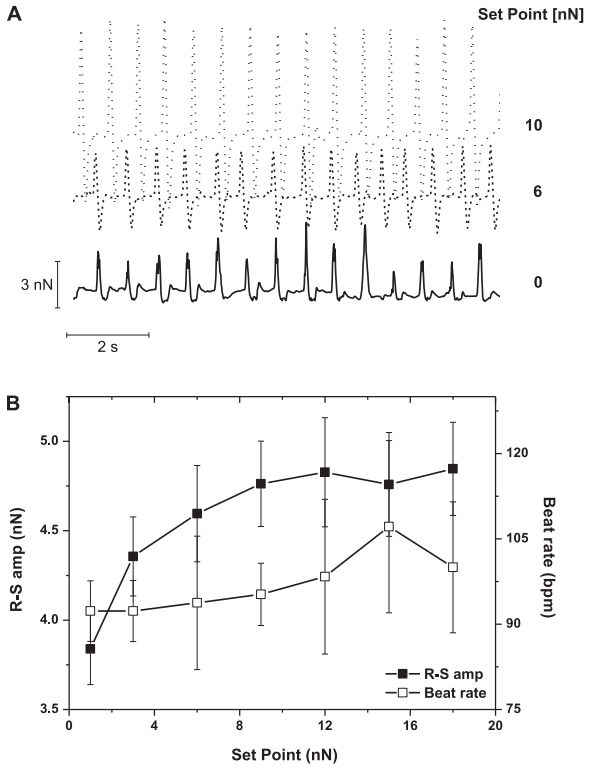



**Fig. 2.** A Comparison of real time curves recorded during the passive (set point value 0 nN) and active mode, with two different values of set point. B Effect of set point value on force (*r*-S amp) and beat rate of EB. Average of median values is shown in the graph, error bars are equal to standard deviation of values, N=2.

insignificant increase in contraction force; however this, based on the curve shape (Fig. 2(A)), can be explained by mechanical stimulation of the cells in the cluster and activation of mechano-sensitive ion channels (e.g. Lin et al., 2007) rather than by inability to record full contraction with SP=6 nN as in case of the passive mode (0 nN).

Therefore, the optimal value of set point for experiments was set at 6 nN, this is also close to the average values of EBs contraction forces. Such set point force allows for the measurement of 95% of maximum contraction force (4.6 nN vs. 4.85 nN, when SP was 6 and 18 nN, respectively), with no effect on BR therefore minimizing the effect of the mechanical stimulation. On the other hand, further increase in SP force, stimulating the mechano-sensitive ion channels and/or adherens junctions present in the syncytium, enables the EB containing biosensor to be useful for modeling and/or drug screening in case of hypertension and stretch related hypertrophy (Yamazaki et al., 1998) or cardiac injury related tension changes between myocyte and fibroblast (Thompson et al., 2011).

### 3.2. Biomechanical properties are homogenous on the EB surface

The effect of localization of the AFM probe on the surface of the cell cluster was tested; the measuring position ideally should not significantly influence the resulting biomechanical parameters. Nine points homogenously located on the EB surface were chosen (Fig. 3) and the contraction force and BR were determined. Furthermore, to evaluate potential influence of the EB phenotype, these experiments were repeated for three different types of EBs including normal control EBs generated under hypoxic conditions (Hypoxia), disease model EBs with pathologicaly affected

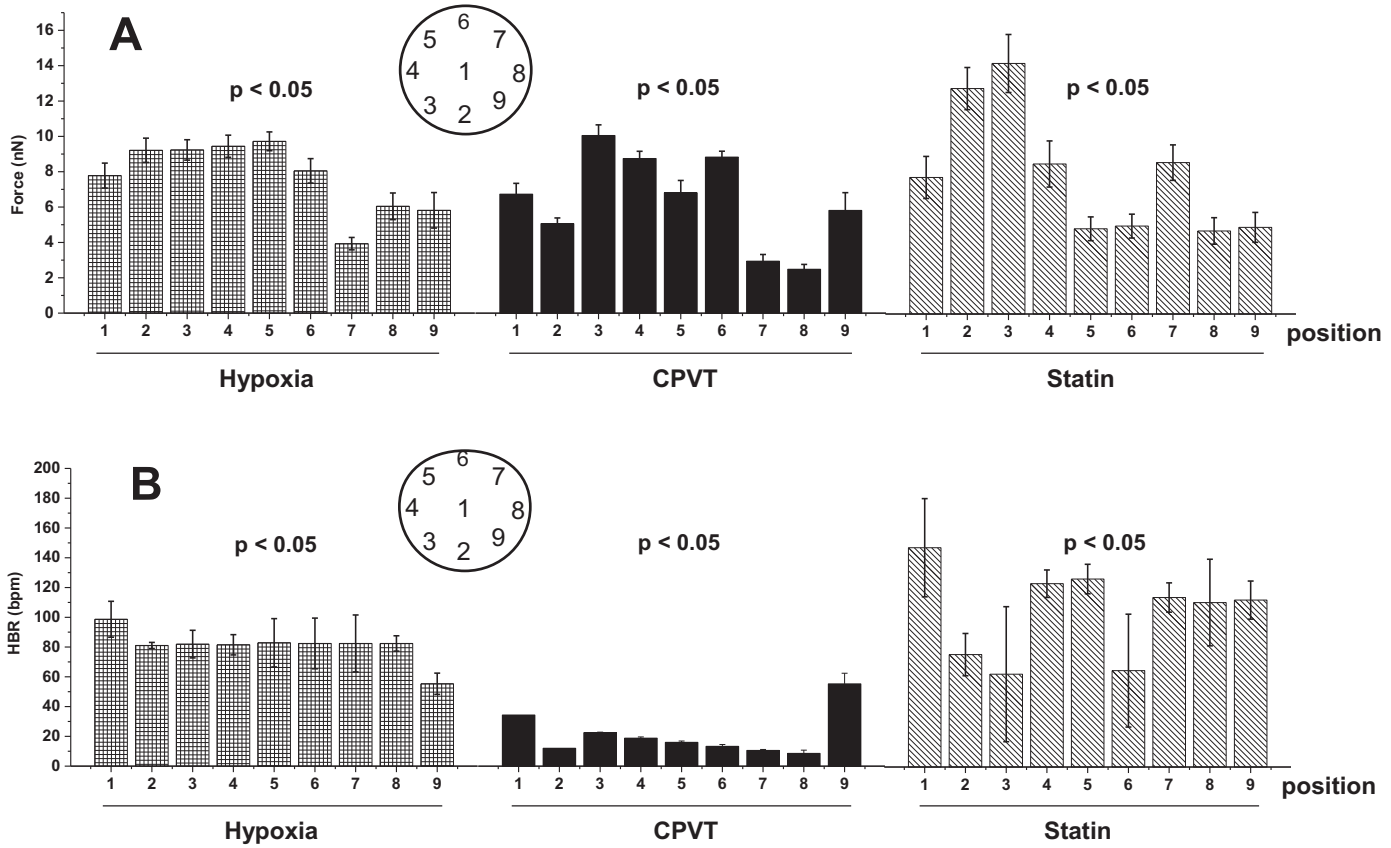



**Fig. 3.** Mapping of the force on the surface of the EB cluster. Average of median values of beating force (A) and beat rate (B) recorded in different positions on cell cluster surface are presented in the graphs as data sets (groups) of values measured for every cell cluster. Map of positions on EB surface is shown in the upper part of both graphs., error bars are equal to standard deviation of values, N=3. The data normality was confirmed by Shapiro Wilk test at 0.05 level. All the data sets were found not to be significantly different from the mean value at the same level (0.05), as indicated in the graph.

excitation-contraction coupling (CPVT) (Meli et al., 2011 and unpublished data), and EBs derived from the cells treated with statins (Jelinkova et al., unpublished).

Consistent values of the contraction force and beating frequency were found by screening of a single EB across the nine detection points and even the EB-to-EB values covered quite narrow interval (Fig. 3; the detailed statistical values are included as Table S1 in SM). However, the contraction force variability on peripheral detection points implicates some positional effect and possibly the effect of biomagnetic fields produced by the EB's electric activity and stresses the importance to choose the detection point with highest response for further analysis. The highest reproducibility was observed for the normal (Hypoxia) EBs. The minor effect of the exact positioning of the microcantilever probe at biosurface seems to be the most important advantage of the cluster of (several hundredths) cells compared to experiments carried out on individual cardiomyocytes. Single cells either separately adhering to the surface or as part of the two-dimensional layer are typically much more affected by the contacting cantilever, and if present, the sharp tip might damage the cell membrane. In the case of cell cluster, damage of few surface-located cells contacting the probe is not very significant. From the practical point of view, this is quite significant advantage of the cluster of cells serving as the biorecognition element.

### 3.3. Effect of temperature on the cardiomyocytes-based biosensor

Temperature affects the beat rate as well as arrhytmogenic cardiomyocyte potential (Chen et al., 2003). Furthermore, temperature affects also stability of the cantilever and its coupling with EB in the biosensor set-up. Contrary to the desired effect of temperature on the cardiomyocyte function (biorecognition process), its effect on the stability of the transducer system should be eliminated by choosing suitable components and optimal conditions.

To characterize the effect of cantilever type and its temperature instability independent of the EB activity, live but non beating EB coupled with variety of AFM probes were evaluated between 30 and 37 °C; details are discussed in SM and shown in Fig. S2. The instability usually results from the bimetallic effect combined with adsorption events on the hydrophobic surface of the coating metal layer (Samori, 2009). Thus, the uncoated silicon nitride cantilever (HYDRA-6R, pyramidal tip) provided most stable force reading and higher reflection of laser beam comparing to the tip-less version (HYDRA TL). Gold-coated SNL-10 probe exhibited the highest variability in the force signal, suggesting limited usefulness of metal coated probes. The cantilever equipped with colloid nanosphere (bio650) provided reasonable temperature stability but high signal noise, probably due to hydration of the colloidal probe, again limiting its use for mechanical transduction. Generally, the work in liquids of elevated temperatures (e.g. physiological) causes instability of the AFM laser signal reflected to the detector (Amano and Takahashi, 2013). Here, the use of non-coated probes eliminated most complications and allowed stable measurements over long time periods.

At the cellular level, temperature modulates contraction force and BR of CMs clusters; this effect can serve as an example of physiological conditions affecting heart function, conveniently studied using the developed EB-based biosensor. Data were collected for the contraction force (median of the *r*-S amplitude) and BR in the range from 26 to 37 °C (Fig. S3).

The temperature dependence showed slightly increasing values of the relative force with rising temperature, with plateau at 34 and 35 °C (88% of maximal force) and absolute maxima (quite fluctuating beating force) at the maximal temperature point. This indicates that the beating EBs are highly sensitive to temperature variation, suggesting that the constant temperature is a major factor for reliable use of the biosensor as well as it provides a great tool for arrhytmogenic drug effect detection under non standard temperature, resembling hypothermia or fever, in agreement with previously described temperature dependency in murine neonatal ventricle slices and hESC co-culture models (Pillekamp et al., 2007).

### 3.4. Effect of extracellular calcium level on contraction force and beat rate

Calcium is a principal mediator of the cardiac excitation-contraction coupling initiating the contraction. We then explored the effect of increased extracellular calcium concentration on EB using this biosensor set-up. The cardiac physiological concentration of $Ca^{2+}$ range from 0.1 to 5 mM (Meli et al., 2011) while 1.8 mM is common for patch clamp and other cardiomyocyte in vitro studies (Bébarová, 2012). Real time force traces (Fig. 4A) recorded with 0.2, 1.0, 1.8, 3.6 and 5.4 mM extracellular $Ca^{2+}$ present not only ability of the biosensor to determine the absolute contraction force (Fig. 3B) and BR (Fig. 3C) data, but also to detect and quantify irregular contractions and arrhythmias evident from traces in Fig. 4A. Such application of the biosensor enables both to detect and characterize the arrhythmias on the cellular level as well as to determine the arrhytmogenic effect of tested drugs or conditions.

Data obtained by evaluation of these curves were relativized as the absolute value for every EB sample is slightly different and therefore difficult for absolute comparison. The contraction force increased with the $Ca^{2+}$ concentration (Fig. 4B), in agreement with well-known fact that the force of contraction is proportional to the calcium uptake in atrial and ventricular cardiomyocytes (Winegrad, 1961, Hellam and Podolsky, 1969; Katz and Lorell, 2000).

Simultaneously, BR decreased with increasing concentration of extracellular calcium (Fig. 4C). This also corresponds to the previously published non reciprocal relationship between force and BR (Burridge et al., 2014; Liu et al., 2012). Interestingly, the BR data presented higher variability for low (0.2 mM) as well as high (3.6 mM) levels of calcium, confirming dependence of coupling of excitation and contraction on calcium (Winegrad, 1961). Winegrad presented periodical drops in BR at 2.5 and 3.75 mM $Ca^{2+}$, almost perfectly matching our data showing uncoupling at 3.6 mM calcium (Fig. 4C). This demonstrates that the EB based biosensor can be used to study both the excitation-contraction coupling as well as to screen drugs targeted for such effects. Moreover, arrhytmogenic effect of higher calcium concentrations (3.6 and 5.4 mM) can be observed in CMG curves (Fig. 4A).

### 3.5. Beta-adrenergic receptors' stimulation/inhibition followed by the biosensor

The cardiomyocytes-based biosensor is not presented as purely analytical tool for measuring concentrations; its principal task is quantification of biochemical activity of the tested drugs affecting biomechanics of the cardiac syncytium. To demonstrate such application, baseline signal for different EBs was initially standardized in Tyrod buffer; afterwards, the tested compound was injected to the working chamber; the experiments included the beta-adrenergic receptor antagonist metoprolol (Beta, final concentration 70 μM), the beta-adrenergic agonist isoproterenol (1 mM) and the calcium discharger caffeine (1 mM) triggering arrhythmia (Fig. 5).

The basal physiological values of the contractile movement were characterized by R-S amplitude corresponding to force of 22.0 nN and beat rate of 67.4 per minute (bpm). In agreement with published data on beta adrenergic antagonizing activity of

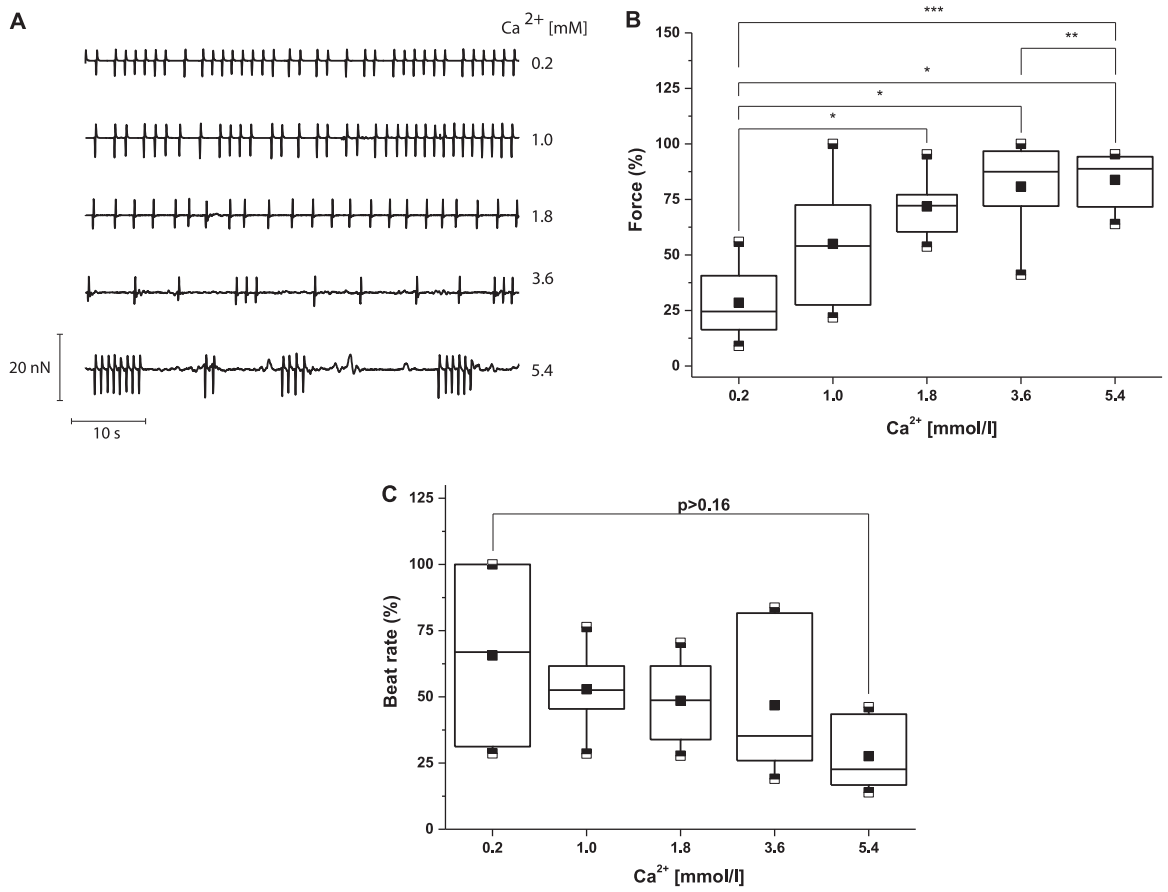



**Fig. 4.** Effect of calcium concentration on the beating force (*r*-S amp) and beating rate (BR) characterized by AFM microscope. Real time curves recorded in the presence of calcium concentrations indicated in the graph A. Corresponding dependencies of force (B) and beat rate (C) on the concentration of calcium. The main bars of data show middle quartile of measured data with line as median and quartiles represented by whiskers (graphs B and C). The main bars show middle quartile of the measured data with line as median and quartiles represented by whiskers (graphs B and C), N=6. Statistical significance of the data was tested by the ANOVA one way method, when the means were compared using the Bonferroni test for their significance at different levels – * $p < 0.05$,** $p < 0.01$,*** $p < 0.005$, the level of significance is indicated numerically in the graph C.

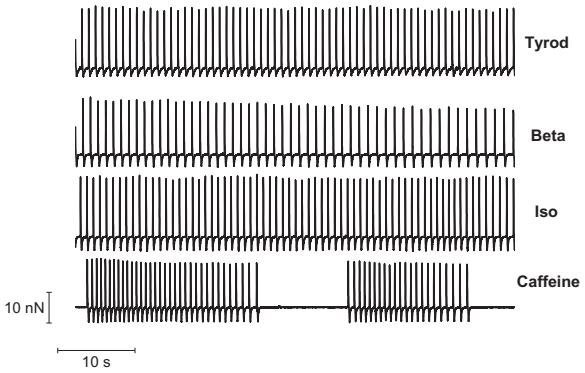



**Fig. 5.** Real traces of force of the beating EB measured by the AFM microscope as a response to the presence of various drugs in the measuring chamber, as indicated close to the curves.

metoprolol (Blinova et al., 2014), its addition decreased the average force down to 18.8 nN accompanied by reduction of beat rate to 53.7 bpm. On the other hand, isoproterenol (Pillekamp et al., 2012), in agreement with published data on its adrenergic stimulatory activity, induced an increase of the beat force value to 23.4 nN and beat rate to 78.8 bpm (Fig. 5).

Finally, the addition of caffeine well illustrates the ability of the biosensor to visualize very fast processes like arrhythmias. From the mathematical point of view, it is difficult to describe the arrhythmic, so called stop-and-go effect. The beating force was rather constant during the active intervals. However, the average frequency provides rather low value (58.9 bpm), it is very high (85.0 bpm) during the active period. The high deviation value stems from the irregular biological movement and not from low measurement reproducibility.

The presented data on beta adrenergic stimulation and inhibition demonstrated that the β-adrenergic signaling was mature in both hESC- and hiPSC-CMs syncytium, rendering the biosensor useful for both studying the mechanism of beta adrenergic stimulation and beta adrenergic modulatory drug screening as well as dissecting the mechanism of induced arrhythmias.

## 4. Conclusions

The cardiomyocytes-based embryoid body as a biorecognition element was coupled to the microcantilever probe from atomic force microscope providing micromechanical cellular biosensor. Beating force and rate of the EB contractions was transduced by AFM cantilever thus providing a robust biosensor platform suitable for whole-day testing. The cellular biosensor was optimized regarding the type of cantilever, thermostating, exchange of media and addition of tested compounds. The resulting reliable biosystem in combination with standardized protocol allowed for complex testing of compounds and conditions affecting the biomechanical properties of the embryoid body. The studied effector molecules included calcium ions, drugs as beta-blocker metoprolol

and stimulant isoprotenol, arrhythmic effects were initiated by caffeine. Furthermore, when embryoid bodies containing cardiomyocytes derived from patient's own cells via reprogrammed pluripotent stem cells are employed, the resulting biosensor can be conveniently used as the in vitro model for detailed biomechanical characterization of heart diseases such as dystrophies, including screening of novel drugs in near physiological conditions.

## Conflict of interest

There is no conflict of interest.

## Acknowledgments

We wish to thank Martina Vodinská and Miroslava Nehybová for their technical support, Guido Caluori from University of Genoa for reading the manuscript. We also thank Majlinda Lako from NewcastleUniversity for the cl1iPSCs line, The work has been supported by CEITEC - Central European Institute of Technology (CZ.1.05/1.1.00/02.0068 and LQ1601), FNUSA-ICRC (CZ.1.05/1.1.00/02.0123 and LQ1605) from the European Regional Development Fund and the National Program of Sustainability II., Grant Agency of the Czech Republic (P302/12/G157 and GA13-19910S). This work has also been supported by SoMoPro – Marie Curie Actions – South Moravian Region and by the European Society of Cardiology (ESC) (R12042FF).

## Appendix A. Supporting information

Supplementary data associated with this article can be found in the online version at http://dx.doi.org/10.1016/j.bios.2016.05.073.

## References

Acimovic, I., Vilotic, A., Pesl, M., Lacampagne, A., Dvorak, P., Rotrekl, V., Meli, A.C., 2014. Biomed. Res. Int. 2014, 512831.
Aistrup, G.L., Shiferaw, Y., Kapur, S., Kadish, A.H., Wasserstrom, J.A., 2009. Circ. Res. 104, 639–649.
Amano, K., Takahashi, O., 2013. ArXiv1, 3053967 (Phys).
Bébarová, M., 2012. Gen. Physiol. Biophys. 31, 131–140.
Blinova, E.V., Skachilova, S.Y., Blinov, D.S., Singh, L.N., Elizarova, Y.N., Meleshkin, A.I., Ivanova, E.A., Salyamova, E.I., 2014. Vestnik aritmologii 77, 53–56.
Burridge, P.W., Metzler, S.A., Nakayama, K.H., Abilez, O.J., Simmons, C.S., Bruce, M.A., Matsuura, Y., Kim, P., Wu, J.C., Butte, M., Huang, N.F., Yang, P.C., 2014. Am. J. Transl. Res. 6, 724–735.
Chen, Y.J., Chen, Y.C., Chan, P., Lin, C.I., Chen, S.A., 2003. J. Biomed. Sci. 10, 535–543.
Dahlmann, J., Kensah, G., Kempf, H., Skvorc, D., Gawol, A., Elliott, D.A., Dräger, G., Zweigerdt, R., Martin, U., Gruh, I., 2013. Biomaterials 34, 2463–2471.
Dvorak, P., Dvorakova, D., Koskova, S., Vodinska, M., Najvirtova, M., Krekac, D., Hampl, A., 2005. Stem Cells 23, 1200–1211.
Fearn, L.A., Bartoo, M.L., Myers, J.A., Pollack, G.H., 1993. IEEE Trans. Biomed. Eng. 40, 1127–1132.
Giaever, I., Keese, C.R., 1984. Proc. Natl. Acad. Sci. USA 81, 3761–3764.
Guo, L., Abrams, R.M.C., Babiarz, J.E., Cohen, J.D., Kameoka, S., Sanders, M.J., Chiao, E., Kolaja, K.L., 2011. Toxicol. Sci. J. Soc. Toxicol. 123, 281–289.
Hane, F.T., Lee, B.Y., Petoyan, A., Rauk, A., Leonenko, Z., 2014. Biosens. Bioelectron. 54, 492–498.
Hellam, D.C., Podolsky, R.J., 1969. J. Physiol. 200, 807–819.
Holzmann, M., Nicko, A., Kühl, U., Noutsias, M., Poller, W., Hoffmann, W., Morguet, A., Witzenbichler, B., Tschöpe, C., Schultheiss, H.-P., Pauschinger, M., 2008. Circulation 118, 1722–1728.
Imamura, T., Kinugawa, K., Nitta, D., Fujino, T., Inaba, T., Maki, H., Hatano, M., Kinoshita, O., Nawata, K., Yao, A., Kyo, S., Ono, M., 2015. Int. Heart J. 56, 67–72.
International Stem Cell Initiative, Adewumi, O., Aflatoonian, B., Ahrlund-Richter, L., Amit, M., Andrews, P.W., Beighton, G., Bello, P.A., Benvenisty, N., Berry, L.S., Bevan, S., Blum, B., Brooking, J., Chen, K.G., Choo, A.B.H., Churchill, G.A., Corbel, M., Damjanov, I., Draper, J.S., Dvorak, P., Emanuelsson, K., Fleck, R.A., Ford, A., Gertow, K., Gertsenstein, M., Gokhale, P.J., Hamilton, R.S., Hampl, A., Healy, L.E., Hovatta, O., Hyllner, J., Imreh, M.P., Itskovitz-Eldor, J., Jackson, J., Johnson, J.L., Jones, M., Kee, K., King, B.L., Knowles, B.B., Lako, M., Lebrin, F., Mallon, B.S., Manning, D., Mayshar, Y., McKay, R.D.G., Michalska, A.E., Mikkola, M., Mileikovsky, M., Minger, S.L., Moore, H.D., Mummery, C.L., Nagy, A., Nakatsuji, N., O'Brien, C.M., Oh, S.K.W., Olsson, C., Otonkoski, T., Park, K.-Y., Passier, R., Patel, H., Patel, M., Pedersen, R., Pera, M.F., Piekarczyk, M.S., Pera, R.A.R., Reubinoff, B. E., Robins, A.J., Rossant, J., Rugg-Gunn, P., Schulz, T.C., Semb, H., Sherrer, E.S., Siemen, H., Stacey, G.N., Stojkovic, M., Suemori, H., Szatkiewicz, J., Turetsky, T., Tuuri, T., van den Brink, S., Vintersten, K., Vuoristo, S., Ward, D., Weaver, T.A., Young, L.A., Zhang, W., 2007. Nat. Biotechnol. 25, 803–816.
Kaneko, T., Kojima, K., Yasuda, K., 2007. Biochem Biophys. Res. Commun. 356, 494–498.
Kaneko, T., Nomura, F., Hamada, T., Abe, Y., Takamori, H., Sakakura, T., Takasuna, K., Sanbuissho, A., Hyllner, J., Sartipy, P., Yasuda, K., 2014. Sci. Rep. 4, 4670.
Katz, A.M., Lorell, B.H., 2000. Circulation 102, Iv-69-Iv-74.
Kelly, D., Mackenzie, L., Hunter, P., Smaill, B., Saint, D.A., 2006. Clin. Exp. Pharmacol. Physiol. 33, 642–648.
Krutá, M., Bálek, L., Hejnová, R., Dobšáková, Z., Eiselleová, L., Matulka, K., Bárta, T., Fojtík, P., Fajkus, J., Hampl, A., Dvořák, P., Rotrekl, V., 2013. Stem Cells 31, 693–702.
Krutá, M., Šeneklová, M., Raška, J., Salykin, A., Zerzánková, L., Pešl, M., Bártová, E., Franek, M., Baumeisterová, A., Košková, S., Neelsen, K.J., Hampl, A., Dvořák, P., Rotrekl, V., 2014. Stem Cells Dev. 23, 2443–2454.
Lavrik, N.V., Sepaniak, M.J., Datskos, P.G., 2004. Rev. Sci. Instrum. 75, 2229–2253.
Lin, W., Laitko, U., Juranka, P.F., Morris, C.E., 2007. Biophys. J. 92 (5) 1559-72.
Liu, J., Sun, N., Bruce, M.A., Wu, J.C., Butte, M.J., 2012. PLoS One 7, e37559.
Meli, A.C., Refaat, M.M., Dura, M., Reiken, S., Wronska, A., Wojciak, J., Carroll, J., Scheinman, M.M., Marks, A.R., 2011. Circ. Res. 22 109(3):281–90.
Mummery, C., Ward, D., Van den Brink, C.E., Bird, S.D., Doevendans, P.A., Opthof, T., La Riviere, D., Brutel, A., Tertoolen, L., Van Der Heyden, M., 2002. (others). J. Anat. 200, 233–242.
Neagoe, C., Opitz, C.A., Makarenko, I., Linke, W.A., 2003. J. Muscle Res. Cell Motil. 24, 175–189.
Obataya, I., Nakamura, C., Han, S., Nakamura, N., Miyake, J., 2005. Biosens. Bioelectron. 20, 1652–1655.
Pesl, M., Acimovic, I., Pribyl, J., Hezova, R., Vilotic, A., Fauconnier, J., Vrbsky, J., Kruzliak, P., Skladal, P., Kara, T., Rotrekl, V., Lacampagne, A., Dvorak, P., Meli, A.C., 2014. Heart Vessel. 29, 834–846.
Pilkerton, C.S., Singh, S.S., Bias, T.K., Frisbee, S.J., 2015. J. Am. Heart Assoc. 4, e001650.
Pillekamp, F., Reppel, M., Rubenchyk, O., Pfannkuche, K., Matzkies, M., Bloch, W., Sreeram, N., Brockmeier, K., Hescheler, J., 2007. Stem Cells Dayt. Ohio 25, 174–180.
Pillekamp, F., Haustein, M., Khalil, M., Emmelheinz, M., Nazzal, R., Adelmann, R., Nguemo, F., Rubenchyk, O., Pfannkuche, K., Matzkies, M., Reppel, M., Bloch, W., Brockmeier, K., Hescheler, J., 2012. Stem Cells Dev. 21, 2111–2121.
Rodriguez, A.G., Han, S.J., Regnier, M., Sniadecki, N.J., 2011. Biophys. J. 101, 2455–2464.
Rodriguez, M.L., Graham, B.T., Pabon, L.M., Han, S.J., Murry, C.E., Sniadecki, N.J., 2014. J. Biomech. Eng. 136, 051005.
Samori, P., 2009. STM and AFM Studies on (Bio) molecular Systems: Unravelling the Nanoworld. Springer Science & Business Media,, Germany.
Sondergaard, C.S., Mathews, G., Wang, L., Jeffreys, A., Sahota, A., Wood, M., Ripplinger, C.M., Si, M.-S., 2012. Ann. Thorac. Surg. 94, 1241–1249.
Stienen, G.J.M., 2015. J. Muscle Res. Cell Motil. 36, 47–60.
Sundararajan, S., Bhushan, B., 2002. Sens. Actuators Phys. 101, 338–351.
Takahashi, K., Tanabe, K., Ohnuki, M., Narita, M., Ichisaka, T., Tomoda, K., Yamanaka, S., 2007. Cell 131, 861–872.
Thompson, S.A., Copeland, C.R., Reich, D.H., Tung, L., 2011. Circulation 123, 2083–2093.
Thomson, J.A., Itskovitz-Eldor, J., Shapiro, S.S., Waknitz, M.A., Swiergiel, J.J., Marshall, V.S., Jones, J.M., 1998. Science 282, 1145–1147.
Vahabi, S., Nazemi Salman, B., Javanmard, A., 2013. Iran. J. Med. Sci. 38, 76–83.
Wang, C., Kim, J., Zhu, Y., Yang, J., Lee, G.-H., Lee, S., Yu, J., Pei, R., Liu, G., Nuckolls, C., Hone, J., Lin, Q., 2015. Biosens. Bioelectron. 71, 222–229.
Wang, J., Wan, Z., Liu, W., Li, L., Ren, L., Wang, X., Sun, P., Ren, L., Zhao, H., Tu, Q., Zhang, Z., Song, N., Zhang, L., 2009. Biosens. Bioelectron. 25, 721–727.
Winegrad, S., 1961. Circullation 24, 523.
Yamazaki, T., Komuro, I., Yazaki, Y., 1998. Cell. Signalling 10, 693–698.
Zhang, L., Yang, F., Cai, J.-Y., Yang, P.-H., Liang, Z.-H., 2014. Biosens. Bioelectron. 56, 271–277.

Biosensors and Bioelectronics 124–125 (2019) 129–135

Contents lists available at ScienceDirect

Biosensors and Bioelectronics

journal homepage: www.elsevier.com/locate/bios

# Non-invasive electromechanical cell-based biosensors for improved investigation of 3D cardiac models

Guido Caluori[a,b,c], Jan Pribyl[a], Martin Pesl[b,d,e], Sarka Jelinkova[d], Vladimir Rotrekl[d], Petr Skladal[a,*], Roberto Raiteri[c,*]

[a] Central European Institute of Technology, Masaryk University, Kamenice 5, 62500 Brno, Czech Republic
[b] International Clinical Research Centre of Saint Anne Hospital Brno, Pekarska 53, 60200 Brno, Czech Republic
[c] Department of Informatics, Bioengineering Robotics and Systems Engineering, University of Genova, Via All'Opera Pia, 13, 16145 Genova, Italy
[d] Department of Biology, Faculty of Medicine, Masaryk University, Kamenice 5, 62500 Brno, Czech Republic
[e] 1st Department of Cardiovascular Diseases, St. Anne's University Hospital and Masaryk University, Pekarska 53, Brno, Czech Republic

ARTICLE INFO

*Keywords:*
Excitation-contraction coupling
Human pluripotent stem cells
Cardiomyocytes
Atomic force microscopy
Microelectrode array
Drug testing

ABSTRACT

Cardiomyocytes (CM) placed on microelectrode array (MEA) were simultaneously probed with cantilever from atomic force microscope (AFM) system. This electric / nanomechanical combination in real time recorded beating force of the CMs cluster and the triggering electric events. Such "organ-on-a-chip" represents a tool for drug development and disease modeling. The human pluripotent stem cells included the WT embryonic line CCTL14 and the induced dystrophin deficient line reprogrammed from fibroblasts of a patient affected by Duchenne Muscular Dystrophy (DMD, complete loss of dystrophin expression). Both were differentiated to CMs and employed with the AFM/MEA platform for diseased CMs' drug response testing and DMD characterization. The dependence of cardiac parameters on extracellular $Ca^{2+}$ was studied. The differential evaluation explained the observed effects despite variability of biological samples. The β-adrenergic stimulation (isoproterenol) and antagonist trials (verapamil) addressed ionotropic and chronotropic cell line-dependent features. For the first time, a distinctive beating-force relation for DMD CMs was measured on the 3D cardiac in vitro model.

## 1. Introduction

In the field of cell-based biosensors, cardiomyocytes (CM) are often used as models to study heart related diseases. The monitoring of electric activities of CMs is typically chosen; (multi)electrode transducers seem well established and widely available as microelectrode arrays (MEA) (Rothermel et al., 2005). The beating of CMs can be followed relatively easily (e.g. by video microscopy, Laurila et al., 2015), though in many situations the missing information on the associated beating force is of paramount importance in heart remodeling pathologies, such as dystrophinopathies and cardiomyopathies (Vatta et al., 2005). Beating force is associated with pathophysiological electro-mechanical coupling, and its alterations result often in mechanical heart failure (Pesl et al., 2016a). Such biomechanical measurements investigating the dilated cardiomyopathy were previously done on CMs using the stretcher device (Knoll et al., 2002). More detailed investigations were later done using cantilevers as nanomechanical transducers and atomic force microscope (AFM) as the evaluation system in real time with individual cardiomyocyte cells (Liu et al., 2012a,2012b) or cell clusters (Pesl et al., 2016a). Thus, combination of AFM for biomechanical changes with MEA sensing electric signals described here seems naturally promising for elucidating complex events in cardiomyocytes obtained from patient derived stem cells. This approach provides a robust and convenient example of the organ-on-a-chip system demonstrating its capabilities on disease related CMs.

Supplementary material related to this article can be found online at doi:10.1016/j.bios.2018.10.021.

The introduction of human pluripotent stem cells (hPSC, either embryonic, hESC, or induced pluripotent, hiPSC) and cardiac differentiation protocols allowed almost two decades of study on the cardiac organogenesis and functionality. In particular, patient-specific hiPSC representing a direct supply of healthy and mutation-carrying samples (Sinnecker et al., 2014) allow for description of the diseases progression involved in heart failure (Moretti et al., 2013). To improve the comparison between in vitro models, CRISPR-Cas9 technology has recently gained an outstanding popularity for its efficiency and flexibility in inducing precise mutations in cell lines, providing researchers with isogenic controls (Motta et al., 2017). hPSC-derived cardiomyocytes

* Corresponding authors.
*E-mail addresses:* skladal@chemi.muni.cz (P. Skladal), roberto.raiteri@unige.it (R. Raiteri).

https://doi.org/10.1016/j.bios.2018.10.021
Received 1 July 2018; Received in revised form 11 October 2018; Accepted 11 October 2018
Available online 16 October 2018
0956-5663/ © 2018 Elsevier B.V. All rights reserved.

and models recapitulate the morphological, genetic and functional characteristics of the heart muscle, specifically the subcellular cascade known as cardiac excitation-contraction coupling (cECC), responsible for heart pumping function (Bers, 2002). Cardiomyocytes from hPSC can be derived as 2D or 3D stem cell cultures. However, the 3D models seem to be superior and more physiologically relevant compared to the 2D ones (Regmi and Jeong, 2016). For monolayer culture, the multiple existing protocols with high differentiation efficiency involve modulation of the canonical Wnt/β-catenin pathway (Lian et al., 2012; Burridge et al., 2014), with high differentiation efficiency. For 3D cultures, the protocols exploit the spontaneous differentiation triggered from the aggregation of hPSC into embryoid bodies, which is driven to cardiac phenotypes using hypoxia and small molecules cocktails (Pesl et al., 2014). The efficiency of differentiation and grade of maturation can vary according to protocol and cell lines, and can be improved by physical methods, as in electro-mechanical stimulation (Bauwens et al., 2016). Purified hPSC-CMs can be further reassembled in precise geometries, such as in the engineered heart tissue (Tzatzalos et al., 2016). From gene expression to functionality, hPSC-CMs present an embryonic-like cardiac phenotype, with immature sarcomeres, sarcoplasmic reticulum and calcium cycling (Mummery et al., 2012; Acimovic et al., 2014). An immature phenotype has also been proven for embryoid body-derived cardiac models (Doevendans et al., 2000). Nevertheless, hPSC-CMs play a key role in future drug development with reduced attrition rate (Liang et al., 2013; Zheng et al., 2013), in cardiotoxicity assays (Takeda et al., 2018), disease modeling (Dell'Era et al., 2015) and in cell-based regenerative therapies (Doppler et al., 2013), and further studies to achieve cardiac maturation are ongoing. This aspect is also investigated by our proposed approach, to assess its robustness.

The hPSC-derived cardiac models can be characterized by functional (or phenotypic) properties though multiple in vitro assays, reviewed in another work from our group (Pesl et al., 2016b). Among these, atomic force microscopy has in the past three decades achieved remarkable role in the evaluation of biological samples mechanics and topography (Alonso and Goldmann, 2003; Kilpatrick et al., 2015) in native culture environment. In particular, it has been employed in important studies on single CMs (Liu et al., 2012a). A combination of AFM and 3D cardiac models has already been proposed as cell-based biosensor (CBB) in our previous work (Pesl et al., 2016a). Most AFM systems are now currently integrated with optical and confocal microscopy, which allows the implementation of combined measures of AFM and calcium imaging (Liu et al., 2012b; Caluori et al., 2018), but further systems can be included if properly miniaturized. Small biosensors, such as microelectrode arrays (MEA), can be engineered to comply with AFM and optical microscopy systems for cardiac investigation (Cogollo et al., 2011). The attractiveness of MEA-based electrophysiology resides in its ability to multiprobe extracellular field potentials (EFP) of electroactive cells in a non-destructive fashion, which allows for prolonged and complex measurements of cells and tissues (Spira and Hai, 2013).

In this work, we present an electromechanical in vitro system for the combined study of cECC on 3D cardiac models, employing both AFM and MEA platforms together. The aim of this work is to provide an improved method for cardiac models characterization and drug testing in the format of an organ (heart)-on-a-chip. For this reason, we have confronted a model of cardiac maturation with respect to its control, and employed a disease model of Duchenne muscular dystrophy (DMD), a progressively invalidating pathology of the striated muscle, including the myocardium (Finsterer and Stöllberger, 2003).

## 2. Materials and methods

### 2.1. hPSC culture and cardiac differentiation

The cardiac cells clusters were obtained using the hESC line CCTL14 (Adewumi et al., 2007) and one hiPSC line reprogrammed from fibroblasts of a patient affected by Duchenne Muscular Dystrophy (DMD). The patient carries a deletion of exons 45–50 of the DMD gene causing a complete loss of dystrophin expression. The line has been fully characterized for pluripotency markers (https://hpscreg.eu/cell-line/MUNIi001-A) and the differentiated CMs were tested for presence of striated pattern of sarcomeres labeled with cardiac troponin T (sc-8121, Santa Cruz), and cytoplasmic presence of dystrophin (NCL-DYSB, Leica) (see Supplementary material, SFig. 1). Pluripotent cells were firstly thawed and seeded on mitotically-inactivated mouse embryonic fibroblasts (feeder cells). The hPSC colonies were cultivated in DMEM-F12 (Thermofisher, Waltham, MA, USA) supplemented with 15% KnockOut fetal bovine serum Serum Replacement (FBS, Life Technologies, Carlsbad, CA, USA), 1% L-glutamine (Thermofisher), 0.5% penicillin/streptomycin (Thermofisher), 1% 2-mercaptoethanol (Thermofisher), 1% non-essential amino acids (Life Technologies), and 4 ng ml$^{-1}$ and 10 ng ml$^{-1}$ human fibroblast growth factor 2 (hFGF2, Peptrotech, London, UK) for hESC and hiPSC, respectively. Medium was changed daily and colonies were propagated for at least 5 passages, by manual fractioning. hESC cells were divided in a control group (CTRL) and another group (DORSO) undergoing an exposure to 500 nM of dorsomorphin (Sigma Aldrich, St. Louis, MO, USA) 4 days to the differentiation protocol, to improve cardiac commitment (Hao et al., 2008).

Cardiac differentiation was started by embryoid body formation, as described elsewhere (Pesl et al., 2013). Briefly, compact, round colonies were manually cut and scratched from the culture surface. For DMD iPSC, the colonies were kept intact, carefully detached from the culturing surface as a whole. The cell leaflets were transferred in hypoxic incubation atmosphere (5% $O_2$) and underwent a sequential cytokine modulation in KnockOut DMEM (Life Technologies), supplemented with 10% FBS, 1% L-glutamine, 1% PS, 1% 2-mercapthoethanol, 1% non-essential amino acids (further referred simply as culture medium). Beating cardiac clusters (BCC, Supplementary Fig. 1) were visible from day 14 and were transferred into normoxic atmosphere. After day 22, they were kept in the culture medium with 10 μg ml$^{-1}$ ascorbic acid (Sigma Aldrich).

### 2.2. Microelectrode arrays cleaning and coating

Before beating CMs cluster plating, 60 channel MEAs (60MEA200/30iR-Ti/ITO, Multichannel Systems, Reutlingen, Germany) were cleaned using a 0.1% w/v solution of Tergazyme detergent (Alconox, White Plains, NY, US) in MilliQ water for at least 8 h. The culture well (i.e. the area inside the plastic ring) was then thoroughly washed with MilliQ water to remove the excess detergent. The preparation of the device was moved to a UV-sterilized clean box (Biosan, Riga, Latvia). Each MEA was placed in 100 mm sterile Petri dish (TPP, Trasadingen, Switzerland), and the MEA culture well was sterilized by filling it with 70% ethanol solution. After 30 min, the sterilizing solution was removed, the culture well on MEA was rinsed twice with 0.2 μm-filtered MilliQ water and let dry. The sensing area (i.e. the electrode array area) was then coated with 20–50 μl of 0.1 mg ml$^{-1}$ laminin (Sigma Aldrich) and fibronectin (Sigma Aldrich) mixture, 1:1 ratio, to promote cell adhesion. The MEAs were put in a cell incubator at 37 °C, 5% $CO_2$, overnight. The next day, MEAs were rinsed twice with filtered MilliQ water to remove excess of adhesion factor from the surface.

### 2.3. BCCs plating on MEA chips

Suspended BCCs were collected and plated on MEA sensing area with 30 μl droplet of the culture medium. This amount of medium was a safe tradeoff between sample wobbling limitation and the need of hydrated environment. Samples were manually placed on top of electrode array, then put in standard cell incubator and kept in this overnight (with loosely fitted lid and additional droplets were placed separately around the well to prevent evaporation). The following day, medium

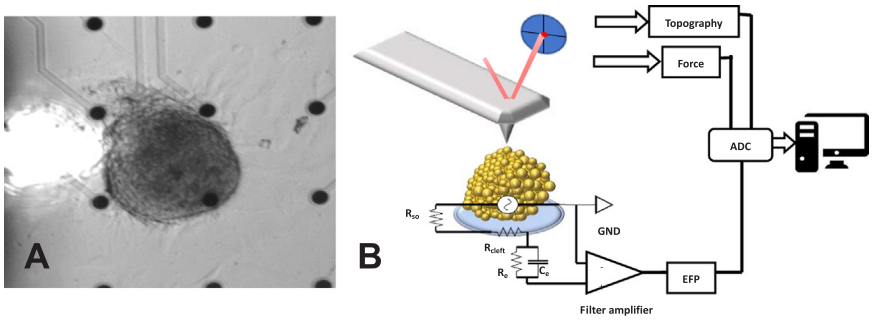



**Fig. 1.** Real case and schematic of the proposed electromechanical cell-based system. A) A beating cardiac cluster (BCC) placed on a microelectrode array (MEA) sensing area. The bright spot on the left side represents the AFM laser reflecting from the cantilever. Scale bar is 200 μm. B) Schematic representation of the implemented setup. The BCC acts as a periodic micro-voltage generator sensed by the planar electrode, while the AFM measures the topographical displacement and the exerted force. The synchronous acquisition is guaranteed by the common acquisition board and computer.

was gently added atop up to 1 ml. The BCCs were allowed to stabilize up to 3 days in vitro to ensure appropriate adhesion, spreading and formation of cell-electrode contacts. Fig. 1A and Supplementary Fig. 3 show typical BCCs properly placed on MEA, before beginning the experiments. Supplementary video recording presents movements of the adhered BCC clearly demonstrating the regular beating events.

### 2.4. Setup preparation and experimental protocols

The MEA chip containing the samples was housed in a customized holder made of an aluminum plate with adhesive heating pads and Pt100 temperature probe (RS Components, Corby, UK), and an electronic board with contacts to interface with the MEA electrodes. The electronic board was equipped with 60-channels unity-gain amplifiers to provide low impedance tracks and noise shielding. A second filtering-amplifying stage provides a pass-band of 10–3000 Hz and a total gain of 60 dB. The described holder was then fixed on the motorized stage of an inverted microscope (Olympus IX-81S1F-3, Tokyo, Japan). An AFM scanner head with 15 μm vertical range (BioAFM NanoWizard 3, JPK, Berlin, Germany) was placed above the sample. A soft silicon nitride cantilever SNL-10-D (Bruker, Billerica, MA, USA; nominal spring constant 30 pN $m^{-1}$) was used as nanomechanical probe to ensure stable contact without applying disruptive forces on the sample. The cantilever spring constant was calibrated before each experiment using the thermal noise method (Butt and Jaschke, 1995). A contact force of 5 nN was found optimal compromise between baseline stability and absence of visible adverse effects on the sample, as previously showed (Pesl et al., 2016a). Each experiment was performed in Tyrode solution (135 mM NaCl, 10 mM HEPES, 5.4 mM KCl, 0.9 mM $MgCl_2$, pH 7.4) supplemented with 10 mM glucose and 1.8 mM $CaCl_2$. After solution exchange, the calibrated cantilever was immersed in liquid and put in contact with the sample several times to identify the superficial center of contraction (i.e. the point with highest vertical positive displacement). Once the center of contraction was found, the drug trials started at an interval of 5 min of recording and 10 min settling time after drug administration or washout (a schematic is provided in Supplementary Fig. 4).

Calcium chloride solution was obtained in Tyrode buffer to give a stepwise increment of 1.1 mM after each addition. Isoproterenol stock solution (30 μM) was made in sterilized MilliQ water to prevent it from quenching: the selected step increment was 300 nM. Finally, Verapamil hydrochloride (Lekoptin, Lek Pharmaceuticals, Ljubljana, Slovinia) stock solutions (127.5 μM) were made in Tyrode, for a step increment of 255 nM. The added volume of drug solution never exceeded 5% of the basal volume in the MEA chip (2 ml).

### 2.5. Data recording and evaluation

All the presented protocols were repeated on 3 biological replicates of each cell line. Electromechanical recordings were acquired at 5 kHz sampling frequency through a LabVIEW virtual instrument and a proprietary data acquisition board PCI6071E (National Instruments, Austin, TX, USA). Fig. 1B shows a schematic of the acquisition system. Cell mechanocardiogram (MCG) comprehends the time-dependent topographical changes (i.e. the vertical displacement of the AFM piezo actuator, in μm) and the uncompensated force (in nN). The cell-cantilever contact was never lost during drug injections or medium washout. The obtained data were post-processed and analyzed using a Matlab R2016b (Natwick, MA, USA) GUI, using state of the art algorithms. From each recording, the parameters listed in Table 1 and defined in Supplementary Fig. 5 were determined. Statistical analysis was performed in Prism 5.0 (GraphPad Software, La Jolla, CA, USA) and numerical results are presented as mean ± SEM, after passing normality test. Datasets were compared for statistical significance using 1-way analysis of variance (ANOVA) with Bonferroni post-test, or repeated measures 2-way ANOVA with matching on drug concentration levels. Statistical significance was accepted with $p$-values below 0.05.

## 3. Results and discussion

### 3.1. Simultaneous electromechanical recording

The implemented setup allowed the simultaneous visualization, synchronous recording and coupled analysis of the electromechanical features of the cECC (Fig. 2A). The lowest observable noise level in the MEA-EP traces was 33.3 μVpp, whereas the average noise in the force and in the Z height traces were 18.3 pN and 24.5 nm respectively. Online and post-processing digital filtration allowed the analysis of

**Table 1**
Description of extracted parameters.

| Parameter name | Description |
|---|---|
| Beating rate | Reciprocal of time distance between two adjacent events |
| Electro mechanical delay | Time between the electrical event and 10% of the next contraction maximum amplitude |
| Contraction time | Time between 10% of the peak amplitude and the peak, on the rising side |
| Relaxation time | Time between the event peak and the point corresponding to 10% of the peak amplitude on the falling side |
| Duration time | The sum of contraction and relaxation times |
| Average speed of contraction | Mean of the first derivative of the rising part of contraction |
| Time constant | Time parameter obtained by fitting the relaxation time interval with a decreasing exponential function |
| Force | The uncompensated force peak-to-peak during the contraction |
| $Z$ height | The peak excursus of the AFM $Z$-piezo following the contraction |

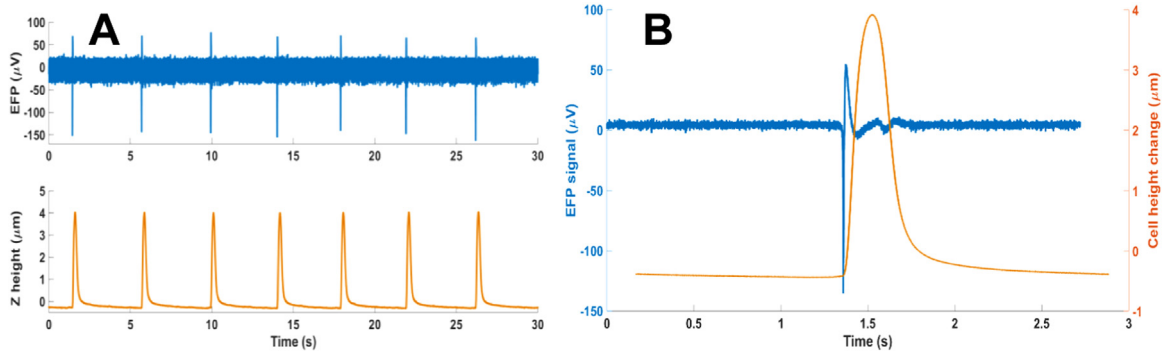



**Fig. 2.** Representative recording obtained with the implemented electromechanical system, and its post-processed part. A) Simultaneously and synchronously acquired extracellular field potential (top) and mechanical contraction (bottom). B) Averaged curves from the same recording; it is possible to appreciate the noise reduction due to filtering. The two traces are separated by the mean calculated delay.

EFPs with signal-to-noise ratio even close to 0 dB. Nevertheless, approximately half of the plated samples were able to produce a visible EFP trace, while mechanically beating. This issue is most probably due to scarcely-conductive coupling between the MEA planar electrodes and the BCC. Extracellular biopotentials morphology is fundamentally dependent on the conductive sample/electrode proximity and high resistance cleft (Spira and Hai, 2013). As BCC present a mixed cell population of cardiomyocytes and fibroblast-like cells (Supplementary Fig. 1A), as also previously reported (Ma et al., 2011); it is plausible that a non-conductive patch might adhere to the electrode area. In fact, fibroblast-like cells are found to be dedicated into BCC adhesion and spreading (Supplementary Fig. 2). This drawback is easily amendable, since it is possible to remove gently and re-plate BCCs in sterile conditions.

Each measurement lasted between 4 and 5 h, without any remarkable alteration of cardiac activity, if not due to drug stimulation. This can be also seen in the absence of morphological alteration between beginning and end of protocol (Supplementary Fig. 3). Although probed in not completely sterile conditions, it was found that if refilled with antibiotics-containing medium, at the end of the experiments, the samples can keep on without visible contamination up to 4 days. This is particularly useful when testing overnight or realizing several-day treatments. Such evidence shows, like previously reported, how the adopted BCC model presents an outstanding resilience. Since an applied force of 5 nN did not elicit any spontaneous change in the measured parameters, in time, one can infer that the implemented CBBs are really following alteration of cECC and not mechano-electric feedback from stretch-induced depolarization (Zhang et al., 2008).

An accurate peak detection and averaging period selection allowed the reconstruction of important physiological parameters described in Table 1, namely beating rate, contraction speed, cardiac cycle duration and, most importantly, a coupled parameter such as the electro-mechanical delay (EMD). To our best knowledge, this is the first time that such parameter is measured on 3D cardiac in vitro model. Fig. 2B shows the obtainable averaged electromechanical events, corrected by the calculated EMD.

### 3.2. Differential drug response and correlation analysis is indispensable to distinguish cell-type dependency of cardiac parameters

Once the feasibility and features of the implemented electromechanical CBBs were assessed, we firstly asked whether basal conditions would be sufficient to distinguish diseased and healthy hPSC derived BCC. The baseline beating frequency for all the cell lines tested was not significantly different (0.327 ± 0.023 Hz for CTRL, 0.325 ± 0.062 Hz for DORSO and 0.468 ± 0.103 Hz for DMD). The same evidence was found for other important functional parameters, such as the basal force (2.1 ± 1.9 nN for CTRL, 12.0 ± 4.7 nN for DORSO and 0.89 ± 0.46 nN for DMD) and EMD (23.0 ± 1.3 ms for CTRL, 22.0 ± 3.0 ms for DORSO and 25.6 ± 5.3 ms for DMD). Therefore, different stimulation / inhibition drug protocols were tested to validate the adopted models versus the expected cardiac response and assess the presence of cell type-dependent differences.

### 3.3. Calcium trials

Initially, the dependence of cardiac parameters on extracellular $Ca^{2+}$ concentration was tested. This ion and its extracellular availability are in fact of primary importance for cECC, particularly for the hPSC-derived CMs, which possess an immature calcium handling toolkit (Keung et al., 2014) and rely mostly on membrane transport (Youm, 2016). Cell type-dependency was found by 2-way ANOVA for beating rate ($p = 0.007$), contraction duration ($p = 0.0003$), time decay ($p < 0.0001$) and EMD ($p = 0.026$). A difference close to significance was reached for the average speed of contraction ($p = 0.069$). The effect of the $Ca^{2+}$ concentration was found significant only in relationship to the beating rate ($p < 0.0001$). All cell lines experienced a decrease in beating rate proportional to $Ca^{2+}$ concentration. The CTRL and DORSO groups plateaued around ¾ of the basal rate (67 ± 10% and 68.6 ± 5.1%, respectively), while the DMD group decreased to 89.5 ± 3.2% of its basal rate. The beating rate phenotype of mutation-carrying cell line correlates with previously described pre-existing calcium stress impairing inward ion flux (Fanchaouy et al., 2009). This frequency decrease was paralleled by an increase of exerted force in all the cell lines (120.3 ± 9.4% for the CTRL group, 110 ± 14% for DORSO and 112 ± 19% for DMD). This phenomenon is due to the immature contractile phenotype of hPSC-derived CMs, which possess negative frequency-force relationship (Pesl et al., 2016b). The observed change of contractile events was found as an increase of the relaxation period, expressed by the decay time constant for the CTRL and DORSO groups (108.1 ± 3.5% and 110.5 ± 4.2%, respectively) and a decrease for DMD (84.3 ± 5.2%). The $Ca^{2+}$ dependent decay time decrease in dystrophin mutation-carrying line is in correlation with previously described pre-existing calcium overload (Fanchaouy et al., 2009), which may limit the contraction dilation due to saturated sarcomere, probably resulting in limited ability of the DMD CBB to employ force imposed reaction during cluster stretch as imposed in healthy tissue by Frank Starling mechanisms. The EMD, a parameter directly connected to electromechanical coupling, did prove statistically significant for cell-type. CTRL did not show a dose-dependent relation with the $Ca^{2+}$ concentration (109–99% variation range); DORSO showed a similar trend with only non-significant increase with respect to CTRL (142–131%), validating the CBB's robustness toward line specific variability in differentiation efficiency. Conversely, the DMD group showed a dose-dependent trend (up to 257 ± 71% of the basal delay); it is possible that increasing calcium levels are gradually

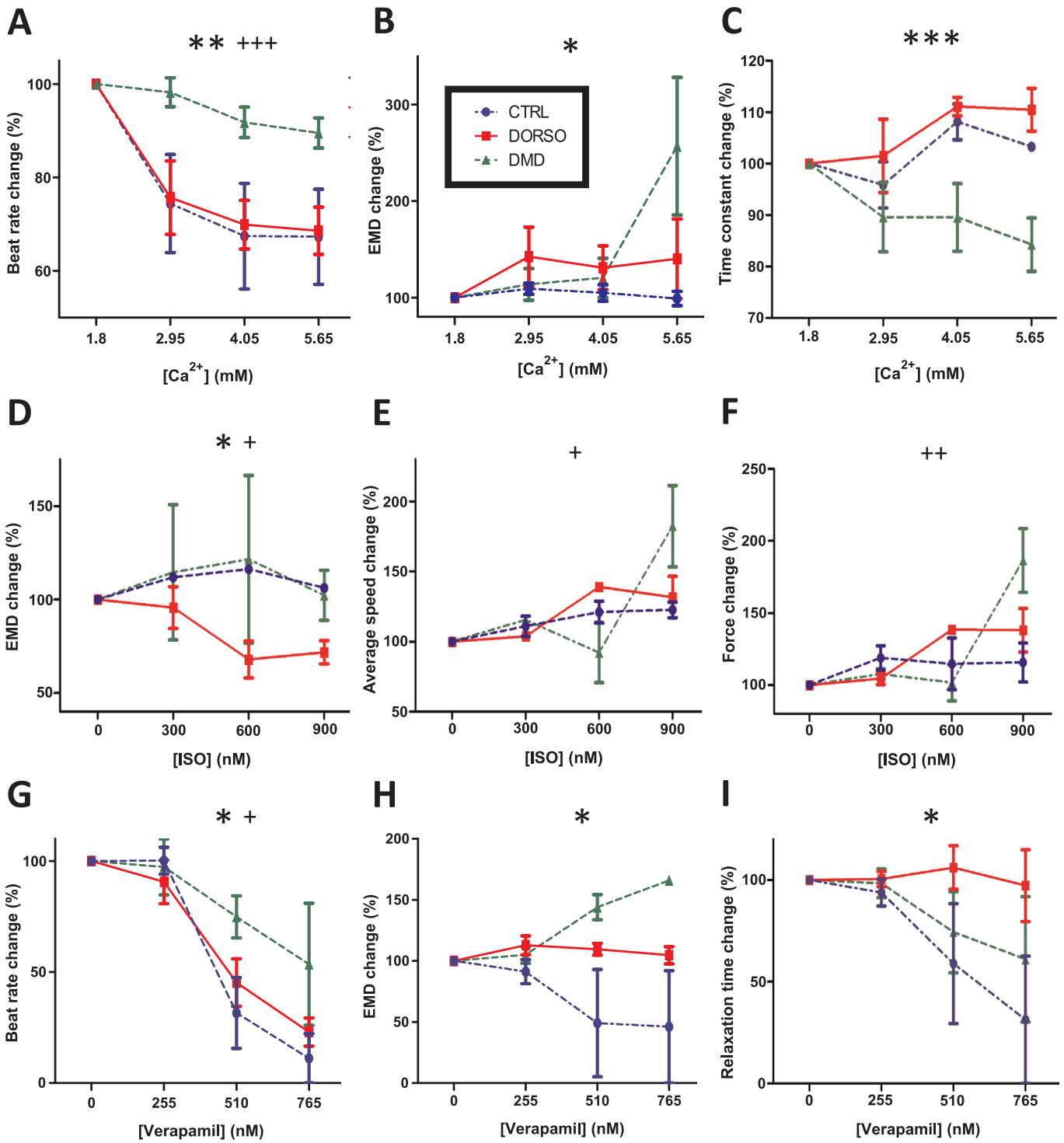



**Fig. 3.** Selected results of drug trials performed with the presented electrochemical cell-based biosensor. The top row (A-B-C) represents extracellular calcium concentration trials. The middle row (D-E-F) β-adrenergic stimulation trials (Isoproterenol). The bottom row (G-H-I) represent class IV antiarrhythmic / calcium channel blocker trial (Verapamil). The * symbol indicates statistically significant difference according to the beating cardiac cluster type. The + symbol indicates statistically significant difference due to the chemical concentration. One symbol indicates a $p$-value $< 0.05$, two symbols $< 0.01$, three symbols $< 0.001$. All the comparisons are carried on with repeated measurements 2-way ANOVA with row matching (drug concentration).

impairing the already elevated activity of an altered ryanodine receptor to coordinate the calcium-induced calcium release (Fauconier et al., 2010). The previous results are summarized in Fig. 3A-C.

### 3.4. Isoproterenol trials

The β-adrenergic stimulation was performed via increasing isoproterenol concentration to assess the ionotropic and chronotropic cell line-dependent features. Surprisingly, no extracted parameter showed significant dependency over the cell type, except for the EMD ($p = 0.0130$), which was also significantly concentration dependent ($p = 0.012$). Other concentration-dependent parameters were the average speed of contraction ($p = 0.031$) and the exerted force ($p = 0.006$), with DMD group showing marked increase at end

concentration (182 ± 29% and 186 ± 22% respectively). In contrast, DORSO experienced roughly 1/3 increase of these parameters (132 ± 15% for average speed and 138 ± 15% for force) and CTRL only 1/5 increase (122.7 ± 5.5% and 116 ± 14% respectively). Isoproterenol effect appears to have a threshold concentration between 300 and 600 nM. After this threshold, the CTRL and DMD groups slightly altered EMD (101.0 ± 6.0% and 96.6 ± 2.7%, respectively), whereas the DORSO group decreased its measured EMD to 73.0 ± 7.6% of the baseline value. This difference might be explained with better differentiation grade of dorsomorphin-treated groups, since dorsomorphin is an inhibitor of BMP signaling and promotes cardiac differentiation (Kattman et al., 2011). It is therefore plausible that an improved differentiation guarantees a better BCC syncytium, able to improve cECC timing in response to adrenergic stimulation. The notable results are shown in Fig. 3D-F. The same negative beating rate/force relationship was also noticed for all the cell lines, except when an arrhythmic behavior (e.g. multiple beating modes) was induced.

### 3.5. Verapamil trials

The antagonist trials were carried on L-type calcium channels to observe the reaction of different BCCs to class IV antiarrhythmics. Verapamil, as an example of this class, was shown to improve skeletal muscle force in DMD patients but led also to adverse cardiac side effect. However, no data on mechanism of such adverse effect exists (Nascimento Osorio et al., 2018). Previously, the growing CMs were coupled to RTCA impedance system, which allowed to quantify only beat rate effects of Verapamil (Wang et al., 2013). Here, the beat rate influence of drug showed to be cell type-dependent ($p = 0.019$) and dose dependent ($p = 0.001$). The EMD parameter was found to be only cell-type dependent ($p = 0.0316$), together with the relaxation time ($p = 0.030$). The measured exerted force and Z height change were found solely dose-dependent ($p = 0.015$ and $p = 0.019$ respectively). The DMD cells showed decrease in beating rate down to 53 ± 27% of baseline, compared to 11 ± 11% of CTRL and 23.0 ± 6.3% of DORSO groups. The EMD shows different trends for each cell line: for the CTRL groups, the delay drops to 46 ± 46% of the baseline; DORSO group upped to 112% of the baseline and ended the trial at 104.0 ± 7.1%; the DMD group showed an increase of 143% to finish the trial at 111 ± 55%. These distinct trends can be due to the different biological backgrounds of the BCC models: CTRL group may respond to L-type channel inhibition by referring to the inositol-3-phosphate complex, which spontaneously produces calcium influx in embryonic cardiac phenotype (Youm, 2016); dorsomorphin-treated BCC might express higher number of functional L-type calcium channels, therefore being more resilient to the same drug concentration and present delayed coupling, with stable force level. DMD samples can present calcium leaking at the membrane level (Burr and Molkentin, 2015), although cECC delay is linearly increasing, which together with the decreasing force suggests impairment of the contractile machinery (Li et al., 2014). The mentioned notable results are shown in Fig. 3G-I.

## 4. Conclusions

We have successfully implemented and tested the electro-mechanical cell-based biosensor for the simultaneous and synchronous probing of cardiac excitation-contraction coupling. The system allows the characterization of cardiac models through differential drug trials and sample-type discrimination. For the first time, to our knowledge, a distinctive beating-force relation was shown for Duchenne muscular dystrophy cardiac models. The bioelectromechanical parameters derived from the cardiomyocyte cluster based models provide important insights into heart pathologies and sometimes (such as in β-adrenergic stimulation assays) serve as the only discriminant between different models.

Current limitations of the systems regard the non-sterility of the measurement environment, and the localized probing of a 3D model with a single MEA electrode and AFM cantilever. The system also suffers from a substantial biological sample variability, which requires more experimental repetitions to achieve better accuracy of results; this can be overcome by suitable choice of drug treatment regimens to focus the data collection toward the desired disease phenotype. Future improvement with higher-density electrode arrays and tip-less cantilevers providing a wider surface contact should provide a higher information content and improve stability of models, respectively.

## Acknowledgments

This research has been financially supported by the Ministry of Education, Youth and Sports of the Czech Republic under the project CEITEC 2020 (LQ1601) and ICRC (LQ1605), the CIISB research infrastructure project LM2015043 supported the AFM measurements at the Core Facility Nanobiotechnology, and the Grant Agency of the Czech Republic (GACR) provided support through grant no. P302/12/G157.

## Conflict of interest

The authors declare no conflict of interest.

## Appendix A. Supporting information

Supplementary data associated with this article can be found in the online version at doi:10.1016/j.bios.2018.10.021.

## References

Acimovic, I., Vilotic, A., Pesl, M., Lacampagne, A., Dvorak, P., Rotrekl, V., Meli, A.C., 2014. Biomed. Res. Int. 2014, 512831.
Adewumi, O., Aflatoonian, B., Ahrlund-Richter, L., Amit, M., Andrews, P.W., Beighton, G., Bello, P.A., Benvenisty, N., Berry, L.S., et al., 2007. International stem cell initiative. Nat. Biotechnol. 25, 803–816.
Alonso, L., Goldmann, W.H., 2003. Life Sci. 72, 2553–2560.
Bauwens, C.L., Toms, D., Ungrin, M., 2016. J. Vis. Exp. 115, e54308.
Bers, D.M., 2002. Cardiac excitation–contraction coupling. Nature 415, 198–205.
Burr, A.R., Molkentin, J.D., 2015. Cell Death Differ. 22, 1402–1412.
Burridge, P.W., Matsa, E., Shukla, P., Lin, Z.C., Churko, J.M., Ebert, A.D., Lan, F., Diecke, S., Huber, B., Mordwinkin, N.M., Plews, J.R., Abilez, O.J., Cui, B., Gold, J.D., Wu, J.C., 2014. Nat. Methods 11, 855–860.
Butt, H.-J., Jaschke, M., 1995. Nanotechnology 6, 1–7.
Caluori, G., Pribyl, J., Cmiel, V., Pesl, M., Potocnak, T., Provaznik, I., Skladal, P., Rotrekl, V., 2018. Simultaneous study of mechanobiology and calcium dynamics on hESC-derived cardiomyocytes clusters. J. Mol. Recognit. e2760.
Cogollo, J.F.S., Tedesco, M., Martinoia, S., Raiteri, R., 2011. Biomed. Microdevice 13, 613–621.
Dell'Era, P., Benzoni, P., Crescini, E., Valle, M., Xia, E., Consiglio, A., Memo, M., 2015. World J. Stem Cells 7, 329–342.
Doevendans, P.A., Kubalak, S.W., An, R.-H., Becker, D.K., Chien, K.R., Kass, R.S., 2000. J. Mol. Cell. Cardiol. 32, 839–851.
Doppler, S.A., Deutsch, M.A., Lange, R., Krane, M., 2013. J. Thorac. Dis. 5, 683–697.
Fanchaouy, M., Polakova, E., Jung, C., Ogrodnik, J., Shirokova, N., Niggli, E., 2009. Cell Calcium 46, 114–121.
Finsterer, J., Stöllberger, C., 2003. Cardiology 99, 1–19.
Hao, J., Daleo, M.A., Murphy, C.K., Yu, P.B., Ho, J.N., Hu, J., Peterson, R.T., Hatzopoulos, A.K., Hong, C.C., 2008. PLOS One 3, e2904.
Kattman, S.J., Witty, A.D., Gagliardi, M., Dubois, N.C., Niapour, M., Hotta, A., Ellis, J., Keller, G., 2011. Cell Stem Cell 18, 228–240.
Keung, W., Boheler, K.R., Li, R.A., 2014. Stem Cell Res. Ther. 5, 17.
Kilpatrick, J.I., Revenko, I., Rodriguez, B.J., 2015. Adv. Healthc. Mater. 4, 2456–2474.
Knoll, R., Hoshijima, M., Hoffman, H.M., Person, V., Lorenzen-Schmidt, I., Bang, M.L., Hayashi, T., Shiga, N., Yasukawa, H., Schaper, W., McKenna, W., Yokoyama, M., Schork, N.J., Omens, J.H., McCulloch, A.D., Kimura, A., Gregorio, C.C., Poller, W., Schultheiss, P., Chien, K.R., 2002. Cell 111, 943–955.
Laurila, E., Ahola, A., Hyttinen, J., Aalto-Setälä, K., 2015. Biochim Biophys. Acta 1863-7B, 1864–1872.
Lian, X., Zhang, J., Azarin, S.M., Zhu, K., Hazeltine, L.B., Bao, X., Hsiao, C., Kamp, T.J., Palecek, S.P., 2012. Nat. Protoc. 8, 162–175.
Li, Y., Zhang, S., Zhang, X., Li, J., Ai, X., Zhang, L., Yu, D., Yu, D., Ge, S., Peng, Y., Chen, X., 2014. Cardiovasc. Res. 103, 60–71.
Liang, P., Lan, F., Lee, A.S., Gong, T., Sanchez-Freire, V., Wang, Y., Diecke, S., Sallam, K., Knowles, J.W., Wang, P.J., Nguyen, P.K., Bers, D.M., Robbins, R.C., Wu, J.C., 2013. Circulation 127, 1677–1691.
Liu, J., Sun, N., Bruce, M.A., Wu, J.C., Butte, M.J., 2012a. PLoS One 7, e37559.

Liu, Y., Feng, J., Shi, L., Niu, R., Sun, Q., Liu, H., Li, J., Guo, J., Zhu, J., Han, D., 2012b. Nanoscale 4, 99–102.
Ma, J., Guo, L., Fiene, S.J., Anson, B.D., Thomson, J.A., Kamp, T.J., Kolaja, K.L., Swanson, B.J., January, C.T., 2011. Am. J. Physiol. Hear. Circ. Physiol 301, H2006–H2017. https://doi.org/10.1152/ajpheart.00694.2011.
Moretti, A., Laugwitz, K.L., Dorn, T., Sinnecker, D., Mummery, C., 2013. Cold Spring Harb. Perspect. Med. 3.
Motta, B.M., Pramstaller, P.P., Hicks, A.A., Rossini, A., 2017. Stem Cells Int. 2017, 8960236.
Mummery, C.L., Zhang, J., Ng, E.S., Elliott, D.A., Elefanty, A.G., Kamp, T.J., 2012. Circ. Res. 111, 344–358.
Nascimento Osorio, A., Medina Cantillo, J., Camacho Salas, A., Madruga Garrido, M., Vilchez Padill, J.J., 2018. Neurologia. https://doi.org/10.1016/j.nrleng.2018.01.001. (In press).
Pesl, M., Acimovic, I., Pribyl, J., Hezova, R., Vilotic, A., Fauconnier, J., Vrbsky, J., Kruzliak, P., Skladal, P., Kara, T., Rotrekl, V., Lacampagne, A., Dvorak, P., Meli, A.C., Fauconnier, J., Vrbsky, J., Kruzliak, P., Skladal, P., Kara, T., Rotrekl, V., Lacampagne, A., Dvorak, P., Meli, A.C., 2013. Heart Vessels 29, 834–846.
Pesl, M., Ivana, A., Pribyl, J., Hezova, R., Vilotic, A., Aimond, F., Fauconnier, J., Vrbsky, J., Kruzliak, P., Skladal, P., Kara, T., Rotrekl, V., Lacampagne, A., Dvorak, P., Meli, A.C., 2014. Biophys. J. 106 (565A–565A).
Pesl, M., Pribyl, J., Acimovic, I., Vilotic, A.A., Jelinkova, S., Salykin, A., Lacampagne, A., Dvorak, P., Meli, A.C., Skladal, P., Rotrekl, V., 2016a. Biosens. Bioelectron. 85, 751–757.
Pesl, M., Pribyl, J., Caluori, G., Cmiel, V., Acimovic, I., Jelinkova, S., Dvorak, P., Starek, Z., Skladal, P., Rotrekl, V., 2016b. J. Mol. Recognit. 30, e2602.
Regmi, S., Jeong, J.H., 2016. Macromol. Res. 24, 1037–1046.
Rothermel, A., Kurz, R., Ruffer, M., Weigel, W., Jahnke, H.G., Sedello, A.K., Stepan, H., Faber, R., Schulze-Forster, K., Robitzki, A.A., 2005. Cell. Physiol. Biochem. 16, 51–58.
Sinnecker, D., Laugwitz, K.-L.L., Moretti, A., 2014. Pharmacol. Ther. 143, 246–252.
Spira, M.E., Hai, A., 2013. Nat. Nanotechnol. 8, 83–94.
Takeda, M., Miyagawa, S., Fukushima, S., Saito, A., Ito, E., Harada, A., Sawa, Y., 2018. Tissue Eng. C Meth. 24, 56–67.
Tzatzalos, E., Abilez, O.J., Shukla, P., Wu, J.C., 2016. Adv. Drug Deliv. Rev. 96, 234–244.
Vatta, M., Sinagra, G., Brunelli, L., Faulkner, G., 2005. J. Cardiovasc. Med. 10, 149–156.
Wang, T., Hu, N., Cao, J., Wu, J., Su, K., Wang, P., 2013. Biosens. Bioelectron. 49, 9–13.
Youm, J.B., 2016. Integr. Med. Res. 5, 3–10.
Zhang, Y., Sekar, R.B., McCulloch, A.D., Tung, L., 2008. Prog. Biophys. Mol. Biol. 97, 367–382.
Zheng, W., Thorne, N., McKew, J.C., 2013. Drug Discov. Today 18, 1067–1073.

Check for updates

Received: 19 January 2018 | Revised: 11 June 2018 | Accepted: 7 July 2018

DOI: 10.1002/jmr.2760

SPECIAL ISSUE ARTICLE

WILEY Journal of Molecular Recognition

# Simultaneous study of mechanobiology and calcium dynamics on hESC-derived cardiomyocytes clusters

Guido Caluori[1,2] | Jan Pribyl[2] | Vratislav Cmiel[3] | Martin Pesl[1,4] | Tomas Potocnak[3] | Ivo Provaznik[3] | Petr Skladal[2] | Vladimir Rotrekl[4]

[1] International Clinical Research Centre of Saint Anne Hospital of Brno (FNUSA-ICRC), Interventional Cardiac Electrophysiology Group, Brno, Czech Republic

[2] Nanobiotechnology Group, Central European Institute of Technology of Masaryk University (CEITEC-MU), Brno, Czech Republic

[3] Department of Biomedical Engineering, Brno University of Technology, Faculty of Electrical Engineering and Communication, Brno, Czech Republic

[4] Department of Biology, Masaryk University, Faculty of Medicine, Brno, Czech Republic

**Correspondence**
Jan Pribyl, Central European Institute of Technology of Masaryk University (CEITEC-MU), Nanobiotechnology Group, Kamenice 5, 62500 Brno, Czech Republic.
Email: jan.pribyl@ceitec.muni.cz

**Funding information**
CIISB research infrastructure, Grant/Award Number: LM2015043; Ministry of Education, Youth and Sports of the Czech Republic, Grant/Award Number: CEITEC 2020 (LQ1601); Czech Science Foundation, Grant/Award Number: GA18-24089S

## Abstract

Calcium ions act like ubiquitous second messengers in a wide amount of cellular processes. In cardiac myocytes, $Ca^{2+}$ handling regulates the mechanical contraction necessary to the heart pump function. The field of intracellular and intercellular $Ca^{2+}$ handling, employing in vitro models of cardiomyocytes, has become a cornerstone to understand the role and adaptation of calcium signalling in healthy and diseased hearts. Comprehensive in vitro systems and cell-based biosensors are powerful tools to enrich and speed up cardiac phenotypic and drug response evaluation.

We have implemented a combined setup to measure contractility and calcium waves in human embryonic stem cells-derived cardiomyocyte 3D clusters, obtained from embryoid body differentiation. A combination of atomic force microscopy to monitor cardiac contractility, and sensitive fast scientific complementary metal-oxide-semiconductor camera for epifluorescence video recording, provided correlated signals in real time. To speed up the integrated data processing, we tested several post-processing algorithms, to improve the automatic detection of relevant functional parameters. The validation of our proposed method was assessed by caffeine stimulation (10mM) and detection/characterization of the induced cardiac response.

We successfully report the first simultaneous recording of cardiac contractility and calcium waves on the described cardiac 3D models. The drug stimulation confirmed the automatic detection capabilities of the used algorithms, measuring expected physiological response, such as elongation of contraction time and $Ca^{2+}$ cytosolic persistence, increased calcium basal fluorescence, and transient peaks. These results contribute to the implementation of novel, integrated, high-information, and reliable experimental systems for cardiac models and drug evaluation.

**KEYWORDS**

atomic force microscopy, biosignals filtering, caffeine, calcium imaging, cardiac differentiation, embryoid bodies, fluorescence microscopy, human stem cell-derived cardiomyocytes

**List of Abbreviations:** AFM, atomic force microscopy; AM, acethoxymethylester; BCC, beating cardiac clusters; CM, cardiomyocytes; EB, embryoid body; ECC, excitation-contraction coupling; EEMD, ensemble empirical mode decomposition; FIR, finite impulse response; hESC, human embryonic stem cells; MCG, mechanocardiogram; PW, peak width; ROI, region of interest; RT/FT, rising time/falling time; RyR, ryanodine receptor; sCMOS, scientific complementary metal-oxide-semiconductor; SNR, signal-to-noise ratio; SR, sarcoplasmic reticulum

Guido Caluori, Jan Pribyl, and Vratislav Cmiel contributed equally to this work.

This article is published in Journal of Molecular Recognition as part of the virtual Special Issue 'AFM BioMed Krakow 2017, edited by Malgorzata Lekka, IFJ PAN, and Pierre Parot, CEA, France, and Jean-Luc Pellequer, IBS, France'.

 © 2018 John Wiley & Sons, Ltd. 

## 1 | INTRODUCTION

The heart muscle provides the necessary pressure to the blood stream to circulate the necessary nutrients, oxygen, and metabolites around the organism. This function is achieved by rhythmic contraction of the cardiac muscle cells, of cardiomyocytes (CMs),[1] through a phenomenon typical of the muscular phenotype called excitation-contraction coupling (ECC).[2] The ECC is a complex and adaptive set of subcellular processes, retained in in vitro cultures of dissociated CMs, both at the single cell level and at the tissue level.[3] The process is triggered by induced/spontaneous cellular depolarization up to the threshold to elicit an action potential, which are subsequently converted into mechanical contraction by the mediation of intracellular $Ca^{2+}$ ions. An appropriate $Ca^{2+}$ handling is of paramount importance for cardiac functionality. Systolic $Ca^{2+}$ cycling has mainly two sources: inward ionic currents flowing through voltage-dependent transmembrane calcium channels (mostly L-type)[4] and a specialized subcellular compartment known as the sarcoplasmic reticulum (SR).[5]

$Ca^{2+}$ release from the SR occurs mostly through a specialized channel known as the ryanodine receptor (RyR), specifically, in cardiac muscle, the RyR2 isoform.[6] Following an action potential, $Ca^{2+}$ ions stored in the SR are massively released, initially triggered by $Ca^{2+}$ inward current, which stimulates the collective opening of grouped RyRs in a process known as calcium-induced calcium release.[7] While contraction occurs, at the membrane level, $Ca^{2+}$ is promptly pumped out by the $Na^{+}/Ca^{2+}$ exchanger or segregated into subsarcolemmal mitochondria by the same mechanism. The high $Ca^{2+}$ concentration inside the SR is re-established by the sarco-endoplasmic reticulum calcium ATPase, which transports calcium ions from the cytosol inside the lumen of the SR. The extremely sophisticated organelles and receptors and buffers for the uptake and release of $Ca^{2+}$ goes generally under the name of calcium-signalling toolkit.[8]

In vitro models of cultured cardiac myocytes offer many advantages for developmental, pathophysiological, and pharmacological studies of cardiac tissue through cell-based biosensors, as they allow direct cell manipulation and control of environmental parameters, without interference from the compensatory feedback mechanisms that exist in vivo.[9] Monolayer cultures of primary neonatal rat ventricular CMs represent a frequently employed model to study cardiac processes,[10] as the isolated CMs retain contractility and reassociate in functional syncytium in vitro.[11] Adult rodent CMs are preferred for single cell study as they present mature morphology (eg, Z-disk structures or ion channels expression) and functional features.[12] Nevertheless, new realistic models are being researched with the use of cellular multilayers[13] or human stem cells-derived CMs.[14] These are able to generate functional cardiac muscle cells that recapitulate existing physiopathological conditions and can be derived in a 2D monolayer form or in a 3D structure from the formation of embryoid bodies (EBs).[15-17] The 3D models derived from EBs have proven to produce beating foetal-like CMs,[18] which control the differentiated cluster contractility and electrophysiology.[19] Recently, these models have also been proved to recapitulated patient-specific disease conditions.[20] For more details on otherwise obtained 3D cardiac constructs, the reader is referred to the dedicated literature.[21] Overall, in vitro cardiac models have allowed to obtain precise physiological insights, such as the difference between atrial and ventricular populations in calcium handling.[22] Furthermore, they have revealed key aspects and consequences of calcium signalling remodelling when cardiac pathologies occur. For example, usually minor calcium toolkits, such as inositol triphosphate (InsP3)/$Ca^{2+}$ signalling can be hyperstimulated by the presence of cardiac hormones due to atrial arrhythmias.[23] Dystrophic mutations (such as Duchenne's muscular dystrophy) severely hamper the $Ca^{2+}$ current inactivation and the SR uptake, leading to $Ca^{2+}$ overload.[24] Genetic mutations can involve specific intracellular receptors, such as in RyR2-specific catecholaminergic polymorphic ventricular tachycardia, which causes leaky SR inducing sudden cardiac death during exercise.[25] It has been demonstrated that induced persistent $Ca^{2+}$ overload, due to prolongation of action potentials, directly induces CMs death through a mitochondria-mediated necrotic pathway.[26] Eventually, reduced $Ca^{2+}$ transients, prolonged duration and impaired uptake lead to abnormal cardiac output, muscular remodelling, and heart failure.[27] Dynamics of $Ca^{2+}$ are becoming an elective drug target to avoid tissue remodelling followed by development of congestive heart failure, ischemia or arrhythmias.[28,29]

$Ca^{2+}$ dynamics are visualized by imaging techniques that require calcium-specific fluorescent probes or fluorophores. These are a class of natural or artificial light-excitables/emitting (bio)molecules able to detect specific chemical species.[30,31] Fluo-4 acethoxymethylester (AM), used in this study, is a high yield nonratiometric (ie, not able to determine concentration) fluoresceine-based dye conjugated with the 1,2-bis (*o*-aminophenoxy)ethane-*N*,*N*,*N*′,*N*′-tetraacetic acid, a calcium-specific chelating agent, linked to AM groups. It is briefly recalled that AM-neutralizing group allows cytosolic irreversible internalization via lipophilic affinity and de-esterification within the cell membrane.[32]

The use of high-performance dyes goes in parallel with the design of high-speed sensitive cameras. Microscopy embedded video imaging[33] and the use of electron multiplying charge coupled device and scientific complementary metal-oxide-semiconductor (sCMOS) cameras[34,35] have been key innovative steps for calcium imaging. The high signal strength of the fluorescent probes in combination with these emerging technologies allowed for real-time fluorescence observations of biological processes at the single-cell level.

As previously mentioned, $Ca^{2+}$ dynamics is directly responsible for the proper function of the contractile machinery and therefore the exerted force by CMs. Cardiac contractility and mechanics in vitro can be assessed by several methodologies (eg, force-transducing elements, optical tweezers, video analysis of particle tracking, and impedance spectroscopy),[15] among which the most sensitive is atomic force microscopy (AFM). Atomic force microscopy-based nanoindentation has been applied for almost 30 years to the investigation of cellular mechanics.[36] Atomic force microscopy can also serve as nanosensitive tool to measure time-resolved cell height change, contractility rate, and transverse exterted force or single CM[37,38] and 3D organoids through mechanocardiograms (MCGs).[39] An important technological integration among experimental systems is the one between optical microscopy (or later confocal microscopy) and AFM. The integration of optical microscopy and confocal microscopy within life sciences has proved particularly beneficial, because it unlocked the ability to simultaneously apply and measure local mechanical forces, while tracking biological responses/pathways with fluorescent dyes,

10991352, 2019, 2, Downloaded from https://onlinelibrary.wiley.com/doi/10.1002/jmr.2760 by National Technical Library, Wiley Online Library on [17/03/2024]. See the Terms and Conditions (https://onlinelibrary.wiley.com/terms-and-conditions) on Wiley Online Library for rules of use; OA articles are governed by the applicable Creative Commons License

antibodies, or genetic incorporation of fluorescent fusion proteins such as green fluorescent protein. Common optical microscopy techniques like bright-field illumination, phase contrast, and especially differential interference contrast, reveal high-contrast topography information, as well as location and/or distribution of internal structural features (eg, cell organelles).[40-42] Fluorescence microscopy has proven to be a powerful tool for selective and specific visualization of labelled molecules down to the single-molecule level, rendering it possible to follow cellular processes and to monitor the dynamics of living cell components.[43] The advantages and benefits of AFM and fluorescence microscopy complement each other, allowing a more detailed characterization of cellular structures and processes.[44,45] A prime example of this is the visualization of calcium dynamics during cardiomyocyte contractions; AFM is used as an ultrasensitive force detector or is measuring the mechanical pulsations of living cells, with cantilever probe touching at a constant force the cell.[42] Employing simultaneous fluorescence-AFM, these local mechanical pulsations can be linked directly to intracellular calcium oscillations.[46] Simoultaneous calcium imaging and AFM contractility recording has been successfully tested for drug response on single CM,[47] but to our best knowledge, no such method has been implemented for 3D cardiac models.

Therefore, we defined an integrated experimental setup that would allow to harness the detecting capabilities of the two techniques simultaneously. In this work, we employed size-controlled EBs, differentiated in beating cardiac clusters (BCCs) from human embryonic stem cells (hESC),[48] as our cell-based biosensors model for detection of cardioactive chemicals. We have expanded our previously established mechanical methods[39] with calcium imaging, to provide combined information of two biophysical aspects of cardiac function. As integrated measures lead to a proportional increase of information, an automatic functional parameter extraction is desirable. The choice of the best automatic analysis algorithm was bound to its versatility in processing different signals and most importantly to performance. Specifically, we looked for increase of the signal-to-noise ratio (SNR) absence of morphological alterations on the baseline and reduction of imposed signal delay for future synchronization. Therefore, we explored different data handling algorithms to put the base of a robust method for automatic analysis.

## 2 | METHODS

### 2.1 | Preparation of hESC-derived CM clusters

In this work, the cardiac models were obtained using the hESC line[43,44] CCTL14. Cells were firstly thawed and seeded on mitotically inactivated mouse embryonic fibroblasts.[49] hESC colonies were cultivated in DMEM-F12 (Thermofisher, Waltham, MA-USA), supplemented with 15% knockout serum replacement (fetal bovine serum (FBS), Life Technologies, Carlsbad, CA-USA), 1% L-glutamine (Thermofisher), 0.5% penicillin/streptomycin (Thermofisher), 1% 2-mercaptoethanol (Thermofisher), 1% nonessential amino acids (Life Technologies), and 4 ng/mL human fibroblast growth factor 2 (hFGF2, Peptrotech, London, UK). Colonies were propagated for at least five passages, by scratching and fractioning using 1-mL pipette tip. To prepare monolayer cultures, colonies were passaged and transferred to 1:100 Matrigel (Corning, Tewksbury, MA-USA) coated dishes. Monolayer cultures were carried on in Modified Eagle's Medium (MEF)-conditioned medium supplemented with 10 ng/mL hFGF2. Upon reaching 80% confluence, hESC were passaged using TrypLE Express dissociating agent (Thermofisher). Cells underwent at least two feeder-free passages. Regular and size-controlled EBs were obtained by forced aggregation of $2 \times 10^6$ cells/millilitres. Aggregation wells were prepared in 1.5% *w/v* agarose gel (VWR, Radnor, PA-USA),[50] and each EB contained approximately 1000 cells. Cardiac differentiation was achieved using our previously described method,[48,51] by sequential cytokine modulation in KnockOut DMEM (Life Technologies), supplemented with 10% FBS, 1% L-Glutamine, 1% penicillin/streptomycin, 1% β-mercapthoethanol, 1% nonessential amino acids, and 10 $\mu g/mL^{-1}$ ascorbic acid. Beating cardiac clusters were visible from day 11, and after day 20, they were counted and divided from nonbeating clusters. Typical dimensions of the measured BCCs ranged between 300 and 400 μm in diameter. By visual observation, BCCs contain both contracting cells and fibroblast-like ones, the latter involved in adhesion to the substrate.

### 2.2 | Clusters seeding and measurement setup

Differentiated BCCs were selected according to spheroidal regular shape and seeded onto 0.1% gelatine-coated (Sigma Aldrich, St. Louis, MO-USA) 34-mm Petri dishes (TPP Technoplastic Products, Trasadingen, Switzerland) and let adhere for 24 hours. Beating cardiac clusters were maintained at 37°C in a standard 5% $CO_2$ incubator. Prior to experiments, the samples were exposed for 60 minutes to a 3μM concentration of Fluo-4 AM (Life Technologies) in culture medium and incubating atmosphere. After loading, the sample were gently rinsed twice with KnockOut DMEM to remove excess of calcium dye, replenished with culture medium, and let in incubator for further 30 minutes to allow fluorophore de-esterification. Ultimately, the medium was removed and replaced by Tyrode solution (135mM NaCl, 10mM HEPES, 5.4mM KCl, 0.9mM $MgCl_2$, 10mM glucose, and 1.8mM $CaCl_2$, pH 7.4). For drug testing, a caffeine (Sigma) solution of 10mM concentration in complete Tyrode was used. All other chemicals when not specified were purchased from Sigma.

The prepared sample dish was equipped with media exchange tubes and placed on the motorized stage of an inverted microscope (Olympus IX-81S1F-3, Tokyo, Japan). An AFM scanner of 15 μm vertical range (BioAFM NanoWizard 3, JPK, Berlin, Germany) was then placed above the sample. A soft semicoated silicon cantilever Hydra2R (AppNano) was used as mechanical probe to ensure a stable contact without applying disruptive forces on the sample. A Petri dish heater (JPK) was used to keep the temperature constant at 37°C. The upper optical path of the optical microscope was used to record fluorescence image sequences with an sCMOS camera Andor Zyla 5.5 (Andor Technology, Belfast, Northern Ireland). A Thorlabs MD498 dichroic mirror was used for light wavelength selection. A Thorlabs FES650 shortpass type optical filter (650 nm) was inserted to the optical path

10991352, 2019, 2, Downloaded from https://onlinelibrary.wiley.com/doi/10.1002/jmr.2760 by National Technical Library, Wiley Online Library on [17/03/2024]. See the Terms and Conditions (https://onlinelibrary.wiley.com/terms-and-conditions) on Wiley Online Library for rules of use; OA articles are governed by the applicable Creative Commons License

before the camera detector to cut off the interference of the AFM laser light.

## 2.3 | Data recording

Beating cardiac cluster contraction and calcium transient signals were obtained simultaneously but in an asynchronous way. Scanning probe microscope Control Software v.5 (JPK) was used for AFM control and data acquisition at 1 kHz rate. The cantilever was placed in contact with the sample using a set point of 5 nN, with feedback loop parameter $I$ = 50 and $P$ = 0.05. This level of force was previously found to be the smallest force necessary to ensure stable contact and showed no visible functional alteration of clusters' contractility rate of exerted force.[39] The location was selected by consecutive trials to find the region with best vertical displacement. The observable MCG showed the temporal displacement on the AFM vertical piezoelectric crystal following the beating of the BCC, to maintain constant force with the sample. Calcium imaging video sequences were recorded at 200× using Andor Solis 64-bit control and acquisition software. The camera was connected via USB 3.0 to the computer station, while a high throughput solid-state drive disc was included to enable fast and long enough video acquisition by increasing the acquisition capacity. Camera resolution was set to 1700 × 1700 px and framerate to 49.67 fps. Data were obtained using spooling mode in form of data fractions and converted to AVI files.

The time points of data acquisition protocol are shown in Figure 1 C. Mechanocardiogram signals were acquired for 10-minute intervals while only 60 seconds of image sequence was recorded from the start point of MCG, due to the memory-consuming data size.

## 2.4 | Data extraction and filtration

Atomic force microscopy data and fluorescence image sequences were processed using Matlab 2015b and its image processing toolbox. Figure 2 shows a schematization of the mixed signal acquisition and post-processing. Contraction signals were extracted as text files while $Ca^{2+}$ traces were obtained from images stacks by selection of appropriate region of interest (ROI). Absolute fluorescence was retrieved as sum of the ROI pixel values ($F_{ROI}$) and corrected using a background fluorescence ROI ($F_{back}$) from each image in the sequence, using the formula

$$\Delta F = \frac{F_{ROI} - F_{back}}{F_{back}}.$$

Raw signals were then filtered and analysed. Linear min-max normalization was performed to allow comparison between filtration and drug stimulation trials. However, to distinguish the change in amplitude of the control and test signal, the relative ratio was recorded prior to normalization. Both MCG were corrected for baseline drift, filtered through different digital algorithms to provide the best noise reduction and parameter detection. The applied filters were

1. finite impulse response low-pass filter, with 5 Hz cut-off frequency;
2. median filter of fixed-length moving window (11 samples for MCG, five for $Ca^{2+}$ transients); and
3. ensemble empirical mode decomposition (EEMD) filter. This method works by analysing the signal to find its main components

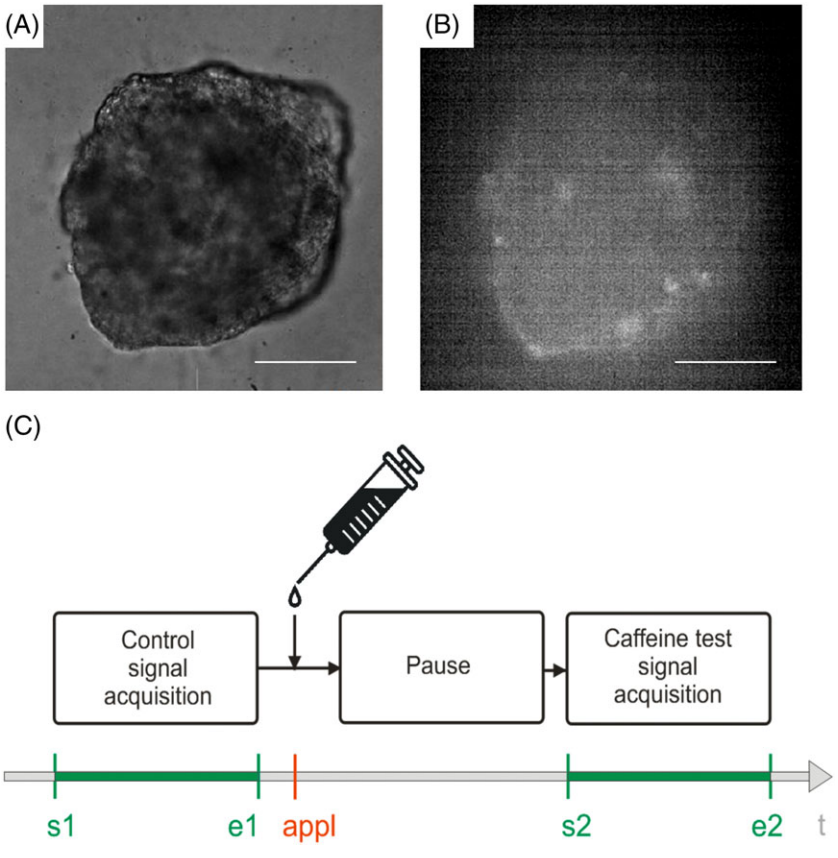



**FIGURE 1** Microscopy images of the cardiac EB loaded with Flou-4 under the combined setup (magnification 20× and scale bar 100 μm). A, Brightfield image of the adhered EB. B, Epifluorescence view, with visible AFM laser artefact on bottom left corner. Biological fluorescence is still visible on the edges. C, Experimental method for caffeine stimulation, all time point distances indicate 10 minutes. E1-S2 restine time of 10 minutes was necessary for appropriate chemical diffusion in the sample

10991352, 2019, 2, Downloaded from https://onlinelibrary.wiley.com/doi/10.1002/jmr.2760 by National Technical Library, Wiley Online Library on [17/03/2024]. See the Terms and Conditions (https://onlinelibrary.wiley.com/terms-and-conditions) on Wiley Online Library for rules of use; OA articles are governed by the applicable Creative Commons License

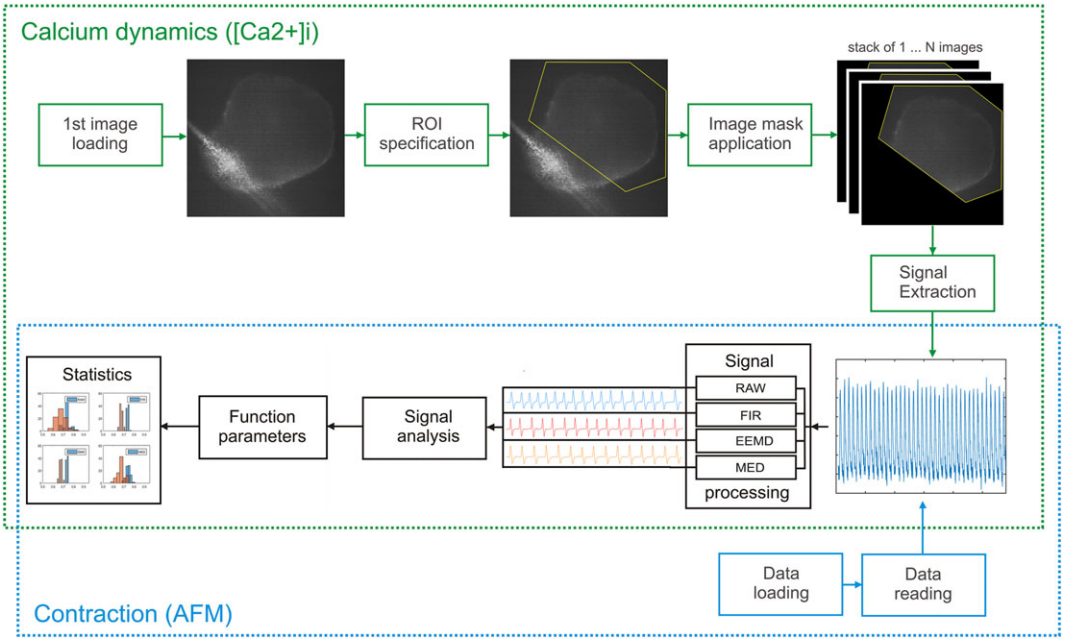



**FIGURE 2** Schematic representation of data manipulation, from extraction to integration, conditioning and parameter extraction

(intrinsic mode functions [IMF]) and remove them selectively in a process called sifting.[52] Two and three IMFs were excluded for $Ca^{2+}$ traces and MCG, respectively, after which the signals were recomposed. The EEMD algorithm was set up to maximum 10 sifting process per IMF with 200 ensembles cycles.

After filtration, signal peaks were detected and parameters of interest (Figure 4, bottom row) were extracted and compared in at least 30 events per sample. For the raw and filtered data sets, the noise reduction was quantified calculating the SNR with the formula

$$\mathrm{SNR} = 20\log_{10}{}^{A_{pp}}/_{4}\sigma,$$

where $A_{pp}$ is the maximum amplitude of the single contraction or transient event, and σ is the standard deviation of the random noise detected on the baseline. Increase of noise standard deviation was considered a sign of undesired morphological artefacts.

## 3 | RESULTS

Repeated recordings were performed after setup optimization over three different clusters. Figure 1A,B show a representative BCC after calcium dye loading. The samples were able to withstand measurement environment for more than 1 hour. The native average beating rate calculated from MCG spanned between 0.74 and 2.35 Hz. The interference coming from the AFM laser module was attenuated on the common path for video acquisition but could not be eliminated. Nevertheless, simultaneous recording was achieved, when AFM backscattering was kept at the edge of the BCC. Figure 3 shows MCG and $Ca^{2+}$ traces recorded from the same sample, before normalization.

### 3.1 | Evaluation of different filtration methods

A correction of MCG drift is achieved by the direct linear interpolation method between two adjacent peaks. $Ca^{2+}$ signal is not affected by baseline drift when corrected appropriately for background intensity. Due to low number of samples, a 1:3 oversampling was performed to

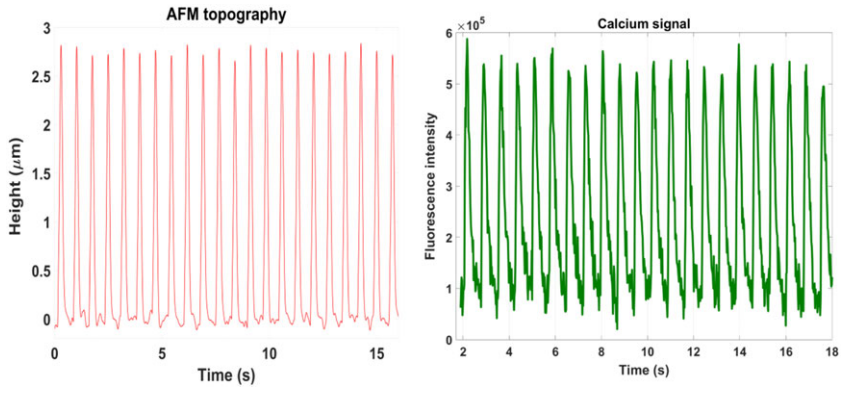



**FIGURE 3** Typical traces of mechanocardiogram (MCG, left) and calcium transients (right) coming from the same recording

10991352, 2019, 2, Downloaded from https://onlinelibrary.wiley.com/doi/10.1002/jmr.2760 by National Technical Library, Wiley Online Library on [17/03/2024]. See the Terms and Conditions (https://onlinelibrary.wiley.com/terms-and-conditions) on Wiley Online Library for rules of use; OA articles are governed by the applicable Creative Commons License

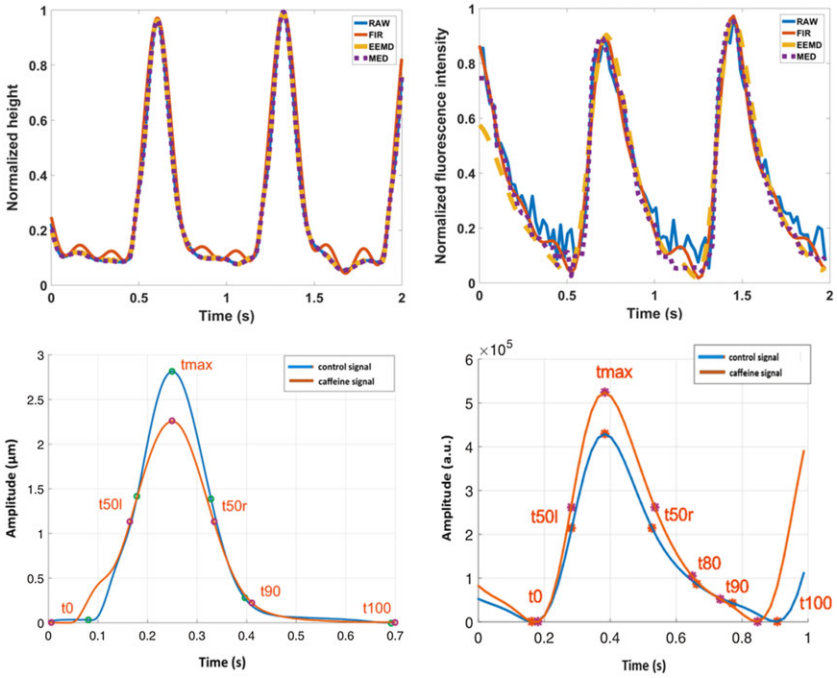



**FIGURE 4** Filtration results and drug effect on the signals traces. MCG traces before and after filtration, where corrugation of the FIR filter is visible (top left). Calcium transients before and after oversampling (1:3) and filtering, where the best effect for EEMD method can be observed (top right). Averaged (n = 39) contraction events detected in MCG before and after caffeine stimulation, where one can see the mean event elongation and the lowering of the peak probably due to contraction pattern changes (bottom left). Averaged (n = 32) calcium cycling events before and after caffeine stimulation, where one can observe the elongating peak width (t50l-t50r), due to persistence of calcium in cytosol, and the increase of peak amplitude most probably due to increased calcium storage depletion (bottom right)

increase filtration working points. Original SNRs of the two signals were 19.73 and 14.11 dB for MCG and calcium transients, respectively.

Finite impulse response filtering increased the SNR to 20.49 and 20.97 dB for MCG and calcium transients, respectively. Overfiltering of MCG produced corrugation artefacts that impaired proper extraction of time-related parameters. For instance, the mean contractile event duration increased up to 15.67% due to filtration-induced error in the automatic detection algorithm. Calcium traces on the contrary were partially smoothed, inducing a mean event time contraction of 4.59%.

Ensemble empirical mode decomposition filtering respected the signal shape with stochastic shifts of peaks on calcium traces, with respect to the raw signals. Signal-to-noise ratio did not improve for MCG (19.71 dB), but it increased for $Ca^{2+}$ transients (21.80 dB). No corrugation of morphological artefact was found using this filtering method. Mean event duration remained stable for MCG (0.08%) and saw a 6.82% elongation of the $Ca^{2+}$ ones.

Median filtering window width was empirically optimized for each separate signal. Signal-to-noise ratio again did not raise for MCG traces (19.73 dB) but saw mild improvement for calcium transients (16.81 dB). Mean duration of the events was slightly elongated in both cases, at 1.98% for calcium transients and 0.56% for contractility. Representative performance of the different filtering methods is summarized in Figure 4, top row. Because of the general best performance of EEMD filtering method, we will show only the results following this filtration method (Table 1). The results of signal filtration efficiency are included in Table 2.

### 3.2 | Evaluation of caffeine effect on calcium and contraction signals

To validate the robustness of our recording system automatic detection approach, we conducted caffeine stimulation on BCCs. The expected cardiac response was seen in contraction signal, as reduction of peak amplitude (24.7%) and increasing peak width (14.5%), as

**TABLE 1** Parameter identification and description

| Parameter | Meaning |
|---|---|
| $t_X$ | Time with x indication percentage of the event total time |
| $t_{max}$ | Time to maximum |
| $T_{50l}/T_{50R}$ | Time to half of maximum in rising/falling |
| PW | Peak width (T50R-T50l) |
| RT/FT | Rising/falling time |

combination of elongation in rising time (25.2%) and falling time (5.1%). Event frequency increased 8.3%. Similar trend was observed in $Ca^{2+}$ signals in frequency increase (8.43%), with corresponding faster rising time (−3.7%) and longer falling time (13.4%). Basal fluorescence increased 3.9 times and peak width rose up of 5.5%. While the MCG traces did not benefit largely from the filtration in terms of SNR (from 20.73 to 20.70 dB), EEMD filtration doubled $Ca^{2+}$ signals SNR (7.35 dB to 14.61 dB), aiding significantly the reliability of the detection. These results are summarized in Tables 2 and 3.

## 4 | DISCUSSION

A trustworthy and rapid investigation of in vitro cardiac cellular models is of fundamental importance to validate new drugs and investigate cardiac pathologies at the level of basic science. So far, in vitro models of CMs are examined through multiple alternative techniques (increasing sample variability) or powerful techniques affected by low throughput (eg, patch clam electrophysiology). $Ca^{2+}$ imaging is a powerful technique that brings precious insights in the adaptation of ECC at the single cell and tissue level.[53] Atomic force microscopy can, due to its versatility, integrate the information of chemical signaling with information on the cell/tissue mechanics, leading to better inference when an abnormal effect is observed.[54] For this reason, we have implemented a combined optical and scanning probe microscopic

10991352, 2019, 2, Downloaded from https://onlinelibrary.wiley.com/doi/10.1002/jmr.2760 by National Technical Library, Wiley Online Library on [17/03/2024]. See the Terms and Conditions (https://onlinelibrary.wiley.com/terms-and-conditions) on Wiley Online Library for rules of use; OA articles are governed by the applicable Creative Commons License

**TABLE 2** Representative effect of different filtration methods on SNR ($N_{events}$ > 30)

| | Contraction Signal (AFM) | | | | Calcium Transients (Optical Measurement) | | | |
|---|---|---|---|---|---|---|---|---|
| SNR, dB | Raw | FIR | EEMD | Median | Raw | FIR | EEMD | Median |
| Control signal | 19.73 | 20.49 | 19.71 | 19.73 | 14.10 | 20.97 | 21.80 | 16.81 |
| Caffeine signal | 20.73 | 21.82 | 20.70 | 20.73 | 7.35 | 14.22 | 14.61 | 11.62 |

Abbreviations: AFM, atomic force microscopy; EEMD, ensemble empirical mode decomposition; FIR, finite impulse response; SNR: signal-to-noise ratio.

**TABLE 3** Representative effect of caffeine stimulation over observed parameters ($N_{events}$ > 30)

| Parameter | Contraction Signal (MCG, % Change) | Calcium Transients (% Change) |
|---|---|---|
| Beating rate | 8.83 | 8.42 |
| Peak amplitude | −24.70 | 20.85 |
| Rising time | 25.20 | −3.70 |
| Falling time | 5.20 | −13.40 |
| Peak width | 14.50 | 5.50 |

Abbreviations: MCG, mechanocardiogram.

setup, tested it on a defined 3D cardiac model, and validated it with a known cardiac drug response. To increase the throughput of the experimental method, we have also tested different data conditioning methods to improve the accuracy of automatic detection of important parameters.

We successfully recorded for the first time, to the best knowledge of the authors, simultaneous $Ca^{2+}$ cycling and contractility of intact BCC. We experienced how hardware technological integration of the two techniques is not a trivial point. Because the sCMOS camera shares the optical path with the AFM infrared laser, the nonreflected portion of the laser beam was often sufficient to disturb epifluorescence emission detection. The interposition of a near infrared filter on the camera optical path greatly attenuated the unwanted artefact, but it could not eliminate it completely. This problem was related to the high sensitivity of the employed camera and the nature of the technique. Similar artefacts were not visible with CCD cameras or confocal microscopy, albeit these two alternatives present different disadvantages: the former one comports the loss of the sensitivity necessary to detect events at high resolution, while the latter is technologically expensive and less flexible. Therefore, great attention on light filtration must be taken into consideration for different AFM producers.

After data extraction, we explored different filtration methods and quantified them in terms of SNR increase and undesired signal alteration. Due to the asynchronous recording, filtration-induced delays were not quantified. The aim behind filtering is to improve the automatic detection of points of interest in noisy signal, when diverse sources of electronic noise are present from distinctive systems. The noise affecting the $Ca^{2+}$ transients comes primarily from the processes associated with image acquisition by sensor array and camera electronics. This electronic and thermal detector noise is typically of high frequency nature with respect to the biological signals of interest. Nevertheless, due to the relatively low acquisition rate, oversampling is recommendable to ensure reliable performance of subsequent filtration. In the contraction signals obtained by AFM, a source of the signal noise comes from uncompensated environmental vibrations, but baseline drift, due to the soft sample creeping or temperature-induced bimetallic effect on the probe, are preeminent disturbances and need to be compensated. Due to the low frequency of drifts, a simple peak-between-peak linear interpolating algorithm is enough correct for this noise source.

In general, all three filtering methods led to beneficial increase of the SNR for the $Ca^{2+}$ signals, in basal condition and in caffeine-stimulated ones. The MCGs present higher SNR due to the AFM detecting method (optical lever amplification) and low noise electronics, which allows force sensing at the nanoscale. In this case, FIR filtering can lead to over-filtration artefacts. Median filtering was the worst performing option in terms of improvement of SNR, although signal parameter alterations were in the order of units of percent. Ensemble empirical mode decomposition filtering met the SNR improvement performance with the low signal alteration; therefore, it became the filtering elective choice for both signals. This algorithm is very adaptive, low-demand, and effective for high-frequency white noise elimination, while at the same time preserving the original signal character. Our selection does not exclude the possibility to employ other harmonic-based methods, like Fourier transform, although EEMD works without the assumption of stationary signals. Averaging filters could also provide an alternative method for functional parameters calculation, provided that the events alignment jitter induced by the noise is neglectable.

To test the detection of biological drug response, we employed caffeine stimulation. Caffeine is a well-known agonist of the RyR2 receptor of cardiac SR, as it induces calcium release in the cytoplasm.[55] This effect can be appreciated by the augmented basal fluorescence, reflecting the presence of more unbound $Ca^{2+}$ in the cytosol.[56] The increase peak amplitude and elongated width of $Ca^{2+}$ transients can also be explained with the stimulated and prolonged depletion of the SR storage. The observed reduction of SNR in caffeine-stimulated conditions can be due to chaotic activation of local calcium sparks.[57] Rise in beating rate can be explained with the depolarized state induced by cytosolic unbound calcium,[58] a condition initiated by caffeine and probably maintained by neighbouring coupled fibroblasts.[59] Consequently to the beating rate increase, $Ca^{2+}$ transients rising time decreased, probably due to the augmented activation of L-type voltage-gated channels.[60] Falling time decreased as well, most probably from enhanced activity of the $Na^{+}/Ca^{2+}$ exchange mechanism,[61] deputed to restore low calcium cytosolic levels.[62] The change of peak amplitude at the MCG level can be attributed to the immature contractile machinery of hESC-derived CMs,[15] and to different activation pattern of the 3D cardiac cluster. Local monitoring of the BCC contraction using a pyramidal tip cantilever, like the one employed in this study, faced the influence of changing contractile patterns in heterogeneous sample. For future study, a colloidal probe with appropriate diameter (over 20 μm), or a tipless cantilever, might suffer less from this phenomenon.

10991352, 2019, 2, Downloaded from https://onlinelibrary.wiley.com/doi/10.1002/jmr.2760 by National Technical Library, Wiley Online Library on [17/03/2024]. See the Terms and Conditions (https://onlinelibrary.wiley.com/terms-and-conditions) on Wiley Online Library for rules of use; OA articles are governed by the applicable Creative Commons License

## 5 | CONCLUSIONS

In the presented work, we have proven the feasibility of the combination of AFM mechanical probing and epifluorescence recording of chemical events in 3D cardiac in vitro models. We have also proposed a best data handling and filtration method to speed up reliable and robust automatic analysis of data. This will hopefully contribute to the implementation of new and reliable integrated experimental systems, with high-information content, for cardiac in vitro models and cardiac drugs evaluation.


## FUNDING INFORMATION

CIISB research infrastructure project LM2015043 funded by MEYS CR is gratefully acknowledged for the financial support of the measurements at the CF Nanobiotechnology. Work was supported by the projects no. LQ1601 (CEITEC 2020) and LQ1605 from the National Program of Sustainability II (MEYS CR) and by the project FNUSA-ICRC no. CZ.1.05/1.1.00/02.0123 (OP VaVpI). Czech Science Foundation GACR supported this work with grant number GA18-24089S.



## ORCID

*Guido Caluori* http://orcid.org/0000-0003-2725-8768


## REFERENCES


1. Nickerson, D. P. Cardiac electro-mechanics: from to the whole heart. 1994, (1994).
2. Bers DM. Cardiac excitation–contraction coupling. *Nature*. 2002; 415(6868):198-205.
3. Rapila R, Korhonen T, Tavi P. Excitation—contraction coupling of the mouse embryonic cardiomyocyte. *J Gen Physiol*. 2008;132(4):397-405.
4. Satin J, Itzhaki I, Rapoport S, et al. Calcium handling in human embryonic stem cell-derived cardiomyocytes. *Stem Cells*. 2008;26(8): 1961-1972.
5. Dibb KM, Trafford AW, Eisner DA. *Calcium Signaling in Cardiac Muscle. Handbook of Glycomics*. 2 Elsevier Inc.; 2010.
6. Liu Y. *Ryanodine Receptor Function in Intracellular Calcium Signaling*. ProQuest; 2008.
7. Fabiato A. Time and calcium dependence of activation and inactivation of calcium-induced release of calcium from the sarcoplasmic reticulum of a skinned canine cardiac Purkinje cell. *J Gen Physiol*. 1985;85(2):247-289.
8. Berridge MJ, Bootman MD, Roderick HL. Calcium signalling: dynamics, homeostasis and remodelling. *Nat Rev Mol Cell Biol*. 2003;4(7):517-529.
9. Bursac N, Papadaki M, Cohen RJ, et al. Cardiac muscle tissue engineering: toward an in vitro model for electrophysiological studies. *Am J Physiol*. 1999;277(2 Pt 2):H433-H444.
10. Martherus RS, Zeijlemaker VA, Ayoubi TAY. Electrical stimulation of primary neonatal rat ventricular cardiomyocytes using pacemakers. *Benchmarks*. 2010;48:65-67.
11. Eschenhagen T, Zimmermann WH. Engineering myocardial tissue. *Circ Res*. 2005;97(12):1220-1231.
12. Yang X, Pabon L, Murry CE. Engineering adolescence: maturation of human pluripotent stem cell-derived cardiomyocytes. *Circ Res*. 2014;114(3):511-523.
13. Sperelakis, N. *Developmental Changes in Membrane Electrical Properties of the Heart*. in 595–623 (Springer, Boston, MA, 1989). doi:https://doi.org/10.1007/978-1-4613-0873-7_29
14. Gepstein L. Derivation and potential applications of human embryonic stem cells. *Circ Res*. 2013;91:866-876.
15. Pesl M, Pribyl J, Caluori G, et al. Phenotypic assays for analyses of pluripotent stem cell-derived cardiomyocytes. *J. Mol. Recognit*. 2016; 30(6):e2602. https://doi.org/10.1002/jmr.2602
16. Davis RP, Casini S, van den Berg CW, et al. Cardiomyocytes derived from pluripotent stem cells recapitulate electrophysiological characteristics of an overlap syndrome of cardiac sodium channel disease. *Circulation*. 2012;125(25):3079-3091.
17. Acimovic I, Vilotic A, Pesl M, et al. Human pluripotent stem cell-derived cardiomyocytes as research and therapeutic tools. *Biomed Res Int*. 2014;2014(512831):1-14.
18. Jung KB, Son YS, Lee H, Jung CR, Kim J, Son MY. Transcriptome dynamics of human pluripotent stem cell-derived contracting cardiomyocytes using an embryoid body model with fetal bovine serum. *Mol Biosyst*. 2017;13(8):1565-1574.
19. Mummery CL, Zhang J, Ng ES, Elliott DA, Elefanty AG, Kamp TJ. Differentiation of human embryonic stem cells and induced pluripotent stem cells to cardiomyocytes: a methods overview. *Circ Res*. 2012; 111(3):344-358.
20. Spitalieri P, Talarico RV, Caioli S, et al. Modelling the pathogenesis of myotonic dystrophy type 1 cardiac phenotype through human iPSC-derived cardiomyocytes. *J Mol Cell Cardiol*. 2018;118:95-109.
21. Mathur A, Ma Z, Loskill P, Jeeawoody S, Healy KE. In vitro cardiac tissue models: current status and future prospects. *Adv Drug Deliv Rev*. 2016;96:203-213.
22. Bootman MD, Smyrnias I, Thul R, Coombes S, Roderick HL. Atrial cardiomyocyte calcium signalling. *Biochim Biophys Acta - Mol Cell Res*. 2011;1813(5):922-934.
23. Berridge MJ. Calcium signalling remodelling and disease. *Biochem Soc Trans*. 2012;40(2):297-309.
24. Koenig X, Rubi L, Obermair GJ, et al. Enhanced currents through L-type calcium channels in cardiomyocytes disturb the electrophysiology of the dystrophic heart. *Am J Physiol Heart Circ Physiol*. 2013;306: H564-H573.
25. Marks AR. Calcium cycling proteins and heart failure: mechanisms and therapeutics. *J Clin Invest*. 2013;123(1):46-52.
26. Nakayama H, Chen X, Baines CP, et al. Ca2+− and mitochondrial-dependent cardiomyocyte necrosis as a primary mediator of heart failure. *J Clin Invest*. 2007;117(9):2431-2444.
27. Gorski PA, Ceholski DK, Hajjar RJ. Altered myocardial calcium cycling and energetics in heart failure—a rational approach for disease treatment. *Cell Metab*. 2015;21(2):183-194.
28. Nattel S, Maguy A, Le Bouter S, Yeh Y-H. Arrhythmogenic ion-channel remodeling in the heart: heart failure, myocardial infarction, and atrial fibrillation. *Physiol Rev*. 2007;87(2):425-456.
29. Driessen HE, Bourgonje VJA, van Veen TAB, Vos MA. New antiarrhythmic targets to control intracellular calcium handling. *Neth Heart J*. 2014;22(5):198-213.
30. Molecular Probes. The Molecular Probes ® Handbook—Introduction to fluorescence techniques. (2010).
31. Bootman MD, Rietdorf K, Collins T, Walker S, Sanderson M. Ca2+-sensitive fluorescent dyes and intracellular Ca2+ imaging. *Cold Spring Harb Protoc*. 2013;2013(2):83-99.
32. Tsien RY. A non-disruptive technique for loading calcium buffers and indicators into cells. *Nature*. 1981;290(5806):527-528.
33. Swandulla D, Hans M, Zipser K, Augustine GJ. Role of residual calcium in synaptic depression and posttetanic potentiation: fast and slow calcium signaling in nerve terminals. *Neuron*. 1991;7(6):915-926.
34. Lasser-Ross N, Miyakawa H, Lev-Ram V, Young SR, Ross WN. High time resolution fluorescence imaging with a CCD camera. *J Neurosci Methods*. 1991;36(2-3):253-261.
35. Bigas M, Cabruja E, Forest J, Salvi J. Review of CMOS image sensors. *Microelectron J*. 2006;37(5):433-451.
36. Radmacher M. Studying the mechanics of cellular processes by atomic force microscopy. *Methods Cell Biol*. 2007;83:347-372.


10991352, 2019, 2, Downloaded from https://onlinelibrary.wiley.com/doi/10.1002/jmr.2760 by National Technical Library, Wiley Online Library on [17/03/2024]. See the Terms and Conditions (https://onlinelibrary.wiley.com/terms-and-conditions) on Wiley Online Library for rules of use; OA articles are governed by the applicable Creative Commons License

37. Domke J, Parak WJ, George M, Gaub HE, Radmacher M. Mapping the mechanical pulse of single cardiomyocytes with the atomic force microscope. *Eur Biophys J*. 1999;28(3):179-186.
38. Sun N, Yazawa M, Liu J, et al. Patient-specific induced pluripotent stem cells as a model for familial dilated cardiomyopathy. *Sci Transl Med*. 2012;4:130ra47-130ra47.
39. Pesl M, Pribyl J, Acimovic I, et al. Atomic force microscopy combined with human pluripotent stem cell derived cardiomyocytes for biomechanical sensing. *Biosens Bioelectron*. 2016;85:751-757.
40. Bank, W. Combined AFM and confocal fluorescence microscope for applications in bio-nanotechnology 217, 109–116 (2005).
41. Madl J, Rhode S, Stangl H, et al. A combined optical and atomic force microscope for live cell investigations. *Ultramicroscopy*. 2006; 106(8-9):645-651.
42. Pelling, A. E., Nicholls, B. M., Silberberg, Y. R. & Horton, M. A. Approaches for investigating mechanobiological dynamics in living cells with fluorescence and atomic force microscopies. 26–28 (2007).
43. Hinterdorfer P, Schütz G, Kienberger F, Schindler H. Detection and characterization of single biomolecules at surfaces. *Rev Mol Biotechnol*. 2001;82(1):25-35.
44. Hards A, Zhou C, Seitz M, Bräuchle C, Zumbusch A. Simultaneous AFM manipulation and fluorescence imaging of single DNA strands. *Chemphyschem Eur J Chem Phys Phys Chem*. 2005; 6(3):534-540.
45. Raiteri R, Caluori G, Tedesco M, Andrade Caicedo HH, Ward CW. A novel AFM-based technique for measuring coupled phenomena in cardiac myocytes. *Biophys J*. 2015;108:168a.
46. Haupt BJ, Pelling AE, Horton M a. Integrated confocal and scanning probe microscopy for biomedical research. *Sci World J*. 2006; 6:1609-1618.
47. Liu Y, Feng J, Shi L, et al. In situ mechanical analysis of cardiomyocytes at nano scales. *Nanoscale*. 2012;4(1):99-102.
48. Pesl M, Acimovic I, Pribyl J, et al. Forced aggregation and defined factors allow highly uniform-sized embryoid bodies and functional cardiomyocytes from human embryonic and induced pluripotent stem cells. *Heart Vessels*. 2013;29:834-846.
49. Dvorak P, Dvorakova D, Koskova S, et al. Expression and potential role of fibroblast growth factor 2 and its receptors in human embryonic stem cells. *Stem Cells*. 2005;23(8):1200-1211.
50. Dahlmann J, Kensah G, Kempf H, et al. The use of agarose microwells for scalable embryoid body formation and cardiac differentiation of human and murine pluripotent stem cells. *Biomaterials*. 2013; 34(10):2463-2471.
51. Krutá M, Šeneklová M, Raška J, et al. Mutation frequency dynamics in HPRT locus in culture adapted human embryonic stem cells and induced pluripotent stem cells correspond to their differentiated counterparts. *Stem Cells Dev*. 2014;23(20):2443-2454.
52. L, S. R., Shih, H. H., i-C, N. Y. & L, H. H. The empirical mode decomposition and the Hilbert spectrum for nonlinear and non-stationary time series analysis. (1998).
53. Herron TJ, Lee P, Jalife J. Optical imaging of voltage and calcium in cardiac cells & tissues. *Circ Res*. 2012;110(4):609-623.
54. Franz CM, Puech P-H. Atomic force microscopy: a versatile tool for studying cell morphology, Adhesion and Mechanics. *Cell Mol Bioeng*. 2008;1(4):289-300.
55. Kong H, Jones PP, Koop A, Zhang L, Duff HJ, Chen SRW. Caffeine induces Ca2+ release by reducing the threshold for luminal Ca2+ activation of the ryanodine receptor. *Biochem J*. 2008; 414(3):441-452.
56. O'Neill SC, Eisner DA. A mechanism for the effects of caffeine on Ca2+ release during diastole and systole in isolated rat ventricular myocytes. *J Physiol*. 1990;430(1):519-536.
57. Izu LT, Xie Y, Sato D, Bányász T, Chen-Izu Y. Ca2+ waves in the heart. *J Mol Cell Cardiol*. 2013;58:118-124.
58. Youm JB. Electrophysiological properties and calcium handling of embryonic stem cell-derived cardiomyocytes. *Integr Med Res*. 2016;5(1):3-10.
59. Vasquez C, Benamer N, Morley GE. The cardiac fibroblast: functional and electrophysiological considerations in healthy and diseased hearts. *J Cardiovasc Pharmacol*. 2011;57(4):380-388.
60. Leroy J, Lignon JM, Gannier F, Argibay JA, Malécot CO. Caffeine-induced immobilization of gating charges in isolated guinea-pig ventricular heart cells. *Br J Pharmacol*. 2002;135(3):721-734.
61. Rodriguez JS, Velez Rueda JO, Salas M, et al. Increased Na+/Ca2+ exchanger expression/activity constitutes a point of inflection in the progression to heart failure of hypertensive rats. *PLoS ONE*. 2014; 9(4):e96400.
62. Ottolia M, Torres N, Bridge JHB, Philipson KD, Goldhaber JI. Na/Ca exchange and contraction of the heart. *J Mol Cell Cardiol*. 2013; 61:28-33.

**How to cite this article:** Caluori G, Pribyl J, Cmiel V, et al. Simultaneous study of mechanobiology and calcium dynamics on hESC-derived cardiomyocytes clusters. *J Mol Recognit*. 2019;32:e2760. https://doi.org/10.1002/jmr.2760

10991352, 2019, 2, Downloaded from https://onlinelibrary.wiley.com/doi/10.1002/jmr.2760 by National Technical Library, Wiley Online Library on [17/03/2024]. See the Terms and Conditions (https://onlinelibrary.wiley.com/terms-and-conditions) on Wiley Online Library for rules of use; OA articles are governed by the applicable Creative Commons License

frontiers in Bioengineering and Biotechnology

ORIGINAL RESEARCH
published: 19 June 2020
doi: 10.3389/fbioe.2020.00535

# DMD Pluripotent Stem Cell Derived Cardiac Cells Recapitulate *in vitro* Human Cardiac Pathophysiology

*Sarka Jelinkova[1,2], Aleksandra Vilotic[1], Jan Pribyl[3], Franck Aimond[4], Anton Salykin[1], Ivana Acimovic[1], Martin Pesl[1,2,5], Guido Caluori[2,5], Simon Klimovic[6], Tomas Urban[1], Hana Dobrovolna[7], Vladimir Soska[7,8], Petr Skladal[5,6], Alain Lacampagne[4], Petr Dvorak[1,2], Albano C. Meli[1,4*†] and Vladimir Rotrekl[1,2*†]*

[1] Department of Biology, Faculty of Medicine, Masaryk University, Brno, Czechia, [2] International Clinical Research Center ICRC, St. Anne's University Hospital Brno, Brno, Czechia, [3] CEITEC, Masaryk University, Brno, Czechia, [4] PhyMedExp, University of Montpellier, INSERM, CNRS, Montpellier, France, [5] First Department of Internal Medicine—Cardioangiology, Faculty of Medicine, Masaryk University, Brno, Czechia, [6] Department of Biochemistry, Faculty of Science, Masaryk University, Brno, Czechia, [7] Department of Clinical Biochemistry, St. Anne's University Hospital of Brno, Brno, Czechia, [8] Second Clinic of Internal Medicine, Masaryk University of Brno, Brno, Czechia

Duchenne muscular dystrophy (DMD) is a severe genetic disorder characterized by the lack of functional dystrophin. DMD is associated with progressive dilated cardiomyopathy, eventually leading to heart failure as the main cause of death in DMD patients. Although several molecular mechanisms leading to the DMD cardiomyocyte (DMD-CM) death were described, mostly in mouse model, no suitable human CM model was until recently available together with proper clarification of the DMD-CM phenotype and delay in cardiac symptoms manifestation. We obtained several independent dystrophin-deficient human pluripotent stem cell (hPSC) lines from DMD patients and CRISPR/Cas9-generated DMD gene mutation. We differentiated DMD-hPSC into cardiac cells (CC) creating a human DMD-CC disease model. We observed that mutation-carrying cells were less prone to differentiate into CCs. DMD-CCs demonstrated an enhanced cell death rate in time. Furthermore, ion channel expression was altered in terms of potassium (Kir2.1 overexpression) and calcium handling (dihydropyridine receptor overexpression). DMD-CCs exhibited increased time of calcium transient rising compared to aged-matched control, suggesting mishandling of calcium release. We observed mechanical impairment (hypocontractility), bradycardia, increased heart rate variability, and blunted β-adrenergic response connected with remodeling of β-adrenergic receptors expression in DMD-CCs. Overall, these results indicated that our DMD-CC models are functionally affected by dystrophin-deficiency associated and recapitulate functional defects and cardiac wasting observed in the disease. It offers an accurate tool to study human cardiomyopathy progression and test therapies *in vitro*.

**Keywords: duchenne muscular dystrophy, DMD, human pluripotent stem cells, cardiomyocytes, intracellular calcium, excitation-contraction coupling, adrenergic response, cardiomyocyte death**

OPEN ACCESS

***Edited by:***
*Monica Boffito, Politecnico di Torino, Italy*

***Reviewed by:***
*Monica Mattioli-Belmonte, Marche Polytechnic University, Italy*
*Hannes Todt, Medical University of Vienna, Austria*

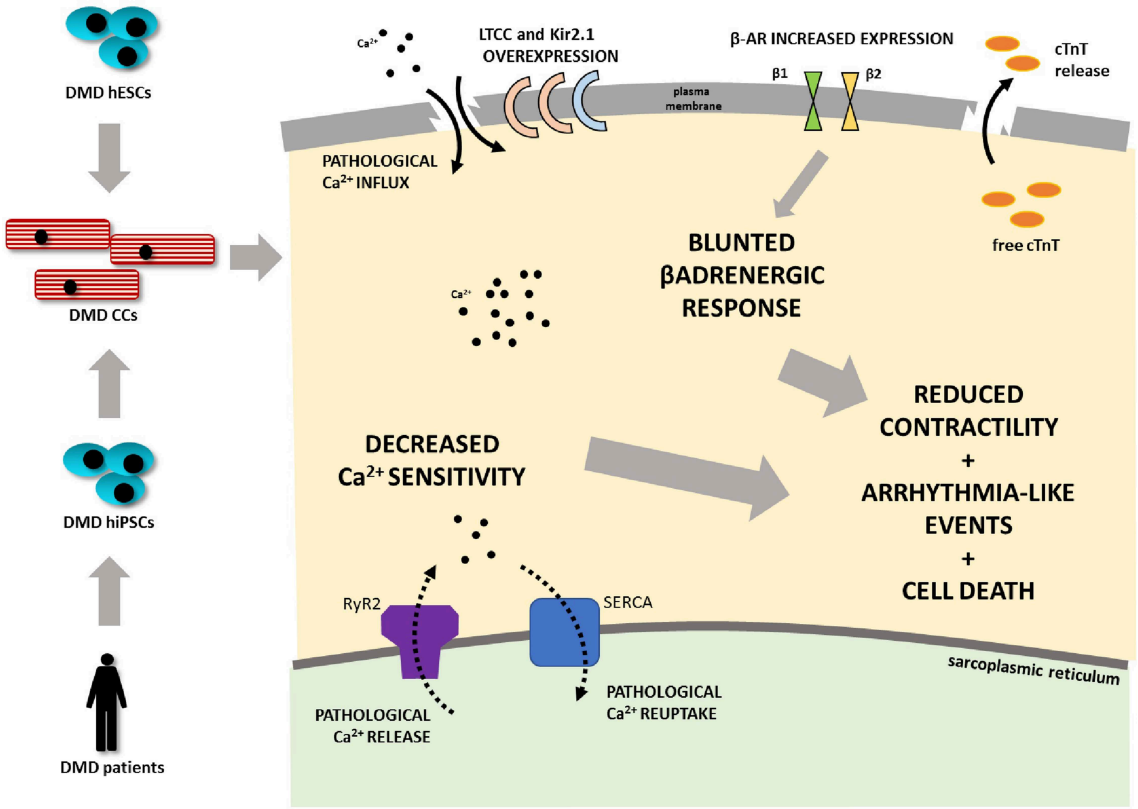
***Correspondence:**
*Albano C. Meli*
*albano.meli@inserm.fr*
*Vladimir Rotrekl*
*vrotrekl@med.muni.cz*

*†These authors have contributed equally to this work*

***Specialty section:***
*This article was submitted to Biomaterials, a section of the journal Frontiers in Bioengineering and Biotechnology*

***Received:*** *15 December 2019*
***Accepted:*** *04 May 2020*
***Published:*** *19 June 2020*

***Citation:***
*Jelinkova S, Vilotic A, Pribyl J, Aimond F, Salykin A, Acimovic I, Pesl M, Caluori G, Klimovic S, Urban T, Dobrovolna H, Soska V, Skladal P, Lacampagne A, Dvorak P, Meli AC and Rotrekl V (2020) DMD Pluripotent Stem Cell Derived Cardiac Cells Recapitulate in vitro Human Cardiac Pathophysiology. Front. Bioeng. Biotechnol. 8:535. doi: 10.3389/fbioe.2020.00535*




**GRAPHICAL ABSTRACT |** Duchenne muscular dystrophy (DMD) is associated with progressive dilated cardiomyopathy eventually leading to heart failure as the main cause of death in DMD patients. A human cardiomyocyte (CM) model was developed from several independent dystrophin-deficient human pluripotent stem cell (hPSC) lines from DMD patients and hESC line with deletion of DMD gene generated by CRISPR/Cas9 technology. DMD hPSC were differentiated into CMs. DMD mutation-carrying cells are less prone to differentiate into CMs. DMD CMs further demonstrate an enhanced cell death rate. Ion channel expression was altered in terms of potassium (Kir2.1 overexpression) and calcium handling (DHPR overexpression). DMD-CMs exhibited mishandling of calcium demonstrated by increased time of calcium release. Further mechanical impairment (hypocontractility), bradycardia, increased beat rate variability, and blunted β-adrenergic response connected with remodeling of β-adrenergic receptors' expression was found in DMD-CMs (LTCC L-type calcium channel, cTnT - cardiac troponin T, Kir2.1 - potassium channel).

**Abbreviations:** ACTC1, cardiac muscle alpha actin; AFM, atomic force microscopy; AP, action potential; APD, action potential duration; AR, adrenergic receptor; BMP4, bone morphogenic factor 4; CC, cardiac cell; cDMD, CRISPR/Cas9 generated DMD-hESC line; cl4, control hiPSC line; CM, cardiomyocyte; cTNT, cardiac troponin T; DAD, delayed after depolarization; DAPI, 4′,6-Diamidine-2′-phenylindole dihydrochloride; DCM, dilated cardiomyopathy; DHPR, dihydropyridine receptor; DMD, Duchenne muscular dystrophy; EB, embryonic body; ECC, excitation-contraction coupling; FGF2, fibroblast growth factor (basic, or 2); FKBP12. 6, calstabin 2; GJA1, connexin43; hESC, human embryonic stem cells; hiPSC, human induced pluripotent stem cells; hPSC, human pluripotent stem cells; IBI, inter-beat variability; ISO, isoproterenol; Kir2.1, Kir2.2, Kir2.3, potassium channels encoded by KCNJ2, KCNJ4, and KCNJ12 genes respectively; LTCC, L-type calcium channel; mdx; mdx:utr, muscular dystrophy on X chromosome, mouse model lacking dystrophin; utrophin and dystrophin lacking mouse model; mEF, mouse embryonic fibroblasts; METO, metoprolol; MYH6, myosin heavy chain α; MYH7, myosin heavy chain β; MYL2, myosin light chain 2; MYL7, myosin light chain 7; NKX2.5, NK homeobox 5; NOS, nitric oxide synthase, inducible (iNOS), neuronal (nNOS); qRT-PCR, quantitative real-time PCR; ROS, reactive oxygen species; RyR2, ryanodine receptor 2; SAC, stretch activated channels; SERCA (ATP2A), Sarcoplasmic/endoplasmic reticulum calcium ATPase 1; SR, sarcoplasmic reticulum; VEGF, vascular endothelial growth factor; WT, wild type control.

## INTRODUCTION

Duchenne muscular dystrophy (DMD, prevalence 1/3,500–6,000 boys) is an X-linked genetic disorder which impairs striated muscles and results in severe disability and premature death in young men (Mah et al., 2014; Vry et al., 2016; Stehlíková et al., 2017). DMD is often associated with dilated cardiomyopathy (Manzur et al., 2008), which develops in affected patients during their teenage years. It is represented by a slowly progressing decline in diastolic function, systolic ejection fraction, and fractional shortening (Markham et al., 2006). Mechanical degeneration is associated with progressive cardiomyocyte (CM) wasting and spreading of fibrosis throughout the ventricular wall (Finsterer and Stöllberger, 2003; Panovský et al., 2019), which leads to intracardiac conduction disturbances, inducing atrial and life-threatening ventricular arrhythmias (Chenard et al., 1993; Himmrich et al., 2000). Gradual dilatation of the ventricle, thinning of the wall (Wagner et al., 2007), and consequent loss of contractility lead to repeated episodes of heart failure, which

recently became the most frequent mortality cause in DMD patients worldwide (Finsterer and Stöllberger, 2003; Fayssoil et al., 2010).

DMD is caused by mutations in the dystrophin gene (*DMD*), which can result in a total lack of functional dystrophin or presence of a truncated inactive form of the protein (Blake et al., 2002). Dystrophin plays a major role in the organization of dystrophin glycoprotein complex (Clarac et al., 2009) responsible for sarcolemmal adhesion to the basal lamina and intracellular pathway regulations. Whereas, skeletal muscle degeneration is extensively studied, the cellular mechanisms of the cardiac pathophysiology are still unclear. Available studies point out the role of oxidative stress and DMD-induced $Ca^{2+}$ mismanagement (Williams and Allen, 2007; Jung et al., 2008; Caluori et al., 2019), with subsequent cytosolic imbalance and cell damage (Gerke et al., 2005).

In DMD (muscular dystrophy on X chromosome, *mdx)* mice, we have shown that dystrophin deficiency caused post-translational remodeling of the cardiac ryanodine receptor (RyR2) macromolecular complex, due to S-nitrosylation and Calstabin2 (FKBP12.6) depletion, which leads to intracellular diastolic $Ca^{2+}$ leak and ventricular arrhythmias (Fauconnier et al., 2010).

Intracellular $Ca^{2+}$ leak from the sarcoplasmic reticulum (SR) was also associated with deregulation of stretch-activated channels (SAC) though reactive oxygen species (ROS)-mediated hyperactivity (Jung et al., 2008).

Further studies in animal models showed misregulation of other ion channels such as voltage-gated Nav1.5 and L-type calcium channel (LTCC) hyperactivation (Koenig et al., 2011), as well as upregulation of inflammation-related induced nitric oxide synthase (iNOS) (Fauconnier et al., 2010; Peterson et al., 2018). Such observations remain to be validated in human DMD. Furthermore, to this day, there are only limited studies of human DMD cardiac cell (CC) models, describing some of the discrepancies eventually leading to DMD-CM damage (Eisen et al., 2019; Pioner et al., 2020). In the present study, we thus focused, for the first time, on evaluating the impact of dystrophin-deficiency on some molecular properties of the excitation-contraction coupling (ECC) and flight-or-fight response in some patient-specific DMD human pluripotent stem cell-derived cardiac cells (DMD-hPSC-CCs) as well as in CRISPR/Cas9 engineered hPSC-CCs (summarized in **Graphical abstract**).

## MATERIALS AND METHODS

A wide selection of methods was used for analysis of the model starting from generation of the hPSC lines to analysis of 3D contracting clusters and dissociated CCs; thus, the methodological approach has been summarized in **Figure 1**.

### Cell Lines, Cultivation, Reprogramming, and hPSC Differentiation Into Cardiomyocytes via Embryoid Bodies

Patient-specific DMD human induced pluripotent stem cell (hiPSC) lines (DMD02 and DMD03) and CRISPR/Cas9 dystrophin-deficient human embryonic stem cell (hESC) line (cDMD) were used (described in Jelinkova et al., 2019a,b). The fibroblasts of two DMD patients were derived from skin/muscle (for DMD02/DMD03, respectively) biopsies. Informed consents approved by Ethics Committee (Faculty of Medicine, Masaryk University) were signed by parents of the patients beforehand and the investigation conformed to the principles outlined in the Declaration of Helsinki.

Control human embryonic stem cell (hESC) line CCTL14 (serving as isogenic control for cDMD) as well as CCTL12 hESC line (further referred to as WT hESC) derived in Masaryk University, Brno, and previously characterized (International Stem Cell Initiative et al., 2007), were used. hiPSC control line UEFhfiPS1.4 (Qu et al., 2013) and cl.4 obtained from Majlinda Lako (NewCastle, UK) (further called WT-hiPSC) were used for comparison with DMD-hiPSC to reduce the effect of reprogramming on the CC phenotype.

All human pluripotent stem cell (hPSC) lines were routinely maintained on feeder layer of mitotically inactivated mouse embryonic fibroblasts (mEF) as previously described (Dvorak et al., 2005; Krutá et al., 2014; Jelinkova et al., 2019a).

Cardiac differentiation and eventual subsequent dissociation of hPSC-CCs were performed for confocal fluorescent intracellular $Ca^{2+}$ measurements, patch-clamp, atomic force microscopy (AFM), and immunocytochemistry as previously described (Pesl et al., 2014) with minor modifications. Briefly, grown colonies were cut into pieces with a pipette tip and clumps were transferred into differentiating embryonic body (EB) medium (86% KnockOut Dulbecco modified eagle medium, 10% fetal bovine serum, 1% L-glutamine, 1% penicillin/streptomycin, 1% nonessential amino acids, 0,1mM 2-mercaptoethanol) with 10 ng/ml bone morphogenic protein 4 (BMP4, R&D) and 10 μg/ml ascorbic acid (Sigma Aldrich) where they formed EBs. After 2 days, the medium was changed into EB medium with 5 ng/ml basic fibroblast growth factor (FGF2, Peprotech), 10 ng/ml BMP4, 6 ng/ml Activin A (R&D) and 10 μg/ml ascorbic acid (Sigma Aldrich) and incubated for 4 days. The next 3 days consisted of EB medium supplemented with 10 ng/ml vascular endothelial growth factor (VEGF, R&D), 10 μM IWR1 (Sigma Aldrich), and 10 μg/ml ascorbic acid. The EBs were further cultivated in EB medium with 10 μg/ml ascorbic acid, 10 ng/ml VEGF, and 5 ng/ml FGF2 for 12 days with medium changed every 4 days, and then with EB medium with 10 μg/ml ascorbic acid until further analysis. The differentiation procedure was performed for 13 days in hypoxic conditions (5% oxygen). Then, the EBs were moved into normoxic conditions (20% oxygen) for further cultivation.

### Immunodetection

Immunocytological analyses utilized [antibody specific against N-terminal (1:50 ICC/1:50-1:300 WB, Cat# NCL-DYSB, Leica Biosystems), and antibody specific against C-terminal (1:100 ICC/1:1000 WB, Abcam, Cat# ab15277)], for cardiac markers cardiac troponin T (cTnT; SantaCruz, Cat# sc-8121, 1:200) α-actinin (SigmaAldrich, Cat# A7180, 1:500) L-type channel (LTCC, dihydropyridine receptor DHPR alpha 2 subunit/CACNA2D1 antibody abcam, Cat# ab2864, 1:200),

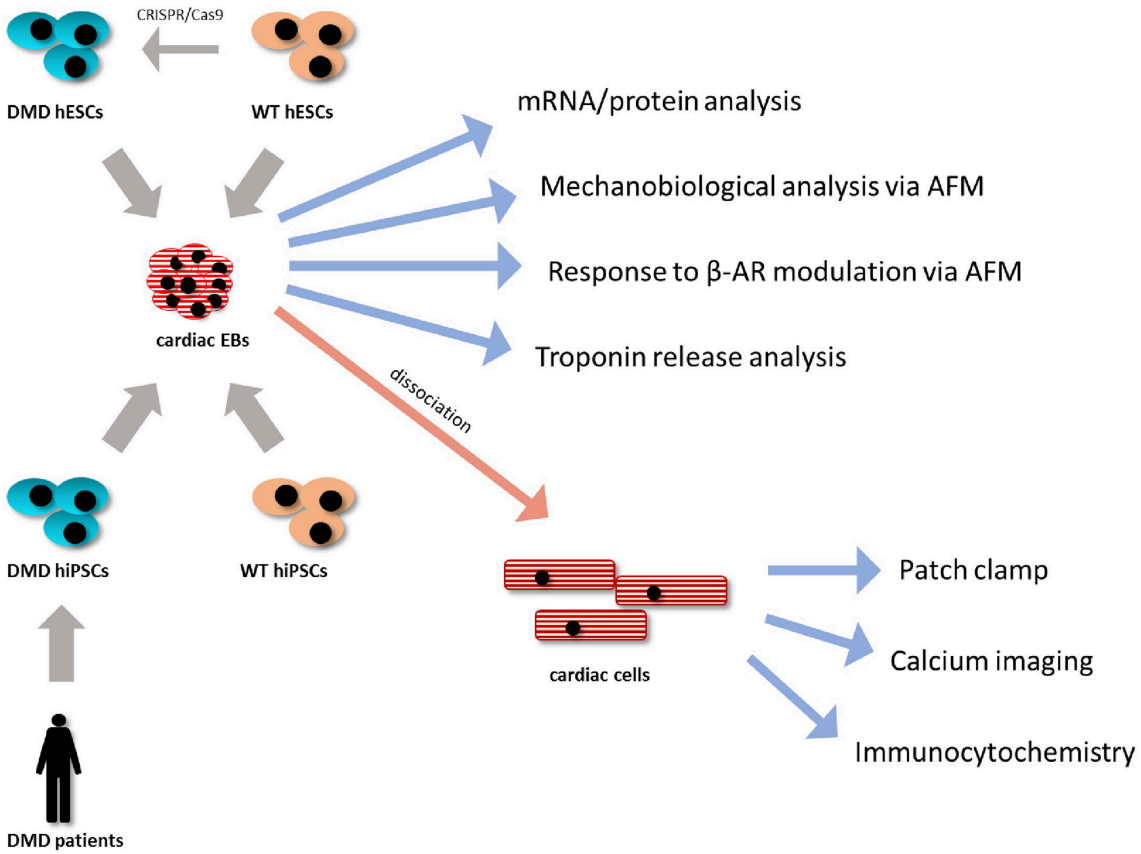



**FIGURE 1 |** Methodological approach. DMD-hiPSC lines from two Duchenne muscular dystrophy (DMD) patients were generated and analyzed compared to WT-hiPSC lines. DMD-hESC line was generated using CRISPR/Cas9 technology by targetted deletion of the DMD gene from a healthy WT hESC line serving as isogenic control. All hPSC lines were differentiated using 3D cell aggregates (embryonic bodies, EBs). These EBs were then used for molecular and mechanobiological analysis methods or were enzymatically dissociated into isolated cardiac cells, which were further analyzed using single cell specific analysis as protein localization and ion fluxes analyses.

assays were performed as described previously (Krutá et al., 2013). For cTnT and α-actinin, cells were fixed using 4% paraformaldehyde at room temperature for 10-15 min. Cells for dystrophin labeling were fixed with 2% paraformaldehyde for 10 min at room temperature, then with ice cold methanol for 5 min, and incubated with pre-extraction buffer (25 mM HEPES, 50 mM NaCl, 1 mM EDTA, 3 mM MgCl2, 200 mM sucrose, 0.5% Triton X-100) before continuing to blocking steps.

The cells were permeabilized and blocked with blocking solution 1 (1% bovine serum albumin, BSA, 0.2% Triton X-100 in phosphate buffer saline, PBS, 15 min on ice) and blocking solution 2 (1% BSA, 1% NaN3, 0.05% Tween 20 in PBS, 60 min on ice). Primary antibodies were diluted in PBS/Tween (0.05%) and incubated overnight at 4°C. Samples were extensively washed with PBS/Tween (0.05%) and incubated with appropriate fluorescent secondary antibody for 1 h at room temperature. For nuclear counterstain, 4′,6-Diamidine-2′-phenylindole dihydrochloride (DAPI) was used. All fluorescent and confocal microscopy experiments were performed using Confocal LSM700 microscope and processed using Zen software (both Carl Zeiss, Oberkochen, Germany).

For dystrophin immunoblots, protein samples from cell lysates were run in 4–12% gradient polyacrylamide gel for 70 min/170V/400mA, blotted at 100 V/300 mA for 2 h, and labeled with antibody against dystrophin protein. After dystrophin detection, the membrane was incubated with antibody against lamin B as loading control (1:1000, Santa Cruz, sc6217). Adrenergic receptors (AR) were analyzed using β1 specific (Thermo Fisher, PA5-28808, 1:500) and β2 specific (abcam, ab137494, 1:500) antibody. Human heart atrial tissue was obtained as procedural surplus material, available during bicaval orthotopic heart transplantation from donor organs and was used as positive control as previously described (Pesl et al., 2020).

## Quantitative Real-Time PCR

Cardiac EBs 30–50 days old and human heart samples (obtained as surplus material from donor hearts during cardiac transplantations) were lysed using RNA Blue reagent (Top-Bio, Prague, Czech Republic) according to the manufacturer's instructions, and the total mRNA was isolated using the RNeasy Micro Kit (Qiagen, Hilden, Germany). RNA concentration and purity were determined using NanoDrop (NanoDrop

technologies, Wilmington, DE, USA). cDNA was synthesized by Moloney Mouse Leukemia Virus (M-MLV) reverse transcriptase (Invitrogen, Carlsbad, CA, USA) at 37°C for 1 h followed by 5 min at 85°C. For quantitative real-time PCR (qRT-PCR), LightCycler® 480 SYBR Green Master kit (Roche, Basel, Switzerland) was used according to manufacturer's instructions, and PCR was performed, with annealing temperature 60°C and 55 cycles on LightCycler LC480 Instrument (Roche). The PCR primers (Generi-Biotech, Hradec Kralove, Czech Republic) are shown in **Supplementary Table 1**.

## Measurements of Intracellular Cytosolic $Ca^{2+}$ Variations by Fluorescent Confocal Microscopy

The contracting EBs were dissociated to single CCs by incubation in $Ca^{2+}$-free solution [120 mM NaCl, 5.4 mM KCl, 5 mM $MgSO_4$, 5 mM sodium pyruvate, 20 mM glucose, 20 mM taurine, 10 mM HEPES (all Sigma Aldrich), pH6.9] at room temperature and enzymatically treated with 0.8 mg/ml type II collagenase (Gibco) and 0.037 mg/ml type XIV proteinase (Sigma Aldrich) in the same solution for 3 min at 37°C. The clusters were then incubated in dissociating solution (85 mM KCl, 30 mM $K_2HPO_4$, 5 mM $MgSO_4$, 1 mM EGTA, 5 mM sodium pyruvate, 5 mM creatine, 20 mM taurine, 20 mM glucose, 2 mM disodium pyruvate, pH = 7.4) for 20 min at 37°C and plated on gelatin coated 35 mm glass bottom culture dishes (MatTek) in EB medium until the next day. On the day of measurements, cells were incubated in a Tyrode's solution (140 mM NaCl, 5 mM HEPES, 4 mM KCl, 1 mM $MgCl_2$, 1.8 mM $CaCl_2$, 10 mM glucose, pH 7.4) with 3 μM Fluo4-AM (Invitrogen, Carlsbad, CA, USA) for 20 min at room temperature. After the incubation with Fluo4-AM, the solution was replaced with the fresh Tyrode's solution and the cells were placed on the stage of an inverted microscope. $Ca^{2+}$ images in line-scan mode were recorded with a laser scanning confocal microscope Zeiss LSM Exciter (Carl Zeiss), with 40x water immersion objective, in x–y mode, 1 image/0.495 s. Electrical pacing was set up with frequency 0.5, 1 Hz (20 V, 0.5 ms duration and 1 ms delay). The kinetic properties of intracellular $Ca^{2+}$ variations including $Ca^{2+}$ transients and diastolic events were analyzed by in-house developed PeakInspector software (https://asalykin.github.io/PeakInspector/) as previously described (Acimovic et al., 2018).

## Electrophysiological Recordings Through Patch-Clamp

Electrophysiological recordings were obtained using whole-cell patch-clamp technique on an Axopatch 200B (Axon Instruments, Foster City, CA) at room temperature (22–24°C). The recording pipettes contained: 120 mM KCl, 8 mM EGTA, 10 mM HEPES, 6.8 mM $MgCl_2$, 3 mM $CaCl_2$, 4 mM $ATPNa_2$, 0.4 mM $GTPNa_2$ (pH 7.2). The bath solution contained: 130 mmol/L NaCl, 4 mM/L KCl, 1.8 mM/L $MgCl_2$, 1.8 mM/L $CaCl_2$, 10 mM/L HEPES, 11 mM/L glucose (pH 7.4). Action potentials (APs) were measured in the current-clamp configuration in response to brief (1–2 ms) depolarizing current injections at 1 Hz. The resting membrane potential, the amplitude and duration (APDs) at 20, 50, and 90% repolarization of the APs were measured (respectively indicated as $APD_{20}$, $APD_{50}$, and $APD_{90}$). 7 DMD-hPSC-derived CCs (DMD-CCs) and 18 WT-hPSC-derived CCs (WT-CCs) were analyzed. Cells arrhythmogenicity was tested using application of successive 10 s runs in the current clamp configuration defined by 5 brief (1 ms) depolarizing current injections at 2 Hz followed by a resting period. Data were analyzed using the Clampfit 10.0 (Axon Instruments) software.

## Atomic Force Microscopy Measurements

Atomic force microscope (JPK NanoWizard 3, JPK, Berlin, Germany), combined with an inverted light microscope (IX-81S1F-3, Olympus, Tokyo, Japan), was used to obtain mechanocardiograms of beating EBs as previously described (Pesl et al., 2014; Caluori et al., 2019; Pribyl et al., 2019). Drug response tests were performed after initial equilibration in Tyrode's solution, followed by addition of 70 μM metoprolol, 10 min of stabilization time, and then 10 min of measurement. Isoproterenol (1 μM) was subsequently added into the solution, and mechanocardiograms were measured after 20 min of stabilization. The mechanical properties of beating EBs were expressed as force of contraction in nN as previously described (Pesl et al., 2014); however, the values were relativized for final comparison.

## Free Troponin Analysis

The EBs were formed and cardiac induction was initiated as described above. On day 18, individual EBs homogenous in size and shape were separated onto 12 well plate coated with gelatin and 1ml of proper induction medium was added. From day 21 to 51 with frequency of 4 days, medium sample was collected, spun, and the supernatant frozen in −20°C until all samples were harvested. The samples were then analyzed for free troponin T concentration using two epitopes based immunochemical system Cobas e602 (Basel, Switzerland) specifically high sensitive short turnaround time (STAT) kit Elecsys Tropo T hs STAT 100 (Roche diagnostics, Basel, Switzerland; Hess et al., 2008) according to the manufacturer's instructions.

## Statistical Analysis

Statistical evaluation was carried out in GraphPad Prism 8.3 software (GraphPad Software, Inc., La Jolla, CA, USA). Available normality tests were performed for the obtained data, and Student's two-tailed *t*-test or ANOVA was used to assess statistically significant differences on normally distributed group pairs. Where normality tests failed, non-parametric tests were used. Individual statistical test used was specified in individual figure legends.

# RESULTS

## DMD-CCs Do Not Express Full-Length Dystrophin Protein

Three previously described patient-specific DMD-hiPSC and one CRISPR/Cas9-mediated DMD-hESC lines (Jelinkova et al., 2019a,b) were differentiated into CMs (Pesl et al., 2014). WT hESC [hESC CCTL12 (hPSCreg name MUNIe005-A, passages

15–61) and CCTL14 (hPSCreg name MUNIe007-A, passages 15–63) derived in Masaryk University, Brno, and characterized previously (International Stem Cell Initiative et al., 2007)] and WT-hiPSC [cl.4 (passages 43–84) obtained from Dr. Majlinda Lako (Newcastle University, UK) (Armstrong et al., 2010) and hfiPSC (passages 20–52) (Qu et al., 2013)] were used as controls. The obtained DMD-CCs were evaluated for dystrophin presence. The strategy for antibody detection is illustrated in **Figure 2A**. Dystrophin expression was evaluated using immunocytology with specific antibodies against high molecular weight isoform of dystrophin (antibody specific to N-terminus detecting the full-length 427 kDa isoform, **Figure 2B**, left panel), as well as shorter isoforms (antibody specific to C-terminus, which is present in various lower molecular weight dystrophin isoforms, **Figure 2B**, right panel). Dystrophin expression was observed with both antibodies in WT-CCs as membranous signal of the antibody (**Supplementary Figure 2**). No membranous/cytoplasmic protein signal was detected in any DMD-CCs (**Figure 2B**). Nuclear signal of dystrophin was detected by C-ter antibody (which can detect shorter dystrophin isoforms, most likely the Dp71 isoform), and no cytoplasmic/membranous signal was observed in CCs derived from either DMD-hPSC lines. Furthermore, western blot analysis with N-ter and C-ter antibodies showed expression of some shorter dystrophin isoforms (Dp140, Dp116, and Dp71) in the DMD cell lines, but none in the full high molecular band (Dp427) (**Figure 2C**, full membranes in **Supplementary Figure 2**).

## Dystrophin Deficiency Leads to Cardiac Differentiation With Lower Yield of Spontaneously Beating EBs

Next, we aimed at characterizing the impact of dystrophin deficiency on the cardiac differentiation of hPSCs through the EB-based method as previously published (Pesl et al., 2014). We compared the yield of beating EBs upon differentiation of all DMD and WT-hPSC lines. First of all, we used the spontaneous beat in 3D EB clusters as a criterion to evaluate the cardiac differentiation success. The differentiation efficacy represented by the fraction of spontaneously beating EBs (detected at day 29 after cardiac differentiation start) was decreased in DMD-EBs compared to WT-EBs (**Figure 3A**, statistical evaluation in **Supplementary Table 2**). At the cellular level, the beating EBs from all tested cell lines contained CCs (**Figure 3B**) with striated pattern of cardiac troponin T (cTnT) and α-actinin. The differentiation efficacy was also measured in age-matched groups of DMD- and WT-EBs aged 25–29 days by qRT-PCR of well-known cardiac markers [*NKX2.5* ($p = 0.42$), myosin heavy chain α (*MYH6*, $p = 0.71$), myosin heavy chain β (*MYH7*, $p = 0.82$), myosin light chain 2 (*MYL2*, $p = 0.17$), myosin light chain 7 (*MYL7*, $p = 0.42$), ryanodine receptor 2 (*RYR2*, $p = 0.61$), cardiac muscle alpha actin (*ACTC1*, $p = 0.78$), connexin43 (*GJA1*, $p = 0.36$)], showing no significant difference in relative mRNA expression. However, a tendency for lower yield of most of the markers in the obtained DMD clusters was observed, with the exception for *MYH7* and *GJA1* (**Figure 3C**). Inward rectifier potassium channels Kir2.1, Kir2.2, and Kir2.3 were also tested (*KCNJ2*, *KCNJ4*, and *KCNJ12*, respectively) with significant increase in Kir2.1 expression ($p = 0.004$); SERCA (*ATP2A*) shows no difference in mRNA expression.

## DMD-CCs Display Altered Electrophysiological Properties

Next, we tested whether dystrophin deficiency alters the cardiac electrophysiological properties and arrhythmogenicity of single hPSC-derived CCs. Action potential (AP) properties (resting membrane potential (RP), amplitude, and duration (APD) in DMD- (26–46 days old) and WT-CCs (36–41 days old) were recorded using the patch clamp technique. Age matching of the CCss was not possible in this instance due to technical reasons as only a limited number of CCs were analyzed. Both DMD- and WT-CCs mostly exhibited triangular-shaped APs with various APD90 durations ranging from 20 to 380 ms (**Figures 4A,B**) similarly to WT with measured APD90 ranging from 20 to 520 ms. More occasionally, plateau-shaped APs with longer (>300 ms) APD90 durations were observed (**Figures 4A,B**, **Supplementary Figure 7**). No significant difference was observed in RP, amplitude, and durations between DMD- ($n = 7$) and WT-CCs ($n = 18$) APs (**Figure 4B**). Occurrence of fast pacing induced delayed afterdepolarization (DAD) events was observed and quantified. No difference ($p = 0.25$) between DMD-CCs (50%; 1.2 ± 0.3 events/10 s, $n = 7$) and WT-CCs (35%; 1.9 ± 0.4 events/10 s, $n = 18$) in the occurrence of DAD was observed (**Figure 4C**).

## DMD-CCs Exhibit Abnormal Intracellular $Ca^{2+}$ Handling

Intracellular SR $Ca^{2+}$ handling has been shown to be affected in several DMD models, in particular through RyR2 mediated $Ca^{2+}$ leak (Andersson and Marks, 2010; Fauconnier et al., 2010; Andersson et al., 2012). Using confocal fluorescent microscopy as we previously showed in hPSC-CCs (Pesl et al., 2014; Acimovic et al., 2018), we investigated the enzymatically dissociated single cell $Ca^{2+}$ handling in DMD and WT-CCs matched between 40 and 50 days after differentiation. We chose this age as a safe timepoint to interpret the eventual differences as prevalently caused by the DMD mutation: it is in fact reported that calcium machinery in hPSC-CCs reaches a "stationary state" between 21 and 30 days after induction (Hwang et al., 2015). We acquired intracellular $Ca^{2+}$ transients in resting state and under physiological pacing conditions (0.5 and 1 Hz). We analyzed spontaneous frequency of calcium transients, together with their time parameters, and occurrence of secondary small diastolic calcium events possibly triggering increased automaticity.

A lower frequency was observed in the major $Ca^{2+}$ transients in DMD- compared to WT-CCs in resting conditions (1.262 ± 1.608 Hz vs. 2.416 ± 3.441 Hz respectively, $p < 0.0001$). $Ca^{2+}$ transient dynamics resulted altered in DMD single CCs: either in resting or in paced conditions, the time to peak, dependent on the SR $Ca^{2+}$ release properties, was significantly elongated in dystrophin deficient cells ($p < 0.0001$, **Figure 5A**). $Ca^{2+}$ transient

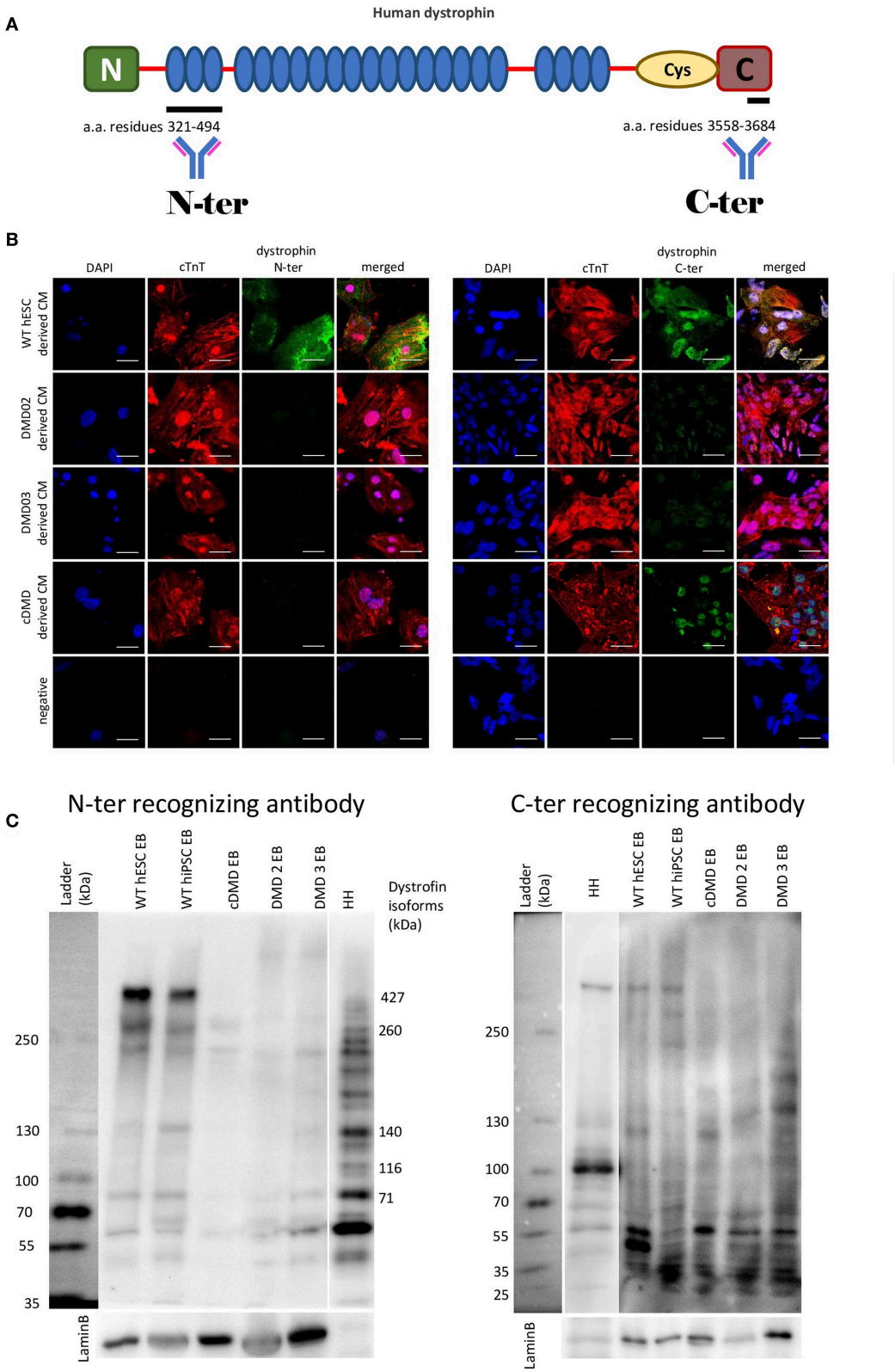



**FIGURE 2 |** DMD-hPSC differentiate into cardiac cells (CCs), which do not express dystrophin. **(A)** Antibodies against dystrophin N-terminal (N) aminoacid (a.a.) residues 321–494 and C-terminal aminoacid residues 3558–3684 were used. **(B)** hPSC derived CCs were analyzed for presence of dystrophin (in green). WT hESC

*(Continued)*

**FIGURE 2 |** derived CCs dissociated from spontaneously beating EBs presenting with positive signal for cardiac troponin T (red) showed positive signal for dystrophin labeled by N-terminus specific antibody as well as by C-terminus specific antibody. None of the DMD-hPSC lines (DMD02, DMD03, and cDMD) derived CCs showed any signal for dystrophin. DAPI was used for nuclear counterstain. Ruler represents 50 μm. **(C)** The differentiated EBs were lyzed and western blot analysis was performed to identify the individual isoforms expressed. Both used WT-hPSC derived EBs show expression of various dystrophin isoforms including Dp427, Dp260, Dp140, and Dp71. The CRISPR/Cas9 generated cDMD-EBs show no expression of either isoform, while only shorter isoforms were identified in patient DMD-hiPSC-EBs with promoters downstream of the patient's mutations. Human heart tissue (HH) was used as positive control. LaminB was used as loading control.

decay time, expression of the features of calcium reuptake, was increased in DMD in resting state (+59.24 ms average increase, $p = 0.013$, **Figure 5B**); this prolongation was non-significant in pacing conditions. Transient duration, which determines the contraction cycle and possible $Ca^{2+}$-induced arrhythmogenicity, was also elongated in DMD-CCs (**Figure 5C**; 63.53 ms in resting state, $p = 0.002$, and 71.51 ms under 0.5 Hz pacing, $p = 0.025$). These data suggest that the lack of dystrophin affects DMD-CCs during spontaneous and triggered SR $Ca^{2+}$ release, affecting overall calcium dynamic.

We then observed and quantified the occurrence of secondary small-amplitude $Ca^{2+}$ release events occurring after a main transient during diastole (relaxation and baseline, **Figure 5D**) and found significantly increased frequency of these events in DMD-CCs ($p = 0.0172$, **Figure 5E**).

## Aberrant L-Type Voltage-Dependent $Ca^{2+}$ Channel Expression in DMD-CCs

To further understand how dystrophin deficiency affects $Ca^{2+}$ homeostasis and ECC in DMD-CCs, we verified the expression pattern of LTCCs using dihydropyridine receptor (DHPR) α2 subunit/CACNA2D1 antibody. At the protein level, DHPR α2 subunit expression was increased in patient-specific DMD-CCs (DMD02 and 03, **Figure 5F**). No difference was observed on the mRNA level of the CACNA1C (encoding Cav1.2) or CACNA1D (encoding Cav1.3) between the WT and DMD groups (**Figure 5G**). We then tested the cellular localization of the L-type channels using DHPR immunostaining. In line with previous protein analysis, DMD-CCs (detected by cTnT labeling) showed stronger signal of the LTCC, and no other difference was detected (**Figure 5H**).

## DMD-EBs Display Hypocontractility, Bradycardia, and Higher Heart Rate Variability

DMD-associated dilated cardiomyopathies is characterized by thinner left ventricle, reduced cardiac output, and hypo-contractility of the heart (Hajjar et al., 1993; Bondue et al., 2018; Amedro et al., 2019). We thus tested whether DMD-CCs contained in 3D cardiac clusters (EBs) exhibit weaker contractile properties by measuring the contraction force and beat rate by AFM as we previously published (Pesl et al., 2014, 2016; Acimovic et al., 2018). We observed weaker spontaneous contraction force in DMD-EBs (**Figure 6A**, $p < 0.0001$) while they exhibited similar overall beat rate compared to WT-EBs (**Figure 6B**, $p = 0.139$; for separate data of each line, see **Supplementary Figure 6**). We noticed a peculiar variability in the inter-beat interval (IBI, **Figure 6C**, $p = 0.0039$) (examples of AFM curves are shown in **Supplementary Figure 6A**) across the different samples. While WT-EBs showed consistent IBI with few exceptions, DMD-EBs showed high heterogeneity (**Figure 6C**, **Supplementary Figures 5B–D**). We observed not only different variability in recorded IBI but also prevalence in shorter IBI in WT-EBs compared to DMD-EBs (1 ± 1.0 s, and 0.96 ± 0.35 s for WT-hESC- and hiPSC-EBs respectively, 2.4 ± 1,6 s for DMD02-EBs, 2.1 ± 1.2 s for DMD03-EBs and 1.9 ± 1.2 s for cDMD-EBs, *p*-values in **Supplementary Table 3**) (**Figures 6D–G**).

Moreover, DMD-EBs displayed more dispersed IBI scatter plot and histogram than WT-EBs (**Figures 6H,I**). Using representative Poincaré plots, a quantitative measure of the evolvement in time of the IBI, we found more scattered inter-contraction pattern in DMD-EBs compared to WT-EBs (**Figures 6J,K**) showing a higher beat rate variability.

## Loss of Dystrophin Leads to β-Adrenergic Remodeling and Cardiomyocyte Wasting

Dystrophin-deficient mouse CMs have been shown to display aberrant response to β-AR stimulation (Li et al., 2014). Thus, we evaluated the β-adrenergic response in DMD-EBs to investigate the effect of stress. We monitored the mechanobiological properties of the contracting clusters upon a selective β1-AR inhibitor (metoprolol, METO) followed by a non-selective β-AR activator (isoproterenol, ISO). In presence of METO, the WT-hPSC-EBs exhibited a significant decrease in contraction force ($p = 0.0042$ for WT hESC, $p = 0.0156$ for WT-hiPSC) and beat rate ($p = 0.0051$ for WT hESC, **Figures 7A,B**). DMD-hiPSC-EBs showed no response in beat rate nor contraction force to modulation by ISO nor METO. cDMD-EBs showed a response in contraction force to METO application similarly to its isogenic control ($p = 0.0003$ for contraction force and $p = 0.103$ for beat rate). WT-EBs responded to subsequent β-adrenergic stimulation by ISO application (partially competing with METO) through marginally significant increase in relative contraction force ($p = 0.0596$ for WT hESC, $p = 0.03$ for WT hiPSC, **Figure 7A**), DMD-EBs did not show statistically significant responses to ISO nor METO. cDMD-hESC line, however, responded similarly to its isogenic WT control in contraction force increase (with significant change in response to modulation, $p = 0.0039$). The pharmacokinetic answer to ISO has been additionally tested by exclusion of METO response using division of Tyrode and ISO value still showing response in WT-EBs ($p = 0.0021$) with no significant change in DMD-EBs ($p = 0.1309$) (as shown in **Supplementary Figure 4C**).

These mechanobiological data suggest that the DMD-EBs exhibit much weaker response to stress conditions in presence of β-AR modulation. Thus, we compared the expression of the β1, β2, and β3 AR at the protein level between DMD- and

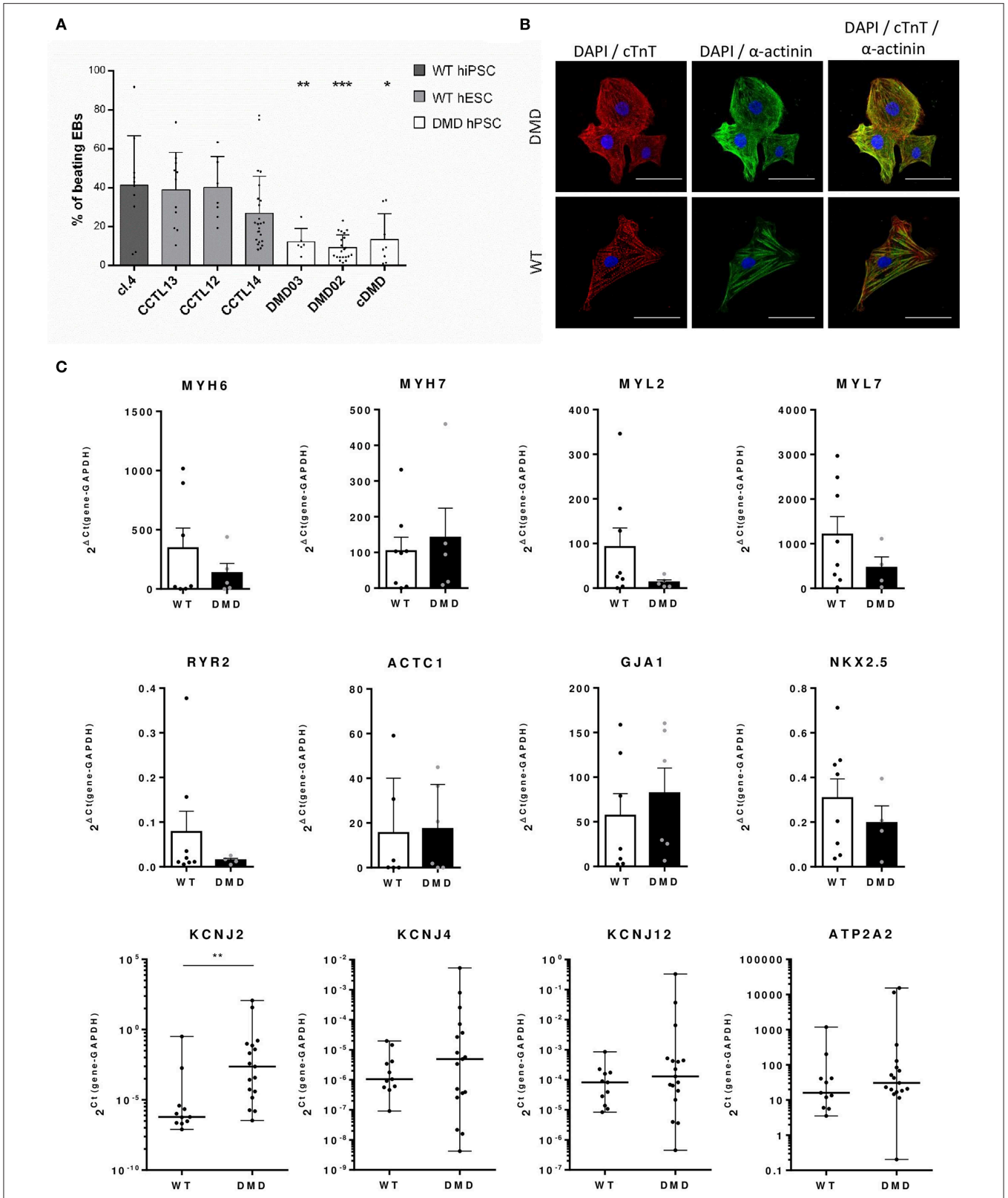



**FIGURE 3 |** Differentiation efficacy is lower in DMD-hPSC lines. **(A)** All DMD-hPSC and WT-hPSC lines were differentiated into spontaneously contracting EBs containing cardiomyocytes and cardiac cells. The ratio of these spontaneously contracting clusters was evaluated and compared to wild-type (WT) controls ($n = 36$

*(Continued)*

**FIGURE 3 |** for CCTL14 EBs, $n = 8$ for CCTL12 EBs, $n = 13$ for CCTL13, $n = 12$ for cl.4 EBs, $n = 25$ for DMD02 EBs, $n = 6$ for DMD03 EBs, $n = 19$ for cDMD-EBs). Lesser yields of beating EBs were identified in all DMD-hPSC lines. Statistical difference was calculated by one-way ANOVA and multiple comparison with Dunn's test. Significance ($^*p < 0.05$, $^{**}p < 0.01$, $^{***}p < 0.01$) is visualized as asterisks for the lowest values; for individual $p$-values, see **Supplementary Table 1**. **(B)** EBs were dissociated and cells labeled for cardiac markers α-actinin (in green) and cardiac troponin T (cTnT, in red) (DAPI is labeling the nuclei). WT and DMD-CCs presented similar level of typical striated pattern of sarcomeres. Line represents 50 μm. **(C)** Differentiation efficacy was evaluated by rt qPCR on mRNA levels of cardiac markers showing only non-significant differences in expression of various markers (MYH6, $n = 7$ for WT and $n = 5$ for DMD; MYL2, $n = 8$ for WT and $n = 4$ for DMD; MYL7, $n = 8$ for WT and $n = 4$ for DMD; RYR2, $n = 8$ for WT and $n = 4$ for DMD; ACTC1 $n = 6$ for WT and $n = 5$ for DMD; NKX2.5, $n = 8$ for WT and $n = 4$ for DMD, ATP2A2, $n = 11$ for WT and $n = 17$ for DMD) and non-significant increase in MYH7 ($n = 8$ for WT and $n = 5$ for DMD) and GJA1 ($n = 7$ for WT and $n = 6$ for DMD). Potassium channels were analyzed using Kir2.x isoforms mRNA expression (KCNJ2 – Kir2.1, KCNJ4 – Kir2.2 and KCNJ12 – Kir2.3, for all $n = 11$ for WT and $n = 17$ for DMD). Statistical significance on pooled DMD and pooled WT data sets was calculated using Mann–Whitney test; exact value for each is represented by • in each graph.

WT-EBs. While DMD-EBs derived from patient hiPSC showed increased β1 ($p = 0.0103$) and β2 AR expression ($p = 0.0162$) compared to isogenic WT-EBs, cDMD-EBs show similar or lower expression of both (**Figures 7C–E**). β3 expression was analyzed by quantitative rt qPCR showing no significant differences in between WT- and DMD-EBs (**Supplementary Figure 4D**).

A pathological overexpression of β-AR together with the blunted drug response and hypocontractility above described lead us to ask whether our derived CCs are already undergoing complex changes leading to their death, with consequential depletion and mechanical function deterioration in our 3D model. Thus, CC death was quantified, over time after differentiation, via cTnT concentration in the culture medium, originating from the dying CCs in the EBs. DMD lines showed from day 35 a significantly increased free cTnT level in their medium, compared to WT samples (**Figure 7F**, statistical evaluation in **Supplementary Table 4**). Interestingly, the DMD-EB kept beating even late after cardiac induction, even over the observed increased CM death (**Supplementary Video 1**).

## DISCUSSION

Dilated cardiomyopathy, ultimately leading to heart failure, is the most common outcome in patients with dystrophin mutations (Kamdar and Garry, 2016; Papa et al., 2017), and it develops in DMD patients due to muscle wasting, but remains mostly unexplained in its dynamics. The DMD (*mdx)* mouse model has critical limitations since it develops only mild symptoms of heart failure with slow progression and unaffected lifespan compared to control mice (Carnwath and Shotton, 1987; Coulton et al., 1988; Shirokova and Niggli, 2013). In the present study, we provided a detailed description of patient-specific hiPSC-CCs and CRISPR/Cas9 engineered hESC-CCs. DMD-CC exhibited several molecular and functional abnormalities including an altered $Ca^{2+}$ handling, irregular bradycardic beating, hypocontractility, and remodeling processes such as βAR alteration and CMs wasting. Our evidences on the alteration of ECC are in agreement with symptoms described in DMD patients.

Our results showed that dystrophin deficiency leads to lower efficacy in differentiating hPSCs into CCs. Interestingly, DMD-CCs exhibited a similar relative expression of known cardiac markers, and with trending increased Connexin 43 expression, similarly observed in *mdx* and *mdx:utr* CMs as a remodeling mechanism following functional dystrophin absence, with potential fatal arrhythmias in presence of β adrenergic stimulation (Patrick Gonzalez et al., 2015). Lower differentiation efficacy can point to cell fate errors: these can result from increased DNA damage caused by deregulated NOS activity (Jelinkova et al., 2019a). This process can lead to loss of stemness both at the commitment and self-renewal level (Rossi et al., 2007; Inomata et al., 2009). DNA damage can also affect multipotent stem cells division, rendering muscular differentiation ineffective (Dumont et al., 2015). Dystrophin loss was recently associated, in advanced CM *in vitro* models, with delayed contractile machinery formation, suggesting a mutation-derived impairment even at the latest stage of CM development (Pioner et al., 2020).

Then, we inquired whether and to what extent the mutation affected the single cell and EB ECC. We measured the electrophysiological properties and found similar AP features between DMD- and WT-CCs. While most of the recorded AP displayed atrial-like AP properties, our results suggested that dystrophin deficiency does not alter the electrophysiological properties of the derived hPSC-CCs. The AP durations we obtained indicate mixed population of various type of excitable cells from ventricular-like CMs (APD90 $\geq$ 300 ms), through atrial- and nodal-like CMs (APD90 $\geq$ 160 ms) and undefined/immature cardiomyocyte-like cells (APD90 $<$ 100 ms) similarly to what others previously found (He et al., 2003; Zhu et al., 2016). Nevertheless, a significant increase of Kir2.1 mRNA expression level point to a possible alteration of APD, which results in reduced effective refractory period during diastole *in vivo*. Furthermore, regarding the voltage-gated ion channels expression, DMD-CCs exhibited increased expression of DHPRα subunit of L-type $Ca^{2+}$ channels but no difference in Cav1.2 and Cav1.3 isoform expression. L-type $Ca^{2+}$ channels presenting gain-of-function mechanism was reported in dystrophic hearts (Koenig et al., 2014). In a recently published work (Eisen et al., 2019), it was shown that prolongation of APD in DMD-CMs was caused by increased $I_{Ca,L}$ density, which can be matched to prolonged diastole in DMD patients (Panovský et al., 2019). APD alterations, both at the potassium and calcium current levels, can lead to ventricular tachycardia (Choi et al., 2002; McNally et al., 2015), or premature ventricular beats, possibly degenerating into Torsades-de-Pointes ventricular fibrillations (Weiss et al., 2010).

Correlated with the mentioned calcium channels alterations, we measured the intracellular $Ca^{2+}$ transients on dissociated CCs and observed a reduced spontaneous firing in DMD-CCs, with a significantly higher occurrence of small $Ca^{2+}$ events in diastolic phase. For $Ca^{2+}$ dynamics, DMD-CCs presented

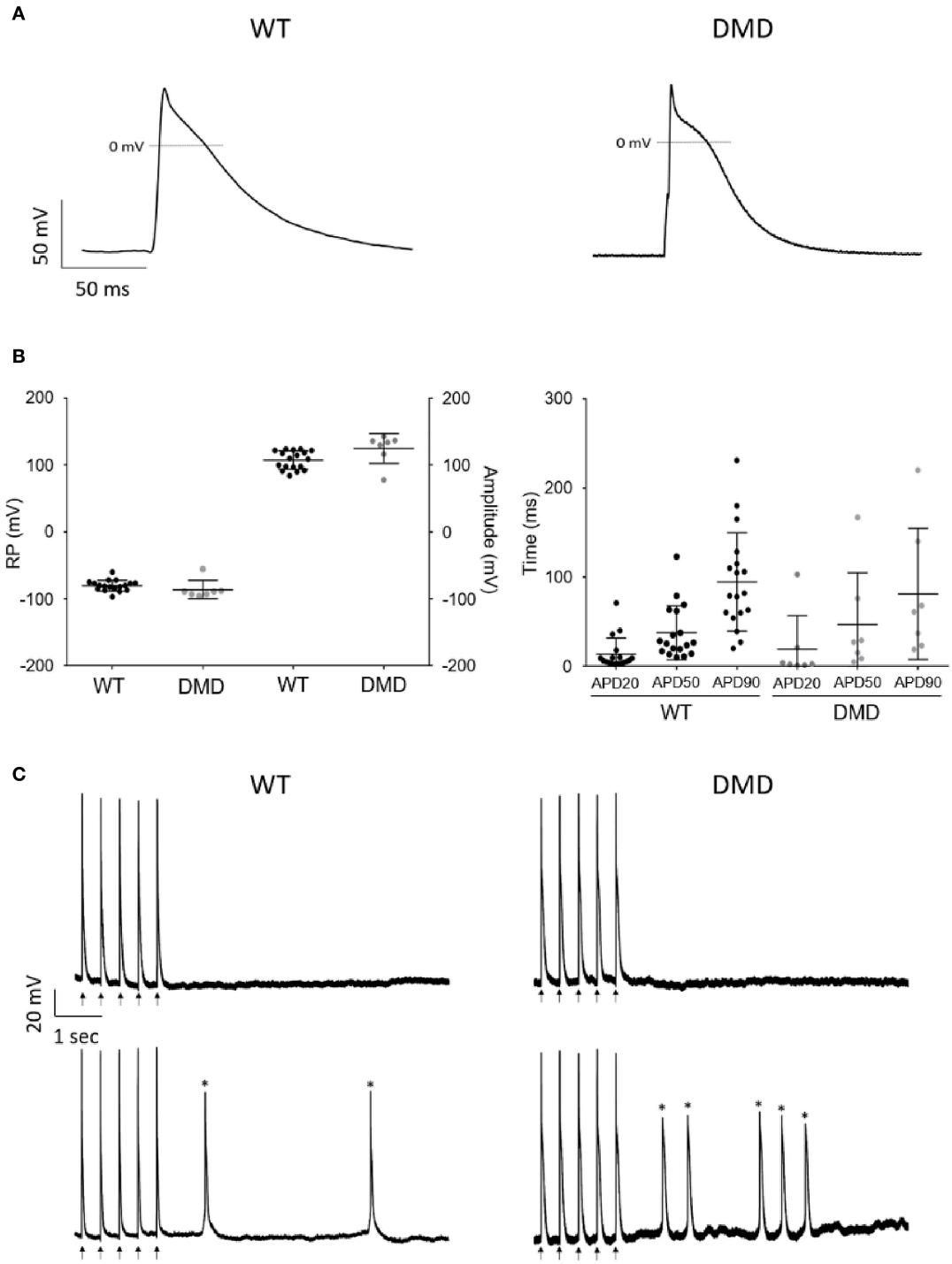



**FIGURE 4 |** AP recordings showed no difference in WT and DMD-CCs. **(A)** Representative AP recordings obtained from WT and DMD-hiPSC derived CCs, under current clamp configuration. **(B)** Scatter plot of RP (mV) and amplitude (mV) (left) and APD 20, 50, and 90 durations (right) of WT ($n = 18$) and DMD ($n = 7$) hPSC-CCs are represented. No significant difference was observed among these parameters between WT and DMD-hPSC-CCs. Exact n value for each is represented by • in each graph. Mean ± SEM are represented. **(C)** Representative arrhythmic events recorded in WT-CCs (left) and DMD-CCs (right). Upper panels show representative recordings of non-arrhythmogenic cells from WT-CCs and DMD-CCs and bottom panels show representative recordings of arrhythmogenic cells showing extra events, such as DAD (Asterisks).

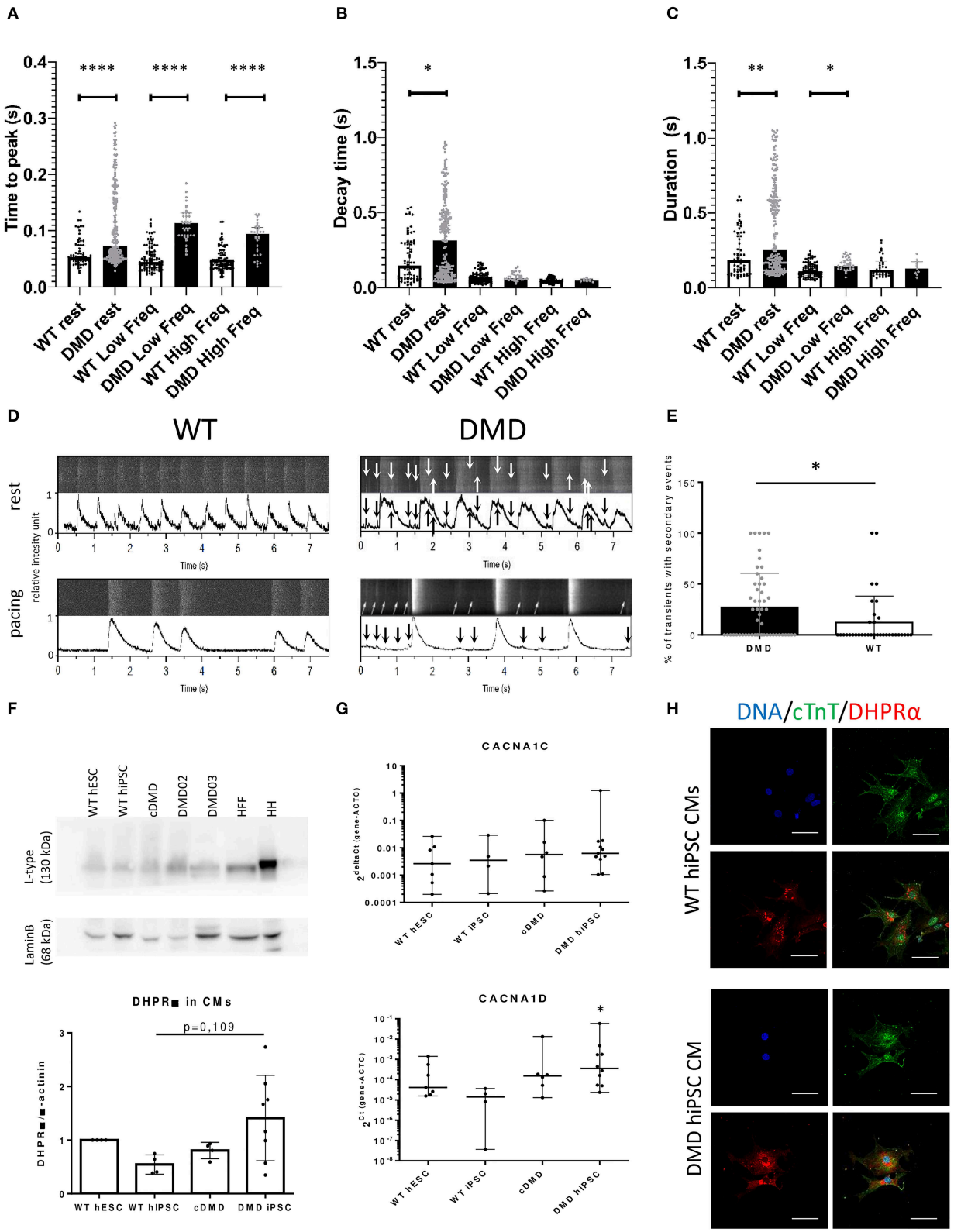



**FIGURE 5 |** The dynamics of $Ca^{2+}$ release and re-pumping is affected by dystrophin deficiency. Release of $Ca^{2+}$ transients was measured using Fluo4 dyes in enzymatically dissociated DMD (91 cells and $n = 278$ transients were analyzed for resting conditions; 20 cells and $n = 83$ transients were analyzed for low frequency

*(Continued)*

**FIGURE 5 |** paced at 0.5 Hz) and WT-CCs (30 cells and $n = 262$ transients were analyzed for resting conditions; 15 cells and $n = 128$ transients were analyzed for low frequency paced at 0.5 Hz) in the age 40–50 days of differentiation. **(A)** Time to peak, **(B)** decay time, and **(C)** contraction duration time were analyzed for the main $Ca^{2+}$ transients. The DMD-CMs showed significantly higher $Ca^{2+}$ amplitude and longer time to release and repump/extrude the $Ca^{2+}$ back into the SR/out of the cell in comparison to WT. The exact values are plotted in the graphs; red line represents the median. Significance ($*p < 0.05$) is visualized as asterisks as calculated by Mann–Whitney one-sided test ($*p < 0.05$, $**p < 0.01$, $****p < 0.0001$). The $Ca^{2+}$ leakage is demonstrated by $Ca^{2+}$ events of low-amplitude (arrows) among the main $Ca^{2+}$ transients [**D**—the obtained data from microscope with line scanning (upper bar) and transferred into peak graph by PeakInspector (lower bar) with and without electrical pacing of 0.5 Hz]. The occurrence of these small events is increased in DMD-CCs transients **(E)** as analyzed by Mann–Whitney test ($n = 54$ and $n = 35$ analyzed cells, for DMD and WT, respectively). **(F)** L-type channel (DHPR subunit) expression was characterized, showing non-significant increase in protein expression in DMD-hiPSC compared to WT-EBs as calculated by one-way ANOVA ($n = 4$, $n = 4$, $n = 4$ and $n = 8$ for WT hESC, WT-hiPSC, cDMD, and DMD-hiPSC-EBs). HH was used as positive control, HFF (human foreskin fibroblasts) as non-CM cell sample. **(G)** CaV isoform's (CACNA1C and CACNA1D) mRNA expression of LTCC subunits were analyzed using rt qPCR showing no difference between the groups. The values were calculated for CMs using ACTC for normalization. At least three biological repetitions were used for the analysis with exact value for each represented by • in the graph. Statistical difference was calculated using one-way ANOVA. **(H)** ICC analysis showed stronger signal for LTCC (in red) in DMD-hiPSC CCs recognized by cTnT labeling (in green). Line represents 50 μm.

prolonged rising time under resting and paced conditions with high variability. The $Ca^{2+}$ transient decay time mean was significantly longer in resting conditions for DMD-CCs, even if this difference was abolished during pacing. This led to a measured prolonged duration of the transients, except under the 1 Hz physiological pacing.

Altered $Ca^{2+}$ transients dynamics correlate with cellular alteration of ECC, as previously shown in our work and others (Sato et al., 2007; Caluori et al., 2019; Pioner et al., 2020). In particular, longer rising time might be correlated to a state of calcium overload, derived from sarcolemmal tears (Danialou et al., 2001) and SR leakage by remodeling of RyR2 by S-nitrosylation (Fauconnier et al., 2010; Oda et al., 2015) or loss of the closed-state stabilizer calstabin2 (Fauconnier et al., 2010). RyR2 misregulation can explain also that the presence of small $Ca^{2+}$ amplitude events by random firing is a state of overload. Prolonged cytosolic $Ca^{2+}$, as expressed by increased duration of the transients, can contribute to arrhythmic events via inverse $Na^{+}$-$Ca^{2+}$-exchange activation (Voigt et al., 2012) and electromechanical dissociation. However, it should be noted that young DMD boys rarely exhibit arrhythmias (Villa Chet et al., 2015). We performed patch-clamp experiments and observed no difference in the number of arrhythmic events in WT- and DMD-CCs. In our previous work, we have shown how DMD-EBs are insensitive to positive chronotropic effect of high extracellular $Ca^{2+}$ concentration, most likely due to low diffusion gradients in case of constant cytosolic overload (Caluori et al., 2019). Nevertheless, WT-EBs tolerated high levels of extracellular $Ca^{2+}$ by modulating their contractile activity, while DMD-EBs presented an increased and erratic electromechanical coupling delay, together with an increased calcium reuptake time. In accordance with the presented evidences, we have previously shown how DMD-EBs are less sensitive to Verapamil L-type channels inhibition.

From the single cell electrochemical experiments, and previous results in the DMD-EB electromechanical alterations, we focused on the study of 3D mechanical behavior and its modulation. EBs showed that the overall spontaneous beat rate of WT and DMD groups did not differ at rest. However, we identified an increased heart rate variability though IBI analysis and its time-dependent correlation, similarly to Eisen et al.'s observations (Eisen et al., 2019), which also showed high heterogeneity in beat rate variability in dissociated DMD-hiPSC-CCs. Heart rate variability via L-type inactivation can be increased and even become pro-arrhythmogenic in case of spontaneous SR leakage (Johnson et al., 2013), a condition proven in the case of DMD models. The measured contraction force in DMD-EBs was significantly lowered compared to WT-EBs, as previously shown in single cell models (Pioner et al., 2020) and correlated to the ejection fraction decrease in reported patient's hearts (Corrado et al., 2002; Villa Chet et al., 2015; Panovský et al., 2019). Both lower contraction force and arrhythmic events occur in DMD patient's heart from a very young age and before dilated cardiomyopathy onset. In fact, 25% of pediatric DMD patients under 10 years old already showed decreased ejection fraction and have developed sinus tachycardia (Sadek et al., 2017). Overall, our model presents functional alterations of an early-stage cardiac manifestation of DMD.

For the first time, we further evaluated the ECC modulation abilities by pharmacological response in DMD-CCs through the β-AR response. We found an impaired response in DMD-EBs through lack of contraction force and beat rate modulation similarly to *mdx* hearts (Meyers et al., 2019). Our data showed visible changes in contraction force and beat rate in WT-EBs in the presence of isoproterenol (non-selective β adrenergic agonist) or metoprolol (β1 receptor inhibitor) but no change of both parameters in DMD-EBs. Surprisingly, the CRISPR/Cas9-induced cDMD-EBs reacted to β adrenergic modulation similarly to WT-EBs. The response might involve an unknown compensatory mechanism proper of the engineered line. As further confirmation, cDMD-CCs presented similar levels of β-AR with respect to its isogenic hESC-derived WT-CCs. In contrast, patient-specific DMD-EBs showed an increased expression in β1 and β2 receptors compared to WT-EBs. It has been previously shown that *mdx* CMs present lowered density of β1-AR (Li et al., 2014) with blunted β-adrenergic signaling pathway (Lu and Hoey, 2000; Li et al., 2014). Here, patient-specific DMD-CCs showed increased protein expression level of both, still with blunted response to adrenergic modulation.

That is also similar to non-DMD heart failure, where β1 overexpression is quite common (Engelhardt et al., 1999); trying to compensate for the weak contractility of the organ and the overactivation of the receptors then leads to receptor dysfunction in signaling, thus their insensitivity (Bristow et al., 1982; Rengo et al., 2009; de Lucia et al., 2018). The impaired contraction

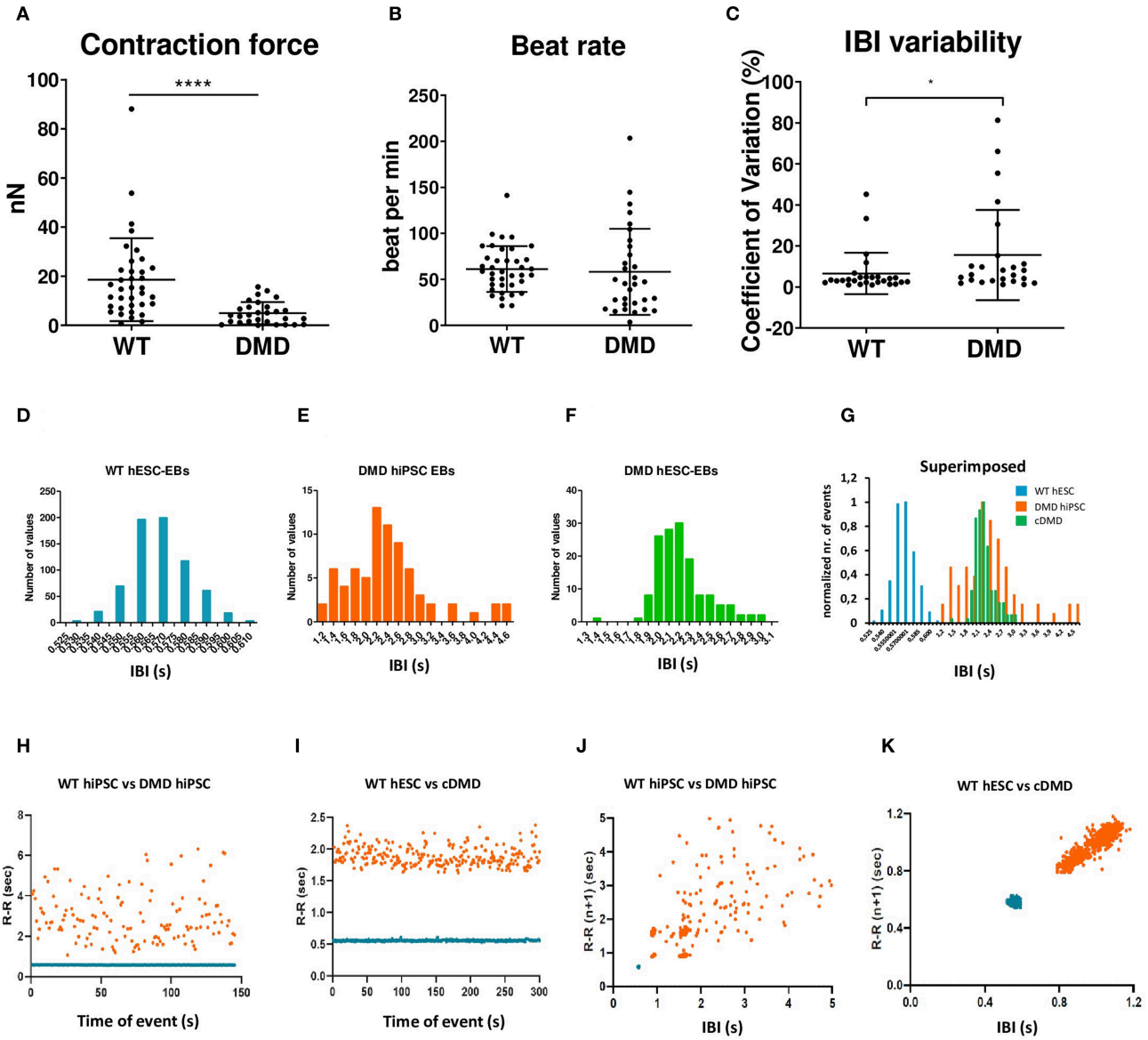



**FIGURE 6 |** The spontaneously contracting EBs lacking dystrophin showed weaker contraction force and signs of arrhythmias. The EBs were analyzed by AFM-based methods. **(A,B)** Contraction force is decreased in DMD-hPSC derived EBs ($n = 36$ for WT, $n = 29$ for DMD-EBs), beat rate is not affected by DMD mutation ($n = 38$ for WT, $n = 31$ for DMD-EBs). The statistical difference was calculated by Mann-Whitney test (*$p < 0.05$, ****$p < 0.0001$). At least five biological repetitions were used in each differentiated line; exact value for each is represented by • in each graph. Beat rate variability was identified in DMD-EBs. Graph shows coefficient of variation analysis **(C)** of pooled control and DMD groups. The data were cleaned of outliers by ROUT test ($q = 1\%$), and normality was tested by available tests showing non-normal distribution. Statistical difference was calculated using Mann–Whitney test. Representative IBI histograms of control (**D**, $n = 712$ peaks of the representative EB analyzed), DMD-hiPSC (**E**, $n = 76$ peaks of the representative EB analyzed), and DMD-hESC (**F**, $n = 165$ peaks of the representative EB analyzed) EBs and superimposed example of all three groups with normalized values **(G)**. Superimposed representative inter-beat-interval (IBI) scatter plots of control hiPSC with DMD-hiPSC-EBs ($n = 145$ time points for each EB) **(H)** and control hESC with DMD-hESC-EBs ($n = 334$ time points for each EB) **(I)**. Superimposed Poincaré plots of control hiPSC with DMD-hiPSC-EBs (**J**, same representative EBs as in **H**) and control hESC with DMD-hESC-EBs (**K**, same representative EBs as in **I**).

force observed in DMD-EBs can also be caused by β3 inhibitory function (Skeberdis, 2004). β3 normally acts as β-adrenergic break, but has been also shown to temper with mechanical properties of skeletal muscle together with nNOS expression increase leading to elevated ROS production (Puzzo et al., 2016). However, our results indicated that β3 expression was unchanged in DMD-CCs although we cannot exclude difference in β3 cellular distribution. The use of β-AR modulators has been shown to be challenging in management of cardiomyopathy in DMD patients due to severe hypotension events (McNally et al., 2015). Investigations using β blockers in DMD cardiomyopathy have turned up mixed results, with some studies demonstrating a

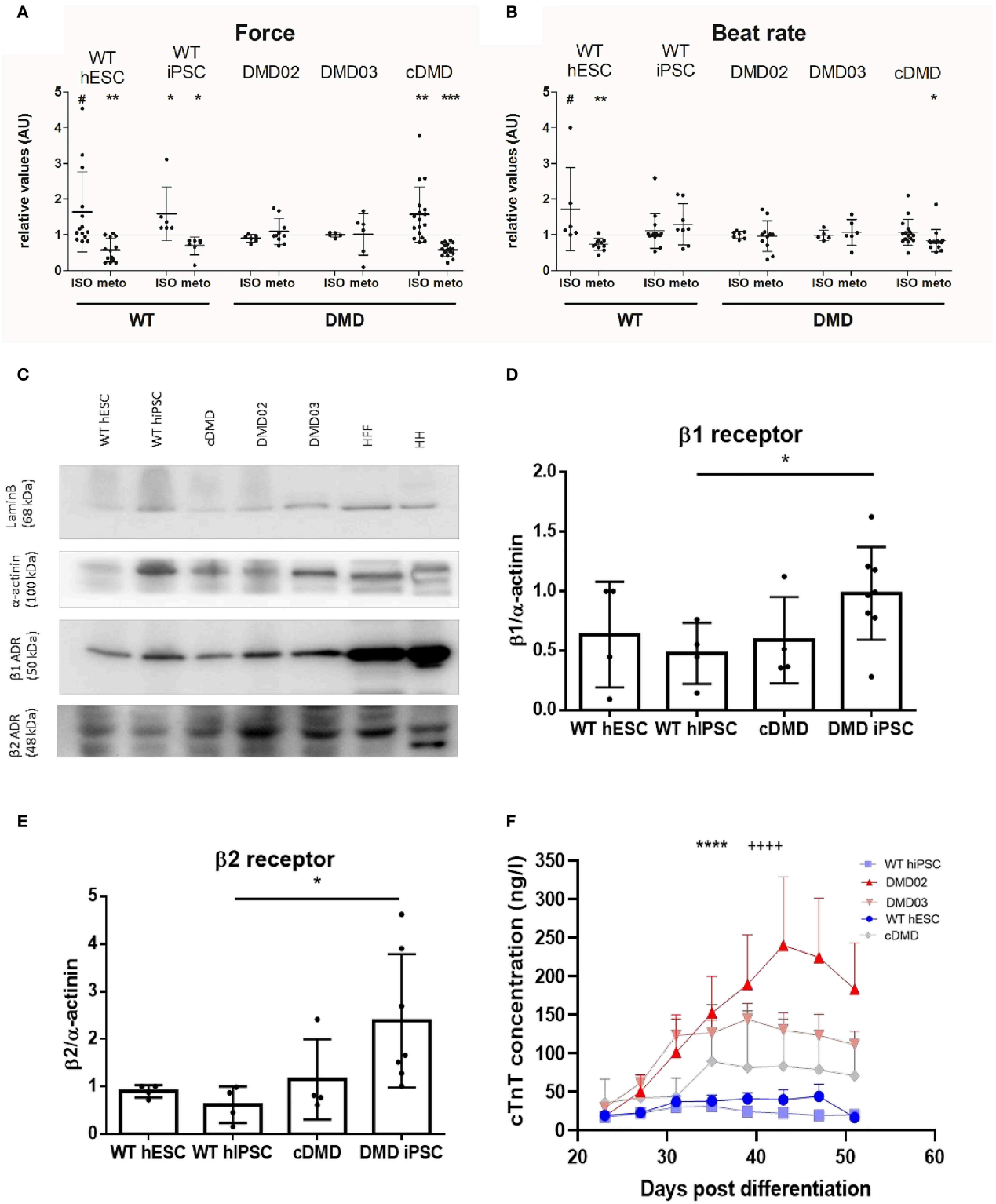



**FIGURE 7 |** DMD-CCs show remodeled β-adrenergic response and increased death. The contraction force and beat rate were measured using an AFM-based method and tested for β adrenergic response with isoproterenol (ISO, activator) and metoprolol (METO, inhibitor) **(A)**. WT-CMs show increase in contraction force ($n$ = ISO/METO: $n$ = 14/13 for WT hESC, $n$ = 6/7 for WT-hiPSC-EBs, $n$ = 6/10 for DMD02 EBs, $n$ = 5/6 for DMD03 EBs, $n$ = 17/17 for cDMD-EBs, exact value for each is represented by • in each graph) and **(B)** beat rate ($n$ = ISO/METO: $n$ = 6/11 for WT hESC, $n$ = 14/8 for WT-hiPSC-EBs, $n$ = 7/11 for DMD02 EBs, $n$ = 5/6 for DMD03 EBs, $n$ = 15/15 for cDMD-EBs, exact value for each is represented by • in each graph) after ISO treatment and decrease in both parameters under METO

*(Continued)*

**FIGURE 7 |** treatment. The DMD-hiPSC-EBs remained unresponsive to any of these stimulations. cDMD derived EBs show similar response in contraction force to its isogenic WT control. The red line represents the ratio of 1 for better orientation in change. Significance calculated by Wilcoxon test (*$p < 0.05$, **$p < 0.01$, ***$p < 0.01$, $^{\#}p < 0.1$) is visualized as asterisks. **(C–E)** Western blot analysis of β receptors shows higher expression of β1 in DMD-hiPSC derived EBs compared to WT-EBs; cDMD line shows similar expression to its isogenic WT control (calculates as β1 signal/actinin signal). β2 receptor showed increased levels in DMD-hiPSC-EBs. Human heart (HH) sample was used as positive control, human foreskin fibroblasts (HFF) as CM negative sample. Lamin B was used as loading control. Exact value for each is represented by • in each graph. Statistical difference was calculated by Mann-Whitney test for both β1 and β2 receptor expression. **(F)** CM death in the EBs was evaluated using free troponin level analysis in the medium. All DMD-EBs show significantly increased free cTnT levels compared to WT-EBs. Statistical difference was calculated using two-way ANOVA with uncorrected Fisher's post hoc test. ****$p < 0.0001$ according to cell line factor (WT vs. DMD) and $++++p < 0.0001$ according to day of differentiation factor.

clear benefit while others showed little effect of β-AR blockade on outcomes signaling lack of response to the modulation (Kajimoto et al., 2006; Matsumura et al., 2010; Viollet et al., 2012). The β-AR responsiveness might as well be linked to the type of mutation of the *DMD* gene, which might explain why one of our models lacked dystrophin expression yet was responsive to adrenergic modulation. Nevertheless, the beat rate and contraction force response to adrenergic modulation in patient-specific DMD-EBs suggested that the human DMD phenotype is accompanied by altered density of the β-AR on the sarcolemma and less sensitive β-AR pathway. The latter can involve a hampered lusitropic effect, resulting in a hypocontractile $Ca^{2+}$-saturated sarcomere (Culligan et al., 2002; Asp et al., 2013).

As a further original contribution, we finally investigated whether ECC alterations and regulatory pathways remodeling were associated in the dish with CCs wasting. Serum concentration of cTnT is a routinely used marker of CMs death, especially for acute myocardial infarction, although with high sensitivity assays it is also a prognostic marker of non-ischemic cardiac diseases (Park et al., 2017). We have indeed observed how even *in vitro* early stage models of DMD undergo progressive CMs injury, with detected levels of free cTnT up to 10 times the one of age-matched control lines. Dystrophin mutations, with severe symptomatology like in Duchenne's or milder like in Becker's, are all characterized with progressive cardiac symptoms stemming from loss of CMs, remodeling of the cardiac tissue with substitutive fibrosis, and ventricular dilation leading to heart failure accompanied by non-CM cell population depletion (Pesl et al., 2020). CM death can be indirectly caused by high levels of cytosolic $Ca^{2+}$, reportedly present in DMD through several mechanisms, which increases proteolysis and triggers mitochondrial dysfunctions with consequent ATP exhaustion (Meyers and Townsend, 2019; Tsurumi et al., 2019). Despite the fact that troponin levels measured by immunoassay methods in the media cannot define the mechanisms of cardiomyocyte injury, nor prove if the cell remains viable after such injury or became apoptotic, our findings confirmed that clinical assays can be used together with our model to follow subclinical stages of DMD cardiac involvement. Remarkably, this progressive CCs death is not correlated with loss of contractility. Pioner at al. demonstrated how up to 100 days of cultivation DMD models preserved their contractile function assuming a hypertrophic phenotype (Pioner et al., 2020). A similar mechanism could explain the similar evidence we observed in our 3D model, where CM depletion might be compensated by surviving CM hypertrophy. This evidence opens further uses of our presented model to study progressive cellular adaptation at different stages of the diseases.

## LIMITATIONS OF THE STUDY

The reported study presents several limitations. The electrophysiological analysis via patch clamp lacks a proper age matching; therefore, the highly variable parameters might have masked mutation-related changes. Furthermore, no channel-specific study was performed to make a causative link between the presented channels overexpression to the calcium handling and contractile alterations observed. We did not directly characterize the age effect on calcium handling and contractility on hPSC-CC. However, we have relied on existent information on the topic to exclude a significant contribution of incomplete maturation to the reported differences.

## CONCLUSIONS

The purpose of this work was to model some key cardiac molecular properties in DMD cardiomyopathy using DMD patient-specific and engineered CRISPR/Cas9 isogenic hPSC derived cardiac cells. Our results indicated that our DMD models in the dish are functionally affected by dystrophin deficiency and recapitulate functional defects and cardiac wasting observed in the disease. This work contributes to determine cardiac defects in DMD patients. It offers an accurate tool to study human cardiomyopathy progression and test therapies in the dish.

## DATA AVAILABILITY STATEMENT

The datasets generated for this study are available on request to the corresponding author.

## ETHICS STATEMENT

The fibroblasts of two DMD patients were derived from skin/muscle biopsies with the patients informed consent and St. Anne's University Hospital (Brno, Czech Republic) Ethics Committee approval under the number 37/2011. Written informed consent to participate in this study was provided by the patient/participants legal guardian.

## AUTHOR CONTRIBUTIONS

All the authors have contributed to the manuscript writing and corrections and were included substantially in the project preparation, conception, and evaluation. SJ has differentiated the cardiomyocytes, ran ICC, PCR, and western blot analyses, evaluated obtained data and interpreted them, prepared the figures, and wrote the draft of the manuscript. AV was included in the experimental design, differentiated cardiomyocytes and performed $Ca^{2+}$ imaging and ICC staining, and helped interpret the data. JP performed the AFM measurements and initial evaluation of the data. FA performed the electrophysiological measurements and interpreted them. MP performed AFM measurement of the EBs. GC participated in AFM measurements and interpretation of the results. AS performed AFM and $Ca^{2+}$ imaging data analysis. IA performed $Ca^{2+}$ imaging of the WT cells and helped interpret the data. VS and HD performed cTnT assays. SK evaluated AFM data. TU performed dystrophin western blot. PS, AL, PD, AM, and VR supervised the project, interpreted the obtained results, and corrected the manuscript. AM and VR were responsible for the experimental design of the project, coordination, and supervision in equal matter.

## FUNDING

This work was supported by the Ministry of Education, Youth, and Sports of the Czech Republic (7AMB13FR011, No. CZ.02.1.01/0.0/0.0/16_013/0001776, No. CZ.02.1.01/0.0/0.0/16_019/0000868), CIISB research infrastructure LM2018127 and supported by funds from the Faculty of Medicine MU to junior researchers SJ and MP. This work was also supported by grants of the European Regional Development Fund (CIISB4HEALTH No. CZ.02.1.01/0.0/0.0/16_013/0001776), South Moravian Centre for International Mobility (SoMoPro No. 2SGA2744), and the European Society of Cardiology (ESC; R12042FF). The French Muscular Dystrophy Association (AFM; project 16073, MNM2 2012, and 20225), the Fondation pour la Recherche Médicale (FRM; SPF20130526710), the PHC Barrande (Duchenstem No. 28379TE), the Institut National pour la Santé et la Recherche Médicale (INSERM) also supported this work.

## SUPPLEMENTARY MATERIAL

The Supplementary Material for this article can be found online at: https://www.frontiersin.org/articles/10.3389/fbioe.2020.00535/full#supplementary-material

## REFERENCES

Acimovic, I., Refaat, M. M., Moreau, A., Salykin, A., Reiken, S., Sleiman, Y., et al. (2018). Post-translational modifications and diastolic calcium leak associated to the novel RyR2-D3638A mutation lead to CPVT in patient-specific hiPSC-derived cardiomyocytes. *J. Clin. Med.* 7:423. doi: 10.3390/jcm7110423

Amedro, P., Vincenti, M., De La Villeon, G., Lavastre, K., Barrea, C., Guillaumont, S., et al. (2019). Speckle-tracking echocardiography in children with duchenne muscular dystrophy: a prospective multicenter controlled cross-sectional study. *J. Am. Soc. Echocardiogr.* 32, 412–422. doi: 10.1016/j.echo.2018.10.017

Andersson, D. C., and Marks, A. R. (2010). Fixing ryanodine receptor Ca leak - a novel therapeutic strategy for contractile failure in heart and skeletal muscle. *Drug Discov. Today Dis. Mech.* 7, e151–e157. doi: 10.1016/j.ddmec.2010.09.009

Andersson, D. C., Meli, A. C., Reiken, S., Betzenhauser, M. J., Umanskaya, A., Shiomi, T., et al. (2012). Leaky ryanodine receptors in β-sarcoglycan deficient mice: a potential common defect in muscular dystrophy. *Skelet. Muscle* 2:9. doi: 10.1186/2044-5040-2-9

Armstrong, L., Tilgner, K., Saretzki, G., Atkinson, S. P., Stojkovic, M., Moreno, R., et al. (2010). Human induced pluripotent stem cell lines show stress defense mechanisms and mitochondrial regulation similar to those of human embryonic stem cells. *Stem Cells* 28, 661–673. doi: 10.1002/stem.307

Asp, M. L., Martindale, J. J., Heinis, F. I., Wang, W., and Metzger, J. M. (2013). Calcium mishandling in diastolic dysfunction: mechanisms and potential therapies. *Biochim. Biophys. Acta* 1833, 895–900. doi: 10.1016/j.bbamcr.2012.09.007

Blake, D. J., Weir, A., Newey, S. E., and Davies, K. E. (2002). Function and genetics of dystrophin and dystrophin-related proteins in muscle. *Physiol. Rev.* 82, 291–329. doi: 10.1152/physrev.00028.2001

Bondue, A., Arbustini, E., Bianco, A., Ciccarelli, M., Dawson, D., De Rosa, M., et al. (2018). Complex roads from genotype to phenotype in dilated cardiomyopathy: scientific update from the working group of myocardial function of the european society of cardiology. *Cardiovasc. Res.* 114, 1287–1303. doi: 10.1093/cvr/cvy122

Bristow, M. R., Ginsburg, R., Minobe, W., Cubicciotti, R. S., Sageman, W. S., Lurie, K., et al. (1982). Decreased catecholamine sensitivity and beta-adrenergic-receptor density in failing human hearts. *N. Engl. J. Med.* 307, 205–211. doi: 10.1056/NEJM198207223070401

Caluori, G., Pribyl, J., Pesl, M., Jelinkova, S., Rotrekl, V., Skladal, P., et al. (2019). Non-invasive electromechanical cell-based biosensors for improved investigation of 3D cardiac models. *Biosens. Bioelectron.* 124–125, 129–135. doi: 10.1016/j.bios.2018.10.021

Carnwath, J. W., and Shotton, D. M. (1987). Muscular dystrophy in the mdx mouse: histopathology of the soleus and extensor digitorum longus muscles. *J. Neurol. Sci.* 80, 39–54. doi: 10.1016/0022-510X(87)90219-X

Chenard, A. A., Becane, H. M., Tertrain, F., de Kermadec, J. M., and Weiss, Y. A. (1993). Ventricular arrhythmia in duchenne muscular dystrophy: prevalence, significance and prognosis. *Neuromuscul. Disord.* 3, 201–206. doi: 10.1016/0960-8966(93)90060-W

Choi, B.-R., Burton, F., and Salama, G. (2002). Cytosolic $Ca^{2+}$ triggers early afterdepolarizations and torsade de pointes in rabbit hearts with type 2 long QT syndrome. *J. Physiol.* 543, 615–631. doi: 10.1113/jphysiol.2002.024570

Clarac, F., Massion, J., and Smith, A. M. (2009). Duchenne, charcot and babinski, three neurologists of la salpetrière hospital, and their contribution to concepts of the central organization of motor synergy. *J. Physiol. Paris* 103, 361–376. doi: 10.1016/j.jphysparis.2009.09.001

Corrado, G., Lissoni, A., Beretta, S., Terenghi, L., Tadeo, G., Foglia-Manzillo, G., et al. (2002). Prognostic value of electrocardiograms, ventricular late potentials, ventricular arrhythmias, and left ventricular systolic dysfunction in patients with Duchenne muscular dystrophy. *Am. J. Cardiol.* 89, 838–841. doi: 10.1016/S0002-9149(02)02195-1

Coulton, G. R., Morgan, J. E., Partridge, T. A., and Sloper, J. C. (1988). The mdx mouse skeletal muscle myopathy: I. A histological, morphometric and biochemical investigation. *Neuropathol. Appl. Neurobiol.* 14, 53–70. doi: 10.1111/j.1365-2990.1988.tb00866.x

Culligan, K., Banville, N., Dowling, P., and Ohlendieck, K. (2002). Drastic reduction of calsequestrin-like proteins and impaired calcium binding in dystrophic mdx muscle. *J. Appl. Physiol.* 92, 435–445. doi: 10.1152/japplphysiol.00903.2001

Danialou, G., Comtois, A. S., Dudley, R., Karpati, G., Vincent, G., Des Rosiers, C., et al. (2001). Dystrophin-deficient cardiomyocytes are abnormally vulnerable

to mechanical stress-induced contractile failure and injury. *FASEB J.* 15, 1655–1657. doi: 10.1096/fj.01-0030fje

de Lucia, C., Eguchi, A., and Koch, W. J. (2018). New insights in cardiac β-adrenergic signaling during heart failure and aging. *Front. Pharmacol.* 9:904. doi: 10.3389/fphar.2018.00904

Dumont, N. A., Wang, Y. X., von Maltzahn, J., Pasut, A., Bentzinger, C. F., Brun, C. E., et al. (2015). Dystrophin expression in muscle stem cells regulates their polarity and asymmetric division. *Nat. Med.* 21, 1455–1463. doi: 10.1038/nm.3990

Dvorak, P., Dvorakova, D., Koskova, S., Vodinska, M., Najvirtova, M., Krekac, D., et al. (2005). Expression and potential role of fibroblast growth factor 2 and its receptors in human embryonic stem cells. *Stem Cells* 23, 1200–1211. doi: 10.1634/stemcells.2004-0303

Eisen, B., Ben Jehuda, R., Cuttitta, A. J., Mekies, L. N., Shemer, Y., Baskin, P., et al. (2019). Electrophysiological abnormalities in induced pluripotent stem cell-derived cardiomyocytes generated from duchenne muscular dystrophy patients. *J. Cell. Mol. Med.* 23, 2125–2135. doi: 10.1111/jcmm.14124

Engelhardt, S., Hein, L., Wiesmann, F., and Lohse, M. J. (1999). Progressive hypertrophy and heart failure in beta1-adrenergic receptor transgenic mice. *Proc. Natl. Acad. Sci. U.S.A.* 96, 7059–7064. doi: 10.1073/pnas.96.12.7059

Fauconnier, J., Thireau, J., Reiken, S., Cassan, C., Richard, S., Matecki, S., et al. (2010). Leaky RyR2 trigger ventricular arrhythmias in duchenne muscular dystrophy. *Proc. Natl. Acad. Sci. U.S.A.* 107, 1559–1564. doi: 10.1073/pnas.0908540107

Fayssoil, A., Nardi, O., Orlikowski, D., and Annane, D. (2010). Cardiomyopathy in duchenne muscular dystrophy: pathogenesis and therapeutics. *Heart Fail Rev.* 15, 103–107. doi: 10.1007/s10741-009-9156-8

Finsterer, J., and Stöllberger, C. (2003). The heart in human dystrophinopathies. *Cardiology* 99, 1–19. doi: 10.1159/000068446

Gerke, V., Creutz, C. E., and Moss, S. E. (2005). Annexins: linking $Ca^{2+}$ signalling to membrane dynamics. *Nat. Rev. Mol. Cell Biol.* 6, 449–461. doi: 10.1038/nrm1661

Hajjar, R. J., Liao, R., Young, J. B., Fuleihan, F., Glass, M. G., and Gwathmey, J. K. (1993). Pathophysiological and biochemical characterisation of an avian model of dilated cardiomyopathy: comparison to findings in human dilated cardiomyopathy. *Cardiovasc. Res.* 27, 2212–2221. doi: 10.1093/cvr/27.12.2212

He, J.-Q., Ma, Y., Lee, Y., Thomson, J. A., and Kamp, T. J. (2003). Human embryonic stem cells develop into multiple types of cardiac myocytes: action potential characterization. *Circ. Res.* 93, 32–39. doi: 10.1161/01.RES.0000080317.92718.99

Hess, G. P. D., Horsch, A. D., and Zdunek, D. D. (2008). *Means and Methods for Optimization of Diagnostic and Therapeutic Approaches in Chronic Artery Disease Based on the Detection of Troponin T and NT-proBNP*. Available online at: https://patents.google.com/patent/EP1925943A1/en/en22 (accessed December 14, 2019).

Himmrich, E., Popov, S., Liebrich, A., Rosocha, S., Zellerhoff, C., Nowak, B., et al. (2000). [Hidden intracardiac conduction disturbances and their spontaneous course in patients with progressive muscular dystrophy]. *Z Kardiol.* 89, 592–598. doi: 10.1007/s003920070208

Hwang, H. S., Kryshtal, D. O., Feaster, T. K., Sánchez-Freire, V., Zhang, J., Kamp, T. J., et al. (2015). Comparable calcium handling of human iPSC-derived cardiomyocytes generated by multiple laboratories. *J. Mol. Cell. Cardiol.* 85, 79–88. doi: 10.1016/j.yjmcc.2015.05.003

Inomata, K., Aoto, T., Binh, N. T., Okamoto, N., Tanimura, S., Wakayama, T., et al. (2009). Genotoxic stress abrogates renewal of melanocyte stem cells by triggering their differentiation. *Cell* 137, 1088–1099. doi: 10.1016/j.cell.2009.03.037

International Stem Cell Initiative, Adewumi, O., Aflatoonian, B., Ahrlund-Richter, L., Amit, M., Andrews, P. W., et al. (2007). Characterization of human embryonic stem cell lines by the international stem cell initiative. *Nat. Biotechnol.* 25, 803–816. doi: 10.1038/nbt1318

Jelinkova, S., Fojtik, P., Kohutova, A., Vilotic, A., Marková, L., Pesl, M., et al. (2019a). Dystrophin deficiency leads to genomic instability in human pluripotent stem cells via NO synthase-induced oxidative stress. *Cells* 8:53. doi: 10.3390/cells8010053

Jelinkova, S., Markova, L., Pesl, M., Valáškova, I., Makaturová, E., Jurikova, L., et al. (2019b). Generation of two duchenne muscular dystrophy patient-specific induced pluripotent stem cell lines DMD02 and DMD03 (MUNIi001-A and MUNIi003-A). *Stem Cell Res.* 40:101562. doi: 10.1016/j.scr.2019.101562

Johnson, D. M., Heijman, J., Bode, E. F., Greensmith, D. J., van der Linde, H., Abi-Gerges, N., et al. (2013). Diastolic spontaneous calcium release from the sarcoplasmic reticulum increases beat-to-beat variability of repolarization in canine ventricular myocytes after β-adrenergic stimulation. *Circ. Res.* 112, 246–256. doi: 10.1161/CIRCRESAHA.112.275735

Jung, C., Martins, A. S., Niggli, E., and Shirokova, N. (2008). Dystrophic cardiomyopathy: amplification of cellular damage by $Ca^{2+}$ signalling and reactive oxygen species-generating pathways. *Cardiovasc. Res.* 77, 766–773. doi: 10.1093/cvr/cvm089

Kajimoto, H., Ishigaki, K., Okumura, K., Tomimatsu, H., Nakazawa, M., Saito, K., et al. (2006). Beta-blocker therapy for cardiac dysfunction in patients with muscular dystrophy. *Circ. J.* 70, 991–994. doi: 10.1253/circj.70.991

Kamdar, F., and Garry, D. J. (2016). Dystrophin-deficient cardiomyopathy. *J. Am. Coll. Cardiol.* 67, 2533–2546. doi: 10.1016/j.jacc.2016.02.081

Koenig, X., Dysek, S., Kimbacher, S., Mike, A. K., Cervenka, R., Lukacs, P., et al. (2011). Voltage-gated ion channel dysfunction precedes cardiomyopathy development in the dystrophic heart. *PLoS ONE* 6:e20300. doi: 10.1371/journal.pone.0020300

Koenig, X., Rubi, L., Obermair, G. J., Cervenka, R., Dang, X. B., Lukacs, P., et al. (2014). Enhanced currents through L-type calcium channels in cardiomyocytes disturb the electrophysiology of the dystrophic heart. *Am. J. Physiol. Heart Circ. Physiol.* 306, H564–H573. doi: 10.1152/ajpheart.00441.2013

Krutá, M., Bálek, L., Hejnová, R., Dobšáková, Z., Eiselleová, L., Matulka, K., et al. (2013). Decrease in abundance of apurinic/apyrimidinic endonuclease causes failure of base excision repair in culture-adapted human embryonic stem cells. *Stem Cells* 31, 693–702. doi: 10.1002/stem.1312

Krutá, M., Šeneklová, M., Raška, J., Salykin, A., Zerzánková, L., Pešl, M., et al. (2014). Mutation frequency dynamics in HPRT locus in culture-adapted human embryonic stem cells and induced pluripotent stem cells correspond to their differentiated counterparts. *Stem Cells Dev.* 23, 2443–2454. doi: 10.1089/scd.2013.0611

Li, Y., Zhang, S., Zhang, X., Li, J., Ai, X., Zhang, L., et al. (2014). Blunted cardiac beta-adrenergic response as an early indication of cardiac dysfunction in duchenne muscular dystrophy. *Cardiovasc. Res.* 103, 60–71. doi: 10.1093/cvr/cvu119

Lu, S., and Hoey, A. (2000). Changes in function of cardiac receptors mediating the effects of the autonomic nervous system in the muscular dystrophy (MDX) mouse. *J. Mol. Cell. Cardiol.* 32, 143–152. doi: 10.1006/jmcc.1999.1063

Mah, J. K., Korngut, L., Dykeman, J., Day, L., Pringsheim, T., and Jette, N. (2014). A systematic review and meta-analysis on the epidemiology of duchenne and becker muscular dystrophy. *Neuromuscul. Disord.* 24, 482–491. doi: 10.1016/j.nmd.2014.03.008

Manzur, A. Y., Kinali, M., and Muntoni, F. (2008). Update on the management of duchenne muscular dystrophy. *Arch. Dis. Child.* 93, 986–990. doi: 10.1136/adc.2007.118141

Markham, L. W., Michelfelder, E. C., Border, W. L., Khoury, P. R., Spicer, R. L., Wong, B. L., et al. (2006). Abnormalities of diastolic function precede dilated cardiomyopathy associated with Duchenne muscular dystrophy. *J. Am. Soc. Echocardiogr.* 19, 865–871. doi: 10.1016/j.echo.2006.02.003

Matsumura, T., Tamura, T., Kuru, S., Kikuchi, Y., and Kawai, M. (2010). Carvedilol can prevent cardiac events in duchenne muscular dystrophy. *Intern. Med.* 49, 1357–1363. doi: 10.2169/internalmedicine.49.3259

McNally, E. M., Kaltman, J. R., Benson, D. W., Canter, C. E., Cripe, L. H., Duan, D., et al. (2015). Contemporary cardiac issues in duchenne muscular dystrophy. *Circulation* 131, 1590–1598. doi: 10.1161/CIRCULATIONAHA.114.015151

Meyers, T. A., Heitzman, J. A., Krebsbach, A. M., Aufdembrink, L. M., Hughes, R., Bartolomucci, A., et al. (2019). Acute AT1R blockade prevents isoproterenol-induced injury in mdx hearts. *J. Mol. Cell. Cardiol.* 128, 51–61. doi: 10.1016/j.yjmcc.2019.01.013

Meyers, T. A., and Townsend, D. (2019). Cardiac pathophysiology and the future of cardiac therapies in duchenne muscular dystrophy. *Int. J. Mol. Sci.* 20:4098. doi: 10.3390/ijms20174098

Oda, T., Yang, Y., Uchinoumi, H., Thomas, D. D., Chen-Izu, Y., Kato, T., et al. (2015). Oxidation of ryanodine receptor (RyR) and calmodulin enhance Ca release and pathologically alter, RyR structure and calmodulin affinity. *J. Mol. Cell. Cardiol.* 85, 240–248. doi: 10.1016/j.yjmcc.2015.06.009

Panovský, R., Pešl, M., Holeček, T., Máchal, J., Feitová, V., Mrázová, L., et al. (2019). Cardiac profile of the czech population of duchenne muscular dystrophy patients: a cardiovascular magnetic resonance study with T1 mapping. *Orphanet J. Rare Dis.* 14:10. doi: 10.1186/s13023-018-0986-0

Papa, A. A., D'Ambrosio, P., Petillo, R., Palladino, A., and Politano, L. (2017). Heart transplantation in patients with dystrophinopathic cardiomyopathy: review of the literature and personal series. *Intractable Rare Dis Res.* 6, 95–101. doi: 10.5582/irdr.2017.01024

Park, K. C., Gaze, D. C., Collinson, P. O., and Marber, M. S. (2017). Cardiac troponins: from myocardial infarction to chronic disease. *Cardiovasc. Res.* 113, 1708–1718. doi: 10.1093/cvr/cvx183

Patrick Gonzalez, J., Ramachandran, J., Xie, L.-H., Contreras, J. E., and Fraidenraich, D. (2015). Selective connexin43 inhibition prevents isoproterenol-induced arrhythmias and lethality in muscular dystrophy mice. *Sci. Rep.* 5:13490. doi: 10.1038/srep13490

Pesl, M., Acimovic, I., Pribyl, J., Hezova, R., Vilotic, A., Fauconnier, J., et al. (2014). Forced aggregation and defined factors allow highly uniform-sized embryoid bodies and functional cardiomyocytes from human embryonic and induced pluripotent stem cells. *Heart Vessels* 29, 834–846. doi: 10.1007/s00380-013-0436-9

Pesl, M., Jelinkova, S., Caluori, G., Holicka, M., Krejci, J., Nemec, P., et al. (2020). Cardiovascular progenitor cells and tissue plasticity are reduced in a myocardium affected by Becker muscular dystrophy. *Orphanet J. Rare Dis.* 15:65. doi: 10.1186/s13023-019-1257-4

Pesl, M., Pribyl, J., Acimovic, I., Vilotic, A., Jelinkova, S., Salykin, A., et al. (2016). Atomic force microscopy combined with human pluripotent stem cell derived cardiomyocytes for biomechanical sensing. *Biosens. Bioelectron.* 85, 751–757. doi: 10.1016/j.bios.2016.05.073

Peterson, J. M., Wang, D. J., Shettigar, V., Roof, S. R., Canan, B. D., Bakkar, N., et al. (2018). NF-κB inhibition rescues cardiac function by remodeling calcium genes in a duchenne muscular dystrophy model. *Nat. Commun.* 9:3431. doi: 10.1038/s41467-018-05910-1

Pioner, J. M., Guan, X., Klaiman, J. M., Racca, A. W., Pabon, L., Muskheli, V., et al. (2020). Absence of full-length dystrophin impairs normal maturation and contraction of cardiomyocytes derived from human-induced pluripotent stem cells. *Cardiovasc. Res*. 116, 368–382.

Pribyl, J., Pešl, M., Caluori, G., Acimovic, I., Jelinkova, S., Dvorak, P., et al. (2019). Biomechanical characterization of human pluripotent stem cell-derived cardiomyocytes by use of atomic force microscopy. *Methods Mol. Biol.* 1886, 343–353. doi: 10.1007/978-1-4939-8894-5_20

Puzzo, D., Raiteri, R., Castaldo, C., Capasso, R., Pagano, E., Tedesco, M., et al. (2016). CL316,243, a β3-adrenergic receptor agonist, induces muscle hypertrophy and increased strength. *Sci. Rep.* 5:37504. doi: 10.1038/srep37504

Qu, C., Puttonen, K. A., Lindeberg, H., Ruponen, M., Hovatta, O., Koistinaho, J., et al. (2013). Chondrogenic differentiation of human pluripotent stem cells in chondrocyte co-culture. *Int. J. Biochem. Cell Biol.* 45, 1802–1812. doi: 10.1016/j.biocel.2013.05.029

Rengo, G., Lymperopoulos, A., and Koch, W. J. (2009). Future g protein-coupled receptor targets for treatment of heart failure. *Curr. Treat. Options Cardiovasc. Med.* 11, 328–338. doi: 10.1007/s11936-009-0033-5

Rossi, D. J., Bryder, D., Seita, J., Nussenzweig, A., Hoeijmakers, J., and Weissman, I. L. (2007). Deficiencies in DNA damage repair limit the function of haematopoietic stem cells with age. *Nature* 447, 725–729. doi: 10.1038/nature05862

Sadek, A. A., Mahmoud, S. M., El-Aal, M. A., Allam, A. A., and El-Halim, W. I. A. (2017). Evaluation of cardiac functions in children with duchenne muscular dystrophy: a prospective case-control study. *Electron. Physician.* 9, 5732–5739. doi: 10.19082/5732

Sato, H., Shiraishi, I., Takamatsu, T., and Hamaoka, K. (2007). Detection of TUNEL-positive cardiomyocytes and c-kit-positive progenitor cells in children with congenital heart disease. *J. Mol. Cell. Cardiol.* 43, 254–261. doi: 10.1016/j.yjmcc.2007.05.011

Shirokova, N., and Niggli, E. (2013). Cardiac phenotype of duchenne muscular dystrophy: insights from cellular studies. *J. Mol. Cell. Cardiol.* 58, 217–224. doi: 10.1016/j.yjmcc.2012.12.009

Skeberdis, V. A. (2004). Structure and function of beta3-adrenergic receptors. *Medicina (Kaunas).* 40, 407–413.

Stehlíková, K., Skálová, D., Zídková, J., Haberlová, J., Vohánka, S., Mazanec, R., et al. (2017). Muscular dystrophies and myopathies: the spectrum of mutated genes in the czech republic. *Clin. Genet.* 91, 463–469. doi: 10.1111/cge.12839

Tsurumi, F., Baba, S., Yoshinaga, D., Umeda, K., Hirata, T., Takita, J., et al. (2019). The intracellular $Ca^{2+}$ concentration is elevated in cardiomyocytes differentiated from hiPSCs derived from a duchenne muscular dystrophy patient. *PLoS ONE* 14:e0213768. doi: 10.1371/journal.pone.0213768

Villa Chet, R., Czosek Richard, J., Ahmed, H., Khoury Philip, R., Anderson Jeffrey, B., Knilans Timothy, K., et al. (2015). Ambulatory monitoring and arrhythmic outcomes in pediatric and adolescent patients with duchenne muscular dystrophy. *J. Am. Heart Assoc.* 5:e002620. doi: 10.1161/JAHA.115.002620

Viollet, L., Thrush, P. T., Flanigan, K. M., Mendell, J. R., and Allen, H. D. (2012). Effects of angiotensin-converting enzyme inhibitors and/or beta blockers on the cardiomyopathy in duchenne muscular dystrophy. *Am. J. Cardiol.* 110, 98–102. doi: 10.1016/j.amjcard.2012.02.064

Voigt, N., Li, N., Wang, Q., Wang, W., Trafford, A. W., Abu-Taha, I., et al. (2012). Enhanced sarcoplasmic reticulum $Ca^{2+}$-leak and increased Na+-Ca2+-exchanger function underlie delayed afterdepolarizations in patients with chronic atrial fibrillation. *Circulation* 125, 2059–2070. doi: 10.1161/CIRCULATIONAHA.111.067306

Vry, J., Gramsch, K., Rodger, S., Thompson, R., Steffensen, B. F., Rahbek, J., et al. (2016). European cross-sectional survey of current care practices for duchenne muscular dystrophy reveals regional and age-dependent differences. *J. Neuromuscul. Dis.* 3, 517–527. doi: 10.3233/JND-160185

Wagner, K. R., Lechtzin, N., and Judge, D. P. (2007). Current treatment of adult duchenne muscular dystrophy. *Biochim. Biophys. Acta* 1772, 229–237. doi: 10.1016/j.bbadis.2006.06.009

Weiss, J. N., Garfinkel, A., Karagueuzian, H. S., Chen, P.-S., and Qu, Z. (2010). Early afterdepolarizations and cardiac arrhythmias. *Heart Rhythm.* 7, 1891–1899. doi: 10.1016/j.hrthm.2010.09.017

Williams, I. A., and Allen, D. G. (2007). Intracellular calcium handling in ventricular myocytes from mdx mice. *Am. J. Physiol. Heart Circ. Physiol.* 292, H846–H855. doi: 10.1152/ajpheart.00688.2006

Zhu, R., Millrod, M. A., Zambidis, E. T., and Tung, L. (2016). Variability of action potentials within and among cardiac cell clusters derived from human embryonic stem cells. *Sci. Rep.* 6:18544. doi: 10.1038/srep18544

**Conflict of Interest:** The authors declare that the research was conducted in the absence of any commercial or financial relationships that could be construed as a potential conflict of interest.

*Copyright © 2020 Jelinkova, Vilotic, Pribyl, Aimond, Salykin, Acimovic, Pesl, Caluori, Klimovic, Urban, Dobrovolna, Soska, Skladal, Lacampagne, Dvorak, Meli and Rotrekl. This is an open-access article distributed under the terms of the Creative Commons Attribution License (CC BY). The use, distribution or reproduction in other forums is permitted, provided the original author(s) and the copyright owner(s) are credited and that the original publication in this journal is cited, in accordance with accepted academic practice. No use, distribution or reproduction is permitted which does not comply with these terms.*

frontiers in Pharmacology

ORIGINAL RESEARCH
published: 17 January 2022
doi: 10.3389/fphar.2021.789730

# Aminophylline Induces Two Types of Arrhythmic Events in Human Pluripotent Stem Cell–Derived Cardiomyocytes

*Simon Klimovic[1,2,3†], Martin Scurek[4,5†], Martin Pesl[2,6,7†], Deborah Beckerova[2,6], Sarka Jelinkova[2], Tomas Urban[2,7], Daniil Kabanov[1,2,3], Zdenek Starek[6,7], Marketa Bebarova[8], Jan Pribyl[1], Vladimir Rotrekl[2,6] and Kristian Brat[4,5,6*†]*

[1]CEITEC, Masaryk University, Brno, Czechia, [2]Department of Biology, Faculty of Medicine, Masaryk University, Brno, Czechia, [3]Department of Biochemistry, Faculty of Science, Masaryk University, Brno, Czechia, [4]Department of Respiratory Diseases, University Hospital Brno, Brno, Czechia, [5]Faculty of Medicine, Masaryk University, Brno, Czechia, [6]International Clinical Research Center, St. Anne's University Hospital, Brno, Czechia, [7]First Department of Internal Medicine—Cardioangiology, Faculty of Medicine, St. Anne's University Hospital, Masaryk University, Brno, Czechia, [8]Department of Physiology, Faculty of Medicine, Masaryk University, Brno, Czechia

OPEN ACCESS

**Edited by:**
*Paulo Correia-de-Sá, University of Porto, Portugal*

**Reviewed by:**
*Bruno Bragança, Centro Hospitalar do Tâmega e Sousa, Portugal, Portugal*
*Jean-Sebastien Rougier, University of Bern, Switzerland*

***Correspondence:**
*Kristian Brat*
*Brat.Kristian@fnbrno.cz*

*[†]These authors have contributed equally to this work*

**Specialty section:**
*This article was submitted to Cardiovascular and Smooth Muscle Pharmacology, a section of the journal Frontiers in Pharmacology*

**Received:** *05 October 2021*
**Accepted:** *17 November 2021*
**Published:** *17 January 2022*

**Citation:**
*Klimovic S, Scurek M, Pesl M, Beckerova D, Jelinkova S, Urban T, Kabanov D, Starek Z, Bebarova M, Pribyl J, Rotrekl V and Brat K (2022) Aminophylline Induces Two Types of Arrhythmic Events in Human Pluripotent Stem Cell–Derived Cardiomyocytes. Front. Pharmacol. 12:789730. doi: 10.3389/fphar.2021.789730*

Cardiac side effects of some pulmonary drugs are observed in clinical practice. Aminophylline, a methylxanthine bronchodilator with documented proarrhythmic action, may serve as an example. Data on the action of aminophylline on cardiac cell electrophysiology and contractility are not available. Hence, this study was focused on the analysis of changes in the beat rate and contraction force of human pluripotent stem cell–derived cardiomyocytes (hPSC-CMs) and HL-1 cardiomyocytes in the presence of increasing concentrations of aminophylline (10 μM–10 mM in hPSC-CM and 8–512 μM in HL-1 cardiomyocytes). Basic biomedical parameters, namely, the beat rate (BR) and contraction force, were assessed in hPSC-CMs using an atomic force microscope (AFM). The beat rate changes under aminophylline were also examined on the HL-1 cardiac muscle cell line via a multielectrode array (MEA). Additionally, calcium imaging was used to evaluate the effect of aminophylline on intracellular $Ca^{2+}$ dynamics in HL-1 cardiomyocytes. The BR was significantly increased after the application of aminophylline both in hPSC-CMs (with 10 mM aminophylline) and in HL-1 cardiomyocytes (with 256 and 512 μM aminophylline) in comparison with controls. A significant increase in the contraction force was also observed in hPSC-CMs with 10 μM aminophylline (a similar trend was visible at higher concentrations as well). We demonstrated that all aminophylline concentrations significantly increased the frequency of rhythm irregularities (extreme interbeat intervals) both in hPSC-CMs and HL-1 cells. The occurrence of the calcium sparks in HL-1 cardiomyocytes was significantly increased with the presence of 512 μM aminophylline. We conclude that the observed aberrant cardiomyocyte response to aminophylline suggests an arrhythmogenic potential

**Abbreviations:** sAFM, atomic force microscope; bpm, beats per minute; CBBs, cell-based biosensors; CCTL, center for cell therapy line; CM, cardiomyocyte; EB, embryoid body; ECC, excitation–contraction coupling; hESC, human embryonic stem cell; hiPSC, human-induced pluripotent stem cell; hPSC, human pluripotent stem cell (hESC and hiPSC); hPSC-CMs, pluripotent stem cell–derived cardiomyocytes.

of the drug. The acquired data represent a missing link between the arrhythmic events related to the aminophylline/theophylline treatment in clinical practice and describe cellular mechanisms of methylxanthine arrhythmogenesis. An AFM combined with hPSC-CMs may serve as a robust platform for direct drug effect screening.

**Keywords: aminophylline, IPSC, hESC, cardiomyocytes, drug cardiotoxicity, atomic force microscopy, arrhythmogenic effects, methylxanthines**

## INTRODUCTION

Theophylline (1,3-dimethylxanthine) and its more soluble form aminophylline (a complex of two theophylline molecules and ethylenediamine) are well-known bronchodilators used mostly for therapy of chronic obstructive pulmonary disease (COPD) and asthma. These drugs are also recommended for the treatment of emphysema (Zatloukal et al., 2020). Other indications have been suggested, for example, treatment of apnea in premature neonates (Ye et al., 2019). Unfortunately, a narrow therapeutic range and frequent adverse effects make their use controversial (Singh et al., 2019). An increased mortality rate in theophylline users has been reported by multiple research teams (Lee et al., 2009; Horita et al., 2016). A higher percentage of cardiovascular deaths was observed in asthma patients who received aminophylline (Suissa et al., 1996), as well as in patients with COPD (Lee et al., 2009), and also in a general patient population overdosed with theophylline (Shannon, 1999).

The adverse effects of theophylline/aminophylline include arrhythmias, even at their therapeutic plasma concentrations (Bittar and Friedman, 1991). In a meta-analysis of several randomized clinical trials, 13% incidence of arrhythmias or palpitations after intravenous aminophylline infusion has been observed (Nair et al., 2012). More than 20% of patients experience cardiac arrhythmias during an aminophylline overdose episode (Shannon, 1999). Supraventricular arrhythmias have been observed most frequently, usually represented by atrial fibrillation (AF) (Varriale and Ramaprasad, 1993; Huerta et al., 2005). Concurrently, COPD is an independent risk factor of AF (Goudis, 2017). The risk of arrhythmias is further enhanced by hypokalemia (Hoppe et al., 2018), which may develop as a side effect of aminophylline treatment, particularly occurring in cases of intentional overdose (Ellis, 1985; Charytan and Jansen, 2003).

Mechanisms of theophylline-/aminophylline-induced arrhythmias are not clear. It is well known that methylxanthines non-specifically inhibit phosphodiesterases (hence increasing the cAMP level) and adenosine receptors (Ukena et al., 1993). These effects may explain the sinus tachycardia often observed in clinical practice. In contrast, this does not explain the origin of AF associated with aminophylline treatment. Effects of theophylline/aminophylline on cardiac electrophysiology were studied mostly in animal models (Komadina et al., 1992; Onodera et al., 2001; Shamsuzzaman et al., 2016). However, a conclusive explanation of their proarrhythmic action has not been provided, and data from human cardiomyocytes (CMs) embedded in cardiac syncytia have been missing completely.

This study was aimed to reveal changes of basic functional characteristics (contraction force and beat rate) of human cardiac tissues induced by aminophylline at a wide range of concentrations. A clinically relevant model was employed, for example, 3D structures called embryoid bodies (EBs) derived from human pluripotent stem cells subsequently differentiated into cardiomyocytes (hPSC-CMs). The model was originally described in previous studies (Burridge et al., 2012; Pesl et al., 2014). Its functional properties were further validated using atomic force microscopy (Liu et al., 2012; Dinarelli et al., 2018; Pribyl et al., 2019), a method enabling real-time monitoring of contractions and thus also beating properties of single cardiomyocytes or cardiac cell clusters, alone or in combination with other methods such as microelectrode array (Caluori et al., 2019b) or calcium imaging (Odstrcilik et al., 2015; Caluori et al., 2019a). This model was recently used for disease modeling in studies by Acimovic et al., 2018; Jelinkova et al., 2019. The effects of aminophylline were further validated on an independent model of HL-1 cardiomyocyte cells. The overall scheme of all experiments within this study is presented in **Figure 1**. This approach has provided the first experimental data well-corresponding with the aminophylline-induced arrhythmias observed in clinical medicine.

## MATERIALS AND METHODS

### Cell Cultivation

The hESC line CCTL14 (46 XX) derived at Masaryk University, Brno, and previously characterized (International Stem Cell Initiative et al., 2007) was routinely maintained on a feeder layer of mitotically inactivated mouse embryonic fibroblasts as previously described (Dvorak et al., 2005; Krutá et al., 2014; Jelinkova et al., 2020).

Differentiation into CMs via embryoid bodies (EBs) and measurements by an AFM were performed as previously described (Pesl et al., 2014), with minor modifications. Briefly, hESC colonies were collected 4 days after seeding and subsequently broken down into smaller clumps which were seeded into the EB medium (86% KO DMEM, 10% FBS, 1% L-glutamine, 1% penicillin/streptomycin, 1% non-essential amino acids, 0.1 mM 2-mercaptoethanol, and 10 μg/ml ascorbic acid) with 10 ng/ml BMP4 (R&D) and placed in hypoxic conditions (5% $O_2$, 5% $CO_2$,) where they spontaneously formed EBs. After 3 days, the medium was removed and replaced with fresh EB medium supplemented with 5 ng/ml FGF2 (Peprotech), 10 ng/ml BMP4, and 6 ng/ml activin A (R&D) for a 4-day incubation. A 3-day incubation in EB

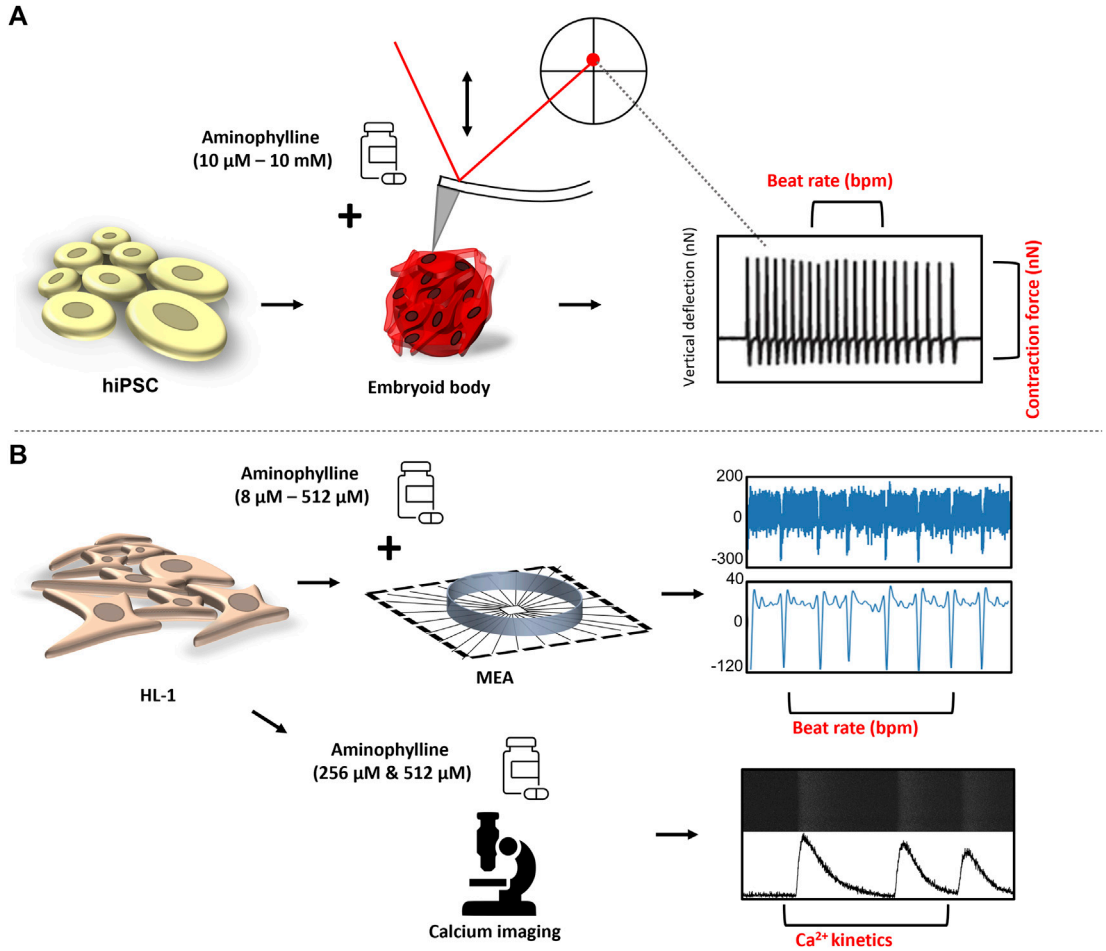



**FIGURE 1 |** Experimental design: **(A)** hPSCs were differentiated in the form of EBs into contracting 3D clusters of cardiomyocytes, and under the influence of increasing concentrations of aminophylline, the mechanocardiogram (MCG) was recorded was recorded by an atomic force microscope. The BR and contraction force values of each contractive event were further analyzed and compared. **(B)** Field potential by the multielectrode array (MEA) system, together with intrinsic $Ca^{2+}$ kinetics via Fluo-8 AM, a calcium-binding dye, was assessed on HL-1 cells to further confirm the arrhythmogenic effect of aminophylline.

medium supplemented with 10 ng/ml VEGF (R&D) and 10 µM IWR1 (R&D). The next induction medium was the EB medium supplemented with 10 ng/ml VEGF and 5 ng/ml FGF2, with a medium exchange every 4 days. After four days in this medium (day 14 of differentiation), the EBs were transferred into a normoxic incubator (21% $O_2$, 5% $CO_2$) for the remaining 8 days of this induction period. From then onward, EBs remained in normoxia and were fed with the EB medium every 4 days until analysis. Beating EBs were selected and transferred on a gelatin-coated PM3 dish to adhere to for measurement. These cellular constructs of the cardiac syncytium were coupled to an AFM force sensor to perform a high-fidelity contraction pattern as an hPSC-CM–based biosensor (Pesl et al., 2014). The constant size of clusters of hPSC-CMs allows comparable and stable beating pattern evaluation allowing for force- and rhythm-related drug effect tracking.

For the immunocytochemistry experiment, either whole or dissociated EBs attached on coverslips were fixed with 4% PFA, blocked and permeabilized by 1% BSA (Sigma) in 0,1% Triton-X (Sigma) or 0,05% TWEEN (Sigma) in PBS, and incubated with anti–troponin T antibody (1:5,000, Cell Signaling, 5,593, Rb) overnight in 4 C. Anti-rabbit Alexa 594 (1:500, Invitrogen) was left to incubate for an hour at room temperature, and the slips were mounted on slides with Mowiol containing DAPI (Sigma). The images were obtained using a Zeiss LSM 700 confocal microscope.

The contracting clusters were previously checked for expression and checked by immunostaining for cardiac troponin T (cTnT) and ryanodine receptor RyR2 as described elsewhere (Pesl et al., 2014; Souidi et al., 2021). The expression of myosin heavy chain MYH6/7 and MYH7, RyR2, and the striated pattern of cTnT in dissociated cardiomyocytes was used to assess the progress in CM maturation. The clusters consisted of all three CM subtypes as described elsewhere; in brief, nodal-like CMs had an AP duration at 90% of repolarization shorter than 100 ms (about 16%), slightly more frequent were atrial-like cells, and recorded AP mainly demonstrated a typical ventricular-like

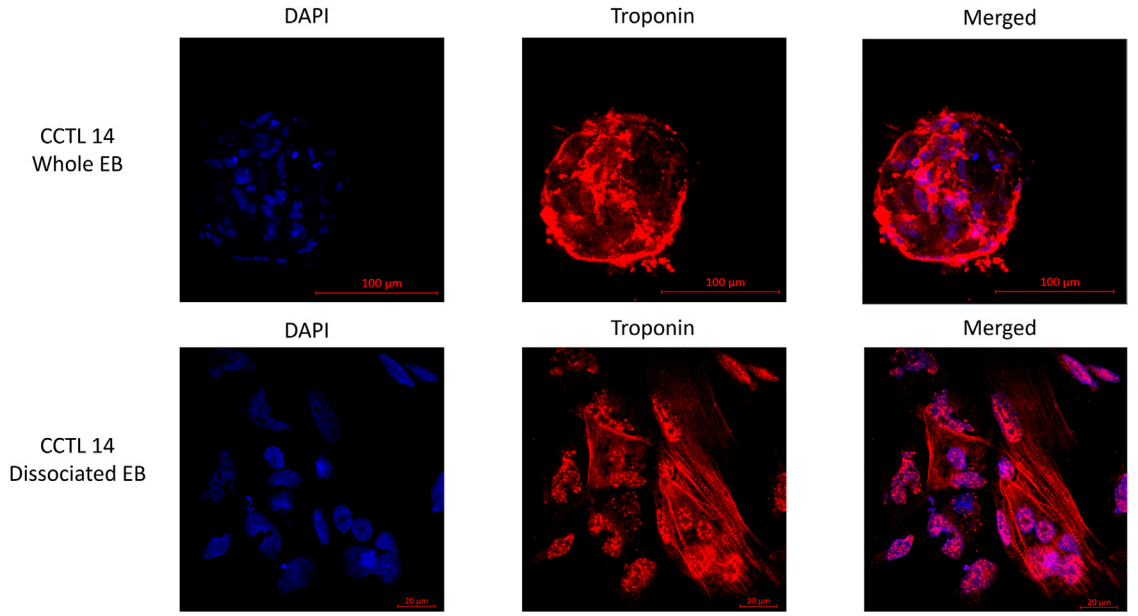



**FIGURE 2 |** Fluorescence staining of whole and dissociated CCTL14 EBs (cell cluster) illustrates the presence of matured cardiomyocytes identified by the presence of troponin T (red color); cells are localized with DAPI staining of the nucleus (blue color).

shape (Acimovic et al., 2018). EB responses to basic heart modulators, such as β adrenoceptor agonist and blocker, isoproterenol, and metoprolol, were previously measured (**Supplementary Figure S1**).

EBs from the same cultivation batch were checked for the presence of cTnT in the clusters as well as in the dissociated EBs by immunostaining to demonstrate the batch-to-batch differentiation consistency (**Figure 2**).

The HL-1 Cardiac Muscle Cell Line (Sigma) was routinely maintained on fibronectin-coated dishes in Claycomb medium (Sigma) supplemented with 10% FBS, 100 U/ml:100 µg/ml penicillin:streptomycin, 0.1 mM norepinephrine, and 2 mM L-glutamine. The cells were passaged with trypsin after reaching full confluency, usually every 3–4 days, in a ratio of 1:3. For experiments with MEA, the HL-1 cells were cultivated on MEA chips coated with fibronectin in 0.02% gelatin (5 mg/ml; Sigma). The HL-1 response to β-adrenoceptor agonist isoproterenol was measured (**Supplementary Figure S1**).

## Atomic Force Microscopy Measurements

NanoWizard 3 AFM (Bruker-JPK) combined with inverted light microscope IX-81 (Olympus) was used to obtain mechanocardiograms (MCGs) of beating EBs as previously described (Pesl et al., 2014; Caluori et al., 2019b; Pribyl et al., 2019).

Drug response tests were performed after initial equilibration of EBs in Tyrode's solution (composition in mM: NaCl 135, KCl 5.4, $MgCl_2$ 0.9, $CaCl_2$ 1.8, HEPES 10, $NaH_2PO_4$ 0.33, and glucose 5.5; pH 7.4 adjusted with 3M NaOH) (Bébarová et al., 2017). The addition of increasing concentrations of aminophylline (10 µM, 100 µM, 1 mM, and 10 mM; Fagron) followed. Each concentration was prepared in Tyrode's solution from 1 mM stock solution of aminophylline. The MCG was recorded for further analysis; each measurement point consisted of 10 min of stabilization time, followed by 10 min of measurement. Control experiments were conducted in the same setting without aminophylline in the treatments.

The contraction of beating EBs was recorded as a force value in time (MCG). In-house built MATLAB-based script located R and S peaks for each contractive event and their respective vertical deflection and time values. From these values, R-R (sec), R-S (contraction force; nN), and BR (beat rate; beats per minute) were calculated, averaged, and normalized to the respective baseline values recorded in Tyrode's solution.

## Multielectrode Array Measurements

The field potential of the HL-1 cells was measured using MEA2100-mini-60 (Multi Channel Systems). Drug responses were measured after initial equilibration in Claycomb medium, followed by the increasing concentrations of aminophylline in Claycomb medium (8, 16, 32, 64, 128, 256, and 512 µM). Measurement points consisted of 3 min of stabilization time, followed by 5 min of measurement. As a monolayer, HL-1 cells are more sensitive to a treatment than hPSC-CM clusters. Therefore, treatment measurement times and concentration ranges were modified.

MEA recordings were analyzed using Multi-Channel Analyzer software and in-house Python script, which processed the data in a similar way; however, the resulting parameters were only R-R (sec) and BR (beat rate; beats per minute). R-S (amplitude; µV) values in case of MEA recordings do not correlate with R-S values measured *via* AFM; therefore, they were not used in this study. Noisy and non-representative MEA channels were eliminated, and at least 3 channels were then used for calculations.

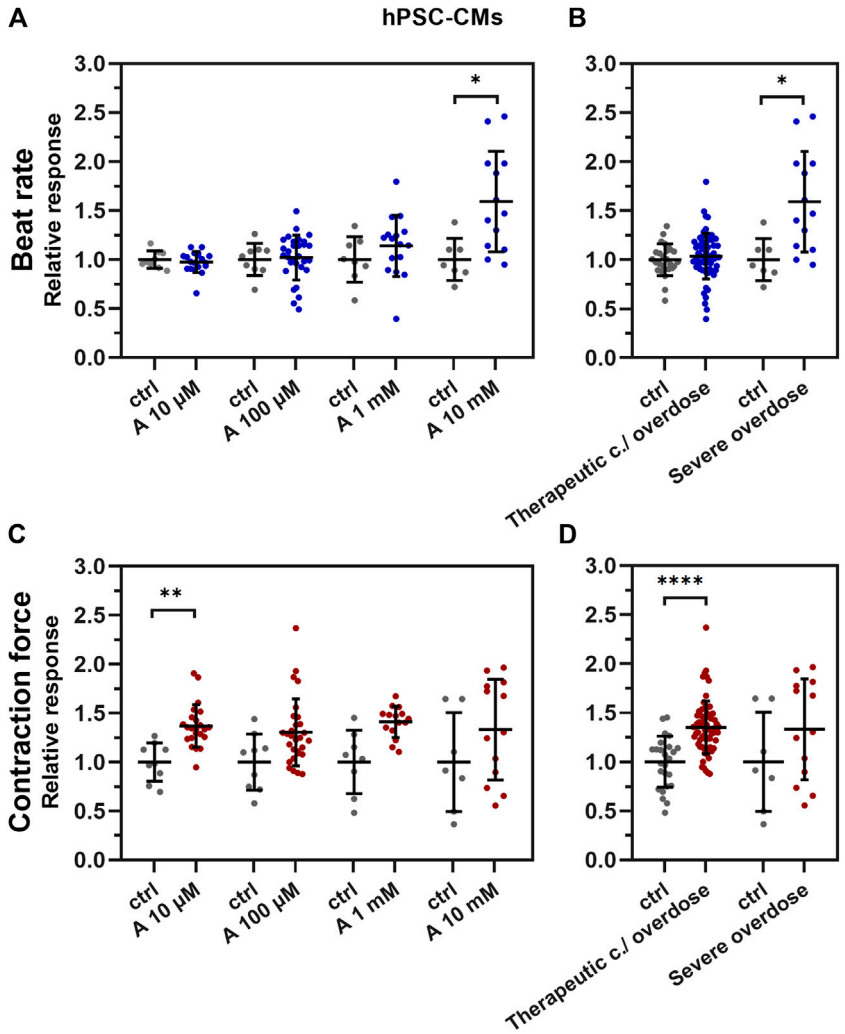



**FIGURE 3 |** Effect of aminophylline (A) on contractile properties of 3D cardiac clusters. Scatterplots (mean ± standard deviation) of the BR (blue) and contraction force (red) overall changes, normalized to a baseline measurement (relative response) and to control measurement means ($n$ = 19 for A 10 µM, $n$ = 30 for A 100 µM, $n$ = 16 for A 1 mM, $n$ = 13 for A 10 mM, $n$ = 9 for BR ctrl and $n$ = 7 for contraction force ctrl). At least four biological repetitions were used in each column. **(A)** BR of the measured EBs with 10 mM aminophylline (A 10 mM) was significantly increased compared to that of the control ($p < 0.05$). **(B)** Similarly, the BR of EBs treated with 10 mM concentration of aminophylline was significantly increased over that of the controls ($p < 0.05$). **(C)** Contraction force of EBs with 10 µM aminophylline treatment was significantly increased over that of the control ($p < 0.05$), with a similar trend in higher concentrations. **(D)** Group analyses then showed a strong statistically significant effect of therapeutic concentration / overdose (10 µM and 100 µM and 1 mM) aminophylline over the controls. (Brown–Forsythe and Welch ANOVA tests were used in all analyses).

## Measurements of Intracellular Cytosolic $Ca^{2+}$

HL-1 cells were passaged and seeded onto an imaging dish with a polymer coverslip bottom (Ibidi) and allowed to adhere. Fluo-8 (490/525; AAT Bioquest) was added into the medium (final concentration 2 µM; stock solution in DMSO 2 mM), and the cells were incubated for 20 min at 37°C. After the incubation, the solution was replaced with fresh medium, and the cells were placed on the heated stage (37°C) of an inverted microscope. $Ca^{2+}$ images in the line-scan (line size 3.37 µm, 100 Hz) mode were recorded using a laser scanning confocal microscope Olympus FL1200 (Olympus) with a ×40 water immersion objective, in the x–y mode. Kinetic properties of intracellular $Ca^{2+}$ were analyzed *via* the in-house Python-based script (Kabanov, 2021).

## Measurement of HL-1 Viability

The HL-1 cells were passaged and mixed with PBS containing aminophylline (final concentration 512 µM) or only PBS for control. The cells were incubated for 8 min after which their viability was analyzed via the trypan blue dye exclusion method (Vicell-XR, Beckman Coulter).

## Statistical Analyses

Statistical evaluation was carried out with the use of GraphPad Prism 8.5 software (GraphPad Software). All data were tested for

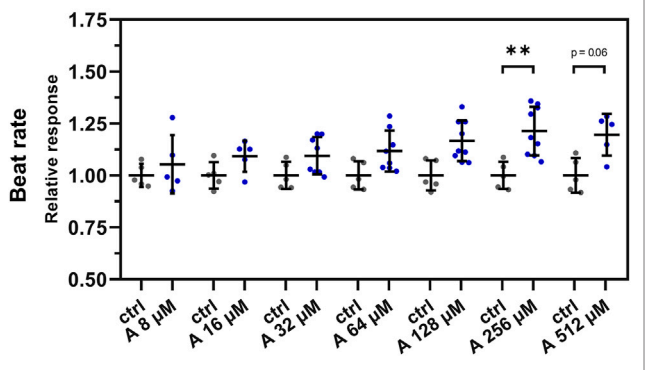



**FIGURE 4 |** Effect of aminophylline (A) on the BR of HL-1 cells. Scatterplots (mean ± standard deviation) of the BR (blue) normalized to a baseline measurement (relative response) and to control measurement means ($n$ = 5 for A 8 and 16 µM, $n$ = 8 for 32 and 64 µM, $n$ = 9 for 128 and 256 µM, $n$ = 5 for 512 µM and $n$ = 5 for ctrl). At least three biological repetitions were used in each column. Results showed linear increase of BR correlating with a higher concentration of aminophylline, with statistically significant and partially significant changes of BR 256 and 512 µM measurements compared that of the control (A 256 vs. ctlr $p < 0.01$, A 526 vs. ctlr $p = 0.06$, ordinary one-way ANOVA).

outliers by the ROUT (Q = 1%) method, and available normality tests were performed for the obtained data. In case of hPSC-CM measurements, Brown–Forsythe ANOVA with Games–Howell multiple comparisons test was used to assess the statistical significance of the differences on normally distributed group pairs. In the case of arrhythmia analysis, R-R for each contractive event was extracted *via* processing scripts as mentioned before. R-R values over 1 or 3 s (cut-off) in HL-1 and hPSC-CMs, respectively, were quantified in all treatment groups and compared to controls. Choice of the cut-off value for hPSC-CMs was based on clinical experience with arrhythmia in human patients. The cut-off value for HL-1 was reduced with respect to the fact that HL-1 is a murine cell line with a higher overall beat rate. The resulting contingency tables were statistically evaluated by using the chi-square test with Yates's correction. The use of the individual statistical test is specified in appropriate figure legends and in Supplementary Data. Additionally, datasets containing complete raw data from all measurements are available at the online open-access repository (Klimovic et al., 2021).

# RESULTS

## Positive Chronotropic and Inotropic Effects of Aminophylline on hPSC-CMs

In the case of hPSC-CMs, two groups of treatment concentrations were determined according to the literature (Aslaksen et al., 1981; Goldberg et al., 1986; Rowe et al., 1988; Higgins et al., 1995; Shannon, 1999). The "therapeutic concentration/overdose" group consisted of 10 µM, 100 µM, and 1 mM of aminophylline treatments, while the 10-mM aminophylline treatment was considered "severe overdose" concentration. Consistent presence of troponin-positive cardiomyocytes in whole and dissociated embryoid bodies (EBs) was confirmed by immunostaining (representative example shown in **Figure 2**).

The positive chronotropic effect of aminophylline on hPSC-CMs was seen only in the 10 mM concentration of aminophylline (**Figures 3A,B**; $p < 0.05$; the remaining $p$-values are given in **Supplementary Table S1** and **Supplementary Table S2**). The positive inotropic effect was evident by a significantly increased contraction force of EBs in lower concentrations of aminophylline that was in contrast to its chronotropic effect (**Figure 3D**; $p < 0.0001$; the remaining $p$-values are given in **Supplementary Table S3**). Statistical analysis showed that this effect was significant in 10 µM concentration, with a similar trend in the concentrations of 100 µM and 1 mM (**Figure 3C**; $p < 0.01$; the remaining $p$-values are given in **Supplementary Table S4**). Linear regression analysis showed that the beat rate increase correlates with the concentration of aminophylline (**Supplementary Figure S2A,B**, $p < 0.0001$). On the contrary, this relationship was not proven in case of contraction force (**Supplementary Figure S2A,B**). To further strengthen the presented results, the washout experiment was performed on hPSC-CMs. The results showed that the BR of EBs increases significantly after administration of aminophylline; however, it decreased again during the washout period, suggesting that the chronotropic and inotropic effects is likely due to the effect of aminophylline and not due to irreversible cellular damage (**Supplementary Figure S3**).

In order to further explain molecular mechanisms, hPSC-CM cells were treated with 1 µM adenosine, followed by a combination of 1 µM adenosine and 1 mM aminophylline, a well-known non-selective adenosine receptor antagonist. The results showed an insignificant trend toward the adenosine-antagonizing aminophylline effect (**Supplementary Figure S3B**).

## Positive Chronotropic Effect of Aminophylline on HL-1

To test whether chronotropic effects of aminophylline are model-independent, field potential measurements of the HL-1 cardiac cell line treated with aminophylline were conducted. The concentrations of aminophylline in a range of 8 up to 512 µM were used. Higher concentrations turned out to be toxic for the cells, which can be explained by higher treatment efficacy on the cellular monolayer of HL-1, as opposed to the cellular cluster of hPSC-CMs. Non-toxicity of selected concentrations was experimentally tested by trypan blue staining (**Supplementary Figure S3C**).

The results of these experiments showed a similar positive chronotropic effect with increasing concentration of aminophylline. Compared to controls, the BR was significantly increased only in the cells treated with 256 µM aminophylline; however, we observed a similar non-significant trend also in the case of the 512-µM treatment (**Figure 4**; 256 µM aminophylline vs. the control $p < 0.05$; 512 µM aminophylline vs. the control $p < 0.06$; the remaining $p$-values are given in **Supplementary Table S5**).

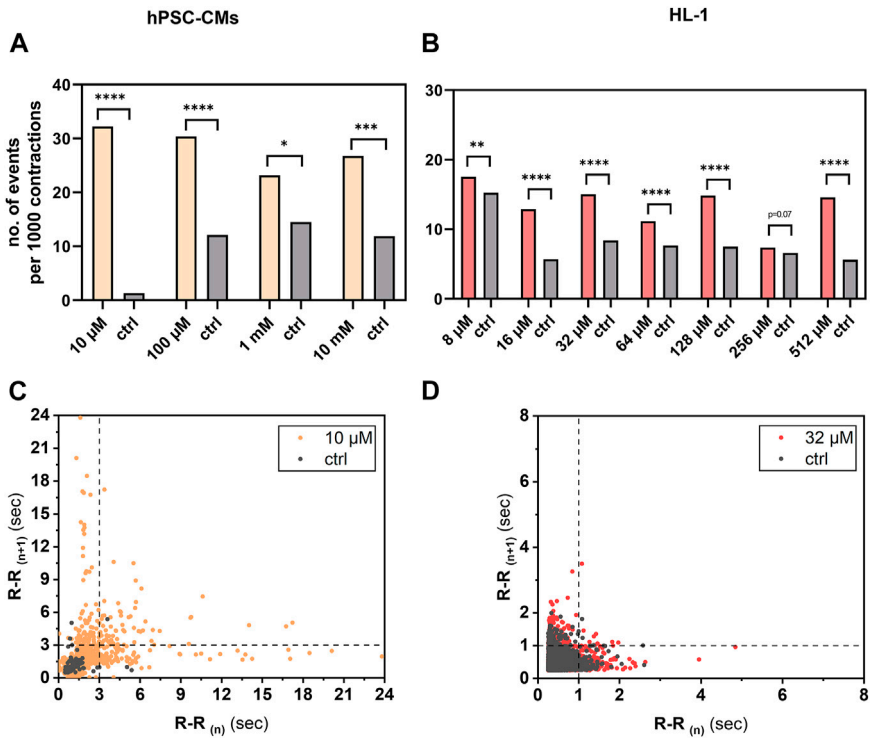



**FIGURE 5 |** Analysis of arrhythmogenic effect of aminophylline on hPSC-CMs and HL-1 cells. R-R values over 3 s in case of hPSC-CM measurements or 1 s in case of HL-1 of aminophylline and control measurements were subtracted, and the resulting contingency tables were statistically analyzed. Column graphs show sums of cutoff R-R values (arrhythmic events) per 1,000 contractions in each treatment group and controls of **(A)** hPSC-CMs and **(B)** HL-1 experiments (chi-square test with Yates' correction). Results show significant or partially significant higher frequency of aminophylline group cutoff values compared to that of the control. Poincaré plots of R-R values of representative concentration for **(C)** hPSC-CMs and **(D)** HL-1 experiments with visible cutoff lines.

## Exposure to Aminophylline Causes Spontaneous $Ca^{2+}$ Releases Leading to Arrhythmia

Among the adverse effects of aminophylline apparent in clinical practice, arrhythmias are most frequent. To test whether this effect is also present in our *in vitro* hPSC-CM model and HL-1 cardiomyocytes, we assessed the number of R-R intervals (inter-beat interval length) over 3 s or 1 s, respectively. Our results showed that the frequency of cutoff R-R values in measurements with aminophylline was significantly higher than that in controls in both models (**Figure 5**; *p*-values in **Supplementary Table S6** and **Supplementary Table S7**).

To further investigate this effect, intracellular cytosolic $Ca^{2+}$ events were measured on HL-1 cells in the presence of 256 and 512 µM aminophylline. A significantly higher number of $Ca^{2+}$ sparks was detected in the presence of 512 µM aminophylline than the control (**Figure 6,** 512 µM aminophylline vs. the control $p < 0.0001$). A similar effect was not detected in the presence of 256 µM aminophylline. Higher concentrations of aminophylline cause arrhythmic events presented by calcium leakage events (sparks). This is in good agreement with the measurement of electrical activity of cells (**Figure 5B**), where the concentration of 256 µM did not cause a significantly higher occurrence of arrhythmia; however, the concentration of 512 µM leads to rhythm irregularities. Last, the time to peak and decay time of main calcium waves were analyzed. While aminophylline caused no change in time to peak, the decay time significantly decreased, corresponding to an increased BR (**Figures 6B,C**).

## DISCUSSION

This is the first study demonstrating the proarrhythmic action of aminophylline on human cardiomyocytes *in vitro*. To monitor aminophylline's effect at a wide range of concentrations, AFM was used on cell clusters [embryoid bodies (EBs)] formed by aggregation of human pluripotent stem cell–derived cardiomyocytes. Furthermore, the effect of aminophylline was investigated *via* a multielectrode array and by means of intracellular cytosolic $Ca^{2+}$ measurement on HL-1 cells. Despite the differences between the models such as monolayer growth, cellular populations, or the fact that it is a murine cell type, HL-1 cells are considered a standard drug screening platform; therefore, we chose them to confirm our findings.

A missing link between the previous experimental data and aminophylline-induced arrhythmias observed in clinical practice was identified. Our most important finding was that aminophylline had two principal actions of arrhythmogenicity, the first being concentration-dependent ("deterministic") and the

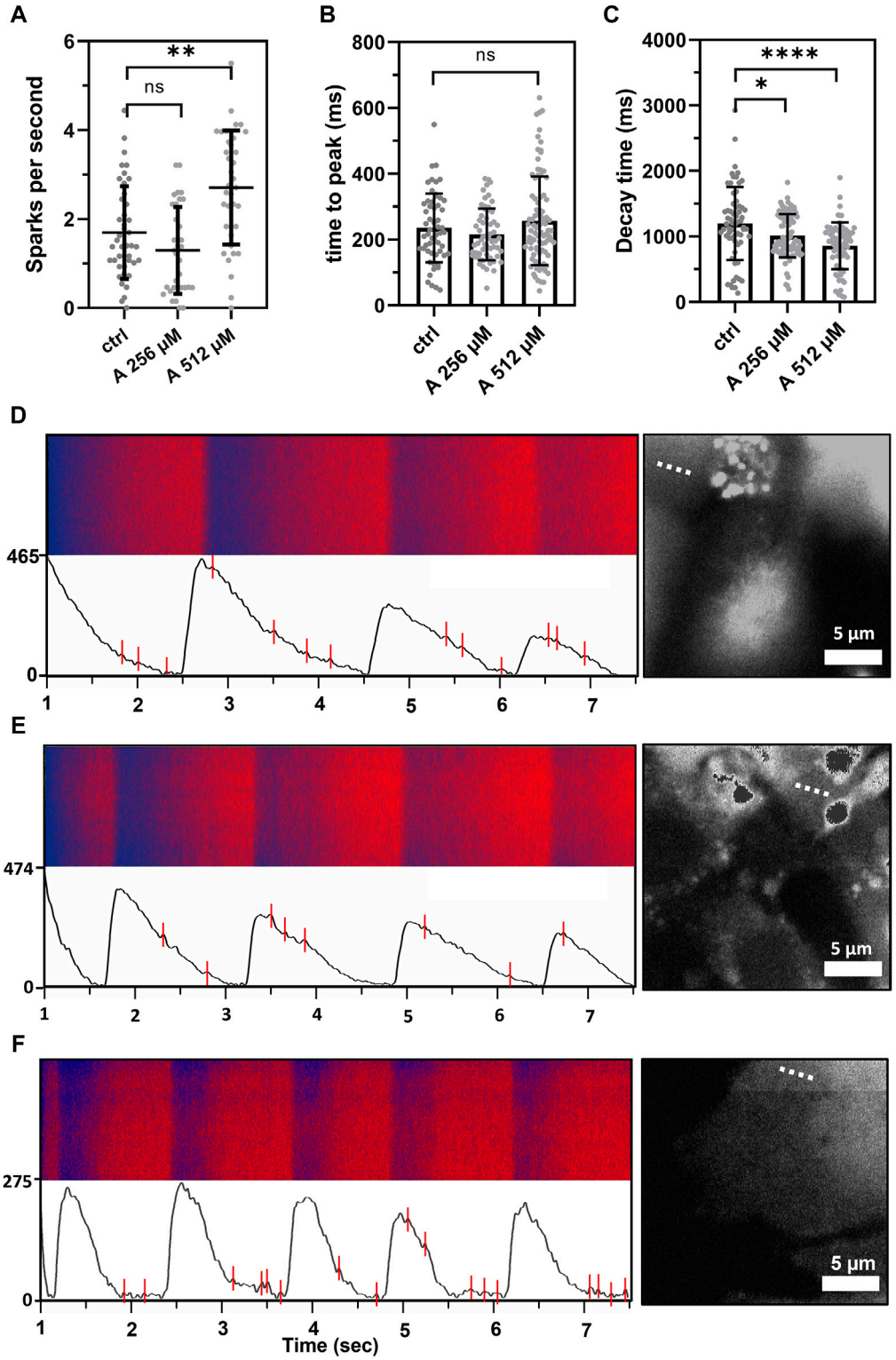



**FIGURE 6 |** Calcium sparks measured as extra events in the fluorescence in-time signal, showing leakage of calcium from the sarcoplasmic reticulum. **(A)** Scatterplot (mean ± standard deviation) showing calcium leakage events in a one-second period in control cells compared to the treatment by 256 and 512 µM aminophylline (A; $n = 43$ for ctlr, $n = 33$ for 256 µM and $n = 37$ for 512 µM). The frequency of calcium leakage events of cells treated with 512 µM aminophylline was significantly higher than that of the control (A 512 vs. ctlr $p < 0.01$, ordinary one-way ANOVA). **(B,C)** Scatterplots (mean ± standard deviation) showing times to peak and decay times of the control compared to the treatments. Aminophylline caused no significant change to time to peak compared to the control; however, decay time

(*Continued*)

**FIGURE 6** | significantly decreased in a linear trend ($n$ = 65 for ctrl, $n$ = 89 for A 256 μM, $n$ = 77 for A 512 μM; ctlr vs. A 256 μM $p < 0.05$, ctlr vs. A 512 μM $p < 00.001$; Kruskal–Wallis test). **(D–F)** Fluorescence line profiles were measured in time, typical recordings together with fluorescence–time curves were filtered for the presence of noise, and calcium sparks were found—labeled as red lines (B = control, C = 256 μM, D = 512 μM). Each recording is accompanied with a fluorescence image showing the exact location of line scan on the cell (dashed line).

second one concentration-independent ("stochastic"). First, we observed a linear concentration-dependent positive chronotropic effect with increasing aminophylline concentrations in hPSC-CMs (**Figures 3A,B** and **Supplementary Figure S2A,B**). Moreover, this effect was also confirmed to an extent on the HL-1 cellular line (**Figure 4**). This may be related to previous clinical findings that demonstrated that theophylline's higher plasmatic levels were associated with an increased heart rate (sinus tachycardia); the relationship was linear and concentration-dependent (Vestal et al., 1983; Nadkarni et al., 1988). This effect is sometimes used to treat severe, atropine-resistant bradycardia (Pasnoori and Leesar, 2004) or other indications (Conte et al., 2017). The inotropic effect was non-linear in our study. An increased inotropic effect was present only in lower aminophylline concentrations. This response may be attributed to reaching peak-shortening amplitude, as a physical parameter of cells and cluster, respectively, and partial immaturity may be responsible for lower number of present sarcomeres and, thus, lower shortening capability of the cells (Fraticelli et al., 1989).

In parallel to the "deterministic" effect, we observed a second arrhythmogenic action of aminophylline expressed as a concentration-independent occurrence of RR interval abnormities. This action was stochastic, independent of the applied aminophylline concentration. It consisted of repeated tachycardia-like periods followed by bradycardia-like periods (not illustrated), which is reflected by the extreme R-R intervals in **Figure 5** that occurred significantly more often in the cells exposed to aminophylline. Even though certain beat rate variability was present in spontaneously beating hPSC-derived CMs in previous studies (Mandel et al., 2012; Binah et al., 2013; Niehoff et al., 2019), similar events have never been previously described to our best knowledge. We speculate that this effect may be an experimental equivalent to the sick sinus syndrome (Tse et al., 2017) or to tachy–brady alternating episodes in patients with AF, an arrhythmia that was previously observed both in aminophylline overdose cases and at therapeutic levels of the drug (Laaban et al., 1988; Bittar and Friedman, 1991; Varriale and Ramaprasad, 1993).

Attempts to reveal mechanisms of the arrhythmogenic action of aminophylline/theophylline have been performed previously, using various animal models. In rats, aminophylline induced tachycardia and elevated blood pressure and potential cardiac ischemia (Shamsuzzaman et al., 2016), which may be related to theophylline-induced myocardial fibrosis found as a long-term concentration-/dose-dependent side effect in a notable portion of rats (Onodera et al., 2001). In a canine model, aminophylline significantly enhanced AV nodal and His–Purkinje conduction; this effect was potentiated in combined therapy with metaproterenol (Komadina et al., 1992).

Studies published so far have not provided a clear clue to the genesis of proarrhythmic effects of aminophylline/theophylline, namely, AF. Aminophylline effects (likely an equivalent of the sinus tachycardia in patients) may be explained by the effect of elevated cAMP and the absence of the inhibitory effect of adenosine (Belardinelli et al., 1995) on cardiac ionic currents (see insignificant trend in **Supplementary Figure S3B**).

As studied in detail by Kong et al. (2008), caffeine (another type of methylxanthine), aminophylline, and theophylline preferentially potentiated luminal $Ca^{2+}$ activation of the ryanodine type 2 (RyR2) receptor, reduced the threshold for spontaneous $Ca^{2+}$ release, and increased the basal activity, inducing repeated quantal $Ca^{2+}$ releases. As is well-known, the accumulation of $Ca^{2+}$ in the cytoplasm may result in delayed afterdepolarizations, which can trigger arrhythmia. Considering the increased occurrence of $Ca^{2+}$ sparks in HL-1 cardiomyocytes treated with 512 μM aminophylline (**Figure 6**), the concentration-independent "stochastic" effect of aminophylline observed in our study may be a consequence of microdomain cAMP level–related diastolic release of $Ca^{2+}$ *via* independent clusters of RyR2 receptors (Berisha et al., 2021). Such transient $Ca^{2+}$ accumulation may induce an increased BR and, following $Ca^{2+}$ depletion, results in a pause in the investigated cardiac cell's beating clusters. Such chain of events might also be amplified by the local cAMP level–induced alteration of the current amplitude *via* modulation of hERG potassium channel phosphorylation (Cui et al., 2000). Detailed subcellular mechanisms of this effect should be studied in the future.

To our best knowledge, this is the first study reporting results of experiments with aminophylline conducted on human cardiomyocytes derived from hPSCs. As such, this set of experiments showed that our comprehensive monitoring system is a unique and valuable tool for cardiotoxicity vs. safety testing of various molecules or drugs. Our results may present the missing link between the described subcellular mechanisms of methylxanthine arrhythmogenesis and the clinical variability of arrhythmic events related to the theophylline treatment in clinical practice.

## CONCLUSION/SUMMARY

We conclude that aminophylline had two parallel arrhythmogenic mechanisms of action on EBs: a concentration-dependent ("deterministic") effect, presenting with an increased beat rate (potential clinical correlate: sinus tachycardia), and a concentration-independent ("stochastic") effect, which was characterized by tachycardia-like episodes alternating with long pauses (potential clinical correlate: atrial fibrillation). Our comprehensive monitoring system is a unique

and valuable tool for cardiotoxicity vs. safety testing of various molecules or drugs.

## STUDY LIMITATIONS

The study presents the effect of aminophylline on contractile properties of human hPSC-CMs along with results of field potential measurements on the HL-1 cardiac cell line that further confirmed the effects. First, it has to be considered that hPSC-derived CMs represented immature/neonatal phenotype possibly affecting drug effect kinetics [e.g., altered IK1 levels which may affect resting potential, repolarization, and depolarization dynamics (Sartiani et al., 2007)]. Second, if different hPSC lines are used to generate embryoid bodies, it is likely that there will be different degrees of maturity and the effect of aminophylline might also differ. The last limitation is that field potential measurements can generate information about the BR but not about contraction force; therefore, the results with HL-1 cells confirmed only the chronotropic effect of aminophylline.

## DATA AVAILABILITY STATEMENT

The original contributions presented in the study are included in the article/**Supplementary Material**; further inquiries can be directed to the corresponding author.

## AUTHOR CONTRIBUTIONS

All the authors have contributed to manuscript writing and corrections and were included substantially in the project preparation, conceptualization, and evaluation. MP, VR, and KB prepared the experimental design. DB, TU, and SJ have differentiated the cardiomyocytes; DB and DK maintained the HL-1 cell line; and SJ performed the immunostaining. SK and MS analyzed the data, interpreted them, prepared the figures, and wrote the manuscript draft. SK and JP performed the AFM measurements and evaluated AFM data; ZS and VR supervised the project, interpreted the obtained results, and corrected the manuscript; MB drafted additional explanations to experimental findings and commented on the manuscript; KB was responsible for the coordination and supervision; and SK, MS, and MP contributed equally to the study. DK performed the MEA measurments and analyzed the MEA data.

## FUNDING

This study was funded by the Ministry of Health of the Czech Republic (Research Grant No. NU20-06-00156).

## ACKNOWLEDGMENTS

We acknowledge further support by the European Regional Development Fund-Project ENOCH (No. CZ.02.1.01/0.0/0.0/16_019/0000868) and the Specific University Research Grants of the Masaryk University MUNI/A/1246/2020, MUNI/A/1700/2020, and MUNI/A/1133/2021 provided by the Ministry of Education, Youth and Sports of the Czech Republic. We also acknowledge the support by the Internal grant agency of Masaryk University - Project MUNI/IGA/1428/2020. CIISB, Instruct-CZ Centre of the Instruct-ERIC EU consortium, funded by the MEYS CR infrastructure project LM2018127, is gratefully acknowledged for the financial support of the measurements at the CF Nanobiotechnology.

## SUPPLEMENTARY MATERIAL

The Supplementary Material for this article can be found online at: https://www.frontiersin.org/articles/10.3389/fphar.2021.789730/full#supplementary-material

## REFERENCES

Acimovic, I., Refaat, M. M., Moreau, A., Salykin, A., Reiken, S., Sleiman, Y., et al. (2018). Post-translational Modifications and Diastolic Calcium Leak Associated to the Novel RyR2-D3638a Mutation Lead to CPVT in Patient-specific hiPSC-Derived Cardiomyocytes. *J. Clin. Med.* 7, 423. doi:10.3390/jcm7110423

Aslaksen, A., Bakke, O. M., and Vigander, T. (1981). Comparative Pharmacokinetics of Theophylline and Aminophylline in Man. *Br. J. Clin. Pharmacol.* 11, 269–273. doi:10.1111/j.1365-2125.1981.tb00533.x

Bébarová, M., Matejovič, P., Švecová, O., Kula, R., Šimurdová, M., and Šimurda, J. (2017). Nicotine at Clinically Relevant Concentrations Affects Atrial Inward Rectifier Potassium Current Sensitive to Acetylcholine. *Naunyn-schmiedeberg's Arch. Pharmacol.* 390, 471–481. doi:10.1007/s00210-017-1341-z

Belardinelli, L., Shryock, J. C., Song, Y., Wang, D., and Srinivas, M. (1995). Ionic Basis of the Electrophysiological Actions of Adenosine on Cardiomyocytes. *FASEB J.* 9, 359–365. doi:10.1096/fasebj.9.5.7896004

Berisha, F., Götz, K. R., Wegener, J. W., Brandenburg, S., Subramanian, H., Molina, C. E., et al. (2021). cAMP Imaging at Ryanodine Receptors Reveals β2-Adrenoceptor Driven Arrhythmias. *Circ. Res.* 129, 81–94. doi:10.1161/CIRCRESAHA.120.318234

Binah, O., Weissman, A., Itskovitz-Eldor, J., and Rosen, M. R. (2013). Integrating Beat Rate Variability: from Single Cells to Hearts. *Heart Rhythm* 10, 928–932. doi:10.1016/j.hrthm.2013.02.013

Bittar, G., and Friedman, H. S. (1991). The Arrhythmogenicity of Theophylline. A Multivariate Analysis of Clinical Determinants. *Chest* 99, 1415–1420. doi:10.1378/chest.99.6.1415

Burridge, P. W., Keller, G., Gold, J. D., and Wu, J. C. (2012). Production of De Novo Cardiomyocytes: Human Pluripotent Stem Cell Differentiation and Direct Reprogramming. *Cell Stem Cell* 10, 16–28. doi:10.1016/j.stem.2011.12.013

Caluori, G., Pribyl, J., Cmiel, V., Pesl, M., Potocnak, T., Provaznik, I., et al. (2019a). Simultaneous Study of Mechanobiology and Calcium Dynamics on hESC-Derived Cardiomyocytes Clusters. *J. Mol. Recognit.* 32, e2760. doi:10.1002/jmr.2760

Caluori, G., Pribyl, J., Pesl, M., Jelinkova, S., Rotrekl, V., Skladal, P., et al. (2019b). Non-invasive Electromechanical Cell-Based Biosensors for Improved Investigation of 3D Cardiac Models. *Biosens. Bioelectron.* 124-125 (125), 129–135. doi:10.1016/j.bios.2018.10.021

Charytan, D., and Jansen, K. (2003). Severe Metabolic Complications from Theophylline Intoxication. *Nephrology (Carlton)* 8, 239–242. doi:10.1046/j.1440-1797.2003.00181.x

Conte, L., Pugliese, N. R., and Giannoni, A. (2017). Reversal of Ticagrelor-Induced Arrhythmias and Cheyne-Stokes Respiration with Aminophylline Infusion. *J. Cardiovasc. Pharmacol.* 70, 290–292. doi:10.1097/FJC.0000000000000518

Cui, J., Melman, Y., Palma, E., Fishman, G. I., and McDonald, T. V. (2000). Cyclic AMP Regulates the HERG K(+) Channel by Dual Pathways. *Curr. Biol.* 10, 671–674. doi:10.1016/s0960-9822(00)00516-9

Kabanov, D. (2021). DaniilKabanov/CardioScripts. Available at: https://github.com/DaniilKabanov/CardioScripts [Accessed September 14, 2021].

Dinarelli, S., Girasole, M., Spitalieri, P., Talarico, R. V., Murdocca, M., Botta, A., et al. (2018). AFM Nano-Mechanical Study of the Beating Profile of hiPSC-Derived Cardiomyocytes Beating Bodies WT and DM1. *J. Mol. Recognit* 31, e2725. doi:10.1002/jmr.2725

Dvorak, P., Dvorakova, D., Koskova, S., Vodinska, M., Najvirtova, M., Krekac, D., et al. (2005). Expression and Potential Role of Fibroblast Growth Factor 2 and its Receptors in Human Embryonic Stem Cells. *Stem Cells* 23, 1200–1211. doi:10.1634/stemcells.2004-0303

Ellis, E. F. (1985). Theophylline Toxicity. *J. Allergy Clin. Immunol.* 76, 297–301. doi:10.1016/0091-6749(85)90645-1

Fraticelli, A., Josephson, R., Danziger, R., Lakatta, E., and Spurgeon, H. (1989). Morphological and Contractile Characteristics of Rat Cardiac Myocytes from Maturation to Senescence. *Am. J. Physiol.* 257, H259–H265. doi:10.1152/ajpheart.1989.257.1.H259

Goldberg, M. J., Park, G. D., and Berlinger, W. G. (1986). Treatment of Theophylline Intoxication. *J. Allergy Clin. Immunol.* 78, 811–817. doi:10.1016/0091-6749(86)90066-7

Goudis, C. A. (2017). Chronic Obstructive Pulmonary Disease and Atrial Fibrillation: An Unknown Relationship. *J. Cardiol.* 69, 699–705. doi:10.1016/j.jjcc.2016.12.013

Higgins, R. M., Hearing, S., Goldsmith, D. J., Keevil, B., Venning, M. C., and Ackrill, P. (1995). Severe Theophylline Poisoning: Charcoal Haemoperfusion or Haemodialysis. *Postgrad. Med. J.* 71, 224–226. doi:10.1136/pgmj.71.834.224

Hoppe, L. K., Muhlack, D. C., Koenig, W., Carr, P. R., Brenner, H., and Schöttker, B. (2018). Association of Abnormal Serum Potassium Levels with Arrhythmias and Cardiovascular Mortality: a Systematic Review and Meta-Analysis of Observational Studies. *Cardiovasc. Drugs Ther.* 32, 197–212. doi:10.1007/s10557-018-6783-0

Horita, N., Miyazawa, N., Kojima, R., Inoue, M., Ishigatsubo, Y., and Kaneko, T. (2016). Chronic Use of Theophylline and Mortality in Chronic Obstructive Pulmonary Disease: A Meta-Analysis. *Arch. Bronconeumol* 52, 233–238. doi:10.1016/j.arbres.2015.02.021

Huerta, C., Lanes, S. F., and García Rodríguez, L. A. (2005). Respiratory Medications and the Risk of Cardiac Arrhythmias. *Epidemiology* 16, 360–366. doi:10.1097/01.ede.0000158743.90664.a7

International Stem Cell InitiativeAdewumi, O., Adewumi, O., Aflatoonian, B., Ahrlund-Richter, L., Amit, M., Andrews, P. W., et al. (2007). Characterization of Human Embryonic Stem Cell Lines by the International Stem Cell Initiative. *Nat. Biotechnol.* 25, 803–816. doi:10.1038/nbt1318

Jelinkova, S., Fojtik, P., Kohutova, A., Vilotic, A., Marková, L., Pesl, M., et al. (2019). Dystrophin Deficiency Leads to Genomic Instability in Human Pluripotent Stem Cells via NO Synthase-Induced Oxidative Stress. *Cells* 8. doi:10.3390/cells8010053

Jelinkova, S., Vilotic, A., Pribyl, J., Aimond, F., Salykin, A., Acimovic, I., et al. (2020). DMD Pluripotent Stem Cell Derived Cardiac Cells Recapitulate *In Vitro* Human Cardiac Pathophysiology. *Front. Bioeng. Biotechnol.* 8, 535. doi:10.3389/fbioe.2020.00535

Klimovic, S., Scurek, M., Pesl, M., Beckerova, D., Jelinkova, S., Urban, T., et al. (2021). *Aminophylline Induces Two Types of Arrhythmic Events in Human Pluripotent Stem Cell-Derived Cardiomyocytes - Dataset*. doi:10.5281/zenodo.4552607

Komadina, K. H., Carlson, T. A., Strollo, P. J., and Navratil, D. L. (1992). Electrophysiologic Study of the Effects of Aminophylline and Metaproterenol on Canine Myocardium. *Chest* 101, 232–238. doi:10.1378/chest.101.1.232

Krutá, M., Šeneklová, M., Raška, J., Salykin, A., Zerzánková, L., Pešl, M., et al. (2014). Mutation Frequency Dynamics inHPRTLocus in Culture-Adapted Human Embryonic Stem Cells and Induced Pluripotent Stem Cells Correspond to Their Differentiated Counterparts. *Stem Cell Dev.* 23, 2443–2454. doi:10.1089/scd.2013.0611

Laaban, J. P., Iung, B., Chauvet, J. P., Psychoyos, I., Proteau, J., and Rochemaure, J. (1988). Cardiac Arrhythmias during the Combined Use of Intravenous Aminophylline and Terbutaline in Status Asthmaticus. *Chest* 94, 496–502. doi:10.1378/chest.94.3.496

Lee, T. A., Schumock, G. T., Bartle, B., and Pickard, A. S. (2009). Mortality Risk in Patients Receiving Drug Regimens with Theophylline for Chronic Obstructive Pulmonary Disease. *Pharmacotherapy* 29, 1039–1053. doi:10.1592/phco.29.9.1039

Liu, J., Sun, N., Bruce, M. A., Wu, J. C., and Butte, M. J. (2012). Atomic Force Mechanobiology of Pluripotent Stem Cell-Derived Cardiomyocytes. *PLoS ONE* 7, e37559. doi:10.1371/journal.pone.0037559

Mandel, Y., Weissman, A., Schick, R., Barad, L., Novak, A., Meiry, G., et al. (2012). Human Embryonic and Induced Pluripotent Stem Cell-Derived Cardiomyocytes Exhibit Beat Rate Variability and Power-Law Behavior. *Circulation* 125, 883–893. doi:10.1161/CIRCULATIONAHA.111.045146

Nadkarni, S., Hay, A. W., Faye, S., and Congdon, P. J. (1988). The Relationship between Theophylline, Caffeine and Heart Rate in Neonates. *Ann. Clin. Biochem.* 25 ( Pt 4) (Pt 4), 408–410. doi:10.1177/000456328802500415

Nair, P., Milan, S. J., and Rowe, B. H. (2012). Addition of Intravenous Aminophylline to Inhaled Beta(2)-Agonists in Adults with Acute Asthma. *Cochrane Database Syst. Rev.* 12, CD002742. doi:10.1002/14651858.CD002742.pub2

Niehoff, J., Matzkies, M., Nguemo, F., Hescheler, J., and Reppel, M. (2019). The Effect of Antiarrhythmic Drugs on the Beat Rate Variability of Human Embryonic and Human Induced Pluripotent Stem Cell Derived Cardiomyocytes. *Sci. Rep.* 9, 14106. doi:10.1038/s41598-019-50557-7

Odstrcilik, J., Cmiel, V., Kolar, R., Ronzhina, M., Baiazitova, L., Pesl, M., et al. (2015). "Computer Analysis of Isolated Cardiomyocyte Contraction Process via Advanced Image Processing Techniques," in 2015 Computing in Cardiology Conference (CinC) (Nice, France: IEEE), 453–456. doi:10.1109/CIC.2015.7408684

Onodera, K., Shibata, M., Kojima, J., Wachi, M., Sogawa, N., Furuta, H., et al. (2001). Toxicity of Theophylline Depends on Plasma Concentration by Single and Also Repeated Dosing in Rats. *Pharmacol. Res.* 44, 81–87. doi:10.1006/phrs.2001.0831

Pasnoori, V. R., and Leesar, M. A. (2004). Use of Aminophylline in the Treatment of Severe Symptomatic Bradycardia Resistant to Atropine. *Cardiol. Rev.* 12, 65–68. doi:10.1097/01.crd.0000096418.72821.fa

Pesl, M., Acimovic, I., Pribyl, J., Hezova, R., Vilotic, A., Fauconnier, J., et al. (2014). Forced Aggregation and Defined Factors Allow Highly Uniform-Sized Embryoid Bodies and Functional Cardiomyocytes from Human Embryonic and Induced Pluripotent Stem Cells. *Heart Vessels* 29, 834–846. doi:10.1007/s00380-013-0436-9

Pribyl, J., Pešl, M., Caluori, G., Acimovic, I., Jelinkova, S., Dvorak, P., et al. (20191886). Biomechanical Characterization of Human Pluripotent Stem Cell-Derived Cardiomyocytes by Use of Atomic Force Microscopy. *Methods Mol. Biol.* 1886, 343–353. doi:10.1007/978-1-4939-8894-5_20

Rowe, D. J., Watson, I. D., Williams, J., and Berry, D. J. (1988). The Clinical Use and Measurement of Theophylline. *Ann. Clin. Biochem.* 25 ( Pt 1), 4–26. doi:10.1177/000456328802500102

Sartiani, L., Bettiol, E., Stillitano, F., Mugelli, A., Cerbai, E., and Jaconi, M. E. (2007). Developmental Changes in Cardiomyocytes Differentiated from Human Embryonic Stem Cells: a Molecular and Electrophysiological Approach. *Stem Cells* 25, 1136–1144. doi:10.1634/stemcells.2006-0466

Shamsuzzaman, M., Kavita, G., and Arunabha, R. (2016). Methylxanthine Induced Cardiotoxicity and its Mechanisms: An Experimental Study. *MJMS* 1, 10.

Shannon, M. (1999). Life-threatening Events after Theophylline Overdose: a 10-year Prospective Analysis. *Arch. Intern. Med.* 159, 989–994. doi:10.1001/archinte.159.9.989

Singh, D., Agusti, A., Anzueto, A., Barnes, P. J., Bourbeau, J., Celli, B. R., et al. (2019). Global Strategy for the Diagnosis, Management, and Prevention of Chronic Obstructive Lung Disease: the GOLD Science Committee Report 2019. *Eur. Respir. J.* 53. doi:10.1183/13993003.00164-2019

Souidi, M., Sleiman, Y., Acimovic, I., Pribyl, J., Charrabi, A., Baecker, V., et al. (2021). Oxygen Is an Ambivalent Factor for the Differentiation of Human Pluripotent Stem Cells in Cardiac 2D Monolayer and 3D Cardiac Spheroids. *Ijms* 22, 662. doi:10.3390/ijms22020662

Suissa, S., Hemmelgarn, B., Blais, L., and Ernst, P. (1996). Bronchodilators and Acute Cardiac Death. *Am. J. Respir. Crit. Care Med.* 154, 1598–1602. doi:10.1164/ajrccm.154.6.8970341

Tse, G., Liu, T., Li, K. H., Laxton, V., Wong, A. O., Chan, Y. W., et al. (2017). Tachycardia-bradycardia Syndrome: Electrophysiological Mechanisms and Future Therapeutic Approaches (Review). *Int. J. Mol. Med.* 39, 519–526. doi:10.3892/ijmm.2017.2877

Ukena, D., Schudt, C., and Sybrecht, G. W. (1993). Adenosine Receptor-Blocking Xanthines as Inhibitors of Phosphodiesterase Isozymes. *Biochem. Pharmacol.* 45, 847–851. doi:10.1016/0006-2952(93)90168-v

Varriale, P., and Ramaprasad, S. (1993). Aminophylline Induced Atrial Fibrillation. *Pacing Clin. Electrophysiol.* 16, 1953–1955. doi:10.1111/j.1540-8159.1993.tb00987.x

Vestal, R. E., Eiriksson, C. E., Musser, B., Ozaki, L. K., and Halter, J. B. (1983). Effect of Intravenous Aminophylline on Plasma Levels of Catecholamines and Related Cardiovascular and Metabolic Responses in Man. *Circulation* 67, 162–171. doi:10.1161/01.cir.67.1.162

Ye, C., Miao, C., Yu, L., Dong, Z., Zhang, J., Mao, Y., et al. (2019). Factors Affecting the Efficacy and Safety of Aminophylline in Treatment of Apnea of Prematurity in Neonatal Intensive Care Unit. *Pediatr. Neonatol* 60, 43–49. doi:10.1016/j.pedneo.2018.03.008

Zatloukal, J., Brat, K., Neumannova, K., Volakova, E., Hejduk, K., Kocova, E., et al. (2020). Chronic Obstructive Pulmonary Disease - Diagnosis and Management of Stable Disease; a Personalized Approach to Care, Using the Treatable Traits Concept Based on Clinical Phenotypes. Position Paper of the Czech Pneumological and Phthisiological Society. *Biomed. Pap. Med. Fac. Univ. Palacky Olomouc Czech Repub* 164, 325–356. doi:10.5507/bp.2020.056

**Conflict of Interest:** The authors declare that the research was conducted in the absence of any commercial or financial relationships that could be construed as a potential conflict of interest.

**Publisher's Note:** All claims expressed in this article are solely those of the authors and do not necessarily represent those of their affiliated organizations, or those of the publisher, the editors, and the reviewers. Any product that may be evaluated in this article, or claim that may be made by its manufacturer, is not guaranteed or endorsed by the publisher.

*Copyright © 2022 Klimovic, Scurek, Pesl, Beckerova, Jelinkova, Urban, Kabanov, Starek, Bebarova, Pribyl, Rotrekl and Brat. This is an open-access article distributed under the terms of the Creative Commons Attribution License (CC BY). The use, distribution or reproduction in other forums is permitted, provided the original author(s) and the copyright owner(s) are credited and that the original publication in this journal is cited, in accordance with accepted academic practice. No use, distribution or reproduction is permitted which does not comply with these terms.*

scientific reports

Check for updates

OPEN

# Salbutamol attenuates arrhythmogenic effect of aminophylline in a hPSC-derived cardiac model

Daniil Kabanov[1,3], Simon Vrana Klimovic[1,3], Deborah Beckerová[2,5], Martin Molcan[5], Martin Scurek[4], Kristian Brat[4], Marketa Bebarova[7], Vladimir Rotrekl[2,5], Jan Pribyl[1,2]✉ & Martin Pesl[2,5,6]✉

**The combination of aminophylline and salbutamol is frequently used in clinical practice in the treatment of obstructive lung diseases. While the side effects (including arrhythmias) of the individual bronchodilator drugs were well described previously, the side effects of combined treatment are almost unknown. We aimed to study the arrhythmogenic potential of combined aminophylline and salbutamol treatment in vitro. For this purpose, we used the established atomic force microscopy (AFM) model coupled with cardiac organoids derived from human pluripotent stem cells (hPSC-CMs). We focused on the chronotropic, inotropic, and arrhythmogenic effects of salbutamol alone and aminophylline and salbutamol combined treatment. We used a method based on heart rate/beat rate variability (HRV/BRV) analysis to detect arrhythmic events in the hPSC-CM based AFM recordings. Salbutamol and aminophylline had a synergistic chronotropic and inotropic effect compared to the effects of monotherapy. Our main finding was that salbutamol reduced the arrhythmogenic effect of aminophylline, most likely mediated by endothelial nitric oxide synthase activated by beta-2 adrenergic receptors. These findings were replicated and confirmed using hPSC-CM derived from two cell lines (CCTL4 and CCTL12). Data suggest that salbutamol as an add-on therapy may not only deliver a bronchodilator effect but also increase the cardiovascular safety of aminophylline, as salbutamol reduces its arrhythmogenic potential.**

**Keywords** Salbutamol, Aminophylline, Atomic force microscopy, iPSC, HESC, Cardiomyocytes, Pulmonary drug screening, Drug cardiotoxicity, Biomechanical properties, Arrhythmogenic effects

**Abbreviations**

| | |
|---|---|
| AFM | Atomic force microscopy |
| BPM | Beats per minute |
| BRV | Beat rate variability |
| CBBs | Cell-based biosensors |
| CCTL | Center for cell therapy line |
| CM | Cardiomyocyte |
| EB | Embryoid body |
| ECC | Excitation-contraction coupling |
| hESC | Human embryonic stem cell |
| hiPSC | Human induced pluripotent stem cell |
| hPSC | Human pluripotent stem cell (hESC and hiPSC) |
| hPSC-CMs | Pluripotent stem cell-derived cardiomyocytes |

[1]CEITEC MU, Masaryk University, Brno, Czech Republic. [2]Department of Biology, Faculty of Medicine, Masaryk University, Brno, Czech Republic. [3]Department of Biochemistry, Faculty of Science, Masaryk University, Brno, Czech Republic. [4]Department of Respiratory Diseases, University Hospital Brno and Faculty of Medicine, Masaryk University, Brno, Czech Republic. [5]International Clinical Research Center, St. Anne's University Hospital, Brno, Czech Republic. [6]First Department of Internal Medicine – Cardioangiology, Faculty of Medicine, Masaryk University, St. Anne's University Hospital, Brno, Czech Republic. [7]Department of Physiology, Faculty of Medicine, Masaryk University, Brno, Czech Republic. ✉email: jan.pribyl@ceitec.muni.cz; pesl@fnusa.cz

| | |
|---|---|
| SDSD | Standard deviation of successive differences |
| $\beta_1$-AR | $\beta_1$-adrenergic receptor |
| $\beta_2$-AR | $\beta_2$-adrenergic receptor |

Bronchodilator drugs were designed to relieve symptoms of obstructive respiratory diseases (e.g., asthma and chronic obstructive pulmonary disease, COPD) by relaxing the smooth muscle apparatus of the lower airways. To date, three main classes of bronchodilators have been introduced in clinical practice, namely beta-2 agonists, anticholinergics, and methylxanthines[1]. These drugs are often used in combination, either in the stable phase of the disease or during asthma or COPD exacerbation[1–3].

Cardiac adverse events are among the most frequent side effects of beta-2 agonists and methylxanthines. While the pro-arrhythmic activity of aminophylline is well described in the clinical setting[4,5] and has recently been examined in our experimental study[6], there is limited evidence on the effect and adverse events of these two bronchodilator classes used in combination[7–9].

Salbutamol (also known as albuterol) is the most frequently used short-acting beta-2 agonist (SABA). A wide variety of side effects have been described with salbutamol treatment, especially when the drug is injected into the bloodstream[10]. Considering its effects on the heart, positive bathmotropic, chronotropic, and inotropic effects were described[11–13]. Salbutamol-induced hypokalemia may also affect cardiac function[14] Serious arrhythmias (even ventricular fibrillation) in patients with preexisting heart diseases were reported[14,15].

Using our established and previously described in vitro three-dimensional model of cardiac tissue formed by clusters of human pluripotent stem cells-derived cardiomyocytes (hPSC), we aimed to evaluate the effect of salbutamol alone and in combination with aminophylline on cardiac excitability and inotropy with a focus on their impact on arrhythmogenesis[6,16–20].

## Materials and methods

### Cell cultivation

hESC line "center for cell therapy line" CCTL14 (46 XX) and CCTL12 (46 XX) derived at Masaryk University, Brno, and previously characterized[21] was routinely maintained on a feeder layer of mitotically inactivated mouse embryonic fibroblasts. For formation of embryonic bodies (EB), hESC colonies were collected 4 days after seeding and subsequently broken down into smaller clumps which were seeded into EB medium (86% KO DMEM, 10% FBS, 1% L-glutamine, 1% penicillin/streptomycin, 1% nonessential amino acids, 0,1mM 2-mercaptoethanol and 10 µg/ml ascorbic acid) with 10 ng/ml BMP4 (R&D) and placed in hypoxic conditions (5% $O_2$, 5% $CO_2$) where they spontaneously formed EBs. After three days, the medium was removed and replaced with fresh EB medium supplemented with 5 ng/ml FGF2 (Peprotech), 10 ng/ml BMP4, and 6 ng/ml Activin A (R&D) for a four-day incubation. A three-day incubation followed this in EB media supplemented with 10 ng/ml VEGF (R&D) and 10 µM IWR1 (R&D). The following induction media was EB medium supplemented with 10 ng/ml VEGF and 5 ng/ml FGF2 with a media exchange every four days. After four days in this media (day 14 of differentiation), the EBs were transferred into a normoxic incubator (21% $O_2$, 5% $CO_2$) for the remaining 8 days of this induction period. From then onward, EBs remained in normoxia and were fed with EB medium every four days. 1 month old EBs with spontaneous contraction activity were used for analysis. Beating EBs were selected and transferred on a gelatin-coated PM3 dish to adhere to for measurement. These cellular constructs of cardiac syncytium were coupled to an AFM force sensor to perform a high-fidelity contraction pattern as an hPSC-CM-based biosensor[22].

### Atomic force microscopy measurements

Contraction of beating EBs was assessed by Nanowizard 3 (Bruker-JPK) AFM combined with inverted light microscope IX-81 (Olympus) as previously described[6,17–19]. Liquid media was preheated to 37 Celsius degree and let to stabilize for at least 10 min before each measurement. Temperature was maintained unchanged during all following measurements[18,22]. A soft silicon nitride cantilever (Nitra-tall B, AppNano) was landed on EB attached to the petri dish (TPP). Real-time changes of force in time applied by contracting EB were recorded while administrating salbutamol (Fagron), its mixes with aminophylline (Fagron) in different concentrations, or butoxamine (Sigma Aldrich). Each measurement was preceded by initial equilibrium in Tyrode solution (composition in mM: NaCl 135, KCl 5.4, $MgCl_2$ 0.9, $CaCl_2$ 1.8, HEPES 10, $NaH_2PO_4$ 0.33, and glucose 5.5; pH 7.4 adjusted with 3 M NaOH), after which increasing concentrations of salbutamol (10 nM, 100 nM, 1 µM, 10 µM), mixes of salbutamol (S) and aminophylline (A) (10–1000 nM salbutamol, 10–100 µM aminophylline) or butoxamine (3 µM) was added[16]. All stock solutions of substances and treatments were prepared using Tyrode buffer, as both compounds show excellent water solubility (approx. 0.2 M for both), and no stock solutions in organic solvents were needed. Mixes were defined based on previous results of individual measurements of salbutamol in this article and aminophylline in our group's previous article[6]. Each measurement point consisted of 10 min of stabilization time, followed by 10 min of measurement. Control experiments were conducted in the same setting with the Tyrode solution alone and tied to individual experiment groups based on the time the treatment was given to the cells. Therefore, some control groups can repeat thought-out results. Control EBs were taken from each batch to account for variances among batches. During all experiments, the temperature was maintained at 37 °C.

The resulting data were processed by a python-based script, which located R and S peaks for all contractive events[23]. Contraction forces (nN), beat rates (bpm), and interbeat intervals (sec) were calculated and statistically evaluated. Representative AFM records of vertical deflection of cells treated with salbutamol, aminophylline, and a mix of both are shown in Figure S5.

### Beat rate variability (BRV) analysis

To ensure reliable and valid data, samples invalid for BRV analysis because of multiple sudden irregular pauses in beat rate were excluded using SignalPlant software (ver. 1.2.8.2)[24]. Resulting interbeat RR-intervals were analyzed by domain BRV analysis methods, which compute variability. For analysis of short-term variability, the standard deviation of successive differences (SDSD) was used[25]. SDSD serves as an index of beat-to-beat variability, primarily determined by external influences on the heart. It measures the variability in the time intervals between successive heartbeats. It is unaffected by linear trends in the heart rate, acting as a statistical filter in which the low-frequency components are removed[26]. In our approximation, R-R intervals that deviated from the median by more than two times were excluded from the analysis to reduce the influence of noise. The PyHRV[27] library for Python was used for SDSD calculations. Internal variability was constant during the measurement and may be related to the mixed population of all three CM subtypes as described elsewhere; in brief, nodal-like CMs had an AP duration at 90% of repolarization shorter than 100 ms (about 16%), slightly more frequent were atrial-like cells, and recorded AP mainly demonstrated a typical ventricular-like shape[28].

### Statistical analysis

Data was processed via the in-house Python-based scripts or Signal plant software as described above. Statistical evaluation was calculated with GraphPad Prism 8.5 software (GraphPad Software). All data were tested for outliers by the ROUT (Q = 1%) method, and their normal distribution was tested via available normality tests. Ordinary one-way ANOVA with the Holm Sidak multiple comparisons test was used to test the statistical significance of the differences in normally distributed group pairs. In cases where equal standard deviations could not be assumed, Brown–Forsythe ANOVA with Games–Howell multiple comparisons test was used. Where normality tests failed, non-parametric tests were used. Cut-off arrhythmia analysis (Figure S2 and S3, Supplementary data) was previously described[6]. Briefly, in that work, inter-beat RR intervals over 3 s were subtracted, and the statistical significance of the differences between treatments and controls were tested by the Chi-square test with Yate's correction. An individual statistical test is specified in appropriate figure legends and in Supplementary Data.

## Results

### Inotropic and anti-arrhythmic effect of salbutamol on hPSC-CMs

The AFM-based setup was used to obtain and calculate the contraction force and beat rate of hPSC-CMs in EBs. The contraction force was significantly increased by 40% in the presence of 100 nM salbutamol compared to the normalized control (Fig. 1A) and increased non-significantly in higher concentrations. Salbutamol didn't significantly increase the beat rate in the concentration range between 10 nM and 10 µM (Fig. 1B). Still, linear regression of beat rate relative responses and measured concentrations showed a significant increase towards 1 µM (Fig. 1CD).

The SDSD of short-term beat rate variability was used for the analysis of arrhythmic effects after salbutamol administration. A higher value corresponds to an elevated beat rate variability, i.e., to an increased pro-arrhythmic activity. Interestingly, salbutamol showed a dose-independent trend to reduce the variability of RR intervals compared to controls (Fig. 2A). This effect is further illustrated in the Poincaré plot, where measurements with salbutamol are clustered in the left bottom corner of the plot (i.e., showing a low variability), compared to the scattered control values (Fig. 2B).

We observed a limited effect of salbutamol on the beat rate and contraction force, with the latter significantly increased at 100 nM salbutamol. While a significant anti-arrhythmic effect was present within all tested concentrations (i.e. 10 nM and 100 nM) of salbutamol.

### Synergic effect of salbutamol and aminophylline on hPSC-CMs

Effects of aminophylline and salbutamol alone were compared with their combined action in various concentrations on EBs prepared from hPSC-CMs derived from the CCTL14 cell line. Significant increases in the beat rate and contraction force were observed when the combinations of 10 nM, 100 nM, and 1 µM salbutamol with 1 mM aminophylline were administered (Fig. 3). Strikingly, a comparison with individual effects of salbutamol and aminophylline in the respective concentrations revealed an amplified effect of the combined drugs. The observed effects on the beat rate and contraction force were also validated using a different cell line (CCTL12 hPSC-CMs; Figure S1 in Supplementary data).

Analysis of the short-term beat rate variability with combined salbutamol and aminophylline treatment showed a decreasing arrhythmia tendency across the concentrations, with a significant decrease if 1 µM salbutamol and 1 mM aminophylline were applied (Fig. 4A, B). In our previous study, we demonstrated the arrhythmogenic potential of aminophylline using the cut-off method of arrhythmia analysis[6]. An analogical cut-off arrhythmia analysis of the current data revealed an anti-arrhythmic effect of salbutamol, alone or administered with aminophylline (Figure S2 and S3).

Overall, we observed a synergic effect of salbutamol and aminophylline as both bronchodilators potentiate their individual effects on the contraction force and beat rate; this effect was most apparent with 1 mM concentration of aminophylline. Finally, anti-arrhythmic effect of salbutamol prevailed even aminophylline was co-administered.

### Activation of nitric oxide synthase (NOS) reduces aminophylline induced arrhythmia

To exclude a contribution of possible non-specific mechanisms of the salbutamol action, we investigated the role of beta-2 adrenergic receptors ($\beta_2$-AR) in the observed effect. We co-administered butoxamine, a β2-selective blocker, with the mixture of salbutamol and aminophylline, and we observed that butoxamine effectively blocked the anti-arrhythmic effects of salbutamol and synergic effects of the salbutamol-aminophylline combination

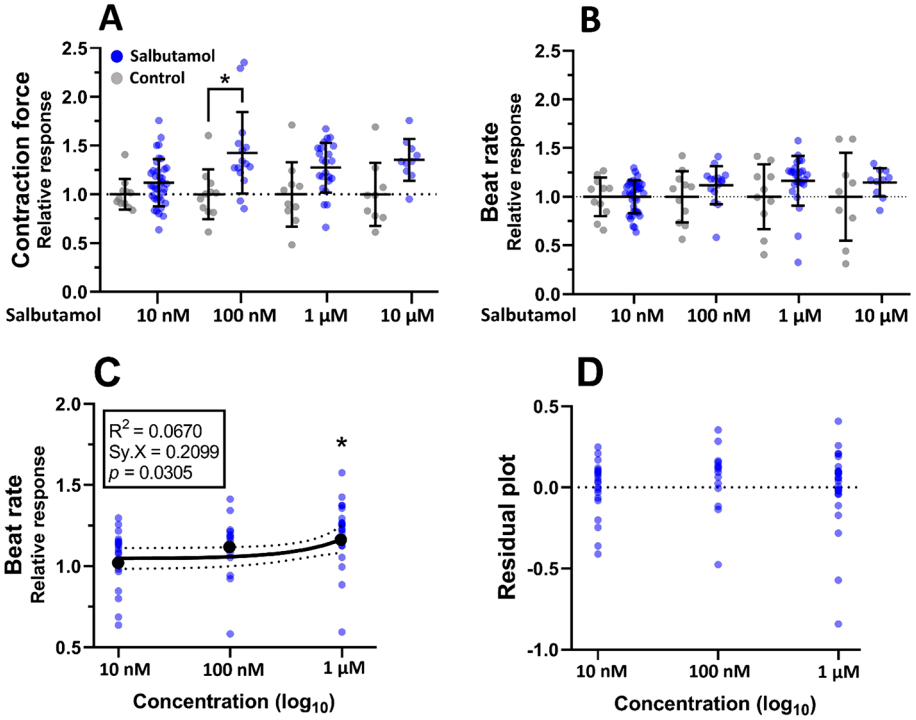



**Fig. 1**. Effect of salbutamol on contraction properties of hPSC-CMs. Scatter plots with indicated means and standard deviation (SD) of the contraction force and beat rate relative responses normalized to the respective baseline control measurement in the case of salbutamol and to mean values of the control measurement in the case of control ($n = 11$ for controls, $n = 15$, 15, 23, and 10 for 10 nM, 100 nM, 1 µM, and 10 µM salbutamol, respectively). At least four biological repetitions were used in each column. **(A)** The contraction force was significantly increased after administration of salbutamol at the concentration of 100 nM (Kruskal-Wallis test with Dunn's multiple comparisons test, $P < 0.05$). **(B)** The beat rate wasn't significantly elevated after administration of salbutamol ($P > 0.05$). **(C, D)** Linear regression of beat rate relative responses and measured concentrations coupled with residual plot. Results show a statistically significant non-zero slope (Wald test, $P = 0.0305$), proving a positive relationship between concentration and relative response.

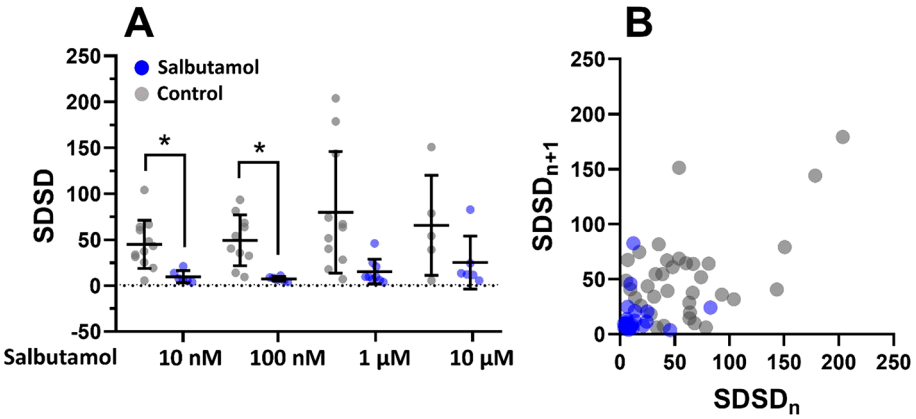



**Fig. 2**. Beat rate variability analysis of hPSC-CMs with salbutamol. **(A)** Scatters plots with indicated means and SD of the standard deviation of successive differences (SDSD) of EBs measured in salbutamol and control ($n = 8$, 9, 9, and 6 for 10 nM, 100 nM, 1 µM, and 10 µM salbutamol, respectively, and $n = 14$, 11, 11, and 5 for the respective controls). SDSD with 10 nM and 100 nM salbutamol were significantly lower compared to controls (Brown-Forsythe and Welch ANOVA test with Holm-Sidak multiple comparisons test, control vs. 10 nM salbutamol, $P = 0.0115$, control vs. 100 nM salbutamol, $P = 0.0139$). **(B)** Poincaré plots with SDSD intervals.

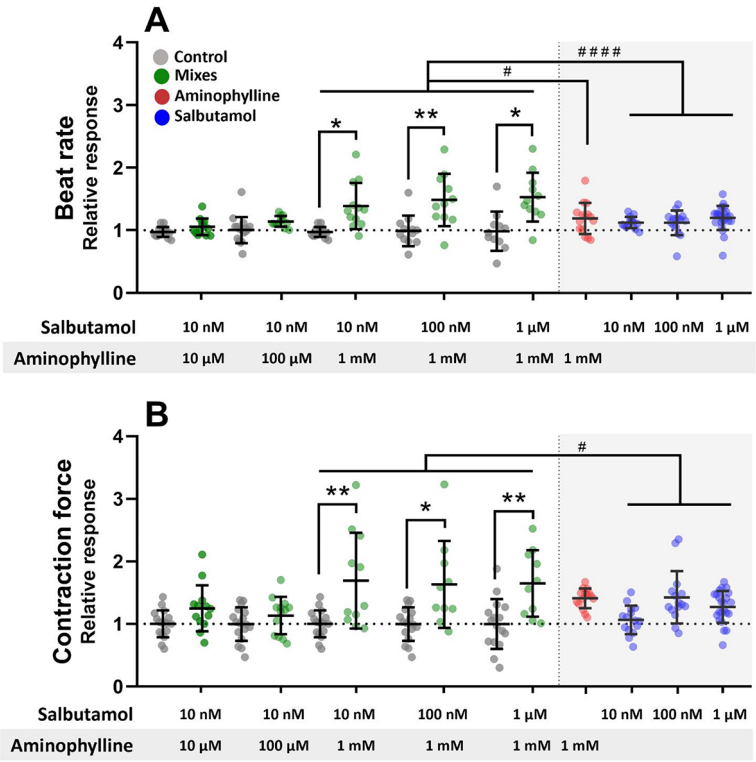



**Fig. 3**. Synergic effect of salbutamol and aminophylline on contractile properties of hPSC-CMs. *stands for $P \leq 0.05$, **$P \leq 0.01$, # stands for $P \leq 0.05$ and #### stands for $P \leq 0.0001$. Scatter plots with indicated means and standard deviation (SD) of the beat rate (**A**) and contraction force (**B**) relative responses normalized to the respective baseline control measurement in the case of salbutamol and aminophylline and to mean values of the control measurement in the case of control ($n = 17$ for controls, $n = 13$, 13, 11, 10, 10, 15, 15, 23, and 15 for treatments, P values in Table S1 in Supplementary data, Brown-Forsythe and Welch ANOVA test was used for contraction force results, ordinary one-way ANOVA for the beat rate results and Kruskal-Wallis test was applied to compare contraction force and beat rate results of mixes with individual treatment). The legend in A applies to the whole graph. The results of the mixes consist of two separate experiments, same control dataset used based on time of measurement (the first two controls are the same as the third and fourth, relating to 20 min and 40 min of treatment). The results of separate aminophylline administration originate from our previous paper[6]. (**A**, **B**) The beat rate and contraction force significantly differed from controls in mixed treatments with 1 mM aminophylline and 10 nM, 100 nM, or 1 µM salbutamol. Still, no significant effect was observed in individual treatments. The effect of mixed treatments was amplified when compared to individual treatments.

(Fig. 5). Interestingly, when treatment containing salbutamol was administered before any treatment containing butoxamine, the anti-arrhythmic effect was apparent even after the addition of pro-arrhythmic aminophylline alone. (Figure S5 in Supplementary data). These results showed that the anti-arrhythmic effect in hPSC-CM is mediated solely through $\beta_2$-AR and could last tens of minutes after salbutamol exposure.

To test whether $\beta_2$-AR activated NOS has a role in antiarrhythmic effect of salbutamol, a well-known non-specific inhibitor of NOS Nω-Nitro-L-arginine methyl (L-NAME) was co-administered with mixture of salbutamol and aminophylline. Figure 6 shows that inhibition of NOS led to significant increase of SDSD value compared to mix without the inhibitor. This increase was comparable to results where sole aminophylline was administered (Fig. 6, $P > 0.01$). These results indicate that mechanism of salbutamol anti-arrhythmic effect depends on activation NOS through $\beta_2$-AR.

## Discussion

In the present study, we observed that salbutamol at clinically relevant concentrations up to 1 µM, which should selectively affect $\beta_2$-AR, caused a significant inotropic effect and a non-significant trend toward a chronotropic effect on hPSC-CM clusters. When salbutamol was applied with aminophylline, inotropic and chronotropic effects were more prominent. Importantly, this is the first report on a significant anti-arrhythmic effect of salbutamol, which reduced the arrhythmia occurrence previously introduced with aminophylline in our hPSC-CMs model. This anti-arrhythmic effect was blocked by a selective $\beta_2$-AR blocker butoxamine and by a non-selective NOS inhibitor L-NAME.

The positive inotropic effect and the concentration-dependent trend to a positive chronotropic effect of salbutamol are consistent with its known stimulatory effect on $\beta_2$-AR[29–32]. This receptor is primarily expressed

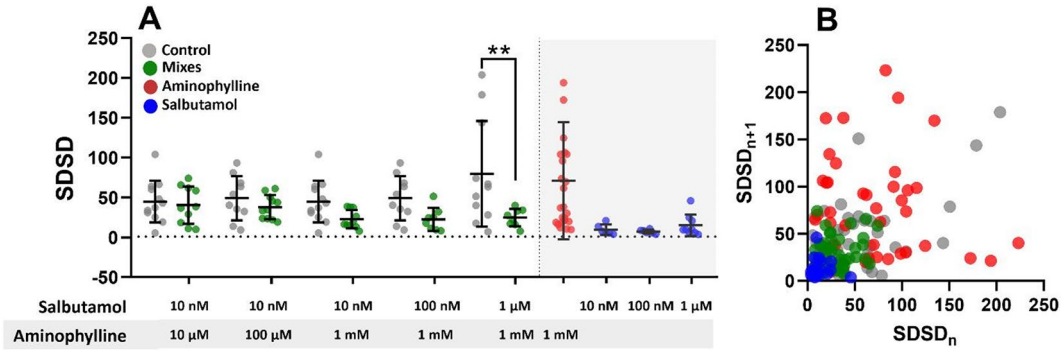



**Fig. 4**. Beat rate variability analysis with combined salbutamol and aminophylline treatments. Scatter plots indicate means and SDs of SDSDs measured with mixed treatments and control ($n = 10$ for controls, $n = 10$, 11, 10, 8, 8, 24, 6, 6, and 9 for treatments, p values in Table S1 in Supplementary data, Ordinary one way ANOVA test was used). **(A)** SDSD results of EBs with indicated concentrations of salbutamol and aminophylline supplemented with separate measurements of both treatments for comparison. The results of the mixes consist of two separate experiments, so the same control dataset was used based on time of measurement (the first two controls are the same as the third and fourth, relating to 20 min and 40 min of treatment). The results of separate aminophylline administration originate from our previous paper[6]. **(B)** Poincaré plots with SDSD intervals.

in cells of the lower respiratory tract, such as in smooth muscle cells, where its activation leads to relaxation and, thus, to bronchodilation[33]. In cardiac cells, there is approximately a 4:1 ratio of $\beta_1$-AR to $\beta_2$-AR; activation of both predominantly leads to chronotropy, inotropy, and lusitropy[34,35]. Similarly, we found lower expression of $\beta_2$ receptors compared to $\beta_1$ in our model (described in our previous work[36]). These effects are mediated by the activation of protein kinase A, which phosphorylates several effector molecules such as phospholamban (PLB), L-type calcium channels (LTCC), or troponin complex[37,38] which plays a key role in the regulation of inotropy [39]. Phosphorylation of troponin during activation of β-adrenergic receptors causes a more intense response even at lower $Ca^{2+}$ concentrations[39,40]. Stimulation of $\beta_1$-AR, but not that of $\beta_2$-AR, may show proarrhythmic effects[41], and as suggested, $\beta_2$-AR receptors may even counteract $\beta_1$-AR mediated arrhythmogenic effect[42]. The minimal but significant chronotropic effect of salbutamol is not surprising considering its $\beta_2$ selectivity and preferential activity in the bronchial smooth muscle[29,32] as well as much lower expression of $\beta_2$ receptors in healthy myocardium compared with $\beta_1$ receptors[35]. The chronotropic effect of isoproterenol, a non-selective β-AR agonist, is much higher. It was shown that salbutamol at concentrations below 1 µM (which primarily stimulate $\beta_2$ receptors and were used in our study) did not cause a chronotropic effect, and its chronotropic effect at higher concentrations was mediated exclusively through $\beta_1$ receptor stimulation[43].

As confirmed in this study (with the use of butoxamine), the observed anti-arrhythmic effect of salbutamol was primarily mediated *via* the $\beta_2$-AR. The chronotropic effect was smaller than that of isoproterenol, which corresponds to clinical experience[44,45]. Nevertheless intrinsic beat rate variability of the model may contribute to the observed trend.

In patients with obstructive lung diseases, various combinations of bronchodilator drugs are used to relieve symptoms[1–3]. While the side effects of individual bronchodilator drugs on cardiac physiology were studied, the side effects of combinations of these substances have not been clarified sufficiently[46–48]. Hence, we decided to analyze the combined effect of different concentrations of salbutamol and aminophylline. We discovered that the combination of salbutamol and aminophylline in concentrations of at least 10 nM and 1 mM had synergic chronotropic and inotropic effects. These effects were significantly stronger compared to controls but also to individual measurements with aminophylline or salbutamol. Aminophylline, similar to other methylxanthines such as caffeine, nonspecifically inhibits phosphodiesterase (PDE) and antagonizes adenosine receptors[49]. Taken together, salbutamol (by activation of $\beta_2$-AR) and aminophylline (by inhibition of PDE and adenosine receptors) co-medication may result in an increased intracellular concentration of cAMP and synergic chronotropic and inotropic effects.

Surprisingly, the pro-arrhythmic effect of aminophylline described in our previous study [6] was reduced in the presence of salbutamol. The previously proposed mechanism of the aminophylline arrhythmic effect was connected to a microdomain cAMP level-related diastolic $Ca^{2+}$ releases *via* independent clusters of ryanodine receptor 2 (RyR2) channels, reducing the threshold for spontaneous $Ca^{2+}$ release[50]. Since the antiarrhythmic action of salbutamol, both alone and in the presence of aminophylline, cannot be logically mediated by the cAMP-PKA pathway, which is generally known to show an opposite effect[51–54]. We were looking for alternative possibilities. Considering the role of the cGMP-eNOS pathway, which may be activated by β2-AR[55–60] and is known to cause a systemic decrease of cytosolic $Ca^{2+}$ concentration and increase in SR load[57–60], thus likely inhibiting spontaneous $Ca^{2+}$ release from SR, we aimed to prove if the non-specific NOS inhibitor L-NAME could mitigate or even prevent the antiarrhythmic effect of salbutamol. The cGMP pathway also depends on cAMP level[55,61]. As apparent from Fig. 6, SDSD was not different if both salbutamol and aminophylline were applied in the presence of L-NAME from SDSD in the presence of aminophylline alone and, vice versa, it was

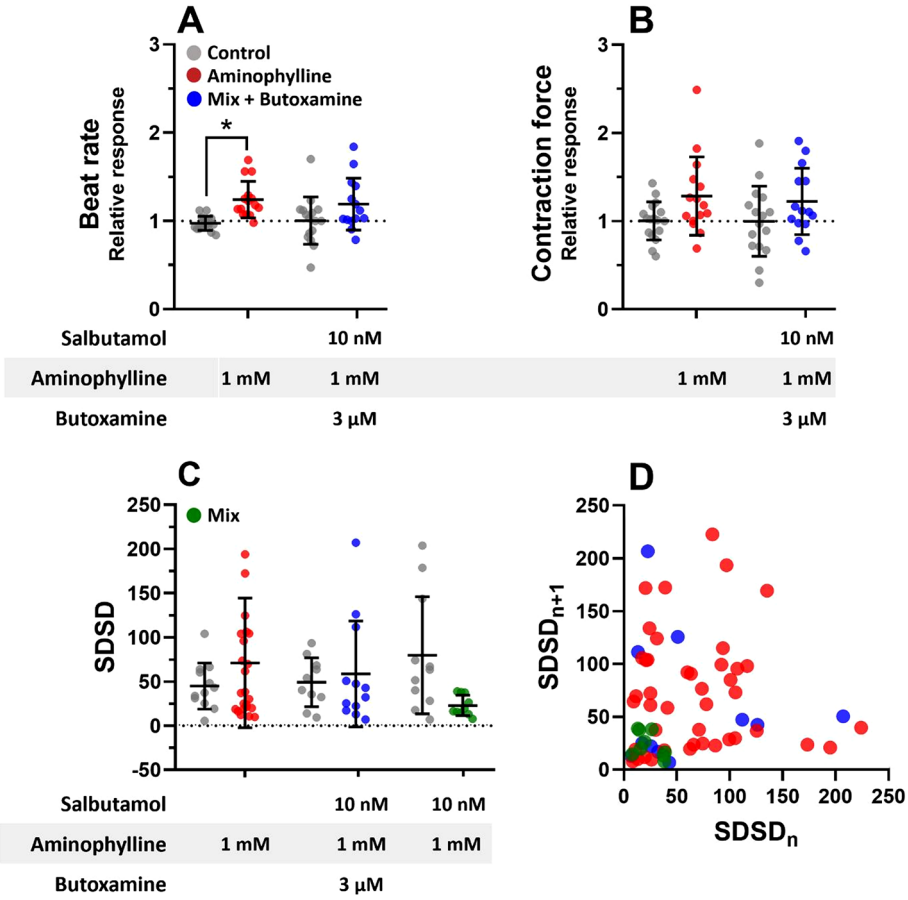



**Fig. 5**. Contractile properties and beat rate variability analysis of hPSC-CMs with salbutamol, aminophylline, and selective $\beta_2$-AR blocker butoxamine. Scatter plots indicate means and standard deviations (SD) of the beat rate and contraction force relative responses normalized to the respective baseline control measurement in the case of salbutamol and mixed treatments and to mean values of the control measurement. Scatter plots with means and SDs of SDSDs measured with mixed treatments and control means (n and P values) are presented in Table S1 in Supplementary data, ordinary one-way ANOVA test was used. **(A, B)** The contraction force and beat rate of EBs treated with the mixes of salbutamol, aminophylline, and butoxamine are indicated at the bottom. **(C)** Analysis of short-term variability SDSD. Control groups were always paired with treatment groups based on the time they were given, so they were repeated from previous figures. **(D)** Poincaré plots with SDSD. If butoxamine was added to the mix, contractile properties were not significantly different from the effect of aminophylline alone. The anti-arrhythmic potential of salbutamol completely diminished when butoxamine was co-administered.

significantly higher to SDSD in the presence of salbutamol and aminophylline mixture, thus, proving the central role of cGMP-eNOS pathway in the antiarrhythmic action of salbutamol.

Our main finding showing that salbutamol reduces the arrhythmogenic effect of aminophylline may be highly clinically relevant. The arrhythmogenic effect of aminophylline is widely known, occurring in about 13% of patients after intravenous administration of the drug or even in 20% of overdosed patients[5,9]. Aminophylline-induced arrhythmia presents most frequently as atrial fibrillation, but more severe arrhythmias may also occur[62]. The dual treatment with salbutamol and aminophylline is a frequently used treatment combination in clinical practice, mainly in the hospital setting during acute exacerbations of asthma or COPD[1–3]. No randomized trials have been reported on the combined effect of aminophylline and salbutamol in patients with COPD or asthma. Only sparse data on the potential toxicity of this combination have been reported previously[8]. Our data show two types of results, i.e., that salbutamol added to aminophylline may cease some arrhythmia mechanisms while enhancing the chronotropic and inotropic effects can lead to increased tachycardia, similar to literature[63,64].

This study first showed that salbutamol at clinically relevant concentrations may reduce the pro-arrhythmic potential of aminophylline if both these drugs are combined. This effect was mediated *via* $\beta_2$-AR activated NOS. The clinical relevance of this finding may be high, representing a potential way to reduce pharmacotoxicity during aminophylline treatment. The combined effect of the two molecules, their safety profile, and potential arrhythmogenicity need further investigation in prospective randomized clinical trials.

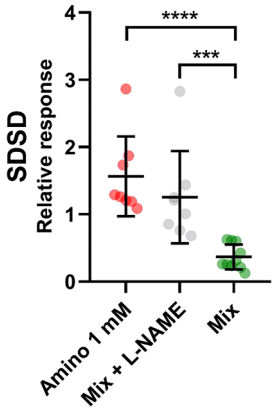



**Fig. 6**. Beat rate variability analysis of hPSC-CMs with salbutamol, aminophylline, and L-NAME, non-selective inhibitor of NOS. Figure shows relative responses to the respective baseline control. Results shows that L-NAME is co-administrated with mix of salbutamol (10 nM) and aminophylline (1 mM), SDSD values are comparable to results with aminophylline (1mM) and significantly increased to salbutamol and aminophylline mix without the inhibitor (Amino 1 mM vs. Mix, $p = 0.0001$, Mix + L-NAME vs. Mix, $p = 0.0065$, Kruskal-Wallis with Dunn's multiple comparisons test, $n = 8$ for Amino 1 mM and Mix + L-NAME, $n = 10$ for Mix).

## Data availability

Data is provided within the manuscript or supplementary information files.

Received: 29 February 2024; Accepted: 17 October 2024
Published online: 09 November 2024

## References

1. Zatloukal, J. et al. Chronic obstructive pulmonary disease - diagnosis and management of stable disease; a personalized approach to care, using the treatable traits concept based on clinical phenotypes. Position paper of the Czech Pneumological and Phthisiological Society. *Biomed. Pap. Med. Fac. Univ. Palacky Olomouc Czechoslov.* **164**, 325–356 (2020).
2. Levy, M. L. et al. Key recommendations for primary care from the 2022 Global Initiative for Asthma (GINA) update. *NPJ Prim. Care Respir. Med.* **33**, 7 (2023).
3. 2023 GOLD Report. *Global Initiative for Chronic Obstructive Lung Disease - GOLD* https://goldcopd.org/2023-gold-report-2/.
4. Bittar, G. & Friedman, H. S. The arrhythmogenicity of theophylline. A multivariate analysis of clinical determinants. *Chest* **99**, 1415–1420 (1991).
5. Shannon, M. Life-threatening events after theophylline overdose: a 10-year prospective analysis. *Arch. Intern. Med.* **159**, 989–994 (1999).
6. Klimovic, S. et al. Aminophylline Induces Two Types of Arrhythmic Events in Human Pluripotent Stem Cell–Derived Cardiomyocytes. *Front. Pharmacol.* **12**, (2022).
7. Rodrigo, C. & Rodrigo, G. Treatment of acute asthma. Lack of therapeutic benefit and increase of the toxicity from aminophylline given in addition to high doses of salbutamol delivered by metered-dose inhaler with a spacer. *Chest* **106**, 1071–1076 (1994).
8. White, S. M., Constantin, P. E. & Claycomb, W. C. Cardiac physiology at the cellular level: use of cultured HL-1 cardiomyocytes for studies of cardiac muscle cell structure and function. *Am. J. Physiol.-Heart Circ. Physiol.* **286**, H823–H829 (2004).
9. Nair, P., Milan, S. J. & Rowe, B. H. Addition of intravenous aminophylline to inhaled beta(2)-agonists in adults with acute asthma. *Cochrane Database Syst. Rev.* **12**, CD002742 (2012).
10. Price, A. H. & Clissold, S. P. Salbutamol in the 1980s. A reappraisal of its clinical efficacy. *Drugs* **38**, 77–122 (1989).
11. Deacon, S. P. Metabolic effects of salbutamol. *Br. Med. J.* **1**, 639 (1977).
12. Engel, B., Einstein, R. & Goodman, A. H. Inotropic selectivity of salbutamol and terbutaline in anaesthetised, areflexic dogs. *Eur. J. Pharmacol.* **116**, 97–104 (1985).
13. Overgaard, K., Nielsen, O. B., Flatman, J. A. & Clausen, T. Relations between excitability and contractility in rat soleus muscle: role of the Na+-K + pump and Na+/K + gradients. *J. Physiol.* **518**, 215–225 (1999).
14. Mettauer, B., Rouleau, J. L. & Burgess, J. H. Detrimental arrhythmogenic and sustained beneficial hemodynamic effects of oral salbutamol in patients with chronic congestive heart failure. *Am. Heart J.* **109**, 840–847 (1985).
15. Uysal, E., Solak, S., Carus, M., Uzun, N. & Cevik, E. Salbutamol Abuse is Associated with Ventricular Fibrillation. *Turk. J. Emerg. Med.* **15**, 87–89 (2016).
16. Bébarová, M. et al. Nicotine at clinically relevant concentrations affects atrial inward rectifier potassium current sensitive to acetylcholine. *Naunyn. Schmiedebergs Arch. Pharmacol.* **390**, 471–481 (2017).
17. Caluori, G. et al. Non-invasive electromechanical cell-based biosensors for improved investigation of 3D cardiac models. *Biosens. Bioelectron.* **124–125**, 129–135 (2019).
18. Pesl, M. et al. Phenotypic assays for analyses of pluripotent stem cell–derived cardiomyocytes. *J. Mol. Recognit.* **30**, e2602 (2017).
19. Pribyl, J. et al. Biomechanical Characterization of Human Pluripotent Stem Cell-Derived Cardiomyocytes by Use of Atomic Force Microscopy. *Methods Mol. Biol. Clifton NJ* **1886**, 343–353 (2019).
20. Ramalho, N. J. D. et al. Aminophylline at clinically relevant concentrations affects inward rectifier potassium current in a dual way. *Pflugers Arch.* **474**, 303–313 (2022).
21. International Stem Cell Initiative et al. Characterization of human embryonic stem cell lines by the International Stem Cell Initiative. *Nat. Biotechnol.* **25**, 803–816 (2007).
22. Pesl, M. et al. Atomic force microscopy combined with human pluripotent stem cell derived cardiomyocytes for biomechanical sensing. *Biosens. Bioelectron.* **85**, 751–757 (2016).
23. Daniil, K., Simon, K., Deborah, B., Vladimír, R., Martin, P., and Jan, P. A comprehensive system of algorithms for characterization of cardiomyocyte mechanical and electrical function. Available at SSRN https://doi.org/10.2139/ssrn.4784992.

24. Plesinger, F., Jurco, J., Halamek, J. & Jurak, P. Signal Plant: an open signal processing software platform. *Physiol. Meas.* **37**, N38–N48 (2016).
25. Shaffer, F. & Ginsberg, J. P. An Overview of Heart Rate Variability Metrics and Norms. *Front. Public Health* **5**, 258 (2017).
26. Malpas, S. C. & Maling, T. J. B. Heart-Rate Variability and Cardiac Autonomic Function in Diabetes. *Diabetes* **39**, 1177–1181 (1990).
27. Highlights — pyHRV - OpenSource Python Toolbox for Heart Rate Variability 0.4 documentation. https://pyhrv.readthedocs.io/en/latest/index.html.
28. Acimovic, I. et al. Post-Translational Modifications and Diastolic Calcium Leak Associated to the Novel RyR2-D3638A Mutation Lead to CPVT in Patient-Specific hiPSC-Derived Cardiomyocytes. *J. Clin. Med.* **7**, 423 (2018).
29. Cullum, V. A., Farmer, J. B., Jack, D. & Levy, G. P. Salbutamol: a new, selective β-adrenoceptive receptor stimulant. *Br. J. Pharmacol.* **35**, 141–151 (1969).
30. Corea, L. et al. Noninvasive assessment of chronotropic and inotropic response to preferential beta-1 and beta-2 adrenoceptor stimulation. *Clin. Pharmacol. Ther.* **35**, 776–781 (1984).
31. Libretto, S. E. A review of the toxicology of salbutamol (albuterol). *Arch. Toxicol.* **68**, 213–216 (1994).
32. Baker, J. G. The selectivity of β-adrenoceptor antagonists at the human β1, β2 and β3 adrenoceptors. *Br. J. Pharmacol.* **144**, 317–322 (2005).
33. Johnson, D. B., Merrell, B. J. & Bounds, C. G. Albuterol. in *StatPearls* (StatPearls Publishing, Treasure Island (FL), 2022).
34. Moniotte, S. et al. Upregulation of beta(3)-adrenoceptors and altered contractile response to inotropic amines in human failing myocardium. *Circulation* **103**, 1649–1655 (2001).
35. Bristow, M. R. et al. Beta 1- and beta 2-adrenergic-receptor subpopulations in nonfailing and failing human ventricular myocardium: coupling of both receptor subtypes to muscle contraction and selective beta 1-receptor down-regulation in heart failure. *Circ. Res.* **59**, 297–309 (1986).
36. Jelinkova, S. et al. DMD Pluripotent Stem Cell Derived Cardiac Cells Recapitulate in vitro Human Cardiac Pathophysiology. *Front. Bioeng. Biotechnol.* **8**, 535 (2020).
37. Post, S. R., Hammond, H. K. & Insel, P. A. β-Adrenergic receptors and receptor signaling in heart failure. *Annu. Rev. Pharmacol. Toxicol.* **39**, 343–360 (1999).
38. Lucia, C. de, Eguchi, A. & Koch, W. J. New Insights in Cardiac β-Adrenergic Signaling During Heart Failure and Aging. *Front. Pharmacol.* **9**, (2018).
39. Keefe, J. A., Moore, O. M., Ho, K. S. & Wehrens, X. H. T. Role of Ca2 + in healthy and pathologic cardiac function: from normal excitation–contraction coupling to mutations that cause inherited arrhythmia. *Arch. Toxicol.* **97**, 73–92 (2023).
40. Lorenz, K., Rosner, M. R., Brand, T. & Schmitt, J. P. Raf kinase inhibitor protein: lessons of a better way for β-adrenergic receptor activation in the heart. *J. Physiol.* **595**, 4073–4087 (2017).
41. Pérez-Schindler, J., Philp, A. & Hernandez-Cascales, J. Pathophysiological relevance of the cardiac β2-adrenergic receptor and its potential as a therapeutic target to improve cardiac function. *Eur. J. Pharmacol.* **698**, 39–47 (2013).
42. Cerbai, E., Pino, R., Rodriguez, M. L. & Mugelli, A. Modulation of the pacemaker current If by beta-adrenoceptor subtypes in ventricular myocytes isolated from hypertensive and normotensive rats. *Cardiovasc. Res.* **42**, 121–129 (1999).
43. Gonzalez-Muñoz, C., Fuente, T., Medin-Aguerre, S. & Hernández-Cascales, J. The increase in rat ventricular automaticity induced by salbutamol is mediated through β1- but not β2-adrenoceptors: Role of phosphodiesterases. *Life Sci.* **88**, 1095–1101 (2011).
44. Akhtar, A. et al. The Acute Effects of the Use of Salbutamol and Ipratropium on the Heart Rates of Patients With Obstructive Airway Disease. *Cureus* **15**, e46409 (2023).
45. Rabbany, M. A. et al. Comparative Efficacy of Levosalbutamol and Racemic Salbutamol in the Treatment of Acute Exacerbation of Asthma. *Mymensingh Med. J. MMJ* **32**, 10–17 (2023).
46. Cazzola, M., Rogliani, P. & Matera, M. G. Ultra-LABAs for the treatment of asthma. *Respir. Med.* **156**, 47–52 (2019).
47. Matera, M. G., Page, C. P., Calzetta, L., Rogliani, P. & Cazzola, M. Pharmacology and Therapeutics of Bronchodilators Revisited. *Pharmacol. Rev.* **72**, 218–252 (2020).
48. Matera, M. G., Rogliani, P., Calzetta, L. & Cazzola, M. Safety Considerations with Dual Bronchodilator Therapy in COPD: An Update. *Drug Saf.* **39**, 501–508 (2016).
49. Ukena, D., Schudt, C. & Sybrecht, G. W. Adenosine receptor-blocking xanthines as inhibitors of phosphodiesterase isozymes. *Biochem. Pharmacol.* **45**, 847–851 (1993).
50. Domeier, T. L., Maxwell, J. T. & Blatter, L. A. β-Adrenergic stimulation increases the intra-sarcoplasmic reticulum Ca2 + threshold for Ca2 + wave generation. *J. Physiol.* **590**, 6093–6108 (2012).
51. Colombe, A.-S. & Pidoux, G. Cardiac cAMP-PKA Signaling Compartmentalization in Myocardial Infarction. *Cells* **10**, 922 (2021).
52. Sucharov, C. C., Dockstader, K., Nunley, K., McKinsey, T. A. & Bristow, M. β-adrenergic receptor stimulation and activation of PKA protect against α1-adrenergic mediated phosphorylation of PKD and HDAC5. *J. Card. Fail.* **17**, 592–600 (2011).
53. Crespo, P., Cachero, T. G., Xu, N. & Gutkind, J. S. Dual Effect of β-Adrenergic Receptors on Mitogen-activated Protein kinase: evidence for a βγ-dependent activation and a gαs-camp-mediated inhibition (∗). *J. Biol. Chem.* **270**, 25259–25265 (1995).
54. Molenaar, P., Chen, L. & Parsonage, W. A. Cardiac implications for the use of β2-adrenoceptor agonists for the management of muscle wasting. *Br. J. Pharmacol.* **147**, 583–586 (2006).
55. Balligand, J.-L. Regulation of cardiac β-adrenergic response by nitric oxide. *Cardiovasc. Res.* **43**, 607–620 (1999).
56. Ghasemi, A. & Jeddi, S. Quantitative aspects of nitric oxide production in the heart. *Mol. Biol. Rep.* **49**, 11113–11122 (2022).
57. Domeier, T. L., Maxwell, J. T. & Blatter, L. A. β-Adrenergic stimulation increases the intra-sarcoplasmic reticulum Ca2 + threshold for Ca2 + wave generation. *J. Physiol.* **590**, 6093–6108 (2012).
58. Tamargo, J., Caballero, R., Gómez, R. & Delpón, E. Cardiac electrophysiological effects of nitric oxide. *Cardiovasc. Res.* **87**, 593–600 (2010).
59. Bhushan, S. et al. Selective β2-Adrenoreceptor Stimulation Attenuates Myocardial Cell Death and Preserves Cardiac Function After Ischemia–Reperfusion Injury. *Arterioscler. Thromb. Vasc. Biol.* **32**, 1865–1874 (2012).
60. E. Burger, D. & Feng, Q. Protective Role of Nitric Oxide Against Cardiac Arrhythmia - An Update. *Open Nitric Oxide J.* **3**, (2011).
61. García-Morales, V., Luaces-Regueira, M. & Campos-Toimil, M. The cAMP effectors PKA and Epac activate endothelial NO synthase through PI3K/Akt pathway in human endothelial cells. *Biochem. Pharmacol.* **145**, 94–101 (2017).
62. Huerta, C., Lanes, S. F. & García Rodríguez, L. A. Respiratory medications and the risk of cardiac arrhythmias. *Epidemiol. Camb. Mass* **16**, 360–366 (2005).
63. Insulander, P., Juhlin-Dannfelt, A., Freyschuss, U. & Vallin, H. Electrophysiologic effects of salbutamol, a beta2-selective agonist. *J. Cardiovasc. Electrophysiol.* **15**, 316–322 (2004).
64. Futyma, P. How to Induce Arrhythmias with Salbutamol. in *Arrhythmia Induction in the EP Lab* (ed. Cismaru, G.) 115–122 (Springer International Publishing, Cham, 2019). https://doi.org/10.1007/978-3-319-92729-9_12.


## Acknowledgements

This work was supported by the Ministry of Health of the Czech Republic, research grant no. NU20-06-00156 and NU22-02-00348. A4L_ACTIONS and A4L_Bridge supported by European Union's Horizon 2020 and Horizon Europe program, under grant agreement No. 964997 and 101136453. CIISB, Instruct-CZ Centre of Instruct-ERIC EU consortium, funded by MEYS CR infrastructure project LM2023042 and European Regional

Development Fund-Project "UP CIISB" (No. CZ.02.1.01/0.0/0.0/18_046/0015974), are gratefully acknowledged for the financial support of the measurements at the CF Nanobiotechnology. The work was furthermore supported by the European Commission's Horizon Europe Framework Program under the Research and Innovation Action MUQUABIS GA no. 101070546, and by the Specific University Research Grants of the Masaryk University , MUNI/A/1410/2022, and MUNI/A/1547/2023 provided by the Ministry of Education, Youth and Sports of the Czech Republic.

## Author contributions

All the authors have contributed to manuscript writing and corrections and were included substantially in the project preparation, conceptualization, and evaluation. DK conducted the experimental work, performed data analysis, and prepared the initial draft of the manuscript. ŠK conducted the experimental work and contributed to data visualization, enhancing the graphical representation of key findings in the study. DB was responsible for cell cultivation and the preparation of embryoid bodies (EBs). MS, MP, and KB contributed to manuscript preparation, secured funding and the clinical perspective of the study, ensuring its relevance to practical applications. MB participated in refining and expanding the explanations related to experimental findings. MP, VR, JP, and MB provided critical feedback and comments on the manuscript. MP, VR, and JP conducted the overall project supervision, including the development of the experimental design, interpretation of results, and manuscript corrections. MM focused on the analysis of data related to HRV/BRV. Each author has reviewed and approved the final version of the manuscript.

## Funding

The work was supported by project National Institute for Research of Metabolic and Cardiovascular Diseases (Programme EXCELES, No. LX22NPO5104) - Funded by the European Union – Next Generation).

## Declarations

## Competing interests

The authors declare no competing interests.

## Additional information

**Supplementary Information** The online version contains supplementary material available at https://doi.org/10.1038/s41598-024-76846-4.

**Correspondence** and requests for materials should be addressed to J.P. or M.P.

**Reprints and permissions information** is available at www.nature.com/reprints.

**Publisher's note** Springer Nature remains neutral with regard to jurisdictional claims in published maps and institutional affiliations.

**Open Access** This article is licensed under a Creative Commons Attribution 4.0 International License, which permits use, sharing, adaptation, distribution and reproduction in any medium or format, as long as you give appropriate credit to the original author(s) and the source, provide a link to the Creative Commons licence, and indicate if changes were made. The images or other third party material in this article are included in the article's Creative Commons licence, unless indicated otherwise in a credit line to the material. If material is not included in the article's Creative Commons licence and your intended use is not permitted by statutory regulation or exceeds the permitted use, you will need to obtain permission directly from the copyright holder. To view a copy of this licence, visit http://creativecommons.org/licenses/by/4.0/.

© The Author(s) 2024

Analytica Chimica Acta 1216 (2022) 339959

Contents lists available at ScienceDirect

Analytica Chimica Acta

journal homepage: www.elsevier.com/locate/aca

# hESC derived cardiomyocyte biosensor to detect the different types of arrhythmogenic properties of drugs

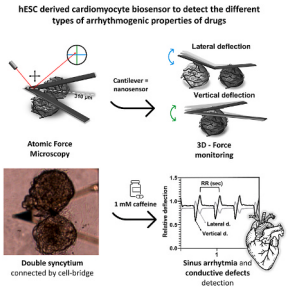
Roberto Pivato [a,b], Simon Klimovic [b,c,d], Daniil Kabanov [c,d], Filip Sverák [a,b], Martin Pesl [a,b,e], Jan Pribyl [d,**], Vladimir Rotrekl [a,b,*]

[a] Department of Biology, Faculty of Medicine, Masaryk University, Kamenice 5, 625 00, Brno, Czech Republic
[b] International Clinical Research Center at St. Anne's University Hospital, Pekarská 53, 65691, Brno, Czech Republic
[c] Department of Biochemistry, Faculty of Science, Masaryk University, Kamenice 753/5, 625 00, Brno, Czech Republic
[d] Central European Institute for Technology, Masaryk University, Kamenice 753/5, 625 00, Brno, Czech Republic
[e] First Department of Internal Medicine - Cardioangiology, Faculty of Medicine, Masaryk University and St. Anne's University Hospital, Pekarská 53, 65691, Brno, Czech Republic

## HIGHLIGHTS

- CBB consists of dual human stem cell-derived CMs cluster forming conductive syncytium.
- AFM based CBB presents relevant arrhythmic response suitable for arrhythmia detection.
- Dual cluster syncytium is able to spontaneously mimic phenotypes present in the neonatal heart.
- CBB derived from patients' specific hiPSCs possesses high potential for precision medicine.

## GRAPHICAL ABSTRACT




## ARTICLE INFO

*Keywords:*
Cell-based biosensor
Atomic force microscopy
Human embryonic stem cells
Cardiac arrhythmia
Cardiomyocytes
Caffeine

## ABSTRACT

In the present work, we introduce a new cell-based biosensor for detecting arrhythmias based on a novel utilization of the combination of the Atomic Force Microscope (AFM) lateral force measurement as a nanosensor with a dual 3D cardiomyocyte syncytium. Two spontaneously coupled clusters of cardiomyocytes form this.

The syncytium's functional contraction behavior was assessed using video sequences analyzed with Musclemotion ImageJ/Fiji software, and immunocytochemistry evaluated phenotype composition.

The application of caffeine solution induced arrhythmia as a model drug, and its spontaneous resolution was monitored by AFM lateral force recording and interpretation and calcium fluorescence imaging as a reference method describing non-synchronized contractions of cardiomyocytes.

The phenotypic analysis revealed the syncytium as a functional contractile and conduction cardiac behavior model. Calcium fluorescence imaging was used to validate that AFM fully enabled to discriminate cardiac arrhythmias in this *in vitro* cellular model. The described novel 3D hESCs-based cellular biosensor is suitable to detect arrhythmic events on the level of cardiac contractile and conduction tissue cellular model. The resulting

* Corresponding author. Department of Biology, Faculty of Medicine, Masaryk University, Kamenice 5, 625 00, Brno, Czech Republic.
** Corresponding author.
*E-mail addresses:* jan.pribyl@ceitec.muni.cz (J. Pribyl), vrotrekl@med.muni.cz (V. Rotrekl).

https://doi.org/10.1016/j.aca.2022.339959
Received 23 February 2022; Received in revised form 16 May 2022; Accepted 17 May 2022
Available online 20 May 2022
0003-2670/© 2022 Published by Elsevier B.V.

biosensor allows for screening of arrhythmogenic properties of tailored drugs enabling its use in precision medicine.

## 1. Introduction

Introduction of induced pluripotent stem cells (iPSCs)-derived cardiomyocytes (CM) allowed the wide development of cell-based biosensors (CBBs). This leap allowed quantification of CMs biomechanical and biochemical properties to study response to various treatments or cardiomyopathies [1]. Sensors are usually based on the multi-electrode array (MEA) [2–4], impedance-based assays (ECIS, xCELLigence®) [5,6], piezoresistive sensor [7] or atomic force microscopy (AFM) [8].

AFM, belonging to the scanning probe microscopy, was at the beginning used predominantly in material research and engineering. Overcoming difficulties related to biological samples allowed it to become a frequently used tool in life sciences. AFM was used to characterize the cell properties, such as phenotype [9,10], cell growth [11] and stiffness of living cells [12]. Moreover, AFM was successfully used as a sensitive cell-based biosensor (CBB), capable of detecting contractile movements of the cardiac cells [13] and their clusters (embryonic bodies EBs) [8], or combined with MEA [14]. Additionally, arrhythmic (i.e., non-periodical) events in the natural beating pattern, often connected with cardiac non-functionality and heart failure, can be identified in the recorded data by adding drugs or other bioactive molecules [15]. AFM microscopy can also be easily combined with other methods such as optical or fluorescence microscopy, as they often create a single unit with AFM [16]. AFM can be further combined with Raman spectroscopy [17], and others to bring a multiparametric description of cardiac cell functions. The main limitation is the need for proper cell adhesion on the surface and maintaining conditions such as a liquid medium and physiological temperature [18].

Cardiac cells within the sinus node generate action potentials spontaneously (cardiac automaticity). This spontaneous activity is retrieved by diastolic depolarization, which brings the membrane potential to the threshold and triggers an impulse propagating through the cardiac conduction system. Cardiac arrhythmia is defined as a deviation from the regular electrical activation of heart contraction, originating in the sinus node [19]. Human heart rate above 100 BPM is tachycardia, and around 50–60 and lower is bradycardia, arrhythmia often presents irregularly [20]. The most prevalent type of arrhythmia is atrial fibrillation (AF), affecting more than 33 million people worldwide, with an estimated increase of 2–3 times by 2050 [21]. AF aggravates the risk of stroke, heart failure, and all-cause mortality [22]. Recent studies say atrial fibrillation is independently associated with an increased risk of sudden cardiac death [23]. The mechanisms of cardiac arrhythmias are divided into two categories - abnormal or enhanced formation of ectopic impulses and conduction disturbances. In a structurally normal heart, the ectopic beats seldom progress to sustained arrhythmia. Thus, conduction disturbances in the myocardial tissue are crucial.

A large body of commonly utilized substances and even drugs causing arrhythmias – i.e., antianginals, antibiotics, narcotics, or bronchodilators [24]. A widely available chemical compound with proarrhythmic effects is caffeine [25] Caffeine acts as a nonselective inhibitor of A1 and A2A adenosine receptors at the cellular level. Cardiovascular effects of caffeine include an increase in blood pressure, changes in heart rate, and neuroendocrine effects. These effects find reason in the blockade of adenosine receptors, causing an increase in intracellular calcium concentrations, the release of norepinephrine, and the sensitization of dopamine receptors [26]. In clinical practice, caffeine finds application alone, e.g., in selected cases of hypotension [27] or in combination with analgesics due to its vasoconstricting and anti-inflammatory effects [26,28]. Due to the high prevalence of arrhythmias in the population, their difficult therapy, it is appropriate to address this abnormality burdening the normal functioning of the heart also at the cellular level. This approach is well served by the presented CBB, which can help describe the arrhythmia, its formation, the treatment, and possibly the effect of therapeutical drugs, as even the treatment medication may cause adverse side effects.

Most of the available cell models are based on single cells or smaller clusters of cells, both of which produce unstable signals [29]. Other models are based on cell monolayers, such as the model proposed by Lian et al. [30]. The major limitation of these monolayer models is that the environment in which cells are grown does not allow to form 3D syncytia with sufficient similarity to physiological tissues [31]. Monolayers present a significantly reduced extracellular matrix, connections between cells only at the periphery of the cells, and the answer to drugs is uniform in all cells. Therefore, 3D models such as embryoid bodies (EBs) are more indicated. EBs are 3D aggregates of cells that imitate structures of the developing embryo and can be differentiated from different lineages such as human embryonic stem cells (hESCs) or patient-specific human induced pluripotent stem cells (hiPSCs), enabling their use in precision medicine [32]. In the present work, hESCs were used. The rationale for using hESCs is that they represent a standard in the field and they do not carry the burden of somatic mutations or reprogramming-induced epigenetic effects [33].

In the present work, we introduce a new biosensor setup based on a combination of atomic force microscope with the hESC derived CMs, where the microcantilever of the microscope creates a sensitive transducer to study cardiac arrhythmias. Computational analysis of image sequences served as a reference method to monitor synchronization of the arrhythmic beating of two cell clusters connected by cardiac conduction-like syncytium. Moreover, the fluorescence calcium imaging supports data obtained by the biosensor setup. The arrhythmic events were induced by caffeine solution. The use of the biosensor setup for a detailed description of the arrhythmia initiation, progression, and termination is presented and discussed.

## 2. Materials and methods

### 2.1. Cell lines, cultivation, and differentiation into embryoid bodies

Human embryonic stem cell (hESCs) CCTL14 and CCTL 12 were used in the present work. These cell lines have been derived in Masaryk University, Brno, approved by Ministry of Education of the Czech Republic (MSMT approval no.14648/2016-5) and were previously characterized and described [34].

Cell lines have been maintained on the feeder layer of mouse embryonic fibroblasts (mEF), that have been inactivated mitotically by irradiation as previously described [35].

Cardiac differentiation was performed as described in Ref. [36].

### 2.2. Cultivation dish preparation and EBs seeding

Standard 30 mm cultivation dishes (TPP, cat no. 93040) and low 35 mm ibidi μ-Dishes (ibidi, cat. no. 80136) had to be modified with an agarose-based mask to increase the probability of seeding two differentiated embryoid bodies next to each other. Consequently, we delimited the area to let the EBs adhere when the following protocol was employed. A 0.5 ml Eppendorf tube was cut to obtain 4 mm external diameter sections. The prepared sections were fixed to the bottom of the cultivation dish with a double-sided scotch. The remaining space in the dish was filled with a 1 mm thick layer of 1% agarose dissolved in PBS. Agarose solution created gel after 20 min of incubation at RT. The addition of 1 ml of PBS stabilized the gel layer after another 10 min. The plastic mask was then removed, the dishes were closed and sealed with a

parafilm. The whole process was finished with sterilization by gamma-irradiation at 100 Gy. Dishes were stored for a maximum of one week at 4° Celsius.

The dish was washed twice with PBS prior to seeding the EBs. The bottom of the holes created by the masking process was coated with 0,1% gelatin for at least 30 min at 37 °C and 5% $CO_2$ to promote the cell adhesion. Then, the excess gelatin was removed, 1 ml of cultivation medium was added, and two differentiated EBs were seeded. Thus, prepared samples were left for at least 24 h in a standard $CO_2$ incubator to produce adhered double-EB structure.

### 2.3. Processing of video sequences

After seeding of EBs, the development of beating synchronization was monitored in real-time by analyzing sequences of optical images. Monitoring was performed by the everyday acquisition of 20-s videos on the Zeiss LSM 700 microscope in the bright field and processing them using ImageJ/Fiji macro Musclemotion (see supplementary material) [37].

### 2.4. Atomic force microscopy

For mechanic contraction measurements Atomic Force Microscopy (AFM) method (JPK Nanowizard 3, JPK-Bruker) was used as described before [8]. In a liquid environment, measurements were conducted in force spectroscopy mode (1 nN setpoint) using MLCT-C cantilever (Bruker). The cantilever was chosen based on its dimensions, allowing it to land on both EBs simultaneously (see Fig. 1). Partially coated cantilevers from silicon nitride were used due to their properties when measuring in liquid. 30 mm cultivation Petri dishes containing either distilled water for calibration or double EB were placed to the motorized stage with a pre-heated Petri dish heater to 37 °C. The laser reflection sum was maximized before each experiment, and the laser detector was centered. After that, cantilever sensitivity and stiffness via the contact-free method in Bruker-JPK software were determined. Vertical and lateral deflection data was collected in 100 Hz frequency as mechanocardiograms (MCG). Sampling frequency was chosen three times higher than the frequency required to sample the fastest event in the QRS complex. Vertical deflection provided information about the R-R interval and its immediate response to caffeine. Beating frequency was calculated as 60s divided by average R-R interval in seconds during post processing. The lateral (horizontal) deflection representing the complex movement of the syncytium was used to report on the different defects of EB synchronization. Each sample was measured for 1 min in a standard cultivation medium (MEF), followed by 1-min measurements of cells treated with 1 mM caffeine in MEF in 0, 5, and 10 after the addition of treatment. Experiments to assess the effect of caffeine (Sigma Aldrich, cat. No. C-0750) on our syncytium has been performed 24 h after synchronization of the syncytium.

Data analysis obtained from AFM was based on the combination of

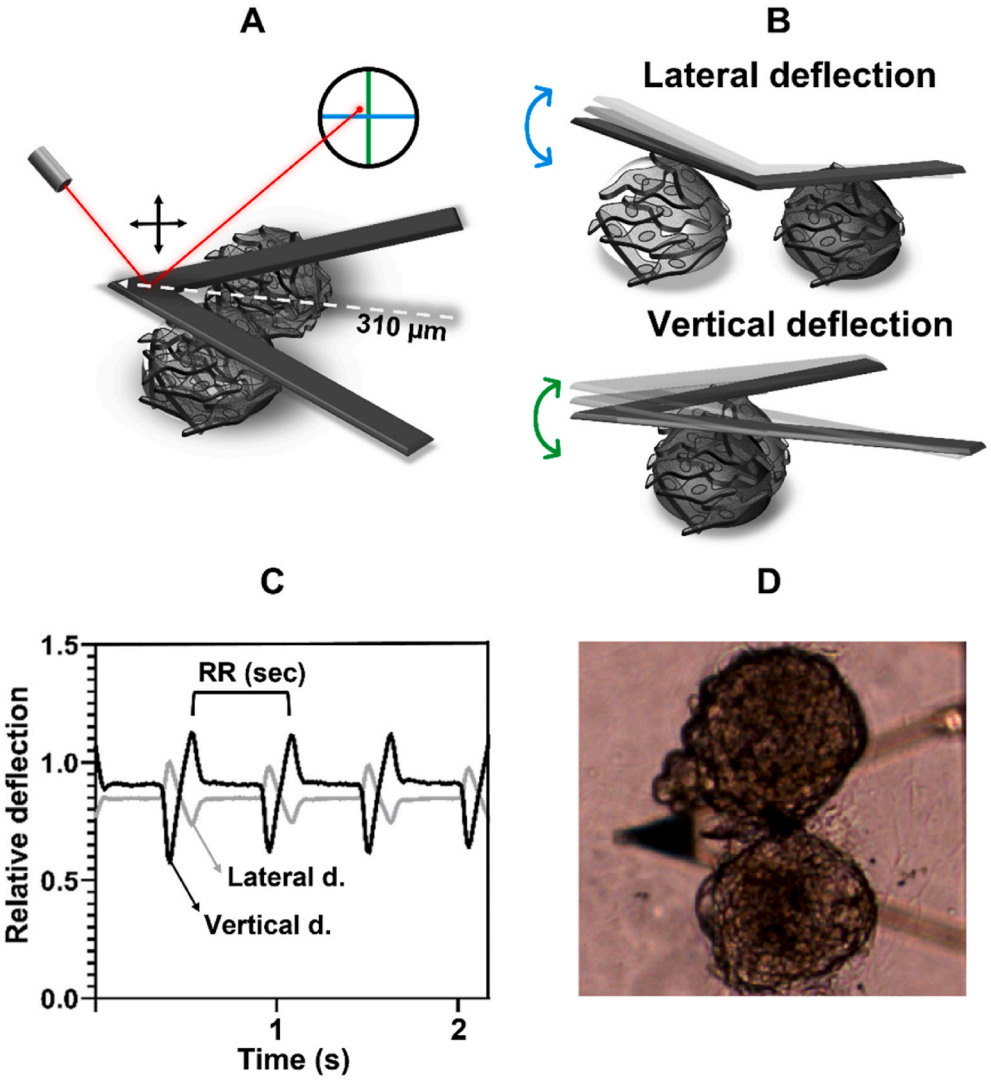



**Fig. 1.** (A) - Schematic description of the AFM methodological approach. The soft silicon-nitride lever measures the contraction movement of the double-EB in both planes, (B) as lateral and vertical force change deflection of the cantilever. (C) – Representative mechanocardiogram with indicated vertical, lateral synchronized deflection and RR length in seconds (D) - Real image from the top optical microscope captures the cantilever in contact with both EBs, magnification 10×. (For interpretation of the references to color in this figure legend, the reader is referred to the Web version of this article.)

average RR length, the distance between two R peaks, and standard deviation of the average RR length in vertical and lateral deflection data (Fig. 1B, D). These values, recorded for each time point, have been normalized concerning the values registered in standard cultivation medium, i.e., without caffeine. Variation of RR length indicates the onset of tachycardia or bradycardia. The onset of arrhythmic events was assessed by comparing the standard deviation value computed after caffeine treatment concerning the value registered in the standard cultivation medium. Data extraction was performed employing our python script [38]. Analysis of typical MCG curve recorded by AFM is shown in Fig. S1.

### 2.5. $Ca^{2+}$ imaging

The fluorescence staining of cytoplasmic calcium with Fluo-4-AM (Invitrogen, cat. no. F14201) dye was used as a supportive analysis of the contraction movements. This allowed for monitoring of the contraction by measuring the $Ca^{2+}$ release from sarcoplasmic reticulum. The samples of double EBs were prepared with the same protocol as for AFM measurements; the $Ca^{2+}$ imaging experiments were performed 24 h after syncytium synchronization.

The staining protocol was adopted from the literature [39] Briefly, 1.5 μM Fluo-4-AM solution in DMSO was added to the cultivation medium. EBs were then incubated for at least 30 min at 37 °C and 5% $CO_2$ in the dark. No washing of the fluorescence dye was necessary.

The measurement of $Ca^{2+}$ fluorescence was performed on Zeiss LSM 700 confocal microscope using software Zen Black. Here, line scan analysis was performed (1000 Hz) by placing the line across our syncytium to cover its full length.

Line scans were then processed on ImageJ/Fiji [40]. Two regions of interest (ROIs) were applied, one over each EB, and evaluated was each ROI average intensity of the fluorescence signal for every timepoint. Data extracted were then plotted in GraphPad software (GraphPad Software) to analyze the evolution of the mutual interaction between the two EBs in real-time.

### 2.6. Immunocytochemistry

To unravel the cellular phenotypes composing our syncytium, immunocytochemistry analysis for three markers was performed. Vimentin (Santa Cruz Biotechnologies, cat. no. sc-7557, dilution 1:250) as a marker of fibroblasts [41]; Discoidin Domain Receptor 2 (DDR2-Santa Cruz Biotechnologies, cat. no. sc-81707, dilution 1:100) marker of cardiac fibroblasts [42]; Cardiac Troponin T (cTnT- R&D Systems, cat. no. MAB1874, dilution 1:100) marker of CMs [43].

Briefly, the samples were fixed in ice-cold paraformaldehyde, after permeabilization with 0.2% Triton X, blocking with 2.5% BSA solution in PBS buffer containing 0.1% Tween detergent followed. The incubation of samples with primary antibodies was performed overnight at 4 °C. The following day, the secondary antibodies were applied, and cover glasses were mounted on the Mowiol® 4–88 (Sigma, cat. no. 9002-89-5) layer with DAPI (Thermo Fisher Scientific, cat. no. 62248). Secondary antibodies labeled with the Alexa Fluor 488 (Invitrogen, cat. no. A-21202) and Alexa Fluor 594 (Invitrogen, cat. no. A-21203) dyes were both applied in dilution 1:500.

## 3. Results and discussion

In this study, we presented a new stem cell-based model for the study of cardiac arrhythmias coupled with AFM forming together a biosensor capable of detecting arrhythmogenic properties of drugs. Starting from hESCs, we have been able to form a suspension of hESC's clusters which were differentiated into CMs syncytium. Two such clusters seeded on adherent plate in vicinity spontaneously formed electrically connected syncytium presenting fundamental phenotypes of the human myocardium and its conductive system. Formation of the syncytium, beating synchronization, and study of arrhythmia monitored by the AFM and calcium release are presented and discussed in the following chapter.

### 3.1. Formation and characterization of functional syncytium

In this work, two beating clusters were seeded in the vicinity on an adhesive surface allowing cell outgrowth from the EBs. The adhesive surface was previously shown to inhibit cardiogenesis via SRC-family kinases [44], promote cell migration [45], and fibroblast proliferation [46]. To investigate the cellular composition of the conductive cell layer connecting the two synchronized EBs, staining of vimentin and discoidin domain receptor 2 (DDR2) was visualized by confocal microscopy (Fig. 2). A positive signal for vimentin evenly spread across the cell layer suggested the presence of fibroblast cells. Most cells between the two EBs ('a bridge') proved to be positive for DDR 2, a specific marker of cardiac fibroblasts. The presence of cardiac fibroblasts has been previously shown to be a key factor in the onset of cardiac syncytia synchronization [47]. Cardiac fibroblasts are also crucial in forming tissue-like architecture [48]. Finally, the syncytium and the bridge were positively stained for cTnT, structural CMse protein, and synchronization of the contractions of the two EBs was observed on day 4. Considering the hESC-derived CMs have a similar phenotype as fetal/-neonatal CMs [49] the composition of the connecting cell layer may resemble the composition of the human fetal heart [50].

Two EBs were seeded in proximity, thus creating a functional syncytium "bridge" during the following days. Sets of EBs with the suboptimal distance between each other were excluded. The beat rate and synchronicity of the EB pairs were observed in time for 4 days from seeding. Syncytia formed by the two EBs connected by conductive cell layer (Fig. 1) with fully synchronized beating were observed at day four for all analyzed samples (Fig. 3; 10 EB sets were analyzed).

The unification of the beating frequency of the two EBs and the synchronization of their beats was associated with cell outgrowth on adhesive tissue culture dishes, stemming from both EBs. Correlation between the amount of the cellular outgrowth and synchronization of the beating was observed, suggesting the formation of a conductive cell layer between the EBs. The cell outgrowth was fundamental for the synchronization of the syncytium. Synchronization may come from the excitable cardiac fibroblast population [47] or gap junctions formed between adjacent CMs [51].

### 3.2. Detection of caffeine-induced arrhythmia by AFM based biosensor and Fluo-4

An extremely sensitive setup based on the microcantilever of AFM acting as a nanosensor was used to analyze the contractile properties of both EBs (Fig. 1). Recorded data were analyzed for both vertical (beating frequency) and horizontal (synchronization) deflections (Fig. 4). Caffeine was used to induce arrhythmic events.

Caffeine addition induced shortening of the RR interval and thus the increase in the beat rate of the syncytium (Fig. 4). This was reflected by both the change in vertical and lateral deflection (Fig. 4a, c). Calculated standard deviation reports on the irregularity/arrhythmic events. A significant increase in standard deviation was observed immediately after caffeine injection (Fig. 4b and d, time 0 min) in comparison to other time points, suggesting an arrhythmic event induced by the caffeine. The caffeine-induced increase in standard deviation was observed for both the lateral and the vertical deflection.

The decrease in average RR length is comparable for vertical and lateral deflection after the addition of caffeine (Table S1), witnessing that the chronotropic effect of caffeine increases with time. The standard deviation of the RR interval, on the other side, increases only immediately after the addition of caffeine in both the vertical and lateral deflection, while it is lower than the control value in all other time intervals (Table S1). The increase in RR standard deviation at time 0 suggests that RR standard deviation reports the caffeine-induced beat rate

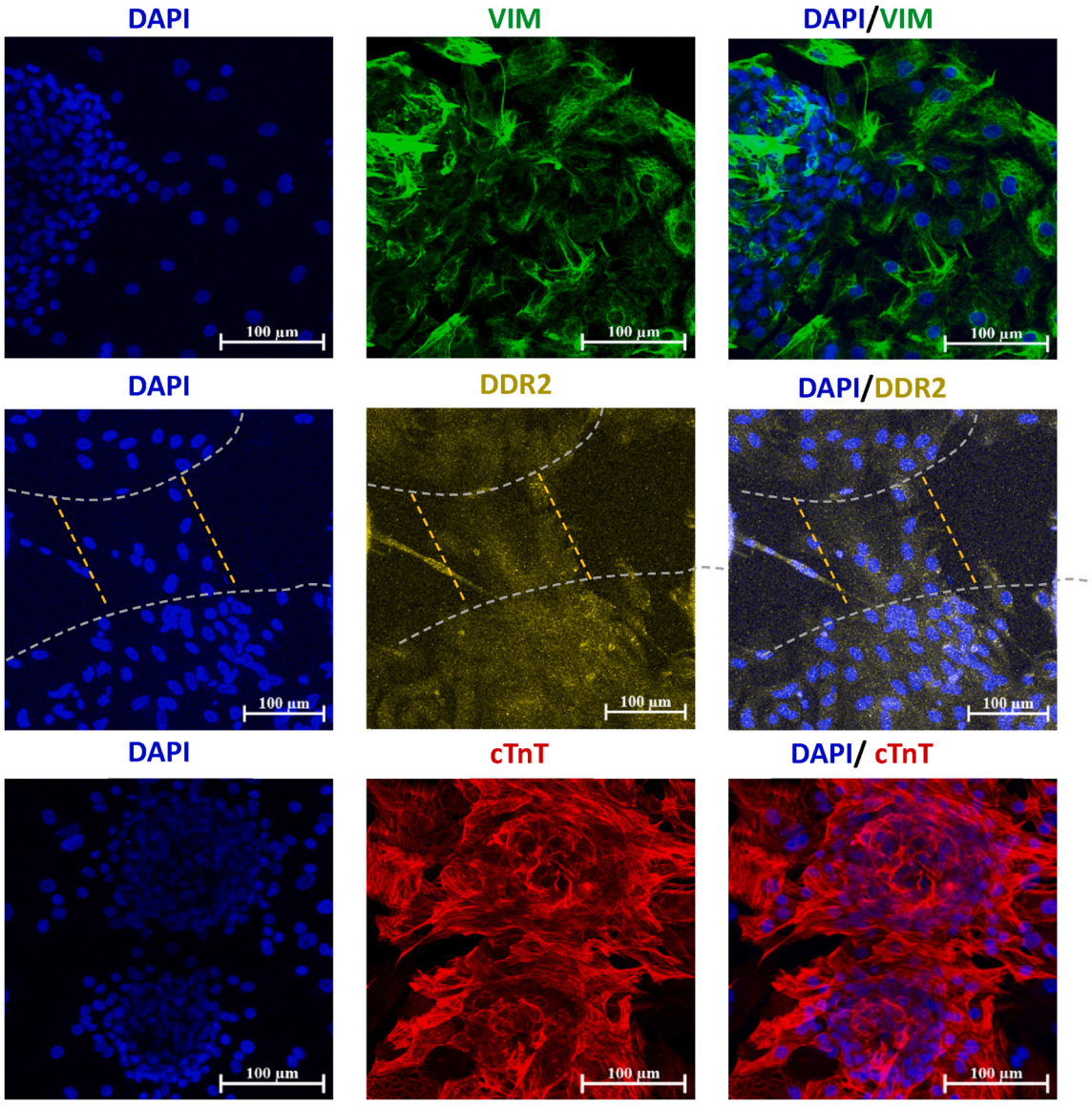



**Fig. 2.** Cell composition of the connective cell layer between the two adjacent EBs 'a bridge'. The cell layer formed by cell outgrowth from the two EBs on the adhesive surface was stained for the presence of the fibroblast marker vimentin (green), cardiac fibroblast marker DDR2 (yellow), and cardiomyocyte marker cTnT (red). The yellow color was obtained in postprocessing. Orange dashed line helps to recognize connecting 'bridge'; the grey dashed line visualizes partial contours of both EBs. (For interpretation of the references to color in this figure legend, the reader is referred to the Web version of this article.)

irregularity (vertical movement) and EBs' synchronization irregularity (lateral movement).

Further, caffeine affected the synchronization of vertical and lateral displacement of the AFM cantilever (Fig. 5). The lateral and vertical deflection peaks followed each other closely before adding caffeine, suggesting the spread of contraction waves through the syncytium (Fig. 5A). Adding caffeine caused a series of small peeks (independent lateral and vertical deflections) and ultimately resulted in complete dyssynchrony of the lateral and vertical movement (Fig. 5B). That suggests arrhythmic-like events caused by defects in signal spreading through the bridge of cells between the two EBs, resulting in the irregular beat of the two EBs (Fig. 5B).

The addition of caffeine induced the loss of synchrony between lateral and vertical deflection resulting in the displacement of the cantilever in both directions (for detail see Fig. 5C).

The novel double EB biosensor benefits from atomic force microscopy's real-time measuring mechanical response. Measuring the displacement of a soft cantilever in time gave us information about both cellular clusters' lateral and vertical movements. We hypothesized that vertical movement reports on the beat rate of the whole syncytium while lateral movement can record excitation waves spreading across the double EB set up and report on asynchronous events due to irregular beat of the adjacent EBs.

To validate our hypothesis, our model consisting of two EBs connected in syncytium was subjected to measurement of intracellular cytosolic $Ca^{2+}$ employing fluorescent calcium-sensitive detector Fluo-4. The line scan across the two EBs and their connective layer allowed for the observation of synchronization of the two EBs (Fig. 6C, D, F). Caffeine induced a progressive increase of beat rate sound with the observation by AFM. The whole syncytium presents a higher beat rate in caffeine's presence than the MEF media without the caffeine. Caffeine further induced beat rate irregularities and beating discrepancies between the two EBs suggesting the presence of synchronization defects of the two EBs in the double EB biosensor (Fig. 6C and D). Fig. 6 also shows a different pacing part of one of the clusters compared to the contraction rate of the syncytium (Fig. 6E and F). To validate our hypothesis, our model consisting of two EBs connected in syncytium was subjected to measurement of intracellular cytosolic $Ca^{2+}$ employing fluorescent

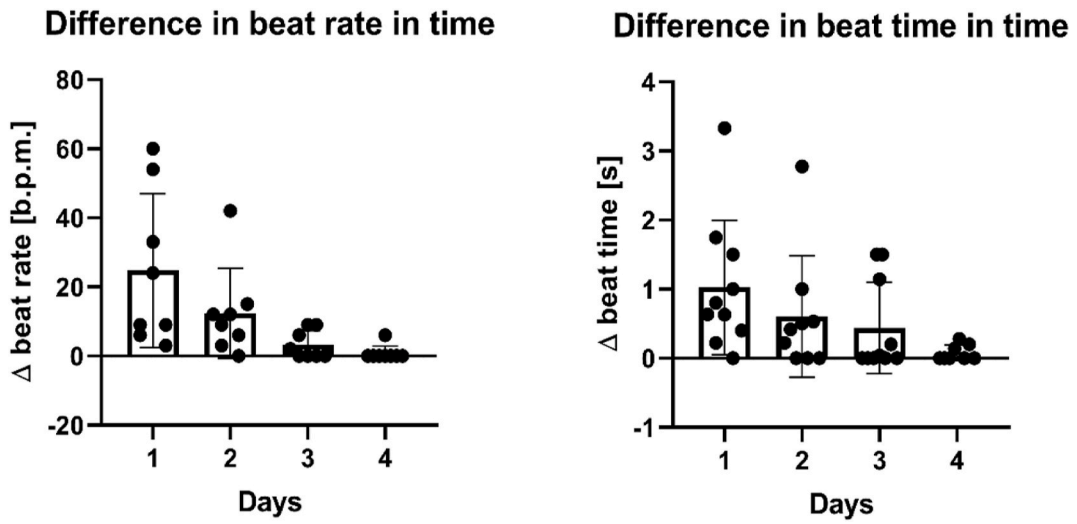



**Fig. 3.** Synchronization of the syncytium. The evolution of the difference between contraction frequency (Δ beat rate) of the two EBs is plotted against time (days) in panel A. Difference between total times of contraction of the two EBs (Δ beat time) is plotted against time (days) in panel B. The two graphs show that full synchronization of the syncytium was achieved on day 4, as they developed a common beating frequency and synchronized their beating. N = 10.

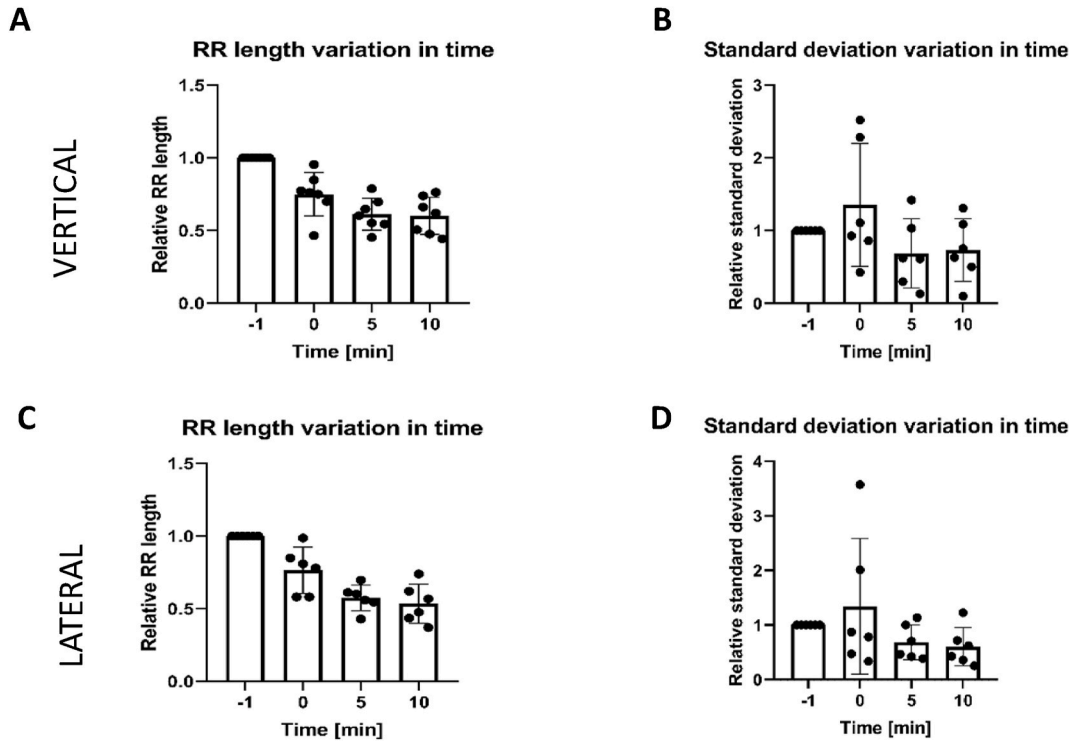



**Fig. 4.** AFM analysis of the caffeine induced changes in vertical and lateral displacement. Time -1 min indicates measurements conducted in MEF media without caffeine. Caffeine was added at 0 min with subsequent measurements at 5 and 10 min. The vertical displacement (VERTICAL) and lateral displacement (LATERAL) were analyzed. The frequencies of the vertical and lateral movement reporting on the chronotropic effect of caffeine are shown on panels A and C, while the variation of the movement in time is plotted as standard deviation values on panels A and B. Both average RR length and standard deviation have been normalized to the average RR length and standard deviation value before caffeine addition. In both cases, the RR length decreases in time, and the standard deviation increases right after adding caffeine medium.

calcium-sensitive detector Fluo-4. The line scan across the two EBs and their connective layer allowed for the observation of synchronization of the two EBs (Fig. 6B, D, F). Caffeine induced a progressive increase of beat rate sound with the observation by AFM. The syncytium presents a higher beat rate in caffeine's presence than the MEF media without the caffeine. Caffeine further induced beat rate irregularities and beating discrepancies between the two EBs suggesting the presence of synchronization defects of the two EBs in the double EB biosensor (Fig. 6C and D).

As already mentioned, in the present work, we used a 3D model derived from the model used by Ref. [52]. Our model and the single EB model agree on the arrhythmic response caused by caffeine except for the stop-and-go effect not observed in the double EB setup. Moreover, the single EB presents a lower degree of complexity as it does not allow to characterize the effects of chemical compounds on the conductive system employing AFM. Indeed, differentiated EBs present a

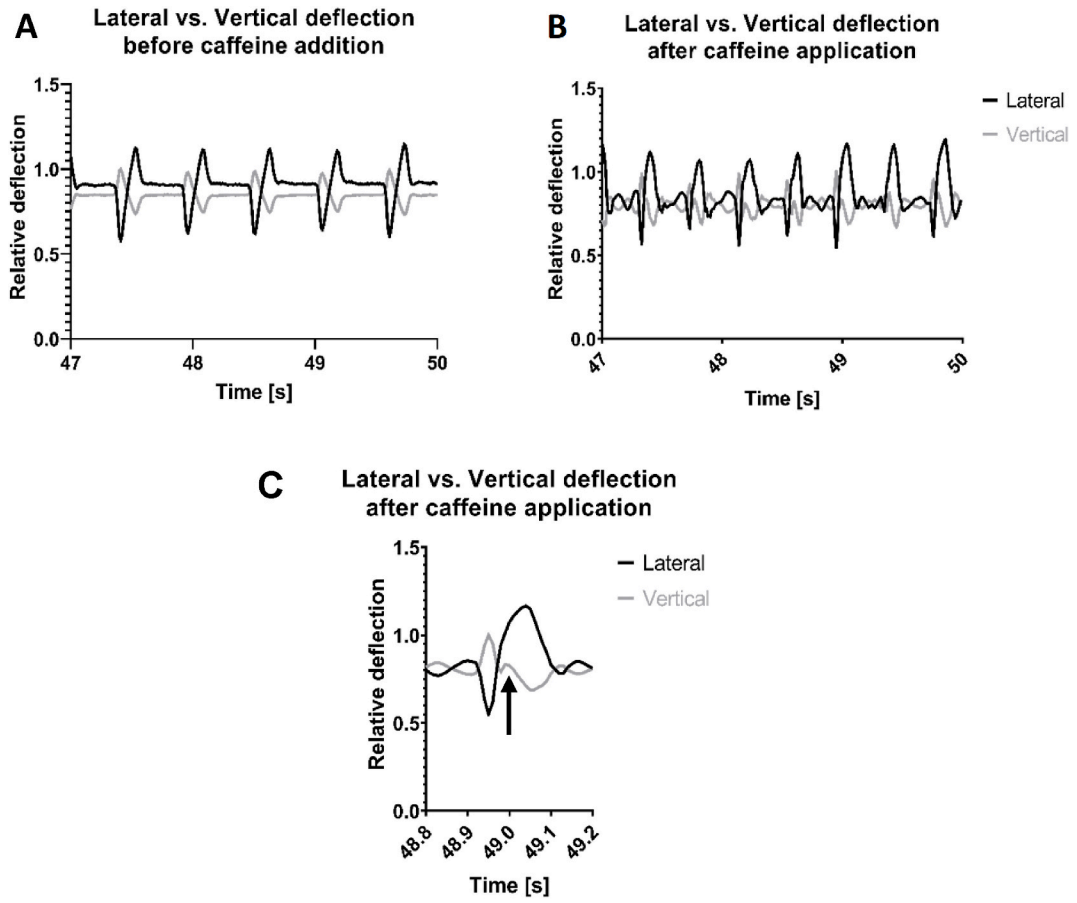



**Fig. 5.** Caffeine-induced dyssynchrony of the lateral and vertical deflections. Comparison of lateral and vertical deflection before caffeine addition (panel a) and after caffeine addition (panel b). In standard culture medium, vertical and lateral deflection appears to be synchronized with slight time shifts. Caffeine induced irregular small deflections and dyssynchrony of lateral and vertical displacements. (c) Detail of the comparison between vertical and lateral deflection after the application of caffeine. The arrow indicates the instant where dyssynchrony is detected.

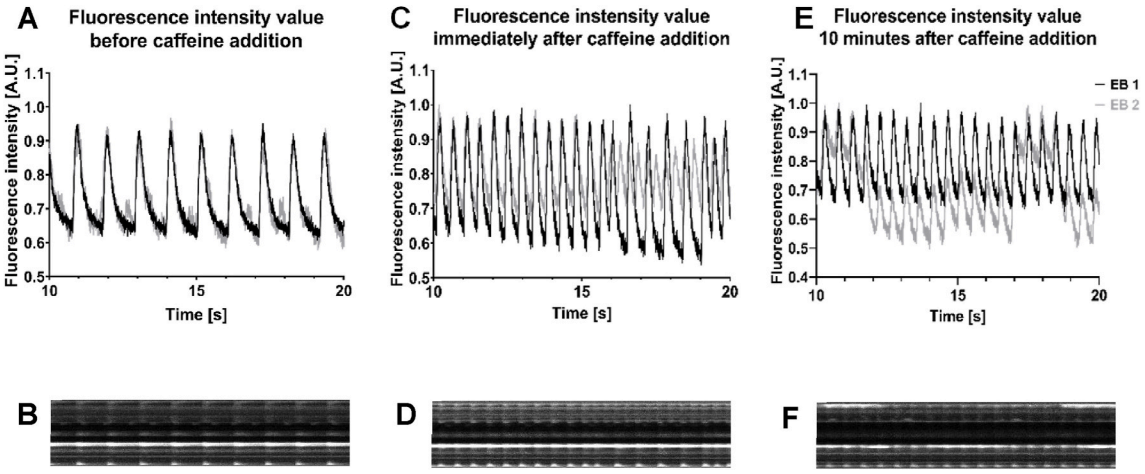



**Fig. 6.** Calcium imaging analysis of caffeine-induced synchronization defects of the double EB biosensor. Evaluation of the time evolution of the synchronicity of the two EBs (EB1 in black and EB2 in grey) of the double EB biosensor by line scan in high sampling frequency. Panels a and b show representative data of the double EB biosensor in MEF media (control). Panels c to f show three types of beat rate and synchronization defects after caffeine addition. Each curve and image represent 10 s recording before (panels A and B) and after caffeine addition (panels C to F).

combination of atrial, ventricular, and nodal CMs [53] Our model can detect rhythm abnormalities on vertical deflection and conductive disorders on a horizontal deflection by comparing vertical and lateral deflection. In the present study, a conductive defect caused by caffeine equals either ventricular or atrial fibrillation-like behavior and a decrease of contractile function. This is a precise picture of proarrhythmogenic loss of complementarity and sequentiality between vertical and horizontal deflection patterns. This proves that our detection method based on AFM is suitably sensitive for detecting arrhythmic events.

The introduction of the effects caused by the conductive cardiac system and the complex behavior of caffeine represents an advantage of our model compared to 2D models. However, the arrhythmic response of our syncytium is coherent with planar models present in the literature, whether analyzing tachycardia-like [54,55], fibrillation-like [56] or conductive anomalies [57] response.

On the other hand, the multicellular system may constitute an eventual limitation as a dual model cannot discreet single-cell phenotype as other 3D [58] or 2D [59] models, thus increasing the difficulty of studying the contribution of single cellular phenotypes on the arrhythmic response. The phenotype is a known hurdle in the process of drug screening [49]. Further, we must acknowledge that our system is unlikely to contain Purkinje bundles, the anatomical structure of the cardiac conduction system, responsible for certain kinds of arrhythmias and it' development [60]. Thus, the involvement of direct Purkinje cells generation from hESCs by cAMP signaling activation [61] might be the next step in developing a complex cardiac conduction system model.

Nevertheless, using this model has a crucial advantage. As a matter of fact, for the differentiation of EBs, it is possible to use both hESCs and hiPSCs [43]. The use of hiPSCs could be used in the future to introduce patient-specific models that would allow ad hoc drug screening [62] to select the most appropriate anti-arrhythmic drug for a given patient/pathology.

AFM also comes with limitations as the samples need to adhere, and the question of sterility comes to mind when measuring for a longer time. Some alternatives can be used for mechanical responses measurements, such as traction force microscopy or optical tweezers [63–65]. Those two, however, lack a straightforward sample preparation in the case of the former or are experimentally complex in the case of the latter. Methods based on image processing software such as Musclemotion [37], Myocyter [66] and others, offer a non-invasive way to measure mechanical response; however, they lack the sensitivity of AFM and information about contraction force. Moreover, optical methods lack exact recognition of CMs cultivated *in vitro* due to their immature morphology compared to isolated CMs and often require dissociation of the syncytium [67]. Compared to AFM, calcium imaging required sophisticated image/video postprocessing and analysis. Finally, impedance assay methods were also used for mechanical contraction measurements [68], but it's unclear whether this method would be feasible with two EBs. Some methods are probing contractile properties in the context of cellular electrophysiology rather than mechanobiology. Those methods include fluorescence voltage-sensitive or calcium-sensitive dyes, arguably suitable for this model, though, become toxic for the cells after a given time [69–71]. Compared to AFM, fluorescent calcium indicators require an incubation period and the intracellular presence of the indicator may interfere with cell physiology. Nevertheless, the fluorescent methods can serve as complementary methods.

On the other hand, a multi-electrode array (MEA) is suitable for this model as each EB can sit on a different electrode, allowing simultaneous field potential monitoring of both EBs. Still, such measurement would be complicated by adhering EBs exactly on the electrode. Optimization in this regard, for example, by different types of coating, is very desirable, as this method can be easily combined with AFM. This MEA-AFM setup would give us complex information about electro-mechanical coupling [14], together with the detection of arrhythmic events demonstrated in this paper.

## 4. Conclusion

Dual cluster CBB using human stem cell-derived CMs based model presents relevant arrhythmic response and confirms AFM as a suitable device for arrhythmia detection.

Dual cluster syncytium can spontaneously mimic phenotypes present in the neonatal heart, yet its heterogeneity might constitute a limitation. On the other hand, this model already possesses high potential for patient-specific drug screening as future application as patients' hiPSCs derived beating EBs have already been successfully differentiated.

## CRediT authorship contribution statement

**Roberto Pivato:** Methodology, Investigation, Writing – original draft. **Simon Klimovic:** Methodology, Investigation. **Daniil Kabanov:** Data curation. **Filip Sverák:** Data curation. **Martin Pesl:** Writing – review & editing. **Jan Pribyl:** Writing – review & editing, Supervision. **Vladimir Rotrekl:** Conceptualization, Writing – review & editing, Supervision.

## Declaration of competing interest

The authors declare that they have no known competing financial interests or personal relationships that could have appeared to influence the work reported in this paper.

## Acknowledgments

The European Regional Development Fund supports this project – Project ENOCH (No. CZ.02.1.01/0.0/0.0/16_019/0000868) and by Brno Ph.D. Talent Scholarship, funded by the Brno City Municipality.

CIISB, Instruct-CZ Centre of Instruct-ERIC EU consortium, funded by MEYS CR infrastructure project LM2018127, is gratefully acknowledged for the financial support of the measurements at the CF Nanobiotechnology.

Ministry of Health of the Czech Republic, grant NU20-06-00156 has financially supported this work.

## Appendix A. Supplementary data

Supplementary data to this article can be found online at https://doi.org/10.1016/j.aca.2022.339959.

## References

[1] N. Gupta, V. Renugopalakrishnan, D. Liepmann, R. Paulmurugan, B.D. Malhotra, Cell-based biosensors: recent trends, challenges and future perspectives, Biosens. Bioelectron. 141 (2019) 111435, https://doi.org/10.1016/J.BIOS.2019.111435.

[2] H. Izumi-Nakaseko, M. Hagiwara-Nagasawa, A.T. Naito, A. Goto, K. Chiba, Y. Sekino, Y. Kanda, A. Sugiyama, Application of human induced pluripotent stem cell-derived cardiomyocytes sheets with microelectrode array system to estimate antiarrhythmic properties of multi-ion channel blockers, J. Pharmacol. Sci. 137 (2018) 372–378, https://doi.org/10.1016/J.JPHS.2018.07.011.

[3] D. Jans, G. Callewaert, O. Krylychkina, L. Hoffman, F. Gullo, D. Prodanov, D. Braeken, Action potential-based MEA platform for in vitro screening of drug-induced cardiotoxicity using human iPSCs and rat neonatal myocytes, J. Pharmacol. Toxicol. Methods 87 (2017) 48–52, https://doi.org/10.1016/J.VASCN.2017.05.003.

[4] L. Wang, L. Liu, X. Li, N. Magome, K. Agladze, Y. Chen, Multi-electrode monitoring of guided excitation in patterned cardiomyocytes, Microelectron. Eng. 111 (2013) 267–271, https://doi.org/10.1016/J.MEE.2012.11.018.

[5] Q. Wang, K. Su, L. Hu, L. Zou, T. Wang, L. Zhuang, N. Hu, P. Wang, A novel and functional assay for pharmacological effects of marine toxins, saxitoxin and tetrodotoxin by cardiomyocyte-based impedance biosensor, Sensor. Actuator. B Chem. 209 (2015) 828–837, https://doi.org/10.1016/J.SNB.2014.11.150.

[6] S. Fleischer, H.G. Jahnke, E. Fritsche, M. Girard, A.A. Robitzki, Comprehensive human stem cell differentiation in a 2D and 3D mode to cardiomyocytes for long-term cultivation and multiparametric monitoring on a multimodal microelectrode array setup, Biosens. Bioelectron. 126 (2019) 624–631, https://doi.org/10.1016/J.BIOS.2018.10.061.

[7] D.S. Kim, Y.J. Jeong, B.K. Lee, A. Shanmugasundaram, D.W. Lee, Piezoresistive sensor-integrated PDMS cantilever: a new class of device for measuring the drug-induced changes in the mechanical activity of cardiomyocytes, Sensor. Actuator. B Chem. 240 (2017) 566–572, https://doi.org/10.1016/J.SNB.2016.08.167.

[8] M. Pesl, J. Pribyl, I. Acimovic, A. Vilotic, S. Jelinkova, A. Salykin, A. Lacampagne, P. Dvorak, A.C. Meli, P. Skladal, V. Rotrekl, Atomic force microscopy combined with human pluripotent stem cell derived cardiomyocytes for biomechanical sensing, Biosens. Bioelectron. 85 (2016), https://doi.org/10.1016/j.bios.2016.05.073.

[9] M. Pesl, J. Pribyl, G. Caluori, V. Cmiel, I. Acimovic, S. Jelinkova, P. Dvorak, Z. Starek, P. Skladal, V. Rotrekl, Phenotypic assays for analyses of pluripotent stem cell–derived cardiomyocytes, J. Mol. Recogn. 30 (2017) 1–14, https://doi.org/10.1002/jmr.2602.

[10] S. Warrier, A.E. Belevych, M. Ruse, R.L. Eckert, M. Zaccolo, T. Pozzan, R.D. Harvey, β-adrenergic- and muscarinic receptor-induced changes in cAMP activity in adult cardiac myocytes detected with FRET-based biosensor, Am. J. Physiol. Cell Physiol. 289 (2005) 455–461, https://doi.org/10.1152/ajpcell.00058.2005.

[11] T. Wang, N. Hu, J. Cao, J. Wu, K. Su, P. Wang, A cardiomyocyte-based biosensor for antiarrhythmic drug evaluation by simultaneously monitoring cell growth and beating, Biosens. Bioelectron. 49 (2013) 9–13, https://doi.org/10.1016/j.bios.2013.04.039.

[12] B.O. Alunda, Y.J. Lee, Review: cantilever-based sensors for high speed atomic force microscopy, Sensors 20 (2020) 1–39, https://doi.org/10.3390/S20174784.

[13] H. Liu, S. Yu, H. Zhang, J. Xu, Angiogenesis impairment in diabetes: role of methylglyoxal-induced receptor for advanced glycation endproducts, autophagy and vascular endothelial growth factor receptor 2, PLoS One 7 (2012), https://doi.org/10.1371/journal.pone.0046720.

[14] G. Caluori, J. Pribyl, M. Pesl, S. Jelinkova, V. Rotrekl, P. Skladal, R. Raiteri, Non-invasive electromechanical cell-based biosensors for improved investigation of 3D cardiac models, Biosens. Bioelectron. (2019) 124–125, https://doi.org/10.1016/j.bios.2018.10.021.

[15] N. Gupta, V. Renugopalakrishnan, D. Liepmann, R. Paulmurugan, B.D. Malhotra, Cell-based biosensors: recent trends, challenges and future perspectives, Biosens. Bioelectron. 141 (2019) 111435, https://doi.org/10.1016/j.bios.2019.111435.

[16] N.A. Geisse, AFM and combined optical techniques, Mater. Today 12 (2009) 40–45, https://doi.org/10.1016/S1369-7021(09)70201-9.

[17] M. Miletić, S. Aškrabić, J. Rüger, B. Vasić, L. Koricánac, A.S. Mondol, J. Dellith, J. Popp, I.W. Schie, Z. Dohčević-Mitrović, Combined Raman and AFM detection of changes in HeLa cervical cancer cells induced by CeO2 nanoparticles – molecular and morphological perspectives, Analyst 145 (2020) 3983–3995, https://doi.org/10.1039/C9AN02518A.

[18] J. Domke, W.J. Parak, M. George, H.E. Gaub, M. Radmacher, Mapping the mechanical pulse of single cardiomyocytes with the atomic force microscope, Eur. Biophys. J. 28 (1999) 179–186, https://doi.org/10.1007/s002490050198.

[19] C. Antzelevitch, A. Burashnikov, Overview of basic mechanisms of cardiac arrhythmia, Card. Electrophys. Clin. 3 (2011) 23–45, https://doi.org/10.1016/j.ccep.2010.10.012.

[20] S.M. Al-Khatib, W.G. Stevenson, M.J. Ackerman, W.J. Bryant, D.J. Callans, A. B. Curtis, B.J. Deal, T. Dickfeld, M.E. Field, G.C. Fonarow, A.M. Gillis, C.B. Granger, S.C. Hammill, M.A. Hlatky, J.A. Joglar, G.N. Kay, D.D. Matlock, R.J. Myerburg, R. L. Page, AHA/ACC/HRS guideline for management of patients with ventricular arrhythmias and the prevention of sudden cardiac death: executive summary: a report of the American college of cardiology/American heart association task force on clinical practice guidelines and the heart rhythm society, 2018, Heart Rhythm 15 (2017) e190, https://doi.org/10.1016/j.hrthm.2017.10.035. e252.

[21] S.S. Chugh, R. Havmoeller, K. Narayanan, D. Singh, M. Rienstra, E.J. Benjamin, R. F. Gillum, Y.H. Kim, J.H. McAnulty, Z.J. Zheng, M.H. Forouzanfar, M. Naghavi, G. A. Mensah, M. Ezzati, C.J.L. Murray, Worldwide epidemiology of atrial fibrillation: a global burden of disease 2010 study, Circulation 129 (2014) 837–847, https://doi.org/10.1161/CIRCULATIONAHA.113.005119.

[22] C.T. January, L.S. Wann, J.S. Alpert, H. Calkins, J.E. Cigarroa, J.C. Cleveland, J. B. Conti, P.T. Ellinor, M.D. Ezekowitz, M.E. Field, K.T. Murray, R.L. Sacco, W. G. Stevenson, P.J. Tchou, C.M. Tracy, J.L. Anderson, J.L. Halperin, N.M. Albert, B. Bozkurt, R.G. Brindis, M.A. Creager, L.H. Curtis, D. DeMets, R.A. Guyton, J. S. Hochman, R.J. Kovacs, E.M. Ohman, S.J. Pressler, F.W. Sellke, W.K. Shen, C. W. Yancy, AHA/ACC/HRS Guideline for the Management of Patients with Atrial Fibrillation: Executive Summary: A Report of the American College of Cardiology/American Heart Association Task Force on Practice Guidelines and the Heart Rhythm Society, 2014, https://doi.org/10.1161/CIR.0000000000000040, 2014.

[23] L.Y. Chen, N. Sotoodehnia, P. Bůžková, F.L. Lopez, L.M. Yee, S.R. Heckbert, R. Prineas, E.Z. Soliman, S. Adabag, S. Konety, A.R. Folsom, D. Siscovick, A. Alonso, Atrial fibrillation and the risk of sudden cardiac death: the atherosclerosis risk in communities study and cardiovascular health study, JAMA Intern. Med. 173 (2013) 29–35, https://doi.org/10.1001/2013.jamainternmed.744.

[24] B.J. Barnes, J.M. Hollands, Drug-induced arrhythmias, Crit. Care Med. 38 (2010), https://doi.org/10.1097/CCM.0b013e3181de112a.

[25] A. Voskoboinik, J.M. Kalman, P.M. Kistler, Caffeine and arrhythmias: time to grind the data, JACC (J. Am. Coll. Cardiol.): Clinic. Electrophys. 4 (2018) 425–432, https://doi.org/10.1016/j.jacep.2018.01.012.

[26] J.W. Daly, D. Shi, O. Nikodijevic, K.A. Jacobson, The role of adenosine receptors in the central action of caffeine, Caffeine and Behavior: current Views & Research Trends, Curr. Views Res. Trends 7 (2020) 1–31, https://doi.org/10.4324/9780429271038-1.

[27] J. Sawynok, Pharmacological rationale for the clinical use of caffeine, Drugs 49 (1995) 37–50, https://doi.org/10.2165/00003495-199549010-00004.

[28] J.L. Temple, C. Bernard, S.E. Lipshultz, J.D. Czachor, J.A. Westphal, M.A. Mestre, The safety of ingested caffeine: a comprehensive review, Front. Psychiatr. 8 (2017) 1–19, https://doi.org/10.3389/fpsyt.2017.00080.

[29] P. Wu, G. Deng, X. Sai, H. Guo, H. Huang, P. Zhu, Maturation strategies and limitations of induced pluripotent stem cell-derived cardiomyocytes, Biosci. Rep. 41 (2021) 1–16, https://doi.org/10.1042/BSR20200833.

[30] X. Lian, C. Hsiao, G. Wilson, K. Zhu, L.B. Hazeltine, S.M. Azarin, K.K. Raval, J. Zhang, T.J. Kamp, S.P. Palecek, Robust cardiomyocyte differentiation from human pluripotent stem cells via temporal modulation of canonical Wnt signaling, Proc. Natl. Acad. Sci. U. S. A. 109 (2012), https://doi.org/10.1073/pnas.1200250109.

[31] C. Zuppinger, 3D culture for cardiac cells, Biochim. Biophys. Acta Mol. Cell Res. 1863 (2016) 1873, https://doi.org/10.1016/j.bbamcr.2015.11.036. –1881.

[32] G. Pettinato, X. Wen, N. Zhang, Formation of well-defined embryoid bodies from dissociated human induced pluripotent stem cells using microfabricated cell-repellent microwell arrays, Sci. Rep. 4 (2014), https://doi.org/10.1038/srep07402.

[33] S. Kobold, A. Guhr, A. Kurtz, P. Löser, Human embryonic and induced pluripotent stem cell research trends: complementation and diversification of the field, Stem Cell Rep. 4 (2015) 914–925, https://doi.org/10.1016/j.stemcr.2015.03.002.

[34] O. Adewumi, B. Aflatoonian, L. Ahrlund-Richter, M. Amit, P.W. Andrews, G. Beighton, P.A. Bello, N. Benvenisty, L.S. Berry, S. Bevan, B. Blum, J. Brooking, K. G. Chen, A.B.H. Choo, G.A. Churchill, M. Corbel, I. Damjanov, J.S. Draper, P. Dvorak, K. Emanuelsson, R.A. Fleck, A. Ford, K. Gertow, M. Gertsenstein, P. J. Gokhale, R.S. Hamilton, A. Hampl, L.E. Healy, O. Hovatta, J. Hyllner, M. P. Imreh, J. Itskovitz-Eldor, J. Jackson, J.L. Johnson, M. Jones, K. Kee, B.L. King, B. B. Knowles, M. Lako, F. Lebrin, B.S. Mallon, D. Manning, Y. Mayshar, R.D. G. McKay, A.E. Michalska, M. Mikkola, M. Mileikovsky, S.L. Minger, H.D. Moore, C.L. Mummery, A. Nagy, N. Nakatsuji, C.M. O'Brien, S.K.W. Oh, C. Olsson, T. Otonkoski, K.Y. Park, R. Passier, H. Patel, M. Patel, R. Pedersen, M.F. Pera, M. S. Piekarczyk, R.A.R. Pera, B.E. Reubinoff, A.J. Robins, J. Rossant, P. Rugg-Gunn, T.C. Schulz, H. Semb, E.S. Sherrer, H. Siemen, G.N. Stacey, M. Stojkovic, H. Suemori, J. Szatkiewicz, T. Turetsky, T. Tuuri, S. Van Den Brink, K. Vintersten, S. Vuoristo, D. Ward, T.A. Weaver, L.A. Young, W. Zhang, Characterization of human embryonic stem cell lines by the International Stem Cell Initiative, Nat. Biotechnol. 25 (2007) 803–816, https://doi.org/10.1038/nbt1318.

[35] S. Jelinkova, P. Fojtik, A. Kohutova, A. Vilotic, L. Marková, M. Pesl, T. Jurakova, M. Kruta, J. Vrbsky, R. Gaillyova, I. Valášková, I. Frák, A. Lacampagne, G. Forte, P. Dvorak, A.C. Meli, V. Rotrekl, Dystrophin deficiency leads to genomic instability in human pluripotent stem cells via NO synthase-induced oxidative stress, Cells 8 (2019) 53, https://doi.org/10.3390/cells8010053.

[36] S. Jelinkova, A. Vilotic, J. Pribyl, F. Aimond, A. Salykin, I. Acimovic, M. Pesl, G. Caluori, S. Klimovic, T. Urban, H. Dobrovolna, V. Soska, P. Skladal, A. Lacampagne, P. Dvorak, A.C. Meli, V. Rotrekl, DMD pluripotent stem cell derived cardiac cells recapitulate in vitro human cardiac pathophysiology, Front. Bioeng. Biotechnol. 8 (2020), https://doi.org/10.3389/fbioe.2020.00535.

[37] L. Sala, B.J. Van Meer, L.G.J. Tertoolen, J. Bakkers, M. Bellin, R.P. Davis, C. Denning, M.A.E. Dieben, T. Eschenhagen, E. Giacomelli, C. Grandela, A. Hansen, E.R. Holman, M.R.M. Jongbloed, S.M. Kamel, C.D. Koopman, Q. Lachaud, I. Mannhardt, M.P.H. Mol, D. Mosqueira, V.V. Orlova, R. Passier, M.C. Ribeiro, U. Saleem, G.L. Smith, F.L. Burton, C.L. Mummery, Musclemotion: a versatile open software tool to quantify cardiomyocyte and cardiac muscle contraction in vitro and in vivo, Circ. Res. 122 (2018), https://doi.org/10.1161/CIRCRESAHA.117.312067 e5–e16.

[38] D. Kabanov, CardioScripts: scripts for calculations of cardiac data such as MEA results and calcium sparks. https://github.com/DaniilKabanov/CardioScripts. (Accessed 12 January 2022).

[39] S. Klimovic, M. Scurek, M. Pesl, D. Beckerova, S. Jelinkova, T. Urban, Z. Starek, M. Bebarova, J. Pribyl, V. Rotrekl, K. Brat, Aminophylline Induces Two Types of Arrhythmic Events in Human Pluripotent Stem Cell-Derived Cardiomyocytes - Dataset, 2021. https://zenodo.org/record/4552607.

[40] J. Schindelin, I. Arganda-Carreras, E. Frise, V. Kaynig, M. Longair, T. Pietzsch, S. Preibisch, C. Rueden, S. Saalfeld, B. Schmid, J.Y. Tinevez, D.J. White, V. Hartenstein, K. Eliceiri, P. Tomancak, A. Cardona, Fiji: an open-source platform for biological-image analysis, Nat. Methods 9 (2012) 7, https://doi.org/10.1038/nmeth.2019, 9 (2012) 676–682.

[41] E. Tarbit, I. Singh, J.N. Peart, R.B. Rose'Meyer, Biomarkers for the identification of cardiac fibroblast and myofibroblast cells, Heart Fail. Rev. 24 (2019) 1–15, https://doi.org/10.1007/s10741-018-9720-1.

[42] P. Camelliti, T.K. Borg, P. Kohl, Structural and functional characterisation of cardiac fibroblasts, Cardiovasc. Res. 65 (2005) 40–51, https://doi.org/10.1016/j.cardiores.2004.08.020.

[43] S. Jelinkova, A. Vilotic, J. Pribyl, F. Aimond, A. Salykin, I. Acimovic, M. Pesl, G. Caluori, S. Klimovic, T. Urban, H. Dobrovolna, V. Soska, P. Skladal, A. Lacampagne, P. Dvorak, A.C. Meli, V. Rotrekl, DMD pluripotent stem cell derived cardiac cells recapitulate in vitro human cardiac pathophysiology, Front. Bioeng. Biotechnol. 8 (2020) 1–19, https://doi.org/10.3389/fbioe.2020.00535.

[44] X. Zhang, C. Simerly, C. Hartnett, G. Schatten, T.E. Smithgall, Src-family tyrosine kinase activities are essential for differentiation of human embryonic stem cells, Stem Cell Res. 13 (2014) 379, https://doi.org/10.1016/J.SCR.2014.09.007.

[45] J. Liu, C. Huang, X. Zhan, Src is required for cell migration and shape changes induced by fibroblast growth factor 1, Oncogene 18 (1999) 48, https://doi.org/10.1038/sj.onc.1203050, 18 (1999) 6700–6706.

[46] D.M. Kilkenny, J.v. Rocheleau, J. Price, M.B. Reich, G.G. Miller, c-Src regulation of fibroblast growth factor-induced proliferation in murine embryonic fibroblasts, J. Biol. Chem. 278 (2003) 17448–17454, https://doi.org/10.1074/JBC.M209698200.

[47] Y. Jang, S.C. Choi, D.S. Lim, J.H. Kim, J. Kim, Y. Park, Modulating cardiomyocyte and fibroblast interaction using layer-by-layer deposition facilitates synchronisation of cardiac macro tissues, Soft Matter 16 (2020) 428–434, https://doi.org/10.1039/c9sm01531k.

[48] A. Eder, I. Vollert, A. Hansen, T. Eschenhagen, Human engineered heart tissue as a model system for drug testing, Adv. Drug Deliv. Rev. 96 (2016) 214–224, https://doi.org/10.1016/j.addr.2015.05.010.

[49] L. Sala, M. Bellin, C.L. Mummery, Integrating cardiomyocytes from human pluripotent stem cells in safety pharmacology: has the time come? Br. J. Pharmacol. 174 (2017) 3749–3765, https://doi.org/10.1111/bph.13577.

[50] J.M. Dewing, V. Saunders, I. O'Kelly, D.I. Wilson, Defining cardiac cell populations and relative cellular composition of the early fetal human heart, bioRxiv (2021) 2021, 10.21.465281.
[51] Y. Aratyn-Schaus, F.S. Pasqualini, H. Yuan, M.L. McCain, G.J.C. Ye, S.P. Sheehy, P. H. Campbell, K.K. Parker, Coupling primary and stem cell-derived cardiomyocytes in an in vitro model of cardiac cell therapy, JCB (J. Cell Biol.) 212 (2016) 389–397, https://doi.org/10.1083/jcb.201508026.
[52] M. Pesl, I. Acimovic, J. Pribyl, R. Hezova, A. Vilotic, J. Fauconnier, J. Vrbsky, P. Kruzliak, P. Skladal, T. Kara, V. Rotrekl, A. Lacampagne, P. Dvorak, A.C. Meli, Forced aggregation and defined factors allow highly uniform-sized embryoid bodies and functional cardiomyocytes from human embryonic and induced pluripotent stem cells, Heart Ves. 29 (2014), https://doi.org/10.1007/s00380-013-0436-9.
[53] N. Naumova, L. Iop, Bioengineering the cardiac conduction system: advances in cellular, gene, and tissue engineering for heart rhythm regeneration, Front. Bioeng. Biotechnol. 9 (2021) 1–21, https://doi.org/10.3389/fbioe.2021.673477.
[54] R. Balasubramaniam, S. Chawla, A.A. Grace, C.L.H. Huang, Caffeine-induced arrhythmias in murine hearts parallel changes in cellular Ca2+ homeostasis, Am. J. Physiol. Heart Circ. Physiol. 289 (2005) 1584–1593, https://doi.org/10.1152/ajpheart.01250.2004.
[55] W. Korohoda, A. Jurkiewicz, I. Figiel, J. Czyz, A new model for the research into rhythmic contraction activity of cardiomyocytes in vitro, Biochem. Cell. Biol. 73 (1995) 431–439, https://doi.org/10.1139/o95-050.
[56] S. Shafaattalab, E. Lin, E. Christidi, H. Huang, Y. Nartiss, A. Garcia, J. Lee, S. Protze, G. Keller, L. Brunham, G.F. Tibbits, Z. Laksman, Ibrutinib displays atrial-specific toxicity in human stem cell-derived cardiomyocytes, Stem Cell Rep. 12 (2019) 996–1006, https://doi.org/10.1016/j.stemcr.2019.03.011.
[57] H. Satoh, Positive and negative chronotropic effects of caffeine in spontaneously beating rabbit sino-atrial node cells, Gen. Pharmacol. 24 (1993) 1223–1230, https://doi.org/10.1016/0306-3623(93)90372-5.
[58] M. Kawatou, H. Masumoto, H. Fukushima, G. Morinaga, R. Sakata, T. Ashihara, J. K. Yamashita, Modelling Torsade de Pointes arrhythmias in vitro in 3D human iPS cell-engineered heart tissue, Nat. Commun. 8 (2017) 1–11, https://doi.org/10.1038/s41467-017-01125-y.
[59] M. Gharanei, S. Shafaattalab, S. Sangha, M. Gunawan, Z. Laksman, L. Hove-Madsen, G.F. Tibbits, Atrial-specific hiPSC-derived cardiomyocytes in drug discovery and disease modeling, Methods (2021), https://doi.org/10.1016/j.ymeth.2021.06.009.
[60] K.H.W.J.T. Tusscher, A.V. Panfilov, Modelling of the ventricular conduction system, Prog. Biophys. Mol. Biol. 96 (2008) 152–170, https://doi.org/10.1016/j.pbiomolbio.2007.07.026.
[61] S.Y. Tsai, K. Maass, J. Lu, G.I. Fishman, S. Chen, T. Evans, Efficient generation of cardiac Purkinje cells from ESCs by activating cAMP signaling, Stem Cell Rep. 4 (2015) 1089–1102, https://doi.org/10.1016/j.stemcr.2015.04.015.
[62] S. Kussauer, R. David, H. Lemcke, hiPSCs derived cardiac cells for drug and toxicity screening and disease modeling: what micro- electrode-array analyses can tell us, Cells 8 (2019) 1331, https://doi.org/10.3390/CELLS8111331, 8 (2019) 1331.
[63] C. Arbore, L. Perego, M. Sergides, M. Capitanio, Probing force in living cells with optical tweezers: from single-molecule mechanics to cell mechanotransduction, Biophys. Rev. 11 (2019) 765–782, https://doi.org/10.1007/s12551-019-00599-y.
[64] M. Lekka, K. Gnanachandran, A. Kubiak, T. Zieliński, J. Zemła, Traction force microscopy – measuring the forces exerted by cells, Micron 150 (2021), https://doi.org/10.1016/j.micron.2021.103138.
[65] J.A. Schaefer, R.T. Tranquillo, Tissue contraction force microscopy for optimization of engineered cardiac tissue, tissue engineering - Part C: methods, 22, https://doi.org/10.1089/ten.tec.2015.0220, 2016, 76-83.
[66] T. Grune, C. Ott, S. Häseli, A. Höhn, T. Jung, The "MYOCYTER" – convert cellular and cardiac contractions into numbers with ImageJ, Sci. Rep. 9 (2019) 1–13, https://doi.org/10.1038/s41598-019-51676-x.
[67] M.L. Rodriguez, B.T. Graham, L.M. Pabon, S.J. Han, C.E. Murry, N.J. Sniadecki, Measuring the contractile forces of human induced pluripotent stem cell-derived cardiomyocytes with arrays of microposts, J. Biomech. Eng. 136 (2014), https://doi.org/10.1115/1.4027145.
[68] H.G. Jahnke, D. Steel, S. Fleischer, D. Seidel, R. Kurz, S. Vinz, K. Dahlenborg, P. Sartipy, A.A. Robitzki, A novel 3D label-free monitoring system of hES-derived cardiomyocyte clusters: a step forward to in vitro cardiotoxicity testing, PLoS One 8 (2013) 1–9, https://doi.org/10.1371/journal.pone.0068971.
[69] A. Ahola, R.P. Pölönen, K. Aalto-Setälä, J. Hyttinen, Simultaneous measurement of contraction and calcium transients in stem cell derived cardiomyocytes, Ann. Biomed. Eng. 46 (2018) 148–158, https://doi.org/10.1007/s10439-017-1933-2.
[70] S. Guatimosim, C. Guatimosim, L.S. Song, Imaging calcium sparks in cardiac myocytes, Methods Mol. Biol. 689 (2011) 205–214, https://doi.org/10.1007/978-1-60761-950-5_12.
[71] T.J. Herron, P. Lee, J. Jalife, Optical imaging of voltage and calcium in cardiac cells & tissues, Circ. Res. 110 (2012) 609–623, https://doi.org/10.1161/CIRCRESAHA.111.247494.